Multiscale variation of 3D tooth forms in selachians and developmental and evolutionary inferences : Odyssey of a scyliorhinid tooth

Fidji Berio

Numéro National de Thèse : 2021LYSEN010

THÈSE de DOCTORAT DE L'UNIVERSITÉ DE LYON

opérée par

l'École Normale Supérieure de Lyon

École doctorale N° 341
Évolution, Écosystèmes, Microbiologie, Modélisation

Spécialité de doctorat : Sciences de la vie et de la santé
Discipline : Biologie

Soutenue publiquement le 07/04/2021 par
Fidji BERIO

Variation multiscalaire des formes dentaires en 3D chez les sélaciens et inférences développementales et évolutives : odyssée d'une dent de scyliorhinidé

Multiscale variation of 3D tooth forms in selachians and developmental and evolutionary inferences: Odyssey of a scyliorhinid tooth

---

Devant le jury composé de :

Adnet, Sylvain	Maître de Conférences	Université de Montpellier	Rapporteur
Kriwet, Jürgen	Professeur	Université de Vienne	Rapporteur
Di Santo, Valentina	*Assistant professor*	Université de Stockholm	Examinatrice
Dean, Mason	*Assistant professor*	Institut Max Planck des colloïdes et des interfaces	Examinateur
Janvier, Philippe	Directeur de Recherche émérite	Museum National d'Histoire Naturelle	Examinateur
Goudemand, Nicolas	Professeur	ENS de Lyon	Directeur
Debiais-Thibaud, Mélanie	Maître de Conférences	Université de Montpellier	Co-directrice

Steve Zissou: *"Now if you'll excuse me, I'm going to go on an overnight drunk, and in ten days I'm going to set out to find the shark that ate my friend and destroy it. Anyone who wants to tag along is more than welcome. [...]"*
Woman: *"That's an endangered species at most. What would be the scientific purpose of killing it?"*
Steve Zissou: *"Revenge."*

– *The Life Aquatic with Steve Zissou*, 2004

"Oui, la mer est tout. [...] C'est l'immense désert où l'homme n'est jamais seul, car il sent frémir la vie à ses côtés."

– *Vingt mille lieues sous les mers*, 1870, Jules Vernes

Abstract

Teeth are serial structures whose evolutionary and developmental history is intricately linked with the emergence of mineralised tissues in vertebrates. Teeth display a broad range of forms and differ in developmental patterns in extant vertebrates, making them remarkable elements to study species diversification. Selachian teeth renew permanently and display morphologies that are correlated with mating and trophic behaviours.

This work first assesses the variation of tooth forms in two scyliorhinids by using 3D geometric morphometrics and machine learning. The emergence of gynandric heterodonty is detailed for the first time along the ontogeny of sharks and it is demonstrated that this natural variation should be first assessed before performing species discrimination.

This work also questions the role of specific proteins on the acquisition of a shark tooth form over development. Functional tests suggest an impact of Shh and Fgf3 in the cusp morphogenesis and in the mineralisation process. These proteins are promising explanatory variables to the inter- and intraspecific tooth differences observed, leading to hypotheses on their role in the evolution of structures with speciation and trophic and mating behaviours.

Histological data on extant chondrichthyan vertebrae finally highlight the unsuspected proportion of extant elasmobranchs exhibiting fibrous mineralisation in the neural arches, a bone-like tissue which occurrence had long been refuted in this group. Evolutionary considerations are discussed in the light of the evolution of jawed vertebrates and question on the ecological factors that led particular tissues to be restricted to specific shark and batoid groups.

Keywords chondrichthyans; evo-devo; geometric morphometrics; histology; machine learning; scyliorhinids; tooth morphology; vertebrae

Acknowledgements

Je remercie mes directeurs, Mélanie et Nicolas d'avoir parié sur moi, financé ma thèse et de m'avoir soutenue durant ces années. Je remercie Nicolas pour avoir discrètement laissé les portes ouvertes sur un chemin engageant nécessairement à l'autonomie.

Je te remercie Mélanie d'avoir exaucé mon rêve de disséquer des raies géantes congelées à la scie rouillée, d'avoir étanché ma soif de meurtre de requins au nom de la science et de m'avoir permis de trouver l'aventure dans les volumineux et millénaires bidons d'alcool dont la fragrance fermentée et la robe opaque et grasse recèlent des mâchoires qui mordent encore. Merci de m'avoir entraînée dans le tourbillon des chondrichtyens que j'espérais intégrer depuis si longtemps. Je te remercie de m'avoir permis de fureter par monts et par vaux et de m'avoir fait confiance par la force des choses. Merci de m'avoir accompagnée jusqu'au bout de ma thèse, d'avoir partagé ta vision d'une science intègre et collaborative. Merci de m'avoir importée dans cette équipe et dans cet institut dans lesquels j'ai trouvé une ambiance de travail idéale, à l'exception bien sûr des clés manquantes, des courants d'air hivernaux, de mon fauteuil rachitique et de la paléopoésie que tu estimes tant.

Je remercie Sylvie, Ronan et Maxence de l'Observatoire Océanologique de Banyuls-sur-mer de nous avoir, Mélanie et moi, laissé salir leurs paillasses, d'avoir tendrement veillé sur nos embryons de roussettes et d'avoir fait tomber des têtes au nom de la science. Je remercie Sophie Germain Pigno de l'Aquarium du Cap d'Agde de m'avoir permis de compléter mon échantillonnage de roussettes, dans le respect des lois du trafic de requins. Je remercie Nicolas Hirel de Planet Ocean Montpellier d'avoir partagé sa passion et sa connaissance des chimères et pour son aimable collaboration à plusieurs projets. Je remercie Nelly et Morgane du Réseau d'Histologie Expérimentale de Montpellier pour avoir généré un arc-en-ciel de coupes histologiques, selon notre lubie passagère. Je remercie Sébastien Enault pour sa gentillesse et pour les jolies coupes histologiques qu'il a laissées après son passage et grâce auxquelles j'ai pu entrevoir un futur qui n'était pas fait que de dents.

I thank Daniel from the Zuse Institute Berlin for having saved a huge amount of my time and for his availability, teaching ability, expertise, and kindness. I thank Mason for allowing me participating to the organisation of the Comparative Cartilage Biology meeting, for being amenable and for bringing fun into science. I thank him, Júlia Chaumel, and Ronald Seidel for inspiring discussions on sharks, science, or sharks in science.

I thank my jury members, Sylvain Adnet, Jürgen Kriwet, Valentina Di Santo, Mason Dean, and Philippe Janvier for accepting to kindly evaluate my work and for that their own research has inspired me during these years.

Je remercie Renaud et Mathilde de m'avoir laissée passer de si longues heures au microCT scan et d'avoir fait germer dans ma tête ces patrons d'art moderne communs à de nombreux collègues dont l'un des défis est bien souvent de maintenir immobile une carcasse dégoulinante d'alcool durant une heure dans le microtomographe.

Je remercie Allowen et Julien d'avoir été les piliers de mon apprentissage de la morphométrie géométrique tout en constituant les pôles changeants d'un même aimant. Je les remercie d'avoir remis mon travail de thèse sur un sentier moins sinueux et d'avoir été peu regardants quant au fatras de mes lignes de code souvent saluées d'un « *error* » fatidique et quant aux principes indérogeables de la Sainte Morphométrie sur lesquels j'ai pris la plaisante liberté de m'asseoir. Je les remercie également de m'avoir permis de constater que tout peut toujours être discuté par Julien Claude.

Je remercie plus généralement Richard, Olivier, Margot, Cyrena, Roxanne, Mathieu, Vincent, Kathleen, Kim, Misha, Laurent, Agathe, Cynthia et Marion de l'Université du Québec à Rimouski d'avoir subrepticement semé autour de moi et sans en avoir l'air les principes du travail d'équipe, de bienveillance, d'égalité et d'entraide et de m'avoir permis de me familiariser avec le fabuleux monde des raies.

Je remercie Sylvain, Guillaume et Henri de m'avoir permis de faire prendre l'air aux mâchoires de requins des collections de l'ISEM et de m'avoir laissée plonger dans les bidons des sous-sols à la recherche d'un précieux spécimen trop longtemps préservé des blocs de paraffine. Je les remercie de m'avoir épargné des heures de lecture de clés d'identification et de m'avoir parfois fait entrevoir leur collection bibliographique millénaire dont l'exhaustivité relègue certainement la bibliothèque d'Alexandrie au rang de collection de timbres.

Je remercie mes compagnons et collègues lyonnais, Pauline G, Louise, Ludivine, Pauline J, Mathilde, Thomas, Jérémie, Sam, Roland et Cyril de m'avoir aidée dans la bonne humeur à chaque fois que je l'ai demandé, de ne pas avoir laissé sommeiller mon indignation et d'avoir reconnu que les conodontes ne sont pas des vertébrés. Je remercie particulièrement Pauline G et Louise qui, un soir au laboratoire, m'ont aidée à parcourir incognito cinquante mètres bien difficiles en respectant les limites de vitesse.

Je remercie les membres de mon comité de thèse, Régis Chirat, Guillaume Guinot, Sophie Pantalacci et Sabrina Renaud de m'avoir écoutée, fait confiance et de ne pas avoir reculé devant les obstacles lorsque de nombreuses autres personnes s'adonnent à cette discipline. Leur aide a largement contribué à ce que je termine ma thèse.

Je remercie mes collègues d'enseignement pour avoir partagé, avec un niveau de sang-froid relatif, les salles de TD et de TP et de n'avoir cédé que virtuellement à l'appel du lancer de scalpel. Si je sais à présent que les années d'enseignement ne préparent en rien aux géniales conclusions des étudiants, elles présentent toutefois l'avantage de former l'esprit à la possibilité de l'existence d'univers parallèles. Je remercie mes stagiaires avec lesquels j'ai pu générer, sinon des résultats révolutionnaires, des discussions enrichissantes et des rires.

Je remercie généralement les isémiens et isémiennes pour leur accueil chaleureux, leur gentillesse et leur disponibilité. L'ambiance qu'ils et elles créent à l'ISEM m'y a fait travailler et vivre avec joie.

Je remercie les personnes de la folle équipe de Montpellier : Sylvie pour m'avoir octroyé le don d'ubiquité par semi-procuration pendant quelques temps entre le microCT scan et la paillasse, Julien pour le cours d'œnologie à Barcelone, son enseignement scientifique et sa démonstration du panache en toutes circonstances. Je remercie Nicolas pour sa disponibilité, ses nombreux services et sa bonne humeur permanente. Je remercie Camille pour sa gentillesse, sa bienveillance, son humanité, sa bonne humeur, son entrain et pour m'avoir laissée entrevoir les miroitements de son royaume adoré et

farouchement gardé : la paillasse. Je remercie Amira de m'avoir accordé son amitié et sa confiance et d'avoir partagé avec moi sa sagesse, sa force et une autre vision du monde.

Te agradezco Faviel por haber aceptado trabajar conmigo sin realmente conocerme, seguir conociéndome y por haber trasformado parte de tus vacaciones en una búsqueda de tiburones. Gracias por tu gentileza y por compartir la experiencia tuya del doctorado.

Je remercie les compagnons avec lesquels j'ai hanté l'ISEM : Arthur pour ta bienveillante maladresse et ta profonde gentillesse, Alexandre pour le trafic d'informations et de clés sous le manteau, Quentin pour chaque jour tenter de nous soustraire, pauvres mortels, à nos obsolètes croyances en la rotondité terrestre et l'évolution des espèces et Marianne pour avoir mis de la vie dans les couloirs inanimés. Je remercie Adèle de m'avoir fait me tenir sur mes gardes au détour des couloirs et d'avoir imprégné ces murs que j'emporte avec moi d'un enthousiasme et d'une bonne humeur à toute épreuve. Je remercie Manon dont la chaleur de l'accueil lors de mon premier jour ne s'est jamais estompée et dont la révolte permanente, la ténacité et les nombreuses convictions et batailles ont achevé de me convaincre que ce pays est géré comme un groupe d'étudiants en littérature devant R, par des mâles obnubilés par la soif inextinguible de notre asservissement. Ton caractère, aussi semblable au mien qu'il y est opposé, nous a offert de rire de l'outrageux au ridicule et du futile au déplorable.

Je te remercie Pauline pour ton exubérance publique qui égale ta discrétion privée et pour avoir su te tenir si longtemps sur ce point exact d'équilibre qui fait les vraies amies. Tu ne seras pas surprise si je te remercie pour cet humour si caustique et parfois, il faut bien l'admettre, si frivole que je recherche tant pour ne le trouver qu'en très peu de personnes, fussent-elles conodontologues.

Je remercie ma belle-famille pour avoir suivi d'un œil distrait mais toujours bienveillant mon travail incompréhensible et à toutes fins relativement inutile.

Je remercie les Fantastic Four et Dou-mi de m'avoir toujours encouragée à condenser, laisser tomber et persévérer lorsqu'il le fallait, d'avoir essayé de comprendre et entretenu ma folie contrôlée pour ce long chemin parcouru ensemble, sans avoir jamais fléchi.

Yann, merci. La longue route est derrière et devant. Elle est sinueuse, vertigineuse, paisible et tourmentée mais de ce béton fibré qui font les dalles sur lesquelles tout repose. Elle est une, indistincte et miroitante, parcourue de frissons entremêlés. Elle est d'une inébranlable évidence, mon phare dans la nuit.

Au palpitant à fond de cale léthargique
Avalant les clapots indistincts de l'ailleurs
Où se glisse un Léviathan usé, erratique :
La mer s'ouvre, la mer éveille et la mer leurre.

Des lames sans octave émerge le profond,
Turbulent grondement de l'Immense et grouillant
Qui vient sans éclairer et dépèce les routes,
Amenuise les voix et érige les rêves.

Tremblante et humble éclate aux vies des naufragés
Cette scélérate qui emporte les voix nues,
Des phares vacillants enlacés et griffant
Le cap chancelant vers les limbes étendues

Mais le grain s'amenuise et le lagon émerge
Scintillant et bleu, bleu des lointaines Marquises.
Sur la berge s'échoue une ridule. Non, non,
S'étire en volupté avant de joindre le large.

Contents

List of figures

List of Tables

List of acronyms

Chapter 1
The rise of odontodes and teeth

1.1 Evolutionary origin and diversity of odontodes

1.1.1 The exoskeleton of early vertebrates

In the beginning of Vertebrates was the exoskeleton, an extensively developed and mineralised version of skeleton that covered the head and body of species [Sire and Huysseune, 2003]. Most of the exoskeleton of early vertebrates was composed of dermal bones, but isolated highly mineralised elements of dentine and enameloid were attached to these bony plates and covered the head and body at various degrees, depending on the species [Janvier, 1996; Sire and Huysseune, 2003; Giles et al., 2013]. Histological features of these early exoskeletons usually revealed multilayered structures made of superficial dentine-enameloid tubercles or a superficial dermal bone-like layer, a medial spongy bone layer, and a basal, compact lamellar bone layer [Donoghue et al., 2006; Giles et al., 2013]. Although some stem gnathostome positions are still phylogenetically unsolved, the ancestral organisation of the exoskeleton could be hypothesised as a three layered structure: a superficial one composed of dentine covered by an enameloid cap, a mesial layer made of osteons, and a basal isopedin-like layer [Keating et al., 2015]. As a consequence, a striking feature emerging from paleontological data is the concomitant evolution of a variety of mineralised tissues in early vertebrates. These early tissues have affinities to the tissues composing both modern teeth and bones.
From the evolution of these early forms, the extant diversity of vertebrates includes agnathans and gnathostomes, in which are the chondrichthyans and osteichthyans that diverged about 422 million years ago [Benton et al., 2009] (Figure 1.1). My work focuses on extant chondrichthyans, a group that includes neoselachians or sharks (galeomorphs and squalomorphs), batoids or batomorphs (both forming the group of elasmobranchs), and holocephalans (chimaeras) (Figure 1.2) [Inoue et al., 2010; Janvier and Pradel, 2015; Last et al., 2016].

The mineralised skeleton of extant vertebrates can be composed of four types of tissues that are characterised by different natures of the extracellular matrix and are synthesised by distinct cell types [Hall, 2015]. The most mineralised tissues are the enamel or enameloid and dentine of teeth and dermal scales, which are respectively produced by the ameloblasts of ectodermal origin and by the odontoblasts derived from the neural crest (ectomesenchymal cells). Lamellar bone tissue is composed of spongy (cancellous or trabecular) bone and of compact bone. Spongy bone is arranged in flat lamellae parallel to the bone element surface that intertwine with bone marrow and blood vessels, while compact bone is organised in concentric lamellae forming

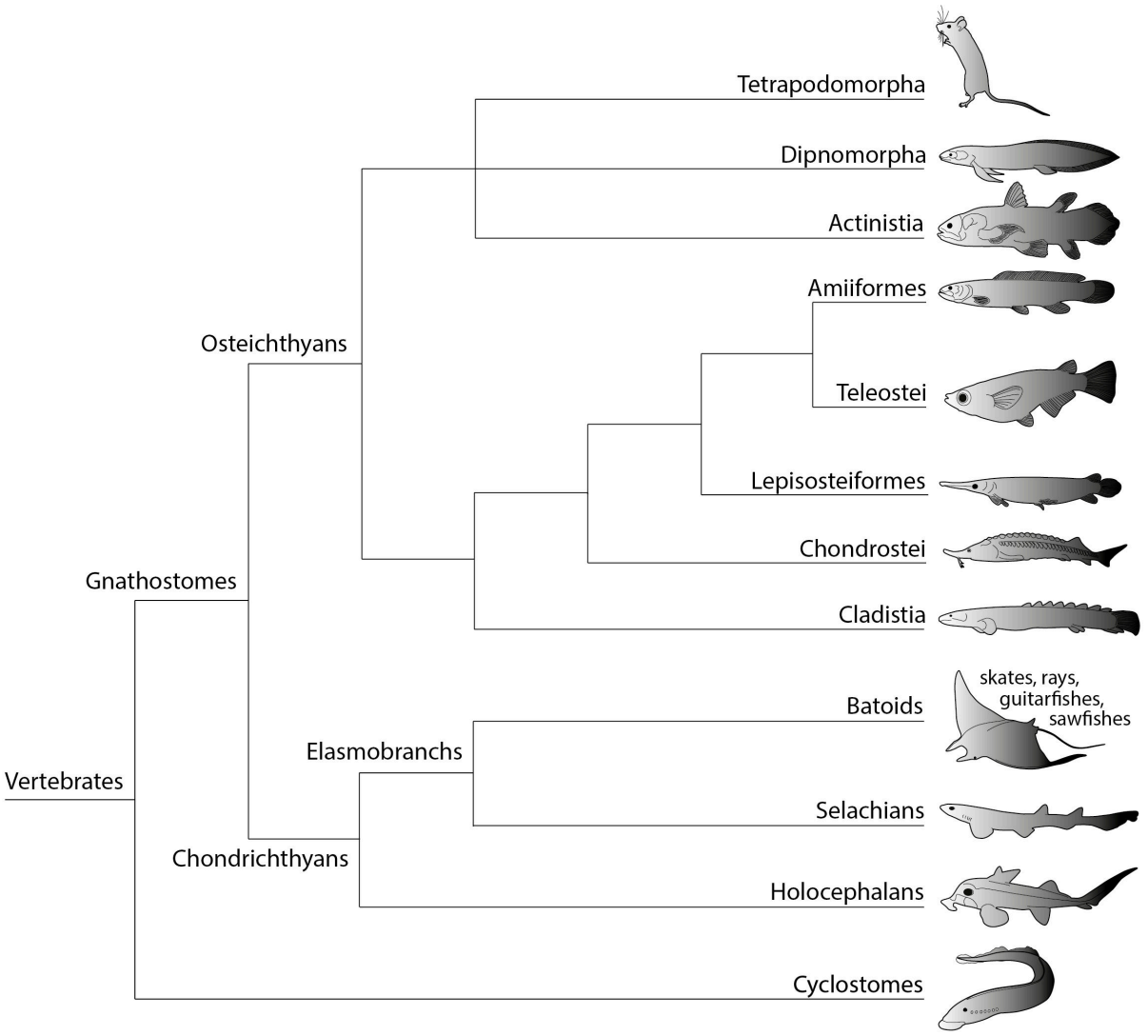

FIGURE 1.1: Simplified phylogeny of extant vertebrates

osteons. Bone tissue is produced by osteoblasts of mesodermal origin (except in head bones) that are progressively enclosed in the matrix, and become osteocytes. Mineralised cartilage is a transitional (during endochondral ossification) or restricted in space in most vertebrates, whereas it is the normal condition in the chondrichthyan endoskeleton. In vertebrates, neural crest cells participate to the production of bone and cartilage in the head. The cells producing the cartilage matrix are chondroblasts and chondrocytes and the cartilage mineralisation can be performed by round chondrocytes and chondrocytes with a fibrocyte shape in fibrocartilage.

The odontodes were first defined by the occurrence of enamel or enameloid covering a dentinous tissue around a vascularized and innervated cavity, and by the anchoring to acellular or cellular bone (first definition of Ørvig [1977], modified in Reif [1982]).

The dermal denticles (also termed placoid scales) of chondrichthyans (Figure 1.1) are serial structures that form the exoskeleton (Figure 1.3) and are considered to be derived from the superficial layers (enameloid and dentine) of the ancestral state of an odontode of which the underlying bony layer has been lost.

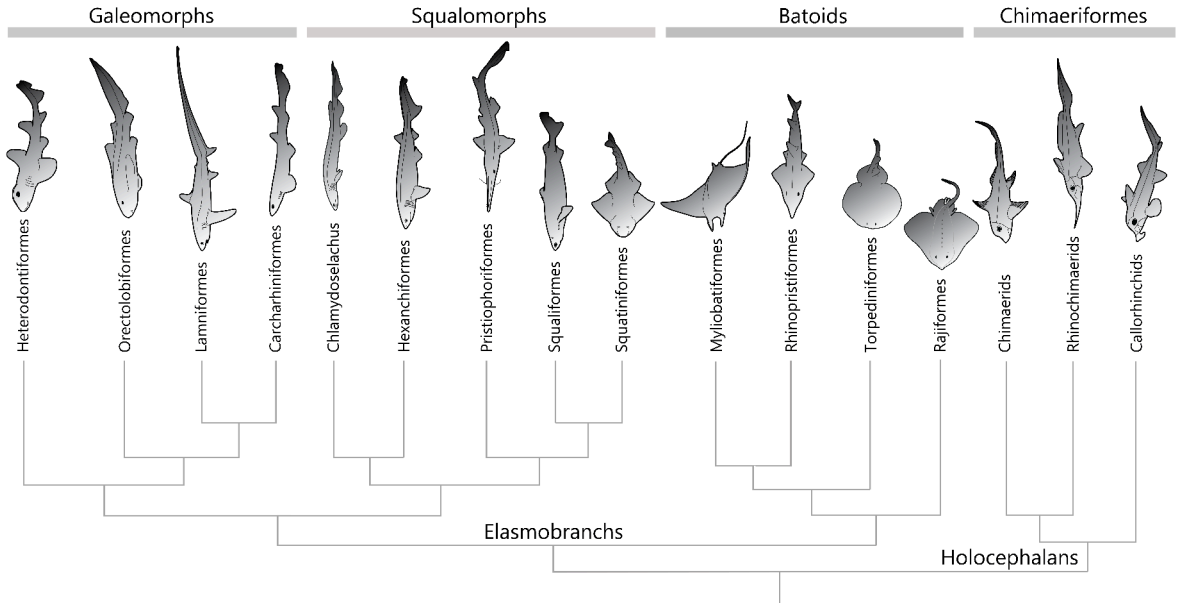

FIGURE 1.2: Phylogeny of extant chondrichthyans. Based on Inoue et al. [2010]; Janvier and Pradel [2015]; Last et al. [2016].

In most osteichthyans, serial exoskeletal elements covering the head and body include a broad diversity of scales (e.g., ganoid, elasmoid) [Sire et al., 2009; Sasagawa et al., 2013; Schultze, 2016; Quan et al., 2018]. Ancient bony fish displayed large bony plates forming an armour, which split into smaller plates through the evolution and now represent the ganoid scales of bichirs and gars [Sasagawa et al., 2013; Quan et al., 2018]. Elasmoid scales occur notably in teleosts and lungfishes and have developed from ganoid scales [Schultze, 2016]. As opposed to placoid scales, the elasmoid scales are formed without the contribution of an epithelial layer and are greatly unmineralised [Sire and Akimenko, 2004; Mondéjar Fernández and Meunier, 2020]. Rhomboid scales (ganoid and cosmoid) still retain enamel and dentine or enamel-like tissues covering a bony layer, whereas elasmoid scales are composed of a superficial bony plate covering an inner layer of connective tissue made of collagen fibers [Sasagawa et al., 2013; Schultze, 2016; Quan et al., 2018].

The fundamental distinction between most teleost (elasmoid) scales, dermal denticles, and teeth is that the first ones are of mesodermal origin, so as the trunk endoskeletal tissues (cartilage and bone), whereas the main tissues of the others originate from ectomesenchyme, a neural crest-derived tissue (further discussed in subsection 3.1.1) [Lee et al., 2013; Mongera and Nüsslein-Volhard, 2013; Shimada et al., 2013; Gillis et al., 2017].

Astonishing similarities have been highlighted between dermal denticles and teeth of elasmobranchs: they (i) exhibit similar gene expression patterns during development, (ii) share the same embryonic origin (see subsection 3.1.1), (iii) display equivalent stages of morphogenesis and differentiation, and (iv) require intimate epithelial-mesenchymal interaction [Debiais-Thibaud et al., 2011, 2015; Smith et al., 2015; Martin et al., 2016; Enault et al., 2018; Berio and Debiais-Thibaud, 2019] (see also chapter 3). However, as opposed to dermal denticles, elasmobranch teeth develop from a dental lamina [Reif, 1982; Witten et al., 2014].

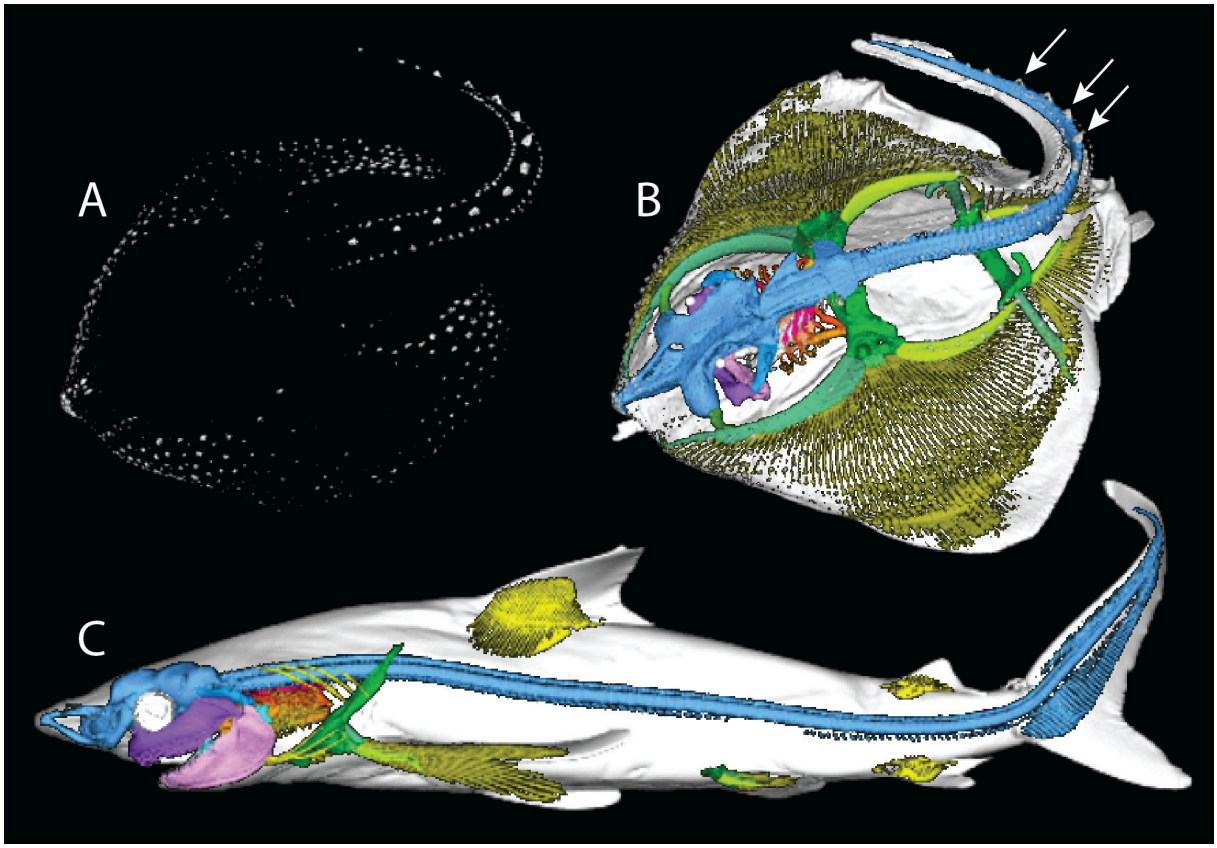

FIGURE 1.3: Endoskeleton and exoskeleton of extant elasmobranchs. A, dermal denticles of the thorny skate *Amblyraja radiata*; B, endoskeleton (colours), dermal denticles (arrows) and skin (white background) of *A. radiata*; C, endoskeleton (colours) and skin (white background) of the Galapagos shark *Carcharhinus galapagensis*. MicroCT images. Images courtesy of Gavin Naylor, extracted by Margot Angibaud from the project `https://sharksrays.org`.

1.1.2 Form diversity of dermal denticles in extant elasmobranchs

Elasmobranchs are key to understand the evolution of odontodes because, as opposed to most extant vertebrates, this group retains placoid scales that first served as a model for the ancestral state of an odontode. The development and forms of elasmobranch placoid scales and teeth provide insights into the evolution of the regulatory networks that control the occurrence of such structures within chondrichthyans and among vertebrates. Batoids (Figure 1.1) and sharks display placoid scales (Figure 1.3) and eventually fin spines on the head and body skin, inside the mouth and sometimes on nictitating membrane and eye [Poscai et al., 2017; de Sousa Rangel et al., 2019a; Tomita et al., 2020]. As opposed to elasmobranchs (Figure 1.2), mature chimaeras retain a very limited number of dermal denticles, notably next to the dorsal spine and to the lateral line canals [Didier and Stehmann, 1996; Didier, 2004; Møller et al., 2004].
To what extent are the elasmobranch placoid scale morphologies driven by ecological factors and phylogeny is still prone to debates. As an example, the low amount of dermal denticle ornamentations is considered to be the plesiomorphic condition in sharks and the increase in ridge number and in microstructure complexity is assumed to have occurred through the evolution of this group [Mello et al., 2013]. However, morphological differences of dermal denticles at intra- and interspecific levels also

suggest a role of biotic and abiotic selective pressures in the final form of dermal denticles [Raschi and Tabit, 1992; Deynat and Séret, 1996; Chernova and Vorob'eva, 2012; Crooks et al., 2013; Mello et al., 2013; Dillon et al., 2017].
The functions of elasmobranch placoid scale patterns over the body, including both morphologies and densities, fall into several categories in which there are protection, and influence on hydrodynamics [Raschi and Tabit, 1992; Dillon et al., 2017; Ankhelyi et al., 2018]. Ridges on oropharyngeal dermal denticles are assumed to increase the efficiency of ram ventilation (e.g., in sharks with decreased mouth size such as hammerhead sharks) but their absence may enhance hydrodynamic drag in species with greater gill surface areas (e.g., shortfin mako sharks) [Atkinson and Collin, 2012; de Sousa Rangel et al., 2019b]. Similarly, multicuspidate and thin body dermal denticles with parallel ridges to the water flow significantly reduce water turbulences during swimming of fast pelagic species, whereas benthic species skin is usually covered by thick and smooth dermal denticles which are expected to prevent from seafloor abrasion [Raschi and Tabit, 1992; Dillon et al., 2017]. The spatial arrangement of dermal denticles also impacts the species hydrodynamics: fast pelagic predators, such as *Isurus* sharks, display an overall dermal denticle density more than 100 times higher than demersal and sedentary species [Díez et al., 2015; Dillon et al., 2017].

Elasmobranch dermal denticles build a permanently restructured dermal armour: they may deter parasite settlements (although it is debated [Raschi and Tabit, 1992]) and provide protection from bites, of predators and mates [Raschi and Tabit, 1992; Dillon et al., 2017]. Bite marks resulting from mating behaviour are commonly observed on elasmobranch skin, because of males grasping females during copulation [Stevens, 1974; Young, 1993; Kajiura et al., 2000; Pratt and Carrier, 2001; Calich and Campana, 2015; Ritter and Amin, 2019].

The modified dermal denticles into alar thorns on the dorsal apices of batoid pectoral fins (and especially of Rajidae) also help males holding females during copulation [de Sousa Rangel et al., 2016]. It has been reported that their cusps undergo a transition from rounded to pointed after sexual maturation of males, concomitant with similar tooth shape transition prior to sexual maturation in males [McEachran, 1977; Braccini and Chiaramonte, 2002; Vinu et al., 2017]. In small shark species (e.g., horn sharks *Heterodontus francisci*, chain catsharks *Scyliorhinus retifer*, and small-spotted catsharks *Scyliorhinus canicula*), males also wrap themselves around females before and during copulation and it has been suggested that sexually dimorphic dermal denticles at specific locations (e.g., pectoral fin, posterior part of the pectoral fin, and pelvic girdle) might help holding such posture to facilitate clasper intromission [Pratt and Carrier, 2001; Crooks et al., 2013].

Regionalisation of placoid scales on the elasmobranch body has thus been highlighted many times, as the result of functional specialisations [Daniel, 1934; Raschi and Tabit, 1992; Díez et al., 2015; de Sousa Rangel et al., 2016; Dillon et al., 2017; Ankhelyi et al., 2018; Soares and de Carvalho, 2019]. The interplay between development and structure of different dermal denticle morphologies at distinct body locations has been investigated in very few elasmobranch species. The first dermal denticles develop and erupt according to sequential patterns: in the little skate *Leucoraja erinacea*, in the Port Jackson shark *Heterodontus portusjacksoni*, in the crested hornshark *Heterodontus galeatus*, and in *S. canicula*, rows of flat and smooth dermal denticles with irregular outlines are first aligned along the caudal fin of the embryo; then enlarged and long dermal

denticles erupt aligned to the dorsal row [Grover, 1974; Ballard et al., 1993; Mellinger and Wrisez, 1993; Miyake et al., 1999; Johanson et al., 2007, 2008; Debiais-Thibaud et al., 2011, 2015; Cooper et al., 2018]. These eruptions are followed by waves of developing body dermal denticles in less organised patterns; they are later subsumed within body dermal denticles and not replaced throughout ontogeny [Cooper et al., 2018]. Divergences between developmental timings, forms, sequential or scattered patterns, and structure of shark dermal denticles led to consider the caudal primary denticles and scattered body denticles to be developmental modules [Johanson et al., 2007, 2008]. However, gene expression patterns between caudal primary denticles and scattered body denticles remain extremely fragmentary and the data gathered hitherto did not challenge this hypothesis [Debiais-Thibaud et al., 2011, 2015; Martin et al., 2016; Cooper et al., 2017, 2018; Berio and Debiais-Thibaud, 2019].
Similar questions about the occurrence of putative dental modules can be asked, however, such investigation requires a detailed examination of tooth forms in different conditions (e.g., ontogenetic stages, location within the jaw) and a comparative framework that is discussed and used in this thesis.

1.1.3 The controversial question of homology

The morphology of biological elements can be compared between species and specimens. From this need of comparison arises the problem of the framework in which structures can be compared within and between organisms. This issue is classically raised when homology relationships are suggested between elements to be compared and is best driven by the two following questions: Are these elements topologically comparable (e.g., Do they display similar anatomical connections in different species and organs?)? [Panchen, 2001] and do they derive from a unique structure displayed by their last common ancestor (*i.e.*, Do the topologically comparable elements result from the most parsimonious, evolutionary, hypothesis?) [Schmitt, 1995]? This latter version of homology is the one used in evolutionary biology, however, it is not always defined nor considered as such when performing Geometric Morphometrics (GM). This assumption is often discussed after performing analyses based on topological homologies, notably between serial structures in a same specimen.

There had been previous attempts to define tooth homologies between shark species and to cluster teeth along the mesio-distal axis of the jaw. The most striking example of teeth categorisation concerns the so-called lamnoid tooth pattern, whose decription involves the use of dental formulas inspired from the work of mammalogists [Shimada, 2002]. It was originally divided into symphyseal, anterior, intermediate, and lateral teeth in the palatoquadrate (upper jaw cartilage), and into symphyseal, anterior, and lateral teeth in the Meckel's cartilage (lower jaw cartilage) [Leriche, 1905]. These tooth families are based on occlusal tooth file patterns, as well as on abrupt changes in tooth morphology and size, notably impacted by the underlying dental bulla, an inflation of the dental cartilage [Leriche, 1905; Shimada, 2002; Purdy and Francis, 2007]. Naming of these tooth families has, however, been subject to internal strife due to homology relationships between lamniform teeth and establishment of the "true" lamnoid pattern [Shimada, 2002, 2005a; Purdy and Francis, 2007; Bemis et al., 2015]. In these studies, the homology concept has been defined from a phylogenetic point of view: homologous structures in distinct species necessarily derive from a single structure in their last

common ancestor [Gans, 1985]. The homologous relationships between lamnoid tooth files at the interspecific level remain, however, debated since variations of a single tooth file identification might shift the whole lamnoid pattern and reassess the previously established lamnoid homology pattern [Shimada, 2002; Purdy and Francis, 2007].

All in all, homology of shark tooth files in a specimen at different growth stages, between specimens of the same species, and between species is strongly challenged by the variability of tooth file insertion within a dental set. In *Heterodontus*, Reif [1976] for example reports "spontaneous divisions of tooth families [in an hemi-jaw] that do not occur in the other half", as well as new tooth families that can be inserted at two locations in a jaw: between the symphyseal teeth and the crushing ones (*i.e.*, among post-symphyseal teeth), and at the commissures [Reif, 1980]. In batoids also, new tooth files can emerge after tooth germ injury, but also in a more normal way, adjacent to symphyseal teeth (e.g., in the bowmouth guitarfish *Rhina ancylostoma*) [Smith et al., 2013]. In addition, intraspecific differences regarding the presence and absence of symphyseal teeth are frequent in Carcharhinidae, as well as the tooth file number of lamniform intermediate teeth. Also, the topologic elements used to determine interspecific homologies are not always present in a given clade (e.g., dental bullae in the basking shark *Cetorhinus maximus* and in the megamouth shark *Megachasma pelagios*, both Lamniformes), which questions the reliability of homology hypotheses [Shimada, 2002; Smith et al., 2013]. Such variability requires adaptability of the "rules" used to determine interspecific homologies: in the goblin shark *Mitsukurina owstoni*, the establishment of the lamnoid pattern only relies on tooth relative sizes and occlusion because the dental bulla borders used to characterise anterior and intermediate teeth of most Lamniformes are difficult to detect [Shimada, 2002].

There is also a lack of *in vivo* surveys on tooth file insertion, and the few developmental data gathered hitherto also indicate that the development of new tooth files follows different patterns in a single jaw [Reif, 1976; Smith et al., 2013; Underwood et al., 2015]. Although tooth files are usually added distal to the most distal tooth file in elasmobranchs, this pattern is distorted by occasional emergence of mesial or random tooth files, which makes intricate to define strict homologies between tooth files [Smith et al., 2013; Underwood et al., 2015, 2016]. Strict tooth file homologies might thus be exclusively used for species which undergo distal tooth file addition until a fixed ontogenetic stage. However, such key stage remains to be determined for each elasmobranch species.

Attempts to homologise shark teeth were originally designed to investigate the robustness of tooth-to-tooth dental homologies outside the traditional mammalian framework [Shimada, 2002]. Fortunately, it turned out that individual tooth files and tooth family designation are currently more a useful tool to compare tooth types in jaw quadrants than the reflect of true homologies [Straube et al., 2007; Cullen and Marshall, 2019; Berio et al., 2020]. The denomination of tooth groups in shark clades other than Lamniformes is more flexible due to more subtle and subjective tooth morphological patterns along the jaw. Among them are for example the symphyseal teeth, whose definition varies from teeth located next to the jaw symphysis to teeth on the jaw symphysis itself, and teeth that must be small for some authors, but not necessarily for others (see Shimada [2002] for historic explanations). In most cases, the tooth family terminology applies differently among species and often depends on the authors goodwill, while others prefer to peel categorisation back by safely using tooth mesio-distal numbering [Straube

et al., 2007; Bemis et al., 2015].

During my PhD, the choice was made to analyse tooth files along the mesial to distal axis of the palatoquadrate and Meckel's cartilages and teeth were numbered accordingly. Tooth numbering was only an attempt to facilitate analyses of gradients of shape and size, along the jaw, and between specimens. The trajectory analyses necessarily implied an homology hypothesis (a one-to-one tooth file identity) but the interpretation of the results was performed under the hypothesis of topologically comparable tooth files, within and between specimens. This latter hypothesis thus does not imply common ancestral structures to each tooth file. The equivalent tooth file numberings along the ontogeny and between sexes were not used in the strict evolutionary meaning of homology and were not used to discuss patterns of evolution over the speciation time. However, they hypothesise a continuity at the locus where new teeth are produced over time: the continuity of topological constraints and of molecular information.

1.2 Developmental origin of odontodes and teeth

1.2.1 Teeth from odontodes or odontodes from teeth?

Arising from the morphological and developmental similarities between dermal denticles and teeth is the tremendous evolutionary question on (i) what is the common embryonic relationship between these structures and (ii) if so, which, of a tooth or a dermal denticle, gave rise to the other?

The first proposed theory has been the outside-in theory (Figure 1.4A), which states that teeth are derived from the external ectodermal-epithelial tissue allowing odontogenesis and that competent-odontode forming cells would have subsequently invaded the oropharyngeal cavity [Huysseune et al., 2009, 2010]. Supports to this hypothesis are the abovementioned striking developmental similarities between teeth and dermal scales, as well as the transitional denticle morphologies on the mouth edges (see chapter 3) [Daniel, 1934; Blais et al., 2011; Debiais-Thibaud et al., 2011, 2015; Martin et al., 2016; Enault et al., 2018; Berio and Debiais-Thibaud, 2019]. Regarding the main cusp orientation in these transitional forms in the extant spiny dogfish *Squalus acanthias*, Daniel [1934, p.38] states that "some of the transitionals [...] are so generalised that the retention of the latter [spine] projection would result in a scale, its loss would result in the formation of a tooth". However, the outside-in theory lacks the support from the fossil record, which was expected to provide anatomical continuity between teeth and denticles [Blais et al., 2011].

The inside-out theory (Figure 1.4B) stipulates that (i) teeth of endodermal origin developed first, in conjunction with odontogenic neural-crest derived mesenchyme and in the posterior pharynx of jawless vertebrates, (ii) evolved independently in the oral cavity in various lineages, and (iii) did not give rise to dermal denticles [Smith and Coates, 1998; Smith, 2003; Johanson and Smith, 2005; Huysseune et al., 2009; Fraser et al., 2010; Witten et al., 2014]. According to this hypothesis, the dental competence was *de novo* acquired by the oral cavity and spread to oral endoderm and external ectoderm, allowing the development of teeth and dermal denticles, respectively, which is consistent with the common gene expressions reported during development of teeth and skin denticles [Smith and Coates, 1998, 2001; Fraser et al., 2010; Donoghue and Rücklin, 2016]. The inside-out theory is based on the assumption that teeth appeared before jaws and before

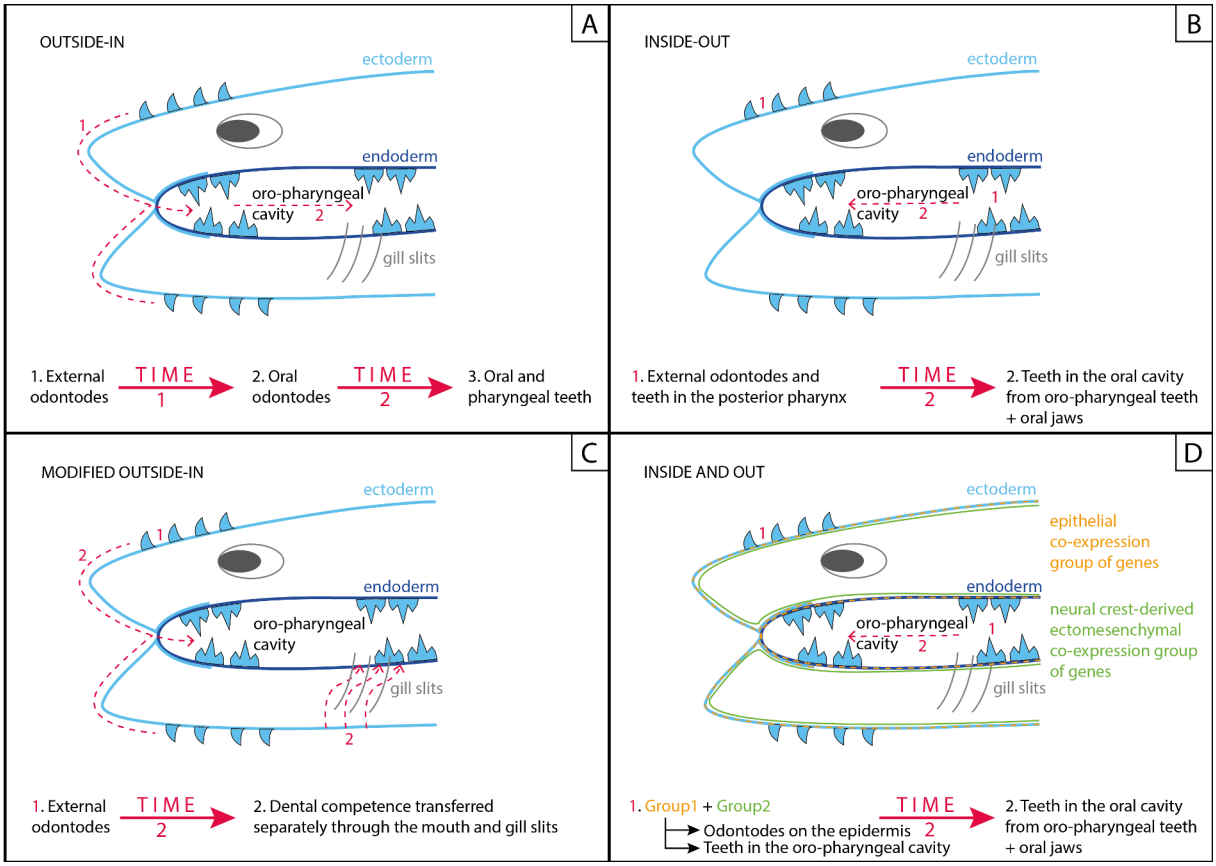

FIGURE 1.4: Theories on the evolutionary history of odontodes. A) Outside-in theory; B) Inside-out theory; C) Modified outside-in theory; D) Inside and out theory. Based on Fraser et al. [2010].

the dermal skeleton [Smith and Coates, 1998, 2001; Murdock et al., 2013]. However, homology between thelodont (agnathan) pharyngeal odontodes, conodont (agnathan) elements, and eugnathostome teeth has been refuted and does not support that true oral teeth predated the development of dermal denticles [Blais et al., 2011; Donoghue and Rücklin, 2016].

A modified outside-in theory (Figure 1.4C) attempted to reconcile paleontological and embryological data, albeit conodonts were not included even though their vertebrate-or-not condition was crucial to the debate [Huysseune et al., 2009, 2010]. It was proposed that teeth arose before jaws because they were produced by odontode-forming ectoderm after inwards migration by gill slits and mouth [Huysseune et al., 2009, 2010]. However, the competence of producing odontodes would have been transferred from ectoderm to endoderm at these sites and teeth would thus have arisen from the interaction between endoderm and neural-crest derived mesenchyme [Huysseune et al., 2009, 2010]. When established, this hypothesis was supported by the absence of pharyngeal teeth in species without gill slits. However, tetrapods with open gill slits (e.g., salamanders and frog tadpoles) still do not exhibit pharyngeal teeth [Huysseune et al., 2009; Berkovitz and Shellis, 2016].

Fraser et al. [2010] proposed a fourth theory named inside and out (Figure 1.4D), focused on an ancestral odontode gene regulation network rather than a tissue or a cell type. The authors suggest that an epithelial co-expression group of genes located in

sensory placodes (e.g., sensory papillae-like) interacted with the gene co-expression group of neural crest-derived ectomesenchymal cells [Fraser et al., 2010]. This new odontode gene regulation network might have allowed the development of an odontode or a tooth anywhere in the body where neural crest-derived ectomesenchymal cells were closely associated with any epithelium [Fraser et al., 2010].

Based on recent data on a stem osteichthyan, Chen et al. [2020] proposed that primordial types of founder odontodes were initially covering the skin and the oropharyngeal cavity and that when covered by the oral epithelium, these structures developed into teeth while the presence of a dermal epithelium determined their development as odontodes. However, this finding is very recent and more fossils are needed to challenge the hypothesis that is suggested.

Overall, the main support is attributed to the classical outside-in hypothesis. First, the euconodont elements are not homologous to vertebrate teeth because their enamel-like crown was absent in their paraconodont ancestors [Murdock et al., 2013]. Evidence of tooth-like pattern and successional replacement of tooth whorls in the pharynx and mouth of the thelodont-derived *Loganellia* also led to favour the hypothesis that teeth evolved before jaws [Van Der Brugghen and Janvier, 1993; Donoghue and Rücklin, 2016]. However, the remote phylogenetic relationship between thelodonts and clades, including gnathostomes, exhibiting successional replacement and tooth-like structures favours a hypothesis of evolutionary convergence of these structures rather than homology [Donoghue and Rücklin, 2016]. Then, the homology of placoderm and crown gnathostome teeth has been established, refuting the convergence of teeth between the latter and advanced placoderms [Rücklin et al., 2012]. Most studies finally agree on the fact that teeth evolved from dermal odontodes and that they evolved once in gnathostomes, albeit the debate is ongoing [Rücklin et al., 2011; Murdock et al., 2013; Witten et al., 2014; Donoghue and Rücklin, 2016; Martin et al., 2016; Haridy et al., 2019].

Nevertheless, Biology is full of exceptions and studies reported the occurrence of extra-oral denticles on head dermal bones of unrelated extant teleost species (e.g., *Denticeps*, *Atherion*, *Xiphias*) [Huysseune and Sire, 1998; Sire, 2001; Sire and Allizard, 2001]. However, these denticles are not directly derived from ancestral odontodes, *i.e.* they are not the consequence of the re-expression of quiescent odontogenetic factors in the skin [Sire, 2001]. They are more likely resulting of an intricate interaction between epidermal cells over the body and odontogenic Neural Crest Cells (NCCs) that migrated outside the mouth [Sire, 2001].

This "tooth-and-odontode" problem well illustrates the need for fossils to challenge evolutionary hypotheses and try to decide which one is the most likely to have occurred. Developmental studies, however, bring insights into how similar is the growth of odontodes and teeth within and between species.

1.2.2 Tooth form diversity and dentition patternings in elasmobranchs

> *Of the Heterodontus francisci biology: "May bite back when harassed."*
> – *www.fishbase.se*, read 02/09/2020

In mammals, teeth develop exclusively on the jaw bones. They are replaced once during life in most species (diphyodonty) and usually display different shapes from the symphysis to the commissures (monognathic heterodonty) [Jernvall and Thesleff, 2012]. Exceptions to this pattern are reported, notably in muroid rodents, bats, and

odontocetes, which are monophyodont, *i.e.* they have a unique dental set during life [Jernvall and Thesleff, 2012]. Rare species such as the little rock wallaby and the manatee have a polyphyodont dentition (with teeth continuously replaced throughout life), which is replaced by the distal addition of new molars [Jernvall and Thesleff, 2012]. As opposed to mammals, most other vertebrates are polyphyodont, which is considered the plesiomorphic condition of tooth replacement in crown gnathostomes [Rücklin et al., 2012]. Bony fishes, amphibians, reptiles, and elasmobranchs renew their teeth several times during life and have teeth developing at various sites in the oro-pharyngeal cavity, patterning a broad diversity of dental formulas and replacement types [Davit-Béal et al., 2007; Cappetta, 2012; Jernvall and Thesleff, 2012; Underwood et al., 2015; Smith et al., 2018]. The teeth can for example develop on the palate bones of salamanders [Ungar and Sues, 2019] and on the pharyngeal arches of teleosts [Wautier et al., 2001], and variants in tooth row number have been reported in caecilians [Ungar and Sues, 2019].

Within chondrichthyans, chimaeras have lost the ability to produce individual teeth during evolution but have six permanently growing dental plates of dentine (trabecular, hypermineralised (whitlockin), and sclerotic (including osteodentine)) [Smith et al., 2020]. Whether extant chimaeras have enameloid or not covering the dentine has long been controversial [Ishiyama et al., 1984; Ørvig, 1985; Enault et al., 2015a] but the tooth plates hypermineralisation is likely due to the occurrence of biomineral whitlockite in the dentinous matrix [Johanson et al., 2020].

Most elasmobranch fishes have teeth on palatoquadrate and Meckel's cartilages exclusively. The externalmost mineralised layer of shark teeth is composed of enameloid, which matrix originates both from the ameloblasts (ectodermal origin) and the odontoblasts (ectomesenchymal origin), as opposed to enamel that is of ectodermal origin only [Sasagawa, 2002; Gillis and Donoghue, 2007; Enault et al., 2015a; Lübke et al., 2015]. The elasmobranch enameloid is not equivalent to the tetrapod enamel [Kemp, 1999; Enault et al., 2015a]. It notably differs from enamel in that the mineral phase of enameloid is composed of fluoroapatite, while it consists of hydroxyapatite in enamel [Enax et al., 2014; Lübke et al., 2015]. Moreover, as opposed to enamel, the elasmobranch enameloid mineralises before dentine [Kemp, 1999]. The elasmobranch and actinopterygian enameloids have been found to be homologous but differ in their organisation and mineralisation patterns [Sasagawa, 2002; Gillis and Donoghue, 2007]. In teleosts, the enameloid is scattered by matrix vesicles containing crystals that further participate to the mineralisation, whereas in elasmobranchs the site of initial mineralisation is the tubular vesicles from the processes of odontoblasts [Sasagawa, 2002]. Also, the elasmobranch enameloid contains less collagen fibrils than teleost enameloid and the crystals do not specifically accumulate along these fibrils [Sasagawa, 2002]. Finally, the initial crystals that participate to enameloid mineralisation in elasmobranch do not gather following a specific pattern, while in teleosts, the mineralisation process starts at the boundary between dentine and enameloid and progresses toward the outer enameloid border [Sasagawa, 2002].

The teeth of extant sharks have been classified according to histological features, notably concerning the occurrence of dentine types in the tooth crown. The histology of extant and extinct shark teeth has been the focus of several studies to understand the diversification of tooth mineralisation in this group and to establish correlations between histotypes (histological patterns of the tooth crown) and phylogenetic or functional signals [Moyer et al., 2015; Jambura et al., 2018, 2019, 2020].

Three tooth histotypes are defined in sharks (Figure 1.5). Orthodont teeth are made of an enameloid cap covering a layer of orthodentine that encloses the pulp cavity [Moyer et al., 2015; Jambura et al., 2020]. They are notably found in most Carcharhiniformes, in the frilled shark *Chlamydoselachus anguineus*, and in the whale shark *Rhincodon typus* (Figure 1.5A) [Moyer et al., 2015; Jambura et al., 2020]. Pseudoosteodont teeth represent the supposed plesiomorphic condition for all modern sharks and are composed of a core of osteodentine enclosed in a layer of orthodentine covered by enameloid (Figure 1.5B) [Jambura et al., 2018, 2020]. Pseudoosteodont teeth are for example observed in Echinorhiniformes, Squaliformes, and in some Orectolobiformes [Jambura et al., 2020]. Osteodont teeth have a crown that is filled with osteodentine and does not contain orthodentine (Figure 1.5C) [Moyer et al., 2015; Jambura et al., 2019, 2020]. It is found in most Lamniformes such as the longfin mako shark *Isurus paucus* and the great white shark *Carcharodon carcharias* [Moyer et al., 2015; Jambura et al., 2019, 2020].

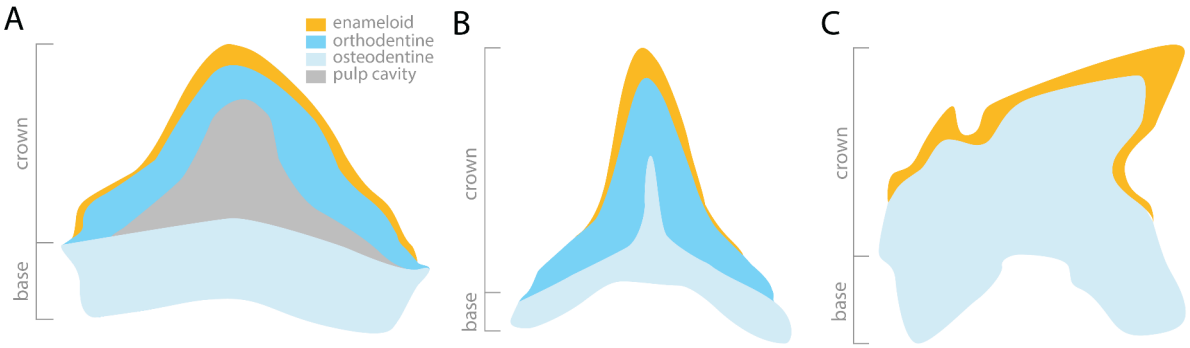

FIGURE 1.5: Tooth histotypes in sharks. A) Orthodont tooth; B) Pseudoosteodont tooth; C) Osteodont tooth.

Elasmobranch teeth are shed and replaced lifelong, with timings depending on species, jaws, and seasonal metabolic rates [Luer et al., 1990; Correia, 1999; Motta and Wilga, 2001; Botella et al., 2009]. These metabolic rates are usually influenced by environmental conditions such as water temperature, but have not been correlated to accidental shedding, such as during feeding or mating [Luer et al., 1990; Correia, 1999; Motta and Wilga, 2001]. Shedding teeth also constitutes a pattern *per se* when teeth are not lost accidentally. The worn teeth are replaced through a conveyor belt process, which pattern diverges between species. Teeth of individual files can be sporadically shed (e.g., in the blue shark *Prionace glauca*, the oceanic whitetip shark *Carcharhinus longimanus*, *I. paucus*, and *C. carcharias*), phased (e.g., following a mesial to distal sinusoidal pattern in the palatoquadrate of the gulper shark *Centrophorus granulosus*), or they can be shed during the complete renewal of the whole, oldest, tooth set of the jaw (e.g., in the cookie cutter shark *Isistius brasiliensis*, in the spiny dogfish *Squalus acanthias*, and in the *C. granulosus* Meckelian cartilage) [Bigelow and Schroeder, 1948; Strasburg, 1963; Motta and Wilga, 2001; Bemis et al., 2015; Moyer and Bemis, 2016] (Figure 1.6).

In elasmobranchs, tooth types can change through ontogenetic replacement. They can undergo a variation in number of tooth elements, for example an addition of cusplets (between the juvenile and mature ontogenetic stages in the bramble shark *Echinorhinus brucus* [Herman et al., 1989] or between the juvenile and mature ontogenetic stages in males of *S. canicula* [Ellis and Shackley, 1995] and *S. stellaris* [Berio et al., 2020] (please also refer to subsection 2.1.2), an addition of serrations (between juvenile and mature

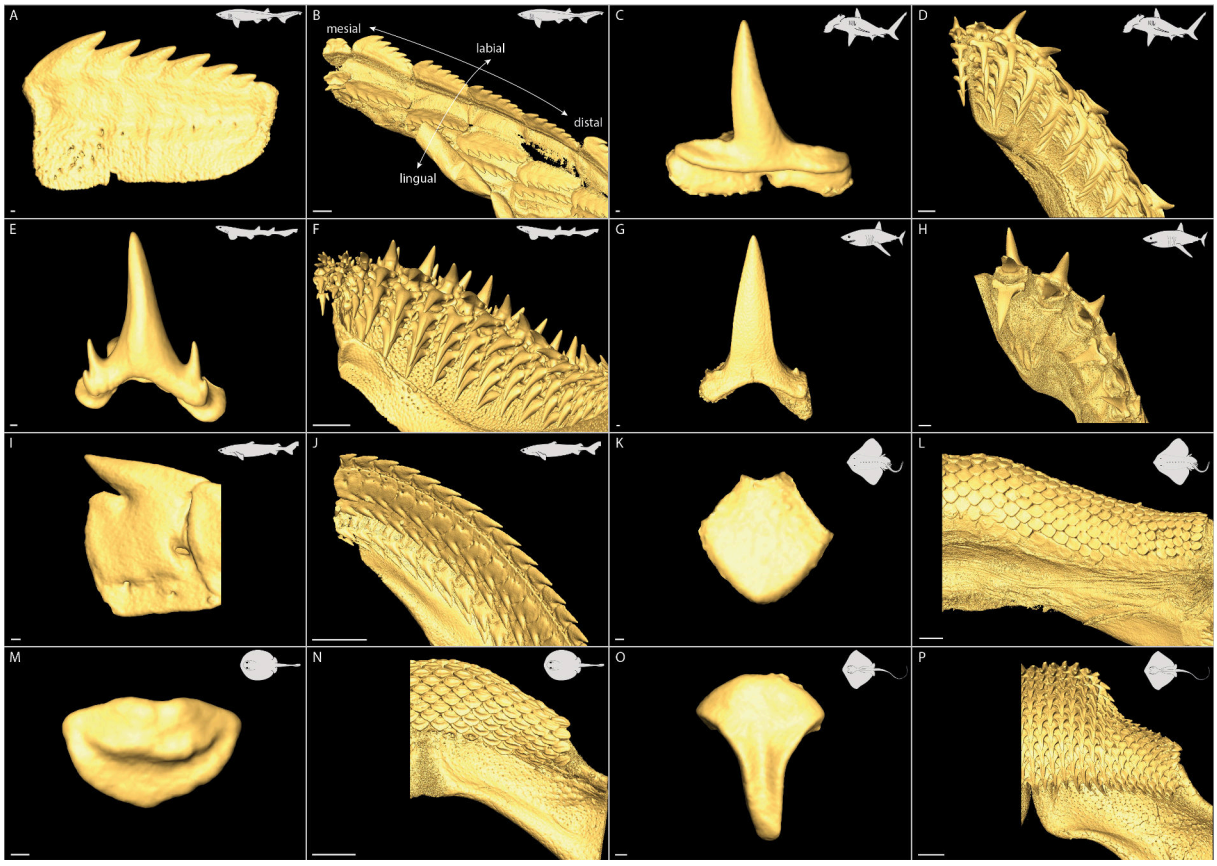

FIGURE 1.6: Diversity of tooth forms and dental patterns in elasmobranchs. A-B) *Hexanchus griseus*, specimen REC1151; C-D) Sphyrna media, specimen REC0142; E-F) *Scyliorhinus stellaris*, specimen REC0189; G-H) *Lamna nasus*, specimen REC0306 ; I-J) *Etmopterus spinax*, specimen REC0718; K-L) *Raja montagui* specimen REC0431; M-N) *Urobatis jamaicensis* specimen REC1092; O-P) *Neotrygon kuhlii* specimen REC0644. Meckelian teeth of the right Meckel's cartilage in labial view. The mesio-distal axis of the jaw and the labio-lingual orientation are exampled in B. The specimens were microCT scanned from the collections of the University of Montpellier, at the ISEM. Scale bars are 100 µm for isolated teeth and 2 mm for jaws.

night sharks *Carcharhinus signatus* [Raschi et al., 1982]) and a loss of serrational cusplets (in mature *C. carcharias* [Bemis et al., 2015]) (Figure 1.7).

The tooth set can also undergo a modification of tooth type proportions: juveniles of *Heterodontus* have a majority of grasping teeth, whereas mature specimens have more molariform teeth [Reif, 1976; Powter et al., 2010] and early-term *C. carcharias* display fang-like crown with no serrations, while full-term embryos have tricuspid teeth with lateral serrations [Tomita et al., 2017]. In elasmobranchs, tooth shapes can vary from cuspidate to molariform between the symphysis and the commissure, and ontogenetic shifts in tooth type proportions have also been observed that correlate with diet modifications [Reif, 1976; Wilga and Motta, 2000; Motta and Wilga, 2001; Powter et al., 2010; Cappetta, 2012]. Besides putative role in trophic ecology, ontogenetic replacement is intricately linked to mating behaviour, at least in some batoids [McEachran, 1977; Kajiura and Tricas, 1996; Schmitt et al., 2015; Vinu et al., 2017; Rutledge et al., 2019]. Mechanical tests with batoid jaws demonstrated the increased grasping efficiency of mature male cuspate teeth compared to juvenile male rounded teeth (tests performed

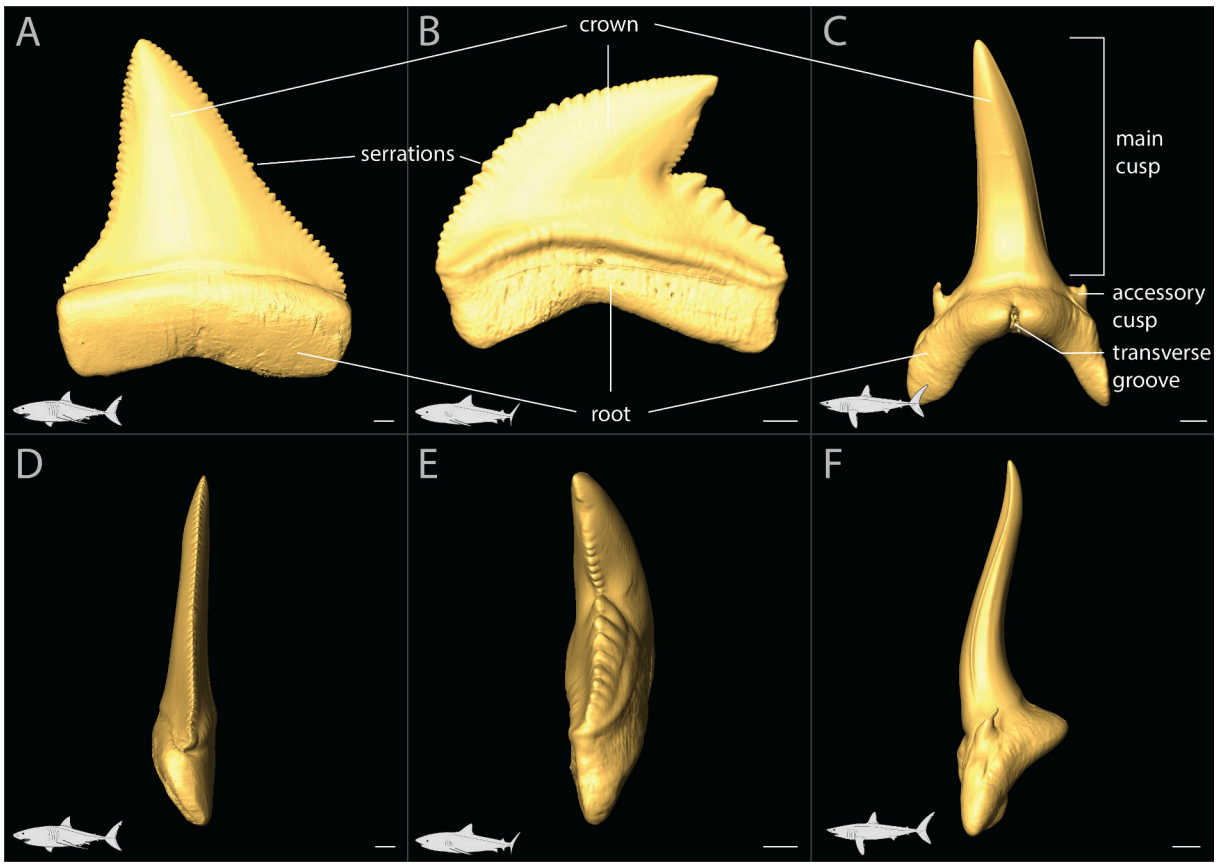

FIGURE 1.7: Shark tooth terminology. A,D) Tooth of a great white shark *Carcharodon carcharias*; B,E) Tooth of a tiger shark *Galeocerdo cuvier*; C,F) Tooth of a mako shark *Isurus* sp. For each species, the tooth is presented labio-lingually (A-C) and from the cutting edge (D-F). Scale bars are 2 mm. Images courtesy of Alexandre Assemat.

with the jaws of the Atlantic stingray *Hypanus sabinus* and the Eastern shovelnose ray *Aptychotrema rostrata*) [Kajiura and Tricas, 1996; Gutteridge and Bennett, 2014]. It is also curious that ontogenetic changes of tooth morphologies can affect certain teeth or tooth families at specific locations of the jaw. The most extreme case concerns the upper first and third teeth of *C. carcharias*, which width and angle are respectively and significantly modified after sexual maturation in males, contrary to females [French et al., 2017]. In *H. portusjacksoni*, more crushing teeth are retained in mature females compared to males, and anterior teeth are more cuspidate in mature than juvenile batoid males, while posterior teeth remain of crushing type (e.g., in the whip stingray *Hemitrygon akajei*, in *H. sabinus*, and in *A. rostrata*) [Taniuchi and Shimizu, 1993; Kajiura and Tricas, 1996; Powter et al., 2010; Gutteridge and Bennett, 2014].

Very few elasmobranchs exhibit monognathic homodonty (e.g., lower teeth of some squaliformes, teeth of the thornback ray *Raja clavata*, of whale sharks *Rhincodon*, and of basking sharks *Cetorhinus*) [Karbhari and Josekutty, 1986; Motta and Wilga, 2001; Underwood et al., 2015, 2016] (Figure 1.6). In most sharks and batoids, the tooth morphologies undergo subtle and continuous modifications along the mesio-distal axis (weak heterodonty), making difficult to determine tooth families [Reif, 1976; Straube et al., 2007] (Figure 1.6 and see subsection 2.1.2). One issue to that matter is the characterisation of tooth morphological changes within a jaw, and to compare these patterns between

specimens. Such issue was challenged during my PhD through the use of 3D GM (see chapter 2).
One of the main advantages of exploring the broad variation of shark tooth forms at the intraspecific and interindividual levels is to provide an overview of extreme tooth shapes a single species can develop according to multiple parameters such as the population considered, the ontogenetic stage, the sex, and the mesio-distal location along the jaw. The range of morphologies that characterise a species can thus be correlated to developmental parameters, whose physical and genetic influence on tooth shapes remains understudied in sharks. These data aim at identifying the proximal causes for morphological variations that build the substrate for natural selection, leading to the incredible diversity of tooth shapes.

1.3 You came for teeth, then go for the endoskeleton

> *"[...] it may be pointed out that until the vertebrae of any particular fish are examined one cannot decide whether they are of interest or not; when the examination has been made, the author is performing a service to science by placing his observations on record, for even if the structures prove to have no very direct bearing on the elucidation of the problem, he spares his successors the labour of an independent examination of the vertebrae."*
>
> – *On the Calcification of the Vertebral Centra in Sharks and Rays*, Walter G. Ridewood, 1921

Anyone who ever worked on teeth knows there is a non-null probability of being irresistibly attracted by the slightest mineralising thing that crosses its way. Reasons for this are to be found in the similar experimental approches used to study odontodes and endoskeletons but also in the initial intrincated evolution of these mineralised structures, which has been reccurently suggested both by paleontological and developmental, including genetic data.

When tooth buds enter the differentiation stage, part of the genes expressed are responsible for the mineralisation step. The corresponding proteins and molecules control the secretion of dentine by the odontoblasts of mesenchymal origin and of enameloid (enamel in mammals) by the ameloblasts, derived from the epithelium. Yet, odontoblasts express type I collagen genes in elasmobranchs, which is also one of the main characteristics of bone producing cells, as well as additional markers that are also common to osteoblasts [James et al., 2004; Simon et al., 2009; Enault et al., 2015b; Hisham Zainal Ariffin et al., 2017; Enault et al., 2018] (see subsection 3.1.1). Until the 80's, the elasmobranch endoskeleton was thought to be devoid of bone tissue, however, neural arch mineralisation patterns and part of the tesserae exhibit elongated cells resembling osteoblasts and markers that are similar to bone [Kemp and Westrin, 1979; Peignoux-Deville et al., 1982, 1989; Eames et al., 2007; Atake et al., 2019]. The fact that all chondrichthyans have odontoblastic ability and few of them exhibit bone-like (lamellar) tissue questions the similarities between the resulting structures (dental and neural arch tissues) in terms of gene expression, cellular types, and extracellular matrix composition. Since odontoblasts and osteoblasts share common gene regulatory expressions, the occurrence of bone-like tissue in elasmobranchs might have been allowed by (i) the only partial loss of bone by the ancestors or (ii) an interplay between loss and re-acquisition

in some fibroblast populations of developing pathways that rule the development of dentine and bone. During my PhD, the choice has been made to start addressing this complex question by investigating the occurrence of bone-like tissue in the main orders of extant chondrichthyans.

The study of the occurrence and diversity of skeletal components in chondrichthyans intertwines with the investigation of the origin of vertebrate mineralised tissues. The origin of the putative absence of bone in extant chondrichthyans is still debated. Endochondral ossification is either suspected to be an innovation of bony fishes [Donoghue and Sansom, 2002], either thought to be the result of a general loss of bone synthesis ability by chondrichthyans, after they diverged from osteichthyans [Donoghue et al., 2006; Brazeau et al., 2020]. The latter hypothesis is the more likely due to the fossil record, which implies that the "osseous" tissue reported in some extant chondrichthyans does not represent the ancestral state of vertebrate endochondral bone. This "osseous" tissue would therefore represent either a remnant of a bony tissue, or a derived feature found only in a subset of extant elasmobranchs.

1.4 Outline of the thesis

In chapter 2, I describe in detail the tooth morphologies of the large-spotted catshark *Scyliorhinus stellaris* by taking advantage of micro-computed tomography and 3D GM. I discuss the preliminary results of a similar study on *S. canicula* teeth and on comparative analysis of scyliorhinid tooth forms. I comment on the contribution of these descriptions for taxonomy, and for the crucial consideration of shark tooth morphologies as being dynamic in time and between sexes. Once finely characterised, these shark tooth morphologies can serve broader questions. Among them, I chose to focus on the potential of *S. canicula* teeth to discriminate between genetically and ecologically different populations. I designed an original framework by combining the advantages of GM and Random Forests [Breiman, 2001], a machine learning algorithm, to classify the teeth of *S. canicula* specimens from Atlantic and Mediterranean environments.

Another question that arises from the morphological diversity of shark teeth concerns the putative factors influencing the final form of a tooth. These factors can be physical and genetic and the latter have been experimentally investigated in this work. In chapter 3, I discuss the importance of combining theoretical and experimental approaches to decipher the role of specific proteins or molecules in designing a tooth form. I also comment on the advantages of comparing the shark and mammalian patterns to understand the evolutionary history of teeth. I present the preliminary results of functional tests performed on tooth buds of *S. canicula* embryos and comment on the bead implantation method, as well as on further experiments that should be conducted to challenge the results obtained hitherto.

The chapter 4 is dedicated to the investigation of the diversity of mineralised tissue types in the neural arches of chondrichthyans. It questions how widespread is bone-like tissue in the phylogeny of extant cartilaginous fishes. A combination of microCT scans and histology provides results that are discussed in light of the evolutionary history of vertebrate mineralised tissues.

Chapter 2
Characterisation of tooth forms and dental sets in sharks

2.1 Explanatory parameters of intraspecific tooth form diversity in *S. stellaris*: Ontogeny and sexual maturation

"Humans are good [...] at discerning subtle patterns that are really there, but equally so at imagining them when they are altogether absent."

– *Contact*, Carl Sagan, 1985

The intraindividual diversity of odontodes and teeth is a recurrent pattern among elasmobranchs and questions the underlying mechanisms affecting the regionalisation of their patterns and forms. As opposed to odontodes, elasmobranch teeth are replaced in a successive way, which allows to follow, in a relative manner (see subsection 1.1.3), tooth forms of comparable files during ontogeny [James, 1953; Reif, 1982; Underwood et al., 2015, 2016; Smith et al., 2018]. Such "monitoring" allows (i) to characterise intraspecific and interspecific tooth form variability and (ii) to address the parameters that impact tooth form generation in elasmobranchs. A first question to be addressed concerns the comparison of tooth files between sharks of different ontogenetic stage and sex. In mammals, this can be done by invoking the underlying developmental homology of tooth development in a species, however, this concept is more controversial when applied to shark tooth files, as presented in subsection 1.1.3. Furthermore, several methods have been proposed during the last decades to compare the morphology of a structure at the intra- and interspecific levels. The main outlines and frameworks commonly used in traditional morphometrics and GM are presented and discussed in this chapter, as well as the potential to combine a classical GM approach with a Machine Learning (ML) algorithm barely used in this field.

2.1.1 Traditional assessment of forms: Linear morphometrics is not enough

"To consult the statistician after an experiment is finished is often merely to ask him to conduct a post mortem examination. He can perhaps say what the experiment died of."

– *Presidential Address to the First Indian Statistical Congress*, 1938, Ronald Fisher

For centuries, the perception of biological diversity has largely involved the comparison of anatomical traits. Taxonomy, but also ecology long rested upon the characterisation and comparison of morphologies. Historically, visual observations and linear measurements were supplanted, at least partially, by geometric analyses. Indeed, while the former can be satisfying to compare familiar elements of similar silhouettes and of low complexity, the second turn out to be necessary when shape similarities are much less evident. Morphometrics used to lie in the distinction of a form into shape and size [Mitteroecker et al., 2013; Klingenberg, 2016]. The *form* of a structure thus refers to geometric aspects of a structure invariant to rotation and space translation, whereas *shape* contains the resulting geometric properties of a form after size component removal [Dryden and Mardia, 1998; Mitteroecker et al., 2013; Klingenberg, 2016]. Size is of major concern in morphometric studies because structures can shape differently relative to their size (positive or negative allometries). The strict comparison of shapes thus usually requires the use of size-free shape variables.

Morphometrics and other methods further employing similar basis rely on measurements to describe shape variation and test its covariation with explanatory variables (e.g., sex, habitat, diet). However, traditional morphometrics and its derivatives employ fundamentally divergent paradigms.

Traditional, linear morphometrics

The response variables used in traditional morphometrics are linear measurements, usually lengths, widths, and angles of a structure (Figure 2.1A) [Marcus, 1990; Rohlf and Marcus, 1993; Zelditch et al., 2004; Marramà and Kriwet, 2017].

Even though traditional morphometrics first succeeded as a taxonomic tool, it rapidly appeared that for lots of biological materials, several methodological points would face pitfalls [Rohlf and Marcus, 1993; Adams et al., 2004] (see Marramà and Kriwet [2017] for exceptions on fossil shark teeth). One would first notice the partial redundancy of such metrics, from the snout to the base of the tail and to the posteriormost gill opening for example (Figure 2.1A). Such redundancy makes difficult the identification of the shape parts that really differ between structures because they are associated with a combination of several measurements. Moreover, the geometric information of a structure is lost when linear measurements only are collected and it is further impossible to reconstruct the shape of the original structure [Rohlf and Marcus, 1993; Adams et al., 2004; Zelditch et al., 2004]. This loss of geometrical information implies that measurement values of two structures can be the same even though these structures display different shapes [Adams et al., 2004]. Furthermore, most traditional morphometric metrics represent biologically meaningful dimensions (e.g., snout-eye distance, dorsal fin-tail tip length) that can intuitively be compared between specimens and species. However, these measurements are, most of the time, not drawn between homologous points from a biological, evolutionary perspective, which makes interspecific and even intraspecific comparisons prone to biases [Adams et al., 2004]. Even more tricky is the definition of measurements in morphometrics because beyond the same metric designation can lie several ways of measurement with distinct anatomical landmarks, such as for body depth [Zelditch et al., 2004].

As stated before, the impact of size on shape must be removed or at least quantified. In traditional morphometrics, one issue to that matter has been the results variability

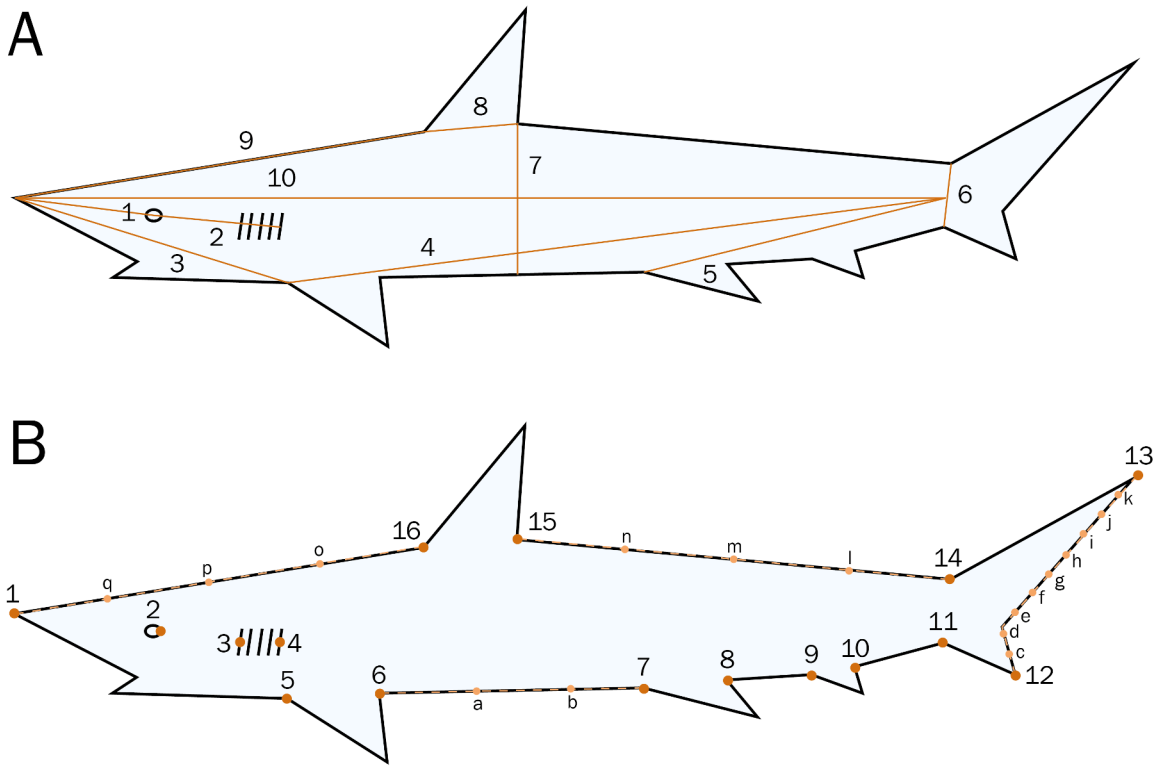

FIGURE 2.1: Traditional *versus* Geometric Morphometric measurements. A) Examples of linear measurements of a shark body in traditional morphometrics; B) Example of landmark (numbers) and semilandmark (letters) setting on the same shark body in geometric morphometrics. Measurements in A are adapted from some originally collected measurements on teleost fish body [Lagler et al., 1962; Zelditch et al., 2004].

of size-free variables after different correction methods, resulting in a lack of strict consensus on which method should be adopted [Adams et al., 2004].

All these partial or inaccurate enough morphometric data and methods led to elaborate new methods and paradigm in the morphometric field and to the subsequent emergence of the so-called "new morphometrics" [Rohlf and Marcus, 1993].

Geometric morphometrics

In the 90's, landmark-based GM were referred to as part of this revolutionary "new morphometrics" because it allows to compare geometries besides linear measures, displays covariation of landmark configurations, and prioritises the use of homologous landmarks, which enhances the robustness of shape comparability [Rohlf and Marcus, 1993]. The term "prioritises" is used here because most homologous points remain hypothetic, either because these points are set on locations that cannot really be homologous, or simply because no study ever proved the homology relationship between the locations. The points are thus set based on a developmental hypothesis about the similar genesis of a structure. For this reason, the homology between two points is more

often a question of structural homology that allows a further biological interpretation rather than a strict evolutionary homology.
Three landmark types are defined in GM that are characterised by two (2D) or three (3D) Cartesian coordinates. In both cases, type I landmarks locate at biologically meaningful boundaries and are defined *per se* (e.g., tissue sutures), type II landmarks locate at geometrically relevant positions (e.g., local maximum curvature of a tooth cusp), and type III landmarks, also termed semilandmarks, are set on extreme positions, relative to some structure (e.g., the furthest point to the eye along the antero-posterior axis) [Bookstein, 1991b; Gunz et al., 2005] (Figure 2.1B). The question whether type I, II, or III landmarks are set is crucial for the results interpretation in a biological context. Different developmental and evolutionary hypotheses could for example be drawn based on shape changes from type I and for type III landmarks. The definition of type I landmarks across species can be challenging when performing interspecific comparisons of forms, especially when the species are morphologically broadly distinct and display body plans that cannot be compared between specimens [Goswami, 2006; Bardua et al., 2019]. Type II landmarks are often easier to define and also allow an increased patching success of the structure as their location and number is less constrained by local homologies than type I landmarks. Because they are defined relative to true (types I and II) landmarks, sliding semilandmarks only provide information that is not contained in these other landmark types (e.g., the bowing of a curve between true landmarks) [Zelditch et al., 2004; Webster and Sheets, 2010]. However, sliding semilandmarks are of primary usefulness when no type I or II landmarks can be reliably identified on curving structures [Bookstein, 1997; Gunz and Mitteroecker, 2013].

Once retrieved, the form coordinates are preprocessed to retain only the shape information, *i.e.* without movement, rotation, and size change of the structure. Yet, some authors chose to investigate forms of landmark configurations without separating shape from size, for example by considering the logarithmic centroid size as an extra dimension of shape tangent space or by superimposing the landmark configurations without scaling them to unit centroid size [Mitteroecker et al., 2004; Goswami, 2006; Mitteroecker et al., 2013; Klingenberg, 2016]. Considering altogether shape and size helps questioning more complex interspecific developmental processes than strict heterochrony, which is a modification in the timing or rate of development of a structure in a specimen as compared to its ancestor [McNamara, 2012].
The separation of shape and size is commonly achieved with a Generalised Procrustes Analysis (GPA) [Bookstein, 1991a; Mitteroecker et al., 2013] (Figure 2.2). During this process, the original landmark configurations in a dataset are spatially translated to the same centroid, normalised, and rotated so the distance between corresponding landmarks of all configurations is minimal to the average location of this landmark position usually with least-squares adjustment [Mitteroecker et al., 2013]. On the course of superimposition, semilandmarks are allowed to slide along the curve they are placed on. Sliding landmarks can be done by minimising the bending energy or by minimising the Procrustes distance between two shapes [Gunz and Mitteroecker, 2013]. The former is historically the first to be defined, it implies that all semilandmarks slide as a whole and relative to true landmarks to minimise the bending energy, which is the amount of local shape deformation [Bookstein, 1989; Gunz and Mitteroecker, 2013]. It is often favoured to the Procrustes distance minimisation between two configurations because in this case semilandmarks are allowed to slide independently one from another and from

the whole superimposition, which can lead to absurd shapes [Gunz and Mitteroecker, 2013].

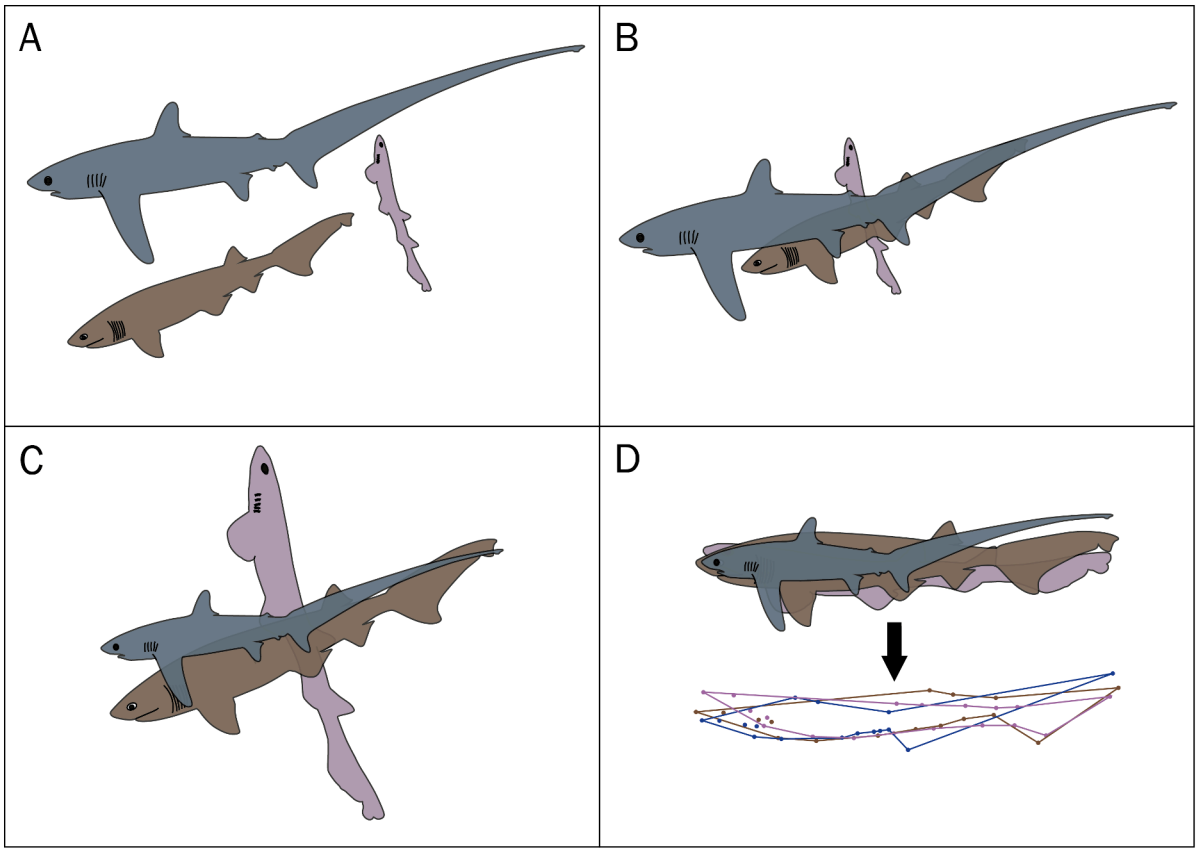

FIGURE 2.2: Superimposition steps achieved by a GPA. A) Original configurations; B) Location differences removed; C) Scale differences removed; D) Orientation removed, resulting in alignment of shapes only. For visual convenience the full shark morphologies are displayed but in reality only the landmark coordinates undergo the superimposition. The landmarks used are in Figure 2.1B.

The centroid size is the common measure of size in geometric morphometrics and it is defined for each conformation as the squared root of the sum of squared distances between each landmark and its configuration centroid [Zelditch et al., 2004; Mitteroecker et al., 2013; Klingenberg, 2016]. The configuration centroid is the average landmark position and the centre of gravity of a configuration [Zelditch et al., 2004; Mitteroecker et al., 2013; Klingenberg, 2016]. Per construction, centroid size and shape are independent; however, this statement only holds for empirical data if all landmarks vary the same in a small area, and in slight proportions (isotropic variation) [Mitteroecker et al., 2013]. Because this is untrue in most biological datasets, the centroid size is often related to shape.
From the resulting Procrustes shape coordinates, it is possible to quantify the shape differences between two landmark configurations by calculating the Procrustes distance. It is the square root of summed squared distances of corresponding —and superimposed— landmarks and intuitively, the higher the Procrustes distance, the more different the shapes.

The superimposition also distributes the landmark coordinates in a shape space that displays the range of shape variation of a dataset.

Finding group differences One of the main goals in GM is to study the variation of shapes and their covariation with other factors (e.g., sex and ontogenetic stage) and thus to find group structures based on shape data. This is usually first achieved with a Principal Component Analysis (PCA) that maximises the variance in a dataset without knowing *a priori* groups. The visualisation of a PCA in GM also provides visual clues of putative groups but does not perform clustering nor classification, as opposed to ML algorithms (see subsection 2.2.1). When coupled with extreme shape visualisation, PCA also allows to describe the main shape changes in a dataset.

A PCA is performed based on variance-covariance matrix of Procrustes coordinates –after superimposition– and allows designing a new shape space in which a combination of the original variables provides new axes of maximised variance. The new variables are termed principal components, they are sought into all space directions and result from linear transformations of original Procrustes coordinates. As opposed to the original morphometric variables, they are uncorrelated and orthogonal one with another.

The principal components are also termed eigenvectors because they are particular vectors whose length, but not direction, is affected by a linear transformation. While an eigenvector represents the rotation of variance-covariance matrix and a direction of data spread, an eigenvalue is the scalar which allows the transformation of a specific vector and indicates the variance of data in this same direction. On the eigenvalues is based the relative importance of eigenvectors even though these elements usually cannot be interpreted as biological meaningful factors [Mitteroecker et al., 2004; Mitteroecker and Gunz, 2009]. For this reason, it is generally suggested not to interpret one principal component separately from the others [Mitteroecker and Gunz, 2009; Fruciano, 2016]. However, in the case of intraspecific or intra-population GM datasets, the first principal component very often represents shape variation relative to size (allometry) and can be used alone [Mitteroecker et al., 2004; Mitteroecker and Gunz, 2009; Fruciano, 2016; Klingenberg, 2016]. Each element of the dataset is now attributed principal component scores (original scores by principal component coefficients) and can be displayed in a low-dimensional shape space defined by any two principal components combination. One interest of the PCA lies in the concentration of a dataset variance in few variables (and dimensions) as compared to the original dataset, which allows reducing data dimensionality while limiting information loss and generally greatly enhancing group separation [MacLeod, 2018]. This reduction of data dimensionality is for example crucial to most classification algorithms (but refer to subsection 2.2.1 for counter examples) to learn on the highest possible diversity of samples and to infer the most discriminant variable values that enhance classification performances. There are several opinions on how the dimensionality of principal component scores should be reduced prior to statistical analyses. Some authors (i) leave the noisy axes and keep those cumulating 90 % or 95 % of the total variation, others keep the axes accounting for more than 5 % of the total variation, and another choice is to consider all the first axes that maximise the cross-validation percentages of correct classification of elements after a Linear Discriminant Analysis (LDA) [Sheets et al., 2006; Evin et al., 2013; Fruciano, 2016; MacLeod, 2017]. However, there is no categorical rule on whether one method should

be adopted rather than another [Sheets et al., 2006; Evin et al., 2013; Fruciano, 2016; MacLeod, 2017].

The LDA belongs to supervised classification algorithms (see subsection 2.2.1) and can be used instead of, or combined with a PCA, which is often done in GM. An LDA is performed after the reduction of data dimensionality, which is, per construction, necessary for the model to perform well at classification task, and predicts the group of an element based on previously analysed data [Kemsley, 1996; Mitteroecker and Bookstein, 2011]. The fundamental difference between PCA and LDA is that the latter computes new axes of variation only in directions that maximise between-group differences, while minimising within-group distinctions, whereas in a PCA all directions are considered. The LD axes are the eigenvectors resulting from the within- and between-group scatter matrices product. They are also associated with eigenvalues whose magnitude define the orders of importance of the linear discriminant axes.
The statistic relevance of the groups characterised with PCAs and LDAs can further be tested with Multivariate ANalyses Of VAriance (MANOVAs) [MacLeod, 2017, 2018]. The purpose of a MANOVA is to test if independent variables (e.g., sex, growth stage, species) do impact a response patterning on dependent variables (e.g., landmark aligned coordinates). For that, a MANOVA computes the mean of each dependent variable for one or more independent variables and performs between-group comparisons. If these vectors are significantly different, it means that the groups do not belong to the same sampling distribution.

Shape visualisations in GM The visual examination of a PCA in GM is aided by modelling shape differences at key points of the morphospace. This can be achieved by producing deformation (warp) grids, which principle was proposed by Thompson [1917] and later formalised and developed by Bookstein [1989] and Rohlf and Slice [1990]. The principle lies in placing a Cartesian coordinate grid upon a reference shape and in further deforming the grid along two principal components of the shape space to reach a target shape [Rohlf and Slice, 1990; Gunz and Mitteroecker, 2013]. A usual choice is to warp each of the configurations with extreme PC1 and PC2 values against the mean shape of the dataset (located at the origin) to produce the extreme PCA shapes and visualise the range of shape deformations along the axes of maximum variance. The article in subsection 2.1.2 provides an example of the use of PCAs and extreme shapes to visualise the tooth shape diversity of different ontogenetic stages and sexes of *S. stellaris*. The transformed grid can be used subsequently to pattern a warped surface that can be compared to the reference one and these objects have been demonstrated to be of prime aid for visual perception of shape deformation [Oxnard and O'Higgins, 2009; Gunz and Mitteroecker, 2013].

Trajectory analyses A phenotypic trajectory represents the length, direction, and shape of the pathway that leads one group of specimens, such as a species, a population, or specimens of the same sex, to reach a specific phenotype [Pistore et al., 2019]. Evolutionary trajectories are drawn between species to understand the shape modification of a structure over long time periods or multiple generations [Adams and Collyer, 2009]. The shape modifications can be affected by biotic (e.g., predation) or abiotic (e.g., temperature) factors [Sheets and Zelditch, 2013]. Ontogenetic trajectories are a specific type of phenotypic trajectories: they represent the shape modification a

structure undergoes throughout the growth of specimens of a same species [Collyer and Adams, 2013; Sheets and Zelditch, 2013]. Growth can be represented by successive ontogenetic stages (e.g., embryonic, juvenile, sexually mature) or by continuous values (e.g., total length of specimens) [Sheets and Zelditch, 2013].

Within each ontogenetic stage or size class, a mean value of all principal components of shape is computed. The Euclidean distances are then computed between the means of sequential growth levels, which is visualised in a morphospace defined by two principal components, usually those containing the most variation. Ontogenetic trajectories are characterised by a location in the morphospace, a length, a direction, and a shape when the trajectory is drawn between more than two points (as can be visualised in Figure 2.3) [Adams and Collyer, 2009; Collyer and Adams, 2013; Sheets and Zelditch, 2013].

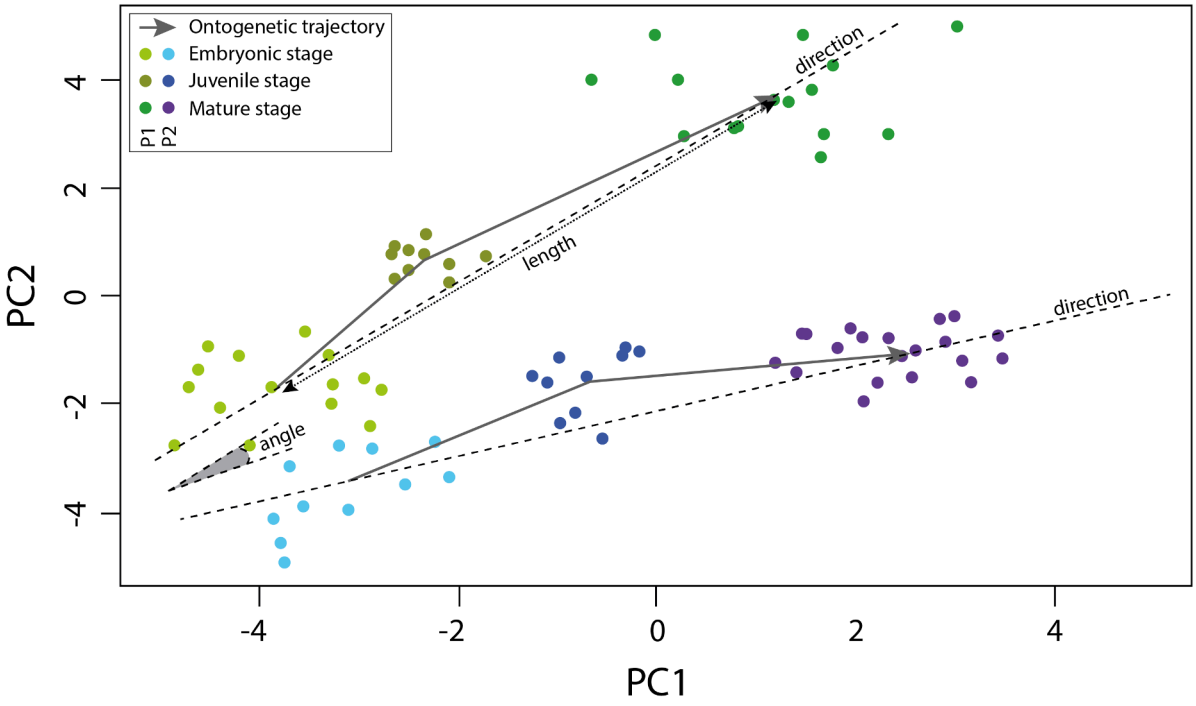

FIGURE 2.3: Characteristics of ontogenetic trajectories. The ontogenetic trajectories are computed between the embryonic, juvenile, and sexually mature stages, in two populations (green and blue shades). The trajectories are visualised in two dimensions but their characteristics are compared based on multiple axes. Each trajectory is characterised by a location, a length, a shape, and a direction that can be compared between trajectories with a measure of angle. P1, population 1; P2, population 2.

The Figure 2.3 depicts how these characteristics can be compared between trajectories with pairwise comparisons, as well as the angles that separate them in the morphospace [Collyer and Adams, 2013]. Differences in trajectory locations in the PCA are interpreted as differences in global shape of a structure between the groups considered [Collyer and Adams, 2013], such as tricuspid teeth in *S. stellaris* mature males and pentacuspid teeth in *S. stellaris* mature females [Berio et al., 2020]. The trajectory length is the sum of vector lengths between successive points in the trajectory and is interpreted as the amount of ontogenetic change in a group [Adams and Collyer, 2009; Collyer and Adams, 2013]. It can be easily stated that the longer the value between equivalent growth stages, the faster the shape change of a specific structure in a group, to the condition that

other trajectory parameters do not differ substantially [Collyer and Adams, 2013]. The trajectory direction represents the covariation of shape variables associated with unit change of the ontogenetic state. Differences in two directional shape changes are computed as an angle between both trajectory directions [Collyer and Adams, 2013] (see Figure 2.3). The comparison of shape trajectories is performed after a least-squares superimposition and differences in shape are quantified by the Euclidean distances between equivalent growth levels. Although they are informative about the general pattern of shape change across ontogeny, the statistical differences should be interpreted carefully, as these differences can arise from length or direction divergences of portions of trajectories, and not of entire trajectories [Collyer and Adams, 2013]. Furthermore, the trajectories are often displayed in 2D morphospaces but are computed on more PC axes than PC1 and PC2 and their comparison should be carefully interpreted in this regard.

Allometry Quantifying allometry relies in predicting a shape change per increase of size unit and then in understanding the relation between shape and size [Klingenberg, 2016]. The use of the log-transformed centroid size as the independent variable is recommended instead of centroid size in multivariate regression when there is an important range of variation, as it is the case between different species or ontogenetic stages [Klingenberg, 2016]. A positive allometry qualifies more size increase of a trait as compared to the others, this is for example the case of the liver weight of sharks, involved in buoyancy [Lingham-Soliar, 2005; Mitteroecker et al., 2013; Klingenberg, 2016; Gleiss et al., 2017]. A negative allometry is characterised by less size increase of a trait as compared to the others, as for the dimensions of large pelagic sharks caudal fin that allows slow swimming in long distances [Lingham-Soliar, 2005; Klingenberg, 2016; Gleiss et al., 2017; Ahnelt et al., 2020]. By contrast, a relationship is termed isometric (as opposed to allometric) when the size of a trait increases as much as the size of other traits or as the overall size of the structure [Klingenberg, 2016].

The size and shape are considered distinctly in the Gould-Mosimann framework, whereas in the Huxley-Jolicoeur framework, size belongs to all morphological variables [Klingenberg, 2016]. To be in line with our previous choice of complete Procrustes superimposition and shape *versus* size-and-shape space, here I introduce the allometry investigation following the Gould-Mosimann framework, in which shape and size are considered independently.

The type of allometry considered depends on the dataset composition and on the question that is asked [Klingenberg and Zimmermann, 1992; Pélabon et al., 2013]. Static allometry is estimated between specimens of same ontogenetic stage [Klingenberg and Zimmermann, 1992; Mitteroecker et al., 2013; Pélabon et al., 2013]. When the dataset involves specimens of different species, evolutionary allometry allows understanding their functional and behavioural adaptations [Klingenberg and Zimmermann, 1992; Mitteroecker et al., 2013; Pélabon et al., 2013]. At the intraspecific level, ontogenetic allometry can be estimated between specimens of different ages [Klingenberg and Zimmermann, 1992; Mitteroecker et al., 2013; Pélabon et al., 2013], which for example highlights sex-specific allometric patterns. Although different, these allometry types are interrelated because they all depend on overall size [Klingenberg and Zimmermann, 1992]. Moreover, the static and evolutionary allometries result from differences and

modifications of ontogenetic allometries: developmental genes for example regulate differently the ontogeny of structures, which results in structure-specific static allometries [Nijhout and McKenna, 2019]. Klingenberg and Zimmermann [1992] also suggested that the relation between ontogenetic and evolutionary allometry results from species-specific environmental adaptations, achieved through initially diverging morphologies and differences in growth trajectory directions.

There have been and still are various ways of exploring allometric patterns in GM. One of the first to be used was the linear regression of PC1 values (considered as composing the allometric vector) against the size variable, which is classically the centroid size of the elements. However, if PC1 often contains a high proportion of size variation, it is also composed of shape variation and in some datasets, most size variation is contained in other PC axes [Mitteroecker et al., 2013]. Several PCA axes usually contain information of size and a better approach to test for allometries is thus to use several axes (a conformation), whose number is determined as discussed in section 2.1.1. When there are several groups (e.g., species, ontogenetic stages, sexes) in the dataset, it can be relevant to compute independent allometric patterns for each of them. The point of this approach is twofold: it allows to pool all specimens in the same allometric analysis when no significant differences between the group-specific allometric patterns are detected, and to compare these allometric patterns when differences are found.
The first step in the allometric analysis is to use Multivariate ANalyses Of COVAriance (MANCOVAs) to test if there is any significant impact of centroid size (or any other size variable) on shape data. If so, two-way MANCOVAs test the homogeneity of allometry between all groups. Several methods allow to compare the allometric patterns between groups, for example by testing the significant differences between the slopes of allometric trajectories, and by computing the angles between them [Klingenberg, 2016]. Although the quantification of allometry is a field *per se* that includes multiple versions and subtleties, the former examples are the most used in GM for preliminary investigation of allometry and were informative enough in the scope of this PhD.

2.1.2 Intraspecific diversity of *Scyliorhinus stellaris* teeth

Stakes of the article

The tooth morphologies of *S. stellaris* have not been described in details along the ontogeny and between specimens of both sexes [Soldo et al., 2000; Soares and de Carvalho, 2019]. We were able to explore such variation using well preserved specimen jaws of different ontogenetic stages and we provide the first detailed description of *S. stellaris* tooth shapes and sizes among specimens of different sexes and ontogenetic stages. A classical GM framework is used on 3D data, as previously described in section 2.1.1 and aims at understanding the tooth morphological changes a specimen undergoes between the hatchling stage and its sexual maturation. This article also focuses on the emergence of gynandric heterodonty (sexual dimorphism in teeth) and on the tooth developmental trajectories that differ between females and males. Through the descriptive approaches used in this work and the one presented in section 2.2, I hope to contribute to a more detailed and comprehensive examination of teeth of extant shark species, including information about the sex, the ontogenetic stage, and the geographical origin to the analyses of shark tooth forms.

Journal article — The intraspecific diversity of tooth morphology in the large-spotted catshark *Scyliorhinus stellaris*: insights into the ontogenetic cues driving sexual dimorphism

Received: 14 March 2020 | Revised: 2 May 2020 | Accepted: 26 May 2020

DOI: 10.1111/joa.13257

ORIGINAL ARTICLE

ANATOMICAL SOCIETY Journal of Anatomy WILEY

The intraspecific diversity of tooth morphology in the large-spotted catshark *Scyliorhinus stellaris*: insights into the ontogenetic cues driving sexual dimorphism

Fidji Berio[1,2] | Allowen Evin[1] | Nicolas Goudemand[2] | Mélanie Debiais-Thibaud[1]

[1]CNRS, IRD, EPHE, UMR5554, Institut des Sciences de l'Évolution de Montpellier, ISEM, Université de Montpellier, Montpellier, France

[2]Centre National de la Recherche Scientifique, École Normale Supérieure de Lyon, Institut de Génomique Fonctionnelle de Lyon, UMR 5242, Université Claude Bernard Lyon 1, Univ. Lyon, Lyon, France

Correspondence
Mélanie Debiais-Thibaud, CNRS, IRD, EPHE, UMR5554, Institut des Sciences de l'Évolution de Montpellier, ISEM, Université de Montpellier, Montpellier, France.
Email: melanie.debiais-thibaud@umontpellier.fr

Funding information
This work was supported by the ENS de Lyon "Attractivite Nouveaux professeurs" fund (attributed to Nicolas Goudemand)

Abstract

Teeth in sharks are shed and replaced throughout their lifetime. Morphological dental changes through ontogeny have been identified in several species and have been correlated with shifts in diet and the acquisition of sexual maturity. However, these changes were rarely quantified in detail along multiple ontogenetic stages, which makes it difficult to infer the developmental processes responsible for the observed plasticity. In this work, we use micro-computed tomography and 3D geometric morphometrics to describe and analyze the tooth size and shape diversity across three ontogenetic stages (hatchling, juvenile, and sexually mature) in the large-spotted catshark *Scyliorhinus stellaris* (Linnaeus, 1758). We first describe the intra-individual variation of tooth form for each sex at each ontogenetic stage. We provide a tooth morphospace for palatoquadrate and Meckelian teeth and identify dental features, such as relative size and number of cusps, involved in the range of variation of the observed morphologies. We then use these shape data to draw developmental trajectories between ontogenetic stages and for each tooth position within the jaw to characterize ontogenetic patterns of sexual dimorphism. We highlight the emergence of gynandric heterodonty between the juvenile and mature ontogenetic stages, with mature females having tooth morphologies more similar to juveniles' than mature males that display regression in the number of accessory cusps. From these data, we speculate on the developmental processes that could account for such developmental plasticity in *S. stellaris*.

KEYWORDS

geometric morphometrics, gynandric heterodonty, monognathic heterodonty, ontogenetic trajectory, scyliorhinids

1 | INTRODUCTION

The fantastic diversity of shark tooth shapes has been studied in relation to the evolutionary history and ecological traits of this iconic group (Bazzi *et al*., 2018). Functionally, convergent tooth shapes between the bonnethead sharks *Sphyrna tiburo* (Sphyrnidae) and horn sharks (Heterodontidae) were associated with the hard prey they feed on (Wilga and Motta, 2000). On the other hand, a strong phylogenetic signal arose from the analysis of the whole dentition of Lamniforms, which have a unique symphyseal to commissural tooth-type patterning (Shimada, 2002, 2005). For this reason, tooth shape is one of the main supports for establishing taxonomic groups and phylogenetic relationships between fossil and extant elasmobranchs (sharks and batomorphs) (Shimada, 2002, 2005; Cappetta, 2012).

One issue in this matter arises from the fact that an elasmobranch is rarely characterized by a single tooth type (molariform, unicuspidate, multicuspidate) within the jaw but by a continuum of different tooth shapes along the jaw axis (monognathic heterodonty) and often displays differences between the palatoquadrate (upper) and Meckelian (lower) teeth (dignathic heterodonty). The continuous and lifelong replacement of teeth in elasmobranchs makes this variation dynamic in time (ontogenetic heterodonty), their tooth types being replaced, linked to dietary shifts (Luer *et al*., 1990; Powter *et al*., 2010) and reproductive status (Reif, 1976; Springer, 1979; Gottfried and Francis, 1996; Motta and Wilga, 2001; Purdy and Francis, 2007; Powter *et al*., 2010; French *et al*., 2017).

In elasmobranchs, tooth replacement occurs at various rates and following different patterns, depending, for instance, on tooth imbrication and water temperature, and may also differ between jaws (Strasburg, 1963; Luer *et al*., 1990; Correia, 1999; Moyer and Bemis, 2016; Meredith Smith *et al*., 2018). Gynandric heterodonty (sexual dimorphism in teeth) is very common in elasmobranchs (Feduccia and Slaughter, 1974; Taniuchi and Shimizu, 1993; Kajiura and Tricas, 1996; Geniz *et al*., 2007; Gutteridge and Bennett, 2014; Underwood *et al*., 2015; French *et al*., 2017) and affects specific tooth files (reported in Dasyatidae, Carcharhinidae, and Leptochariidae) to the whole dental set at various degrees during the sexually mature stage (Cappetta, 1986). The higher and sharper mature male teeth are indeed assumed to function in grasping females and consequently to facilitate clasper introduction during copulation (Springer, 1966; McEachran, 1977; McCourt and Kerstitch, 1980; Cappetta, 1986; Ellis and Shackley, 1995; Kajiura and Tricas, 1996; Pratt Jr. and Carrier, 2001; Litvinov and Laptikhovsky, 2005; Gutteridge and Bennett, 2014). This feature has been recorded as a seasonal variation in the Atlantic stingray *Dasyatis sabina* (Kajiura and Tricas, 1996), while it is assumed to be a fixed-in-time feature in other elasmobranch species for which it has been described (Gutteridge and Bennett, 2014; de Sousa Rangel *et al*., 2016). Gynandric heterodonty has also been only described at sexually mature stages, suggesting that sex-hormone signals triggering the reproductive activity may also be involved in the development of the observed dental sexual dimorphism (McEachran, 1977; Cappetta, 1986; Snelson *et al*., 1997; Powter *et al*., 2010).

Shark tooth shapes have been mostly evaluated through semi-quantitative studies based on asymmetry, number, sharpness, and relative bending or size of cusps (Cappetta, 1986; Frazzetta, 1988). Moreover, studies that performed morphometrics on extant species mainly focused on tooth crown dimensions (height, width, and angle) of specific teeth (small-spotted catshark *Scyliorhinus canicula* (Linnaeus, 1758) Ellis and Shackley, 1995), Lamniforms (Shimada, 2002), and Port Jackson shark *Heterodontus portusjacksoni* (Meyer, 1793) (Powter *et al*., 2010). These approaches mainly base the tooth shape analysis on main cusp dimensions, which do not capture complex heterodonty patterns (Whitenack and Gottfried, 2010). Recent publications, however, have focused on quantitative tooth traits in sharks by using geometric morphometrics (Marramà and Kriwet, 2017; Soda *et al*., 2017; Cullen and Marshall, 2019), providing more subtle information on tooth size and shape quantitative variation. These comparative studies allow to infer developmental and phylogenetic hypotheses and refine our knowledge about the inter- and intraspecific tooth shape variation in several shark species. Overall, the authors highlight the benefits of a quantitative investigation of complete tooth shape patterns in sharks to understand ontogenetic and evolutionary shifts.

Scyliorhinids are emerging models for shark studies (Coolen *et al*., 2008) and among them, *S. canicula* tooth morphologies have been the most studied. Mature *S. canicula* specimens display gynandric heterodonty that has been qualitatively described (Brough, 1937; Ellis and Shackley, 1995; Erdogan *et al*., 2004; Debiais-Thibaud *et al*., 2015; Soares and Carvalho, 2019), but quantification of scyliorhinids dental variation is still fragmentary. In particular, the nursehound *S. stellaris* (Linnaeus, 1758) is a phylogenetically close relative of *S. canicula* (Iglésias *et al*., 2005; Vélez-Zuazo and Agnarsson, 2011) and has mostly been studied for physiological aspects (Piiper *et al*., 1977; Heisler and Neumann, 1980). To our knowledge, the study of Soldo *et al*. (2000) is the only one focusing on *S. stellaris* tooth shape patterns. However, this study did not test the impact of ontogeny on tooth morphology and did not detect sexual dimorphism although gynandric heterodonty is known to be a common feature to Scyliorhinidae (Cappetta, 1986; Soldo *et al*., 2000; Soares and Carvalho, 2019).

Here, we provide the first detailed description of *S. stellaris* tooth form (shape and size) using microCT images and quantitative 3D geometric morphometrics. We characterize the ontogenetic and sexually dimorphic trajectories of tooth shapes and highlight the emergence of gynandric heterodonty with sexual maturation. We also describe intra-individual tooth morphological variation and we discuss the developmental hypotheses that could be involved in the observed tooth diversity of *S. stellaris*.

2 | MATERIALS AND METHODS

2.1 | Biological material

In total, 33 specimens of *Scyliorhinus stellaris* (16 females, 17 males; 2,467 teeth) were analyzed. Total length (TL, in cm) was used to define the groups of same ontogenetic stages. Female *S. stellaris* are considered sexually mature at 79 cm TL and males at 77 cm TL (Fischer *et al*., 1987; Musa *et al*., 2018), but longer mature specimens were chosen to avoid biases due to potential later maturation. Juveniles were twice shorter than the mature specimens and hatchling specimens were chosen as close as possible from hatching (Musa *et al*., 2018) although umbilical scars were never observed. We cannot evaluate how these time points are distributed along the ontogeny of the specimens because we have no information on the age of each specimen, and no growth curve has been published for this species beyond the hatchling stage (Musa *et al*., 2018). Growth rates may be sex-specific in elasmobranchs (Hale and Lowe, 2008) so we may expect age differences between males and females of similar total length. Hatchling specimens were 17.7 ± 3.3 cm TL (7 females, 5 males), juveniles were 57.7 ± 3.2 cm TL (5 females, 5 males), and mature ones were 102.7 ± 7.2 cm TL (4

females, 7 males; Table 1). Dried jaws were provided by the Institute of Evolution Sciences of Montpellier (France), and jaws preserved in ethanol were provided by the Aquarium du Cap d'Agde (France).

2.2 | MicroCT scans

Jaws were microCT scanned using a Phoenix Nanotom S with voxel sizes ranging from (10.7 µm) to (30.0 µm), and 3D volumes were reconstructed using the corresponding phoenix datos x2 reconstruction software (v2.3.0).

2.3 | Tooth selection

For each specimen, all 3D teeth were isolated from the right palatoquadrate and Meckelian cartilages with Amira software (v6.2.0) (Stalling *et al.*, 2005). Each tooth was identified within a file (or family) along the mesio-distal axis and by the generation within a tooth file (Figure 1a). Within each tooth file, we analyzed 1–4, functional but not worn, generations.

The teeth were not clustered into classically used tooth-type denominations (e.g., symphyseal, parasymphyseal, lateral, commissural) (Reif, 1976; Lucifora *et al.*, 2001) on purpose since we did not visually identify abrupt tooth shape or size change along the mesio-distal axis,

TABLE 1 Scanned *Scyliorhinus stellaris* specimens.

Specimen	Sex	Stage (TL, cm)	Cartilage	Preservation	Scanning resolution (µm)
100418A	F	Hat (22)	Both	etOH	13.18
100418B	F	Hat (21)	Both	etOH	13.18
100418D	F	Hat (14)	Both	etOH	8.64
100418E	M	Hat (17.5)	Both	etOH	13.00
100418F	M	Hat (14)	Both	etOH	9.41
100418G	F	Hat (14)	Both	etOH	9.41
100418H	M	Hat (17)	Both	etOH	14.26
160118B	F	Hat (17)	Both	etOH	10.88
160118C	F	Hat (17)	Both	etOH	11.16
160118D	F	Hat (17.5)	Both	etOH	11.40
160118E	M	Hat (16.5)	Both	etOH	10.51
230918A	M	Hat (24.5)	Both	etOH	10.00
000000B	F	Juv (64)	Pq	Air	16.61
000000C	M	Juv (56)	Pq	Air	16.61
UM REC0371M	M	Juv (53)	Pq	Air	15.60
UM REC0778M	M	Juv (59)	Both	Air	19.17
UM REC1068M	F	Juv (55)	Both	Air	16.56
UM REC1073M	M	Juv (60)	Both	Air	14.29
UM REC1074M	F	Juv (57)	Both	Air	18.33
UM REC1075M	F	Juv (59)	Both	Air	12.50
UM REC1076M	F	Juv (55)	Both	Air	16.00
UM REC1077M	M	Juv (59)	Both	Air	21.28
UM REC0185M	M	Mat (112)	Mc	Air	26.93
UM REC0187M	M	Mat (106)	Mc	Air	26.93
UM REC0188M	M	Mat (113)	Pq	Air	26.93
UM REC0189M	F	Mat (93)	Both	Air	26.93
UM REC0353M	F	Mat (95)	Mc	Air	18.52
UM REC1312M	M	Mat (98)	Both	Air	30.00
UM REC1496M	M	Mat (102)	Both	Air	29.75
UM REC1497M	M	Mat (105)	Both	Air	30.00
UM REC1498M	M	Mat (110)	Both	Air	30.00
UM REC1499M	F	Mat (94)	Both	Air	25.00
UM REC1500M	F	Mat (102)	Both	Air	30.00

Abbreviations: etOH, 70% ethanol; F, female; Hat, hatchling stage; Juv, juvenile stage; M, male; Mat, mature stage; Mc, Meckel cartilage; and Pq, palatoquadrate.

except for the symphyseal teeth on the lower jaw (Figure 1a). These symphyseal teeth are located between the right and left Meckelian cartilages and are not located above jaw cartilages, contrary to all other teeth. All subsequent analyses were performed under the hypothesis of homology between tooth files of different specimens, which, for example, means that the most symphyseal Meckelian tooth file of a given hatchling male is considered equivalent to the most symphyseal Meckelian tooth file of a mature female.

2.4 | Geometric morphometrics

Seven 3D landmarks and 31 semilandmarks were placed on the cutting edge of each tooth (Figure 1b) with the Landmark software (v3.0.0.6) (Wiley *et al*., 2005), and the data were preprocessed with Scyland3D (v1.1.0) (Berio and Bayle, 2020). The semilandmark density was made higher in the lateral sides of the teeth because gynandric heterodonty in scyliorhinids is known to involve the addition of lateral accessory cusps (Gosztonyi, 1973; Ellis and Shackley, 1995; Debiais-Thibaud *et al*., 2015; Soares and Carvalho, 2019). Our form comparison analyses will be interpreted in light of this choice: the centroid size and shape parameters will be more affected by variations in the lateral zones (with higher density of semilandmarks) than in the main cusp and crown base zones. All analyses were performed separately for Meckelian and palatoquadrate teeth.

Crown base width was computed based on the distance between landmarks 1 and 33 (d1–33, Figure 1b), while main cusp height was the mean of the distances between the main cusp and each side of the tooth (mean of d1–17 and d17–33, see Figure 1b). We also used these measures to generate a ratio between main cusp height and crown base width, later referred to as the cusp-crown ratio. Tooth

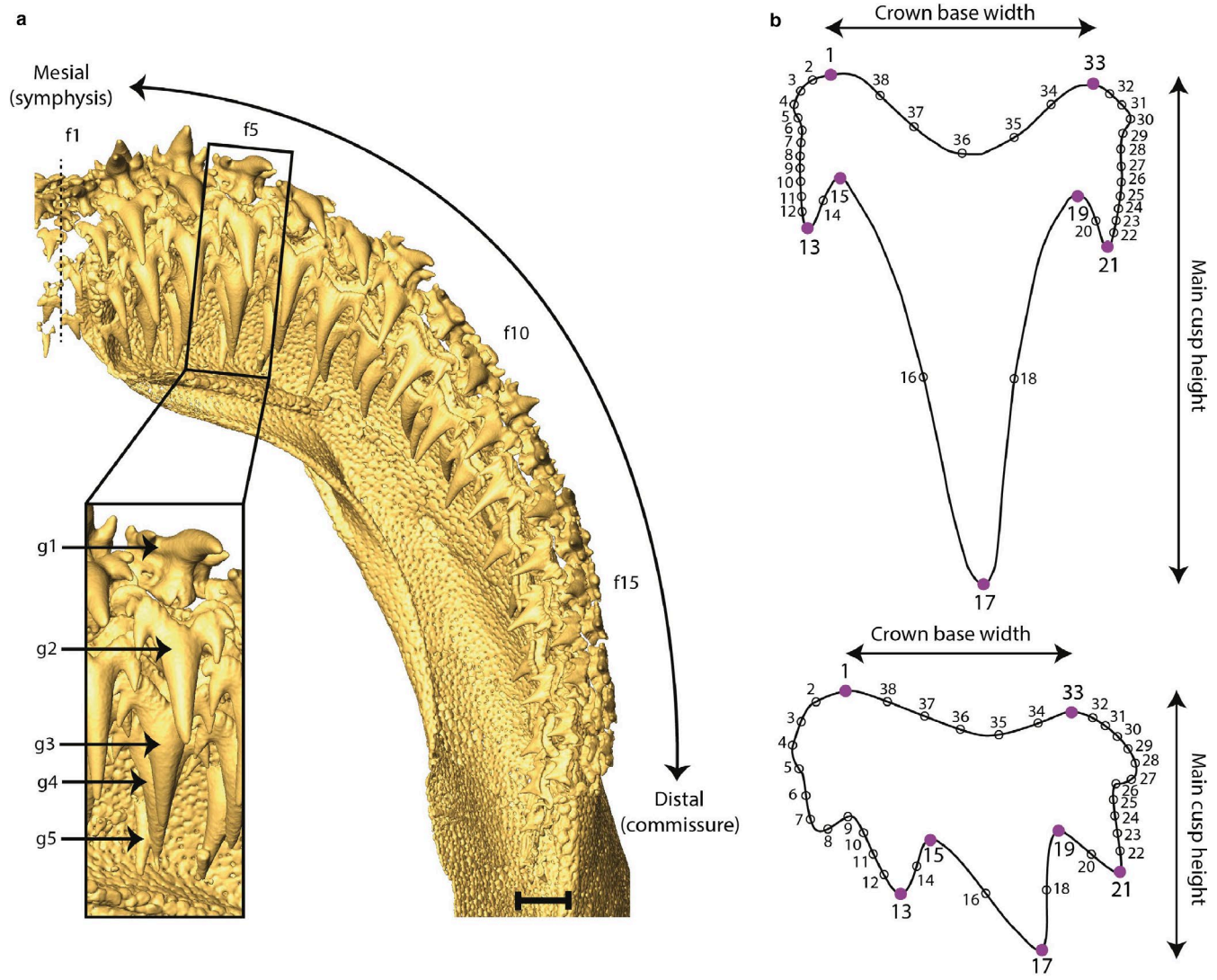

FIGURE 1 Tooth identification within a jaw and landmarking. (a) microCT image of a right lower jaw of a juvenile female *Scyliorhinus stellaris*, dorsal view. f, file as defined from the symphysis (dotted line) to the commissure; g, generation. Scale bar represents 5 mm for the jaw and 3 mm for the zoomed teeth; (b) examples of landmark (purple) and semilandmark (empty dots) setting on mesial (top) and distal (bottom) teeth of a juvenile female.

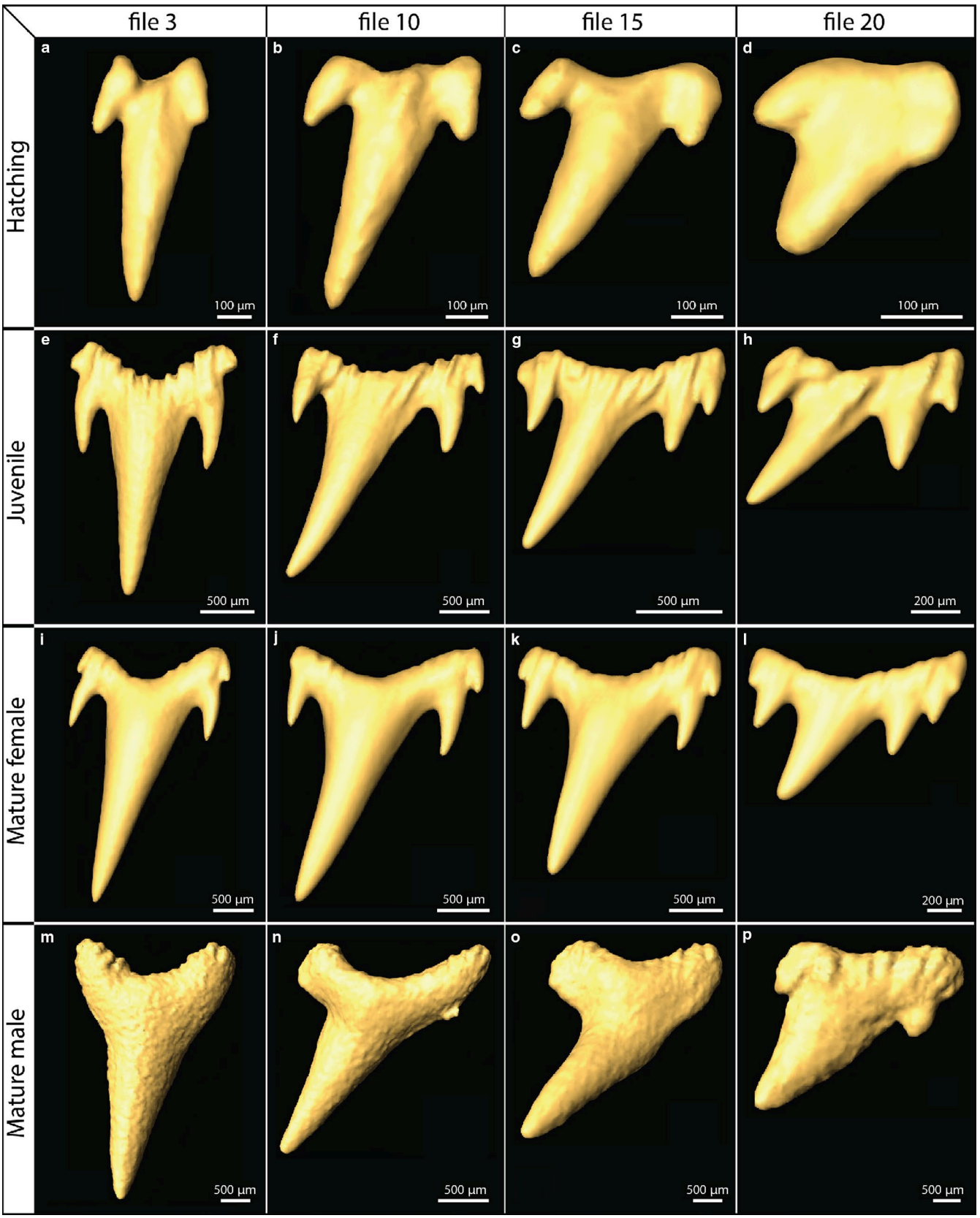

FIGURE 2 Palatoquadrate tooth shape diversity in *Scyliorhinus stellaris*. (a–d) Hatchling female teeth; (e–h) juvenile female teeth; (i–l) mature female teeth; (m–p) mature male teeth. Symphyseal (mesial) pole to the left.

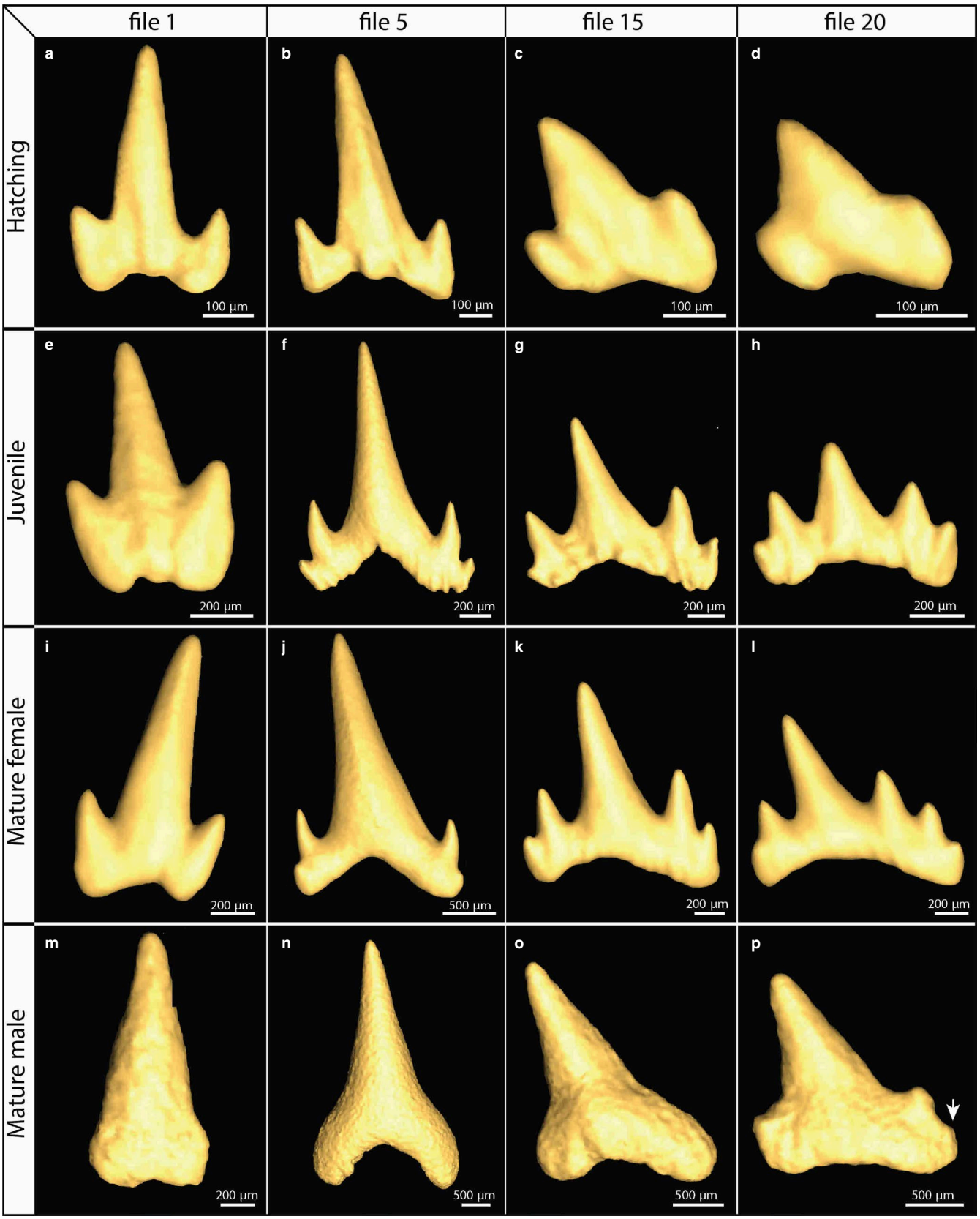

FIGURE 3 Meckelian tooth shape diversity in *Scyliorhinus stellaris*. (a–d) Hatchling female teeth; (e–h) juvenile female teeth; (i–l) mature female teeth; (m–p) mature male teeth. Symphyseal (mesial) pole to the left.

symmetry was measured by the ratio between d1–17 and d17–33 and a value of 1 implies a symmetric tooth.

A Generalized Procrustes Superimposition (GPA) was performed (Bookstein, 1991) during which the semilandmarks were slided based on minimizing bending energy (Bookstein, 1997). The tooth size patterns were investigated using centroid sizes computed based on the GPA, and the tooth shape variation was displayed with principal component analyses (PCAs). In order to reduce the high dimensionality of the aligned coordinates, the data were reduced prior to multivariate analyses of variance (MANOVAs) to the axes containing 95% of the total variation (14 and 13 PCA axes for Meckelian and palatoquadrate teeth, respectively, out of 114 available axes). We defined the random variable as the tooth generation within a given tooth file, in a specimen. We used these generations as internal replicates from which we generated an average tooth shape per tooth file, for each specimen. One-way analyses of variance (ANOVAs) and MANOVAs were then computed on tooth mean centroid size and tooth shape for each tooth position, each sex, at each ontogenetic stage, to avoid biases due to unbalanced sampling between tooth files (from one to four sampled teeth within one tooth file). Two-way ANOVAs and MANOVAs were subsequently used on tooth mean centroid size and shape to test the interaction between sex, stage, and tooth position along the jaw. Within each jaw, inter-group differences in shape were first investigated between sexes without considering ontogenetic stages nor tooth positions. The differences due to sex and tooth position within the jaw were subsequently tested within given ontogenetic stages.

Trajectory analyses were performed to evaluate the developmental tooth shape changes within each tooth position. The trajectories were computed and compared (a) between sexes and (b) between two consecutive ontogenetic stages within sexes (e.g., from hatchling to juvenile, and juvenile to mature). The statistical tests were performed on the length, direction, and shape of the trajectory in the morphospace (Adams and Otárola-Castillo, 2013).

Geometric morphometric superimposition and analyses were carried out in R (v3.4.3) with the geomorph library (v3.2.1) (Adams and Otárola-Castillo, 2013).

3 | RESULTS

3.1 | Visual inspection of tooth morphology

There were no symphyseal teeth on the palatoquadrate, but one symphyseal file on the Meckelian cartilage (for 41% of the specimens). Although the second Meckelian tooth file is partially located above the Meckelian mesial edge, the teeth display size and morphological similarities to the symphyseal ones (for 59% of the specimens). We report no significant difference in tooth file counts between right and left sides of the jaw within each ontogenetic stage for each sex (Wilcoxon matched-pairs signed rank tests, *p*-val > $4.60e^{-2}$ for all tests; we observed a maximum difference of two tooth files between the right and left jaws, in 13/51 comparisons). Palatoquadrate number of tooth files does not differ significantly between ontogenetic stages in males and in females (one-way permutation ANOVAs, *p*-vals > $5.00e^{-2}$). Conversely, in both sexes, there are significantly more Meckelian tooth files in juvenile and mature specimens compared to hatchling ones (one-way permutation ANOVAs, *p*-vals < $5.00e^{-2}$), but no difference was detected between the juvenile and mature ontogenetic stages. Moreover, there is no significant difference in tooth file counts between males and females (Wilcoxon tests, *p*-val > $3.10e^{-1}$ for all tests).

A graded decrease of tooth size is observed along the mesio-distal axis of the jaw, except for the symphyseal teeth which are smaller than parasymphyseal ones (see Figures 1, 2e, and 3e,i). In all sexes and stages, there is a graded increase of lateral bending of teeth from the symphysis to the commissure, producing asymmetric teeth (Figures 2 and 3). Teeth of male and female hatchlings are visually similar in shape with tricuspid teeth in both jaws (Figures 2a–d and 3a–d).

Juvenile female and male teeth display little variability in cusp number along the jaw: Mesial palatoquadrate teeth (Figure 2e) often display one main cusp and four accessory cusps, while the more distal ones have four to five cusps and often more accessory cusps in the mesial than in the distal part of the crown (Figure 2e–h). A similar pattern is observed in Meckelian teeth (Figure 3e–h), except for tricuspid symphyseal ones. Mature female teeth are similar in shape to those of juveniles except at the most distal positions where they exhibit up to six cusps (Figures 2i–l and 3i–l). Mature male mesial teeth are always un-bent and unicuspidate, while more distal teeth undergo an addition of one to two accessory cusps (Figures 2m–p and 3m–p). Mature male teeth rarely display more than two accessory cusps (Figures 2m–o and 3m–p); however, a small third accessory cusp was detected on the distalmost teeth of some specimens (see arrow on Figure 3p).

3.2 | Morphometric analyses

3.2.1 | Tooth size patterns

To support and quantify visual observations, morphometric measurements were performed and ratios of the main cusp height and the crown base width were computed. Ratio values are higher than 1, showing that the main cusp is higher than the crown base is wide (Figure 4a,d).

In all groups, this ratio decreases along the mesio-distal axis of the jaw (Figure 4a,d), with exceptions in the distalmost positions in Meckelian teeth of mature males and juvenile females (Figure 4a,d). The variation of this ratio follows the gradual decrease of both measures, although stronger decrease is observed in the main cusp height (Figure S1). At each position, the measured cusp–crown ratio is very comparable between ontogenetic stages, but in the palatoquadrate teeth of hatchling specimens, we report higher ratios (1.5-fold increase), with a minimum of 1.6 along the mesio-distal axis

(see position 19 in hatchling males in Figure 4d). The raw data on main cusp height and crown base width show that hatchling palatoquadrate teeth are different from Meckelian teeth because of their smaller crown base (Figure S1A,B). Overall, these observations point to similar developmental constraints on the overall geometry of teeth at all ontogenetic stages on Meckelian teeth and to a transition of these developmental constraints between the hatchling and juvenile ontogenetic stages in palatoquadrate teeth.

3.2.2 | Tooth asymmetry

Teeth of *S. stellaris* undergo a global increase of bilateral asymmetry from the symphysis to the commissure although we also report a sudden fall of asymmetry values in the distalmost tooth files (Figure 4b,e). In Meckelian teeth, the tooth asymmetry values of all groups (ontogenetic stages) are overlapping until the 15th tooth file, but female teeth distal to this position tend to display higher asymmetries than teeth of other groups (Figure 4b). A similar pattern is observed in the palatoquadrate: asymmetry values of all groups are very similar until the 14th tooth file (Figure 4e). However, contrary to Meckelian teeth, asymmetry patterns of hatchling teeth distal to the 14th tooth file are distinct from those of juveniles with lower asymmetry values (Figure 4e). Mature males display teeth whose symmetry values are in between those of hatchling and juvenile specimens (Figure 4e). As for Meckelian teeth, mature female teeth are the most asymmetrical (Figure 4e) with maximum values between the 19th and 23rd files (Figure 4b). In the palatoquadrate, these maxima are reached between the 22nd and 24th tooth files in all groups (Figure 4e). We also highlight that the anteriormost teeth (1st file in

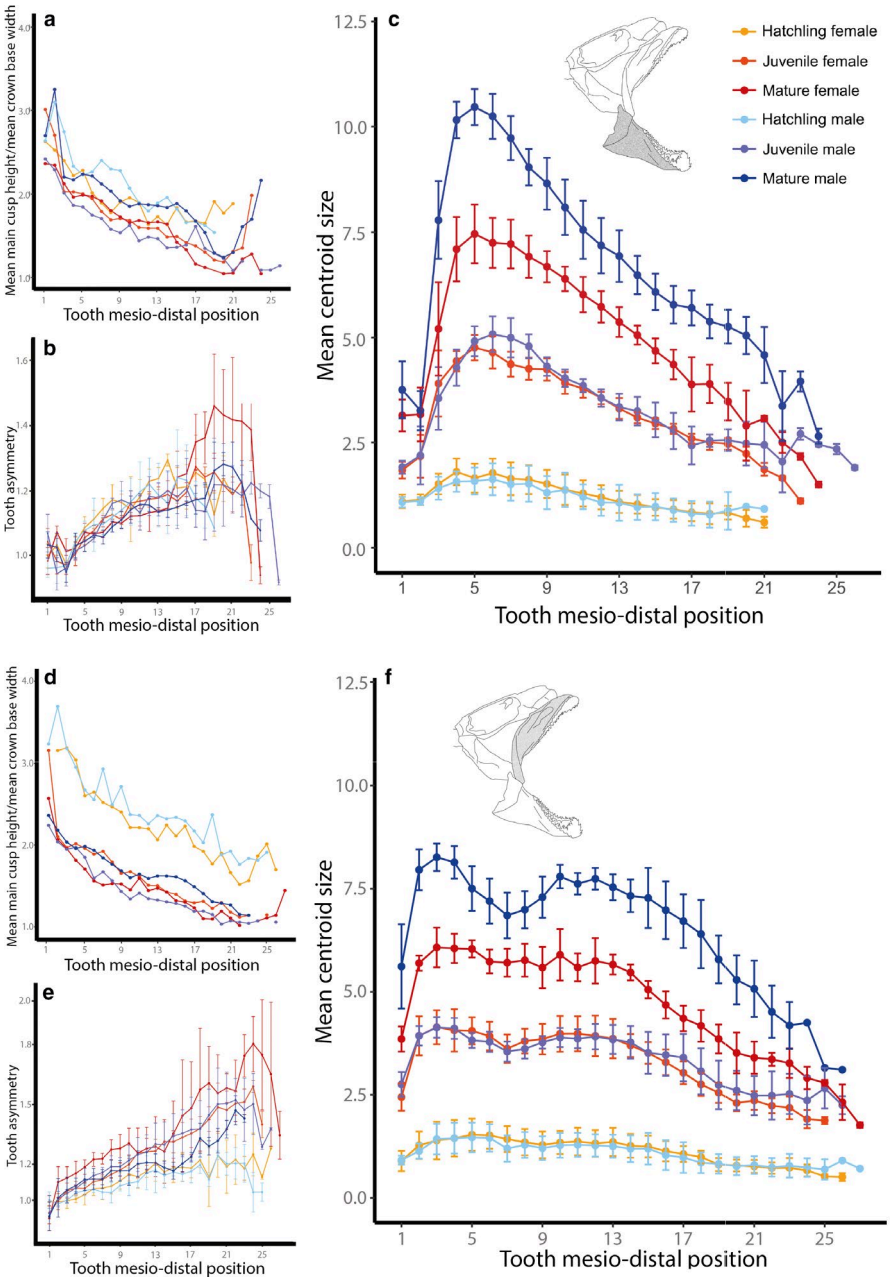

FIGURE 4 Tooth dimensions of *Scyliorhinus stellaris* right Meckelian and palatoquadrate teeth. (a and d) Morphometric measure of the ratio between main cusp height and crown base width; (b and e) deviation to tooth bilateral symmetry: difference between the tooth tip and each crown base extremity distances. (c and f) Tooth centroid sizes. At each tooth position, mean values are computed among all tooth generations (internal replicates), before being computed among all specimens. Error bars are standard deviations among replicates and specimens.

the palatoquadrate and up to the 3rd file in the Meckelian cartilage) are close to bilateral symmetry (Figure 4b,e). These measurements highlight similar tooth mesio-distal asymmetry patterns within hatchling and juvenile specimens and higher asymmetry values in mature females compared to all other groups (Figure 4b,e).

3.3 | Geometric morphometric analyses

In the previous two morphometric analyses, the mesio-distal variation of tooth shape could be discriminated in terms of relation of cusp height and crown width and in terms of asymmetry for juvenile and mature teeth. However, no strong difference of these parameters could be seen between sexes in either jaws of all three ontogenetic stages. In the following, we established the tooth centroid size patterns of variation along the mesio-distal jaw axis for each group.

3.3.1 | Meckelian teeth

Both sexes show similar tooth centroid size patterns along the mesio-distal axis of the jaw at hatchling and juvenile stages (Figure 4c). Hatchling males and females display very little tooth centroid size variation along the jaw (Figure 4c), as opposed to juvenile and mature specimens that share a maximum tooth centroid size in file 5 or 6 (Figure 4c): values for juvenile teeth are intermediate between the hatchling and mature values. Overall, the mesio-distal tooth centroid size pattern is similar between juvenile and mature specimens (Figure 4c), but mature males display an exacerbated tooth size pattern compared to mature females, except at the symphyseal tooth positions (Figure 4c).

3.3.2 | Palatoquadrate teeth

Similar to the Meckelian teeth, palatoquadrate tooth centroid sizes do not differ between sexes at hatchling or juvenile stages, centroid sizes increase with ontogeny, and mature males display higher values compared to females (Figure 4f). Juvenile males and females have two local maxima tooth centroid sizes at the 3rd and 12th and 4th and 10th files, respectively, and a minimum centroid size at file 7 (Figure 4f). Mature specimens display a clear bimodal tooth centroid size pattern from the symphysis to the commissure, with local maximum values in the 3rd and 10th files and a local minimum value in the 7th file (Figure 4f). Topologically, the Meckelian file 5 (maximal value in adult males) faces the palatoquadrate file 7 (local minimum in adult males) which suggests functional constraints for these variation of tooth size along the mesio-distal axis.

Our statistical tests corroborated the observation that tooth centroid size varies according to the ontogenetic stage in both cartilages (one-way ANOVAs, p-vals < $2.00e^{-16}$, Table 2). Within all ontogenetic stages, the Meckelian and palatoquadrate tooth mesio-distal position also significantly impacts the tooth centroid size (one-way ANOVAs, p-vals < $9.37e^{-4}$, Table 2). The Meckelian and palatoquadrate tooth centroid size of mature specimens is also significantly impacted by sex (one-way ANOVAs, p-vals < $1.54e^{-2}$, Table 2). We finally report a significant interaction between sex and ontogenetic stage in the Meckelian and palatoquadrate full datasets (two-way ANOVAs, p-vals < $3.24e^{-3}$, Table 2), as well as between ontogenetic stage and

TABLE 2 ANOVA results on centroid sizes.

	All	Hatchling	Juvenile	Mature
	F value (*p*-val)	F value (*p*-val)	*F* value (*p*-val)	*F* value (*p*-val)
Meckelian teeth				
Sex	2.37 ($1.26e^{-1}$)	$1.47e^{-1}$ ($7.04e^{-1}$)	$4.00e^{-2}$ ($8.42e^{-1}$)	6.33 (**$1.54e^{-2}$**)
Stage	$1.03e^{2}$ (**$<2.00e^{-16}$**)	-	-	-
ToothMD	1.09 ($3.61e^{-1}$)	$2.43e^{1}$ (**$2.67e^{-10}$**)	$1.48e^{1}$ (**$4.69e^{-9}$**)	5.39 (**$5.77e^{-5}$**)
Sex:Stage	5.99 (**$3.24e^{-3}$**)	–	–	–
Sex:ToothMD	$2.20e^{-2}$ (1.00)	–	–	–
Stage:ToothMD	2.14 ($2.49e^{-3}$)	–	–	–
Palatoquadrate teeth				
Sex	2.83 ($9.48e^{-2}$)	$4.52e^{-1}$ ($5.04e^{-1}$)	$1.00e^{-3}$ ($9.70e^{-1}$)	$1.48e^{1}$ (**$3.32e^{-4}$**)
Stage	$2.24e^{2}$ (**$2.00e^{-16}$**)	–	–	–
ToothMD	$8.29e^{-1}$ ($7.03e^{-1}$)	$1.91e^{1}$ (**$3.44e^{-11}$**)	$2.72e^{1}$ (**$1.33e^{-12}$**)	3.56 (**$9.37e^{-4}$**)
Sex:Stage	$1.59e^{1}$ (**$5.48e^{-7}$**)	–	–	–
Sex:ToothMD	$1.50e^{-2}$ (1.00)	–	–	–
Stage:ToothMD	1.33 ($1.28e^{-1}$)	–	–	–

Significant p-values after Benjamini and Hochberg correction are in bold.
Abbreviation: MD, mesio-distal.

tooth mesio-distal position in Meckelian teeth (two-way ANOVA, *p*-val < $2.49e^{-3}$, Table 2).

3.4 | Developmental trajectories

We performed independent PCAs in each jaw, and the extreme shapes on the PC1 and PC2 axes illustrate how similar shape parameters generate the main Meckelian and palatoquadrate variations of tooth shapes. This first observation highlights the fact that, although we treated them separately, teeth of the upper and lower jaw show similar shape variations along the first PCs. In both cases, the main axis of tooth shape variation relates to the main cusp proportions and to the variation in the number of lateral accessory cusps (Figure 5a,b). The second axis of variation seems to relate to the size of lateral cusps relative to the main cusp size (Figure 5a,b).

The shape of Meckelian and palatoquadrate teeth of *S. stellaris* is mostly impacted by ontogenetic stage (one-way MANOVAs, *p*-vals < $2.20e^{-16}$, $3.04e^{1}$ < *F* approx < $4.58e^{1}$, Table 3) although the sex of the specimens and the tooth position along the mesio-distal axis of the jaw also significantly impact the tooth shape (one-way MANOVAs, Sex: *p*-val < $6.13e^{-8}$, 5.39 < *F* approx < 7.61; tooth position: *p*-val < $3.12e^{-14}$, 1.80 < *F* approx < 1.89, Table 3). Within ontogenetic stages, the mesio-distal position of a tooth significantly impacts the tooth shape of juveniles (one-way MANOVAs, *p*-vals < $1.16e^{-4}$ for both jaws, Table 3) and palatoquadrate teeth of hatchling specimens (one-way MANOVA, *p*-val < $2.28e^{-6}$, Table 3). Conversely, for both jaws and within each ontogenetic stage, a sexual dimorphism of tooth shape was detected (one-way MANOVAs, *p*-vals < $5.37e^{-3}$, Table 3). We finally report that the sexual dimorphism differs between stages and tooth mesio-distal positions for Meckelian and palatoquadrate teeth (two-way MANOVAs, *p*-vals < $1.02e^{-2}$, Table 3).

3.4.1 | Comparison of developmental trajectories between sexes

The full shape developmental trajectories (from hatchling to juvenile, and to mature stage) differ between sexes for most of the palatoquadrate tooth files that are distal to the 3rd file and for all Meckelian tooth files distal to the 8th file (*p*-vals < $1.60e^{-2}$, Tables 4 and 5). These differences arise from divergent juvenile-to-mature developmental directions between males and females (45/46 significant *p*-values, *p*-vals < $3.10e^{-2}$, Tables 4 and 5). Significant differences between males and females for juvenile-to-mature trajectory lengths are also reported for most tooth files and always involve longer trajectories in males than females (*p*-vals < $3.40e^{-2}$, Tables 4 and 5). We report no such differences between male and female hatchling-to-juvenile trajectory lengths and angles (Tables 4 and 5). This pattern highlights a shift between male and female tooth shape developmental trajectories only after the juvenile stage.

3.4.2 | Comparison of developmental trajectories within sexes

Significant differences were observed for all tooth files of both jaws between the hatchling-to-juvenile and the juvenile-to-mature trajectory angles within sexes (*p*-vals < $1.20e^{-2}$, Tables S1 and S2), showing that whatever the mesio-distal position of a tooth, the shape modifications between juvenile and mature stages cannot be considered a prolongation of the hatchling-to-juvenile modifications. Significant differences in trajectory lengths are reported for most female palatoquadrate files (19/25 significant *p*-values, Table S1) and for female Meckelian files distal to the 8th file (*p*-vals < $4.40e^{-2}$, Table S2). In all these cases, the hatchling-to-juvenile trajectory is longer than the juvenile-to-mature one (Tables S1 and S2), showing that, in females, tooth shapes generated at sexual maturation are less dissimilar to juveniles than in males. In contrast, male trajectory lengths significantly differ only in a few tooth files (6/46 significant *p*-values, Tables S1 and S2, *p*-vals < $4.60e^{-2}$).

4 | DISCUSSION

4.1 | Capturing the intra-individual and ontogenetic-stage variations of tooth shape in *Scyliorhinus stellaris*

In this study, we generated 3D images and collected 3D coordinates of landmarks and semilandmarks on the cutting edge of the tooth surface. Despite the 3D nature of the surface data, the described tooth outline finally includes very little information in the third dimension. While the use of 2D data would have probably been less time-consuming, working on 3D data avoids biases due to parallax (Mullin and Taylor, 2002; Fruciano, 2016). Moreover, 3D surfaces can provide insights into topological aspects such as ornamentations, which can be of interest for future studies.

From our analyses, we described the wide range of blade-shaped to crown-shaped teeth in *S. stellaris*, which we characterized through classical and geometric morphometric analyses. In *S. stellaris*, we quantified how classical tooth shape parameters (asymmetry and cusp–crown ratio) vary in a gradual and linear way along the mesio-distal axis of both jaws, with extreme variations at the mesial-most and distalmost tooth positions. Also, we captured a higher cusp–crown ratio for palatoquadrate hatchling teeth compared to other ontogenetic stages. Because the lack of asymmetry is a shared feature of hatchling teeth and symphyseal teeth of older specimens, we show that palatoquadrate and Meckelian teeth undergo similar transition in their development (asymmetry) once the hatching stage is passed, to the exception of the symphyseal teeth. According to visual observations, the palatoquadrate and Meckelian teeth of *S. stellaris* are very similar in shape (dignathic homodonty or weak dignathic heterodonty), which is consistent with previous works on scyliorhinids (Herman *et al*., 1990; Ellis and Shackley, 1995; Soares and Carvalho, 2019). As opposed to Scyliorhinidae,

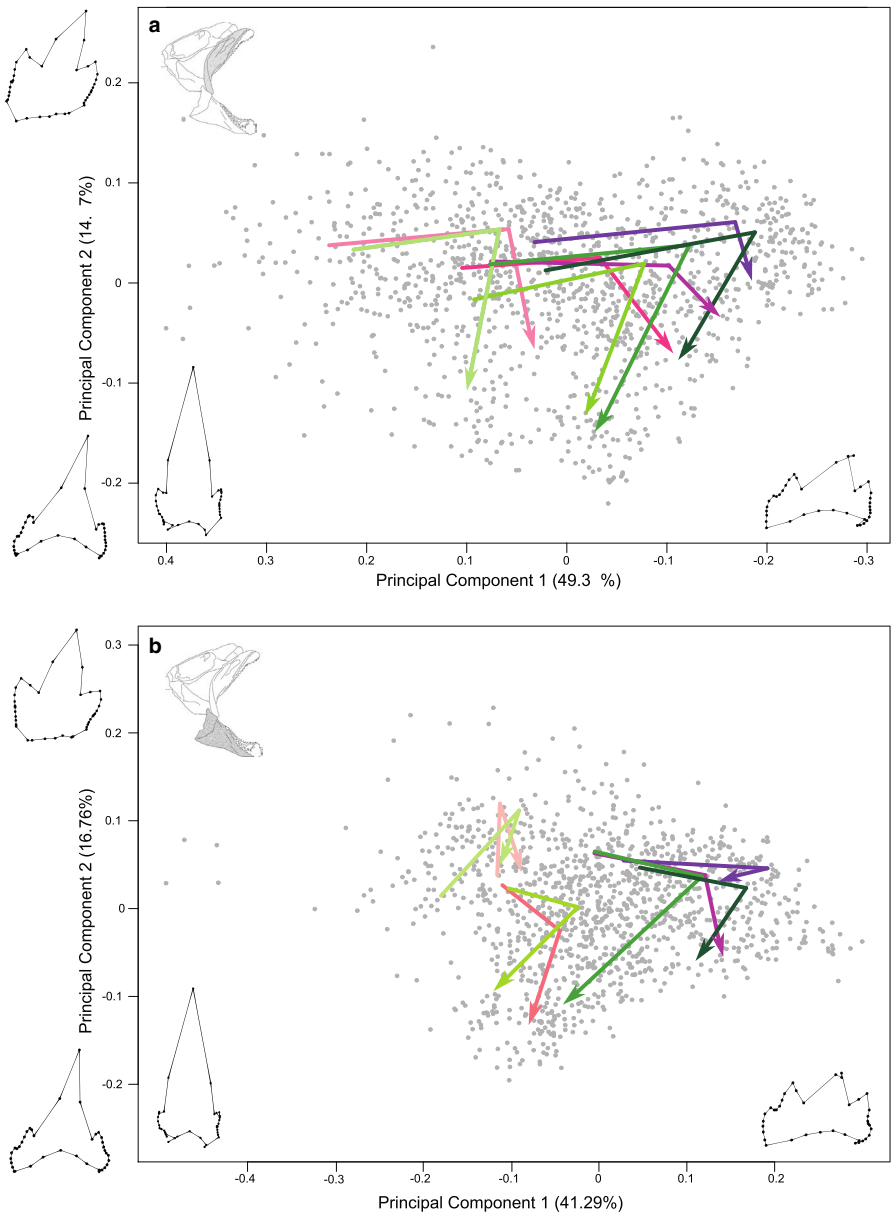

FIGURE 5 2D representation (PC1×PC2) of tooth developmental trajectories in *Scyliorhinus stellaris*. (a) 2D trajectories for palatoquadrate tooth files 3, 10, 15, and 20; (b) 2D trajectories for Meckel's tooth files 1, 5, 15, and 20. The trajectory representations are drawn between the mean shape of hatchling (starting point), juvenile, and mature (arrow tip) specimen teeth. Purple and green shades are for females and males trajectories, respectively. Mesial-to-distal files appear in light-to-deep shades. Wireframes depict extreme deformations of the mean shape at the positive and negative extremities of the PC1 and PC2 axes.

dignathic heterodonty is very common in other shark groups, such as in Hexanchidae and most Squaliformes. The tooth-type discrepancies between palatoquadrate and Meckelian teeth have been correlated with different functions in feeding: Upper grasping teeth might help catching and holding a prey, whereas blade-shaped lower teeth might function in tearing a prey to pieces (Cappetta, 1986; Frazzetta, 1988; Cappetta, 2012). Beyond ecology, dignathic heterodonty might also convey a phylogenetic signal: Sharks from distinct taxonomic groups might have overlapping trophic habits (especially in the case of opportunistic behavior) and, however, display different dignathic heterodonty patterns that diet alone cannot explain. Regarding whether the gynandric heterodonty follows similar patterns between both jaws, the data gathered hitherto on sharks are insufficient to answer.

Our results notably suggest a developmental transition between hatchlings and juveniles, especially on the palatoquadrate, that involves a global increase of the crown size. Note that asymmetry and cusp–crown ratio poorly discriminate between the three ontogenetic stages because they are corrected for size. As expected, the variation of tooth centroid size strongly discriminates between ontogenetic stages (Table 2) and shape analyses also recover growth stage significant differences (Table 3).

4.2 | The ontogenetic tempo and pattern of gynandric heterodonty

In previous works, classical shape parameters did not discriminate sex-dependent variation of tooth shape in *S. stellaris*, although gynandric heterodonty is well known in scyliorhinids (Gosztonyi, 1973; Ellis and Shackley, 1995; Cappetta, 2012; Debiais-Thibaud *et al.*, 2015; Soares and Carvalho, 2019). In our geometric morphometric

TABLE 3 MANOVA results on shape data.

	All	Hatchling	Juvenile	Mature
	F approx (*p*-val)	*F* approx (*p*-val)	*F* approx (*p*-val)	*F* approx (*p*-val)
Meckelian teeth				
Sex	5.39 (**6.13e^{-8}**)	4.02 (**9.54e^{-4}**)	1.86e^{1} (**5.72e^{-12}**)	2.67e^{1} (**5.39e^{-14}**)
Stage	3.04e^{1} (**<2.20e^{-16}**)	–	–	–
ToothMD	1.80 (**3.12e^{-14}**)	1.09 (2.36e^{-1})	1.50 (**1.16e^{-4}**)	1.03 (4.12e^{-1})
Sex:Stage	1.05e^{1} (**<2.20e^{-16}**)	–	–	–
Sex:ToothMD	8.73e^{-1} (9.33e^{-1})	–	–	–
Stage:ToothMD	1.18 (**1.02e^{-2}**)	–	–	–
Palatoquadrate teeth				
Sex	7.61 (**2.67e^{-11}**)	2.88 (**5.37e^{-3}**)	4.84 (**7.58e^{-5}**)	5.99e^{1} (**<2.20e^{-16}**)
Stage	4.58e^{1} (**<2.20e^{-16}**)	–	–	–
ToothMD	1.89 (**3.36e^{-16}**)	1.65 (**2.28e^{-6}**)	1.52 (**9.56e^{-5}**)	1.17 (7.37e^{-2})
Sex:Stage	7.32 (**<2.20e^{-16}**)	–	–	–
Sex:ToothMD	8.63e^{-1} (9.53e^{-1})	–	–	–
Stage:ToothMD	1.50 (**4.16e^{-9}**)	–	–	–

Abbreviation: MD, mesio-distal.

Significant *p*-values after Benjamini and Hochberg correction are in bold.

analyses of *S. stellaris* teeth, we detected no significant centroid size differences between sexes at hatching and juvenile ontogenetic stages, while we observed such difference at mature stages with male tooth centroid sizes being larger than female ones. Centroid size is, per construction, a feature with little sensitivity to shape. However, because we weighted tooth zones by positioning the majority of semilandmarks in the lateral sides and in the crown base of the teeth (see Material and Methods, and Figure 1b), the abovementioned differences in centroid size might be marginally affected by differences in tooth shape at these locations (Webster and Sheets, 2010). For most specimens, these crown sides and bases include lateral cusps (between landmarks 1–13 and 21–33, Figure 1), but also other aspects of tooth shape such as the labial notch where two successive teeth can be in contact (between landmarks 33-1, Figure 1). Statistical analyses supported the observed sexual dimorphism of the centroid size and shape among mature specimens, as well as a visually undetected sexual dimorphism in tooth shape at hatching and juvenile stages (Tables 2 and 3).

We generated developmental trajectories between the three ontogenetic stages at all tooth positions in order to compare the shape transitions along jaws and ontogeny. Our analyses were performed under the hypothesis of homology (equivalence between compared structures) between tooth files of different specimens, to allow the developmental comparisons of forms over the lifetime of specimens of a given sex. However, the biological support for this hypothesis is questionable as the number of tooth files is not a fixed parameter over time. In *S. stellaris*, we also observed variation in the number of tooth files between specimens of similar total length. We chose to accept this hypothesis of homology based on the fact that newly formed tooth files are generally considered to be added at the jaw distal extremity in elasmobranchs (see Smith (2003), Smith *et al*. (2009); Underwood *et al*. (2016) for sharks and Underwood *et al*. (2015) for batoids). However, they also might be inserted between already existing tooth files (Reif, 1976, 1980; Smith *et al*., 2013), which would skew the continuity of tooth file numbering over time (see Underwood *et al*. (2015), Smith *et al*. (2013) for similar remarks on batoids). Finally, we want to highlight that this homology (comparability) hypothesis is based under the assumption that the genesis of a tooth bud happens from a defined and continuous source, which is a strongly mammal-centered view of tooth morphogenesis. In contrast, tooth bud initiation in elasmobranchs is considered to happen through self-organization of the dental lamina, the invaginated epithelial fold from which new teeth develop (Reif, 1982; Rasch *et al*., 2016). For all these reasons, we interpreted our results as trends along the mesio-distal axis of a jaw but never under a strict homology hypothesis that would allow the comparison of a single given file between specimens, to the exception of the developmental trajectory analyses that necessitate a one-to-one comparison.

Over the time of sexual maturation, the juvenile-to-mature tooth shape developmental trajectories diverged between males and females at all tooth positions. In both sexes, these juvenile-to-mature developmental trajectories differed from the hatchling-to-juvenile ones (Tables 4 and 5). However, this deviation is increased in mature males ("angle cor" values are higher in males than in females in Tables 4 and 5). In males, mature tooth morphogenesis is characterized by an elongation of the main cusp and a reduction of the number of accessory cusps, generating unicuspid to tricuspid teeth similar to hatchling ones (Figures 2 and 3). In contrast, mature female tooth shape patterns resemble those of juveniles although the most distal teeth of mature females can reach a maximum of six accessory cusps (Figures 2

TABLE 4 Developmental trajectory values between sexes for palatoquadrate teeth.

File	All stages	Juvenile-to-mature stage		Hatchling-to-juvenile stage	
	M/F shape (*p*-val)	dL (M-F) (*p*-val)	MF angle cor (*p*-val)	dL (M-F) (*p*-val)	MF angle cor (*p*-val)
1	$3.08e^{-1}$ ($6.10e^{-2}$)	$7.39e^{-2}$ (**$3.00e^{-3}$**)	1.21 (**$1.00e^{-3}$**)	$2.12e^{-2}$ ($4.89e^{-1}$)	$6.57e^{-1}$ ($1.20e^{-2}$)
2	$1.13e^{-1}$ ($5.90e^{-1}$)	$4.14e^{-2}$ ($9.60e^{-2}$)	1.04 (**$1.00e^{-3}$**)	$4.77e^{-2}$ ($1.97e^{-1}$)	$4.90e^{-1}$ ($3.10e^{-2}$)
3	$3.34e^{-1}$ ($3.20e^{-2}$)	$7.05e^{-2}$ (**$1.70e^{-2}$**)	$9.63e^{-1}$ (**$1.00e^{-3}$**)	$-3.45e^{-2}$ ($4.05e^{-1}$)	$3.35e^{-1}$ ($1.23e^{-1}$)
4	$3.86e^{-1}$ (**$1.40e^{-2}$**)	$6.29e^{-2}$ (**$3.40e^{-2}$**)	$9.19e^{-1}$ (**$1.00e^{-3}$**)	$-3.66e^{-2}$ ($3.64e^{-1}$)	$4.24e^{-1}$ ($2.40e^{-2}$)
5	$4.41e^{-1}$ (**$2.00e^{-3}$**)	$6.58e^{-2}$ (**$2.90e^{-2}$**)	1.05 (**$1.00e^{-3}$**)	$-9.50e^{-3}$ ($7.45e^{-1}$)	$6.44e^{-1}$ ($2.30e^{-2}$)
6	$4.95e^{-1}$ (**$1.00e^{-3}$**)	$7.13e^{-2}$ (**$1.10e^{-2}$**)	1.03 (**$1.00e^{-3}$**)	$-2.10e^{-3}$ ($9.45e^{-1}$)	$4.35e^{-1}$ ($1.90e^{-2}$)
7	$4.58e^{-1}$ (**$1.00e^{-3}$**)	$6.88e^{-2}$ (**$5.00e^{-3}$**)	1.22 (**$1.00e^{-3}$**)	$4.67e^{-2}$ ($1.44e^{-1}$)	$3.64e^{-1}$ ($1.90e^{-2}$)
8	$4.54e^{-1}$ (**$1.00e^{-3}$**)	$7.85e^{-2}$ (**$5.00e^{-3}$**)	$9.69e^{-1}$ (**$1.00e^{-3}$**)	$5.60e^{-3}$ ($8.51e^{-1}$)	$3.37e^{-1}$ ($1.07e^{-1}$)
9	$2.93e^{-1}$ ($4.60e^{-2}$)	$7.64e^{-2}$ (**$3.00e^{-3}$**)	$7.97e^{-1}$ (**$1.00e^{-3}$**)	$1.59e^{-2}$ ($6.25e^{-1}$)	$2.74e^{-1}$ ($1.17e^{-1}$)
10	$3.32e^{-1}$ (**$1.20e^{-2}$**)	$5.17e^{-2}$ ($6.60e^{-2}$)	1.04 (**$1.00e^{-3}$**)	$2.76e^{-2}$ ($3.66e^{-1}$)	$3.47e^{-1}$ ($8.30e^{-2}$)
11	$3.14e^{-1}$ ($3.50e^{-2}$)	$9.38e^{-2}$ (**$3.00e^{-3}$**)	$6.26e^{-1}$ (**$4.00e^{-3}$**)	$1.30e^{-2}$ ($7.25e^{-1}$)	$3.07e^{-1}$ ($2.20e^{-2}$)
12	$4.11e^{-1}$ (**$3.00e^{-3}$**)	$1.02e^{-1}$ (**$1.00e^{-3}$**)	$8.58e^{-1}$) (**$2.00e^{-3}$**)	$-5.80e^{-3}$ ($8.75e^{-1}$)	$3.47e^{-1}$ ($1.00e^{-2}$)
13	$2.55e^{-1}$ ($1.82e^{-1}$)	$8.29e^{-2}$ (**$1.20e^{-2}$**)	$6.53e^{-1}$ (**$2.60e^{-2}$**)	$3.48e^{-2}$ ($4.18e^{-1}$)	$3.68e^{-1}$ ($1.80e^{-2}$)
14	$4.76e^{-1}$ (**$5.00e^{-3}$**)	$1.23e^{-1}$ (**$1.00e^{-3}$**)	1.06 (**$1.00e^{-3}$**)	$-3.50e^{-3}$ ($9.46e^{-1}$)	$3.59e^{-1}$ ($4.00e^{-3}$)
15	$4.85e^{-1}$ (**$1.00e^{-3}$**)	$1.25e^{-1}$ (**$2.00e^{-3}$**)	1.22 (**$1.00e^{-3}$**)	$3.48e^{-2}$ ($3.43e^{-1}$)	$3.05e^{-1}$ ($2.00e^{-2}$)
16	$4.88e^{-1}$ (**$1.00e^{-3}$**)	$1.17e^{-1}$ (**$1.00e^{-3}$**)	$8.27e^{-1}$ (**$3.00e^{-3}$**)	$-1.13e^{-2}$ ($7.59e^{-1}$)	$2.90e^{-1}$ ($2.60e^{-2}$)
17	$3.68e^{-1}$ (**$1.20e^{-2}$**)	$1.09e^{-1}$ (**$1.00e^{-3}$**)	1.15 (**$1.00e^{-3}$**)	$2.40e^{-2}$ ($5.14e^{-1}$)	$3.63e^{-1}$ ($1.20e^{-2}$)
18	$4.63e^{-1}$ (**$2.00e^{-3}$**)	$6.49e^{-2}$ (**$3.30e^{-2}$**)	1.38 (**$1.00e^{-3}$**)	$1.99e^{-2}$ ($5.33e^{-1}$)	$3.45e^{-1}$ ($6.90e^{-2}$)
19	$4.41e^{-1}$ (**$2.00e^{-3}$**)	$9.03e^{-2}$ (**$4.00e^{-3}$**)	1.58 (**$1.00e^{-3}$**)	$5.27e^{-2}$ ($2.07e^{-1}$)	$2.60e^{-1}$ ($1.18e^{-1}$)
20	$3.54e^{-1}$ (**$4.00e^{-3}$**)	$8.28e^{-2}$ (**$1.00e^{-3}$**)	1.17 (**$3.00e^{-3}$**)	$2.24e^{-2}$ ($5.34e^{-1}$)	$3.25e^{-1}$ ($3.40e^{-2}$)
21	$3.36e^{-1}$ (**$9.00e^{-3}$**)	$8.08e^{-2}$ (**$1.00e^{-3}$**)	1.08 (**$1.00e^{-3}$**)	$3.72e^{-2}$ ($2.54e^{-1}$)	$2.26e^{-1}$ ($7.50e^{-2}$)
22	$3.31e^{-1}$ ($3.90e^{-2}$)	$4.88e^{-2}$ (**$1.90e^{-2}$**)	1.25 (**$9.00e^{-3}$**)	$4.20e^{-3}$) ($9.16e^{-1}$)	$2.95e^{-1}$ ($2.50e^{-2}$)
23	$3.77e^{-1}$ ($1.14e^{-1}$)	$3.16e^{-2}$ ($2.44e^{-1}$)	1.37 (**$2.00e^{-3}$**)	$1.71e^{-2}$ ($7.15e^{-1}$)	$3.29e^{-1}$ ($2.00e^{-2}$)
24	NA	NA	NA	$2.44e^{-2}$ ($5.69e^{-1}$)	$5.88e^{-1}$ ($4.00e^{-3}$)
25	NA	NA	NA	$2.63e^{-2}$ ($7.13e^{-1}$)	$8.04e^{-1}$ ($2.20e^{-2}$)

Significant *p*-values after Benjamini and Hochberg correction are in bold. Due to the difference in total tooth file number between stages, some comparisons could not be done (NAs). –, difference; dL, delta length; F, females; and M, males.

TABLE 5 Developmental trajectory values between sexes for Meckelian teeth.

File	All stages	Juvenile-to-mature stage		Hatchling-to-juvenile stage	
	M/F shape (*p*-val)	dL (M-F) (*p*-val)	MF angle cor (*p*-val)	dL (M-F) (*p*-val)	MF angle cor (*p*-val)
1	$3.30e^{-1}$ ($7.20e^{-2}$)	$4.88e^{-2}$ (**$2.10e^{-2}$**)	1.14 (**$1.00e^{-3}$**)	$2.14e^{-2}$ ($3.11e^{-1}$)	$9.65e^{-1}$ ($1.10e^{-2}$)
2	$3.11e^{-1}$ ($2.56e^{-1}$)	$1.54e^{-1}$ (**$1.00e^{-3}$**)	1.49 (**$1.00e^{-3}$**)	$4.04e^{-2}$ ($1.04e^{-1}$)	$9.16e^{-1}$ ($3.00e^{-3}$)
3	$1.11e^{-1}$ ($7.19e^{-1}$)	$5.95e^{-2}$ (**$8.00e^{-3}$**)	$7.61e^{-1}$ (**$3.00e^{-3}$**)	$3.88e^{-2}$ ($1.86e^{-1}$)	$7.27e^{-1}$ ($5.00e^{-3}$)
4	$2.07e^{-1}$ ($1.19e^{-1}$)	$5.46e^{-2}$ (**3.40e−2**)	$5.05e^{-1}$ (**$2.40e^{-2}$**)	$5.40e^{-2}$ ($6.00e^{-3}$)	$7.20e^{-1}$ (**$1.00e^{-3}$**)
5	$1.98e^{-1}$ ($2.19e^{-1}$)	$5.20e^{-2}$ ($9.70e^{-2}$)	$7.55e^{-1}$ (**$1.30e^{-2}$**)	$3.39e^{-2}$ ($1.02e^{-1}$)	$6.32e^{-1}$ ($1.70e^{-2}$)
6	$2.44e^{-1}$ ($1.54e^{-1}$)	$8.06e^{-2}$ (**$1.40e^{-2}$**)	$6.96e^{-1}$ (**$8.00e^{-3}$**)	$3.17e^{-2}$ ($1.54e^{-1}$)	$6.41e^{-1}$ ($1.50e^{-2}$)
7	$3.14e^{-1}$ ($5.20e^{-2}$)	$6.35e^{-2}$ (**$3.00e^{-2}$**)	$7.71e^{-1}$ (**$3.10e^{-2}$**)	$5.19e^{-2}$ ($1.07e^{-1}$)	$6.76e^{-1}$ ($2.90e^{-2}$)
8	$2.52e^{-1}$ ($1.78e^{-1}$)	$9.04e^{-2}$ (**$4.00e^{-3}$**)	$7.58e^{-1}$ (**$1.70e^{-2}$**)	$5.65e^{-1}$ ($2.10e^{-2}$)	$7.69e^{-1}$ ($8.00e^{-3}$)
9	$4.01e^{-1}$ (**$1.60e^{-2}$**)	$1.01e^{-1}$ (**$1.00e^{-3}$**)	$8.20e^{-1}$ (**$1.00e^{-2}$**)	$3.85e^{-2}$ ($2.20e^{-1}$)	$6.42e^{-1}$ ($1.10e^{-2}$)
10	$4.82e^{-1}$ (**$6.00e^{-3}$**)	$1.15e^{-1}$ (**$1.00e^{-3}$**)	$9.85e^{-1}$ (**$3.00e^{-3}$**)	$8.46e^{-3}$ ($7.74e^{-1}$)	$5.45e^{-1}$ ($5.70e^{-2}$)
11	$3.76e^{-1}$ (**$1.40e^{-2}$**)	$1.03e^{-1}$ (**$1.00e^{-3}$**)	$9.61e^{-1}$ (**$4.00e^{-3}$**)	$3.86e^{-2}$ ($1.84e^{-1}$)	$4.83e^{-1}$ ($2.10e^{-2}$)
12	$3.88e^{-1}$ (**$1.60e^{-2}$**)	$1.05e^{-1}$ (**$1.00e^{-3}$**)	$8.80e^{-1}$ (**$2.00e^{-3}$**)	$3.01e^{-2}$ ($2.92e^{-1}$)	$4.74e^{-1}$ ($5.10e^{-2}$)
13	$4.97e^{-1}$ (**$2.00e^{-3}$**)	$1.23e^{-1}$ (**$1.00e^{-3}$**)	$8.04e^{-1}$ (**$1.00e^{-3}$**)	$3.61e^{-2}$ ($2.20e^{-1}$)	$3.94e^{-1}$ ($1.00e^{-1}$)
14	$4.72e^{-1}$ (**$4.00e^{-3}$**)	$1.43e^{-1}$ (**$1.00e^{-3}$**)	1.02 (**$1.00e^{-3}$**)	$6.14e^{-2}$ ($4.20e^{-2}$)	$4.14e^{-1}$ ($1.20e^{-2}$)
15	$5.51e^{-1}$ (**$2.00e^{-3}$**)	$1.33e^{-1}$ (**$1.00e^{-3}$**)	1.02 (**$1.00e^{-3}$**)	$1.19e^{-2}$ ($7.40e^{-1}$)	$2.78e^{-1}$ ($2.43e^{-1}$)
16	$5.11e^{-1}$ (**$2.00e^{-3}$**)	$1.07e^{-1}$ (**$1.00e^{-3}$**)	1.01 (**$1.00e^{-3}$**)	$-3.27e^{-3}$ ($9.17e^{-1}$)	$3.68e^{-1}$ ($1.39e^{-1}$)
17	$5.99e^{-1}$ (**$2.00e^{-3}$**)	$1.15e^{-1}$ (**$1.00e^{-3}$**)	1.17 (**$3.00e^{-3}$**)	$-4.49e^{-2}$ ($2.42e^{-1}$)	$7.78e^{-1}$ ($2.90e^{-2}$)
18	$5.02e^{-1}$ (**$1.00e^{-3}$**)	$9.26e^{-2}$ (**$6.00e^{-3}$**)	1.23 (**$5.00e^{-3}$**)	$-1.33e^{-2}$ ($7.28e^{-1}$)	$3.75e^{-1}$ ($1.42e^{-1}$)
19	$4.43e^{-1}$ (**$1.00e^{-3}$**)	$5.94e^{-2}$ (**$1.50e^{-2}$**)	1.47 (**$3.00e^{-3}$**)	$-4.71e^{-2}$ ($1.78e^{-1}$)	$3.93e^{-1}$ ($2.30e^{-2}$)
20	NA	$4.02e^{-2}$ ($1.42e^{-1}$)	$9.81e^{-1}$ ($1.09e^{-1}$)	NA	NA
21	NA	$4.10e^{-3}$ ($8.47e^{-1}$)	1.57 (**$1.00e^{-3}$**)	NA	NA
22	NA	$7.71e^{-2}$ ($5.40e^{-2}$)	1.18 (**$2.80e^{-2}$**)	NA	NA
23	NA	$-5.97e^{-2}$ ($3.12e^{-1}$)	2.21 (**$1.00e^{-3}$**)	NA	NA

Significant *p*-values after Benjamini and Hochberg correction are in bold. Due to the difference in total tooth file number between stages, some comparisons could not be done (NAs). –, difference; dL, delta length; F, females; and M, males.

and 3). As a conclusion, during sexual maturation, all tooth files in *S. stellaris* are affected by a slighter (females) or stronger (males) modification of developmental trajectories, compared to their hatchling-to-juvenile trajectories.

On the one hand, it is tempting to speculate on dietary differences between sexes that would correlate with morphological differences in teeth. It was reported that *S. stellaris* juvenile and mature specimens mostly feed on cephalopods and, to a lesser extent, on teleosts and crustaceans (Capape, 1975). Juvenile females were reported to feed more on crustaceans than males and mature females (Capape, 1975). These observations do not fit with any of the morphological shifts in tooth shape described in this study, so we cannot discuss any putative link between *S. stellaris* trophic ecology and tooth shape variation. On the other hand, the gynandric heterodonty of mature *S. stellaris* is consistent with reports on the role of teeth during copulation in elasmobranchs (Springer, 1967; McEachran, 1977; Kajiura and Tricas, 1996; Pratt and Carrier, 2001; Gutteridge and Bennett, 2014). The increased main cusp height of mature male teeth might indeed enhance gripping, as compared to teeth with more accessory cusps and smaller main cusp. However, this remains speculative as there are no experimental data on comparative gripping efficiency for shark teeth, only a few studies that compared flat versus cuspidate teeth in batoids (Kajiura and Tricas, 1996; Gutteridge and Bennett, 2014).

4.3 | Developmental cues linked to tooth development plasticity

Our analyses highlight features linked to tooth developmental plasticity in several ontogenetic dimensions. The notion of developmental plasticity classically refers to the building of distinct phenotypes from the expression of a same genome in different environments (Moczek, 2015). Here, we want to use a modified version of this concept and apply it to tooth shape variation: (a) of different teeth at the intra-individual level and (b) of comparable teeth between successive ontogenetic stages. First, the intra-individual variation points to developmental plasticity which is here dependent on the mesio-distal position of the tooth bud and which we could name "positional developmental plasticity". Second, the comparison between different ontogenetic stages—although an extrapolation of a situation with constant genome—questions developmental plasticity in the temporal dimension, assuming comparable tooth files between successive ontogenetic stages. We name this process "successive developmental plasticity," generated through tooth successional replacement. Here we have quantified a peculiarity of successive developmental plasticity: the divergence of its developmental trajectory between males and females during sexual maturation.

From these observations, we want to speculate on the potential developmental mechanisms that might generate these developmental plasticities, considering the physical and molecular cues acting on tooth bud growth within the dental lamina. To our knowledge, there are very scarce genetic data available on tooth morphogenesis in *S. stellaris* (Rasch *et al*., 2016) but gene regulatory networks involved in elasmobranch tooth development have been investigated in *S. canicula*. The expression of classical developmental genes was characterized in tooth buds (Debiais-Thibaud *et al*., 2011, 2015; Martin *et al*., 2016; Rasch *et al*., 2016), including the well-known signaling factor *Shh* that acts as both a tooth bud initiation signal and a proliferation signal during tooth morphogenesis (Berio and Debiais-Thibaud, 2019; Hosoya *et al*., 2020). Data on the physical features that could constrain tooth bud growth within the dental lamina are even scarcer although previous studies on mammals emphasized that a modification of the tooth bud physical environment can modify the final shape of a tooth (Renvoisé *et al*., 2017). Several observations of the jaw morphology may still help discuss how these physical constraints can be linked to tooth development. Of course, these genetic and physical cues acting on tooth development should not be considered as acting independently of one another on tooth development: It is likely that developmental signaling pathways impact morphogenesis by modifying physical parameters at the cellular level, while geometrical and physical constraints at the jaw cartilage or dental lamina levels can induce differential diffusion of molecules (Salazar-Ciudad, 2008; Renvoisé *et al*., 2017; Calamari *et al*., 2018). The parameters of this complex system that may be relevant for specific aspects of tooth morphology and its variational properties in time or space are essentially unknown. However, from our results in *S. stellaris*, we wish to draw three main discussion points on the putative sources of: (1) mesio-distal patterning, (2) asymmetry, and (3) gynandric heterodonty.

4.3.1 | Sources of the mesio-distal patterning

The graded variation of cusp-crown ratio is a shared feature of all ontogenetic stages and both jaws: this observation suggests the occurrence of a graded signal along the mesio-distal axis of a jaw at all developmental stages. This signal may be of two non-mutually exclusive origins: a gradient of physical constraints and a gradient of molecular signals along the jaw.

Very little is known on the potential variation of the shape, thickness, and curvature of the dental lamina at any developmental stage. However, previous observations of catshark jaws showed that hatchling tooth buds develop very close to the Meckel's cartilage surface (observations in *S. canicula* in Debiais-Thibaud *et al*. (2015)), suggesting the gradient of dental lamina invagination is weak or non-existent at this stage, contrary to older specimens whose dental lamina is more deeply invaginated. Therefore, the physical constraints on the dental lamina do not seem to explain the observed gradients of cusp-crown ratios. The overall jaw geometry may also be considered as another potential driver of the mesio-distal patterning. As for the dental lamina, its effects on the mesio-distal patterning may however be non-linear: The sexually dimorphic heads in mature scyliorhinids would also affect the shape of jaw cartilages (Ellis and Shackley, 1995; Soares, 2019; Soares and Carvalho, 2019). This

would suggest a sexual dimorphism in the gradient of cusp–crown ratio by affecting differently the labial-lingual local curvature of the dental lamina where the tooth buds develop. However, this is not obvious from our observations, although mature males tend to have a higher cusp–crown ratio in Meckelian teeth than females do and compare best to juveniles in that respect.

On the other hand, the mesio-distal patterning of jaws by developmental genes was demonstrated in model organisms (Van Otterloo *et al*., 2018) and molecular signaling is known to generate the mesio-distal gradient in tooth morphology in mouse (reviewed in Cobourne and Sharpe (2003)). The genes involved in jaw patterning and tooth morphogenesis of mammals are also expressed in *S. canicula* (Debiais-Thibaud *et al*., 2013, 2015; Rasch *et al*., 2016). Yet, there is no available empirical evidence about how this signaling gradient may change during the ontogeny of scyliorhinids and whether it does correlate with the cusp–crown ratio gradient.

4.3.2 | Sources of asymmetry

The first generation of tooth buds in embryos or just hatched specimens of *S. canicula* develops very close to the surface of the jaw epithelium, within a superficial dental lamina (Debiais-Thibaud *et al*., 2011, 2015; Rasch *et al*., 2016). In addition, given the topology of the jaw symphysis (without underlying cartilage), we speculate that the situation is similar for symphyseal teeth. We therefore consider the possibility of tooth asymmetry as being correlated with the depth and topology of the dental lamina invagination. Some of our preliminary tests on modeling tooth development in sharks suggest that the mechanical stresses exerted on a tooth bud by the surrounding tissues (the dental lamina and the underlying cartilage) may be key to breaking the symmetry of the tooth morphology. We speculate that the deeper the dental lamina, the higher the likelihood of an asymmetry in the boundary conditions of the growing tooth bud reflecting into its final shape.

4.3.3 | Sources of gynandric heterodonty

Sex-related tooth shape dimorphism is visually detectable only in mature specimens. This dimorphism stands strongly in the relative size of the main cusp versus accessory cusps (higher in males) and in the number of accessory cusps (higher in females). Previous studies and modeling of mammalian tooth morphogenesis have recovered patterns of covariation between main cusp sharpness and the number and spacing of accessory cusps (Jernvall, 2000; Salazar-Ciudad and Jernvall, 2010). Although highly speculative to infer mammalian developmental patterns to sharks, the 2D-tooth shapes computed in this case study are very similar to the *S. stellaris* lateral teeth (especially those of the ringed seal *Phoca hispida*, see Salazar-Ciudad and Jernvall, 2010). In this case study, the authors have interpreted the observed relationship between the height of the main cusp and the height of accessory cusps as a product of the enamel knot signaling center spacing: the closer the secondary enamel knots as compared to the primary enamel knot, the higher and the more blunt the accessory cusps (Jernvall, 2000; Salazar-Ciudad and Jernvall, 2010). Conversely, when the distance between primary and secondary enamel knots is greater, sharper teeth with fewer and smaller accessory cusps develop (Jernvall, 2000, Salazar-Ciudad and Jernvall, 2010). The successive activation of enamel knots and their spacing is strongly regulated by the diffusion rate of signaling molecules such as Shh and Fgfs (Thesleff and Mikkola, 2002; Du *et al*., 2017). Another developmental parameter in which variation was associated with this shape relationship is epithelial growth rate (Salazar-Ciudad and Jernvall, 2010), for example, the rate of cell division in the tooth bud that is growing from the dental lamina. Finally, the dental lamina characteristics (acting on diffusion rates and cell division rate) might exhibit sexual dimorphism, as a consequence of sexually dimorphic head dimensions in Scyliorhinidae (Ellis and Shackley, 1995; Soares, 2019). The longer and narrower jaw in males compared to females at mature stage is actually a recurrent feature in elasmobranchs and gives support to this hypothesis (Ellis and Shackley, 1995; Braccini and Chiaramonte, 2002; Erdogan *et al*., 2004; Geniz *et al*., 2007; Soares *et al*., 2016; Soares, 2019). Labial curvature of the jaw cartilages may then impact the physical constraints on dental lamina. A second hypothetical source, which might interact with the previous one, is based on the sex-hormone dependence of the molecular signalization involved in tooth bud growth. This is supported by previous identification of a sex-hormone dependency for *Shh* expression in vertebrates, including elasmobranchs (Ogino *et al*., 2004; Chew *et al*., 2014; O'Shaughnessy *et al*., 2015). Gene regulatory networks involved in elasmobranch tooth development have been most extensively investigated in *S. canicula*, where the expression of classical developmental genes was characterized (Debiais-Thibaud *et al*., 2011, 2015; Martin *et al*., 2016; Rasch *et al*., 2016). If the situation in *S. stellaris* is comparable to what was observed in *S. canicula*, then a modification of balance between developmental genes (e.g., *Shh*) under the reception of sex-hormone signals in mature specimens could modify the balance between cell proliferation and differentiation that impacts the final shape of a tooth.

As discussed here, a variety of hypothetical physical and molecular factors might be involved in the generation of tooth shape plasticity in elasmobranchs. To test these influences, morpho-anatomical and functional studies are still necessary although they are difficult to realize in non-model and threatened species such as most elasmobranchs. We expect that our extensive description of the actual tooth form diversity in *S. stellaris* will help to orientate the hypotheses to be further tested to identify the sources of heterodonty in elasmobranchs.

5 | CONCLUSION

Teeth are involved in two main functions in elasmobranchs: feeding and reproduction. Although ontogenetic shifts in tooth morphologies have been reported in different shark orders, very few

studies focused on the changes from an embryonic to a mature dentition in males and females separately. Here we gave a description of the wide, natural, and intraspecific variation of tooth shapes in *S. stellaris*. We detailed the tooth form transitions between three ontogenetic stages and focused on: (a) graded variation of several morphometric parameters along the mesio-distal axis of a jaw, only starting during the juvenile stage, and (b) gynandric heterodonty at mature stage generated by a stronger change in developmental trajectory for males (unicuspid to tricuspid teeth) than for females (addition of lateral cusps). We hope that the detailed morphospaces we provide here for *S. stellaris* teeth will be extended in an interspecific framework to challenge hypotheses on the developmental mechanisms that generate the known elasmobranch tooth shape diversity.

ACKNOWLEDGEMENTS

We are indebted to Sylvain Adnet, Henri Cappetta, Guillaume Guinot, and Suzanne Jiquel for giving access to the collections (University of Montpellier). We also thank Sophie Germain-Pigno from the Aquarium du Cap d'Agde for providing fresh specimens, Sabrina Renaud for her advices on geometric morphometrics, and Yann Bayle, Julien Claude, Guillaume Guinot, and Roland Zimm for insightful proofreading. We acknowledge the contribution of SFR Biosciences (UMS3444/CNRS, US8/Inserm, ENS de Lyon, UCBL) facilities: AniRA-ImmOs (Mathilde Bouchet-Combe) and the contribution of MRI platform, member of the national infrastructure France-BioImaging supported by the French National Research Agency (ANR-10-INBS-04, "Investments for the future"), the labex CEMEB (ANR-10-LABX-0004) and NUMEV (ANR-10-LABX-0020) (Renaud Lebrun). The authors declare no conflict of interest. The datasets generated and analyzed in the current study are not publicly available due to ongoing other project but are available from the corresponding author on reasonable request.

AUTHOR'S CONTRIBUTIONS

FB generated and analyzed the data; FB and AE designed the statistical analyses; FB, NG, and MDT designed the experimental setup; FB and MDT drafted the manuscript.

DATA AVAILABILITY STATEMENT

The datasets generated and analyzed in the current study are not publicly available due to ongoing other project but are available from the corresponding author on reasonable request.

ORCID

Fidji Berio https://orcid.org/0000-0003-0810-9783

REFERENCES

Adams, D.C. and Otárola-Castillo, E. (2013) geomorph: an R package for the collection and analysis of geometric morphometric shape data. *Methods in Ecology and Evolution*, 4, 393–399.

Bazzi, M., Kear, B.P., Blom, H., Ahlberg, P.E. and Campione, N.E. (2018) Static dental disparity and morphological turnover in sharks across the end-cretaceous mass extinction. *Current Biology*, 28, 2607–2615. e3.

Berio, F. and Bayle, Y. (2020) Scyland3D: Processing 3D landmarks. *Journal of Open Source Software*, 5, 1262.

Berio, F. and Debiais-Thibaud, M. (2019) Evolutionary developmental genetics of teeth and odontodes in jawed vertebrates: a perspective from the study of elasmobranchs. *Journal of Fish Biology*.

Bookstein, F.L. (1991) *Morphometric Tools for Landmark Data: Geometry And Biology*. Cambridge: Cambridge University Press.

Bookstein, F.L. (1997) Landmark methods for forms without landmarks: morphometrics of group differences in outline shape. *Medical Image Analysis*, 1, 225–243.

Braccini, J.M. and Chiaramonte, G.E. (2002) Intraspecific variation in the external morphology of the sand skate. *Journal of Fish Biology*, 61, 959–972.

Brough, J. (1937) On certain secondary sexual characters in the common dogfish (*Scyliorhinus caniculus*). *Journal of Zoology*, 107, 217–223.

Calamari, Z.T., Hu, J.-K.-H. and Klein, O.D. (2018) Tissue mechanical forces and evolutionary developmental changes act through space and time to shape tooth morphology and function. *BioEssays*, 40, 1800140.

Capapé, C. (1975) Contribution à la biologie des Scyliorhinidae des côtes tunisiennes. IV *Scyliorhinus stellaris* (Linné, 1758). Régime alimentaire. *Archives de l'Institut Pasteur de Tunis*, 52, 383–394.

Cappetta, H. (1986) Types dentaires adaptatifs chez les sélaciens actuels et post-paléozoïques. *Palaeovertebrata*, 16, 57–76.

Cappetta, H. (2012) *Handbook of Paleoichthyology, Vol 3E: Chondrichthyes - Mesozoic and Cenozoic Elasmobranchii: Teeth*. Munich: Verlag Dr. Friedrich Pfeil.

Chew, K., Pask, A., Hickford, D., Shaw, G. and Renfree, M. (2014) A dual role for SHH during phallus development in a marsupial. *Sexual Development*, 8, 166–177.

Cobourne, M.T. and Sharpe, P.T. (2003) Tooth and jaw: molecular mechanisms of patterning in the first branchial arch. *Archives of Oral Biology*, 48, 1–14.

Coolen, M., Menuet, A., Chassoux, D., Compagnucci, C., Henry, S., Lévèque, L. *et al* (2008) The dogfish *Scyliorhinus canicula*: a reference in jawed vertebrates. *Cold Spring Harbor Protocols*, 2008(12), pdb.emo111.

Correia, J.P. (1999) Tooth loss rate from two captive sandtiger sharks (*Carcharias taurus*). *Zoo Biology*, 18, 313–317.

Cullen, J.A. and Marshall, C.D. (2019) Do sharks exhibit heterodonty by tooth position and over ontogeny? A comparison using elliptic Fourier analysis. *Journal of Morphology*, 280, 687–700.

de Sousa Rangel, B., Santander-Neto, J., Rici, R.E.G. and Lessa, R. (2016) Dental sexual dimorphism and morphology of *Urotrygon microphthalmum*. *Zoomorphology*, 135, 367–374.

Debiais-Thibaud, M., Chiori, R., Enault, S., Oulion, S., Germon, I., Martinand-Mari, C. *et al* (2015) Tooth and scale morphogenesis in shark: an alternative process to the mammalian enamel knot system. *BMC Evolutionary Biology*, 15, 292.

Debiais-Thibaud, M., Metcalfe, C.J., Pollack, J., Germon, I., Ekker, M., Depew, M. *et al* (2013) Heterogeneous conservation of *Dlx* paralog co-expression in jawed vertebrates. *PLoS One*, 8, e68182.

Debiais-Thibaud, M., Oulion, S., Bourrat, F., Laurenti, P., Casane, D. and Borday-Birraux, V. (2011) The homology of odontodes in gnathostomes: insights from Dlx gene expression in the dogfish, *Scyliorhinus canicula*. *BMC Evolutionary Biology*, 11, 307.

Du, W., Hu, J.K.H., Du, W. and Klein, O.D. (2017) Lineage tracing of epithelial cells in developing teeth reveals two strategies for building signaling centers. *Journal of Biological Chemistry*, 292, 15062–15069.

Ellis, J.R. and Shackley, S.E. (1995) Ontogenic changes and sexual dimorphism in the head, mouth and teeth of the lesser spotted dogfish. *Journal of Fish Biology*, 47, 155–164.

Erdogan, Z., Koc, H., Cakir, T., Nerlovic, V. and Dulcic, J. (2004) Sexual dimorphism in the small-spotted catshark *Scyliorhinus canicula* from the Edremit Bay (Turkey). *Series Historia Naturalis*, 14, 165–170.

Feduccia, A. and Slaughter, B.H. (1974) Sexual dimorphism in skates (Rajidae) and its possible role in differential niche utilization. *Evolution*, 8, 164–168.

Fischer, W., Bauchot, M.-L. and Schneider, M. (1987) Fiches FAO d'identification des espèces pour les besoins de la pêche (Révision 1). Méditerranée etMer Noire. Zone de pêche 37. *Vertébrés*. FAO, 2, 761–1530.

Frazzetta, T.H. (1988) The mechanics of cutting and the form of shark teeth (Chondrichthyes, Elasmobranchii). *Zoomorphology*, 108, 93–107.

French, G.C.A., Stürup, M., Rizzuto, S., van Wyk, J.H., Edwards, D., Dolan, R.W. *et al* (2017) The tooth, the whole tooth and nothing but the tooth: tooth shape and ontogenetic shift dynamics in thewhite shark *Carcharodon carcharias*. *Journal of Fish Biology*, 91, 1032–1047.

Fruciano, C. (2016) Measurement error in geometric morphometrics. *Development Genes and Evolution*, 226, 139–158.

Geniz, J., Nishizaki, O. and Perez, J. (2007) Morphological variation and sexual dimorphism in the California skate, *Raja inornata* Jordan and Gilbert, 1881 from the Gulf of California, Mexico. *Zootaxa*, 1545, 1–16.

Gosztonyi, A.E. (1973) About sexual and secondary dimorphism of *Halaelurus bivius* (Muller & Henle, 1841) Garman 1913 (Elasmobranchii, Scyliorhinidae) in Patagonian-Fueguinas waters. *Physis A*, 32, 317–323.

Gottfried, M.D. and Francis, M.P. (1996) Developmental changes in white shark tooth morphology: implications for studies on fossil sharks. *Journal of Vertebrate Paleontology*, 16, 50.

Gutteridge, A.N. and Bennett, M.B. (2014) Functional implications of ontogenetically and sexually dimorphic dentition in the eastern shovelnose ray, *Aptychotrema rostrata*. *The Journal of experimental biology*, 217, 192–200.

Hale, L.F. and Lowe, C.G. (2008) Age and growth of the round stingray *Urobatis halleri* at Seal Beach, California. *Journal of Fish Biology*, 73, 510–523.

Heisler, N. and Neumann, P. (1980) The role of physicochemical buffering and of bicarbonate transfer processes in intracellular pH regulation in response to changes of temperature in the larger spotted dogfish (*Scyliorhinus stellaris*). *Journal of Experimental Biology*, 85, 99–110.

Herman, J., Hovestadt-Euler, M. and Hovestadt, D.C. (1990) Contributions to the study of the comparative morphology of teeth and other relevant ichthyodorulites in living supraspecific taxa of Chondrichthyan fishes. Part A: Selachii. No. 2b: Order: Carcharhiniformes - Family: Scyliorhinidae. *Bulletin de l'Institut Royal des Sciences Naturelles de Belgique*, 60, 181–230.

Hosoya, A., Shalehin, N., Takebe, H., Shimo, T. and Irie, K. (2020) Sonic Hedgehog signaling and tooth development. *International Journal of Molecular Sciences*, 21, 1587.

Iglésias, S.P., Lecointre, G. and Sellos, D.Y. (2005) Extensive paraphylies within sharks of the order Carcharhiniformes inferred from nuclear and mitochondrial genes. *Molecular Phylogenetics and Evolution*, 34, 569–583.

Jernvall, J. (2000) Linking development with generation of novelty in mammalian teeth. *Proceedings of the National Academy of Sciences of the United States of America*, 97, 2641–2645.

Kajiura, S.N. and Tricas, T.C. (1996) Seasonal dynamics of dental sexual dimorphism in the Atlantic stingray *Dasyatis sabina*. *Journal of Experimental Biology*, 199, 2297–2306.

Litvinov, F.F. and Laptikhovsky, V.V. (2005) *Methods of investigations of shark heterodonty and dental formulae's variability with the blue shark*. In ICES CM, p. 15.

Lucifora, L.O., Menni, R.C. and Escalante, A.H. (2001) Analysis of dental insertion angles in the sand tiger shark, *Carcharias taurus* (Chondrichthyes: Lamniformes). *Cybium*, 25, 23–31.

Luer, C.A., Blum, P.C. and Gilbert, P.W. (1990) Rate of tooth replacement in the nurse shark, *Ginglymostoma cirratum*. *Copeia*, 1990, 182–191.

Marramà, G. and Kriwet, J. (2017) Principal component and discriminant analyses as powerful tools to support taxonomic identification and their use for functional and phylogenetic signal detection of isolated fossil shark teeth. *PLoS One*, 12, e0188806.

Martin, K., Rasch, L. and Cooper, R. (2016) Sox2+ progenitors in sharks link taste development with the evolution of regenerative teeth from denticles. *PNAS*, 113, 14769–14774.

McCourt, R. and Kerstitch, A. (1980) Mating behavior and sexual dimorphism in dentition in the stingray, *Urolophus concentricus*, from the Gulf of California. *Copeia*, 1980, 900–901.

McEachran, J.D. (1977) Reply to "Sexual dimorphism in skates (Rajidae)". *Evolution*, 31, 218–220.

Meredith Smith, M., Underwood, C., Clark, B., Kriwet, J. and Johanson, Z. (2018) Development and evolution of tooth renewal in neoselachian sharks as a model for transformation in chondrichthyan dentitions. *Journal of Anatomy*, 232, 891–907.

Moczek, A.P. (2015) Developmental plasticity and evolution—*quo vadis*? *Heredity*, 115, 302–305.

Motta, P.J. and Wilga, C.D. (2001) Advances in the study of feeding behaviors, mechanisms, and mechanics of sharks. In: Tricas, T.C. and Gruber, S.H. (Eds.), *The Behavior and Sensory Biology Of Elasmobranch Fishes: An Anthology In Memory Of Donald Richard Nelson*. Dordrecht: Springer, pp. 131–156.

Moyer, J.K. and Bemis, W.E. (2016) Tooth microstructure and replacement in the gulper shark, *Centrophorus granulosus* (Squaliformes: Centrophoridae). *Copeia*, 104, 529–538.

Mullin, S.K. and Taylor, P.J. (2002) The effects of parallax on geometric morphometric data. *Computers in Biology and Medicine*, 32, 455–464.

Musa, S.M., Czachur, M.V. and Shiels, H.A. (2018) Oviparous elasmobranch development inside the egg case in 7 key stages. *PLoS One*, 13, e0206984.

Ogino, Y., Katoh, H. and Yamada, G. (2004) Androgen dependent development of a modified anal fin, gonopodium, as a model to understand the mechanism of secondary sexual character expression in vertebrates. *FEBS Letters*, 575, 119–126.

O'Shaughnessy, K.L., Dahn, R.D. and Cohn, M.J. (2015) Molecular development of chondrichthyan claspers and the evolution of copulatory organs. *Nature Communications*, 6, 6698.

Piiper, J., Meyer, M., Worth, H. and Willmer, H. (1977) Respiration and circulation during swimming activity in the dogfish *Scyliorhinus stellaris*. *Respiration Physiology*, 30, 221–239.

Powter, D.M., Gladstone, W. and Platell, M. (2010) The influence of sex and maturity on the diet, mouth morphology and dentition of the Port Jackson shark, *Heterodontus portusjacksoni*. *Marine and Freshwater Research*, 61, 74.

Pratt, H.L. Jr and Carrier, J.C. (2001) A review of elasmobranch reproductive behavior with a case study on the nurse shark, *Ginglymostoma cirratum*. *Environmental Biology of Fishes*, 60, 157–188.

Purdy, R.W. and Francis, M.P. (2007) Ontogenetic development of teeth in *Lamna nasus* (Bonnaterre, 1758) (Chondrichthyes: Lamnidae) and its implications for the study of fossil shark teeth. *Journal of Vertebrate Paleontology*, 27, 798–810.

Rasch, L.J., Martin, K.J., Cooper, R.L., Metscher, B.D., Underwood, C.J. and Fraser, G.J. (2016) An ancient dental gene set governs development and continuous regeneration of teeth in sharks. *Developmental Biology*, 415, 347–370.

Reif, W.-E. (1976) Morphogenesis, pattern formation and function of the dentition of *Heterodontus* (Selachii). *Zoomorphology*, 83, 1–47.

Reif, W.-E. (1980) A mechanism for tooth pattern reversal in sharks: the polarity switch model. *Wilhelm Roux's Archives of Developmental Biology*, 188, 115–122.

Reif, W.-E. (1982) Evolution of dermal skeleton and dentition in vertebrates: the odontode regulation theory. In: Hecht, M.K., Wallace, B. and Prance, G.T. (Eds.) *Evolutionary Biology*. New York: Plenum Press, pp. 287–368.

Renvoisé, E., Kavanagh, K.D., Lazzari, V., Häkkinen, T.J., Rice, R., Pantalacci, S. *et al* (2017) Mechanical constraint from growing jaw facilitates mammalian dental diversity. *Proceedings of the National Academy of Sciences of the United States of America*, 114, 9403–9408.

Salazar-Ciudad, I. and Jernvall, J. (2010) A computational model of teeth and the developmental origins of morphological variation. *Nature*, 464(7288), 583–586. https://doi.org/10.1038/nature08838

Salazar-Ciudad, I. (2008) Tooth morphogenesis in vivo, in vitro, and in silico. *Current Topics in Developmental Biology*, 81, 341–371.

Shimada, K. (2002) Dental homologies in lamniform sharks (Chondrichthyes: Elasmobranchii). *Journal of Morphology*, 251, 38–72.

Shimada, K. (2005) Phylogeny of lamniform sharks (Chondrichthyes: Elasmobranchii) and the contribution of dental characters to lamniform systematics. *Paleontological Research*, 9, 55–72.

Smith, M.M. (2003) Vertebrate dentitions at the origin of jaws: when and how pattern evolved. *Evolution and Development*, 5, 394–413.

Smith, M.M., Fraser, G.J., Chaplin, N., Hobbs, C. and Graham, A. (2009) Reiterative pattern of sonic hedgehog expression in the catshark dentition reveals a phylogenetic template for jawed vertebrates. *Proceedings of the Royal Society B: Biological Sciences*, 276, 1225–1233.

Smith, M.M., Johanson, Z., Underwood, C. and Diekwisch, T.G.H. (2013) Pattern formation in development of chondrichthyan dentitions: a review of an evolutionary model. *Historical Biology*, 25, 127–142.

Snelson, F.F., Rasmussen, L., Johnson, M.R. and Hess, D.L. (1997) Serum concentrations of steroid hormones during reproduction in the Atlantic stingray, *Dasyatis sabina*. *General and Comparative Endocrinology*, 108, 67–79.

Soares, K., Gomes, U. and De Carvalho, M. (2016) Taxonomic review of catsharks of the *Scyliorhinus haeckelii* group, with the description of a new species (Chondrichthyes: Carcharhiniformes: Scyliorhinidae). *Zootaxa*, 4066, 501–534.

Soares, K.D.A. (2019) Sexually dimorphic body proportions in the catshark genus *Scyliorhinus* (Chondrichthyes: Carcharhiniformes: Scyliorhinidae). *Journal of Fish Biology*, 95, 683–685.

Soares, K.D.A. and Carvalho, M.R.D. (2019) The catshark genus *Scyliorhinus* (Chondrichthyes: Carcharhiniformes: Scyliorhinidae): taxonomy, morphology and distribution. *Zootaxa*, 4601, 1–147.

Soda, K., Slice, D. and Naylor, G. (2017) Artificial neural networks and geometric morphometric methods as a means for classification: a case-study using teeth from *Carcharhinus sp.* (Carcharhinidae). *Journal of Morphology*, 278, 131–141.

Soldo, A., Dulcic, J., Cetinic, P. and Cetinic, P. (2000) Contribution to the study of the morphology of the teeth of the nursehound *Scyliorhinus stellaris* (Chondrichthyes: Scyliorhinidae). *Scientia Marina*, 64, 355–356.

Springer, S. (1966) A review of western Atlantic cat sharks, Scyliorhinidae, with descriptions of a newgenus and five new species. *Fishery Bulletin*, 65, 581–624.

Springer, S. (1967) Social organization of shark populations. In: Gilbert, P.W., Mathewson, R.F. and Rall, D.P. (Eds.) *Sharks, Skates and Rays*. Baltimore: Johns Hopkins Press, pp. 149–174.

Springer, S. (1979) *A revision of the catsharks, family Scyliorhinidae*. Tech. rep., US Department of Commerce.

Stalling, D., Westerhoff, M. and Hege, H.C. (2005) Amira: A highly interactive system for visual data analysis. In: Hansen, C.D. and Johnson, C.R. (Eds.) *The Visualization Handbook*. Oxford: Elsevier.

Strasburg, D.W. (1963) The diet and dentition of *Isistius brasiliensis*, with remarks on tooth replacement in other sharks. *Copeia*, 33–40.

Taniuchi, T. and Shimizu, M. (1993) Dental sexual dimorphism and food habits in the stingray *Dasyatis akajei* from Tokyo Bay, Japan. *Nippon Suisan Gakkaishi*, 59, 53–60.

Thesleff, I. and Mikkola, M. (2002) The role of growth factors in tooth development. *International Review of Cytology*, 217, 93–135.

Underwood, C., Johanson, Z. and Smith, M.M. (2016) Cutting blade dentitions in squaliform sharks form by modification of inherited alternate tooth ordering patterns. *Open Science*, 3, 160385.

Underwood, C.J., Johanson, Z., Welten, M., Metscher, B., Rasch, L.J., Fraser, G.J. and *et al* (2015) Development and evolution of dentition pattern and tooth order in the skates and rays (Batoidea; Chondrichthyes). *PLoS One*, 10, e0122553.

Van Otterloo, E., Li, H., Jones, K.L. and Williams, T. (2018) AP-2α and AP-2β cooperatively orchestrate homeobox gene expression during branchial arch patterning. *Development*, 145, dev157438.

Vélez-Zuazo, X. and Agnarsson, I. (2011) Shark tales: a molecular species-level phylogeny of sharks (Selachimorpha, Chondrichthyes). *Molecular Phylogenetics and Evolution*, 58, 207–217.

Webster, M. and Sheets, H.D. (2010) A practical introduction to landmark-based geometric morphometrics. *The Paleontological Society Papers*, 16, 163–188.

Whitenack, L.B. and Gottfried, M.D. (2010) A morphometric approach for addressing tooth-based species delimitation in fossil mako sharks, *Isurus* (Elasmobranchii: Lamniformes). *Journal of Vertebrate Paleontology*, 30, 17–25.

Wiley, D., Amenta, N., Alcantara, D., Ghosh, D., Kil, Y., Delson, E. *et al* (2005) Evolutionary morphing. In *Proceedings of the IEEE International Conference on Visualization*. Minneapolis: Institute of Electrical and Electronics Engineers (IEEE), pp 431–438.

Wilga, C.D. and Motta, P.J. (2000) Durophagy in sharks: feeding mechanics of the hammerhead *Sphyrna tiburo*. *The Journal of Experimental Biology*, 203, 2781–2796.

SUPPORTING INFORMATION

Additional supporting information may be found online in the Supporting Information section.

How to cite this article: Berio F, Evin A, Goudemand N, Debiais-Thibaud M. The intraspecific diversity of tooth morphology in the large-spotted catshark *Scyliorhinus stellaris*: insights into the ontogenetic cues driving sexual dimorphism. *J. Anat*. 2020;00:1–19. https://doi.org/10.1111/joa.13257

Conclusions of the article

This paper highlights the emergence of gynandric heterodonty in *S. stellaris* between the juvenile and sexually mature stages. The mature females retain a juvenile-like tooth morphology, as opposed to the mature males. This pattern is characterised by mature females having much more accessory cusps than mature males, which in turn have longer main cusps. Several hypotheses could explain these divergent morphologies, among them is the differential expression of sex hormones that might impact the jaw cartilage bending or the expression of the proteins involved in tooth development. Overall, this study improves knowledge on teeth of extant sharks and shows how diverse the tooth shapes can be at the intraspecific level. This aspect is of primary importance for the taxonomy of extinct sharks that are recognised and classified largely based on their tooth morphologies. The characterisation of intraspecific tooth morphologies aims at refining a species description, as well as comparing similar traits with other scyliorhinids to understand evolutionary, developmental, and ecological relationships within this group of sharks.

2.1.3 Intraspecific tooth form diversity in *S. canicula*

The interspecific comparison of tooth forms within scyliorhinids would allow to decipher the characteristics that are specific to a species and elaborate hypotheses on the potential dental regulatory factors that are common to this group of sharks. Furthermore, a detailed examination of the tooth form diversity in *S. canicula* will provide new information to better know this shark model species [Coolen et al., 2008] and provide knowledge that will be necessary for preparing and interpreting further functional tests. Two populations (Atlantic and Mediterranean) of *S. canicula* were sampled to explore the dental diversity at the intraspecific level, and to further classify the tooth form diversity within this species (see section 2.2 for the second part of the project). Within each population, specimens of both sexes and three ontogenetic stages (hatchling, juvenile, and sexually mature) were sampled (N_{teeth}=3,299). The sampling and scanning information are detailed in section 2.2. The scanning and GM protocols used are identical to the ones performed with *S. stellaris* teeth (see subsection 2.1.2).

Visual inspection of *S. canicula* tooth morphologies

Because this project is paired with the population classification project with Random Forests described in subsection 2.2.2, here we only describe the tooth morphology patterns along the ontogeny and between sexes at the specific level.

In females, the tooth cusp number increases from hatchling to mature stages (Figure 2.4A-D and Y-AB; I-L and AG-AJ; Q-T and AO-AR and Figure 2.5A-D and Y-AB; I-L and AG-AJ; Q-T and AO-AR).

FIGURE 2.4: Diversity of palatoquadrate tooth morphology of North Atlantic and Mediterranean *Scyliorhinus canicula*. A-H and Y-AF) Teeth of hatchlings; I-P and AG-AN) Teeth of juveniles; Q-X and) Teeth of sexually mature specimens. Symphyseal (mesial) pole to the left. Scale bars are 100 µm.

FIGURE 2.5: Diversity of Meckelian tooth morphologies of North Atlantic and Mediterranean *Scyliorhinus canicula*. A-H and Y-AF) Teeth of hatchlings; I-P and AG-AN) Teeth of juveniles; Q-X and AO-AV) Teeth of sexually mature specimens. Symphyseal (mesial) pole to the left. Scale bars are 100 µm.

Male teeth undergo an addition of up to two cusps between the hatchling and juvenile stages (Figure 2.4E-H and AC-AF, M-P and AK-AN and Figure 2.5E-H and AC-AF, M-P and AK-AN), whereas they undergo a decrease in accessory cusps number between the juvenile and mature stages (Figure 2.4M-P and AK-AN, U-X and AS-AV). The teeth of mature *S. canicula* females display more accessory cusps than in males (Figure 2.4 and Figure 2.5). These ontogenetic, visual trends are similar to those described for *S. stellaris* teeth, although some aspects of the tooth shapes, such as the number of accessory cusps differ between the two scyliorhinid species [Berio et al., 2020].

Geometric morphometrics

Tooth centroid size patterns For both populations and sexes, hatchlings display little variation in centroid sizes along the jaw and tooth centroid sizes of Atlantic specimens are slightly higher than in the Mediterranean population (Figure 2.6).

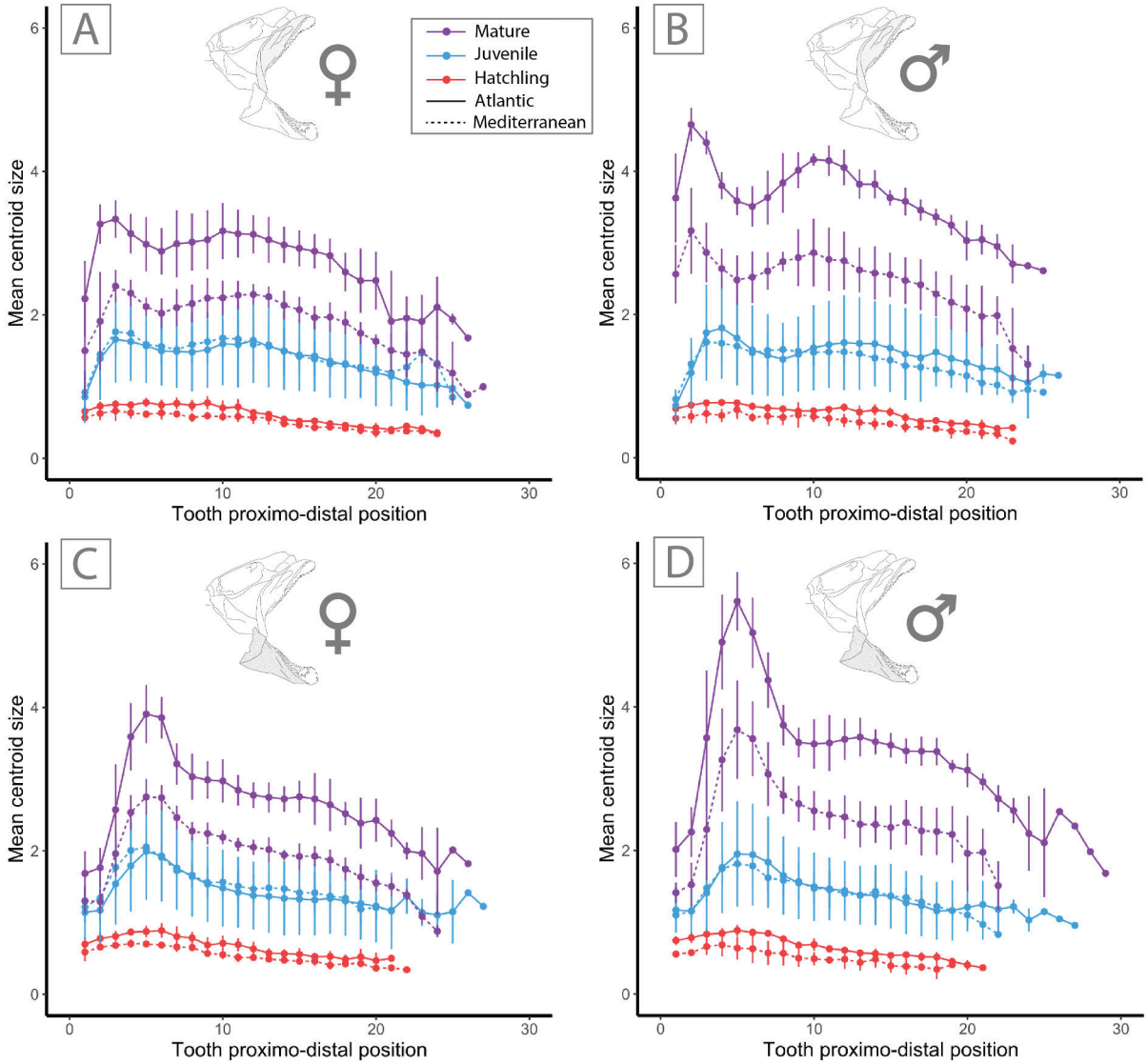

FIGURE 2.6: Tooth centroid size patterns in two *Scyliorhinus canicula* populations. A) Female palatoquadrate teeth; B) Male palatoquadrate teeth; C) Female Meckelian teeth; D) Male Meckelian teeth.

Within juveniles, the tooth centroid size patterns are similar between populations and sexes, however we report pattern differences between both jaws: a bimodal pattern in the palatoquadrate and a unimodal in the Meckelian cartilage, similar to those described by Berio et al. [2020] (Figure 2.6). The centroid size patterns of mature specimens are similar along the jaw between both populations but Atlantic specimens display higher values than Mediterranean specimens (Figure 2.6). We report overlapping values between mature females and juveniles at some locations (Figure 2.6).

Tooth shape differences

PCA patterns The morphospaces of the two *S. canicula* populations are displayed in Figure 2.7. In both palatoquadrate and Meckelian teeth, the three main axes (74.0 % and 70.1 % for the palatoquadrate and Meckelian teeth respectively) of variation indicate a modification of the number of accessory cusps (Figure 2.7). However, the main cusp bending is only displayed for palatoquadrate teeth (Figure 2.7).

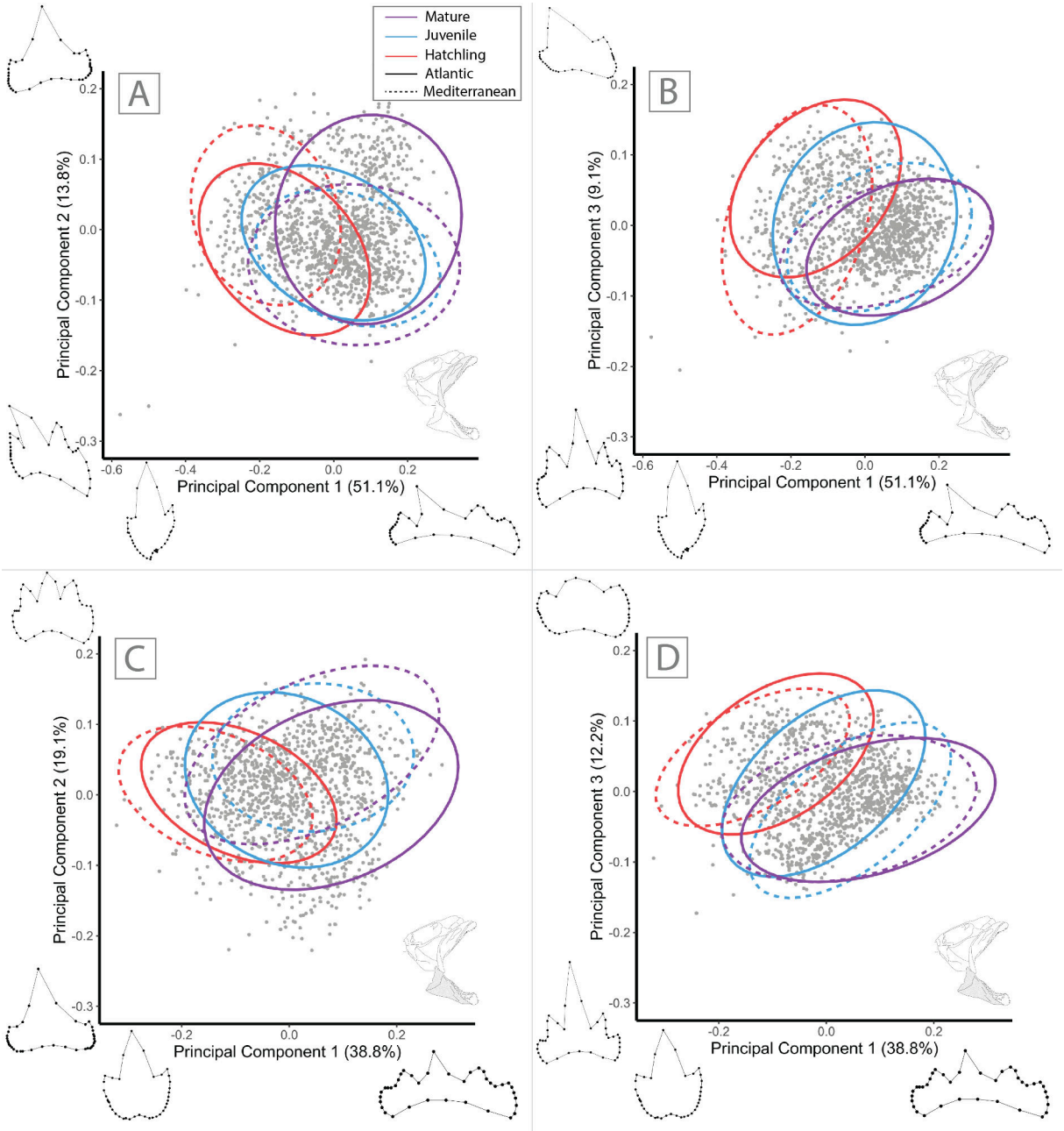

FIGURE 2.7: PCAs of tooth shapes in two *Scyliorhinus canicula* populations. A) PC1xPC2 for palatoquadrate teeth; B) PC1xPC3 for palatoquadrate teeth; C) PC1xPC2 for Meckelian teeth; D) PC1xPC3 for Meckelian teeth. Wireframes depict extreme deformations of the mean shape at the positive and negative extremities of the PC1, PC2, and PC3 axes.

In the two populations and in palatoquadrate and Meckelian teeth, the teeth of

specimens of different ontogenetic stages overlap but also share ontogenetic-specific locations in the morphospaces. Teeth of hatchlings have less accessory cusps than juvenile and mature specimens (albeit this trend is less clear as compared to mature males), which is consistent with the observations reported in Figure 2.4 and Figure 2.5.

Statistical tests The number of axes to be used in ANalyses Of VAriance (ANOVAs) and MANOVAs is determined following Evin et al. [2013]. Ten axes are used for palatoquadrate (91.61 %) and for Meckelian (90.89 %) teeth.

Regarding the centroid size, we report significant influence of the sex factor for all specimens in both jaws, while within each ontogenetic stage, the impact is significant only in mature specimens (Table 2.1).

TABLE 2.1: ANOVA results on centroid sizes. Significant p-values after Benjamini and Hochberg correction are in bold. ToothMD, tooth mesio-distal location along the jaw.

	Palatoquadrate teeth			
	All	Hatchling	Juvenile	Mature
	F value (p-val)	F value (p-val)	F value (p-val)	F value (p-val)
Sex	16.55 (**$5.04e^{-5}$**)	1.50 ($2.22e{-}1$)	6.10 ($4.35e{-}1$)	145.1 (**$< 2.00e^{-16}$**)
Stage	1358.00 (**$< 2.00e^{-16}$**)	-	-	-
ToothMD	2.18 (**$5.87e^{-4}$**)	19.91 (**$< 2.00e^{-16}$**)	6.49 (**$< 2.00e^{-16}$**)	5.96 (**$< 2.00e^{-16}$**)
Population	37.32 (**$1.33e^{-9}$**)	55.49 (**$1.21e^{-12}$**)	7.50 ($7.85e^{-1}$)	285.40 (**$< 2.00e^{-16}$**)
Sex:Stage	93.98 (**$< 2.00e^{-16}$**)	-	-	-
Sex:ToothMD	$7.90e^{-2}$ (1.00)	-	-	-
Sex:Population	7.71 (**$5.56e^{-3}$**)	-	-	-
Stage:ToothMD	2.10 (**$< 2.33e^{-5}$**)	-	-	-
Stage:Population	146.00 (**$< 2.00e^{-16}$**)	-	-	-
ToothMD:Population	$4.20e{-}2$ (1.00)	-	-	-
	Meckelian teeth			
	All	Hatchling	Juvenile	Mature
	F value (p-val)	F value (p-val)	F value (p-val)	F value (p-val)
Sex	14.37 (**$1.58e^{-4}$**)	3.72 ($5.50e{-}2$)	2.066 ($1.51e{-}1$)	75.98 (**$< 2.00e^{-16}$**)
Stage	946.50 (**$< 2.00e^{-16}$**)	-	-	-
ToothMD	3.98 (**$2.77e^{-11}$**)	14.79 (**$< 2.00e^{-16}$**)	8.05 (**$< 2.00e^{-16}$**)	11.66 (**$< 2.00e^{-16}$**)
Population	26.02 (**$3.92e^{-7}$**)	56.88 (**$9.01e^{-13}$**)	1.79 ($1.82e^{-1}$)	159.1 (**$< 2.00e^{-16}$**)
Sex:Stage	57.23 (**$< 2.00e^{-16}$**)	-	-	-
Sex:ToothMD	$9.80e^{-2}$ (1.00)	-	-	-
Sex:Population	4.71 (**$3.00e^{-2}$**)	-	-	-
Stage:ToothMD	4.86 (**$< 2.00e^{-16}$**)	-	-	-
Stage:Population	99.26 (**$< 2.00e^{-16}$**)	-	-	-
ToothMD:Population	$1.30e{-}1$ (1.00)	-	-	-

In both jaws, the centroid size significantly differs according to the ontogenetic stage (Table 2.1). All tests are significant relative to the tooth mesio-distal location along the jaw and within each ontogenetic stage and this result is also reported for the population factor except within juvenile palatoquadrate and Meckelian teeth (Table 2.1). The significant interactions detected between the factors considered are the same in both jaws, which are between sex and ontogenetic stage, sex and population, ontogenetic stage and tooth mesio-distal location, and ontogenetic stage and population (Table 2.1). In both jaws, the ontogenetic stage is the factor that impacts the most the tooth centroid size ($F>946.50$), followed by the ontogenetic stage-population interaction ($F>99.26$) and the sex-ontogenetic stage interaction ($F>57.23$) (Table 2.1).

In the whole dataset, the sex of the specimens significantly impacts the tooth shape in both jaws, but also significantly impacts the tooth shape in specific groups of given ontogenetic stage: in hatchling, juvenile, and mature specimens for palatoquadrate teeth and in juvenile and mature specimens for Meckelian teeth (Table 2.2).

TABLE 2.2: MANOVA results on shape data. Significant p-values after Benjamini and Hochberg correction are in bold. ToothMD, tooth mesio-distal location along the jaw.

	Palatoquadrate teeth			
	All	Hatchling	Juvenile	Mature
	F approx (p-val)	F approx (p-val)	F approx (p-val)	F approx (p-val)
Sex	20.61 (**$< 2.20e^{-16}$**)	7.43 (**$2.11e^{-10}$**)	8.37 (**$1.01e^{-12}$**)	87.41 (**$< 2.20e^{-16}$**)
Stage	143.97 (**$< 2.20e^{-16}$**)	-	-	-
ToothMD	5.96 (**$< 2.20e^{-16}$**)	2.21 (**$< 2.20e^{-16}$**)	4.52 (**$< 2.20e^{-16}$**)	3.71 (**$< 2.20e^{-16}$**)
Population	14.94 (**$1.92e^{-13}$**)	25.59 (**$< 2.20e^{-16}$**)	36.89 (**$< 2.20e^{-16}$**)	19.80 (**$< 2.20e^{-16}$**)
Sex:Stage	31.01 (**$< 2.20e^{-16}$**)	-	-	-
Sex:ToothMD	$7.38e^{-1}$ (1.00)	-	-	-
Sex:Population	5.87 (**$1.04e^{-8}$**)	-	-	-
Stage:ToothMD	2.57 (**$< 2.20e^{-16}$**)	-	-	-
Stage:Population	31.01 (**$< 2.20e^{-16}$**)	-	-	-
ToothMD:Population	$7.61e-1$ (1.00)	-	-	-
	Meckelian teeth			
	All	Hatchling	Juvenile	Mature
	F approx (p-val)	F approx (p-val)	F approx (p-val)	F approx (p-val)
Sex	31.66 (**$< 2.00e^{-16}$**)	1.69 ($7.75e^{-2}$)	10.70 (**$< 2.20e^{-16}$**)	79.66 (**$< 2.20e^{-16}$**)
Stage	169.06 (**$< 2.20e^{-16}$**)	-	-	-
ToothMD	5.93 (**$< 2.20e^{-16}$**)	2.60 (**$< 2.20e^{-16}$**)	3.76 (**$< 2.20e^{-16}$**)	3.26 (**$< 2.20e^{-16}$**)
Population	19.27 (**$< 2.20e^{-16}$**)	9.73 (**$1.78e^{-14}$**)	50.84 (**$< 2.20e^{-16}$**)	12.31 (**$< 2.20e^{-16}$**)
Sex:Stage	24.73 (**$< 2.20e^{-16}$**)	-	-	-
Sex:ToothMD	$9.37e^{-1}$ ($7.69e^{-1}$)	-	-	-
Sex:Population	5.55 (**$1.00e^{-8}$**)	-	-	-
Stage:ToothMD	2.56 (**$< 2.00e^{-16}$**)	-	-	-
Stage:Population	20.79 (**$< 2.00e^{-16}$**)	-	-	-
ToothMD:Population	1.08 ($1.75e^{-1}$)	-	-	-

The *S. canicula* tooth shape is significantly impacted by the ontogenetic stage, as well as by the tooth mesio-distal location and the population and this is also true within each ontogenetic stage for both jaws (Table 2.2). The significant interactions between the factors considered are the same as the ones detected by the ANOVAs, *i.e.* between the sex and the ontogenetic stage, the sex and the population, the ontogenetic stage and the mesio-distal location of the tooth, and between the ontogenetic stage and the population (Table 2.2). In all teeth, the shape is the most impacted by the ontogenetic stage (F>143.97) (Table 2.2). Palatoquadrate tooth shapes also highly depend on the interaction between the sex of the specimens and their ontogenetic stage and by the interaction between the ontogenetic stage and the population of the specimens (F=31.01 for both tests) (Table 2.2). The Meckelian tooth shapes are then highly impacted by the sex of the specimens (F=31.66), and by the interaction between the sex and the ontogenetic stage (F=24.73) (Table 2.2).

Conclusions on *S. canicula* tooth forms

Between the hatching and juvenile ontogenetic stages, the specimens undergo the addition of up to two accessory cusps, resulting in a modification from tricuspid to pentacuspid teeth in both sexes and jaws. The number of accessory cusps also increases in palatoquadrate teeth of mature females, as opposed to Meckelian teeth that do not undergo such modification. Mature males generally exhibit tricuspid teeth with small accessory cusps in both jaws. The teeth of specimens of different ontogenetic stages are visually separated in the PCAs. Centroid size patterns are similar to what has been described in *S. stellaris* [Berio et al., 2020]: they are bimodal in palatoquadrate teeth of juveniles and mature specimens and unimodal for Meckelian teeth of juveniles and mature specimens. The differences between populations are detailed further in section 2.2 but we briefly report sharper teeth in the Mediterranean than in the Atlantic population and more accessory cusps in mature females from the Atlantic Ocean than from the Mediterranean Sea. The tooth centroid sizes are larger for mature specimens from the Atlantic than from the Mediterranean Sea and there are very few visual differences between populations in the PCAs.

2.1.4 Interspecific comparisons of tooth morphologies in sharks: preliminary results on *S. canicula* and *S. stellaris*

Shark tooth morphologies can be correlated with a species' diet [Cappetta, 1986; Wilga and Motta, 2000] but also convey a phylogenetic signal [Shimada, 2002, 2005a]. We aimed at visualising the interspecific boundaries and tooth morphological specificities of *S. canicula* and *S. stellaris* using a GM framework. We combined the GM dataset of these two species and performed GPAs and PCAs separately for palatoquadrate and Meckelian teeth. For each jaw, we display the tooth morphospaces for PC1 and PC2, and PC1 and PC3, accounting for 72.6 % and 71.2 % of the total variation for palatoquadrate and Meckelian teeth respectively (Figure 2.8).

According to the extreme PC shapes, the morphological differences in *Scyliorhinus* palatoquadrate teeth in the three PCA axes are a modification of number of accessory cusps, the relative size of the main cusp as compared to the accessory ones, and the mesio-distal bending of the main cusp (Figure 2.8A and B). In Meckelian teeth, the extreme shapes depict a modification of number of accessory cusps, as well as the main cusp length relative to the accessory cusps length (Figure 2.8C and D). The PCAs for palatoquadrate teeth display more inter- than intraspecific differences and the *S. stellaris* tooth morphologies mostly vary along PC1 (number of accessory cusps, Figure 2.8A and B). The *S. canicula* teeth also slightly vary along PC2 and PC3 (number of accessory cusps and relative size and bending of the main cusp respectively, Figure 2.8A and B). Female Meckelian teeth and male *S. stellaris* teeth mostly vary along PC1 (number of accessory cusps), while *S. canicula* male teeth undergo more variation along PC2 (number of accessory cusps and main cusp length as compared to the tooth base, Figure 2.8C). In the PC1xPC3 morphospace, Meckelian teeth are separated by species rather than sex or population and undergo most morphological changes along PC1 (Figure 2.8).

These preliminary data show that the two scyliorhinid species considered share a great range of tooth morphologies. Such overlap might be a source of taxonomic confusion, for example if the teeth are examined when isolated (see section 2.3 for

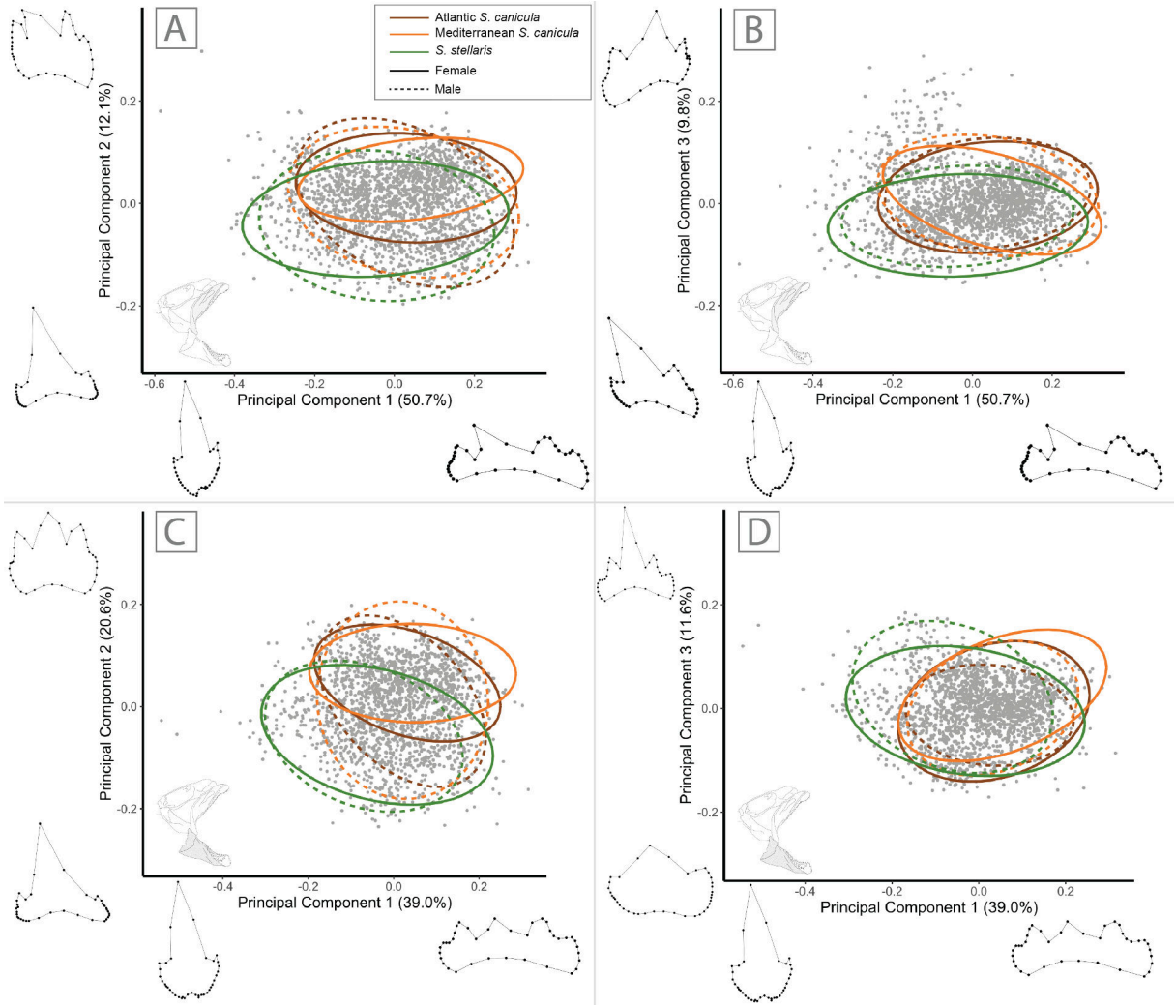

FIGURE 2.8: PCAs of tooth shapes from two *Scyliorhinus canicula* populations and from *Scyliorhinus stellaris*. A) PC1xPC2 for palatoquadrate teeth; B) PC1xPC3 for palatoquadrate teeth; C) PC1xPC2 for Meckelian teeth; D) PC1xPC3 for Meckelian teeth. Wireframes depict extreme deformations of the mean shape at the positive and negative extremities of the PC1, PC2, and PC3 axes. S. canicula populations originate from North East Atlantic Ocean and from West Mediterranean Sea.

detailed discussion). However, *S. canicula* and *S. stellaris* species can still be identified based on some of their tooth morphologies, especially when considering the sex and the ontogenetic stages of the specimens, which remains to be investigated in this project. More difficult is to discriminate populations within a same species, at least with the PCAs displayed here. It thus remains to be determined to what extent the teeth of the two Atlantic and Mediterranean *S. canicula* populations considered can be reliably differentiated and further classified. This question is at the core of the project presented in the next section.

2.2 Same species, same teeth? Insights from two *S. canicula* populations

The following project aims at classifying one Atlantic and one Mediterranean population of *S. canicula* based on their tooth morphologies. In the traditional GM framework, the shape and form differences between structures are usually tested with MANOVAs and discriminated with LDAs. However, this framework might not be optimal to every GM dataset, especially when the sought morphological differences are slight, and when the dataset includes a large number of items. The goal was thus to compare the classification results obtained with a LDA and another ML algorithm, the Random Forests. GM data are used as input data (3D shape coordinates and centroid size) and comments are made on the potential causes of the differences observed between the two populations considered. A more detailed introduction to the project is presented in subsection 2.2.2, as well as the samples and specific parameters used in the models and the conclusions of the project. Before exposing the research core of the project, it is first necessary to provide an overview of ML use in GM and a detailed description of functioning of Random Forests.

2.2.1 Machine learning

> *"In God we trust, all others bring data."*
> – attributed to William Edward Deming, 1900-1993

To morphometrics and beyond

The recent use of ML algorithms (different from LDA) on GM data allowed overcoming unsatisfying classification results gathered by morphometricians. Their aim is to thoroughly differentiate —*a priori* or not— groups (e.g., species) with up to 100 % certainty, a performance that might not be reached with the usual GM framework [Lorenz et al., 2015; Courtenay et al., 2019; MacLeod and Kolska Horwitz, 2020; Quenu et al., 2020]. In some cases, comparisons between traditional classification methods used in GM and ML algorithms reveal equivalent performances, and this is notably true with the linear discriminate function analysis and the multilayered perceptron model applied to Procrustes coordinates of requiem sharks (*Carcharhinus*) teeth [Soda et al., 2017]. However, it appears that the second method was more generalistic because it did provide more evenly dispersed accuracies on all species and it performed well even on small groups [Soda et al., 2017]. Moreover, combinations of supervised and unsupervised ML methods on GM data also provided promising results on a refined structure of populations and cases of hybridisations (e.g., of the land snail *Placostylus*), as well as on complex taxonomic recognitions (e.g., on braconid parasitoid wasps *Bassus* and on the mosquitoes *Anopheles*, *Aedes*, and *Culex*) [Baylac et al., 2003; Lorenz et al., 2015; Quenu et al., 2020].

In a recent comparative study of GM and ML results on digital images of skulls, MacLeod [2017] reported that "machine-learning approaches delivered more consistent, accurate, and stable results than a standard geometric morphometric analysis on either landmark shape-coordinate or boundary outline semilandmark shape-coordinate data".

Moreover, the advantages of using ML methods over the GM framework are also beyond the precision of the results because the ML framework first does not require *a priori* decisions from the user on the putative most relevant features and zones to include in the analysis, and second because the user does not need to place landmarks and semilandmarks before to the analysis (input data are usually raw images), which is highly time-consuming [Lorenz et al., 2015; Sonnenschein et al., 2015; MacLeod, 2017; Soda et al., 2017; Quenu et al., 2020]. The GM framework is finally more domain-driven, whereas the broad diversity of ML algorithms is more data-driven and generalistic, which means the use of these ML algorithms is less restricted to a specific field than to a structure of data.

So why, you may ask, not directly using ML on shark tooth surfaces? As opposed to the previously mentioned studies, the aim here is less to achieve classification with 100 % certainty than to discriminate groups based on features that bear developmental meanings and can be used for species identification. Such features are not known by ML algorithms and still need to be manually specified by the user [Baylac et al., 2003; Sonnenschein et al., 2015]. The choice was thus made to place landmarks on tooth deeps and tips whose development has been characterised in *S. canicula*, and to use a ML algorithm on Procrustes coordinates to discriminate between geographic populations [Debiais-Thibaud et al., 2011, 2015; Martin et al., 2016; Rasch et al., 2016] (see subsection 2.2.2). As shown by Sonnenschein et al. [2015], better performances of classification can also be achieved if landmark data, as opposed to automatically extracted anatomical features, are wisely chosen and provided as input to ML algorithms. Furthermore and as detailed in subsection 2.1.1, the use of GM data gives access to shape and size dissociated features, which respective characteristics must be considered for our task of population discrimination.

Choose your algorithm wisely

ML algorithms fall into two types of classification methods: unsupervised and supervised. Unsupervised classification, also termed clustering, is used on datasets whose groups are not known *a priori*. Clustering is precisely designed to create groups and find a structure among data. Clustering methods are used on fixed datasets and new data cannot be recursively added without modifying the model and the established data pattern. As opposed to clustering, the aim of supervised classification is precisely to learn from the *a priori* data structure to further predict which group a new item belongs to. Supervised classification methods are thus designed to reveal to what extent one or several groups are differentiated and new data can reliably be assigned to one of them. The items are classified based on a set of features used by ML algorithms.

The tooth Procrustes coordinates gathered during my PhD already belong to groups: Information is available about the mesiodistal location of a tooth along the jaw, and about the sex, the ontogenetic stage, and the geographic population of the specimens whose teeth are characterised. ML algorithms perform mathematical operations on features (in our case, the Procrustes coordinates and eventually the centroid sizes) to link them to a set of labels [Hastie et al., 2009]. There are plenty of ML algorithms that perform these operations (e.g., neural networks, decision trees, nearest neighbours, and support vector machine) but there is no universal rule to decide whether a given one is better than another to classify a specific set of features. Moreover, the "No Free Lunch

Theorem" stipulates that there is no better ML algorithm than another so that the only way to get the best ML results as possible is to adapt the algorithm to the problem, by tuning parameters [Wolpert, 1996; Wolpert and Macready, 1997].

The choice of a ML algorithm depends on the problem and the expected results (metrics): does an increased classification performance prime over the interpretation of parameter values? For example, in cases of targeted advertising (e.g., by Google, Amazon), the aim is primarily to maximise the metric values, while the meaning of parameters is of lesser importance. Typical ML methods that can achieve such tasks are the neural network-based algorithms (also termed "black box" algorithms) because there is no tangible meaning beyond the characteristics of each neuron, neither beyond the number of neuron layers [Alain and Bengio, 2016; Schwartz-Ziv and Tishby, 2017]. For our classification purpose, however, we favour parameter understanding over metrics maximisation, albeit our goal is of course also to perform the best classification as possible.

Model's performances: metrics

In the following, I detail the metrics used to interpret the ML classification results. Let us consider a classification of features into two groups, A and B. One would want the true A items to be classified as A, and so on for B. The ML algorithm then produces a confusion matrix that indicates the successes and errors of classification (Table 2.3).

TABLE 2.3: Confusion matrix after item classification into the two A and B groups. Actual groups are in columns and predicted groups in rows. FN, false negative; FP, false positive; TN, true negative; TP, true positive.

Groups	**A**	**B**
A	TP	FP
B	FN	TN

A confusion matrix must be interpreted from a one-group view so here let's consider group A as the reference. True positive (TP) elements are A items that have been correctly assigned to group A during classification. False positives (FP) are real B items that have been classified as A, and this misclassification corresponds to type I error. On the contrary, false negatives (FN) are type II errors and are interpreted as true A items assigned to B group. True negatives (TN) are finally B items whose classification group is also B.

The performances of a model are evaluated through a set of metrics, which are based on the results provided by the confusion matrix. The precision, accuracy, and recall were the ones used in my PhD. The first metric to be used is the precision of classification (Equation 2.1). The precision relates to each group so that there are as many precision values as groups in the analysis. The precision is interpreted from the classification view: it is the number of items correctly assigned to a group (A), as compared to all items (A and B) classified in this same group (A). Precision ranges from 0 to 1 and the

best classification for a group is achieved for a value of 1.

$$Precision_A = \frac{TP_A}{TP_A + FP_A} \tag{2.1}$$

However, it is difficult to evaluate the performances of a model using several precision values (one per group). The model accuracy (Equation 2.2, where g is one group, G represents all groups and N is the total number of elements in the dataset) encompasses this issue by combining the multiple-precision values provided for each group. The accuracy ranges from 0 to 1 and the higher the value, the better the classification.

$$Accuracy = \frac{1}{N} \sum_{g=A}^{G} TP_g \tag{2.2}$$

A third metric commonly used is the recall (Equation 2.3), which depends on the group that is considered. As opposed to precision, it must be understood from the reality view: it is the number of items from a group (A) that have been correctly assigned to this group (A). The recall ranges from 0 to 1 and a value of 1 indicates that all items of a given real group have been classified in this group.

$$Recall_A = \frac{TP_A}{TP_A + FN_A} \tag{2.3}$$

To summarise, the accuracy measures the ability of a model to generate groups of well-classified items, while the recall indicates how good is the model at correctly identifying all the items of a given group from the dataset.

We chose to classify the Procrustes coordinates and eventually the centroid sizes of *S. canicula* teeth into geographical populations with a Random Forest algorithm based on decision trees, whose steps are described in Figure 2.9.

The Random Forest method has been proposed by Breiman [2001] to improve the classification robustness by iteratively computing a large number of decision trees. Random Forests usually outperforms other machine learning algorithms for supervised classification [Caruana and Niculescu-Mizil, 2006; Domínguez-Rodrigo and Baquedano, 2018; Püschel et al., 2018; Courtenay et al., 2019], provide intuitive and interpretable importance measures of feature contribution to classification, and does not require feature reduction prior to the analysis to achieve good performances [Archer and Kimes, 2008]. As for all supervised classification algorithms, the Random Forest process is achieved following two key steps: training and testing. For that purpose, the original dataset is divided into train and test sets, which usually represent about 80 % and 20 % respectively, albeit slight variants of these proportions can also be used [Adelabu et al., 2015; Nguyen and Bui, 2018; Scornet, 2018]. Populations are a categorical variable, as opposed to continuous, so classification trees are used instead of regression trees.
Chawla et al. [2002] state that a dataset is unbalanced: "if the classes are not approximately equally represented", which evidences for the lack of strict, objective limits that define unbalanced classes. Yet, these authors mention an order of 100 to 1 to term an unbalanced dataset in ML [Chawla et al., 2002].

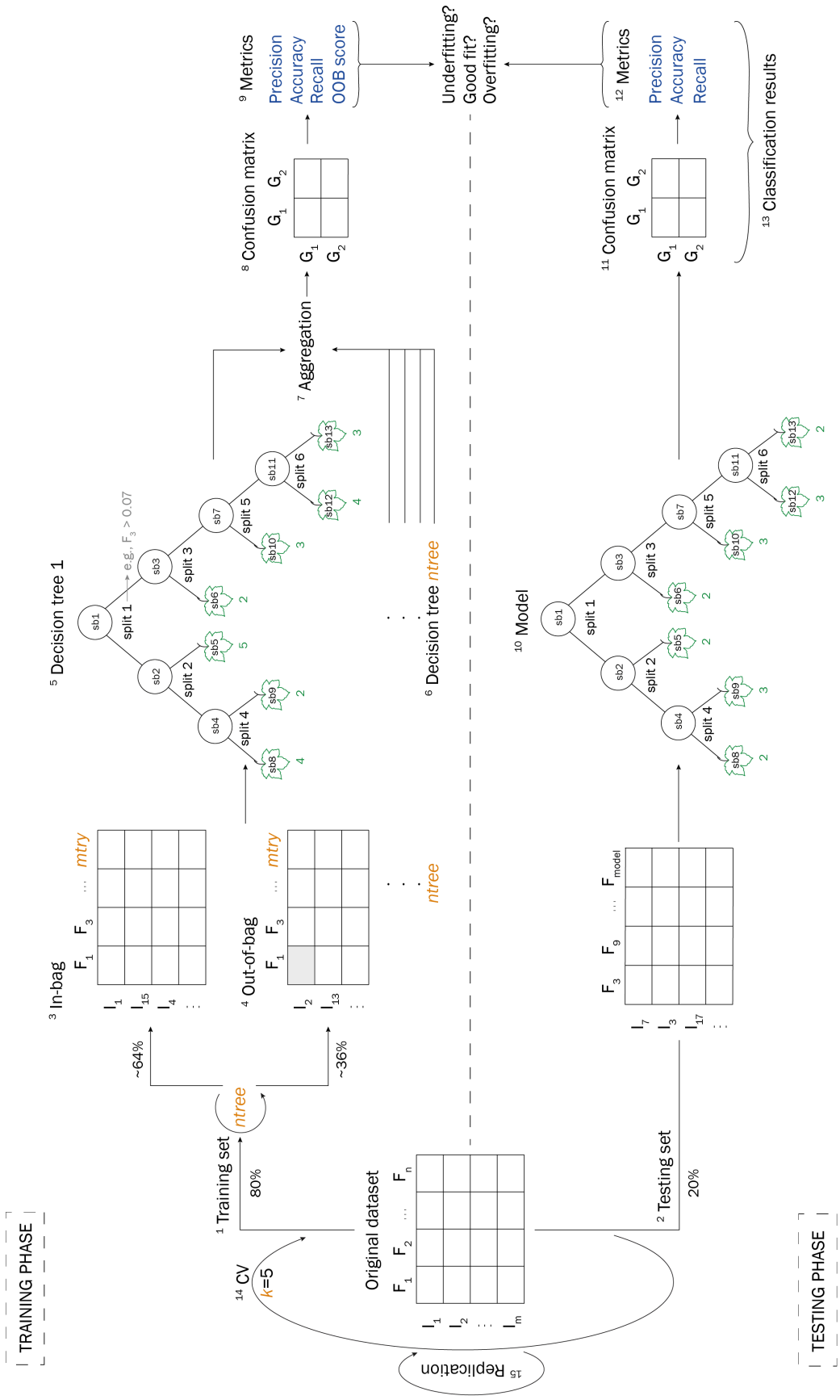

FIGURE 2.9: Scheme detailing the steps characterising the Random Forests algorithm. CV, cross-validation; F, feature; G, group; I, item; sb, subset; OOB, out-of-bag. k, ntree, and mtry are the model parameters that respectively indicate the number of cross-validation steps, the number of trees to be computed, and the number of features to be used for each tree [Liaw and Wiener, 2002].

That classes have similar sizes is necessary for the ML to perform an accurate classification task; if not fullfilled, this condition leads to prediction results for the minority class to be biased toward the majority class [Li et al., 2018]. The *S. canicula* dataset is sufficiently balanced to avoid such bias because it contains the form coordinates for 1,757 teeth of Atlantic specimens and 1,542 teeth of Mediterranean specimens.
The decision tree principle lies in binary splits: the original dataset is split into two subsets based on the most discriminant feature sampled from the set of features available (see section 2.2.1 and Figure 2.9) [Breiman et al., 1984]. The composition of these two subsets is subsequently analysed based again on a newly most discriminant feature, and so on. A subset can be split into two subsets to be split again (nonterminal, internal or split nodes), or to terminal subsets (leaf nodes). The classification is achieved when the maximum number of splits or the minimum number of items per subset allowed by the user is reached. Once all items have been classified into leaf nodes, the algorithm attributes a group to each of these leaf nodes.

Training phase

> *"They were like a kelp forest, they cast a weird green light, you could get lost there, become tangled and drown."*
>
> – *White Oleander*, Janet Fitch, 1999

The randomisation process is achieved during the training phase (Figure 2.9). The training phase can be subdivided into two steps: the building of decision trees, and the model validation. For each decision tree to be built, the randomisation process is twofold: (i) it is computed based on randomly sampled items and (ii) randomly sampled features. The number of items and features must be the same for all decision trees in the forest. The selected items for each decision tree are termed in-bag or bootstrap samples, while the remaining items of the original training set, which are left-out, are termed out-of-bag samples and compose the validation set. Following this sampling, each decision tree is trained on its in-bag samples. Then comes the model validation step: after all decision trees of the forest have been built, each decision tree predicts the group of its out-of-bag sample, based on the rules established with its in-bag samples. At the end of this process, every item of the original dataset has usually been in-bag and out-of-bag in different decision tree. Per construction, each item is on average out-of-bag 36 % of the time [Liaw and Wiener, 2002]. The final group of each item in the original dataset is subsequently defined by a majority vote based on the outcomes of all decision trees [Breiman, 2001]. These steps provide the out-of-bag error, which indicates the average misclassification of each item during the training phase, as well as the relative importance of all features to discriminate groups. The overall model performances are also computed on the classification results of out-of-bag samples.

Testing phase

Once the training phase is achieved, the Random Forest model is built and can be used to predict the groups of now unknown items contained in the test set. During this phase, the model accesses the item features but not their groups. The model builds a decision tree based on the features and rules it learned during the training phase. This final decision tree assigns probabilities to each combination between a succession of internal

nodes (feature values) and a leaf node. For each item, the most probable combination thus leads to the group it is assigned to. Among the outputs of this testing phase are a new confusion matrix and associated metrics.
To evaluate and correct potential under- and overfitting effects, it is of primary importance to compare the training and testing phase metrics.

Underfitting, overfitting, and good fit

Underfitting occurs when metric values on the validation set are better than equivalent metric values on the train set. This arises when the train set does not contain enough data to fully learn the whole variation that can be found in the test set, or when the algorithm parameters have not been tuned properly to reach the same purpose. As opposed to underfitting, overfitting is characterised by better classification results on the train set as compared to the test set. The problem beyond overfitting thus comes from that the ML algorithm intimately learns the train set characteristics and is unable to reach the same performance level on unknown test sets because it is unable to generalise what it had learned. To avoid overfitting, a common process is precisely to use cross-validation sets, to train the algorithm on the first one and test the model on the second one. As previously mentioned, the split is usually 80:20, which means that the train set is randomly separated in 80 % and 20 % subsets to build several decision trees (see section 2.2.1) and that this step is performed four more times on the training set (see k=5 in Figure 2.9). Using randomly selected samples within cross-validation sets also allows to reduce the variance in the classification results without altering biases of the original dataset. To evaluate the model's robustness against the results variability, it is also common to replicate the cross-validation process. This produces errorbars for the metrics considered, and the smaller the variability, the more robust the model.
To summarise, rectifying under- and overfitting respectively allows to increase classification (e.g., precision, accuracy, and recall) and generalisation results (same precision, accuracy, and recall for the train and test sets). A good fit between the model and the data is reached once the metrics from the training and testing phases are balanced. Furthermore, a good fit state means that the model contains the optimal parameter values to classify the original data.

Parameters tuning

The parameter names we use here are those defined in the randomForest function from the randomForest R package (v.4.6-14) [Liaw and Wiener, 2002]. All Random Forest parameters to be tuned must be selected in the light of metric values. As in most studies, we chose to maximise both accuracy and recall. The first Random Forest parameter to be tuned is the number of decision trees (*ntree*) to be built in the forest. A satisfying *ntree* value is when a maximum accuracy value is reached. A second parameter is the number of features, among all original features, that can be used to discriminate items in a decision tree (*mtry*). We remind that even though *mtry* is fixed and is the same for all decision trees, the features are randomly sampled for each decision tree (except in Bagging, see below). It is crucial to evaluate the number of features to be used per decision tree because if too low, the model performances can still be improved, whereas if too high, the results might contain noise. Moreover, large *mtry* values allow optimised split of items because they offer the model to consider many split directions [Scornet,

2018]. If *mtry=f*, the original number of features, then a special case of a Random Forest model is built, termed Bagging [Liaw and Wiener, 2002]. Random Forests also allow specifying the decision tree depth by tuning the *nodesize* and *maxnodes*, which respectively constrains the size and number of leaf nodes [Liaw and Wiener, 2002]. Both values can be modified and have a mutual impact. In conclusion, it is crucial to adapt the ML parameter values to the dataset and be aware of Scornet's warning that "there are no theoretical findings to support the default values used for [the] parameters in Breiman's algorithm" [Soda et al., 2017; Scornet, 2018]. Thus, all parameter combinations must be tested to find the most suited for a specific task.

2.2.2 Journal article — Hide and seek shark teeth in Random Forests: Machine learning applied to *Scyliorhinus canicula* populations

Stakes of the project

The following study aims at classifying the teeth of two *S. canicula* populations that significantly differ in body length at sexual maturity: one from the North Atlantic Ocean and another from the Mediterranean Sea [Capapé et al., 2014]. A traditional framework used in landmark-based GMs is to use LDAs to discriminate groups of objects, however, ML classification algorithms have been demonstrated to perform better than LDA at this task with various types of data [Pang et al., 2006; Perdiguero-Alonso et al., 2008; Shang and Chisholm, 2014]. In this project, we combine GM with Random Forests and compare the classification results with those obtained with a LDA on 3D coordinates of tooth shapes and forms and identify the tooth zones that differ the most between the populations considered.

Introduction

The recognition of disjunct shark populations has opened to new questionings on marine ecosystem connectivity and consequences of gene flows on species evolution. Shark population distributions are structured by ecological habits of species (e.g., degree of habitat fidelity), reproductive strategies (e.g., use of nursery areas by females), dispersal ability (e.g., type of reproduction, migratory behaviour), and environmental barriers to gene flow (e.g., oceanic basins, geological climatic events) [Lucifora et al., 2003; Rodríguez-Cabello et al., 2004; Portnoy et al., 2010; Veríssimo et al., 2010; Karl et al., 2012; Kousteni et al., 2015]. Populations of a same shark species sometimes display vicariance patterns of the number of vertebrae [Gruber and Compagno, 1981], and tooth files [McEachran and Martin, 1977; Templeman, 1984; Lucifora et al., 2003]. In some species, the total length of a specimen at sexual maturity also differs between populations, as in bonnethead sharks *Sphyrna tiburo* [Parsons, 1993; Lombardi-Carlson et al., 2003], shortspine spurdogs *Squalus mitsukurii* [Taniuchi and Tachikawa, 1997], starspotted smooth-hounds *Mustelus manazo* [Yamaguchi et al., 1998, 2000], and cloudy catsharks *Scyliorhinus torazame* [Horie and Tanaka, 2002]. Such differences in specimen size at sexual maturity that are reported among shark populations have been hypothesized to result from genetic, or environmental constraints or both, but the combination between these factors is difficult to evaluate [Lombardi-Carlson et al., 2003].
When observed, these size differences at sexual maturity are often distributed alongside the latitudinal gradient, and shark populations inhabiting higher and colder latitudes are

significantly bigger [Leloup and Olivereau, 1951; Parsons, 1993; Taniuchi and Tachikawa, 1997; Yamaguchi et al., 2000; Horie and Tanaka, 2002; Lombardi-Carlson et al., 2003]. The warmer temperatures at lower latitudes [Blackburn et al., 2008] are thought to limit the energy allowed for somatic growth by inducing increased energy expenditure [Parsons, 1993; Carlson and Parsons, 1997] and also trigger early sexual maturity [Parsons, 1993; Yamaguchi et al., 2000; Goren, 2014].

S. canicula is an abundant benthic species in Western Atlantic (from Senegal to the UK) and Mediterranean Sea and inhabits depths from a few meters to 500 m (most commonly found around 110 m) [Ellis and Shackley, 1997; Compagno, 1984; Rodríguez-Cabello et al., 2004]. The disjunct geographical distribution of *S. canicula* coupled with divergent life history traits and genetic structures led to consider separate populations within its whole distribution range [Leloup and Olivereau, 1951; Mellinger et al., 1984; Rodríguez-Cabello et al., 2004; Barbieri et al., 2014; Capapé et al., 2014; Kousteni et al., 2015]. Such population genetic structures have been attributed to the philopatric behaviour of *S. canicula* and to its low dispersal ability across basins [Compagno, 1984; Rodríguez-Cabello et al., 2004; Barbieri et al., 2014; Kousteni et al., 2015].
However, if different genetic structures have been reported in Mediterranean *S. canicula*, these Mediterranean populations exhibit no significant body size differences at sexual maturity [Barbieri et al., 2014; Capapé et al., 2014; Kousteni et al., 2015]. Conversely, populations differ in maximal body size between the North Atlantic Ocean (Bristol Channel, UK) to the Mediterranean Sea [Leloup and Olivereau, 1951; Mellinger et al., 1984; Rodríguez-Cabello et al., 1998a; Kousteni et al., 2010; Capapé et al., 2014]. However, morphological differences between *S. canicula* populations remains unclear except for sexually mature specimens that differ in body length along a vast latitudinal gradient and between disjunct marine environments.

Tooth morphology is one of the main tools used for shark taxonomy, they are among the anatomical structures that may undergo morphological changes with ontogeny, sexual maturation, and diet of the specimen [Powter et al., 2010; Moyer and Bemis, 2016; Tomita et al., 2017; Cullen and Marshall, 2019; Berio et al., 2020]. Besides, different life history traits between Atlantic and Mediterranean *S. canicula* populations could also involve morphological tooth differences.

Sharks usually have long generation time and many are currently considered endangered species (International Union for Conservation of Nature status (IUCN)) because they struggle withstanding or recovering from accidental catches and fishing [Smith et al., 1998; Cortés, 2000; Dulvy et al., 2014]. Commercial frauds are regularly checked but the identification of species relies on a framework based on DNA barcoding [Barbuto et al., 2010; Melo Palmeira et al., 2013; Almerón-Souza et al., 2018], whose cost and time are limitations to the current inspection process.

This work proposes an alternative, feature-based framework to reliably discriminate shark populations based on their tooth morphological characteristics. The assessment of shark tooth form differences is successfully achieved with geometric morphometrics [Whitenack and Gottfried, 2010; Soda et al., 2017; Cullen and Marshall, 2019; Berio et al., 2020]. LDA is a frequently used machine learning algorithm to discriminate between groups based on geometric morphometric data [Mitteroecker and Bookstein, 2011; MacLeod, 2017; Doyle et al., 2018]. The performances of LDA are particularly dependent on a much higher number of items (e.g., teeth) as compared to the number of features (e.g., aligned coordinates). These conditions are often difficult to meet in

biological datasets, which often implies a feature reduction step through a PCA [Fort and Lambert-Lacroix, 2005; Pechenizkiy et al., 2006; Sheets et al., 2006; Archer and Kimes, 2008]. However, subtle discriminant patterns can also be missed when reducing data dimensionality to the first PCA axes prior to the classification task [MacLeod, 2018]. As opposed to LDA, Random Forests [Breiman, 2001] usually outperform other machine learning algorithms for supervised classification [Caruana and Niculescu-Mizil, 2006; Domínguez-Rodrigo and Baquedano, 2018; Doyle et al., 2018; Püschel et al., 2018; Courtenay et al., 2019]. Random Forests provide intuitive and interpretable importance measures of feature contribution to classification, is highly resistant to overfitting, and do not require feature reduction prior to the analysis to achieve good performances [Díaz-Uriarte and Alvarez de Andrés, 2006; Archer and Kimes, 2008; Doyle et al., 2018].

This work is a proof of concept that shark populations can be discriminated based on tooth morphologies. We take advantage of geometric morphometrics and machine learning methods to question differences of *S. canicula* teeth from North Atlantic and Mediterranean populations whose body size at maturity differ by around 35 % [Capapé et al., 2014]. Random Forests outperform LDA at classifying the tooth shape data. Random Forest models on tooth shape and form data highlight the crucial contribution of tooth size to enhance the classification performances. This work challenges the traditional geometric morphometrics workflow and provides valued indications of discriminant form features between the *S. canicula* populations considered, which are further discussed in light of developmental and ecological hypotheses.

Materials and Methods

Sampling *S. canicula* populations were sampled in 2018 and 2019 in two localities separated by over 2,000 nautical miles: Roscoff (France, Northeast Atlantic Ocean) and Banyuls-sur-mer (France, Western Mediterranean Sea). The Atlantic specimens were sampled at the Roscoff fishmarket and were provided by the Station Biologique de Roscoff, and the University of Montpellier, while the Mediterranean specimens were provided by the Observatoire Océanologique de Banyuls-sur-Mer. All specimens were preserved in 70 % ethanol. Three ontogenetic stages, hereafter referred to as "hatchling", "juvenile", and "mature", are defined within each population according to total body length (TL, from the tip of the snout to tip of the tail). Attempts were made to equally sample specimens from both sexes (female: F, male: M) within each category and to provide regularly sampled sizes. The TL of mature Mediterranean and Atlantic specimens was selected according to Ivory et al. [2004] and Capapé et al. [2014]. Hatchling specimens were sampled just after hatching while juveniles were approximately half the size of mature specimens, for each population respectively. The Mediterranean sampling is composed of six hatchling (3F, 3M; 9.1±0.3 cm TL), 10 juvenile (5F, 5M; 26.8±4.1 cm TL), and nine mature (5F, 4M, 42.9±2.7 cm TL) specimens while the Atlantic sampling includes 11 hatchling (6F, 5M, 11.9±1.4 cm TL), 10 juvenile (5F, 5M, 34.4±1.5 cm TL), and 10 mature (5F, 5M, 58.9±2.7 cm TL) specimens. In addition, we estimated the age of the specimens using the von Bertalanffy growth parameters for the Atlantic and Mediterranean specimens provided by Ivory et al. [2004] and Bendiab et al. [2012] because these studies provide sex-specific growth curves.

We confirmed the consistency of different growth parameters between the Atlantic and Mediterranean populations using supplementary literature data [Rodríguez-Cabello et al., 1998b; Jennings et al., 1999; Henderson and Casey, 2001; Ivory et al., 2004; Rodríguez-Cabello et al., 2005; Bendiab et al., 2012; Ozcan and Başusta, 2018] (Figure 2.10). Based on the Von Bertalanffy growth curves, we estimated the age of hatchlings to be 0 years and 0.2 years in the Mediterranean and Atlantic populations respectively. The Mediterranean juveniles are estimated to be 0.7 years old, while the Atlantic juveniles and Mediterranean matures are 3.5 years old, and the Atlantic matures are 9.6 years.

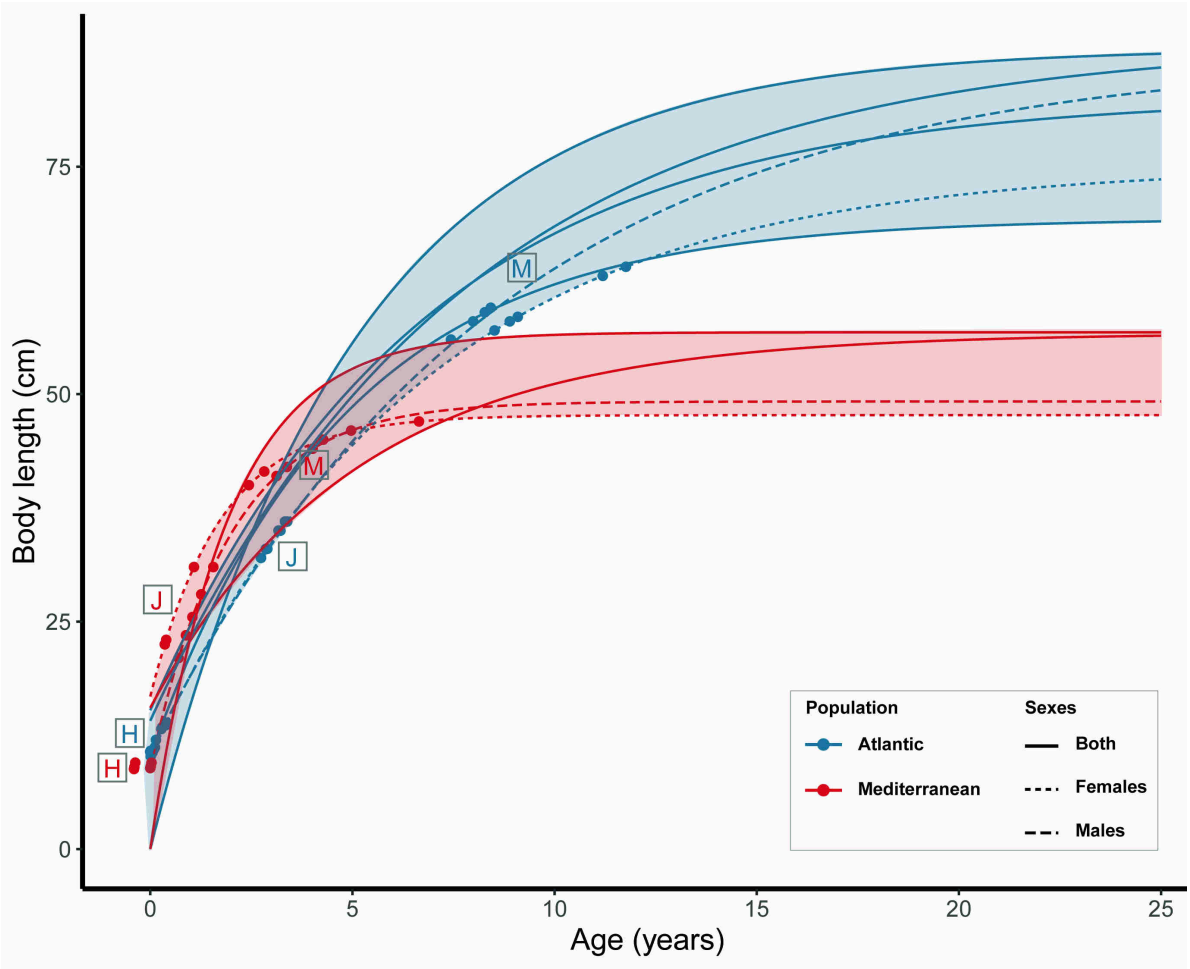

FIGURE 2.10: Growth curves of *Scyliorhinus canicula* from Northeast Atlantic Ocean and Mediterranean Sea. Von Bertalanffy growth parameters retrieved from [Rodríguez-Cabello et al., 1998b; Jennings et al., 1999; Henderson and Casey, 2001; Ivory et al., 2004; Rodríguez-Cabello et al., 2005; Bendiab et al., 2012; Ozcan and Başusta, 2018]. Dots are the specimens used in the current study. H, hatchling; J, juvenile; M, mature.

Data acquisition The jaws were microCT scanned using a Phoenix Nanotom S or an EasyTom 150 with voxel sizes ranging from 6.0 µm to 30.8 µm and 3D volumes were reconstructed using the phoenix datos x2 (v2.3.0) reconstruction or xact softwares (v.11025).

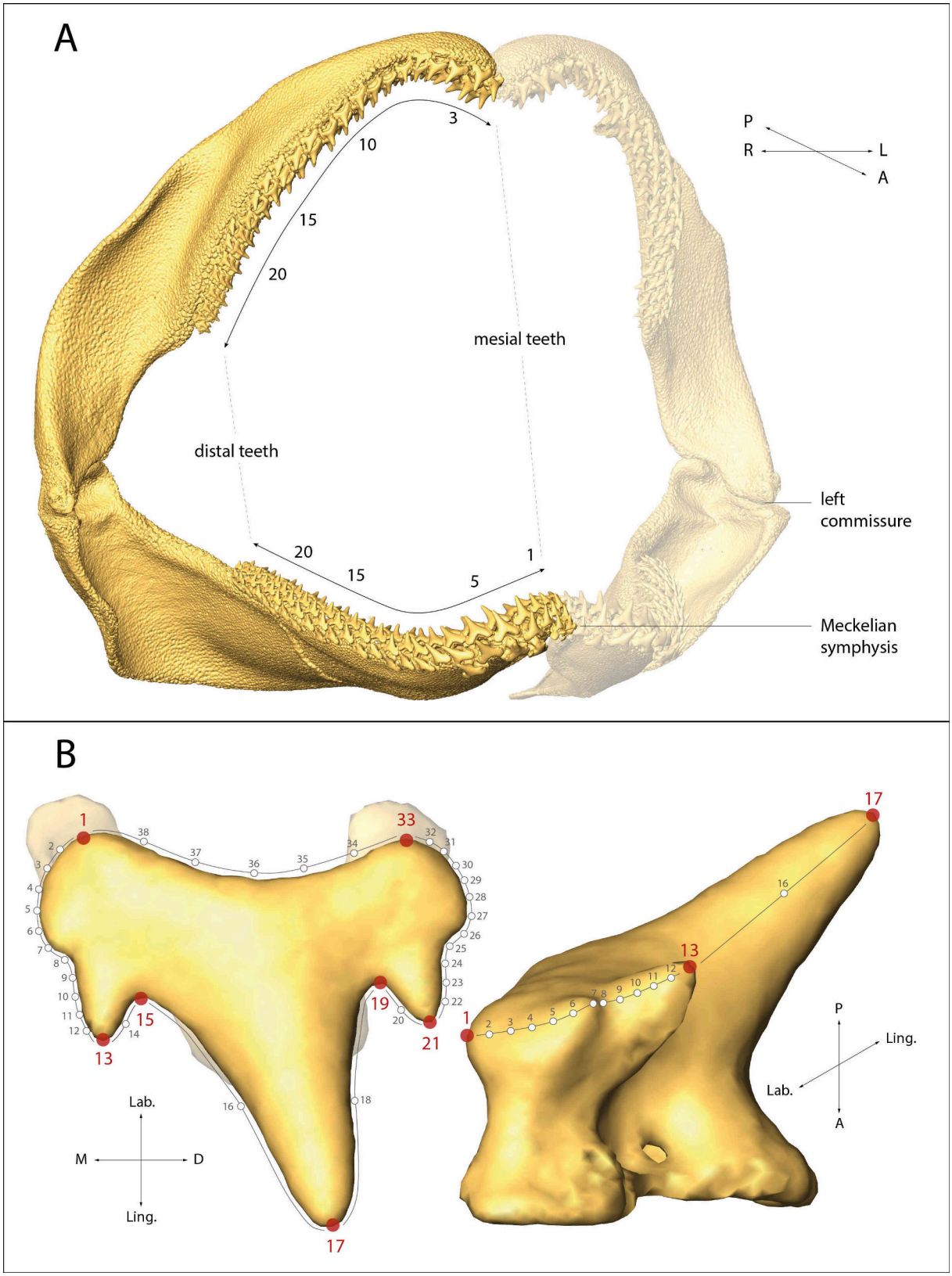

FIGURE 2.11: Labelling and landmarking of *Scyliorhinus canicula* teeth. A) Mesio-distal numbering of right palatoquadrate and Meckelian teeth in a mature male from the Atlantic population (59 cm TL); B) Right Meckelian lateral tooth of the specimen in A with numbering of landmarks (red dots) and semilandmarks (grey lines). Dorsal (left) and mesial (right) views. A, anterior; D, distal; L, left; Lab., labial; Ling., lingual; P, posterior; R, right.

3D surfaces of right palatoquadrate (upper) and Meckelian (lower) teeth were generated with AmiraZIBEdition software, extracted using the ContourTreeSegmentation module [Stalling et al., 2005], and were labelled according to their mesio-distal position along the jaw ($N_{Atlantic}$ = 1,757 and $N_{Mediterranean}$ = 1,542, Figure 2.11A). Seven landmarks (respectively numbered 1, 13, 15, 17, 19, 21, and 33 in Figure 2.11 and in section 6.2 and section 6.3) and 31 semilandmarks were placed on each 3D tooth surface and the semilandmarks were made denser on the lateral sides of the teeth, where modifications of accessory cusp number are reported during *S. canicula* ontogeny [Debiais-Thibaud et al., 2015] (Figure 2.11B and see Berio et al. [2020] for similar trend in *S. stellaris*).

Landmarks and semilandmarks were placed with the Landmark software (v3.0.0.6) [Wiley et al., 2005] and the data were preprocessed with Scyland3D (v1.1.0) [Berio and Bayle, 2020] (see section 6.1).

Data analyses A Generalized Procrustes Analysis was performed and coordinates and semilandmarks were allowed to slide based on minimised bending energy [Bookstein, 1991c]. The structure of the dataset was first investigated through PCA and centroid size patterns, and tooth centroid sizes are used as a proxy for tooth size. The centroid size is computed as the square root of the sum of squared distances between all landmarks and semilandmarks and the centroid of a form [Webster and Sheets, 2010; Klingenberg, 2016]. The slopes of allometric patterns between populations of same sex was assessed with ANalyses Of COVAriance (ANCOVAs) and the interaction between shape data and size was tested using linear regression models. The shape data used to test for allometry were PC axes, which number was determined following [Evin et al., 2013]. The relationship between shape data and size was tested using centroid size values of teeth and the specimens TL. Allometric vectors were computed with linear models and pairwise comparisons allowed to compare the lengths and angles between the vectors of populations of same sex.

Supervised classification of teeth from Atlantic and Mediterranean populations is first achieved with LDA on the same PC axes used for testing allometry and the results are compared with those obtained with Random Forests on shape (Procrustes coordinates) raw data [Breiman, 2001]. A five-fold cross-validation is performed in both methods (train set = 80 % and test set = 20 %).
In Random Forest models, the number of trees is set to 500 and the minimal node size was set to 1. Input features are (i) the tooth shapes (Procrustes coordinates), and (ii) the tooth forms (Procrustes coordinates (*i.e.* shape) + centroid size) [Klingenberg, 2016], to evaluate the contribution of the centroid size to population discrimination. The models are allowed to sample among 114 (shape) to 115 (form) variables to split each internal node. A good fit of the models is determined through the comparison between the accuracies reached on the train and test sets, and for both models (on shape and form), the difference between these metrics is 2 %. The performances of the models are evaluated with precision, accuracy, and recall metrics for the Atlantic and Mediterranean populations. Additionally, a confusion matrix of classification results for populations is detailed to identify which teeth, of males, females, and hatchling, juvenile, and mature specimens are classified the best. The feature importance for the classification is assessed with a measure of Mean Decrease Accuracy (MDA) and features with importance values >1 % are commented [Breiman, 2001].

The geometric morphometric analyses are performed using the geomorph package (v3.1.2) and supervised classification is computed using the MASS package (v7.3.53) for LDA and the randomForest package (v4.6.14) for Random Forests with R software (v3.6.1) [Liaw and Wiener, 2002; Venables and Ripley, 2002; Adams et al., 2019].

Results

Visual observations The tooth diversity presented in Figure 2.12 is a selection of examples among the whole variation observed in the dataset and provides a broad overview of the main morphological differences and associated factors in *S. canicula* tooth forms. Differences in mesio-distal location of a tooth are usually linked with an addition of accessory cusps (Figure 2.12A-B) and an increase of the main cusp bending. Gynandric heterodonty at sexually mature stage is characterised by more accessory cusps in females as compared to males (Figure 2.12C-D). Along the ontogeny, a specimen's tooth undergoes size increase, as well as the addition of accessory cusps, except after sexual maturation (Figure 2.12E-F). The interpopulational tooth form differences involve less accessory cusps and blunter teeth in the Atlantic population than in the Mediterranean population (Figure 2.12G-H).

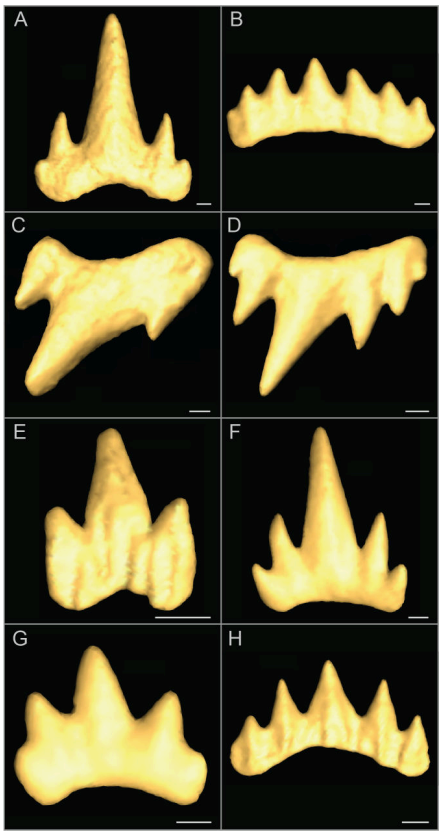

FIGURE 2.12: Examples of tooth morphological differences in *Scyliorhinus canicula*. A-B) Form differences between tooth files: teeth from file 5 (A) and 20 (B) in the Meckelian cartilage of an Atlantic mature female; C-D) Form differences between sexes: Teeth from file 15 in the palatoquadrate cartilage of Mediterranean mature male (C) and female (D); E-F) Form differences between ontogenetic stages: Teeth from file 5 in the Meckelian cartilage of Atlantic hatchling (E) and juvenile (F) males; G-H) Form differences between populations: Teeth from file 15 in the Meckelian cartilage of Atlantic (G) and Mediterranean (H) juvenile males. Scale bars are 100 µm.

We report significantly more Meckelian tooth files in Atlantic juvenile females (23 ± 2) as compared to the Mediterranean ones (20 ± 1) (permutation t test, t=3.29, p-val = 0.02), all other interpopulation tests being not statistically significant (permutation t tests, p-vals > 0.11).

Geometric morphometrics The first two principal components gather 61 % of the total variation in the dataset. The Atlantic and Mediterranean populations are not visually discriminated in the morphospace (Figure 2.13). Extreme shapes for PC1 and PC2 suggest that most variation of the dataset relates to the number of accessory cusps, to their relative size compared to the main cusp, and to the mesio-distal bending of the main cusp (Figure 2.13). In addition, shape variation along PC1 might also involve the relative width of the crown base, as compared to the main cusp height (Figure 2.13).

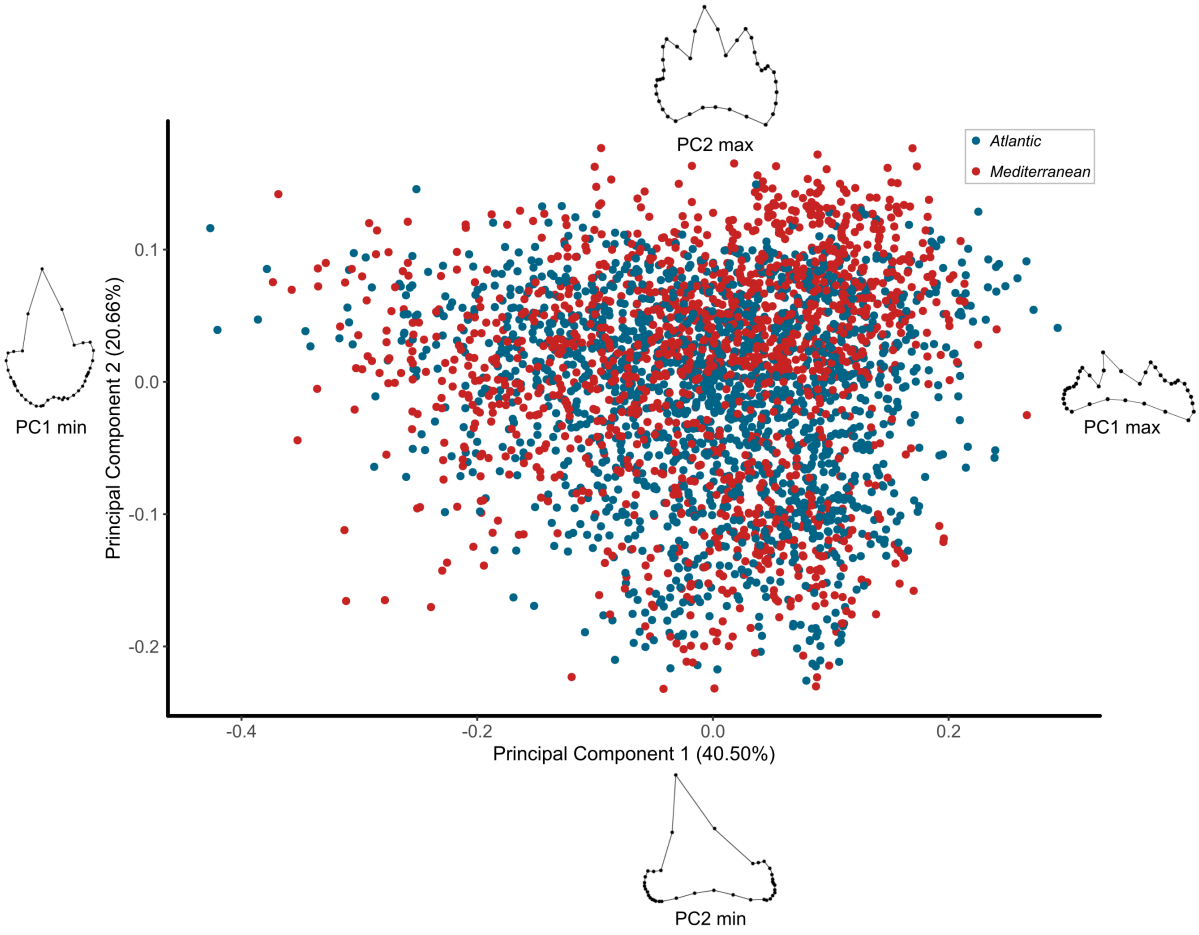

FIGURE 2.13: Morphospace with all *Scyliorhinus canicula* teeth contained in the dataset. Wireframes are the extreme shapes for PC1 and PC2.

The tooth centroid size patterns in the *S. canicula* dataset are exemplified for female Meckelian teeth (Figure 2.14) but similar trends are observed for both jaws and sexes. In hatchlings, the tooth centroid size patterns display no variation along the jaw nor visual differences between populations (Figure 2.14). The centroid size pattern of juveniles and mature specimens is unimodal along the jaw axis and bimodal in the palatoquadrate (data not shown) [Berio et al., 2020], similar to data previously shown in *S. stellaris*

[Berio et al., 2020]. The patterns overlap between juveniles of both populations, while teeth of mature Atlantic females are 35 % bigger than teeth of mature Mediterranean females (Figure 2.14). In mature specimens of both populations, the tooth centroid sizes are overall higher for the Atlantic population, whose body length is also higher as compared to Mediterranean specimens (Figure 2.10 and Figure 2.14). However, no such trend is observed for juveniles, whose differences in body length do not appear in their centroid size patterns (Figure 2.10 and Figure 2.14).

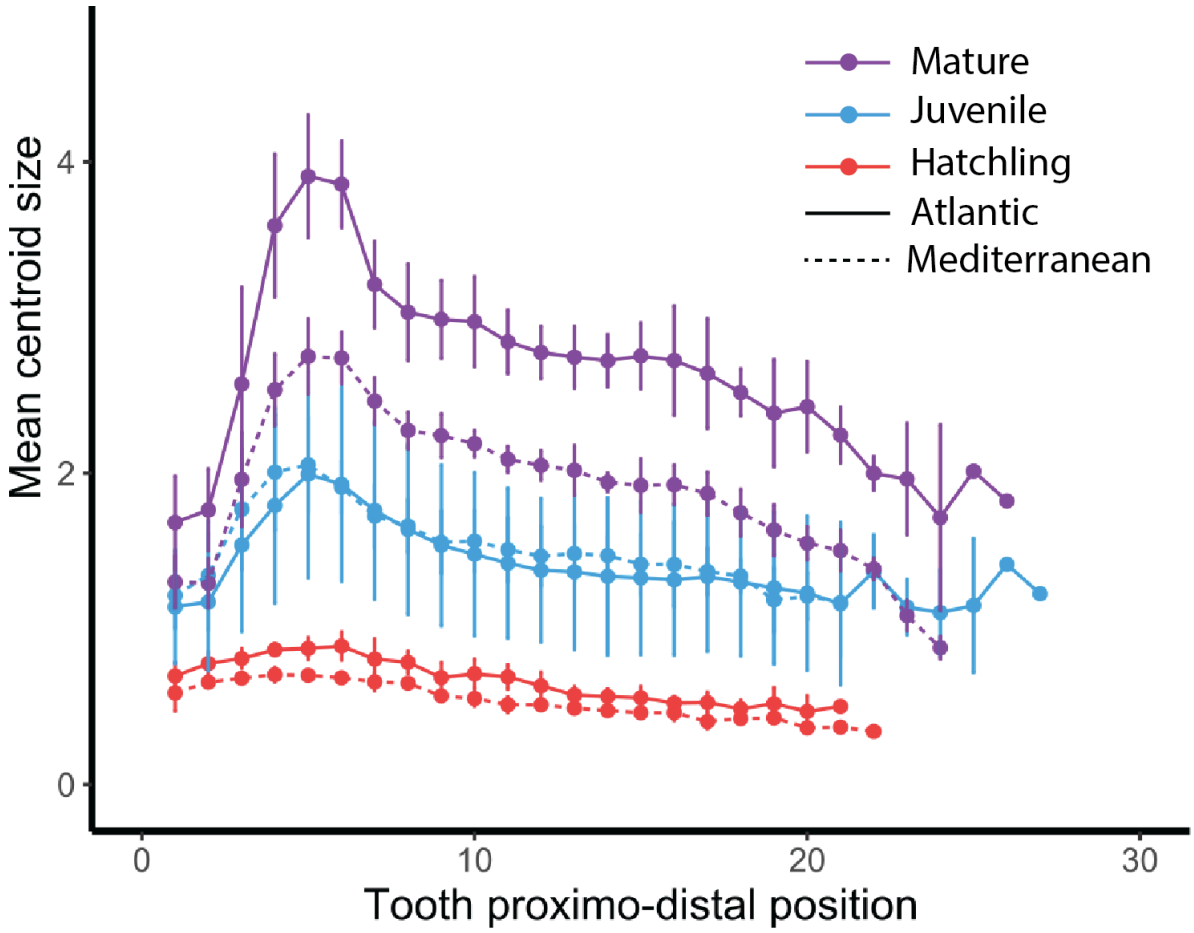

FIGURE 2.14: Tooth centroid size patterns of North Atlantic and Mediterranean populations of *Scyliorhinus canicula*: Example of female Meckelian teeth.

The first 12 PCs (93.43 %) are selected to represent the tooth shape in the following tests and are used as LDA features. The tooth centroid size and the TL of specimens significantly impact the tooth shape in all subgroups (e.g., Mediterranean x females) (One-Way MANOVAs, p-vals $< 2.20e^{-16}$), meaning for example that bigger teeth in larger specimens constrain the global shape of their teeth. The slopes of allometric patterns significantly differ between females and between males of both populations, indicating that the relation between tooth size and shape is not equivalent between populations (Two-Way ANCOVAs, p-vals $< 2.20e^{-16}$). The strength of relationship between shape and tooth centroid size is similar between females from Atlantic and Mediterranean populations (linear regressions, adjusted R-squared respectively of 0.83 and 0.81, p-vals $< 2.20e^{-16}$), as well as between Atlantic and Mediterranean males

(linear regressions, adjusted R-squared respectively of 0.86 and 0.84, p-vals $< 2.20e^{-16}$). The allometric relationship between shape and TL is also similar between Atlantic and Mediterranean populations (linear regressions, adjusted R-squared respectively of 0.73 and 0.69 in females and of 0.82 and 0.81 in males, p-vals $< 2.20e^{-16}$), which indicates that the tooth shapes are similarly modified over the ontogeny of both populations.

Supervised classification

Linear Discriminant Analysis The LDA classification reached an accuracy of 64.5 % $\pm$ 0.7 %. The precisions reached for Atlantic and Mediterranean specimens are 63.5 % and 65.7 % respectively and the recalls are 74.3 % and 53.6 %.

To get further indications of the classification performances, we detail the confusion matrix for each sex-stage subclass in the dataset (Table 2.4). We remind, however, that these values are still computed based on the population class (Atlantic and Mediterranean) only and the performances for subclasses (e.g., Atlantic female hatchling) are detailed after the classification process.

TABLE 2.4: LDA and Random Forest performances of tooth shape and form classification from Atlantic and Mediterranean *Scyliorhinus canicula* populations. Atl, Atlantic; Med., Mediterranean.

Class	LDA		Random Forests			
	Shape		Shape		Form	
	Precision	Recall	Precision	Recall	Precision	Recall
Atl. *(female hatchling)*	57.1 %	63.8 %	83.3 %	83.3 %	83.3 %	83.3 %
Atl. *(female juvenile)*	74.5 %	75.0 %	84.1 %	81.5 %	89.1 %	87.7 %
Atl. *(female mature)*	73.6 %	61.3 %	85.5 %	75.6 %	87.0 %	85.9 %
Atl. *(male hatchling)*	49.3 %	59.6 %	79.3 %	76.7 %	82.8 %	80.0 %
Atl. *(male juvenile)*	78.4 %	79.0 %	87.5 %	92.1 %	93.2 %	89.5 %
Atl. *(male mature)*	50.9 %	92.2 %	76.6 %	94.4 %	86.5 %	100 %
Med. *(female hatchling)*	41.9 %	35.3 %	70.6 %	70.6 %	70.6 %	70.6 %
Med. *(female juvenile)*	65.7 %	65.1 %	76.5 %	79.6 %	84.0 %	85.7 %
Med. *(female mature)*	72.8 %	82.4 %	77.9 %	87.0 %	85.9 %	87.0 %
Med. *(male hatchling)*	45.2 %	35.2 %	63.2 %	66.7 %	68.4 %	72.2 %
Med. *(male juvenile)*	71.7 %	71.0 %	89.8 %	84.1 %	87.9 %	92.1 %
Med. *(male mature)*	57.1 %	10.5 %	88.9 %	60.7 %	100 %	78.8 %

The lesser performances are achieved in teeth of hatchlings of both sexes and mature males, in which the less complex tooth shapes are visually identified. Atlantic specimens are overall better classified than Mediterranean ones (Table 2.4), which might be a consequence of teeth from Atlantic mature specimens potentially exhibiting specific extreme shapes due to extreme tooth size. Within females, the precision is higher for the Atlantic population (Table 2.4). This means that, among all specimens classified as Atlantic, the number of real Atlantic specimens is higher than the number of Mediterranean specimens found in the Mediterranean class. The recall for Mediterranean mature females is higher than the recall in the Atlantic population. This means that, as compared to the total number of actual Mediterranean specimens, more Mediterranean specimens

have been correctly assigned to their class than have been the Atlantic specimens (Table 2.4). The recall is interpreted as the number of specimens correctly assigned to a class, as compared to the total number of specimens actually belonging to this class. As for females, Atlantic juvenile males are better classified than Mediterranean juvenile males and within mature males, the precision reached is higher in the Mediterranean population but the recall is much higher in Atlantic mature males (Table 2.4).

Random Forests The classification task performed by the Random Forests reaches accuracies of 81.7 % $\pm$ 1.1 % for tooth shapes and 87.4 % $\pm$ 1.7 % for tooth forms, indicating a significant contribution of the centroid size information at improving the discrimination between populations. This means using the same methodology on any *S. canicula* tooth from the Mediterranean or Atlantic population determines the correct population with 85.7 % to 89.1 % accuracy. The precisions reached for Atlantic and Mediterranean specimens with tooth shapes are 82.5 % and 80.5 % respectively. Among Atlantic specimens, 85.4 % are correctly detected as such with shape data, while this recall for the Mediterranean population is 76.9 %. With features of form as compared to shapes only, the precision for the Atlantic and Mediterranean populations are 87.8 % (+6.4 %) and 86.5 % (+7.5 %) respectively, and the recalls are 89.7 % (+5.0 %) for the Atlantic specimens and 84.1 % (+9.4 %) for Mediterranean specimens.

The classification usually reaches lesser performance values for the hatchling subclasses than for the juvenile and mature ones (Table 2.4). Moreover, the models (for tooth shape and tooth form) achieve better classification of Atlantic than Mediterranean hatchlings, and reach higher precision and recall for hatchling females than for males in both populations (except for the recall of Mediterranean hatchling males with form data, Table 2.4). Among juveniles, the metrics are better for Atlantic females than Mediterranean females, whereas more contrasting values are reported for males, the precision being higher with shape data in the Mediterranean population than in the Atlantic one, while the recall is better for the Atlantic population, and conversely with form data (Table 2.4). The classification also performs better for males than for females in both populations (Table 2.4). In the mature subclass, the precision values are higher in Atlantic than Mediterranean females, while the opposite is true for the recall values (Table 2.4). As opposed to females, the classification reaches better precision values for Mediterranean than for Atlantic males, and better recall in Atlantic as compared to Mediterranean specimens (Table 2.4).

In most subclasses, the contribution of centroid size enhances the classification results. However, exceptions to this trend are the hatchling females of both populations, for which there is no impact of the centroid size on the classification performances, as compared to those based on shape data (83.3 % and 70.6 % in the Atlantic and Mediterranean populations respectively, Table 2.4), and the Mediterranean mature females whose recall also remains unchanged after the centroid size is included in the dataset (87.0 %, Table 2.4). Among the subclasses of juveniles, the impact of centroid size can lead to lesser performances, as for the recall of Atlantic males (-2.8 %), and the precision of Mediterranean males (-2.1 %) (Table 2.4). Except for the abovementioned recall of Mediterranean mature females, the classification performances of mature specimens is always enhanced when the centroid size is included: the recall for Atlantic mature males for example reaches 100 % (+5.6 %), and the precision for Mediterranean mature males is also 100 % (+12.5 %) based on form data (Table 2.4).

With shape data, the most important feature lies in the semilandmark 11 (5.2 % in x), followed by landmark 13 (1.9 % in y), landmark 1 (1.5 % in y), semilandmark 12 (1.4 % in x), semilandmark 24 (1.7 % in y and 1.1 % in x), and semilandmarks 23 and landmarks 15 and 19 (respectively 1.1 % in y, 1.1 % in z, and 1.0 % in x) (Additional section 6.2). With form data, however, the feature that contributes the most to the classification is the centroid size (12.3 %). The following most important features with form data are the semilandmark 11 (5.5 % in x and 1.7 % in y), the semilandmark 24 (2.3 % in x), the landmark 19 (1.7 % in y), the semilandmark 23 (1.7 % in x), the semilandmark 12 (1.3 % in y), and the landmark 1 (1.2 % in y) (section 6.3).

Discussion

Visual observations and GM struggle discriminating between populations This work highlights that inter-population tooth differences lie in the lateral cusps. We first visually examined *S. canicula* teeth from both populations and, except in hatchlings, the teeth in the Mediterranean population appear sharper than in the Atlantic at all locations and display more accessory cusps for equivalent mesio-distal positions of teeth.

On centroid size patterns, very few elements discriminate between the two populations: hatchling and juvenile of both populations display very similar tooth centroid size patterns and amplitude along the jaw. The main difference between populations arises between the juvenile and mature stages because mature Atlantic specimens have teeth whose centroid size is about 35 % higher than those of mature Mediterranean *S. canicula*. The similarities between the Atlantic and Mediterranean hatchling tooth centroid size patterns are consistent with their very close estimated age and TL (Figure 2.10). In mature specimens also, the amplitude delta in tooth centroid size patterns can be easily interpreted in light of their TL and age differences (Figure 2.10). Yet, the age estimations we provide remain approximative because we chose among several available growth parameters on *S. canicula*. The similar amplitude of tooth centroid size patterns between juveniles of both populations could also be a consequence of our specimens and of their very close ranges of size (Figure 2.10). Regarding allometric patterns, differences in slopes were detected between populations, meaning that the difference in growth rate between teeth and body size is not the same between the Atlantic and Mediterranean populations considered.

In summary, the reported differences between the populations' tooth centroid size patterns seem to relate to the TL of mature specimens but they do not discriminate within hatchling and juvenile teeth of both populations.

The contribution of Random Forest to decipher inter-population differences Machine learning models have already improved the understanding of subtle structures in geometric morphometric data [Lorenz et al., 2015; Soda et al., 2017; Doyle et al., 2018; Courtenay et al., 2019; Quenu et al., 2020], especially when the shapes between groups share common quadrants in a morphospace, as it is the case for the *S. canicula* populations considered in this study. Furthermore, even though the algorithms perform well at classifying geometric morphometric data, the choices made by these models to make groups are usually unknown and deprived of biological meaning [Lorenz et al., 2015; Quenu et al., 2020].

We aimed at comparing the classification performances achieved by the traditional geometric morphometrics workflow, which is achieved by a LDA on the main PC axes, with the classification performances obtained with Random Forests on raw shape data. Doyle et al. [2018] already compared the classification performances of LDA and Random Forests on the shells of populations of common periwinkles (*Littorina littorea*) distributed in different niches. They recommend the use of Random Forests over LDA because the former is more straightforward and robust, does not make assumptions about the data nor necessitate the user to check the violation of LDA assumptions [Doyle et al., 2018]. However, the models of Doyle et al. [2018] do overfit and the results obtained might not be optimal.

With our dataset, the global accuracy, precisions, and recalls reach higher values with Random Forests than LDA (respectively around +21 %, +22 %, and +22 %), which can be due to information loss following the necessary data reduction prior to LDA, as opposed to Random Forests. We used LDA for classification as in the majority of geometric morphometric articles, e.g. without considering the data distribution nor the homogeneity of variance. That such criteria for optimality are not met does not prevent from performing a LDA. The LDA algorithm is robust to such violations and still achieves good performances when assumptions of normality and common covariance matrix among groups are not met [Lachenbruch and Goldstein, 1979; Li et al., 2006]. Furthermore, Doyle et al. [2018] showed similar performances between LDA and Random Forests on geometric morphometric data and conclude that LDA is robust enough to the abovementioned violated conditions to achieve good classification performances Doyle et al. [2018].

The contribution of Random Forests models to our work is four-fold: needing less preprocessing steps than LDA, performing better than LDA at the classification task, achieving good performances at classifying teeth from two *S. canicula* populations based on raw data, and determining the most discriminant features to perform this task. Among landmark and semilandmark features, it is clear that the most discriminant information is contained in two dimensions (x and y), whereas the third dimension brings less information. This implies that running the models with 2D landmark data would have probably achieved similar classification performances as those obtained here, as this has also been evidenced in some traditional geometric morphometric studies [Cardini, 2014; Buser et al., 2018; Wasiljew et al., 2020]. Nevertheless, 3D landmarking avoids parallax biases [Cardini, 2014] and none of the landmarks and semilandmarks did cause a decrease of the metrics, indicating that, even though the z dimension contains little information, this still cannot be considered as noise. Furthermore, the landmarks (1, 15, 19) and semilandmarks (11, 12, 23, 24) contributing the most to the classification are located at geometrical extrema, at extreme mesial and distal locations of the teeth and on the lateral edges, where the accessory cusps emerge. It is also likely that the spacing of these points makes them useful to the algorithm and that spatially close points would bring less information. Overall, the results show that a few points, especially on the lateral sides of the teeth, provide enough information to represent most differences between the tooth shapes of the *S. canicula* populations considered in this work, and this is consistent with our visual observations on the variation of accessory cusps number.

The use of form features instead of shape only greatly improves the overall classification. While we expected such impact in the classification of mature specimens due

to their amplitude differences of centroid size patterns (likely caused by TL, and putative age discrepancies, Figure 2.10), the reason for the significant contribution of tooth centroid size to the classification improvement of the teeth of juveniles and hatchlings is less intuitive. We first assume that the very slight differences in tooth centroid size patterns we visually interpret as part of the inter-populational variability might actually be considered useful information for the model to discriminate between populations. The centroid size is theoretically independent of shape, however, the placement and density of landmarks and semilandmarks modify the contribution of certain parts of a tooth (e.g., the lateral sides of the crown as compared to the main cusp) to the centroid size value. We thus assume that slight changes in centroid size values between populations might also convey relevant shape information for the Random Forest model, which is cryptic to the observer. For a minority of subclasses, however, the addition of centroid size to shape features does not improve the classification performances or even diminish them in rare cases. In the first case, the centroid size is probably too similar between the two hatchling subgroups to allow the model to discriminate against the populations. In the second case, the centroid size information confuses the model and this might indicate that these form data contain more noise than in other groups, which could be overcome by increasing the sampling effort for such groups.

Ecological origins of anatomical divergence between populations The inter- and intraspecific diversity of shark tooth shapes correlates with their feeding behaviour, molariform teeth for example help crushing hard-bodied preys, while cutting teeth allow to remove pieces from larger items [Cappetta, 1986]. *S. canicula* is considered a generalist predator with opportunistic behaviour, whose favourite preys are teleosts, cephalopods, and crustaceans but it also occasionally feeds on macroalgae and echinoderms [Olaso, 1998; Mnasri et al., 2012; Kousteni et al., 2017]. Within the same population, however, slight differences in diet composition can occur between specimens of different sex and ontogenetic stages [Lyle, 1983; Olaso, 1998; Rodríguez-Cabello et al., 2007; Mnasri et al., 2012; Kousteni et al., 2017]. *S. canicula* displays seasonal diet shifts that differ according to the geographic area: more cephalopods are eaten in the winter than in autumn by a Cantabrian Sea (North Atlantic Ocean) population, while a population from eastern Mediterranean Sea feeds most on teleosts in spring and on molluscs in autumn [Olaso, 1998; Kousteni et al., 2017]. Molluscs are far less important in the diet composition of Atlantic populations than in Mediterranean ones, whereas Atlantic specimens feed more on teleosts [Kousteni et al., 2017]. However, the diet differences between several Atlantic and Mediterranean *S. canicula* populations are probably due to the variability of available prey items in contrasted habitats, as suggested by the opportunistic behaviour of this species [Lyle, 1983; Kousteni et al., 2017]. Additionally, we show in this work that *S. canicula* tooth shapes differ between one Atlantic and one Mediterreanean populations. Then, we can hypothesize that diet differences between populations correlate with their distinct tooth forms: sharper teeth of the Mediterranean population may enhance grasping molluscs such as cephalopods, whereas teeth of Atlantic specimens might perform better at catching benthic teleosts. However, the specific diet of the specimens sampled in this study is not known and the relationship between the tooth morphologies depicted here and broad dietary trends in all Atlantic and Mediterranean *S. canicula* remains hypothetical. Overall, several studies already suggested that diet composition of *S. canicula*, as well as of other elasmobranchs, is

correlated to the length of the specimen, rather than to other factors [Lyle, 1983; Bethea et al., 2006; Ellis and Musick, 2007; Borrell et al., 2011; Šantić, M and RaĐa, B and Pallaoro, A, 2012]. Furthermore, we show that tooth shape variation and total body length of *S. canicula* are related, which could suggest that there is an association between diet shifts and tooth shape modifications over a specimen lifetime.

S. canicula has a philopatric behaviour and most specimens do not move further than 30 km over the years [Rodríguez-Cabello et al., 2004]. Additionnally, shared haplotypes between specimens caught off Portugal and specimens from the Mediterranean Sea demonstrate past communication occurrences between the populations, probably resulting from colonisation events from the Atlantic or retention of ancestral polymorphism [Kousteni et al., 2015; Ramírez-Amaro et al., 2018]. High gene flow between Eastern and Western Mediterranean basins has been evidenced, whereas the gene flow between the Atlantic and Mediterranean populations of *S. canicula* is currently very low [Barbieri et al., 2014]. The communication between these Atlantic and Mediterranean populations would indeed only be permitted through the Strait of Gibraltar, yet the hydrographic fronts and bottom topography limit the migration between populations to a few specimens. That tooth morphologies differ between one Atlantic and one Mediterranean *S. canicula* populations is thus consistent with the genetic differentiation between the Atlantic and Mediterranean stocks [Barbieri et al., 2014].

Contributors

The people who also contributed to this work are Yann Bayle, Daniel Baum, Nicolas Goudemand, and Mélanie Debiais-Thibaud.

Conclusions of the article

We combined a geometric morphometric and a machine learning approach to discriminate between teeth of two shark populations. The traditional framework used in geometric morphometrics reached lesser performances at distinguishing the tooth shapes of *S. canicula* specimens from an Atlantic and a Mediterranean localities. However, these shape data combined with centroid sizes allow our proposed Random Forest model to classify the *S. canicula* teeth with up to 100 % precision. This framework should be further tested in more *S. canicula* populations, especially within the Mediterranean Sea, to decipher tooth morphological differences between spatially and genetically closely-related populations. We hope this emergent framework to be further tuned by ichthyologists by including geographical parameters and life history traits to discriminate between subtle shark tooth morphologies and to provide a basis for facilitating the identification procedures of shark stocks and improving fisheries management.

Conclusions of the project

In this work, we show that the Random Forest model on tooth shape data achieves about 21 % better at classifying the teeth from the *S. canicula* populations considered than the LDA. Furthermore, the use of form data instead of shape only increases the classification performances of about 7 %. The Random Forest models provide insights into the most discriminant, biologically interpretable features between the teeth of both populations, which are the tooth centroid size, and the semilandmarks on the lateral

sides of the teeth, where accessory tooth cusps develop. The same framework as used in this study has, to our knowledge, already been tested once on shells of populations of common periwinkles (*Littorina littorea*) but the models did largely overfit [Doyle et al., 2018], which is not the case in our work. We propose a proof of concept that evidences the advantages of using Random Forests models instead of the systematically used LDA in GM analyses to classify shark teeth. The interpopulation differences that are highlighted might arise from genetic differences rather than trophic habits but further tests remain to be performed to challenge this hypothesis.

2.3 Vast (un)known tooth morphospaces and implications

The teeth of extant elasmobranch species are regularly shed in the environment, depending mostly on the season (and water temperature) that impacts the feeding activity and growth rate [Wass, 1973; Luer et al., 1990]. Tooth replacement occurs from several days per tooth row (e.g., in the dusky smooth-hound *Mustelus canis* and in the lemon shark *Negaprion brevirostris*) to several weeks (e.g., in *S. canicula* and in the horn shark *Heterodontus francisci*) [Ifft and Zinn, 1948; Applegate, 1967; Moss, 1967; Märkel and Laubier, 1969; Luer et al., 1990]. Moreover, because enameloid and dentine are very hard to decay —as opposed to calcified cartilage—, most fossil remains of elasmobranchs are teeth [Shimada, 2005b; Pollerspöck and Straube, 2019]. The identification of isolated teeth is thus largely based on characters such as the location, number and size of root foramina, the presence and extension of cutting edges on the crown, the occurrence of accessory cusps, and homodonty and heterodonty patterns [Herman et al., 1989, 1990; Cappetta, 2012; Pollerspöck and Straube, 2019]. The latter are, however, difficult to evaluate, especially in the fossil record when complete tooth sets are most often lacking. Also, shark tooth sets contain different information, depending for example on whether the teeth belong to the same specimen or to several specimens of the same species [Shimada, 2005b]. Attempts to reconstruct dentitions of fossil sharks have been made but the results are criticized since they might be largely based on teeth from different specimens and are "artificial" and not repeatable [Shimada, 2005b]. If the reliability of such reconstructions is questionable [Shimada, 2005b], they still provide insights into the dental set characteristics of the earliest sharks (e.g., into putative heterodonty patterns like those in modern Lamniformes) to the condition they have been elaborated based on "an adequate sample size and a reasonable modern analog" [Welton and Farish, 1993, p.17]. And here is a main limitation for paleoichtyologists: details are lacking on the dental morphologies of extant elasmobranchs to base their reconstructions on, identify species, and infer phylogenies [Guinot et al., 2018]. So far, there are several occurrences of shark species that have been finally assimilated to a same species because the putative inter-specific tooth differences were in fact morphological variations due to ontogeny. Extant night sharks *Hypoprion bigelowi* are for example now reassigned to *Carcharhinus signatus* [Raschi et al., 1982] and the gulper sharks *Centrophorus acus* and *C. niaukang* are now considered junior synonyms of *C. granulosus* [White et al., 2013].

These taxonomic revisions of extant shark species are isolated cases but it might be because, as stated by Moyer and Bemis [2016], "There has been little comprehensive study of ontogenetic changes in dentition in the vast majority of elasmobranch species". The neoselachian classification is not only impacted by the underestimated morphological variation of teeth within a single shark species but also by insufficient knowledge

on interspecific differences. Purdy and Francis [2007] pointed out the "morass of fossil taxa and the propagation of evolutionary scenarios" resulting from "paleontologists who have studied fossil shark teeth [that] have failed to investigate the morphological variations in the teeth of Recent sharks. They [paleontologists] have named numerous species and genera ignorant of this variation [...]".

Chapter 3
Tooth development, a molecular view

3.1 Dental development

3.1.1 "Give me neural crest cells, I'll make an odontode"

The evolution of vertebrates is intricately indebted to the neural crest [Hall, 2001]. NCCs derived from ectoderm are assumed to have allowed the emergence of, among others, a pharyngeal musculature that was little developed in urochordates and cephalochordates, and to have facilitated an active predatory behaviour [Gans and Northcutt, 1983]. The NCCs also participate to form the central and peripheral nervous systems, as well as the endo- and exoskeletons (Figure 3.1) [Le Douarin et al., 2004]. Because it gives rise to more cellular types than mesoderm, neural crest has been suggested to be the fourth germ layer unique to vertebrates, distinct from the ectodermal, endodermal (diploblastic organisms), and mesodermal (tribloblastic organisms) germ layers (Figure 3.1) [Hall, 2001; Vickaryous and Hall, 2006; Hall and Gillis, 2013; Le Douarin and Dupin, 2018].

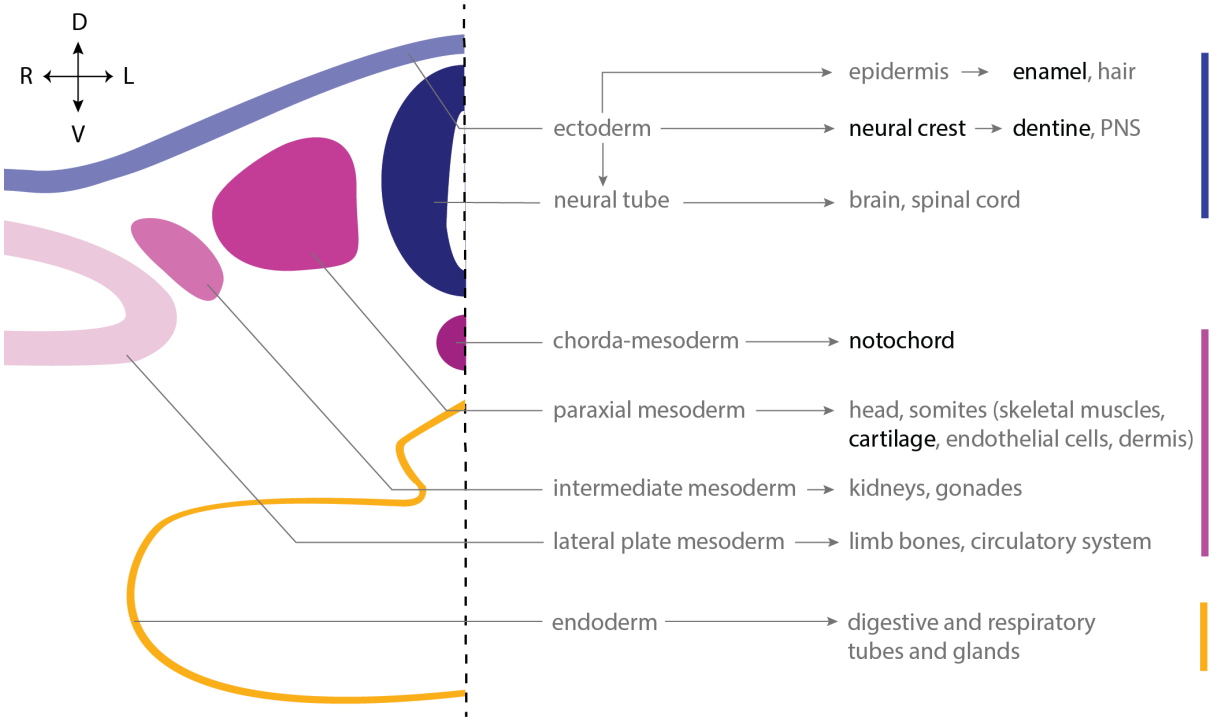

FIGURE 3.1: Embryonic tissues and their fate in an amniote embryo. The tissues of interest in my PhD are in bold. PNS, peripheral nervous system; D, dorsal; L, left; R, right; V, ventral.

NCCs are multipotent cells and form antero-posteriorly during neurulation. During neurulation, the neural plate of ectodermal origin elongates and starts to fold until the neural folds converge and adhere one to the other to form the neural tube [Gilbert and Barresi, 2016]. Once the neural tube is closed, the neural fold apex cells delaminate to form NCCs (this is true for chick embryos; in mouse embryos delamination starts before neural tube closure) [Miletich and Sharpe, 2004; Mayor and Theveneau, 2012; Gilbert and Barresi, 2016]. During this process, the cells undergo an epithelium-to-mesenchyme transition during which the columnar cells undergo modifications of cell-cell junctions and acquire both motility and multiple polarity [Müller, 2006; Mayor and Theveneau, 2012; Hall and Gillis, 2013; Gilbert and Barresi, 2016]. At this stage, the cells spread into the whole embryo, following molecular and physical pathways, and differentiate in a broad diversity of cell types (e.g., fibroblasts, melanocytes, myocytes, endocrine cells, neurones and for some populations, osteocytes, and chondrocytes) [Graveson, 1993; Donoghue et al., 2008; Mayor and Theveneau, 2012; Hall and Gillis, 2013]. The NCCs are subdivided into several populations along the body antero-posterior axis [Mayor and Theveneau, 2012; Gilbert and Barresi, 2016]. In the following, we focus on the cephalic and trunk NCCs because of their role in tooth and odontode development.

The teeth and odontodes of extant species are partly composed of dentinous tissue, as was the dermal skeleton of early gnathostomes (see subsection 1.1.1). Tooth dentine is secreted by odontoblasts that are derived from cephalic NCCs [Chai et al., 2000]. The neural crest likely formed ectomesenchymal cells in stem vertebrates, giving rise to most facial cartilages and bones and to the dentinous tissue composing the postcranial dermal armour [Meulemans and Bronner-Fraser, 2002; Donoghue et al., 2008]. This dermal armour was, however, progressively reduced during gnathostome evolution and restricted to isolated plates in sparse groups of organisms, and to teeth [Quan et al., 2018]. The cephalic NCCs kept this skeletogenic potential because they give rise to the osteoblasts producing most cranial endochondral bones (although some of them are derived from head paraxial mesoderm), and to the odontoblasts producing tooth dentine (Figure 3.1) [Miletich and Sharpe, 2004; Gilbert and Barresi, 2016]. As opposed to cephalic NCCs, trunk NCCs are generally regarded as nonskeletogenic because the cells involved in the development of postcranial amniote endoskeleton (e.g., chondroblasts and osteoblasts) are derived from paraxial mesoderm (Figure 3.1) [Shimada et al., 2013; Gillis et al., 2017]. In teleost fishes also, the trunk NCCs has no ability no produce scale and fin ray osteoblasts, which in turn derive from paraxial mesoderm [Lee et al., 2013; Shimada et al., 2013]. However, given the ancestral contribution of NCCs to dentine synthesis, a latent skeletogenic potential of trunk NCCs was still suspected, notably in extant chondrichthyans [Lee et al., 2013; Green et al., 2015; Gillis et al., 2017]. Based on these data, the postcranial dentine in extant chondrichthyans could have a neural crest origin or could be produced by another embryonic germ layer which had been transferred an ancestral odontogenetic competence.

The retention of skeletogenic potential by trunk NCCs has been first proved during the development of the endoskeleton in osteichthyans. The mesenchymal precursors of medial fins and caudal fin lepidotrichial rays in the zebrafish *Danio rerio* originate from NCCs [Smith et al., 1994]. Moreover, grafts of quail trunk NCCs in the head of chick embryos contributed to form skeletal elements such as eye scleral and Meckel's cartilages, indicating that a skeletogenic potential still characterises the trunk NCCs of extant tetrapods [McGonnell and Graham, 2002].

Two main hypotheses were proposed to explain the embryonic origin of dentine in the chondrichthyan odontodes. A first hypothesis states that during early development, cephalic NCCs migrate to postcranial parts of the embryo and differentiate into odontoblasts, while according to a second hypothesis, trunk NCCs retain a vestigial odontogenic competence and can differentiate into odontoblasts [Smith and Hall, 1990; McGonnell and Graham, 2002]. Gillis et al. [2017] questionned the embryonic origin of odontoblasts involved in the dentine production of postcranial odontodes in the little skate (*Leucoraja erinacea*). They used cell tracking and *in situ* hybridisations to detect migrating trunk NCCs through the postcranial exoskeleton and locate the expression of *FoxD3*, which characterises emergent and early migrating NCCs [Sasai et al., 2001; Stewart et al., 2006; Gillis et al., 2017]. They conclude about a neural crest origin of some odontoblasts, confirming the long suspected vestigial skeletogenic ability of trunk NCCs in non-tetrapod vertebrates also [Gillis et al., 2017].

To conclude, it has been suggested that non-skeletogenic potential of trunk NCCs in extant vertebrates may be less a inherent cell property than a lack of inductive environment [Smith and Hall, 1990; Graveson, 1993; McGonnell and Graham, 2002; Miletich and Sharpe, 2004; Green et al., 2015]. Furthermore, the ability of NCCs to give rise to ectomesenchyme and to chondroblasts, osteoblasts, and odontoblasts is inherited from the dermal armour of bone and dentine of stem gnathostomes [Donoghue et al., 2008; Green et al., 2015]. The trunk NCCs competence of producing exoskeletons might have been lost during the vertebrate evolution, except in several groups including chondrichthyans [McGonnell and Graham, 2002].

From mammals to sharks

Studies on tooth development and dentition patterning have long been mammal-centered and most current developmental studies focus on human or rodent teeth [Hulsey et al., 2020]. One advantage of this tradition is that of providing strong baseline about tooth morphological characterisation, as well as putative features (molecular and physical) influencing tooth form. On the other hand, it is tempting —and actually a common practice— to apply knowledge about mammalian tooth development to many other clades, until the point we forget that "Mammals are atypical vertebrates in many ways" [Butler, 1995] and that they display specific and highly derived characteristics whose developmental patterns should be considered as such. The tooth replacement and morphologies in mammals are for example highly derived and does not represent the ancestral character of tetrapods [Ungar and Sues, 2019].

The development from NCCs to an erupted tooth has been especially well described in mammals. In mouse, a population of cephalic neural crest-derived cells first migrate to form the caudal midbrain and rostral hindbrain [Chai et al., 2000; Miletich and Sharpe, 2004]. Part of this population then colonises the first pharyngeal arch, becomes ectomesenchyme under Fgfs signalling, and gets tightly associated with the ectoderm above, which is a prerequisite to any placode formation [Chai et al., 2000; Miletich and Sharpe, 2004; Som and Miletich, 2018]. During bud stage (see section 3.2 for details on this stage), the condensing mesenchyme exhibits a high proportion of neural crest-derived cells, as opposed to the inner enamel epithelium and oral ectoderm [Chai et al., 2000]. As tooth morphogenesis continues, mesenchymal derivatives form (e.g., dental

papilla, dental sac, and pre-odontoblasts) but cells of non neural crest origin are also included [Chai et al., 2000].

Besides, the tooth development also runs through a decisive interplay between gene expressions that promote cell division (e.g., *Sonic Hedgehog* (*Shh*) and the *Fibroblast Growth Factors* (*Fgf*s)) and cell differentiation (e.g., *Bone Morphogenetic Protein 4* (*Bmp4*)) [Thesleff and Sharpe, 1997]. The development of a mouse molar starts with the dental epithelium thickening at locations termed placodes and this epithelium, termed dental lamina, expresses *Bmp*s, *Fgf*s, *Shh*, and *Wnt* until bud stage [Thesleff and Sharpe, 1997] (Figure 3.2).

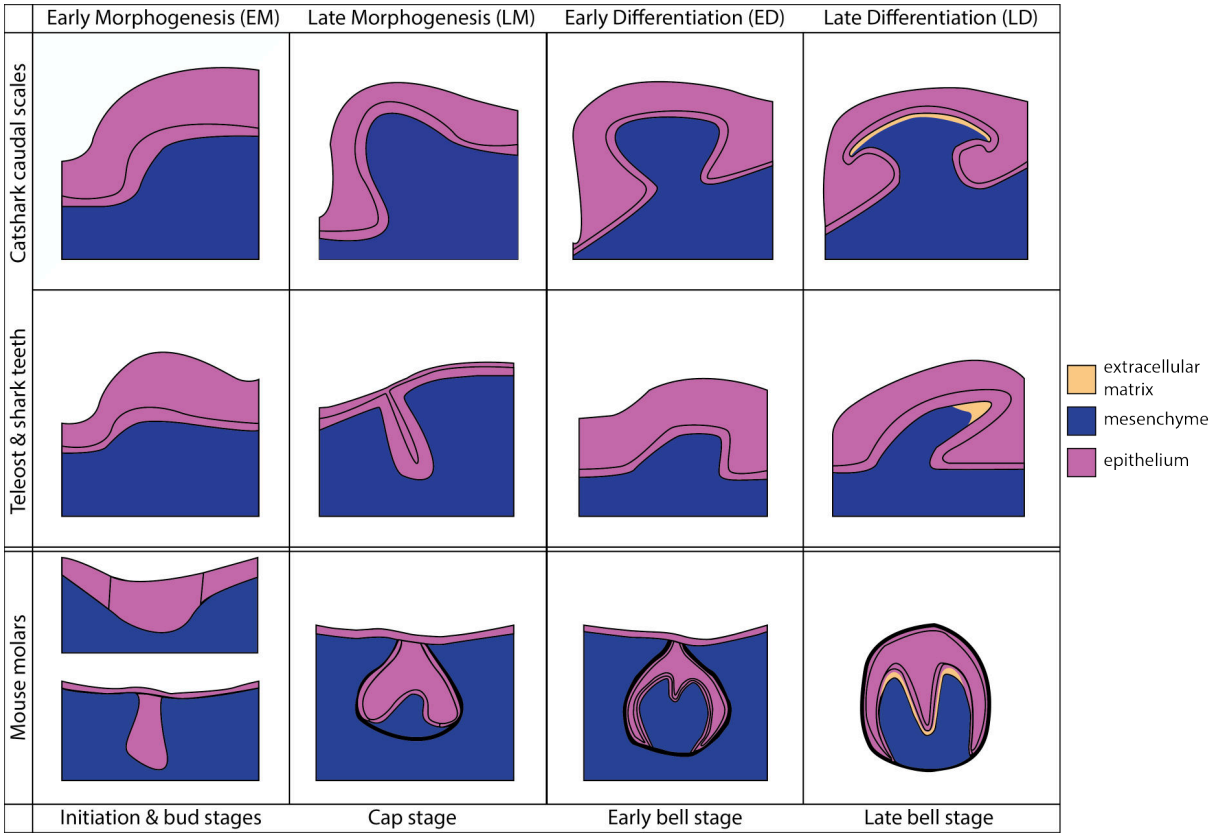

FIGURE 3.2: Simplified four equivalent developmental stages of tooth and tooth-like structures in the catshark *Scyliorhinus canicula*, in teleosts, and in the house mouse *Mus musculus*. Modified after Berio and Debiais-Thibaud [2019].

During this stage, the underlying mesenchyme promotes cellular proliferation of mesenchymal cells through the expression of *Msx* genes, whereas the expression of *Bmp*s triggers the transition to cap stage [Thesleff and Sharpe, 1997]. The primary Enamel Knot (EK) signalling centre is defined during the cap stage and expresses factors that stimulate both cell proliferation and differentiation, however, no cell division is reported in the EK, which is later characterised by apoptosis signals [Jernvall et al., 1994; Thesleff and Sharpe, 1997]. Secondary EKs then develop and shape the cusps and valleys of the molar.

The mammalian tooth identity (incisor, canine, premolar, and molar) is determined through ectodermal signals involving specific pathways [Jernvall and Thesleff, 2000]. The inhibition of Bmp4 in developing mice incisors allows the expression of *Barx-1*, which contributes to acquire a molar tooth bud morphology [Tucker et al., 1998]. Also,

differences in *Dlx5* and *Dlx6* expressions distinctly shape the upper and lower mouse molars [Qiu et al., 1997; Thomas et al., 1997].

Although shark tooth development has been far less studied than in mammals, developmental and evolutionary results are of key importance and deserve to be highlighted. First, the regulatory pathways involved in *S. canicula* tooth development are homologous to those described in mouse [Debiais-Thibaud et al., 2015], which predates these pathways to the emergence of gnathostomes. Second, there is no EK in sharks since the proliferation and differentiation inducers are not expressed in the same signalling centre, which is in conflict with the definition of the mammalian EK [Debiais-Thibaud et al., 2015]. Nevertheless, since homologous signalling factors are involved into shark and mammalian tooth development, it seems reasonable to elaborate preliminary research hypotheses about the role of these factors in shark teeth, based on what is already known in mammals. Moreover, and although authors focused on few, very specific genes —the most well-known in mammals—, the data gathered on gene expression patterns are beginning to provide pictures of the whole shark tooth development [Debiais-Thibaud et al., 2011, 2015; Martin et al., 2016; Rasch et al., 2016].

Many are the steps and pitfalls until elaborating correspondences between the role of signalling factors on tooth shape. Such work has been made in mammals, however, this has not been achieved in sharks [Jernvall et al., 2000]. First, do we have enough and detailed knowledge about shark tooth morphologies? Obviously, more data are always desirable but especially in this case, many detailed descriptions are lacking in extant species [Guinot et al., 2018]. Proofs of this are the aforementioned taxonomic revisions in section 2.3 due to ontogenetic diversity, and more generally to the lack of anatomic, descriptive work on teeth of extant sharks. If acquired, however, this kind of data enables to assess interspecific, intraspecific, and intraindividual tooth shape and form diversity in sharks. In theory, morphological data combined with experimental gene expression patterns in developing tooth buds would then allow to understand how tooth diversity in sharks is generated. Nevertheless, *S. canicula* is the only shark model in which dental gene expressions have been studied, and tooth development has been investigated in embryos only. This results in incomplete patterns as for the role of signalling factors in the acquisition of juvenile and mature tooth morphologies, and of gynandric heterodonty. Moreover, it arises that the gathered gene expression data are incomplete because of the focus on specific genes and not on the gene family, and because the data were not regularly collected for all developmental stages of a shark tooth bud (early morphogenesis, late morphogenesis, early differentiation, and late differentiation), which had then to be done [Berio and Debiais-Thibaud, 2019]. Subsequent hypotheses on the impact of gene expressions on shark tooth shape can be done but they are still mostly based on the results from functional tests in mouse teeth and, in rare cases, in shark odontodes and intromittent organs termed claspers [O'Shaughnessy et al., 2015; Cooper et al., 2018].

It appears that not only molecular factors and proteins might play a role in tooth patterning, but also the physical environment of the tooth bud. This for example includes the topology and bending of the jaw, the spacing between tooth buds, and the dental lamina conformation that hosts the tooth bud growth. As illustrated in Figure 3.3, the dental lamina lies on the jaw cartilage and its folding might be affected by the labio-lingual and mesio-distal bending of this cartilage.

Cells behave differently according to mechanical constraints. There is evidence that

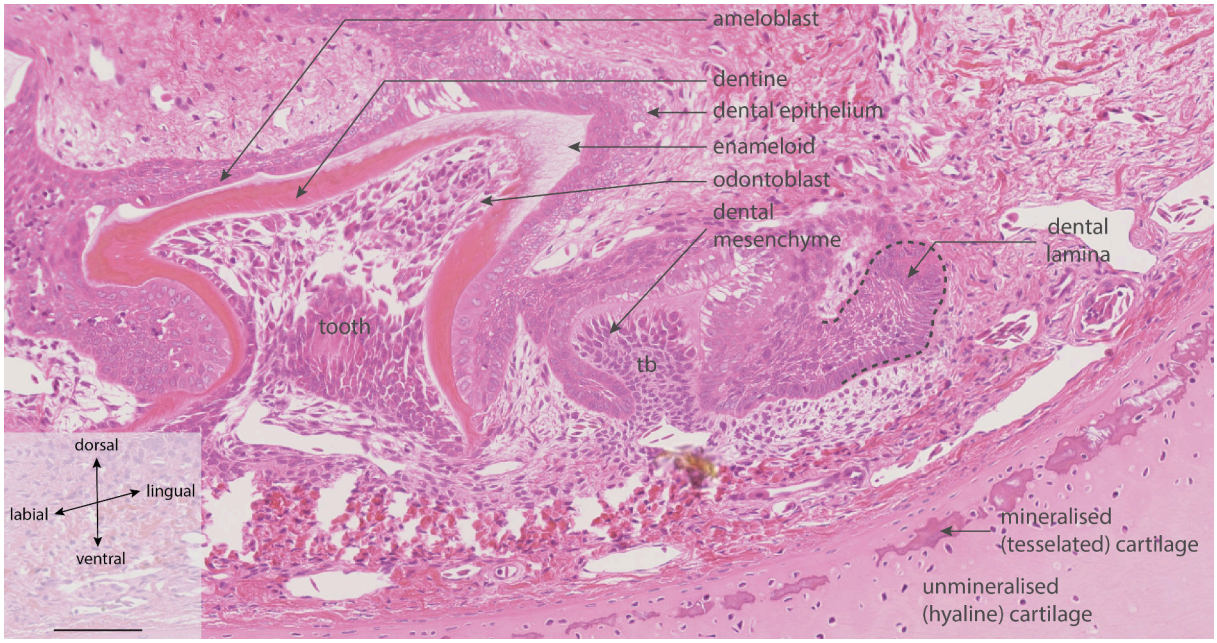

FIGURE 3.3: Successional development of *Scyliorhinus canicula* teeth. Histological section of the Meckelian cartilage and associated tooth files stained with Hematoxylin-Eosin-Saffron. The specimen is 20 cm long. tb, tooth bud. Scale bar is 100 µm. Image courtesy of Mélanie Debiais-Thibaud and Sébastien Enault.

the direction of a mechanical strain impacts the proliferation of mesenchymal cells, as well as their gene expressions [Kurpinski et al., 2006, 2009]. The shape of a mouse molar is also partly driven by mechanical forces, generated by differential growth rates between peripheral and internal epithelial cells [Takigawa-Imamura et al., 2015].
Most lamniform sharks share a unique dental pattern characterised by tallest teeth —termed anterior teeth— located in front of dental bullas and a row of immediately posterior teeth of noteworthy smaller size —termed intermediate teeth [Shimada, 2002] (see subsection 1.1.3). Although it has not been investigated, it is likely that the size patterns of anterior and intermediate teeth are impacted by the physical and spacing constraints imposed by the dental bullas. Furthermore, sexual dimorphism in head and mouth dimensions is a common feature among sexually mature scyliorhinids, so as the gynandric heterodonty (subsection 2.1.3) [Ellis and Shackley, 1995; Soares and de Carvalho, 2019; Berio et al., 2020]. It is thus tempting to correlate these two anatomical observations, since the cartilage morphology can impact the conformation of the dental lamina, which in turn affects the tooth bud growth (Figure 3.3).

3.2 Gene expression patterns in teeth and odontodes of jawed vertebrates

3.2.1 Stakes of the article

In an attempt to provide an overview of the molecular aspects of shark tooth and odontode development, the following article gathers literature data on *in situ* hybridisations obtained from *S. canicula* tooth and dermal denticle buds. The data found in literature

are classified into the four developmental stages of teeth and dermal denticles previously defined in *S. canicula* [Debiais-Thibaud et al., 2011, 2015], and compared to the data available for mouse and teleost teeth. The gene expression patterns are compared at the intraspecific and interspecific levels to provide insights into the evolution of these regulatory pathways in mammals and in teleost and cartilaginous fishes.

3.2.2 Journal article — Evolutionary developmental genetics of teeth and odontodes in jawed vertebrates: a perspective from the study of elasmobranchs

Received: 3 May 2019 | Accepted: 9 December 2019

DOI: 10.1111/jfb.14225

SPECIAL ISSUE REVIEW PAPER

JOURNAL OF FISH BIOLOGY fsbi

Evolutionary developmental genetics of teeth and odontodes in jawed vertebrates: a perspective from the study of elasmobranchs

Fidji Berio[1,2] | Mélanie Debiais-Thibaud[1]

[1]Institut des Sciences de l'Evolution de Montpellier, ISEM, Univ Montpellier, CNRS, IRD, EPHE, Montpellier, France

[2]University of Lyon, Ecole Normale Supérieure de Lyon, Centre National de la Recherche Scientifique, Université Claude Bernard Lyon 1, Institut de Génomique Fonctionnelle de Lyon, UMR5242, 46 Allée d'Italie, Lyon, France

Correspondence
Mélanie Debiais-Thibaud, Institut des Sciences de l'Evolution de Montpellier, ISEM, Univ Montpellier, CNRS, IRD, EPHE, Montpellier, France.
Email: melanie.debiais-thibaud@umontpellier.fr

Abstract

Most extant vertebrates display a high variety of tooth and tooth-like organs (odontodes) that vary in shape, position over the body and nature of composing tissues. The development of these structures is known to involve similar genetic cascades and teeth and odontodes are believed to share a common evolutionary history. Gene expression patterns have previously been compared between mammalian and teleost tooth development but we highlight how the comparative framework was not always properly defined to deal with different tooth types or tooth developmental stages. Larger-scale comparative analyses also included cartilaginous fishes: sharks display oral teeth and dermal scales for which the gene expression during development started to be investigated in the small-spotted catshark *Scyliorhinus canicula* during the past decade. We report several descriptive approaches to analyse the embryonic tooth and caudal scale gene expressions in *S. canicula*. We compare these expressions wih the ones reported in mouse molars and teleost oral and pharyngeal teeth and highlight contributions and biases that arise from these interspecific comparisons. We finally discuss the evolutionary processes that can explain the observed intra and interspecific similarities and divergences in the genetic cascades involved in tooth and odontode development in jawed vertebrates.

KEYWORDS

development, evolution, morphogenesis, odontode, *Scyliorhinus canicula*, tooth

1 | THE EVOLUTION OF TEETH AND ODONTODES

Odontodes are mineralised skeletal units of some extant and extinct vertebrates, sometimes referred to as 'the units of the vertebrate exoskeleton' (Hall, 2005; Janvier, 1996). They share with teeth their histological organisation: a vascularised core covered by dentine or dentine-like tissue that, most often, is covered with a hypermineralised layer of enamel or enameloid (Huysseune & Sire, 1998; Rivera-Rivera & Montoya-Burgos, 2017; Sire & Huysseune, 2003; Witten *et al*., 2014). Extant vertebrates retain pharyngeal and oral teeth, as well as odontodes (*e.g*., placoid scales in elasmobranchs; Figure 1: dermal denticles and scale ornamentations in some osteichthyans; Fraser *et al*., 2010; Huysseune & Sire, 1998; Reif, 1982). Vertebrate odontodes first evolved in a jawless ancestor as structures made of dentine and enameloid and were most probably ornamental units covering superficial dermal bones (Keating & Donoghue, 2016; Reif, 1980; Rücklin & Donoghue, 2015; Sire & Huysseune, 2003). Within species, odontodes or teeth develop as serial repeated structures that can differ in size, shape and body location (Huysseune & Sire, 1998; Martin *et al*., 2016; Rasch *et al*., 2016). Different teeth, different denticles, as well as teeth and denticles altogether, have often been referred to as 'serial homologues' at the intra-individual level (Debiais-Thibaud *et al*., 2011; Donoghue, 2002; Fraser *et al*., 2009; Schaefer, 1997; Smith *et al*., 2016; Young & Hallgrímsson, 2005).

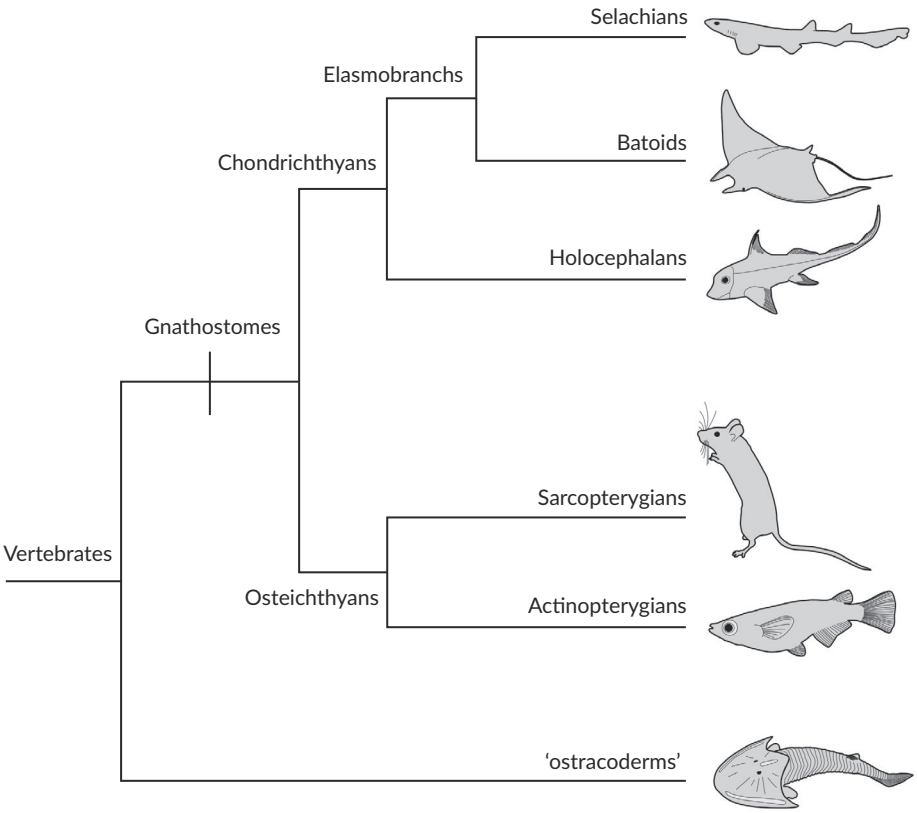

FIGURE 1 Phylogenetic relationships of tooth and odontode bearing vertebrates cited in this study (after Janvier, 1996)

These may be confusing terms because the operational meaning beyond serial homology is most of the time strictly developmental. Indeed, the structures within a specimen are considered to develop from multiple initiations of identical or similar genetic pathways with divergent expression patterns or in different tissue environments (Blais *et al*., 2011; Donoghue, 2002; Griffiths, 2007; Hall, 1999; Hecht *et al*., 2008; Schmitt, 1995). However, a theoretical evolutionary dimension is also implied in the use of serial homology through the hypothesis of a single ancestral genetic pathway that evolved in vertebrate lineages to give rise to all dental and odontode structures (Brigandt, 2003; Donoghue & Rücklin, 2016). The role of this single ancestral genetic pathway in the intra-individual diversification of odontodes and teeth has been part of the debate about the developmental origin of teeth, which are now considered to have evolved from the co-option of dermal denticle development processes (Blais *et al*., 2011; Fraser *et al*., 2010). In this review, we wish to focus on the developmental genetic data obtained in an elasmobranch species and used in a comparative framework and discuss the evolutionary perspectives obtained from these results.

2 | TOOTH AND ODONTODE DEVELOPMENT IN ELASMOBRANCHS

Extant elasmobranch fishes display serial oral teeth that undergo lifelong replacement and dermal scales that are continuously shed and develop to cover the scale-free skin as the specimens grow (Kemp, 1999; Martin *et al*., 2016; Rasch *et al*., 2016; Reif, 1982; Smith *et al*., 2018). Consequently, tooth shape and organisation may depend on the specimen growth stage: *e.g*., tooth shape displays sexual dimorphism in many species of elasmobranchs (Powter *et al*., 2010; Rasch *et al*., 2016; Smith *et al*., 2018; Underwood *et al*., 2015, 2016). Distinct phases of scale development and organisation also depend on developmental stages (Figure 2): embryos first develop (i) embryonic caudal primary scales, as observed in the Port Jackson shark *Heterodontus portusjacksoni* (Meyer 1793) and in the crested hornshark *Heterodontus galeatus* (Günther 1870) by Johanson *et al*. (2007) and in the small-spotted catshark *Scyliorhinus canicula* (L. 1758) by Mellinger & Wrisez (1993) and Johanson *et al*. (2008) and (ii) two rows of embryonic dorsolateral denticles that are later included in the whole post-embryonic body scalation (observed in *S. canicula* by Mellinger & Wrisez (1993) and Cooper *et al*. (2018)). Embryonic scales differ in terms of shape, size, patterning along the skin surface and in their type of dentine, compared with later developing juvenile scales (Johanson *et al*., 2008). As a consequence, morphological and molecular data underlying tooth and scale development in elasmobranchs provide a useful framework to compare developmental constraints and infer evolutionary processes involved in organ diversification patterns (Fraser *et al*., 2010; Huysseune *et al*., 2009).

Developmental and structural studies have pointed out similarities between the nature of the tissues and the morphology of developmental stages involved in shark first tooth generation and caudal primary scale genesis (Debiais-Thibaud *et al*., 2011; Fraser *et al*., 2010; Hecht *et al*., 2008). Debiais-Thibaud *et al*. (2011) used the following developmental stages in the zebrafish *Danio rerio* (Hamilton 1822), adapted from Huysseune *et al*. (1998) to describe the development of embryonic teeth and scales in *S. canicula* (Figure 2): (1) during early morphogenesis (EM), the epithelium thickens into a placode and the underlying mesenchyme

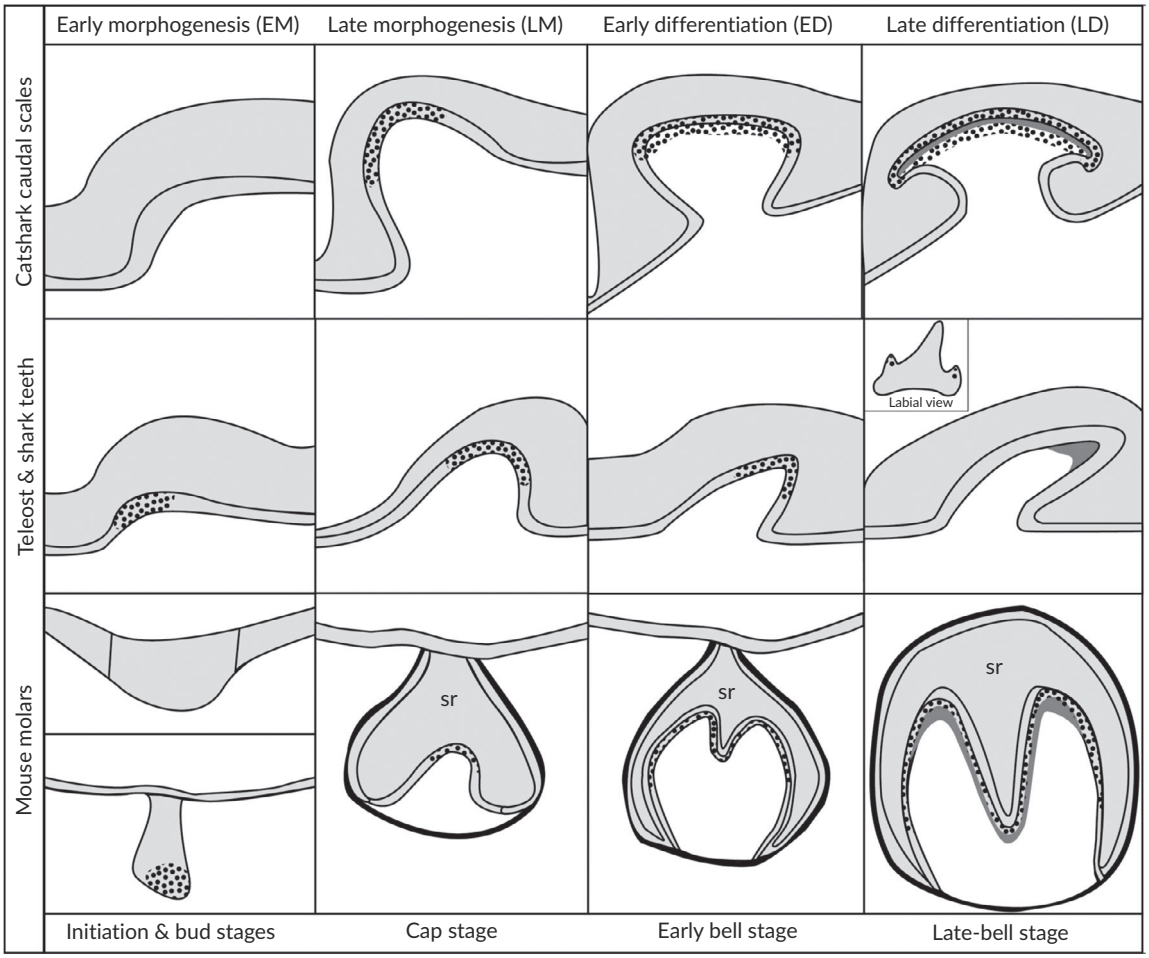

FIGURE 2 Simplified four equivalent developmental stages of tooth and tooth-like structures in the catshark *Scyliorhinus canicula*, in teleosts and in *Mus musculus*. *Shh* expression (after Bitgood and McMahon, 1995; Cooper *et al*., 2017; Debiais-Thibaud *et al*., 2015; Martin *et al*., 2016; Rasch *et al*., 2016) is shown as a dotted surface; dark grey: extracellular matrix; light grey: epithelium; white: mesenchyme; sr, stellate reticulum

condensates; (2) the epithelium encloses the underlying mesenchyme, giving rise to a hemispherical bud during late morphogenesis (LM), with partial (teeth) or without (scales) epithelial invagination; (3) during early differentiation (ED), the organ shape including cusps is acquired and epithelial cells differentiate into the inner and outer epithelial layers; (4) during late differentiation (LD), the polarised inner epithelial cells (ameloblasts) and the mesenchymal cells (odontoblasts) differentiate and start secreting extracellular matrix that then mineralises to form enameloid and dentine respectively. Equivalence between these stages and the ones in mammalian tooth development are powerful comparative tools to infer evolutionary changes in genetic pathways (Borday-Birraux *et al*., 2006; Debiais-Thibaud *et al*., 2015).

3 | GENE EXPRESSIONS DURING TOOTH AND ODONTODE DEVELOPMENT IN *S. CANICULA*

The genetic cascades regulating tooth morphogenesis have been best identified for *Mus musculus* odontogenesis (Tummers & Thesleff, 2009; gene expression in tooth: http://bite-it.helsinki.fi). Tooth development stages and histology are well described for mammalian molars (Thesleff & Mikkola, 2002) but cannot be used as such to compare with teeth and tooth-like structures of other jawed vertebrates as they may differ in terms of developmental timing, body location and structure (Borday-Birraux *et al*., 2006). In mammals, for example, an epithelial signalling centre, the enamel knot, is responsible for tooth-bud shape acquisition (Jernvall *et al*., 1994). In *S. canicula*, however, cusp morphogenesis differs from the mammalian enamel knot system in terms of histology and of gene expression (Debiais-Thibaud *et al*., 2015). Nevertheless, the gene sets involved in murine tooth development provide a strong reference to identify candidate genes, from which putative genetic cascades regulating tooth and odontode morphogenesis in other organisms can be explored. Furthermore, experimental data for expression patterns in the mouse have been used to build *in silico* models of tooth development (Salazar-Ciudad & Jernvall, 2002, 2010). However, the genetic parameters used in these models are not specific to mammals, as they have been generalised to signals that induce cellular differentiation (*i.e*., activators; including bone morphogenetic proteins (*Bmps*) in the mouse), or promote cell division and

TABLE 1 Expression patterns of *Scyliorhinus canicula* genes involved in embryonic tooth and caudal scale development. Expressions are reported for epithelium (E) and mesenchyme (M) for four developmental stages

		Development stage							
		Early morphogenesis		Late morphogenesis		Early differentiation		Late differentiation	
Gene	Tissue	Tooth	Caudal scale	Tooth	Caudal scale	Tooth	Caudal scale	Tooth	Caudal scale
Shh	E	+ (2, 4)	– (2, 5)	+ (2, 3, 4)	+ (2)	+ (2, 4)	+ (2, 3, 5†)	+ (2)	+ (2, 5 †)
	M	– (2, 4)	– (2, 5)	– (2, 3, 4)	– (2)	– (2, 4)	+ (5†)	– (2)	+ (5†)
Fgf3	E			+ (3, 4)	+ (1, 5)	+ (4)	+ (3, 5)	– (3, 4)	+ (5)
	M			+ (3, 4)	+ (1, 5)	+ (4)	+ (3, 5)	– (3, 4)	+ (5)
Fgf8	E	– (2)	– (2, 5)	+ (2)	+ (2, 5†)	+ (2)	+ (2, 5†)	+ (2)	+ (5†)
	M	– (2)	– (2, 5)	– (2)	+ (5†)	– (2)	+ (5†)	– (2)	+ (2†)
Fgf10	E			+ (4)		+ (3, 4)	+ (3)		
	M			– (4)		– (3, 4)	– (3)		
Fgfr1	E						+ (5)		
	M						– (5)		
Fgfr2	E						+ (5)		
	M						– (5)		
Ptc2	E			+ (4)		+ (4)			
	M			+ (4)		+ (4)			
Midkine	E			+ (4)		+ (4)			
	M			+ (4)		+ (4)			
Bmp4	E	+ (2, 4†)	– (2)	+ (2, 4†)	+ (5†)	+ (2)	+ (2, 5)	+ (2, 4†)	+ (2, 5†)
	M	+ (4†)	+ (2)	+ (4†)	+ (2, 5†)	– (2)	+ (2, 5)	+ (3, 4†)	+ (3, 5†)
Lef1	E	+ (3, 4)		+ (3, 4)	+ (3)				– (3)
	M	– (3, 4)		+ (3, 4)	+ (3)				– (3)
β-cat	E	+ (4)				+ (3, 4)	+ (3)	+ (4)	
	M	+ (4)				+ (3, 4)	+ (3)	– (4)	
Eda	E				+ (5)				
	M				– (5)				
Edar	E						+ (5)		
	M						– (5)		
Gli2	E						+ (5)		
	M						– (5)		
Dlx1	E	+ (1)	– (1)	+ (1)	+ (1)	+ (1)	+ (1)	+ (1)	+ (1)
	M	– (1)	– (1)	– (1)	– (1)	+ (1)	+ (1)	– (1)	– (1)
Dlx2	E	– (1)	+ (1, 5)	– (1)	+ (1, 5)	– (1)	+ (1, 5)	– (1)	+ (1)
	M	– (1)	+ (1, 5)	– (1)	+ (1, 5)	– (1)	+ (1, 5)	– (1)	– (1)
Dlx3	E	+ (1)	+ (1)	+ (1)	+ (1)	+ (1)	+ (1)	+ (1)	+ (1)
	M	– (1)	– (1)	+ (1)	+ (1)	+ (1)	+ (1)	+ (1)	– (1)
Dlx4	E	+ (1)	+ (1)	+ (1)	+ (1)	+ (1)	+ (1)	+ (1)	+ (1)
	M	– (1)	– (1)	+ (1)	+ (1)	+ (1)	+ (1)	+ (1)	+ (1)
Dlx5	E	+ (1)	+ (1)	+ (1)	+ (1)	+ (1)	+ (1)	+ (1)	+ (1)
	M	– (1)	– (1)	+ (1)	+ (1)	+ (1)	+ (1)	+ (1)	– (1)
Dlx6	E	– (1)	– (1)	– (1)	– (1)	– (1)	– (1)	– (1)	– (1)
	M	– (1)	– (1)	– (1)	– (1)	– (1)	– (1)	– (1)	– (1)
Msx1	E	+ (2)	+ (2)	+ (2)	– (2)	+ (2)	– (2)	+ (2)	+ (2)
	M	+ (2)	– (2)	– (2)	+ (2)	+ (2)	+ (2)	– (2)	+ (2)

(Continues)

TABLE 1 (Continued)

		Development stage							
		Early morphogenesis		Late morphogenesis		Early differentiation		Late differentiation	
Gene	Tissue	Tooth	Caudal scale	Tooth	Caudal scale	Tooth	Caudal scale	Tooth	Caudal scale
Msx2	E	+ (2)	– (2)	+ (2)	+ (2)	+ (2)	+ (2)	+ (2)	+ (2)
	M	+ (2)	– (2)	+ (2)	– (2)	– (2)	+ (2)	– (2)	– (2)
Msx3	E	+ (2)	– (2)	+ (2)	+ (2)	+ (2)	+ (2)	+ (2)	+ (2)
	M	– (2)	– (2)	+ (2)	– (2)	+ (2)	+ (2)	+ (2)	– (2)
Pitx1	E	+ (2)	+ (2)	+ (2)	+ (2)	+ (2, 4)	+ (2)	+ (2, 4)	+ (2)
	M	– (2)	– (2)	– (2)	– (2)	– (2, 4)	– (2)	– (2, 4)	– (2)
Pitx2	E	+ (2, 4)	– (2)	+ (2)	– (2)	+ (2, 3)	– (2)	+ (2, 4)	– (2)
	M	+ (2, 4)	– (2)	+ (2)	– (2)	+ (2, 3)	– (2)	+ (2, 4)	– (2)
Pitx3	E	– (2)	– (2)	– (2)	– (2)	– (2)	– (2)	– (2)	– (2)
	M	– (2)	– (2)	– (2)	– (2)	– (2)	– (2)	– (2)	– (2)
Sox2	E	+ (4)				+ (3)			
	M	– (4)				– (3)			
Pax9	E			– (4)		– (4)			
	M			+ (4)		+ (4)			
Col1a1	E				– (6)	– (6)		– (6)	– (6)
	M				+ (6)	+ (6)		+ (6)	+ (6)
Col1a2	E				– (6)	– (6)		– (6)	– (6)
	M				+ (6)	+ (6)		+ (6)	+ (6)
Col2a1	E					+ (6)	– (6)	– (6)	– (6)
	M					– (6)	– (6)	+ (6)	– (6)
Sparc	E				– (3)		– (3, 6)	– (3, 6)	– (6)
	M				+ (3)		+ (3, 6)	+ (3, 6)	+ (6)
Sparc–l	E						– (6)	+ (6)	+ (6)
	M						– (6)	– (6)	– (6)

Note: –, no expression; +, expression; †, conflicting expression data; (1), Debiais-Thibaud *et al*., 2011; (2), Debiais-Thibaud *et al*., 2015; (3), Martin *et al*., 2016; (4), Rasch *et al*., 2016; (5), Cooper *et al*., 2017; (6), Enault *et al*., 2018.

therefore structure growth (*i.e*., inhibitors; including fibroblast growth factors (*Fgfs*) and sonic hedgehog (*Shh*) in the mouse; Salazar-Ciudad & Jernvall, 2002, 2010). As a consequence, the use of *M. musculus* as a reference model organism, as well as the parameters in emerging models for tooth development may have influenced the choice of gene expressions primarily investigated (*e.g*., *Shh*, *Fgf* and *Bmp* families) during tooth and odontode development in non-model organisms. However, developmental genes often belong to multigenic families that arose from duplications before jawed vertebrate origin: these members of a given gene family are called paralogues and they are known to be, at least initially, highly redundant genes. The divergence time between the mouse and *S. canicula* is estimated to 450–500 million years (Inoue *et al*., 2010) leading to potential differential evolution of paralog function between lineages. Other approaches have thus included the study of all members of a given gene family to account for potential paralogue function shuffling. In the following section, we review the published gene expressions involved in tooth and embryonic caudal scale development in elasmobranchs (Cooper *et al*., 2017; Debiais-Thibaud *et al*., 2011, 2015; Martin *et al*., 2016; Rasch *et al*., 2016) with special attention for transcription and signalling factors (proliferation or differentiation factors), as used in *in silico* models of tooth development (Salazar-Ciudad & Jernvall, 2002, 2010). A more complete set of data is summarised in Table 1 and the results for two general experimental approaches are discussed below: the candidate-gene approaches, where specific genes well described in mouse are explored in *S. canicula*, and the total-gene-family approach, where gene expression patterns are described for all members of paralogous genes.

3.1 | Candidate-gene approaches

3.1.1 | Cell division activators

Members of two gene families that are known to activate cell proliferation during tooth development in the mouse have been explored in

S. canicula: *Shh* (Figure 2) and the *Fgfs*. *Shh* expression is restricted to the epithelium throughout the development of *S. canicula* teeth (Debiais-Thibaud *et al*., 2015; Martin *et al*., 2016; Rasch *et al*., 2016; Smith *et al*., 2009). In caudal scales, however, no expression is observed during the initiation stage (EM; Cooper *et al*., 2017; Debiais-Thibaud *et al*., 2015), while it is expressed in the epithelium and in the mesenchyme during ED and LD stages (Cooper *et al*., 2017). In tooth and scale epithelium, *Shh* expression is restricted to a focal zone located at the tip of the forming bud–cusps (Cooper *et al*., 2017; Debiais-Thibaud *et al*., 2015; Martin *et al*., 2016; Rasch *et al*., 2016).

The *Fgf* family includes several members (22 in the mouse; Itoh & Ornitz, 2008) and the expression of only two of them was explored in *S. canicula*. *Fgf3* has an epithelial and mesenchymal expression in teeth (from LM to ED stage) and caudal scales (from LM to LD stage; Cooper *et al*., 2017; Debiais-Thibaud *et al*., 2011; Martin *et al*., 2016; Rasch *et al*., 2016). *Fgf8* has an epithelial expression from LM to LD stage in teeth (Debiais-Thibaud *et al*., 2015). In caudal scales, it is either detected in both epithelium and mesenchyme (Cooper *et al*., 2017), either only in the epithelium (Debiais-Thibaud *et al*., 2015) during LM and ED stages and is detected as restricted to the epithelium (Cooper *et al*., 2017) and to the mesenchyme (Debiais-Thibaud *et al*., 2015) during LD stage. These discrepancies may come from different probe sequences, but the *Fgf8* sequence used by Cooper *et al*. (2017) is not available from the original publication to compare with the probe sequence used in Debiais-Thibaud *et al*. (2015).

3.1.2 | Cell differentiation inducers

A recurrent marker for cell proliferation arrest in mouse tooth development is *Bmp4*. However, similar to *Fgf8*, inconsistent *Bmp4* expression patterns were reported in *S. canicula* teeth and caudal scales. Indeed, in the study of Debiais-Thibaud *et al*. (2015), *Bmp4* expression was found restricted to the epithelium throughout tooth development, while it was also expressed in the dental mesenchyme during EM, LM and LD stages in Rasch *et al*. (2016), but also see Martin *et al*. (2016). In caudal scales, *Bmp4* expression differs according to the study considered: it is detected in epithelium and mesenchyme from LM to LD stages in Cooper *et al*. (2017), while Debiais-Thibaud *et al*. (2015) reported mesenchymal (LM stage), epithelial and mesenchymal (ED stage) and epithelial (LD stage) expression. Because the RNA probes used in these studies are only partly overlapping and one is much longer (Rasch *et al*., 2016) than the other (Debiais-Thibaud *et al*. 2015), these discrepancies might have arisen because of unidentified alternative transcripts of the *Bmp4* gene, not captured in Debiais-Thibaud *et al*. (2015).

3.2 | Total-gene-family approaches

Three transcription factor families, well described in murine tooth development, were thoroughly studied in *S. canicula*: the *Dlx*, *Msx* and *Pitx* families. Because expression patterns for *Dlx* and *Msx* genes have been the focus of previous developmental analyses at the intraspecific level (Debiais-Thibaud *et al*., 2011, 2015), we summarise these observations here.

The *Dlx* gene family has ancestrally six members in jawed vertebrates. Expression patterns are very similar between *Dlx3*, *Dlx4* and *Dlx5*, as well as between tooth and caudal scale development (Debiais-Thibaud *et al*., 2011). They have indeed an exclusively epithelial expression during EM and an epithelial and mesenchymal expression from LM to LD in both structures, except for caudal scales where *Dlx3* and *Dlx5* expression is strictly epithelial during LD stage (Debiais-Thibaud *et al*., 2011). Expression of *Dlx1* is similar between both structures and is mainly epithelial, whereas *Dlx2* is expressed in the epithelium and in the mesenchyme of caudal scales only, with expression restricted to the epithelium in LD stage (Debiais-Thibaud *et al*., 2011). *Dlx6* expression was not detected in teeth or scales (Debiais-Thibaud *et al*., 2011).

The *Msx* gene family has ancestrally three members in jawed vertebrates. *Msx1* expression is restricted to the epithelium during EM and LM stages while *Msx2* expression is also detected in the mesenchyme (Debiais-Thibaud *et al*., 2015) and these patterns are inverted during the ED and LD stages. In caudal scales, *Msx1* expression is first epithelial only (EM stage), then mesenchymal only (LM and ED stages) and finally both epithelial and mesenchymal (LD stage; Debiais-Thibaud *et al*., 2015). The *Msx2* and *Msx3* expressions in caudal scales are identical: in the epithelium from the LM to the LD stage, with transient expression in the mesenchyme during the ED stage (Debiais-Thibaud *et al*., 2015). In teeth, however, *Msx3* expression differs from that in caudal scales as it is epithelial during the initiation stage and in both tissues from LM to LD stage (Debiais-Thibaud *et al*., 2015).

The *Pitx* gene family has ancestrally three members in jawed vertebrates. *Pitx1* expression is restricted to the epithelium throughout tooth and caudal scale development (Debiais-Thibaud *et al*., 2015; Rasch *et al*., 2016). *Pitx1* expression is never detected in caudal scale buds and this stands in sharp contrast with its dental expression, both epithelial and mesenchymal, from EM to LD stages (Debiais-Thibaud *et al*., 2015). However, we report an exclusively mesenchymal expression of *Pitx2* during ED stage, as also illustrated in the study of Martin *et al*. (2016). The expression of *Pitx3* was not detected in teeth or scales (Debiais-Thibaud *et al*., 2015). Overall, these data show that genes involved in the development of teeth and scales are generally the same, but that their expression patterns may differ from one structure to another. Below, we question how these discrepancies can be interpreted in a comparative context.

4 | METHODOLOGICAL LIMITATION LINKED TO DEVELOPMENTAL STAGING IN A COMPARATIVE FRAMEWORK

To make intra and interspecific comparisons between gene expression patterns, comparable developmental stages are necessary for teeth and tooth-like structures (Borday-Birraux *et al*., 2006; Debiais-Thibaud *et al*., 2011; Jernvall & Thesleff, 2012). However, odontode

TABLE 2 Expression patterns of genes involved in embryonic tooth development of *Mus musculus*, *Danio rerio*, *Oryzias latipes*, *Oncorhynchus mykiss*, and Malawi cichlid fishes in epithelium (E) and mesenchyme (M) for four developmental stages: Early morphogenesis (EM); Late morphogenesis (LM); Early differentiation (ED); Late differentiation (LD) in fishes and Initiation and bud (IB), Cap, Bell and Late-bell (LB) stages in *Mus musculus*

Gene	Tissue	*Mus musculus* (molars)				*Danio rerio* (pharyngeal teeth)				*Oryzias latipes* (oral teeth)				*Oryzias latipes* (pharyngeal teeth)				*Oncorhynchus mykiss* (oral teeth)				Malawi cichlids (oral teeth)			
		IB	Cap	Bell	LB	EM	LM	ED	LD	EM	LM	ED	LD	EM	LM	ED	LD	EM	LM	ED	LD	EM	LM	ED	LD
Shh	E	+ (5, 11, 8)	+ (5, 11, 8)	+ (5)	+ (5)	+ (31)	+ (33)	+ (33)	+ (33)									+ (22, 25)	+ (25)	+ (22, 25)	+ (22, 25)	–(32)	+ (30,32)	+ (30,32)	+ (30,32)
	M	– (5, 11, 8)	– (5, 11, 8)	– (5)	– (5)	– (31)	– (33)	– (33)	– (33)									– (25)	– (25)	+ (22, 25)	+ (22, 25)	–(32)	– (30,32)	+ (30,32)	+ (30,32)
Fgf3	E	+ (16)	+ (16)	– (16)	– (16)		+ (23)																+ (32)		+ (32)
	M	+ (16)	+ (16)	+ (16)	+ (16)		– (23)																+ (32)		+ (32)
Fgf8	E	– (15)	– (15)	– (15)	– (15)	– (23)	– (23)	– (23)	– (23)																
	M	– (15)	– (15)	– (15)	– (15)	– (23)	– (23)	– (23)	– (23)																
Fgf10	E	– (16)	– (16)	– (16)	– (16)																	+ (32)		+ (32)	– (32)
	M	+ (16)	+ (16)	+ (16)	+ (16)																	+ (32)		+ (32)	+ (32)
Fgfr1	E	– (14)	+ (14)	+ (14)	+ (14)																				
	M	+ (14)	+ (14)	+ (14)	+ (14)																				
Fgfr2	E	+ (14)	+ (14)	+ (14)	+ (14)																				
	M	+ (14)	+ (14)	+ (14)	– (14)																				
Ptc2	E					+ (31)																			
	M					+ (31)																			
Midkine	E	+ (7, 6)	– (6)	+ (6)	+ (6)																				
	M	+ (7, 6)	+ (6)	+ (6)	+ (6)																				
Bmp4	E	– (3, 9, 8)	+ (15, 8)	+ (3, 5)	+ (9, 13)	–(27)	+ (27)	+ (27)	+ (27)					+ (27)	–(27)			– (22)	– (22)	– (22)	– (22)	+ (32)		+ (32)	+ (32)
	M	+ (3, 9, 8)	+ (15, 8)	+ (3, 5)	+ (9, 13)	–(27)	–(27)	+ (27)	+ (27)					+ (27)	+ (27)			+ (22)	+ (22)	+ (22)	+ (22)	+ (32)		+ (32)	+ (32)
Lef1	E	+ (13)	+ (13)	+ (13)	+ (13)																	+ (32)			+ (32)
	M	+ (13)	+ (13)	+ (13)	+ (13)																	+ (32)			+ (32)
β-cat	E																					+ (32)			
	M																					+ (32)			
Eda	E	+ (20)	+ (18, 20)	+ (18, 20)																					
	M	– (20)	– (18, 20)	– (18, 20)																					
Edar	E	+ (18, 20)	+ (18, 20)	+ (18, 20)																					
	M	– (18, 20)	– (18, 20)	– (18, 20)																					
Gli2	E	+ (11)	+ (11)																						
	M	+ (11)	+ (11)																						
Dlx1	E	– (19)	– (19)	– (19)	– (19)	– (24)	– (24)	– (24)	– (24)	– (29)	– (29)	– (29)	– (29)	– (29)	– (29)	– (29)	– (29)								
	M	– (19)	+ (19)	+ (19)	+ (19)	– (24)	– (24)	– (24)	– (24)	– (29)	– (29)	– (29)	– (29)	– (29)	– (29)	– (29)	– (29)								
Dlx2 (dlx2a)	E	+ (19)	– (19)	– (19)	+ (19)	+ (24)	+ (24)	+ (24)	– (24)	– (29)	– (29)	– (29)	– (29)	– (29)	– (29)	– (29)	– (29)						+ (32)		– (32)
	M	+ (19)	+ (19)	+ (19)	– (19)	+ (24)	+ (24)	+ (24)	+ (24)	+ (29)	+ (29)	+ (29)	– (29)	+ (29)	+ (29)	+ (29)	– (29)						+ (32)		+ (32)
Dlx2b	E	absence				+ (23, 24)	+ (23, 24)	+ (24)	+ (24)	loss (29)															
	M					– (23, 24)	+ (23, 24)	+ (24)	+ (24)																
Dlx3a	E	absence				loss (29)				– (29)	– (29)	– (29)	– (29)	– (29)	– (29)	– (29)	– (29)								
	M									– (29)	– (29)	– (29)	– (29)	– (29)	– (29)	– (29)	– (29)								
Dlx3 (dlx3b)	E	+ (19†)	– (19, 4)	– (19)	– (19)	+ (24)	+ (24)	+ (24)	+ (24)	+ (29)	+ (29)	+ (29)	+ (29)	+ (29)	+ (29)	+ (29)	+ (29)								
	M	+ (4†)	+ (19, 4)	(19)	(19)	– (24)	+ (24)	– (24)	– (24)	+ (29)	+ (29)	+ (29)	+ (29)	+ (29)	+ (29)	+ (29)	+ (29)								

(Continues)

TABLE 2 (Continued)

Gene	Tissue	*Mus musculus* (molars)				*Danio rerio* (pharyngeal teeth)				*Oryzias latipes* (oral teeth)				*Oryzias latipes* (pharyngeal teeth)				*Oncorhynchus mykiss* (oral teeth)				Malawi cichlids (oral teeth)			
		IB	Cap	Bell	LB	EM	LM	ED	LD	EM	LM	ED	LD	EM	LM	ED	LD	EM	LM	ED	LD	EM	LM	ED	LD
dlx4a	E	absence				–(24)	+ (24)	+ (24)	+ (24)	loss (29)															
	M					–(24)	+ (24)	+ (24)	+ (24)																
Dlx4 (dlx4b)	E	– (24)	– (24)	– (24)	– (24)	+ (24)	+ (24)	+ (24)	+ (24)	– (29)	– (29)	– (29)	– (29)	– (29)	– (29)	– (29)	– (29)								
	M	– (24)	+ (24)	+ (24)	+ (24)	+ (24)	+ (24)	– (24)	+ (24)	– (29)	– (29)	+ (29)	+ (29)	– (29)	– (29)	+ (29)	+ (29)								
Dlx5	E	– (19)	– (19)	– (19)	– (19)	+ (24)	+ (24)	+ (24)	+ (24)	+ (29)	+ (29)	+ (29)	+ (29)	– (29)	– (29)	+ (29)	+ (29)								
	M	– (19)	+ (19)	+ (19)	+ (19)	– (24)	+ (24)	+ (24)	+ (24)	+ (29)	+ (29)	+ (29)	+ (29)	+ (29)	+ (29)	+ (29)	+ (29)								
Dlx6	E	– (19)	– (19)	– (19)	+ (19)	– (24)	– (24)	– (24)	– (24)	– (29)	– (29)	– (29)	– (29)	– (29)	– (29)	– (29)	– (29)								
	M	– (19)	– (19)	– (19)	+ (19)	– (24)	– (24)	– (24)	– (24)	– (29)	– (29)	+ (29)	+ (29)	– (29)	– (29)	+ (29)	+ (29)								
Msx1	E	– (15, 13)	– (15)	– (13)	– (15)																				
	M	+ (15, 13)	+ (15)	+ (13)	+ (15)																				
Msx2	E	+ (15)	+ (15, 12)	+ (13)	+ (15)																				
	M	+ (15)	– (15, 12)	+ (13)	+ (15)																				
Msx3	E																								
	M																								
Pitx1	E	+ (17)	+ (17)		+ (17)																				
	M	+ (17)	– (17)		– (17)																				
Pitx2	E	+ (17)	+ (17)		+ (17)	+ (23)	+ (23)											+ (25, 26)	+ (22, 26)	+ (22, 26)	+ (25)	+ (32)		+ (32)	+ (30)
	M	– (17)	– (17)		– (17)	– (23)	– (23)											– (25, 26)	– (22, 26)	– (22, 26)	+ (25)	– (32)		– (32)	– (30)
Pitx3	E																								
	M																								
Sox2	E																					–(32)		+ (32)	
	M																					–(32)		– (32)	
Pax9	E	– (21, 10)	– (21)			– (23)	– (23)	– (23)	– (23)									– (25, 28)	– (25, 28)	– (25, 28)	– (25, 28)				
	M	+ (21, 10)	+ (21)			– (23)	– (23)	– (23)	– (23)									– (25, 28)	– (25, 28)	– (25, 28)	– (25, 28)				
Col1a1	E			– (2)	– (2)																				
	M			+ (2)	+ (2)																				
Col1a2	E																								
	M																								
Col2a1	E																								
	M																								
Sparc	E				+ (1)																				
	M				+ (1)																				
Sparc-l	E																								
	M																								

Note: (–), no expression; (+), expression; †, conflicting expression data; (1), Holland *et al*., 1987; (2), Lukinmaa *et al*., 1993; (3), Vainio *et al*., 1993; (4), Robinson & Mahon, 1994; (5), Bitgood & McMahon, 1995; (6), Mitsiadis *et al*., 1995a; (7), Mitsiadis *et al*., 1995b; (8), Vaahtokari *et al*., 1996; (9), Åberg *et al*., 1997; (10), Neubüser *et al*., 1997; (11), Hardcastle *et al*., 1998; (12), Jernvall *et al*., 1998; (13), Keränen *et al*., 1998; (14), Kettunen *et al*., 1998; (15), Kettunen & Thesleff, 1998; (16), Kettunen *et al*., 2000; (17), St. Amand *et al*., 2000; (18), Tucker *et al*., 2000; (19), Zhao *et al*., 2000; (20), Laurikkala *et al*., 2001; (21), Åberg *et al*., 2004; (22), Fraser *et al*., 2004; (23), Jackman *et al*., 2004; (24), Borday-Birraux *et al*., 2006; (25), Fraser *et al*., 2006a; (26), Fraser *et al*., 2006b; (27), Wise & Stock, 2006; (28), Debiais-Thibaud *et al*., 2007; (29), Debiais-Thibaud *et al*., 2008; (30), Fraser *et al*., 2008; (31), Jackman *et al*., 2010; (32), Fraser *et al*., 2013; (33), Yu *et al*., 2015.

and tooth morphogenesis is a continuous biological process. As a consequence, artificial boundaries between developmental stages do necessarily miss subtle transient processes of gene expression patterns and morphological changes during the development of a structure (Dassule & McMahon, 1998; Debiais-Thibaud *et al*., 2015; Vainio *et al*., 1993). In addition, developmental stages during morphogenesis have been considered equivalent between species, even though they are known to show different time intervals and also divergent morphogenetic or differentiation processes between species or between structures (Borday-Birraux *et al*., 2006; Sire *et al*., 2002). As an example, only a few hours are necessary to achieve the development of a small conical tooth in *D. rerio* (Borday-Birraux *et al*., 2006), while Vandenplas *et al*. (2016) mention several weeks in the case of a larger lance-shaped *S. canicula* tooth. Also, the differentiation stage might be highly different in a species where cells produce enamel *versus* a species that produces enameloid (Debiais-Thibaud *et al*., 2019; Enault *et al*., 2018). These staging artefacts might result in differences in gene expression patterns that resemble heterochronies, but they do not necessarily reflect true time shifts, only improper definition of growth stages for a given developmental process. Short heterochronies (one developmental stage difference) between species have often been reported, as is the case of *dlx4* mesenchymal expression differences between *S. canicula* (starting during LM stage; Table 1) and *D. rerio* teeth (starting during ED stage; Table 2; Borday-Birraux *et al*., 2006; Debiais-Thibaud *et al*., 2011). Intraspecific short heterochronies, as observed for mesenchymal *Dlx5* in *S. canicula* teeth and caudal scales (Debiais-Thibaud *et al*., 2011) may also be products of staging artefacts. True shifts in timing of developmental process or gene expression have previously been identified in mouse upper and lower molars, but this study also included a detailed shape description of teeth (Pantalacci *et al*., 2017) that has not been performed in most studies we review here. For this reason, we will not take short heterochronies (one developmental stage differences) into account in the following comparisons between gene expression patterns.

5 | INTRASPECIFIC ROBUSTNESS OF TOOTH AND ODONTODE GENETIC CASCADES

Based on the data available on tooth and caudal scale development in *S. canicula* (Table 1), gene expression patterns have been explored to explain the morphogenetic divergences that arose among vertebrate teeth and odontodes (Tschopp & Tabin, 2017). Identification of the genetic pathways involved in the development of such structures provides clues for investigating tooth-related evolutionary mechanisms as well as intra-specific diversification of odontodes (Fraser *et al*., 2010). Actinopterygians display a high variety of tooth locations within the mouth (jaws, palate roof and pharyngeal regions) that, combined with location-specific shapes of teeth, raises questions about the developmental processes involved in such differences (Debiais-Thibaud *et al*., 2007; Fraser *et al*., 2013; Renz *et al*., 2011). Despite shape differences, oral and pharyngeal intra-individual tooth types in teleosts only differ in expression of just a few genes. For instance, only *dlx5* showed differential gene expression in the medaka *Oryzias latipes* (Temminck & Schlegel 1846) between oral (in epithelium and mesenchyme from EM to LD) and pharyngeal (restricted to mesenchyme during EM and LM and in both tissues during ED and LD) teeth (Debiais-Thibaud *et al*., 2008). However, most of the other data published in teleosts were not acquired by systematically comparing equivalent stages of development and thus do not allow to compare the gene sets involved in both structures. In *S. canicula*, the expression patterns of only five genes (out of 16 nearly complete developmental expression series) significantly differ between tooth and caudal scale development. These five genes are either expressed in only one of these two structures, or restricted to the epithelium or to the mesenchyme in one of them (see Table 1 for *Dlx2*, *Fgf8*, *Msx2*, *Pitx2* and *Shh)*. In contrast, the remaining 11 genes show expression patterns that are similar in teeth and dermal scales. Altogether, these data suggest that differences of expression of only a small number of genes might be sufficient to drive developmental differences of serial homologous structures, both within teleosts and *S. canicula*. This supports the view that a single intraspecific gene regulatory cascade is involved in the development of teeth and odontodes, as postulated in the outside-in model of tooth evolution (Fraser *et al*., 2010).

Another level of complexity is raised with gene expression pattern variations that depend on tooth generation and location. In *M. musculus*, *Dlx1* and *Dlx2* expression are necessary for upper but not lower molar development (Qiu *et al*., 1997; Thomas *et al*., 1997). More global heterochrony in gene expressions between mouse upper and lower molars has also been demonstrated (Pantalacci *et al*., 2017). Similarly, in *D. rerio*, *dlx2a* is expressed only in the first formed tooth ($4V^1$) but not in the adjacent ones ($3V^1$ and $5V^1$) (Borday-Birraux *et al*., 2006). In mouse, these gene expression discrepancies were interpreted as the genetic basis for morphological differences between serial teeth (*e.g*., upper and lower molars (Pantalacci *et al*., 2017)). However, only little morphological differences have been reported between *D. rerio* first generation teeth (Borday-Birraux *et al*., 2006), which suggests that, in this case, the development of each structure may be canalised to produce morphologically similar teeth despite gene expression differences during the development. In cichlids, however, dietary differences (between hard and soft food) are known to affect the shape of newly developed teeth (Gunter *et al*., 2013; Huysseune, 1995). In this case, differences in dental gene expression patterns in association to environmental cues, if shown, may be responsible for tooth shape differences between populations.

As a conclusion, intra and interspecific comparisons are currently limited by restricted expression datasets for more than one type of serial structure within one individual. A more complete dataset would help test the robustness of a given gene expression pattern in one type of structure. In *S. canicula*, for example, caudal and embryonic and post-embryonic body scales could theoretically also exhibit differential gene expression patterns. To the best of our knowledge, however, only two studies provide gene expression data on *S. canicula* embryonic and post-embryonic body denticle development and such data remain largely fragmentary (Cooper *et al*., 2017, 2018) and

difficult to compare to those in caudal scale development. Detailed comparison of these patterns might bring insights into genetic divergences potentially responsible for the structural differences observed among intra individual types of *S. canicula* scales, or for the occurrence of developmental canalisation of serial organs, or both.

6 | DIVERSIFICATION OF A GENETIC CASCADE AMONG LINEAGES: FUNCTIONAL SELECTION, DRIFT, OR BOTH?

The dermal plates of ostracoderms (extinct jawless vertebrates; Figure 2) are the oldest occurrence of odontodes in the fossil record (Keating & Donoghue, 2016). As a consequence, a common working hypothesis is that the gene set involved in the development of the first odontodes may have diverged along vertebrate lineages and generated the tooth and odontode interspecific diversity within gnathostomes (see the 'deep homology' concept in Tschopp & Tabin, 2017). In the data reviewed here, most of the observed divergences come from a mesenchymal-restricted expression in a given species compared with all other species who exhibit the same gene expression in both the epithelium and mesenchyme. This is the case of *dlx2* in *O. latipes* teeth, of *Dlx5* and *Msx1* in *M. musculus* molars and of *bmp4* in rainbow trout *Oncorhynchus mykiss* (Walbaum 1792) teeth (Borday-Birraux *et al*., 2006; Debiais-Thibaud *et al*., 2008; Fraser *et al*., 2004; Zhao *et al*., 2000). Conversely, some gene expressions are restricted to the epithelium, albeit this pattern is less frequent (based on the available data) than a mesenchymal-restricted expression. For instance, *Pitx2* has an epithelial expression in teleost teeth (*D. rerio*, *O. mykiss*, cichlids) and an epithelial-mesenchymal one in *S. canicula* teeth (Debiais-Thibaud *et al*., 2015; Fraser *et al*., 2004, 2008, 2013; Jackman *et al*., 2004).

Some of these interspecific differences can be related to functional redundancies between sister proteins within a given gene family. Functional redundancy was clearly shown in most developmental genes: transcription factors (*Dlx1–Dlx2* genes in mouse, (Qiu *et al*., 1997; Thomas *et al*., 1997)) and signalling factors (*Bmp2–4* in mouse (Vainio *et al*., 1993); *Fgf2–Fgf4*, *Fgf4–Fgf8* and *Fgf9* in mouse, (Jernvall *et al*., 1994; Kettunen & Thesleff, 1998)). However, *Bmp4* expression is far more studied during odontode and tooth development in vertebrates than other *Bmp* genes, which makes it difficult to draw evolutionary hypotheses about expression pattern divergences among species within this gene family. For example, *O. mykiss* and the Atlantic salmon *Salmo salar* (L. 1758) display very divergent *bmp4* dental expression patterns (Fraser *et al*., 2004; Koop *et al*., 2008; Huysseune *et al*., 2008; see Table 2 and http://fberio.github.io/Genetic-building-of-teeth-and-odontodes). In contrast, no expression difference is detected between *S. salar* and *M. musculus* (in both tissues during LM to LD (Åberg *et al*., 1997; Bitgood & McMahon, 1995; Keränen *et al*., 1998; Kettunen & Thesleff, 1998; Vaahtokari *et al*., 1996; Vainio *et al*., 1993)). The trout–salmon differences might come from technical discrepancies (gene expression patterns observed in sections of various thickness or orientation) but they could also reflect an actual difference in very closely related species, which may be explained if a redundant paralogue took over the Bmp4 function. Under the redundancy hypothesis, members of a given gene family (paralogues) can substitute for each other without affecting the development of a given structure. Sub-functionalisation in a gene family happens when regulatory sequences evolve so that different copies inherit the ancestral expression pattern in different lineages (Force *et al*., 1999). Because these transcription and signalisation factors are under strong purifying selection, they still largely conserve their ancestral functions (Carroll, 2008) and regulatory sequences may evolve *de novo* to switch on one gene that previously lost a site of expression. This process of redundant paralog shuffling, when considering the totality of developmental gene families, may be largely responsible for the divergence of a genetic cascade in different lineages. This process would result in a developmental drift: the global conservation of a phenotype while the genetic cascade, considered at the level of individual genes, is very different between species (Robinson, 2011).

Unlike *Bmp4*, *Shh* does not display known functional redundancies with any other gene. It bears a critical role during dental placode initiation and is known to have an epithelial expression in mouse molar development (Li *et al*., 2015; Thesleff & Sharpe, 1997). Yet, in this review we also highlight a mesenchymal *Shh* expression in Malawi cichlids (from ED to LD stages (Fraser *et al*., 2008, 2013)) and in *S. canicula* caudal scales (Cooper *et al*., 2017). Although we cannot invalidate a hypothesis of canalisation (where such differences in *Shh* expression would not have any impact on the final tooth shape), the discrepancies in *Shh* location, timing and intensity of expression between species is most often interpreted as a result of natural selection to explain interspecific evolution of tooth shape. As a conclusion, unravelling the potential major changes in the odontode developmental cascade that led to the diversity of tooth and scale shape in jawed vertebrates is still a complex problem. Testing protein redundancy and function, together with variation in gene expression patterns, in a comparative framework is a difficult task in non-model and highly different organisms. However, this step is probably necessary to test which modified genetic factors can actually account for the evolution of odontodes and teeth in vertebrates.

7 | CONCLUSION

In this review, we report intraspecific and interspecific differences and similarities that are not easily related to evolutionary distances between species or structures. Previous work pointed out that some gene families display more similar expression patterns between different structures within a species than between similar structures across species (Debiais-Thibaud *et al*., 2008, 2011). However, such studies are in the minority and there is still a need for data to validate this trend for multigenic families involved in tooth and odontode development. In the future, particular attention should be given to the investigation of complete gene families and of all developmental stages of the structures.

Here, we wished to highlight how the hypothesis linking gene cascade evolution to morphological evolution is still currently difficult to test both because of staging artefacts and of functional redundancies between paralogs. Computer models for tooth development were proposed as a complementary approach to tackle this issue, as far as the genetic components of these models can be linked to the experimentally studied genes (Salazar-Ciudad & Jernvall, 2002, 2010). Simulations of tooth growth also use different levels of proliferation (*Fgf*, *Shh*) and differentiation (*Bmp*) signals, as well as mechanical constraints such as cell adhesion or tissue bending elasticity (Salazar-Ciudad & Jernvall, 2002, 2010; Takigawa-Imamura *et al*., 2015). The combination of these parameters, mimicking tooth growth in distinct environments, succeeded in producing *in silico* teeth that follow the natural variation of tooth shape, within and among species (Salazar-Ciudad & Jernvall, 2010). These new tools raise the question about the relative importance of variables that affect the shape of a tooth or an odontode: besides chemical signals, mechanical interactions between tissues and cells determine the final shape of a structure (Dassule & McMahon, 1998; Huysseune, 1995; Pantalacci *et al*., 2017; Takigawa-Imamura *et al*., 2015). Hence, the identification of the evolutionary processes that led to the diversity of tooth and odontode development still requires more experimental genetic data but also physical approaches to better describe morphogenesis.

CONTRIBUTIONS

F.B. and M.D.T. drafted the manuscript.

ORCID

Fidji Berio https://orcid.org/0000-0003-0810-9783
Mélanie Debiais-Thibaud https://orcid.org/0000-0002-1377-2515

REFERENCES

Åberg, T., Wang, X.-P., Kim, J.-H., Yamashiro, T., Bei, M., Rice, R., … Thesleff, I. (2004). Runx2 mediates FGF signaling from epithelium to mesenchyme during tooth morphogenesis. *Developmental Biology*, *270*, 76–93.

Åberg, T., Wozney, J., & Thesleff, I. (1997). Expression patterns of bone morphogenetic proteins (*Bmps*) in the developing mouse tooth suggest roles in morphogenesis and cell differentiation. *Developmental Dynamics*, *210*, 383–396.

Bitgood, M. J., & McMahon, A. P. (1995). *Hedgehog* and *Bmp* genes are coexpressed at many diverse sites of cell–cell interaction in the mouse embryo. *Developmental Biology*, *172*, 126–138.

Blais, S. A., MacKenzie, L. A., & Wilson, M. V. H. (2011). Tooth-like scales in early Devonian eugnathostomes and the 'outside-in' hypothesis for the origins of teeth in vertebrates. *Journal of Vertebrate Paleontology*, *31*, 1189–1199.

Borday-Birraux, V., Heyden, C., Debiais-Thibaud, M., Verreijdt, L., Stock, D. W., Huysseune, A., & Sire, J.-Y. (2006). Expression of *dlx* genes during the development of the zebrafish pharyngeal dentition: Evolutionary implications. *Evolution & Development*, *8*, 130–141.

Brigandt, I. (2003). Homology in comparative, molecular and evolutionary developmental biology: The radiation of a concept. *Journal of Experimental Zoology*, *299B*, 9–17.

Carroll, S. B. (2008). Evo-Devo and an expanding evolutionary synthesis: A genetic theory of morphological evolution. *Cell*, *134*, 25–36.

Cooper, R. L., Martin, K. J., Rasch, L. J., & Fraser, G. J. (2017). Developing an ancient epithelial appendage: FGF signalling regulates early tail denticle formation in sharks. *EvoDevo*, *8*, 8.

Cooper, R. L., Thiery, A. P., Fletcher, A. G., Delbarre, D. J., Rasch, L. J., & Fraser, G. J. (2018). An ancient turing-like patterning mechanism regulates skin denticle development in sharks. *Science Advances*, *4*, eaau5484.

Dassule, H. R., & McMahon, A. P. (1998). Analysis of epithelial–mesenchymal interactions in the initial morphogenesis of the mammalian tooth. *Developmental Biology*, *202*, 215–227.

Debiais-Thibaud, M., Borday-Birraux, V., Germon, I., Bourrat, F., Metcalfe, C. J., Casane, D., & Laurenti, P. (2007). Development of oral and pharyngeal teeth in the Medaka (*Oryzias latipes*): Comparison of morphology and expression of *Eve1* gene. *Journal of Experimental Zoology Part B: Molecular and Developmental Evolution*, *308B*, 693–708.

Debiais-Thibaud, M., Chiori, R., Enault, S., Oulion, S., Germon, I., Martinand-Mari, C., … Borday-Birraux, V. (2015). Tooth and scale morphogenesis in shark: An alternative process to the mammalian enamel knot system. *BMC Evolutionary Biology*, *15*, 292.

Debiais-Thibaud, M., Germon, I., Laurenti, P., Casane, D., & Borday-Birraux, V. (2008). Low divergence in *dlx* gene expression between dentitions of the medaka (*Oryzias latipes*) versus high level of expression shuffling in osteichtyans. *Evolution & Development*, *10*, 464–476.

Debiais-Thibaud, M., Oulion, S., Bourrat, F., Laurenti, P., Casane, D., & Borday-Birraux, V. (2011). The homology of odontodes in gnathostomes: Insights from *dlx* gene expression in the dogfish, *Scyliorhinus canicula*. *BMC Evolutionary Biology*, *11*, 307.

Debiais-Thibaud, M., Simion, P., Ventéo, S., Muñoz, D., Marcellini, S., Mazan, S., & Haitina, T. (2019). Skeletal mineralisation in association with type X collagen expression is an ancestral feature for jawed vertebrates. *Molecular Biology and Evolution*. Advance online publication, *36*, 2265–2276. https://doi.org/10.1093/molbev/msz145.

Donoghue, P. C. J. (2002). Evolution of development of the vertebrate dermal and oral skeletons: Unraveling concepts, regulatory theories and homologies. *Paleobiology*, *28*, 474–507.

Donoghue, P. C. J., & Rücklin, M. (2016). The ins and outs of the evolutionary origin of teeth. *Evolution & Development*, *18*, 19–30.

Enault, S., Muñoz, D., Simion, P., Ventéo, S., Sire, J.-Y., Marcellini, S., & Debiais-Thibaud, M. (2018). Evolution of dental tissue mineralization: An analysis of the jawed vertebrate *SPARC* and *SPARC-L* families. *BMC Evolutionary Biology*, *18*, 127.

Force, A., Lynch, M., Pickett, F. B., Amores, A., Yan, Y. L., & Postlethwait, J. (1999). Preservation of duplicate genes by complementary, degenerative mutations. *Genetics*, *151*, 1531–1545.

Fraser, G. J., Berkovitz, B. K., Graham, A., & Smith, M. M. (2006a). Gene deployment for tooth replacement in the rainbow trout (*Oncorhynchus mykiss*): A developmental model for evolution of the osteichthyan dentition. *Evolution & Development*, *8*, 446–457.

Fraser, G. J., Bloomquist, R. F., & Streelman, J. T. (2008). A periodic pattern generator for dental diversity. *BMC Biology*, *6*, 32.

Fraser, G. J., Bloomquist, R. F., & Streelman, J. T. (2013). Common developmental pathways link tooth shape to regeneration. *Developmental Biology*, *377*, 399–414.

Fraser, G. J., Cerny, R., Soukup, V., Bronner-Fraser, M., & Streelman, J. T. (2010). The Odontode explosion: The origin of tooth-like structures in vertebrates. *BioEssays*, *32*, 808–817.

Fraser, G. J., Graham, A., & Smith, M. M. (2004). Conserved deployment of genes during odontogenesis across osteichthyans. *Proceedings of the Biological Sciences*, *271*, 2311–2317.

Fraser, G. J., Graham, A., & Smith, M. M. (2006b). Developmental and evolutionary origins of the vertebrate dentition: Molecular controls for Spatio-temporal organisation of tooth sites in Osteichthyans. *Journal of Experimental Zoology Part B: Molecular and Developmental Evolution*, *306B*, 183–203.

Fraser, G. J., Hulsey, C. D., Bloomquist, R. F., Uyesugi, K., Manley, N. R., & Streelman, J. T. (2009). An ancient gene network is co-opted for teeth on old and new jaws. *PLoS Biology*, *7*, e31.

Griffiths, P. E. (2007). The phenomena of homology. *Biology and Philosophy*, *22*, 643–658.

Gunter, H. M., Fan, S., Xiong, F., Franchini, P., Fruciano, C., & Meyer, A. (2013). Shaping development through mechanical strain: The transcriptional basis of diet-induced phenotypic plasticity in a cichlid fish. *Molecular Ecology*, *22*, 4516–4531.

Hall, B. (2005). *Bones and cartilage: Developmental and evolutionary skeletal biology*. San Diego, CA: Academic Press.

Hall, B. K. (1999). Development evolves: The Dilemna for homology. In *Evolutionary developmental biology* (pp. 335–352). Dordrecht, The Netherlands: Springer Netherlands.

Hardcastle, Z., Mo, R., Hui, C. C., & Sharpe, P. T. (1998). The Shh signalling pathway in tooth development: Defects in *Gli2* and *Gli3* mutants. *Development*, *125*, 2803–2811.

Hecht, J., Stricker, S., Wiecha, U., Stiege, A., Panopoulou, G., Podsiadlowski, L., … Seitz, V. (2008). Evolution of a core gene network for skeletogenesis in chordates. *PLoS Genetics*, *4*, e1000025.

Holland, P. W. H., Harper, S. J., McVey, J. H., & Hogan, B. L. M. (1987). *In vivo* expression of mRNA for the Ca^{++}-binding protein SPARC (Osteonectin) revealed by in situ hybridization. *The Journal of Cell Biology*, *105*, 473–482.

Huysseune, A. (1995). Phenotypic plasticity in the lower pharyngeal jaw dentition of *Astatoreochromis alluaudi* (Teleostei: Cichlidae). *Archives of Oral Biology*, *40*, 1005–1014.

Huysseune, A., & Sire, J.-Y. (1998). Evolution of patterns and processes in teeth and tooth-related tissues in non-mammalian vertebrates. *European Journal of Oral Sciences*, *106*, 437–481.

Huysseune, A., Sire, J.-Y., & Witten, P. E. (2009). Evolutionary and developmental origins of the vertebrate dentition. *Journal of Anatomy*, *214*, 465–476.

Huysseune, A., Takle, H., Soenens, M., Taerwe, K., & Witten, P. E. (2008). Unique and shared gene expression patterns in Atlantic salmon (*Salmo salar*) tooth development. *Development Genes and Evolution*, *218*, 427–437.

Huysseune, A., Van der heyden, C., & Sire, J.-Y. (1998). Early development of the zebrafish (*Danio rerio*) pharyngeal dentition (Teleostei, Cyprinidae). *Anatomy and Embryology*, *198*, 289–305.

Inoue, J. G., Miya, M., Lam, K., Tay, B.-H., Danks, J. A., Bell, J., … Venkatesh, B. (2010). Evolutionary origin and phylogeny of the modern Holocephalans (Chondrichthyes: Chimaeriformes): A mitogenomic perspective. *Molecular Biology and Evolution*, *27*, 2576–2586.

Itoh, N., & Ornitz, D. M. (2008). Functional evolutionary history of the mouse *Fgf* gene family. *Developmental Dynamics*, *237*, 18–27.

Jackman, W. R., Draper, B. W., & Stock, D. W. (2004). *fgf* signaling is required for zebrafish tooth development. *Developmental Biology*, *274*, 139–157.

Jackman, W. R., Yoo, J. J., & Stcok, D. W. (2010). Hedgehog signaling is required at multiple stages of zebrafish tooth development. *BMC Developmental Biology*, *10*, 119.

Janvier, P. (1996). *Early vertebrates*. Oxford, UK: Clarendon Press.

Jernvall, J., Åberg, T., Kettunen, P., Keranen, S., & Thesleff, I. (1998). The life history of an embryonic signaling center: BMP-4 induces p21 and is associated with apoptosis in the mouse tooth enamel knot. *Development*, *125*, 161–169.

Jernvall, J., Kettunen, P., Karavanova, I., Martin, L. B., & Thesleff, I. (1994). Evidence for the role of the enamel knot as a control center in mammalian tooth cusp formation: Non-dividing cells express growth stimulating *fgf-4* gene. *The International Journal of Developmental Biology*, *38*, 463–469.

Jernvall, J., & Thesleff, I. (2012). Tooth shape formation and tooth renewal: Evolving with the same signals. *Development*, *139*, 3487–3497.

Johanson, Z., Smith, M. M., & Joss, J. M. P. (2007). Early scale development in *Heterodontus* (Heterodontiformes; Chondrichthyes): A novel chondrichthyan scale pattern. *Acta Zoologica*, *88*, 249–256.

Johanson, Z., Tanaka, M., Chaplin, N., & Smith, M. (2008). Early palaeozoic dentine and patterned scales in the embryonic catshark tail. *Biology Letters*, *4*, 87–90.

Keating, J. N., & Donoghue, P. C. J. (2016). Histology and affinity of anaspids and the early evolution of the vertebrate dermal skeleton. *Proceedings of the Royal Society B: Biological Sciences*, *283*, 20152917.

Kemp, N. E. (1999). Integumentary system and teeth. In W. C. Hamlett (Ed.), *Sharks, skates and rays. The biology of elasmobranch fishes* (pp. 43–68). Baltimore, MD: Johns Hopkins University Press.

Keränen, S. V. E., Åberg, T., Kettunen, P., Jernvall, J., & Thesleff, I. (1998). Association of developmental regulatory genes with the development of different molar tooth shapes in two species of rodents. *Development Genes and Evolution*, *208*, 477–486.

Kettunen, P., Karavanova, I., & Thesleff, I. (1998). Responsiveness of developing dental tissues to fibroblast growth factors: Expression of splicing alternatives of FGFR1, –2, –3 and of FGFR4; and stimulation of cell proliferation by FGF-2, –4, –8 and –9. *Developmental Genetics*, *22*, 374–385.

Kettunen, P., Laurikkala, J., Itäranta, P., Vainio, S., Itoh, N., & Thesleff, I. (2000). Associations of FGF-3 and FGF-10 with signaling networks regulating tooth morphogenesis. *Developmental Dynamics*, *219*, 322–332.

Kettunen, P., & Thesleff, I. (1998). Expression and function of FGFs-4, –8 and –9 suggest functional redundancy and repetitive use as epithelial signals during tooth morphogenesis. *Developmental Dynamics*, *211*, 256–268.

Koop, B. F., von Schalburg, K. R., Leong, J., Walker, N., Lieph, R., Cooper, G. A., … Davidson, W. S. (2008). A salmonid EST genomic study: Genes, duplications, phylogeny and microarrays. *BMC Genomics*, *9*, 545.

Laurikkala, J., Mikkola, M., Mustonen, T., Åberg, T., Koppinen, P., Pispa, J., … Thesleff, I. (2001). TNF signaling via the ligand–receptor pair Ectodysplasin and Edar controls the function of epithelial signaling centers and is regulated by Wnt and Activin during tooth organogenesis. *Developmental Biology*, *229*, 443–455.

Li, J., Feng, J., Liu, Y., Ho, T. V., Grimes, W., Ho, H. A., … Chai, Y. (2015). BMP-SHH signaling network controls epithelial stem cell fate via regulation of its niche in the developing tooth. *Developmental Cell*, *33*, 125–135.

Lukinmaa, P. L., Vaahtokari, A., Vainio, S., Sandbeg, M., Waltimo, J., & Thesleff, I. (1993). Transient expression of type III collagen by odontoblasts: Developmental changes in the distribution of Pro-$_{\alpha 1}$ (III) and Pro-$_{\alpha 1}$ (I) collagen mRNAs in dental tissues. *Matrix*, *13*, 503–515.

Martin, K., Rasch, L., & Cooper, R. (2016). Sox2+ progenitors in sharks link taste development with the evolution of regenerative teeth from denticles. *PNAS*, *113*, 14769–14774.

Mellinger, J., & Wrisez, F. (1993). Etude des écailles primaires de l'embryon de la roussette *Scyliorhinus canicula* (Chondrichthyes: Scyliorhinidae) au microscope électronique à balayage. *Annales des Sciences Naturelles. Zoologie et Biologie Animale*, *14*, 13–22.

Mitsiadis, T. A., Muramatsu, T., Muramatsu, H., & Thesleff, I. (1995b). Expression of the heparin-binding cytokines, midkine (MK) and HB-GAM (pleiotrophin) is associated with epithelial-mesenchymal interactions during fetal development and organogenesis. *Development*, *121*, 37–51.

Mitsiadis, T. A., Salmivirta, M., Muramatsu, T., Muramatsu, H., Rauvala, H., Lehtonen, E., … Thesleff, I. (1995a). Midkine (MK), a heparin-binding growth/differentiation factor, is regulated by retinoic acid and epithelial-Mesenchymal interactions in the developing mouse tooth and affects cell proliferation and morphogenesis. *The Journal of Cell Biology*, *129*, 267–281.

Neubüser, A., Peters, H., Balling, R., & Martin, G. R. (1997). Antagonistic interactions between FGF and BMP signaling pathways: A mechanism for positioning the sites of tooth formation. *Cell*, *90*, 247–255.

Pantalacci, S., Guéguen, L., Petit, C., Lambert, A., Peterkovà, R., & Sémon, M. (2017). Transcriptomic signatures shaped by cell proportions shed light on comparative developmental biology. *Genome Biology*, *18*, 29–53.

Powter, D. M., Gladstone, W., & Platell, M. (2010). The influence of sex and maturity on the diet, mouth morphology and dentition of the port

Jackson shark, *Heterodontus portusjacksoni*. *Marine and Freshwater Research*, *61*, 74–85.

Qiu, M., Bulfone, A., Ghattas, I., Meneses, J. J., Christensen, L., Sharpe, P. T., … Rubenstein, J. L. R. (1997). Role of the *Dlx* homeobox genes in proximodistal patterning of the branchial arches: Mutations of Dlx-1, Dlx-2 and Dlx-1 and -2 alter morphogenesis of proximal skeletal and soft tissue structures derived from the first and second arches. *Developmental Biology*, *185*, 165–184.

Rasch, L. J., Martin, K. J., Cooper, R. L., Metscher, B. D., Underwood, C. J., & Fraser, G. J. (2016). An ancient dental gene set governs development and continuous regeneration of teeth in sharks. *Developmental Biology*, *415*, 347–370.

Reif, W.-E. (1980). Development of dentition and dermal skeleton in embryonic *Scyliorhinus canicula*. *Journal of Morphology*, *166*, 275–288.

Reif, W.-E. (1982). Evolution of dermal skeleton and dentition in vertebrates: The Odontode regulation theory. In M. K. Hecht, B. Wallace, & G. T. Prance (Eds.), *Evolutionary Biology* (pp. 287–368). New York, NY: Plenum Press.

Renz, A. J., Gunter, H. M., Fischer, J. M., Qiu, H., Meyer, A., & Kuraku, S. (2011). Ancestral and derived attributes of the *dlx* gene repertoire, cluster structure and expression patterns in an African cichlid fish. *Evo-Devo*, *2*, 1.

Rivera-Rivera, C. J., & Montoya-Burgos, J. I. (2017). Trunk dental tissue evolved independently from underlying dermal bony plates but is associated with surface bones in living odontode-bearing catfish. *Proceedings of the Royal Society B: Biological Sciences*, *284*, 20171831.

Robinson, G. W., & Mahon, K. A. (1994). Differential and overlapping expression domains of *Dlx-2* and *Dlx-3* suggest distinct roles for *Distal-less* homeobox genes in craniofacial development. *Mechanisms of Development*, *48*, 199–215.

Robinson, R. (2011). Different paths, same structure: "Developmental systems drift" at work. *PLoS Biology*, *9*, e1001113.

Rücklin, M., & Donoghue, P. C. J. (2015). *Romundina* and the evolutionary origin of teeth. *Biology Letters*, *11*, 20150326.

Salazar-Ciudad, I., & Jernvall, J. (2002). A gene network model accounting for development and evolution of mammalian teeth. *PNAS*, *99*, 8116–8120.

Salazar-Ciudad, I., & Jernvall, J. (2010). A computational model of teeth and the developmental origins of morphological variation. *Nature*, *464*, 583–586.

Schaefer, S. A. (1997). The Neotropical Cascudinhos: Systematics and biogeography of the Otocinclus catfishes (Siluriformes: Loricariidae). *Proceedings of the Academy of Natural Sciences of Philadelphia*, *148*, 1–120.

Schmitt, M. (1995). The homology concept - still alive. In O. Breidbach & W. Kutsch (Eds.), *The nervous systems of invertebrates: An evolutionary and comparative approach* (pp. 425–438). Boston, MA: Birkhäuser Basel.

Sire, J.-Y., Davit-Beal, T., Delgado, S., Van Der Heyden, C., & Huysseune, A. (2002). First-generation teeth in nonmammalian lineages: Evidence for a conserved ancestral character? *Microscopy Research and Technique*, *59*, 408–434.

Sire, J.-Y., & Huysseune, A. (2003). Formation of dermal skeletal and dental tissues in fish: A comparative and evolutionary approach. *Biological Reviews of the Cambridge Philosophical Society*, *78*, 219–249.

Smith, M. M., Fraser, G. J., Chaplin, N., Hobbs, C., & Graham, A. (2009). Reiterative pattern of *sonic hedgehog* expression in the catshark dentition reveals a phylogenetic template for jawed vertebrates. *Proceedings of the Royal Society B: Biological Sciences*, *276*, 1225–1233.

Smith, M. M., Fraser, G. J., & Johanson, Z. (2016). Origin of teeth in jawed vertebrates. *Infocus: Proceedings of the Royal Microscopical Society*, *42*, 4–17.

Smith, M. M., Underwood, C., Clark, B., Kriwet, J., & Johanson, Z. (2018). Development and evolution of tooth renewal in neoselachian sharks as a model for transformation in chondrichthyan dentitions. *Journal of Anatomy*, *232*, 891–907.

St. Amand, T. R., Zhang, Y., Semina, E. V., Zhao, X., Hu, Y., Nguyen, L., … Chen, Y. (2000). Antagonistic signals between BMP4 and FGF8 define the expression of *Pitx1* and *Pitx2* in mouse tooth-forming anlage. *Developmental Biology*, *217*, 323–332.

Takigawa-Imamura, H., Morita, R., Iwaki, T., Tsuji, T., & Yoshikawa, K. (2015). Tooth germ invagination from cell–cell interaction: Working hypothesis on mechanical instability. *Journal of Theoretical Biology*, *382*, 284–291.

Thesleff, I., & Mikkola, M. (2002). The role of growth factors in tooth development. *International Review of Cytology*, *217*, 93–135.

Thesleff, I., & Sharpe, P. (1997). Signalling networks regulating dental development. *Mechanisms of Development*, *67*, 111–123.

Thomas, B. L., Tucker, A. S., Qui, M., Ferguson, C. A., Hardcastle, Z., Rubenstein, J. L., & Sharpe, P. T. (1997). Role of *Dlx-1* and *Dlx-2* genes in patterning of the murine dentition. *Development*, *124*, 4811–4818.

Tschopp, P., & Tabin, C. J. (2017). Deep homology in the age of next-generation sequencing. *Philosophical Transactions of the Royal Society B*, *372*, 20150475.

Tucker, A. S., Headon, D. J., Schneider, P., Ferguson, B. M., Overbeek, P., Tschopp, J., & Sharpe, P. T. (2000). Edar/Eda interactions regulate enamel knot formation in tooth morphogenesis. *Development*, *127*, 4691–4700.

Tummers, M., & Thesleff, I. (2009). The importance of signal pathway modulation in all aspects of tooth development. *Journal of Experimental Zoology Part B: Molecular and Developmental Evolution*, *312B*, 309–319.

Underwood, C. J., Johanson, Z., Welten, M., Metscher, B., Rasch, L. J., Fraser, G. J., & Smith, M. M. (2015). Development and evolution of dentition pattern and tooth order in the skates and rays (Batoidea; Chondrichthyes). *PLoS One*, *10*, e0122553.

Underwood, C. J., Johanson, Z., & Smith, M. M. (2016). Cutting blade dentitions in squaliform sharks form by modification of inherited alternate tooth ordering patterns. *Royal Society Open Science*, *3*, 160385.

Vaahtokari, A., Åberg, T., Jernvall, J., Keränen, S., & Thesleff, I. (1996). The enamel knot as a signaling center in the developing mouse tooth. *Mechanisms of Development*, *54*, 39–43.

Vainio, S., Karavanova, I., Jowett, A., & Thesleff, I. (1993). Identification of BMP-4 as a signal mediating secondary induction between epithelial and mesenchymal tissues during early tooth development. *Cell*, *75*, 45–58.

Vandenplas, S., Vandeghinste, R., Boutet, A., Mazan, S., & Huysseune, A. (2016). Slow cycling cells in the continuous dental lamina of *Scyliorhinus canicula*: New evidence for stem cells in sharks. *Developmental Biology*, *413*, 39–49.

Wise, S. B., & Stock, D. W. (2006). Conservation and divergence of Bmp2a, Bmp2b and Bmp4 expression patterns within and between dentitions of teleost fishes. *Evolution & Development*, *8*, 511–523.

Witten, P. E., Sire, J. Y., & Huysseune, A. (2014). Old, new and new-old concepts about the evolution of teeth. *Journal of Applied Ichthyology*, *30*, 636–642.

Young, N. M., & Hallgrímsson, B. (2005). Serial homology and the evolution of mammalian limb covariation structure. *Evolution*, *59*, 2691–2704.

Yu, J. C., Fox, Z. D., Crimp, J. L., Littleford, H. E., Jowdry, A. L., & Jackman, W. R. (2015). Hedgehog signaling regulates dental papilla formation and tooth size during Zebrafish Odontogenesis. *Developmental Dynamics*, *244*, 577–590.

Zhao, Z., Stock, D. W., Buchanan, A. V., & Weiss, K. M. (2000). Expression of dlx genes during the development of the murine dentition. *Development Genes and Evolution*, *210*, 270–275.

How to cite this article: Berio F, Debiais-Thibaud M. Evolutionary developmental genetics of teeth and odontodes in jawed vertebrates: a perspective from the study of elasmobranchs. *J Fish Biol*. 2020;1–13. https://doi.org/10.1111/jfb.14225

3.2.3 Conclusions of the article

This paper highlights the advantages of using the same baseline to compare the tooth and dermal denticle developments in different clades. However, the morphological equivalences between these interspecific levels might be considered cautiously because they do not necessarily imply strict comparable processes, notably because the timings between two stages differ even within a same clade. Moreover, slight differences in the tooth and denticle regulatory patterns suggest a common, ancestral origin consistent with the outside-in theory (detailed in subsection 1.2.1). The interspecific differences in gene expressions might be attributed to the functional redundancy of some genes. Overall, this review highlights the need for more descriptive and experimental data to correlate the role of a protein with a specific tooth or dermal denticle morphology.

3.3 Tooth models: from *in vivo* to *in silico* teeth

The first computational tooth model was developed about 20 years ago for mammalian teeth by Salazar-Ciudad and Jernvall [2002] and further modified, to link morphological modifications with experimental gene expressions in developing teeth [Salazar-Ciudad and Jernvall, 2002, 2010] (Figure 3.4A).

To us, one of the most relevant findings of this work is that the modification of few parameters, among them the epithelial growth rate, rate of activator secretion, and lateral force in lingual direction, may be sufficient to generate the major transitions in the evolution of an iconic tooth, the so-called mammalian molar [Salazar-Ciudad and Jernvall, 2002]. Similar conclusions have already been pointed out in an experimental study on teeth of *Phoca*: the variation of shape and number of accessory cusps likely emerges from slight differences in activatory and inhibitory fields in a growing tooth bud [Jernvall, 2000; Salazar-Ciudad and Jernvall, 2010] (Figure 3.4). The authors suggested that a cascade effect on successively and slightly distinct inhibitory fields around EKs would generate either sharper teeth with few cusps or blunter teeth with more cusps [Jernvall, 2000; Salazar-Ciudad and Jernvall, 2010] (Figure 3.4A).

As suggested by George Box's famous quote: "all models are wrong but some are useful", computational models are a simplification of reality and, in this sense, are always wrong [Box, 1979]. The trade-off lies in simplifying the reality enough to capture the essence of a phenomenon, while not neglecting factors that could be of —putative— primary importance, in other, Box's, words, "It is inappropriate to be concerned about mice when there are tigers abroad" [Box, 1976]. One simplification consists for example in applying a model based on the gene network topology of a species to another one. Such transfer was achieved from mouse molar developmental rules to postcanine seal teeth and *in silico* results were consistent with the experimental, geometric morphometric findings on seal teeth [Salazar-Ciudad and Jernvall, 2010]. The success of transferring the model between species might, however, rely on the highly conserved dental developmental steps and patterns within mammals, for example on the constitution and functioning of the EKs [Jernvall and Thesleff, 2012]. As stated above, shark tooth buds are not patterned by EKs as defined in mammals [Debiais-Thibaud et al., 2015]. However, because the tooth models are based on mammalian tooth development, one key assumption is the tooth patterning by iterative signalling

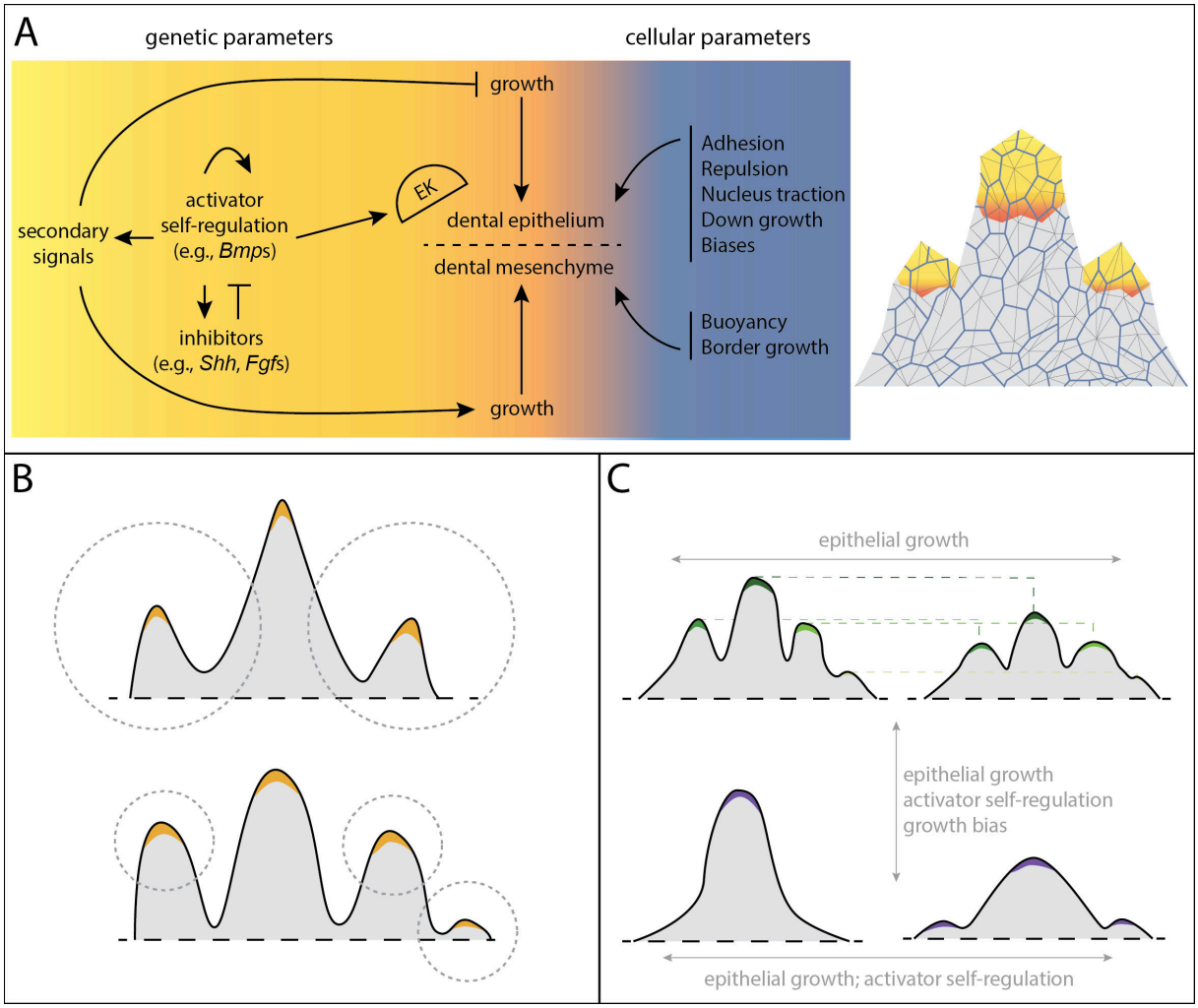

FIGURE 3.4: Results of computational tooth models on mammals. A) Genetic and cellular parameters included in the model of Salazar-Ciudad and Jernvall [2010] (left) and the resulting tooth model (right). EK, enamel knot. Adapted from Salazar-Ciudad and Jernvall [2010]; B) Tooth shapes are impacted by the size of the inhibitory field (dotted circles) of the developing accessory cusps: large inhibitory fields result in teeth with sharp accessory cusps, while small inhibitory fields result in blunt accessory cusps. Scheme adapted from Jernvall [2000]; C) The cusp length is affected by the level of epithelial growth, while the number of accessory cusps is also determined by the activator self-regulation. Scheme adapted from Salazar-Ciudad and Jernvall [2010].

centres mimicking EKs [Salazar-Ciudad and Jernvall, 2002, 2010; Takigawa-Imamura et al., 2015].

That point reached, there are several options to generate realistic shark teeth *in silico* to understand the parameters controlling tooth morphogenesis. In the first, a new model is built from the ground up. However, this might be inefficient because existing models have already be tuned to fit (mammalian) tooth development [Salazar-Ciudad and Jernvall, 2002, 2010] and the regulatory networks are conserved between sharks and mammals [Debiais-Thibaud et al., 2015; Berio and Debiais-Thibaud, 2019]. The second option would be to use brute-force search until the parameters combination that produces the closest morphological result to an actual tooth are reached. Nevertheless,

several combinations of parameters could theoretically produce similar or identical tooth morphologies [Salazar-Ciudad and Jernvall, 2002], which makes it difficult to choose which of the sets is the most likely to drive the tooth shaping in reality. In absence of other decision elements, the most parsimonious combination of parameters as compared to a reference combination (for other species for example) should still be favoured over others. In order to be able to adapt the mammalian models to other groups of organisms, a third option is then to perform functional tests on tooth buds of these organisms to decipher the impact of a given protein or molecule on their final tooth shape. Overall, the best option is to perform functional tests based on the assumptions made by the most parsimonious model so that there is a limited number of parameters to be tested experimentally.

3.4 Project: Functional tests on *S. canicula* tooth buds

"[...] by becoming interested in the cause, we are less likely to dislike the effect."
– How to Win Friends and Influence People, Dale Carnegie, 1936

The following project on functional tests on *S. canicula* tooth buds is still ongoing and the findings presented are only preliminary. The emerging trends and the hypotheses concerning their occurrence should be considered as such.

3.4.1 Introduction

Shark teeth are hypermineralised structures that are permanently shed and replaced by new teeth during lifetime [Reif, 1982; Luer et al., 1990; Powter et al., 2010]. Interspecific tooth forms have been first reported to coincide with sharks feeding habits and phylogenetic relationships [Shimada, 2002, 2005a; Cappetta, 2012]. Intraspecific differences are also reported that result from sexual dimorphism in teeth (gynandric heterodonty) and ontogenetic shifts (ontogenetic heterodonty), and intra-individual variation of tooth forms is correlated with the mesio-distal axis of the jaw [Powter et al., 2010; French et al., 2017; Tomita et al., 2017; Cullen and Marshall, 2019; Berio et al., 2020]. The investigation of the molecular signals involved in shark tooth morphogenesis is a recent field that is largely based on decades of knowledge about mammalian tooth development [Jernvall et al., 1994; Tucker and Sharpe, 1999; Salazar-Ciudad and Jernvall, 2010; Debiais-Thibaud et al., 2011, 2015; Sahlberg, 2015; Martin et al., 2016; Rasch et al., 2016]. In mammals, tooth cusps are patterned by EKs, which are signalling centres expressing a variety of genes including *Shh*, *Fgf*s, and *Bmp*s [Jernvall et al., 1994; Vaahtokari et al., 1996]. As opposed to mammals, shark tooth cusps do not exhibit EKs because the gene expressions that co-locate in the mammalian EKs spatially segregate in sharks [Debiais-Thibaud et al., 2015].

However, if some of the developmental pathways involved in shark tooth patterning have been identified, the functional roles of key proteins in tooth form patterning remain unknown [Debiais-Thibaud et al., 2011, 2015; Martin et al., 2016; Rasch et al., 2016]. Functional tests rely on the *in vivo* modification of the internal or external environment of a specimen and allow to evaluate the impact of such modification on a structure composition and growth. The insertion of soaked beads has been broadly used to perform functional tests: for example to test the role of Shh during limb development

in the chick [Yang et al., 1997] and axolotl [Torok et al., 1999], during molar growth in mouse [Zhang et al., 2008], clasper development in skates [O'Shaughnessy et al., 2015], and shark dermal denticle morphogenesis [Cooper et al., 2018].

3.4.2 Materials and Methods

Sampling

S. canicula embryos were obtained from adults provided by the Observatoire Océanologique de Banyuls-sur-mer (South of France, Mediterranean Sea). Batches of embryos were kept developing at 15 °C until the first tooth row erupts (approximately four months). Detailed sampling is presented in section 6.4 and a summary of the specimens used for the different experiments is displayed in Table 3.1.

TABLE 3.1: Summary of the samples included in each bead experiment. Bmp, bone morphogenetic protein; BSA, bovine serum albumin 0.1 %; DMSO, dimethyl sulfoxide; E, end of the experiment; F, female; Fgf, fibroblast growth factor; HCl, hydrogen chloride; M, male; na, not available; NA, not applicable; PBS, phosphate buffered saline 1X; S, start of the experiment; Shh, sonic hedgehog; TL, total body length.

Number	F:M	TL S:E (cm)	Duration (days)	Protein	Buffer
19	6:13	6.9±0.2:na	32	Shh	NA
8	4:4	6.9±0.4:8.7±0.9	33	none	DMSO
20	6:14	7.4±0.8:9.2±0.7	34	Bmp4	HCl + BSA
11	3:8	8.0±0.4:9.4±0.5	35	none	HCl + BSA
31	17:14	7.5±0.5:8.8±0.4	31	Fgf3	PBS + BSA

The teeth of an untreated embryo were also microCT scanned to provide an overview of the tooth morphologies, as an informal control.

Experimental protocol

Bead preparation Affi-Gel blue gel (Bio-Rad, reference 1537301) beads of 100 µm are selected and stored in PBS at 4 °C. The beads are soaked in the control solutions or solutions containing the proteins (Table 3.2). The proteins are selected according to the role of signalling pathways involved in tooth development in mammals (Figure 3.5) and the proteins used are Shh (human origin, R&D Systems, 8908-SH-005), Fgf3 (human origin, R&D Systems, 1206-F3-025), and Bmp4 (human origin, R&D Systems, 314-BP-010).

TABLE 3.2: Details of bead incubations for the Bmp4, Fgf3, and Shh experiments. Bmp, bone morphogenetic protein; BSA, bovine serum albumin 0.1 %; Fgf, fibroblast growth factor; HCl, hydrogen chloride; PBS, phosphate-buffered saline 1X; Shh, sonic hedgehog.

Experiment	Mix/protein	Composition	Incubation
Shh	Shh	5 µg Shh, 0.2 filtered solution in 20 mM MES, 0.5 M NaCl, 0.5 % CHAPS	1 h, on ice
Shh	PBS	PBS	1 h, on ice
Bmp4	HCl-BSA	4 µL HCl, 1 mg BSA, 896 µL water	1 h, 37 °C
Bmp4	Bmp4	10 µg Bmp4, 100 µL HCl-BSA solution	1 h, 37 °C
Fgf3	PBS-BSA	25 µL BSA, 225 µL PBS	1 h, room temperature
Fgf3	Fgf3	25 mg Fgf3, 25 µL BSA, 225 µL PBS	1 h, room temperature

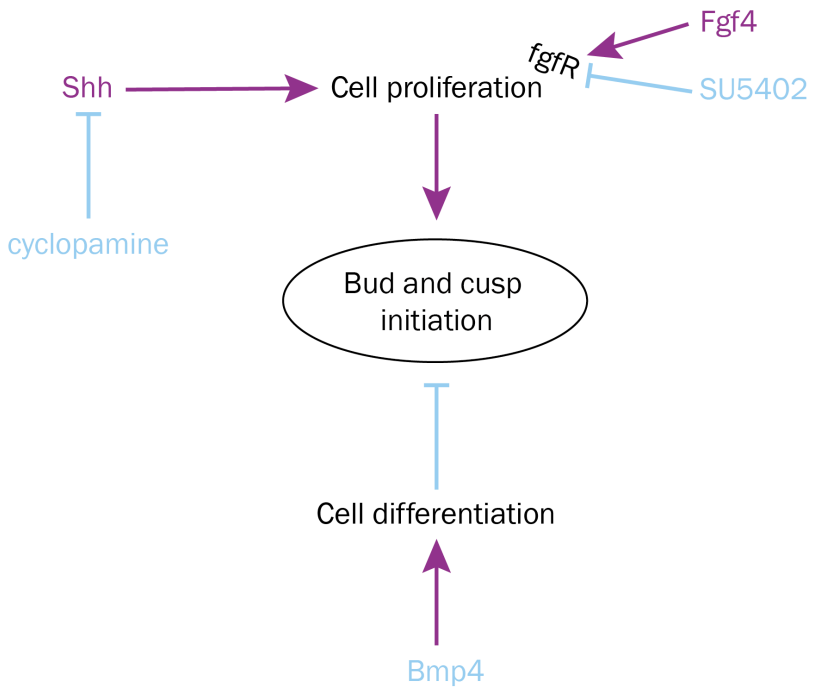

FIGURE 3.5: Proteins and molecules of interest for the functional tests and their putative impacts on tooth bud and cusp initiation in *Scyliorhinus canicula* embryos. Bmp, Bone morphogenetic protein; Fgf, fibroblast growth factor; Shh, Sonic hedgehog.

Bead implantation Once the required total length is reached, the embryos are gently removed from their egg-case (Figure 3.6A-C) and anaesthetised in a buffered tricaine solution (0.17 mg/mL in seawater) for 6 to 8 minutes, depending on the embryo movements (Figure 3.6D and E). The embryo is positioned dorsally so the palatoquadrate teeth can be located (Figure 3.6F). The bead is implanted with a pliers following the alternate tooth pattern in *S. canicula* [Ellis and Shackley, 1995]: in the dental lamina, between two erupted teeth and where the putative youngest tooth bud develops (Figure 3.7). In the Shh and Bmp4 experiments, the control and treated beads are implanted in different specimens, whereas in the Fgf3 experiment, the control and treatment conditions occur in the right and left palatoquadrate, respectively. The sex and total length of each embryo is recorded, the embryo then recovers in seawater. It is enclosed in a small bag to keep developing in seawater during 33 to 35 days, which corresponds to the tooth replacement time in *S. canicula* [Märkel and Laubier, 1969].

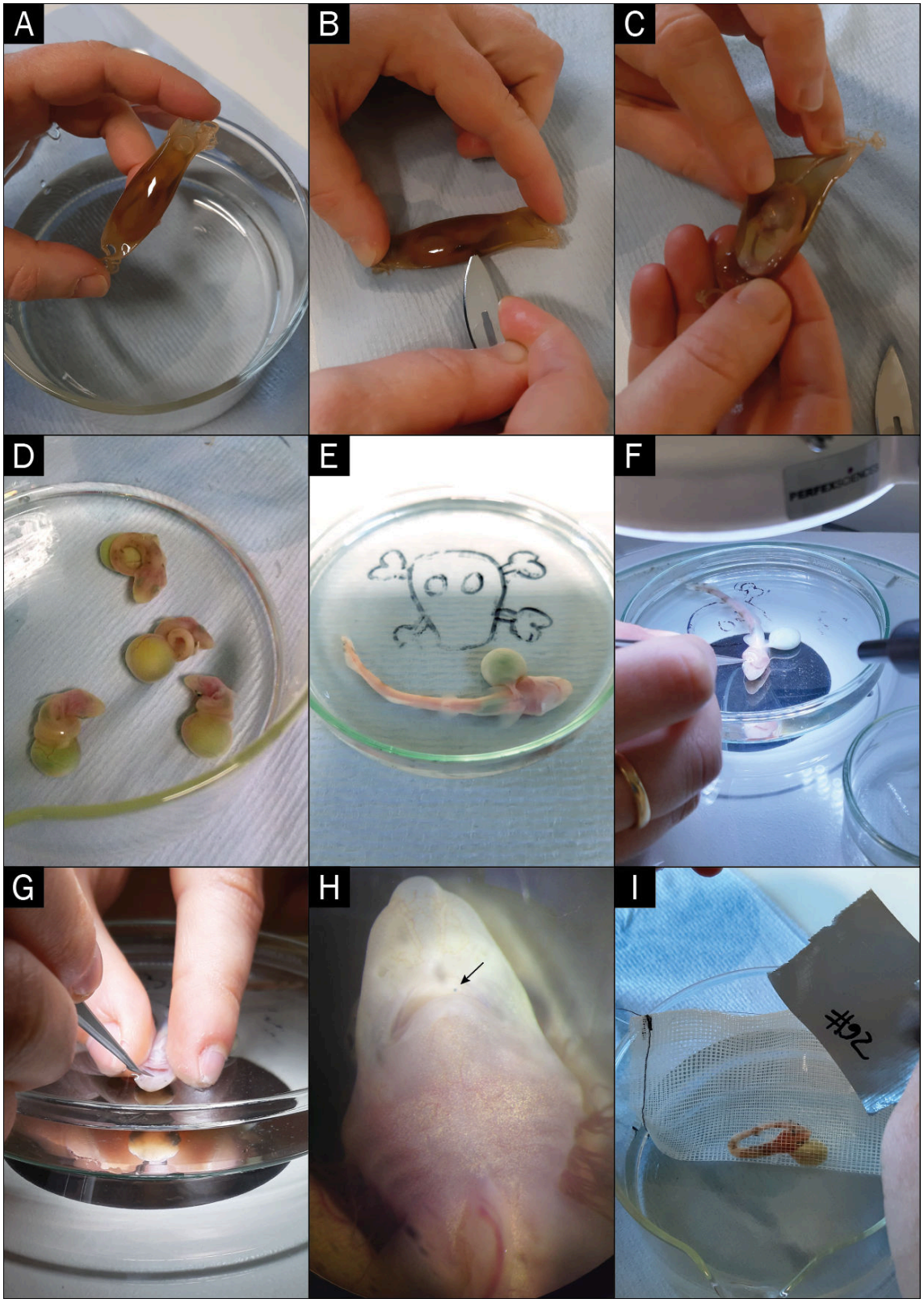

FIGURE 3.6: Experimental protocol of bead insertion in the dental lamina of *Scyliorhinus canicula* embryos. A) *S. canicula* embryo in closed eggcase; B) Eggcase opening with scalpel blade; C) Release of the embryo; D) Embryos are wrapped around themselves just after being released and are left in a tricaine solution until anaesthetised; E) An anaesthetised embryo with now loose body; F) Tracking of tooth rows under binocular loupe to place the bead; G) Bead insertion; H) Checking that the bead (blue point, arrow tip) is locked in place; ventral view; I) The embryo wakes up in sea water, it is identified and placed in a small bag for one month to develop. Pictures by Fidji Berio, Mélanie Debiais-Thibaud, and Adèle Barroil.

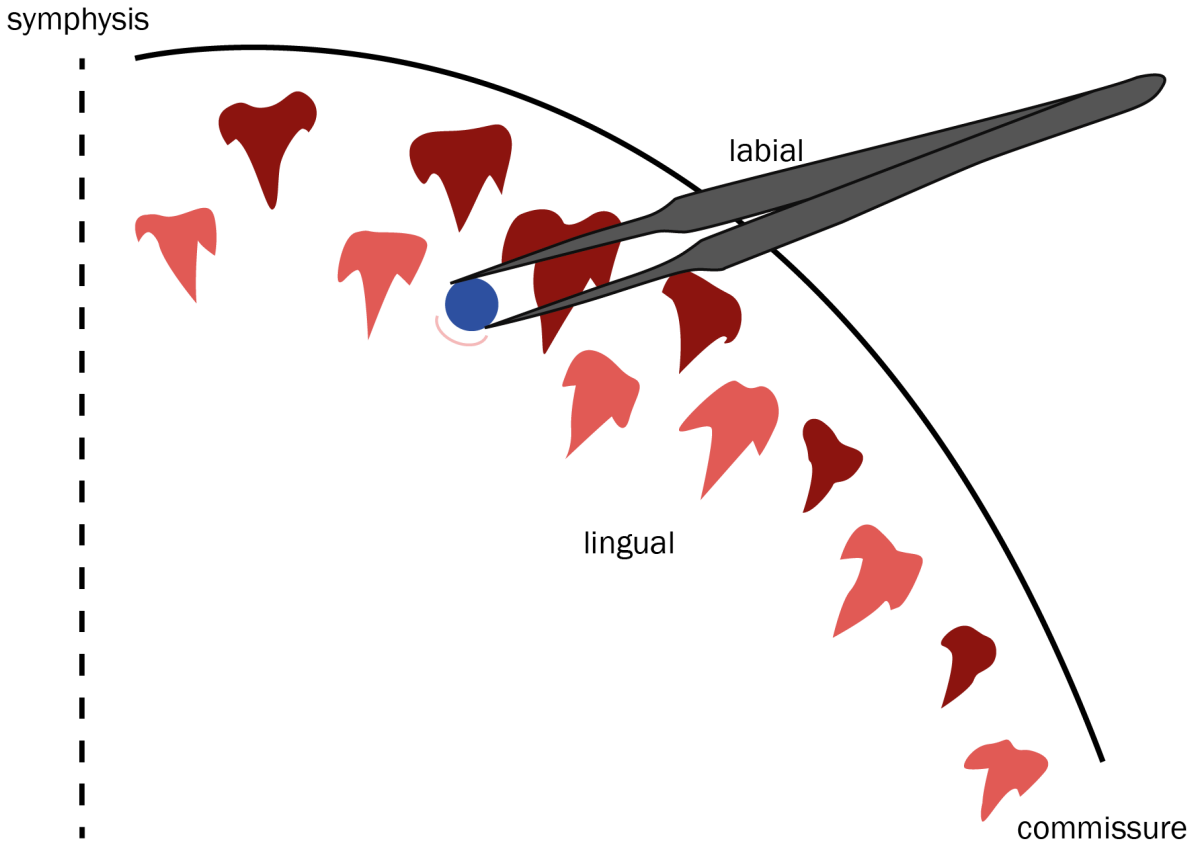

FIGURE 3.7: Bead insertion in the dental lamina of a *Scyliorhinus canicula* embryo. The bead is inserted with a plier in a lingual space in the dental lamina of the palatoquadrate, between two erupted teeth, due to the alternate tooth pattern in *S. canicula*. Blue circle, bead; dark teeth, oldest teeth; lighter teeth, youngest teeth. Plier not to scale.

The embryos are then euthanized in tricaine, measured, fixed in 4 % PFA, and stored at 4 °C. The heads of the embryos are microCT scanned and reconstructed in 3D with Xact softwares (v.11355 and v.11025) and the 3D teeth neighbouring the bead are isolated virtually usuing Avizo Lite (v2019.3).

3.4.3 Results

Teeth of a *S. canicula* embryo are symmetrical or subsymmetrical and look similar when comparing the right and left palatoquadrate, indicating that this is the control morphology (Figure 3.8).

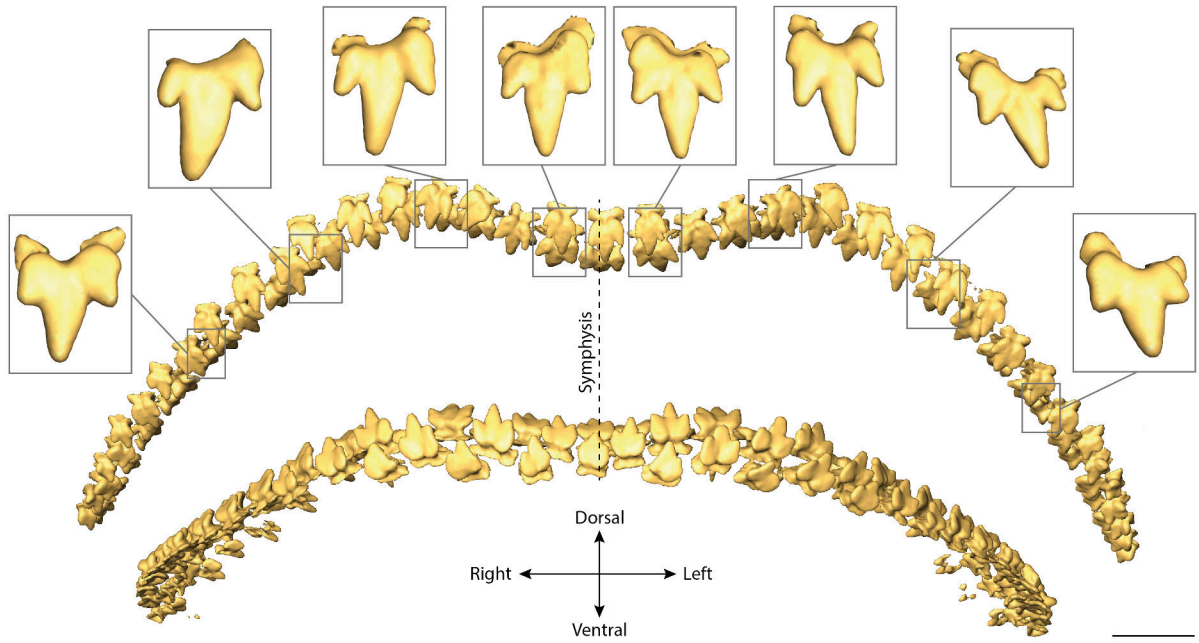

FIGURE 3.8: Tooth morphologies of a *Scyliorhinus canicula* embryo. The tooth morphologies are symmetrical between the right and left palatoquadrate. Scale bar is 300 µm.

Shh

Control. The Shh functional tests included 19 *S. canicula* embryos. Nine specimens died before the end of the experiment and are not included in the following results. In the specimens with no bead insertion, six out of eight teeth have a normal phenotype (Figure 3.9A, C, E, G, I, and O). One has an accessory cusp that is not fully developed (Figure 3.9S) and another displays incomplete mineralisation (Figure 3.9Q). In the specimens with control bead inserted, we report one normal phenotype (Figure 3.9M), one missing tooth (Figure 3.9R), and three teeth with missing cusps (Figure 3.9B, P, and T). Two teeth display a lack of mineralisation (Figure 3.9K and T) and one tooth bud has been split (Figure 3.9T).

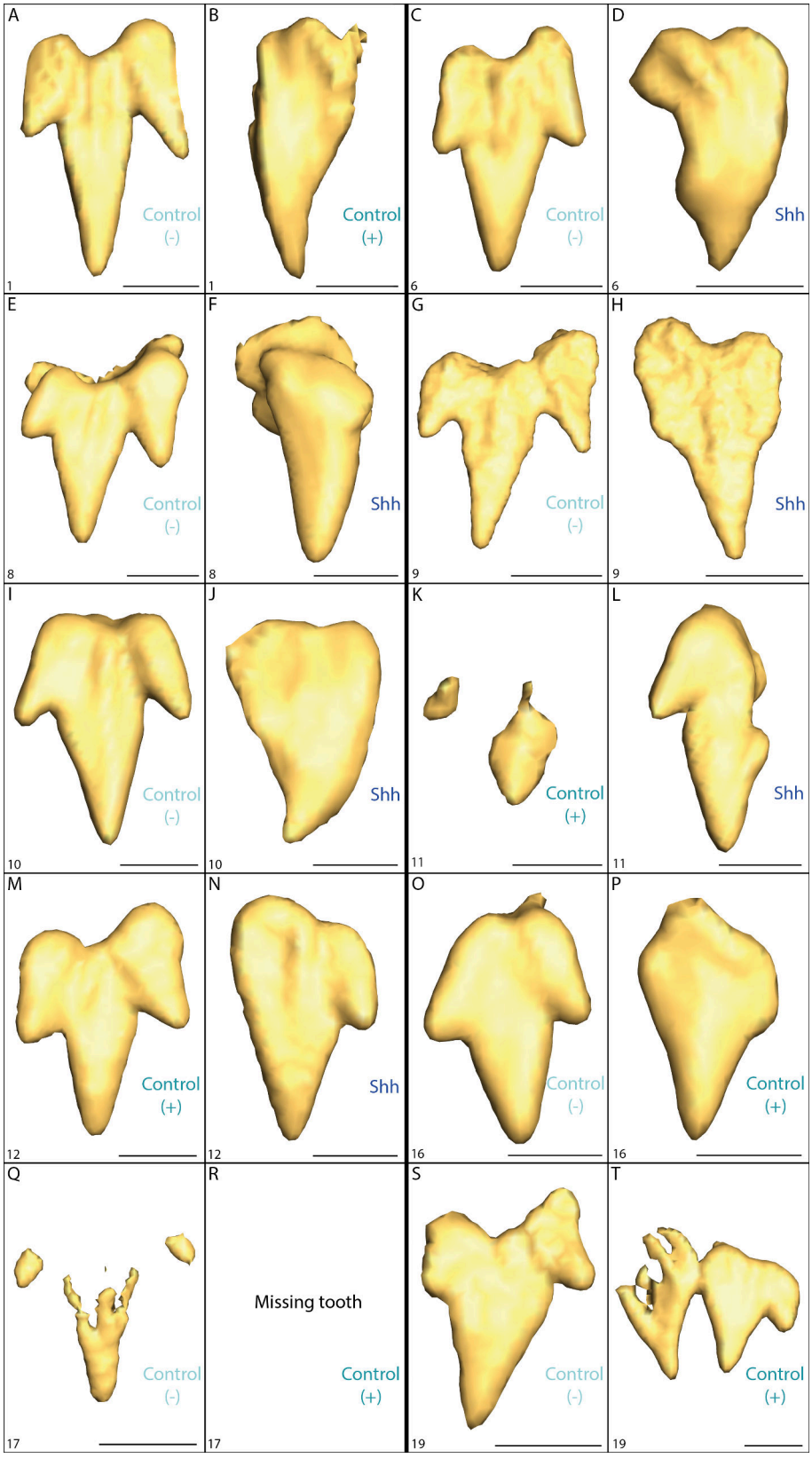

FIGURE 3.9: Morphologies of teeth in *Scyliorhinus canicula* for the Shh functional tests. Control (-) indicates control teeth when no bead is inserted; Control (+) indicates control teeth located next to a bead soaked in PBS; Shh indicates teeth that developed next to a bead soaked in Shh. Identifiers of the specimens are in the bottom left corner. Scale bars are 100 µm.

Treated. All teeth next to the bead soaked in Shh have one or two missing cusps (Figure 3.9D, F, H, J, L, and N) and one is thinner and has a twisted morphology (Figure 3.9L).

Bmp4

Control Two out of the 11 specimens in the control condition died before the end of the experiment and are not included in the following results. Among the remaining specimens, we report one missing tooth (in specimen 33), two with normal morphology (Figure 3.10A and E), and four with missing accessory cusps (Figure 3.10B, F, G, and H). Three specimens exhibit smaller accessory (Figure 3.10D, G, and H) and main (Figure 3.10H) cusps, and one has an accessory cusp with abnormal shape (Figure 3.10C).

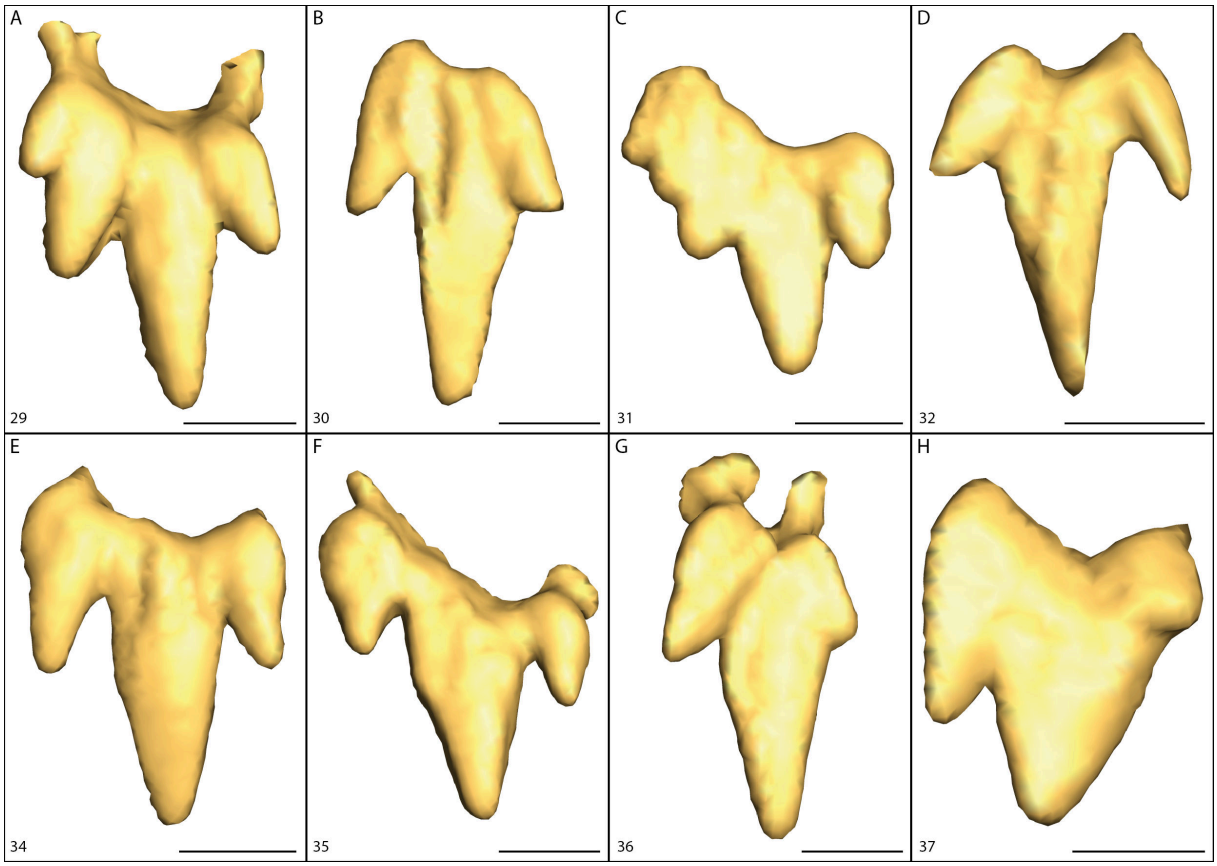

FIGURE 3.10: Morphologies of control teeth in *Scyliorhinus canicula* for the Bmp4 functional tests. The beads are soaked in HCl and BSA. Identifiers of the specimens are in the bottom left corner. Scale bars are 100 µm.

Treated Seven specimens out of the 20 specimens died before the end of the experiment. We report five specimens with normal tooth phenotype (Figure 3.11A, B, C, D, and H) and three specimens with missing tooth at the location of the bead insertion (in specimens 48, 50, and 52). Three specimens have teeth with missing accessory cusps (Figure 3.11E, F, and J), four have small accessory cusps (Figure 3.11E, F, G, and I), and four teeth are thinner than the control teeth (Figure 3.11F, G, I, and J).

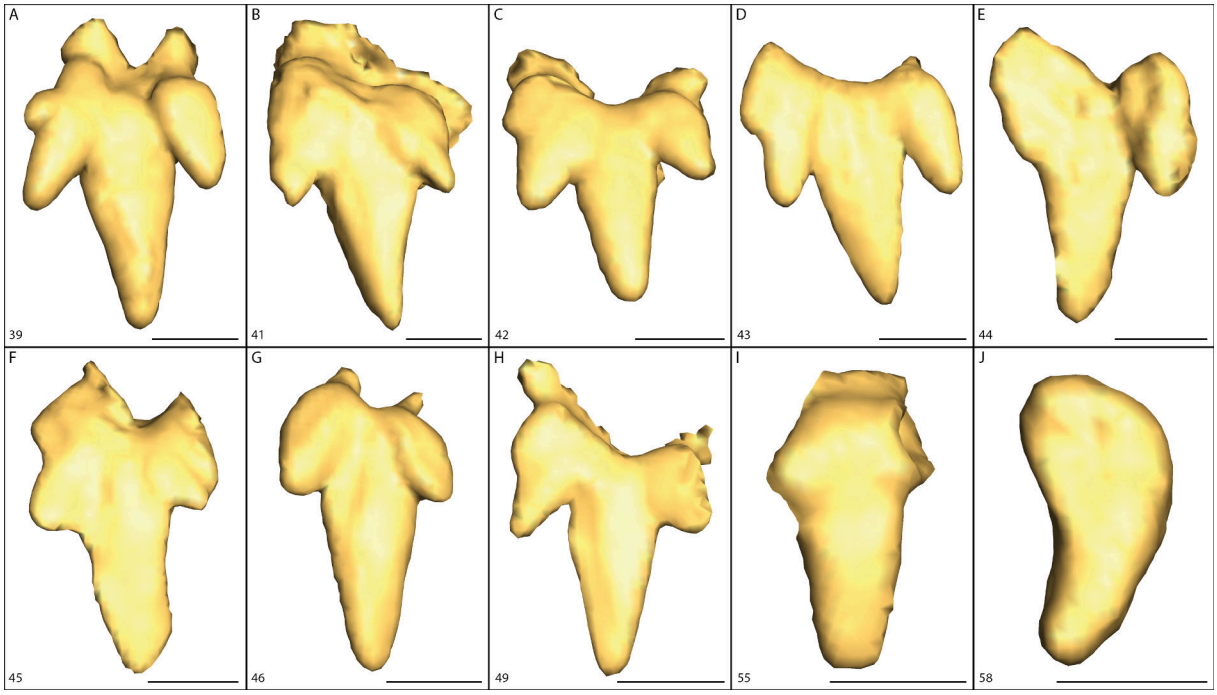

FIGURE 3.11: Morphologies of teeth in *Scyliorhinus canicula* resulting from Bmp4-soaked beads insertion. The beads are soaked in a Bmp4 solution. Identifiers of the specimens are in the bottom left corner. Scale bars are 100 µm.

Fgf3

Nine (three females, six males) out of the 31 specimens died before the end of the experiment and, except for the specimen 83 (Figure 3.12O and P), they could not be used in the following results.

Control Eighteen of the 23 control teeth have a normal morphology, as compared to the adjacent teeth. Out of the other control teeth, one is missing (Figure 3.14AI) and four have missing or underdeveloped accessory cusps (Figure 3.13S and AE and Figure 3.14AM and AO).

Treated Two treated teeth up to 23 have a normal morphology (Figure 3.12L and Figure 3.13V) and one is missing (Figure 3.12B). One tooth cannot be compared to the corresponding control that is missing (Figure 3.14AI and AJ). Nine teeth have missing accessory cusps (Figure 3.12D, N, and P, Figure 3.13Z, AB, AD, and AF, and Figure 3.14AN and AT), four tooth buds are split (Figure 3.12D, Figure 3.13AB and AD, and Figure 3.14AT), and six teeth lack mineralisation, as compared to the controls (Figure 3.12H and J, Figure 3.13T and AB, and Figure 3.14AL and AT). Four teeth exhibit underdeveloped accessory (Figure 3.12F and Figure 3.14AH and AR) and main (Figure 3.13AF) cusps. One tooth has an extra accessory cusp (Figure 3.13X), one tooth has a twisted main cusp (Figure 3.14AR), and two teeth exhibit an abnormal shape of accessory cusps (Figure 3.13R and Figure 3.14AP).

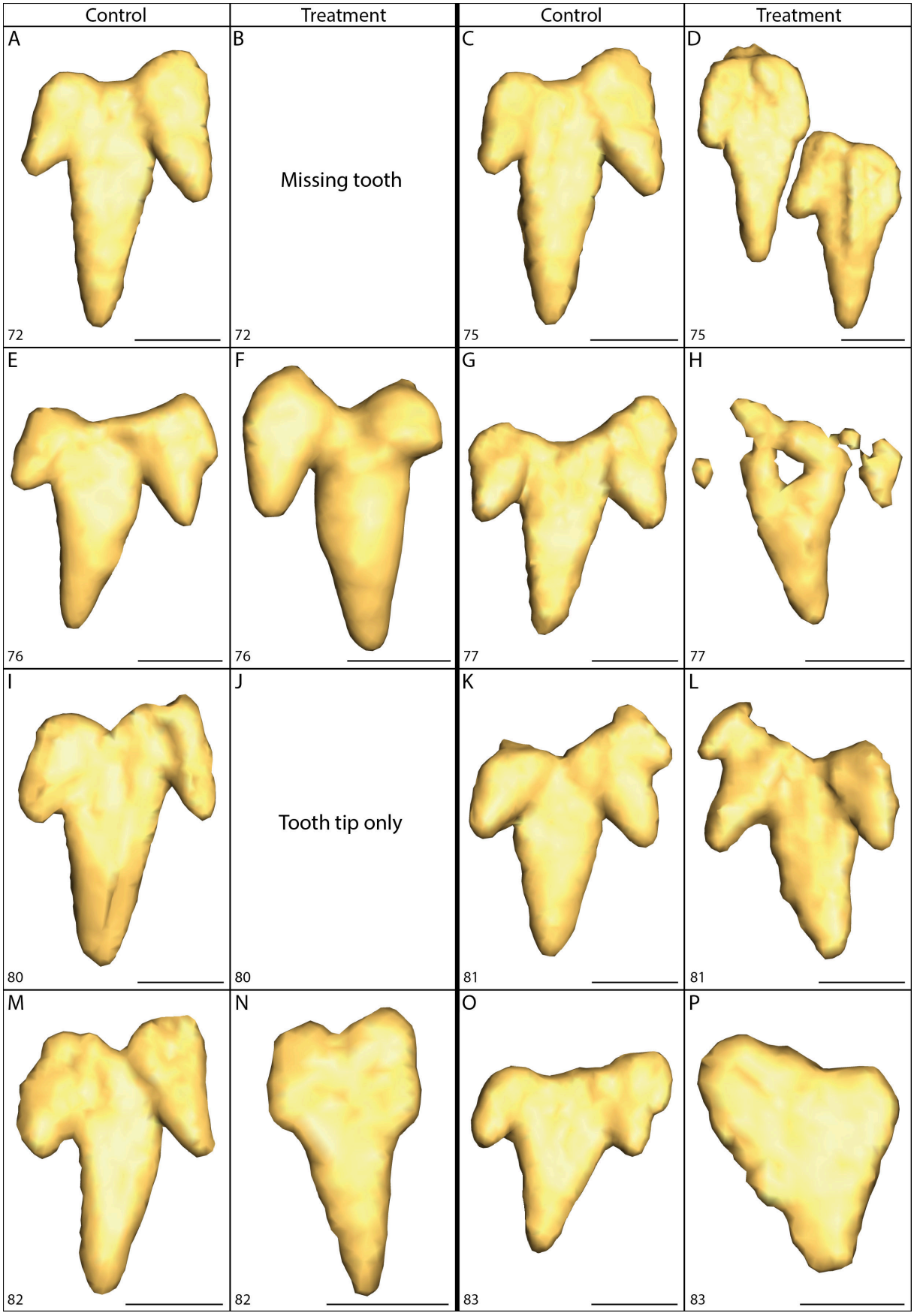

FIGURE 3.12: Morphologies of teeth in *Scyliorhinus canicula* resulting from Fgf3 functional tests – Part 1. In the control condition, beads soaked in PBS-BSA are implanted in the right palatoquadrate and beads soaked in Fgf3 with PBS and BSA are implanted in the left palatoquadrate. Identifiers of the specimens are in the bottom left corner. Scale bars are 100 µm.

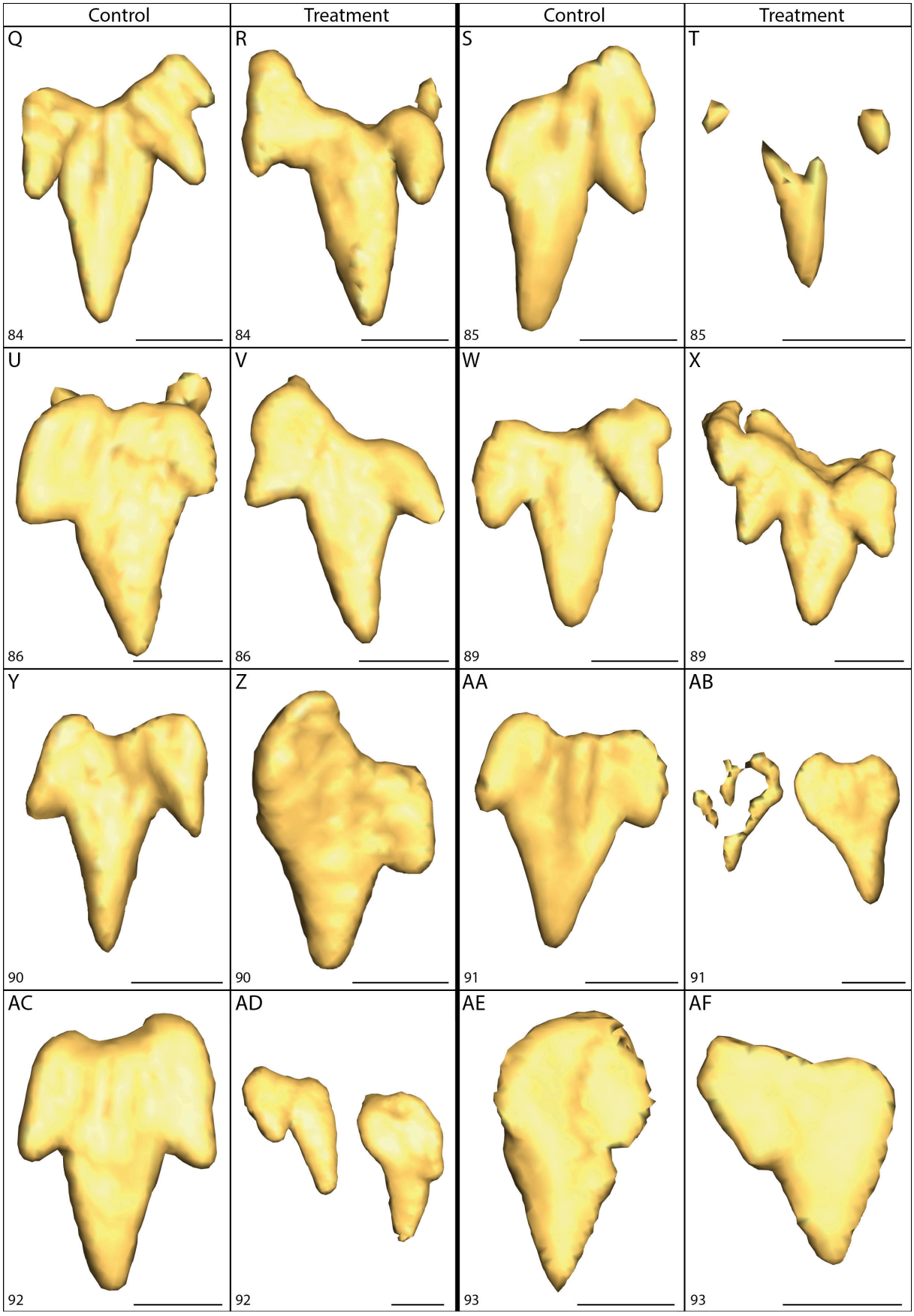

FIGURE 3.13: Morphologies of teeth in *Scyliorhinus canicula* resulting from Fgf3 functional tests – Part 2. In the control condition, beads soaked in PBS-BSA are implanted in the right palatoquadrate and beads soaked in Fgf3 with PBS-BSA are implanted in the left palatoquadrate. Identifiers of the specimens are in the bottom left corner. Scale bars are 100 µm.

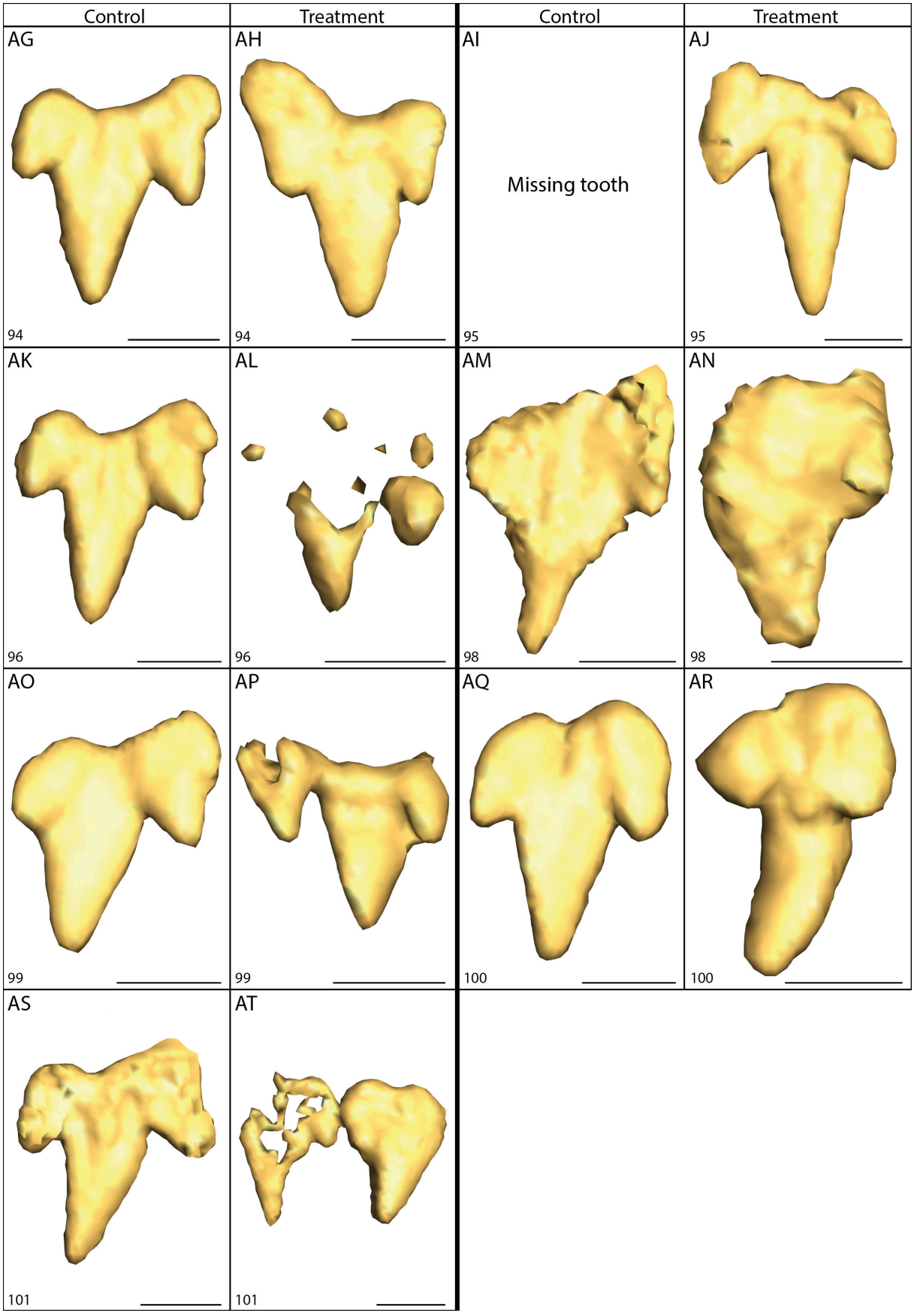

FIGURE 3.14: Morphologies of teeth in *Scyliorhinus canicula* resulting from Fgf3 functional tests – Part 3. In the control condition, beads soaked in PBS-BSA are implanted in the right palatoquadrate and beads soaked in Fgf3 with PBS-BSA are implanted in the left palatoquadrate. Identifiers of the specimens are in the bottom left corner. Scale bars are 100 µm.

The results gathered with the Shh, Bmp4, and Fgf3 experiments are summarised in Figure 3.15.

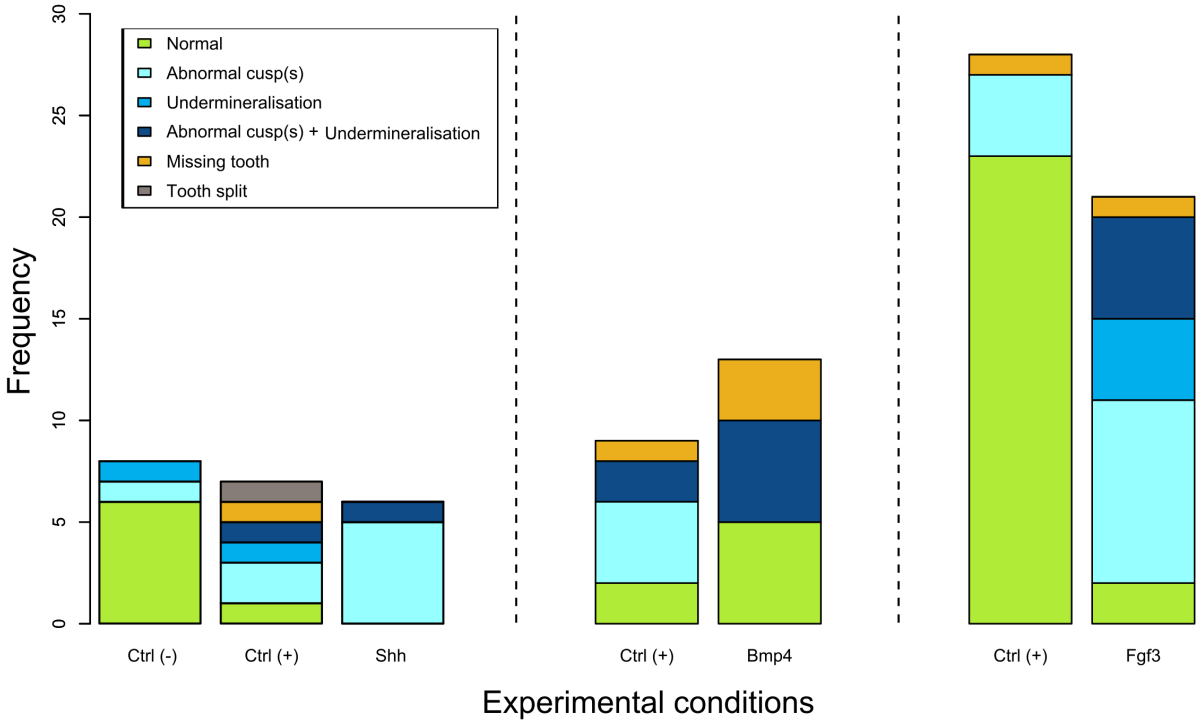

FIGURE 3.15: *Scyliorhinus canicula* tooth phenotypes obtained following the Shh, Bmp4, and Fgf3 functional tests. Ctrl (-), no bead is inserted; Ctrl (+), a bead soaked in buffer is implanted; Shh, Bmp4, and Fgf3, a bead soaked in one of these proteins is inserted next to a developing tooth bud. Abnormal cusp(s), main or accessory cusp(s) are not developed, less developed than in the control condition, or twisted.

3.4.4 Discussion

Technical issues of an unprecedented protocol

The mortality rates of embryos is 47 % in the Shh tests, 9 % in the HCl-BSA controls, 35 % in the Bmp4 tests, and 29 % in the Fgf3 tests. The Shh tests were the first to be performed and the higher mortality as compared to other tests is likely due to the experimental protocol adjustments: of anaesthesia timing, technical handling, and monitoring of embryos. Most embryo losses before the end of the experiments occurred because of umbilical cord twist and yolk sac rupture during growth in the small bags, leading to bacterial contamination and lack of nutrients supply. We improved the protocol by using bags of more flexible material with smaller netting (about 1.1 mm), to reduce the probability of yolk sac being caught in meshes. Smaller bags also reduced the embryos mobility, in an attempt to mimic the available space in the egg-case, which improved the survival rates. Nevertheless, the number of embryos that reached the end of the experiments is still insufficient to elaborate reliable scientific conclusions about the role of Shh, Bmp4, and Fgf3 in shark tooth development and the results only provide preliminary trends to be explored in further experiments.

The location of bead insertion was determined between two erupted teeth of the same generation, next to the putative developing bud of the next generation (Figure 3.7). The bead was inserted within the superficial epithelium, which is supposed to be the dental lamina. Even though this protocol is based on literature data on the jaw topology and tooth patterning of *S. canicula* embryos [Debiais-Thibaud et al., 2011; Rasch et al., 2016], there is no evidence that the bead is inserted at the optimal location to impact the tooth bud development. Because the bead cannot be seen in microCT images, it could be located with a binocular magnifier at the end of the experiment to determine if it locates next to a newly erupted tooth.

Once inserted, the bead must stay in place during the next 24 hours, during which the protein is released in the tissues [Yang et al., 1997]. Out of the 11 inserted beads, six were observed in the dental lamina of *S. canicula* embryos at the end of the Shh experiment (Figure 3.9B, H, J, K, P, and R). The others might thus have been lost at the very beginning of the tests or during the following month of growth, which disrupts the interpretation of what the observed tooth morphologies are due to, protein, bead only or surgical injury, at the end of the experiment.

Heterogeneity of the results: injuries, physical disturbances, and hazardous developmental stages

The bead insertion, with or without protein, interfered with two main processes during tooth growth: cusp development and tooth mineralisation. However, the limits discussed above are likely responsible for other isolated morphologies: the bead insertion or the surgical incision might have split developing tooth buds and created the observed duplicates (Figure 3.9T, Figure 3.12D, Figure 3.13AB and AD, Figure 3.14AT) or may have injured the tissues so that no tooth could have developed at all (Figure 3.9R, Figure 3.12B, and Figure 3.14AI).

The location of the bead relative to the developing tooth bud also conditions its impact on the resulting morphology. If too close, it physically disturbs the tooth development by occupying a space the tooth would have needed to grow accessory cusps and if too far, the control solution or protein would not have reached the developing tooth bud receptors (distance of signalling between 90 and 480 µm, based on *Shh* experiments in the chick limb [Yang et al., 1997]). Although attempts were made to implant beads following a constant pattern in all embryos, microscopic differences may have generated the variation observed within the same condition of an experiment (e.g., Figure 3.12H, L, and P).

Tooth growth achieves through four key developmental stages in *S. canicula*: early morphogenesis, late morphogenesis, early differentiation, and late differentiation [Debiais-Thibaud et al., 2011, 2015; Berio and Debiais-Thibaud, 2019]. During morphogenesis, the epithelium and mesenchyme form a wave-shaped bud, while the cusps are formed during early differentiation and the tooth mineralises during late differentiation, after the tooth form is finally acquired [Debiais-Thibaud et al., 2011; Berio and Debiais-Thibaud, 2019]. *Shh* is expressed in the dental lamina during the four stages in *S. canicula*, while *bmp4* is expressed in both dental lamina and mesenchyme (except in early differentiation in the mesenchyme) in these stages (reviewed in Berio and Debiais-Thibaud [2019]). *Fgf3* expression has not been investigated during early morphogenesis, it is reported during late morphogenesis and early differentiation in the

dental lamina and in the mesenchyme, and is absent during late differentiation [Berio and Debiais-Thibaud, 2019]. These expressions indicate that the genes considered in this work do not play a role in tooth patterning in the same tissues at the same time. This implies that if a bead is inserted deep in the mesenchyme instead of in the dental lamina, the control solution or the protein might not affect the tooth bud development. Moreover, the receptors of these proteins might not be expressed by the tooth bud during its whole growth. The proteins considered in this study were selected based on the previously reported gene expressions on shark tooth buds but the expression of their respective receptors has never been reported in *S. canicula* tooth buds. This information would have helped us to determine the location and timing in which the selected proteins might impact the tooth bud development because if the bead releases the protein next to a tooth bud that does not undergo the responsive developmental stage, the final tooth form will not be patterned according to this protein supply. Furthermore, if the tooth replacement rate is of 35 days per row in *S. canicula* [Märkel and Laubier, 1969], the duration of each bud stage during this time has not been investigated and the 48 hours during which the beads release a protein could for example never impact a short lasting stage. Also, even though the protein interacts with tooth bud receptors, it is not known how resilient the tooth bud is to the disruption and if the exposure duration will impact the long-term morphology of the tooth. This resilience might also depend on the protein concentration and, so far, there is no quantification of such protein amounts in shark tooth buds. The concentrations used in this work are based on previous experimental studies that were not performed in sharks nor necessarily in tooth buds, which also conditions the impact of a protein on *S. canicula* tooth buds.

Impacts of Shh, Fgf3, and Bmp4 on *S. canicula* tooth shape

Several hypotheses about the putative impact of Shh, Fgf3, and Bmp4 on *S. canicula* tooth bud morphology can still be proposed despite the limitations discussed above.

Shh and Fgf3 impact accessory cusp development and tooth mineralisation Shh and Fgf3 are cell division activators of tooth development [Kettunen et al., 2000; Cobourne et al., 2001]. In *S. canicula*, *fgf3* is expressed at the apical epithelial bud, in both epithelium and underlying mesenchyme during late morphogenesis and early differentiation [Rasch et al., 2016]. *Shh* is expressed during early differentiation in the epithelium and restricted to the epithelium of developing accessory cusps during late differentiation [Debiais-Thibaud et al., 2015; Martin et al., 2016]. Shh and Fgf3 were expected to produce bigger teeth with more accessory cusps, as the latter occurs in mouse molars [Zhang et al., 2008] and computational model on seal teeth [Salazar-Ciudad and Jernvall, 2010]. However, no size differences are visually detected in overall teeth between the control and Shh conditions but all teeth treated with Shh have missing or abnormally shaped accessory cusps, while such phenotype was observed in only one tooth exposed to a control bead (Figure 3.9). It is thus possible that the addition of Shh counteracts the differentiation signals expressed in the developing accessory cusps even though it does not promote main cusp growth. The teeth treated with Fgf3 also exhibit missing accessory cusps but also incomplete mineralisation, whereas the control teeth display normal phenotypes in most specimens (Figure 3.12, Figure 3.13, and Figure 3.14). Similar to the Shh impact, Fgf3 could inhibit the shaping process of accessory cusps

by maintaining cell proliferation in a unicuspid tooth. Assuming that a shift in local expressions of *Shh* and *Fgf3* is necessary to initiate the development of accessory cusps after the main cusp is fully patterned, it is possible that such shift might have been obliterated by the diffusion of Shh and Fgf3 at the whole tooth bud scale. Moreover, Fgf signalling is involved in tooth mineralisation in rodent molars and incisors [Du et al., 2018]. Of our three experiments, the Fgf3 is the only one to produce treated teeth with mineralisation deficit. This might suggest an interaction between the genes responsible for the tooth bud mineralisation during late differentiation and the occurrence of Fgf3 around the whole tooth bud. Fgf3 might promote cell division, even at slow rates, leading to the inhibition of cell differentiation in odontoblasts and ameloblasts.

Bmp4 treatment fails to impact the tooth bud shape in this experiment As opposed to *shh* and *fgf* genes, *bmp*s are cell differentiation inducers [Åberg et al., 1997; Cobourne et al., 2001; Gritli-Linde et al., 2002; Du et al., 2018; Malik et al., 2018, 2020]. We thus expected *Bmp4* signal to alter the cusps growth and to generate more accessory cusps than in control teeth. However, we report no strong or consistent signal in tooth morphologies that challenges this hypothesis because altered tooth morphologies, with missing or abnormally shaped accessory cusps, are observed in the control and treated teeth (Figure 3.10 and Figure 3.11). Because no such trend was observed in the Shh and Fgf3 tests, we attribute the abnormal morphologies to the physical bead insertion only and not to the protein effect. Previous work on *S. canicula* tooth development reported a *bmp4* expression in both epithelium and mesenchyme during early and late morphogenesis, as well as during late differentiation, whereas *bmp4* has a strict epithelial expression during early differentiation [Debiais-Thibaud et al., 2015; Rasch et al., 2016; Berio and Debiais-Thibaud, 2019]. The absence of morphological signal after the insertion of Bmp4-soaked beads might thus be due to a bead location farther from the developing tooth bud, an inappropriate Bmp4 concentration or timing of insertion, or a combination of several of these possibilities. Also, because the Bmp4 protein used is human-derived, the *S. canicula* receptors might also have not been able to recognize this protein conformation. The Bmp family finally contains several members with some involved in tooth morphogenesis [Åberg et al., 1997; Malik et al., 2018, 2020] and the absence of altered phenotype in the *S. canicula* embryos would also result from the fact that Bmp members different from Bmp4 would critically control the tooth shape acquisition in sharks.

3.4.5 Conclusion

The experimental protocol and results presented here face several pitfalls, among which are the bead insertion and the associated physical injury that potentially induce physical damages to the developing tooth bud, as well as the subjective choice of protein concentrations that might affect the *S. canicula* tooth development. Nevertheless, the results allow designing trends about the putative roles of Shh and Fgf3 on tooth bud development, which should be further tested in a finer tuned protocol, with wide ranges of protein concentrations, and less invasive bead insertion methods. Furthermore, sexually mature *S. canicula* specimens exhibit gynandric heterodonty, a feature that is involved in mating behaviour in several elasmobranch species because males bite females during copulation [McCourt and Kerstitch, 1980; Kajiura and Tricas, 1996;

Domi et al., 2000; Kajiura et al., 2000; Pratt et al., 2005; Gutteridge and Bennett, 2014]. The interplay between sex hormone signalling, the proteins involved in tooth bud development, and tooth bud shape in sharks is thus a promising path that remains to be explored.

3.4.6 Acknowledgements

The project MORDENT was funded by the European Marine Biological Resources Centre (EMBRC). We thank Sylvie Mazan and Ronan Lagadec from the Oceanological Observatory of Banyuls-sur-mer for providing embryos and giving access to the laboratory. We acknowledge the contribution of the MRI platform, member of the national infrastructure France-BioImaging supported by the French National Research Agency (ANR-10-INBS-04, "Investments for the future"), the labex CEMEB (ANR-10-LABX-0004) and NUMEV (ANR-10-LABX-0020) and thank Renaud Lebrun for his help with microCT scans.

3.4.7 Dental curiosities: clues to decipher the classical tooth development?

The artificial induction of tooth shape modification during bud development can be coupled with the examination of natural variants to draw hypotheses on the causes of the acquisition of a specific tooth shape in sharks.
In some specimens, mostly *S. canicula*, I report sporadic tooth curiosities that could provide clues about the factors impacting tooth morphogenesis in sharks (Figure 3.16). First, and as already pointed out by some authors, I document tooth bud splits that may have been caused by tooth injury, likely during feeding (Figure 3.16A and B) [Reif, 1980; Smith et al., 2013]. In my observations, these splits occasionally doubled the initial bud but did not give rise to a new tooth file, as this had previously been observed in other species [Reif, 1980]. Overall, these occasional curiosities may be indicative of the high resilience ability of shark tooth buds because a physical disturbance in a restricted location of the dental lamina or bud does not seem to affect the morphology of subsequently developing tooth buds. This is of importance when performing functional tests on shark dentitions because injured tooth buds during an experiment might not affect the observed results on neighbouring teeth.
I also report curiosities that extend over entire tooth files, which might not obviously result from tooth bud injury. In one of them, there is a modification of number of accessory cusps from one tooth (four accessory cusps) to the younger one (two accessory cusps), in the same file (Figure 3.16E, three files that likely undergo similar transition). Although a change in number of accessory cusps is well-known in scyliorhinids [Soares and de Carvalho, 2019; Berio et al., 2020], such transition has, to my knowledge, never been reported in a same jaw. The reduction of accessory cusps number is reported during sexual maturation of males [Soares and de Carvalho, 2019; Berio et al., 2020] but the observation in Figure 3.16E is in a mature female. This pattern is not consistent with the normal morphological transition of teeth in *S. canicula* and might result from a developmental disruption.

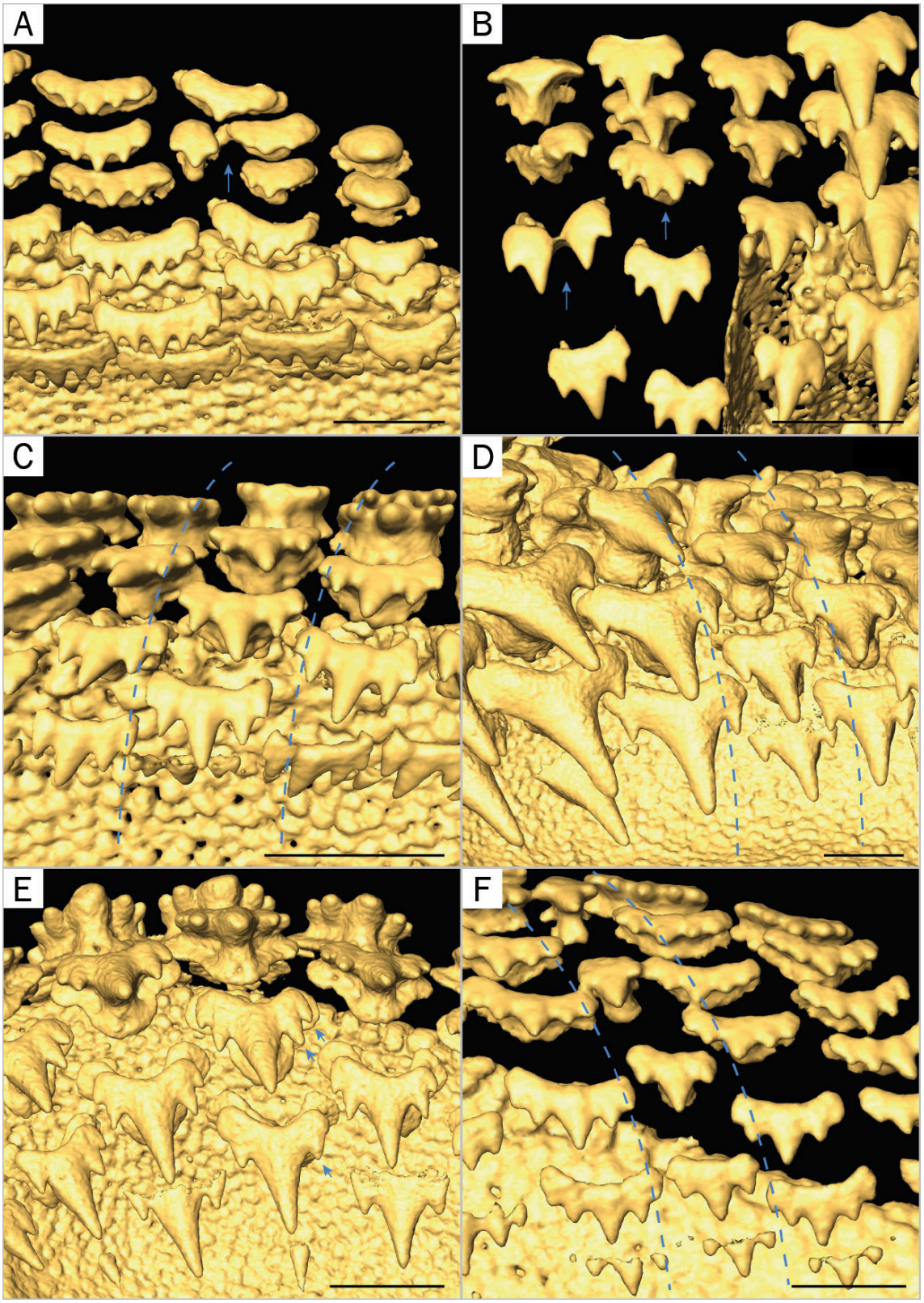

FIGURE 3.16: Tooth curiosities in *Scyliorhinus canicula*. A) A tooth bud has likely been split, resulting in fragmented teeth in a same tooth file; B) A tooth file has likely been split (left arrow) and a split of the main cusp may also have occurred (right arrow); C) A tooth file has a cusp bending reversed (toward the symphysis) as compared to the surrounding tooth files (toward the commissure); D) Tooth dimensions in one file are smaller than the neighbouring tooth files; E) The youngest fully formed tooth has not developed as many accessory cusps as the older teeth in the same tooth file; F) Tooth number of accessory cusps in one file is lower than in the neighbouring tooth files. Scale bars represent 1 mm.

The causes of this local transition could involve a modification of local expressions of receptors that allow the development of accessory cusps, or a particular dental lamina configuration in which protein diffusion might differ from that of the neighbouring files. The occurrence of a two-accessory cusps tooth file between four-accessory cusps tooth files might also arise from similar modifications (Figure 3.16F). The physical configuration of tissues could also explain other curiosities at the tooth file scale. A modification of the dental lamina configuration could generate "reverted" teeth, maybe because of a tooth bud split after injury (Figure 3.16C and see Reif [1980]) but this remains to be investigated with functional tests. Finally, local reduction of tooth dimensions in a single file have been observed, which could be caused by increased space constraints from the neighbouring tooth files (Figure 3.16D).
Albeit they do not provide evidences, the abovementioned dental curiosities surely provide directions for questioning the functioning of molecular and physical regulations of shark tooth morphogenesis.

Chapter 4
Mineralisation patterns in the chondrichthyan endoskeleton

"Mmmh... Y aurait-il un os là-dessous ?"

– Hadès in *Hercules*, 1997

4.1 Stakes of the article

The endoskeleton of extant vertebrates is made of cartilage only (hagfishes and lampreys), and bone and cartilage (e.g., mammals, teleost fishes, and birds) [Witten et al., 2010; Ota et al., 2011; Hall, 2015; Seidel et al., 2017]. In most mature tetrapods, cartilage is found in lesser proportions than bone tissue, being restricted to few body areas (e.g., ear, nose). It is often considered a soft tissue, also functioning as a transition between embryonic skeletal and mature, bony elements, or as composing articular structures. Primary cartilage develops before bone (e.g., at locations of future endochondral, mostly postcranial, bones), while secondary cartilage develops after bone (in the case of membrane, mostly cranial, bones, in groups such as teleosts, mammals, and birds but not in lissamphibians) [Gillis et al., 2006; Bailleul et al., 2012; Hirouchi et al., 2018]. Cartilage is broadly defined by the occurrence of chondrocytes secreting a collagen II and mucopolysaccharides-rich extracellular matrix with limited repair abilities. As opposed to cartilage, bone contains type I collagen that is secreted by osteoblasts and undergoes constant remodelling. However, these definitions are highly restrictive and ignore the extremely diverse forms of cartilaginous and bony tissues found in the vertebrate phylogeny. Cartilage and bone are most likely a continuum of intermediate tissues rather than dichotomous, opposed tissues in function and constitution [Witten et al., 2010]. In teleosts, Witten et al. [2010] for example identified five cartilage types including hyaline, fibrous, calcified, degrading, and intermediate between cartilage and connective tissue. Hyaline cartilage is considered the normal state in tetrapods, whereas transitory calcified cartilage is known in the process of endochondral ossification, surrounding hypertrophic chondrocytes [Von der Mark and Von der Mark, 1977; Pazzaglia et al., 2016]. In other cases in tetrapods, calcified cartilage appears pathologic, resulting from calcific deposits altering the articular function of this tissue [Goldring and Goldring, 2006; Golub, 2011].

It is commonly accepted that the endoskeleton of chondrichthyans is primarily made of cartilage and that endochondral ossification is an innovation of bony fishes [Donoghue and Sansom, 2002], albeit some fossils suggest that endochondral bone

may have predated the split between chondrichthyans and osteichthyans and that chondrichthyans lost the ability to synthesize bone more than 400 million years ago [Donoghue et al., 2006; Brazeau et al., 2020]. Chondrichthyans have, however, a rigid cartilaginous endoskeleton that undergoes mineralisation on its surface as the specimen grows [Dean et al., 2009]. Most endoskeletal elements of chondrichthyans (e.g., jaws, most vertebral elements, and fins) are covered by small blocks of hydroxyapatite, called tesserae [Dean and Summers, 2006; Dean et al., 2009; Debiais-Thibaud, 2019]. These tesserae are composed of two mineralisation types: a prismatic pattern at the perichondral surface ("cap" of the tesserae), and a globular pattern at the chondral side ("body" of the tesserae) [Dean and Summers, 2006; Seidel et al., 2016, 2017]. Areolar mineralisation is restricted to the centrum of elasmobranchs and to the centrum of some chimaeras, it is synthesised by the cells of the notochordal sheath and is characterised by internal fibrous mineralisation and external globular mineralisation [Debiais-Thibaud, 2019]. Another mineralisation type characterising the elasmobranch endoskeleton has been discovered 40 years ago and assimilated to bone because it exhibits Sharpey's fibers-like fibers and a type I collagen-rich extracellular mineralised matrix [Peignoux-Deville et al., 1982, 1989]. This "osseous tissue" has first been evidenced in the neural arches of *S. canicula* (Selachians, Carcharhiniformes) and put on standby until 2007, when Eames et al. [2007] highlighted the occurrence of similar mineralisation pattern in the swellshark *Cephaloscyllium ventriosum* (Selachians, Carcharhiniformes) neural arches. This pattern was then cautiously renamed lamellar mineralisation, because experiments on its composition and growth had not been performed enough to term it bone, in the tetrapod meaning [Eames et al., 2007]. More recently, lamellar mineralisation has been described in the neural arches of the little skate *Leucoraja erinaca* (Batoids, Rajiformes) and the Eaton's skate *Bathyraja eatonii* (Batoids, Rajiformes), in which it exhibits subperichondral lamellae engulfing elongated cells similar to osteocytes [Atake et al., 2019].

The question of whether or not chondrichthyans do have "true" bone is still pending and experimental work needs to be performed to compare the lamellar tissue of elasmobranch neural arches to bone. Another question, however, also conditions our understanding of the evolution of vertebrates: how widespread is the lamellar mineralisation within extant chondrichthyans? Has it be retained in the only Carcharhiniformes and Rajiformes or does it also contribute to the neural arch mineralisation of other groups? The answer to that question might challenge our consideration of cartilaginous fishes as having a fully cartilaginous endoskeleton. The aim of this work is to provide a more diverse overview of the chondrichthyan diversity of neural arches mineralisation (see an overview of sampling in Figure 4.1). It is designed to investigate the occurrence of bone-like patterns in species from different orders to infer about the evolution, modification, and loss of bone-like tissue in the chondrichthyan endoskeleton.

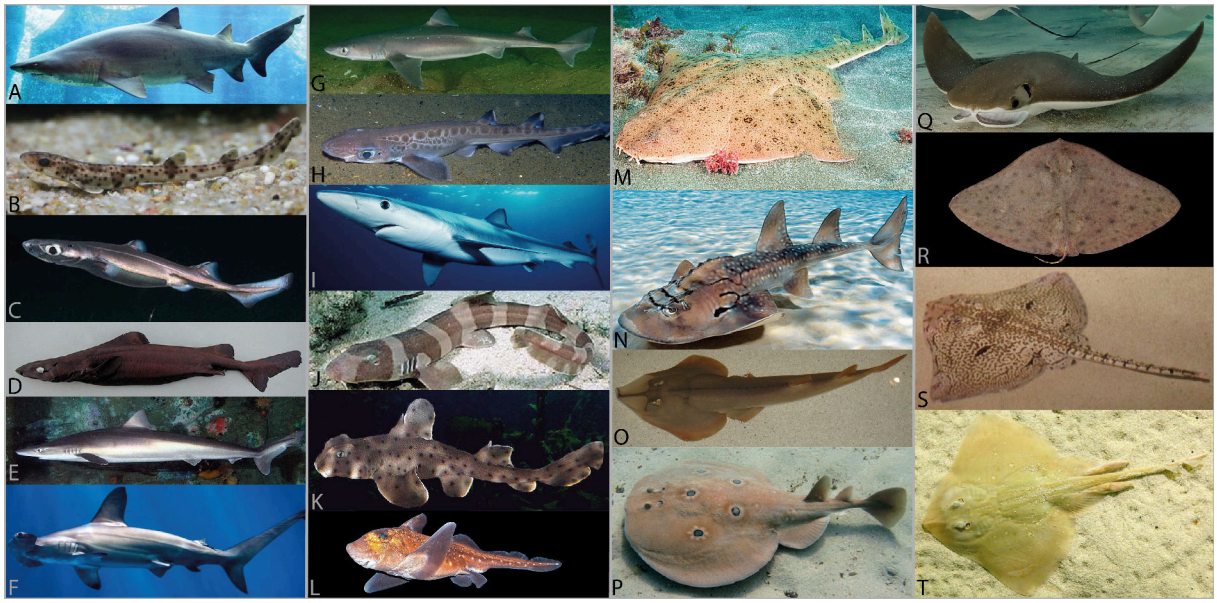

FIGURE 4.1: Chondrichthyan species included in the histological study of neural arch mineralisation patterns. A) *Carcharias taurus* (Amada44); B) *Scyliorhinus canicula* (Vladimir Wrangel); C) *Etmopterus spinax* (Andy Murch); D) *Centroscymnus crepidater* (Cambraia Duarte); E) *Galeorhinus galeus* (D. Ross Robertson); F) *Sphyrna lewini* (Monterey Bay Aquarium); G) *Squalus acanthias* (Andy Murch); H) *Galeus melastomus* (Florian Graner); I) *Prionace glauca* (Mark Conlin); J) *Chiloscyllium punctatum* (Doug Perrine); K) *Heterodontus francisci* (D. Ross Robertson); L) *Hydrolagus colliei* (Giuseppe Mazza); M) *Squatina californica* (David Fleetham); N) *Rhina ancylostoma* (Newport Aquarium); O) *Pseudobatos productus* (Maggie Hammond); P) *Torpedo torpedo* (Roberto Pillon); Q) *Rhinoptera bonasus* (Michael S. Nolan); R) *Gymnura micrura* (Tomas Willems); S) *Raja clavata* (Roberto Pillon); T) *Raja asterias* (Frédéric André).

4.2 Journal article — Diversity and evolution of the mineralised tissues of the neural arches in chondrichthyans

frontiers in Ecology and Evolution

ORIGINAL RESEARCH
published: 22 April 2021
doi: 10.3389/fevo.2021.660767

Diversity and Evolution of Mineralized Skeletal Tissues in Chondrichthyans

Fidji Berio [1,2], Morgane Broyon [3,4], Sébastien Enault [1], Nelly Pirot [3,4], Faviel A. López-Romero [5] and Mélanie Debiais-Thibaud [1]**

[1] ISEM, CNRS, EPHE, IRD, Univ. Montpellier, Montpellier, France, [2] University of Lyon, ENS Lyon, CNRS, Université Claude Bernard Lyon 1, Institut de Génomique Fonctionnelle de Lyon, UMR 5242, Lyon, France, [3] BCM, CNRS, INSERM, Univ. Montpellier, Montpellier, France, [4] IRCM, ICM, INSERM, Univ. Montpellier, Montpellier, France, [5] Department of Palaeontology, University of Vienna, Vienna, Austria

The diversity of skeletal tissues in extant vertebrates includes mineralized and unmineralized structures made of bone, cartilage, or tissues of intermediate nature. This variability, together with the diverse nature of skeletal tissues in fossil species question the origin of skeletonization in early vertebrates. In particular, the study of skeletal tissues in cartilaginous fishes is currently mostly restrained to tessellated cartilage, a derived form of mineralized cartilage that evolved at the origin of this group. In this work, we describe the architectural and histological diversity of neural arch mineralization in cartilaginous fishes. The observed variations in the architecture include tessellated cartilage, with or without more massive sites of mineralization, and continuously mineralized neural arches devoid of tesserae. The histology of these various architectures always includes globular mineralization that takes place in the cartilaginous matrix. In many instances, the mineralized structures also include a fibrous component that seems to emerge from the perichondrium and they may display intermediate features, ranging from partly cartilaginous to mostly fibrous matrix, similar to fibrocartilage. Among these perichondrial mineralized tissues is also found, in few species, a lamellar arrangement of the mineralized extracellular matrix. The evolution of the mineralized tissues in cartilaginous fishes is discussed in light of current knowledge of their phylogenetic relationships.

Keywords: cartilaginous fishes (chondrichthyes), gnathostomes, lamellar mineralization, neural arches, perichondrium, tesserae

OPEN ACCESS

Edited by:
Alessandro Minelli, University of Padua, Italy

Reviewed by:
Zerina Johanson, Natural History Museum, United Kingdom
Ann Huysseune, Ghent University, Belgium

****Correspondence:***
Fidji Berio
fidji.berio@umontpellier.fr
Mélanie Debiais-Thibaud
melanie.debiais-thibaud@umontpellier.fr

Specialty section:
This article was submitted to Evolutionary Developmental Biology, a section of the journal Frontiers in Ecology and Evolution

Received: *29 January 2021*
Accepted: *23 March 2021*
Published: *22 April 2021*

Citation:
Berio F, Broyon M, Enault S, Pirot N, López-Romero FA and Debiais-Thibaud M (2021) Diversity and Evolution of Mineralized Skeletal Tissues in Chondrichthyans. Front. Ecol. Evol. 9:660767. doi: 10.3389/fevo.2021.660767

1. INTRODUCTION

The classical view in vertebrate skeletal biology is mainly driven by the extensive work made in tetrapod species, in which clear distinctions are made between several cartilaginous and bony tissues (Hall, 2015). According to this classical view, cartilaginous tissues are retained in only a few sites in the adult skeleton and are classified into hyaline, elastic, and fibro-cartilages that display various assemblages of collagen fibers (Wachsmuth et al., 2006). Hyaline cartilage appears as a transparent tissue whose extracellular matrix does not display histologically observable fibers. The extracellular matrix of hyaline cartilage is characterized by type II collagen running through high contents of proteoglycans with acidic glycosaminoglycans that sequestrate water (Hall, 2015). Bone is defined by the deposition of type I collagen-rich extracellular matrix with little to no acidic glycosaminoglycans deposited, which undergoes mineralization through the activity of osteocytes (Hall, 2015).

Molecular and paleontological evidence has allowed the elaboration of a timeframe for the emergence of the various vertebrate skeletal tissues. Hyaline cartilage is ancestral to vertebrates (Zhang and Cohn, 2006) and most probably evolved earlier than vertebrates (Tarazona et al., 2016), while dermal and perichondrial bone, but also globular mineralized cartilage, is found in early agnathan vertebrates (Donoghue and Sansom, 2002). Among jawed vertebrates, the skeleton of extant cartilaginous fishes (chondrichthyans) is considered to be made exclusively of cartilage, with different types of mineralization that were described in early classical works (Hasse, 1879; Ridewood and MacBride, 1921; Ørvig, 1951; Applegate, 1967). Cartilage mineralization in chondrichthyans mainly occurs under the form of tesserae that are small articulated units of cartilage impregnated with apatite and are a shared derived character of this group (reviewed in Maisey et al., 2020). Paleontological evidence, therefore, implies that cartilaginous fishes have lost dermal and perichondrial bone more than 400 million years ago (Donoghue and Sansom, 2002). Several genetic data were interpreted in light of this evolutionary framework for skeletal tissues, however, our knowledge of chondrichthyan genomes remains scarce (Ryll et al., 2014; Enault et al., 2015; Debiais-Thibaud et al., 2019; Leurs et al., 2021).

More recent studies have reassessed the diversity of poorly described features of mineralization in cartilaginous fishes (Eames et al., 2007; Enault et al., 2015; Seidel et al., 2017, 2020; Atake et al., 2019; Debiais-Thibaud, 2019; Smith et al., 2019; Chaumel et al., 2020; Pears et al., 2020), raising new questions on the origin and evolution of mineralized tissues in this clade and therefore in vertebrates. Comparative studies of skeletal tissues in non-tetrapods have uncovered a wide range of skeletal tissues that had remained unknown from the sole study of tetrapods (discussed by Witten and Huysseune, 2009 and Hall and Witten, 2019). Teleost fishes display for example a wide variety of skeletal tissues with intermediate features (e.g., hyaline, elastic, fibrous, whether mineralized or not) of what is classically associated to either bone or cartilage and for which standard characterization by histology has been proposed (Witten et al., 2010; Hall and Witten, 2019). A wider description of the diversity of skeletal tissues in non-tetrapod species is therefore still needed to understand the origin and the diversification of mineralized tissues in vertebrates. In this study, we chose to focus on the comparative analysis of mineralized cartilage in the neural arches of chondrichthyans.

Extant chondrichthyans include three major clades. Holocephalans are divided into the three extant families Callorhinchidae, Chimaeridae, and Rhinochimaeridae and have long been considered to have a non-mineralized cartilaginous endoskeleton but are now recognized to have tesserae (Finarelli and Coates, 2014; Maisey et al., 2020; Pears et al., 2020; Seidel et al., 2020). Sister to holocephalans, elasmobranchs include selachians (sharks) that are grouped into Galeomorphii (orders: Carcharhiniformes, Heterodontiformes, Lamniformes, and Orectolobiformes) and Squalomorphii (orders: Hexanchiformes, Pristiophoriformes, Squaliformes, Squatiniformes, and the family Echinorhinidae) and batoids (rays, guitarfishes, skates, and sawfishes) that are divided into Myliobatiformes, Rhinopristiformes, Rajiformes, and Torpediniformes (Naylor et al., 2012; Ebert et al., 2013; Last et al., 2016). Most cartilaginous endoskeletal elements of selachians and batoids are covered by tesserae (e.g., the jaws, fins, and most vertebral elements) (Dean et al., 2009; Chaumel et al., 2020). The tesseral body (the internal part of a tessera) contains type II collagen, round cells enclosed in lacunae, and Liesegang lines typical of globular mineralization (Kemp and Westrin, 1979; Seidel et al., 2017; Chaumel et al., 2020). The tesseral cap zone (the external part of a tessera) is located on the perichondrial side and is characterized by flatter cells engulfed in a type I collagen matrix (Ørvig, 1951; Kemp and Westrin, 1979; Seidel et al., 2017; Chaumel et al., 2020). This cap zone has been discussed as a remnant, or derived version of an ancestral bony tissue in jawed vertebrates (Kemp and Westrin, 1979; Seidel et al., 2017).

Less studied than tesserae are two other mineralized tissues, also reported in the elasmobranch endoskeleton by Ørvig (1951), and reviewed by Dean and Summers (2006) and Debiais-Thibaud (2019). On the one hand, areolar mineralization characterizes the vertebral centra of elasmobranchs (Ridewood and MacBride, 1921). On the other hand, a type of lamellar mineralization has been identified only in the vertebral neural arches and repeatedly compared to bone tissue (Peignoux-Deville et al., 1982; Eames et al., 2007; Atake et al., 2019). Until now, this lamellar mineralization, or bone-like tissue, was reported in two shark species within Carcharhiniformes [the small-spotted catshark *Scyliorhinus canicula* (Peignoux-Deville et al., 1982) and the swellshark *Cephaloscyllium ventriosum* (Eames et al., 2007)], and in two batoid species belonging to Rajiformes [the Eaton's skate *Bathyraja eatonii* and the little skate *Leucoraja erinacea* (Atake et al., 2019)]. The similarity between lamellar mineralization and bone tissue was raised several times—it was first termed osseous tissue by Peignoux-Deville et al. (1982)—because of the occurrence of elongated cells similar to osteoblasts in bone (Peignoux-Deville et al., 1982) that express type I collagen genes (Enault et al., 2015) and because these cells are enclosed in a type I collagen-rich extracellular matrix, which is able to mineralize (Eames et al., 2007). This type of mineralization differs from the classical globular mineralization described in the cartilage of fossils (Ørvig, 1951) and the body zone of tesserae (Kemp and Westrin, 1979; Seidel et al., 2017).

In this study, we first provide microCT images to visualize the architecture of mineralized tissues in the neural arches in ten orders of elasmobranchs and one holocephalan family. We then use classical histology to illustrate cell shape and extracellular matrix characteristics (e.g., fibrous or hyaline nature, presence of acidic proteoglycans) to describe the mineralized tissues. The results provide insights into the evolutionary history of endoskeletal mineralization among chondrichthyans and question the nature of the mineralized tissues described in early gnathostomes and vertebrates.

2. MATERIALS AND METHODS

2.1. Biological Sampling

The dataset includes 19 specimens from 16 species of chondrichthyans (**Table 1**) and covers six of the eight orders

TABLE 1 | Chondrichthyan samples used for histology and microCT scanning.

Subclass	Superorder	Order	Family	Species	Growth stage	Fixation	Decalcification	Section
Elasmobranchii	Galeomorphii	Heterodontiformes	Heterodontidae	*Heterodontus francisci*	Subadult (Meese and Lowe, 2020)	80% ethanol	Yes	posterior
Elasmobranchii	Galeomorphii	Orectolobiformes	Hemiscyllidae	*Chiloscyllium punctatum*	Juvenile (Compagno, 1984)	4% PFA	No	anterior
Elasmobranchii	Galeomorphii	Lamniformes	Odontaspididae	*Carcharias taurus*	Sexually mature (Lucifora et al., 2002)	4% PFA	Yes	anterior
Elasmobranchii	Galeomorphii	Carcharhiniformes	Triakidae	*Galeorhinus galeus*	Juvenile (Lucifora et al., 2004)	80% ethanol	Yes	anterior
Elasmobranchii	Galeomorphii	Carcharhiniformes	Carcharhinidae	*Prionace glauca*	Juvenile (Bustamante and Bennett, 2013)	100% ethanol	Yes	posterior
Elasmobranchii	Galeomorphii	Carcharhiniformes	Scyliorhinidae	*Scyliorhinus canicula*	Embryo (Enault et al., 2016)	4% PFA	No	anterior
Elasmobranchii	Galeomorphii	Carcharhiniformes	Scyliorhinidae	*Scyliorhinus canicula*	Juvenile (Capapé et al., 2008)	4% PFA	No	anterior
Elasmobranchii	Galeomorphii	Carcharhiniformes	Sphyrnidae	*Sphyrna lewini*	Juvenile (Bejarano-Álvarez et al., 2011)	80% ethanol	Yes	posterior
Elasmobranchii	Squalomorphii	Squaliformes	Somniosidae	*Centroscymnus crepidater**	Juvenile (Moore et al., 2013)	70% ethanol	No	posterior
Elasmobranchii	Squalomorphii	Squaliformes	Etmopteridae	*Etmopterus spinax**	Juvenile (Porcu et al., 2014)	70% ethanol	No	posterior
Elasmobranchii	Squalomorphii	Squatiniformes	Squatinidae	*Squatina californica*	Sexually mature (Romero-Caicedo et al., 2016)	80% ethanol	Yes	posterior
Elasmobranchii	Batoidea	Myliobatiformes	Gymnuridae	*Gymnura micrura**	Sexually mature (Yokota et al., 2012)	70% ethanol	Yes	posterior
Elasmobranchii	Batoidea	Rhinopristiformes	Rhinobatidae	*Pseudobatos productus*	Sexually mature (Márquez-Farías, 2007)	80% ethanol	Yes	posterior
Elasmobranchii	Batoidea	Rhinopristiformes	Rhinidae	*Rhina ancylostoma*	147 cm TL	4% PFA	Yes	posterior
Elasmobranchii	Batoidea	Torpediniformes	Torpedinidae	*Torpedo* sp.*	16 cm DW	70% ethanol	Yes	posterior
Elasmobranchii	Batoidea	Rajiformes	Rajidae	*Raja clavata*	Hatchling	4% PFA	No	ant, posterior
Elasmobranchii	Batoidea	Rajiformes	Rajidae	*Raja clavata*	Juvenile (Capapé et al., 2007)	70% ethanol	No	posterior
Holocephali	–	Chimaeriformes	Chimaeridae	*Hydrolagus colliei*	Hatchling	100% ethanol	No	anterior (sy)
Holocephali	–	Chimaeriformes	Chimaeridae	*Hydrolagus colliei**	Juvenile (Barnett et al., 2009)	70% ethanol	No	anterior (sy)

DW, disc width; PFA, paraformaldehyde; sy, synarcual; TL, total length. When no literature data are available on the size at sexual maturity for a species, the TL or DW are indicated. Asterisks indicate the specimens that have been preserved in ethanol for several decades.

of extant sharks, the four orders of extant batoids, and one of the three families of extant Chimaeriformes (Naylor et al., 2012; Ebert et al., 2013; Last et al., 2016). The samples were kindly provided by the University of Montpellier, by the Aquarium of Montpellier (Planet Ocean Montpellier), or were bought at fish markets. No handling of live specimens was necessary for this study. The ontogenetic stages were determined based on literature data, using the total length (TL) or disc width (DW) as proxies (**Table 1**). When no data were available about the ontogenetic stages of the species sampled, the TL, DW, or both were provided (**Table 1**). When fresh or frozen material was available, the vertebra or neural arch were sampled and fixed in 4% paraformaldehyde in Phosphate-Buffered Saline 1X (PBS 1X). Anterior and posterior vertebrae were sampled anterior and posterior to the pelvic girdle, respectively. Samples made from long-term stored material were first rinsed in fresh ethanol for 48 h before further processing (note that some specimens come from collections in ethanol that date back from the 90's, see details in **Table 1**).

2.2. Histological Staining

Alizarin Red S staining on thick (circa 1 mm) slices was performed overnight in a potassium hydroxide (KOH) 0.5% solution with a concentration of Alizarin Red S of 0.005% for samples of *S. canicula* and the thornback ray *Raja clavata*, or 0.05% for samples of the spotted ratfish *Hydrolagus colliei*. Stained samples were progressively equilibrated in 25% glycerol in KOH 0.5%, 50% glycerol in KOH 0.5%, 75% glycerol in KOH 0.5%, and glycerol 100% before being imaged under a binocular (Leica Microsystems). Only samples fixed in paraformaldehyde were used for this staining procedure.

A double Alizarin Red S and Alcian Blue staining was performed on a 14 μm-thick cryostat section made in a non-demineralized portion of the anterior vertebral column of an embryonic lesser spotted catshark fixed in 4% PFA. The section was rinsed in PBS 1X, then in KOH 0.5% before a bath of Alizarin Red S 0.005% in KOH 0.5% for 1 min. The slide was rinsed once in PBS 1X, incubated for 2 min in a 0.02% Alcian blue 8G solution (8:2 ethanol/glacial acetic acid), washed once in EtOH 100%, and once in PBS 1X before being mounted in Mowiol.

For other histological staining protocols, samples exhibiting strong vertebral mineralization were first rehydrated and then demineralized with Thermo Scientific Shandon TBD-2 decalcifier during 24–48 h before the embedding process (**Table 1**). Samples were progressively dehydrated in 70, 96, and 100% ethanol before paraffin embedding. Paraffin-embedded tissue was cut into 7 μm-thick sections, mounted on slides in an alternate consecutive fashion, and dried at 37 °C overnight. Tissue sections were stained with Hematoxylin, Eosin, and Saffron with HMS 740 autostainer (MM France) for preliminary analysis. The Hematoxylin-Eosin-Saffron (HES) protocol stains basophilic components in deep violet [nuclei and basophilic extracellular matrices (H)], cytoplasm in pink (E), and collagen fibers in bright orange (S), allowing a fine description of cell and matrix morphologies. HES has poor staining contrast on hyaline cartilage (gray or beige uniform staining) but allows contrasting the cartilaginous matrix with perichondrial tissue because of the eosinophilic and Saffron-positive staining of the fibrous matrix (Hilton et al., 2005). The modified cartilaginous extracellular matrix in cartilage mineralizing zones is also contrasted in HES (Mayoral et al., 2014), possibly because it is basophilic. Tissue sections were also stained with PAS-AB, which associates the standard Alcian blue method (AB, pH 2.5, standard staining for acid mucins in hyaline cartilage matrix, blue staining) with the Periodic Acid Schiff (PAS) technique to distinguish with neutral mucins (magenta staining). PAS-AB staining is a standard for the detection of hyaline cartilage matrix, as the staining is associated with the acidic glycosaminoglycan content of the matrix (Whiteman, 1973). Previous work has shown that Alcian blue stains best in the proliferative and resting chondrocyte zone of endochondral bone, while the PAS magenta stains both the fibrous perichondrium and the hypertrophic chondrocyte zones (Xiong et al., 2005). Some variation in the intensity and color of HES and PAS-AB assays between samples are observed, which most probably results from variations in the fixation, decalcification, and storage solutions, but also from an important variation in the storage time of our samples. Despite these variations, cell shape was still well-preserved and there was good correspondence between the locations of mineralization (as defined by microCT images) and the places of modified staining with HES in the cartilaginous and fibrous extracellular matrices. Mounted histological slides were scanned with a Hamamatsu NanoZoomer 2.0-HT scanner in the local MRI platform and images were visualized with the NDP.view software (v1.2.47).

2.3. Micro-Computed Tomography

Micro-computed tomography (microCT) was performed on selected vertebral samples preserved in alcohol with EasyTom 150 and reconstructed with the Xact software (v11025). The images were subsequently analyzed with the Avizo Lite software (v2019.3).

2.4. Ancestral Character State Reconstruction

For each character identified in our results, we built a character matrix and used phylogenetic relationships from Licht et al. (2012), Naylor et al. (2012), and Last et al. (2016). We reconstructed the ancestral state for each character (globular mineralization, fibrous mineralization, and lamellar mineralization: presence/absence; mineralization architecture: continuous/semi-discontinuous/discontinuous (tessellated or reduced) with Mesquite (v3.61) (Maddison and Maddison, 2019).

3. RESULTS

3.1. Anatomical and Histological Features of Neural Arches in Three Reference Species

We first selected reference species among the three main chondrichthyan clades: *S. canicula* (Carcharhiniformes, Galeomorphii) (**Figures 1**, **2**), *R. clavata* (Rajiformes, Batoidea) (**Figure 3**), and *H. colliei* (Chimaeriformes, Holocephali)

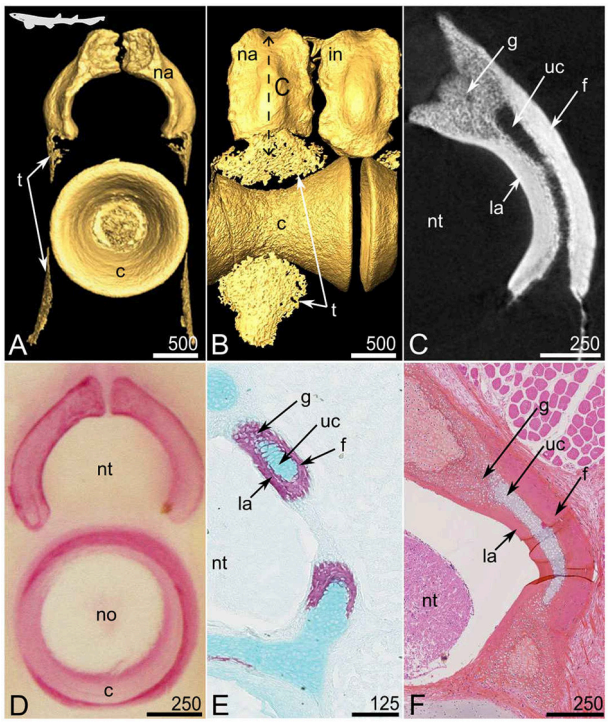

FIGURE 1 | Mineralized tissues in the anterior vertebrae of the small-spotted catshark *Scyliorhinus canicula* at juvenile stages [20 cm TL in **(A–C)** and 31 cm TL in **(F)**] and embryonic stages [8.4 cm TL in **(D)** and 8.0 cm TL in **(E)**]. **(A–C)** Micro-computed tomography imaging, frontal view **(A)** and lateral view **(B)** of 3D isosurfaces and virtual section (**C**, as located by the double sided dashed arrow on **B**). **(D)** Alizarin Red S staining of a thick section. **(E)** Alizarin Red S and Alcian Blue double staining on a cryostat section. **(F)** HES, histological staining; c, centrum; f, fibrous perichondrial mineralization; g, globular mineralized cartilage; in, interneural element; la, lamellar perichondrial mineralization; na, neural arch; no, notochord; nt, neural tube; t, tesserae; uc, unmineralized cartilage. Scale bars are in μm.

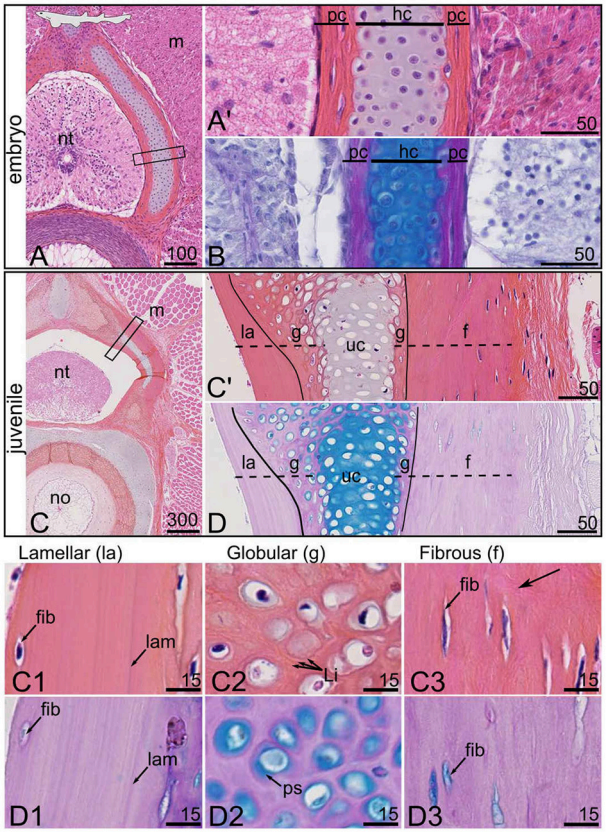

FIGURE 2 | Histological characterization of the mineralized tissues in the anterior vertebrae of the small-spotted catshark *Scyliorhinus canicula* at an embryonic stage [7 cm TL in **(A,B)**] and a juvenile stage [31 cm TL in **(C,D)**]. Serial sections were stained with HES **(A,C)** and PAS-AB **(B,D)**. **(A',C')** Close-ups of the boxed zones in **(A,C)**, respectively. Close-up on the lamellar (la), globular (g), and fibrous (f) mineralized tissues: **(C1–C3,D1–D3)** are details of **(C',D)**, respectively. f, fibrous perichondrial mineralization; fib, fibrocyte-shaped cell; g, globular mineralized cartilage; hc, hyaline cartilage; la, lamellar perichondrial mineralization; lam, lamella; Li, Liesegang lines; m, muscle tissue; no, notochord; nt, neural tube; pc, perichondrium; ps, pericellular space; uc, unmineralized cartilage. Vertical lines in **(C',D)** delimit the fibrous and hyaline cartilaginous matrices. Dashed lines in **(C',D)** locate the zones of mineralized matrix. Black arrow points to fibrous extracellular matrix. Scale bars are in μm.

(**Figure 4**). The description of the vertebrae of these species is provided first because of their representativeness in the chondrichthyan phylogeny, also because literature data shows a strong variation in the type of mineralized tissues in their neural arches (Debiais-Thibaud, 2019), and because we had specimens of successive ontogenetic stages allowing developmental comparisons.

3.1.1. Neural Arch Mineralization in *Scyliorhinus canicula*

Each anterior (thoracic) vertebra of *S. canicula* includes a mineralized, hourglass-shaped, centrum (**Figures 1A,B**). Each centrum is dorsally overlaid by a mineralized neural arch that alternates with interneural elements, both (neural and interneural elements) appearing similar in shape but interneurals are located dorsal to the junction between two centra (**Figures 1A,B**). The vertebral body surface also shows thin zones of mineralization (lace-like mineralization, **Figures 1A,B**) that are small tesserae (see details below and in **Figure 5**). The neural arches and interneural elements externally appear as continuously mineralized structures (**Figures 1A,B**) but the virtual (microCT) and histological sections reveal that the mineralized layer encloses an inner core of unmineralized tissue (**Figures 1C,E,F**) of cartilaginous nature (**Figures 1E,F**). In the following, we used HES and PAS-AB histological staining protocols to characterize cells and their extracellular matrix in each vertebral tissue. We previously successfully used HES staining to characterize cartilaginous matrix mineralization in chondrichthyans (Enault et al., 2015; Debiais-Thibaud, 2019). Mineralized zones (stained with Alizarin Red S in **Figure 1D**) appear dark pink in comparison to the unmineralized matrix (**Figure 1F**, compare g with uc zones), probably because of an eosinophilic nature. The comparison between the virtual and

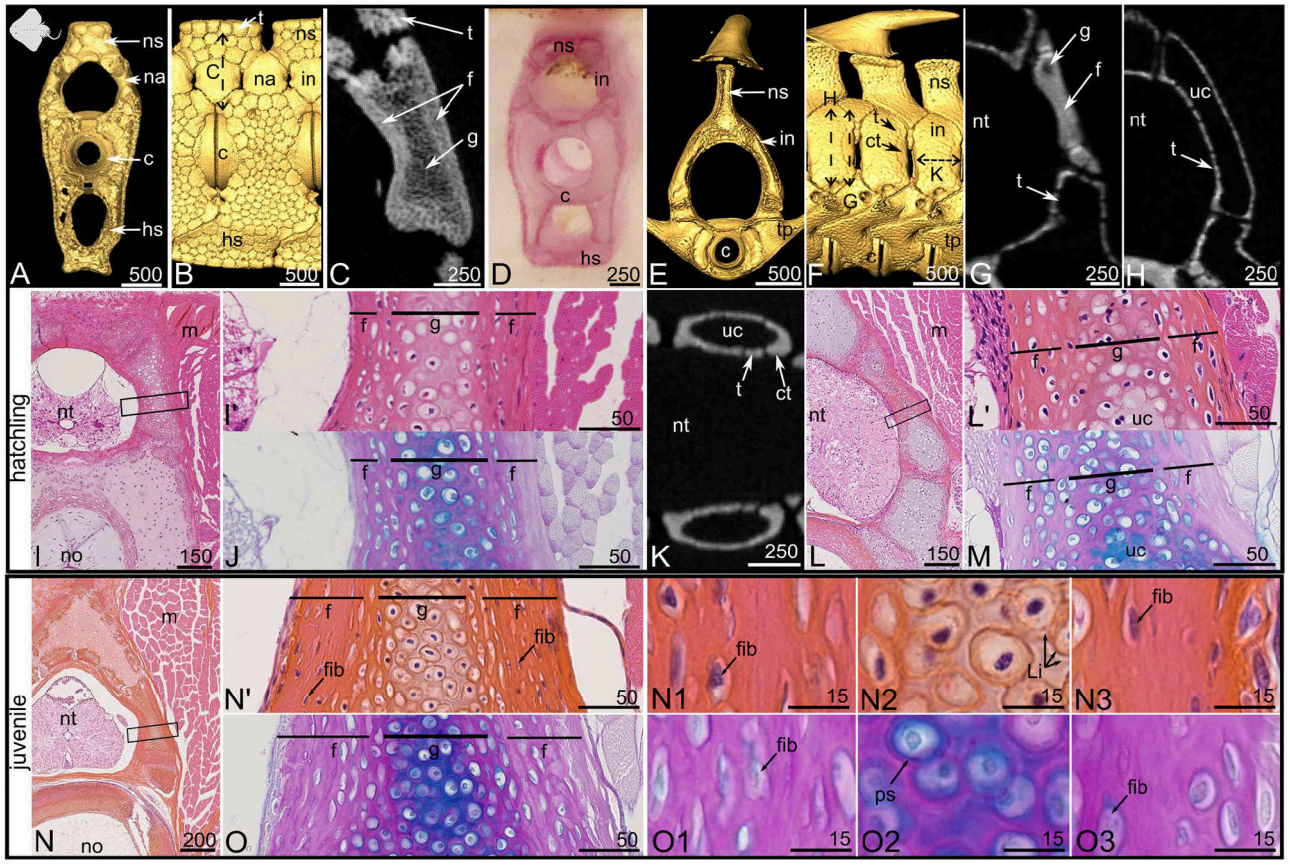

FIGURE 3 | Mineralized tissues in the vertebrae of the thornback ray *Raja clavata* at hatching [8.0 cm DW **(A–M)**] and juvenile stage [13.0 cm DW **(N,O)**]. **(A–D,I,J,N,O)** Posterior vertebrae, **(E–H,K–M)** anterior vertebrae. **(A–C,E–H,K)** Micro-computed tomography imaging, frontal views **(A,E)** and lateral views **(B,F)** of 3D isosurfaces and closer views on virtual sections (**C**: as located by the double sided dashed arrow on **B**; **G,H,K**: as located by the double sided dashed arrows on **F**). **(D)** Alizarin Red S staining of a thick section. **(I,J,L–O)** Histological staining on serial sections with HES **(I,L,N)** and PAS-AB **(J,M,O)**. **(I',L',N')** Close-ups of the boxed zones in **(I,L,N)**, respectively. Cellular details from the proximal **(N1,O1)**, central **(N2,O2)**, and distal **(N3,O3)** zones are zooms taken from the sample in **(N',O)**. c, centrum; ct, corner tessera; f, fibrous perichondrial mineralization; fib, fibrocyte-shaped cell; g, globular mineralized cartilage; hs, hemal spine; in, interneural element; Li, Liesegang lines; m, muscle tissue; na, neural arch; no, notochord; ns, neural spine; nt, neural tube; ps, pericellular space; t, tesserae; tp, transverse process; uc, unmineralized cartilage. Scale bars are in μm.

histological sections (**Figures 1C,F**) allows identifying several types of mineralized tissue. First, there is a zone displaying cell spherical lacunae, where mineralization is less dense (lower gray level in **Figure 1C**), and that is located in the dorsal-most zone of the cartilaginous core (g in **Figure 1**). Denser mineralized zones (deeper white in **Figure 1C**) cover the inner unmineralized cartilage rod (uc in **Figure 1**). These perichondrial zones are further differentiated in the proximal perichondrium (facing the neural tube, la in **Figure 1**) and the distal perichondrium (facing the thoracic muscles, f in **Figure 1**) through the HES and PAS-AB staining protocols.

In the embryonic developing neural arches (**Figures 2A,B**), at a stage when mineralization initiates (Enault et al., 2016), the fibrous perichondrial tissue is characterized by flat cells enclosed in a fibrous extracellular matrix (pc in **Figure 2A'**), while the internal cartilaginous tissue stains positive for Alcian blue (hc in **Figure 2B**).

In the juvenile specimen in which structures are fully mineralized, the neural arch is organized as a central, unmineralized cartilaginous rod (uc in **Figures 2C',D**). This internal cartilaginous rod is no more than 100 μm wide in the juvenile specimen, which is similar to what is observed in the hatchling specimen, suggesting that this internal tissue does not significantly grow between these ontogenetic stages (**Figures 2A,C**). In continuity with this cartilaginous unmineralized rod, the most dorsal and ventral aspects appear mineralized (**Figures 1C,E,F, 2C',D**) together with the contact surface with the perichondrium (g in **Figures 2C',D**). The perichondrium is characterized by low to absent Alcian blue staining in the PAS-AB assay (**Figure 2D**) and by elongated cells engulfed in a Saffron stained extracellular matrix in the HES assay (**Figure 2C'**). Several differences in cell density and matrix organization can be detected when comparing the distal mineralized perichondrium (toward the trunk muscles) with the

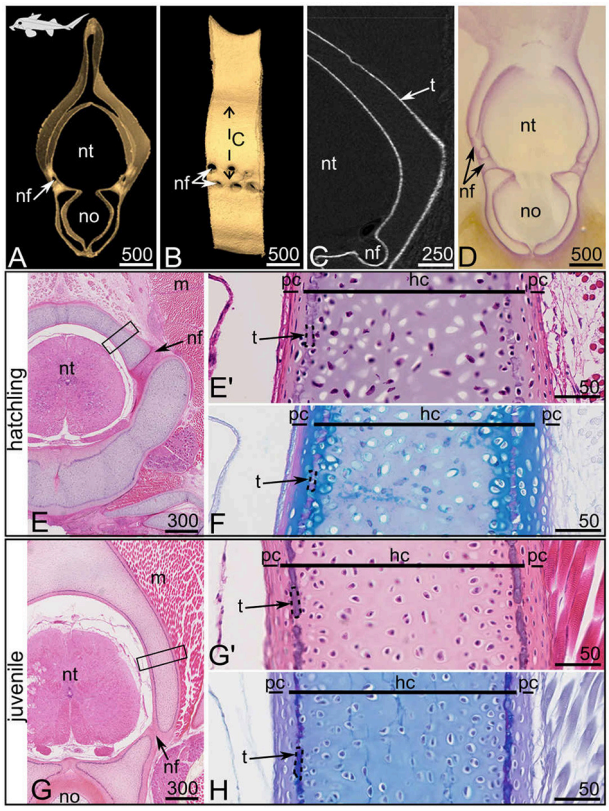

FIGURE 4 | Anterior synarcual mineralization in the spotted ratfish *Hydrolagus colliei* at hatchling [9.5 cm TL, **(A–F)**] and juvenile [14.0 cm TL **(G,H)**] stages. **(A–C)** Micro-computed tomography imaging, frontal view **(A)** and lateral view **(B)** of 3D isosurfaces and virtual section on a closer view (**C**, as located by the double sided dashed arrow on **B**). **(D)** Alizarin Red S staining of a thick section. **(E–H)** Histological staining on serial sections with HES **(E,E',G,G')** and PAS-AB **(F,H)**. **(E',G')** are close-ups of the boxed zones in **(E,G)**, respectively. hc, hyaline cartilage; m, muscle tissue; nf, nerve foramina; no, notochord; nt, neural tube; pc, perichondrium; t, tesserae (dashed contours delineate single tessera). Scale bars are in μm.

proximal mineralized perichondrium (facing the neural tube) (compare **Figures 2C1,C3,D1,D3**).

As a result, three mineralized histotypes can be described in the neural arch of *S. canicula*. The first one is superficial lamellar mineralization that arises from the perichondrium located in the proximal side of the neural arch. The mineralized matrix displays a lamellar organization, cell density appears very low, and the few cells found in the mineralized matrix are elongated (**Figures 2C1,D1**). The second type is globular mineralization, which occurs in the matrix surrounding chondrocytes in the dorsal part of the neural arch and the contact zone with perichondrial mineralized tissues. HES staining in the mineralized matrix shows concentric rings around the chondrocyte lacunae that we interpret as the marks of previously described Liesegang lines (**Figure 2C2**), typical of globular mineralization in hyaline cartilage (Ørvig, 1951; Peignoux-Deville et al., 1982; Seidel et al., 2016). The pericellular space is positive for Alcian blue (ps in **Figure 2D2**). The third type is a fibrous mineralized tissue in the perichondrium that is located in the distal side of the neural arch. The cells also appear elongated as expected with fibrocytes and their matrix is characterized by loosely arranged fibers that stain with Saffron (arrows in **Figure 2C3**). The thin pericellular space is positive for Alcian blue (**Figure 2D3**).

3.1.2. Neural Arch Mineralization in *Raja clavata*

The posterior vertebrae of *R. clavata* are composed of a centrum associated with one neural arch located dorsally, at the junction between two neural spine-interdorsal complexes (**Figures 3A,B**). The neural arches and interneural elements are not covered by tesserae, as opposed to the neural spines (**Figure 3B**). The virtual section shows that the whole depth of the posterior neural arches is mineralized (**Figure 3C**). In both hatchling and juvenile specimens, this architecture is similar in the posterior vertebral column (not shown). HES histological staining highlights the presence of subspherical cells in the center of these neural arches (**Figures 3I',J,N',O,N2,O2**). Their extracellular matrix displays Liesegang lines with HES and an Alcian blue positive pericellullar space with PAS-AB, making this zone similar to the globular mineralization observed in *S. canicula* (**Figures 3N2,O2**). This internal mineralized cartilaginous rod does not seem to differ in size between the hatchling and juvenile specimens, suggesting little growth of this internal zone between the corresponding ontogenetic stages (**Figure 3**, compare the g zone in I' with N').

Surrounding this mineralized cartilage core is a tissue with fibrocyte-shaped cells, engulfed in a fibrous matrix devoid of Alcian blue staining except for a thin pericellular matrix (**Figures 3I',J,N',O,N1,N3,O1,O3**). This mineralized fibrous tissue lines both the proximal and distal sides of the neural arch and is thicker in the juvenile than in the hatchling specimen (compare **Figures 3I',N'**). We assume this tissue to have a perichondrial nature, and it appears similar to the fibrous mineralization in the distal perichondrium of the *S. canicula* neural arches. Similar to the observations in *S. canicula*, perichondrial mineralization appears denser than globular cartilage mineralization (**Figure 3C**). In contrast to *S. canicula*, no lamellar organization of the extracellular matrix was observed in either the proximal or distal perichondrium of *R. clavata* (**Figures 3N1,N3,O1,O3**). In *S. canicula*, the architecture of neural arch mineralization is the same along the anterior-posterior axis of the vertebral column (no difference is observed between the anterior and posterior vertebrae) although the timing of centrum mineralization differs between these regions (Enault et al., 2016). In *R. clavata*, the mineralization architecture in the neural arches differs between anterior and posterior vertebrae (**Figures 3B,F**). In anterior vertebrae, we identified only interneural elements, located dorsal to the junctions between two centra and that were partly covered with tesserae (**Figures 3F,H**), while more massive mineralized units cover the anterior and posterior faces of the interneural elements (**Figures 3F,K**). A longitudinal frontal section in an interneural element shows that these massive units have a U-shape delineating the anterior and posterior faces of each interneural element (**Figure 3K**). As such, we considered them to be "corner tesserae" as previously proposed in the jaw of

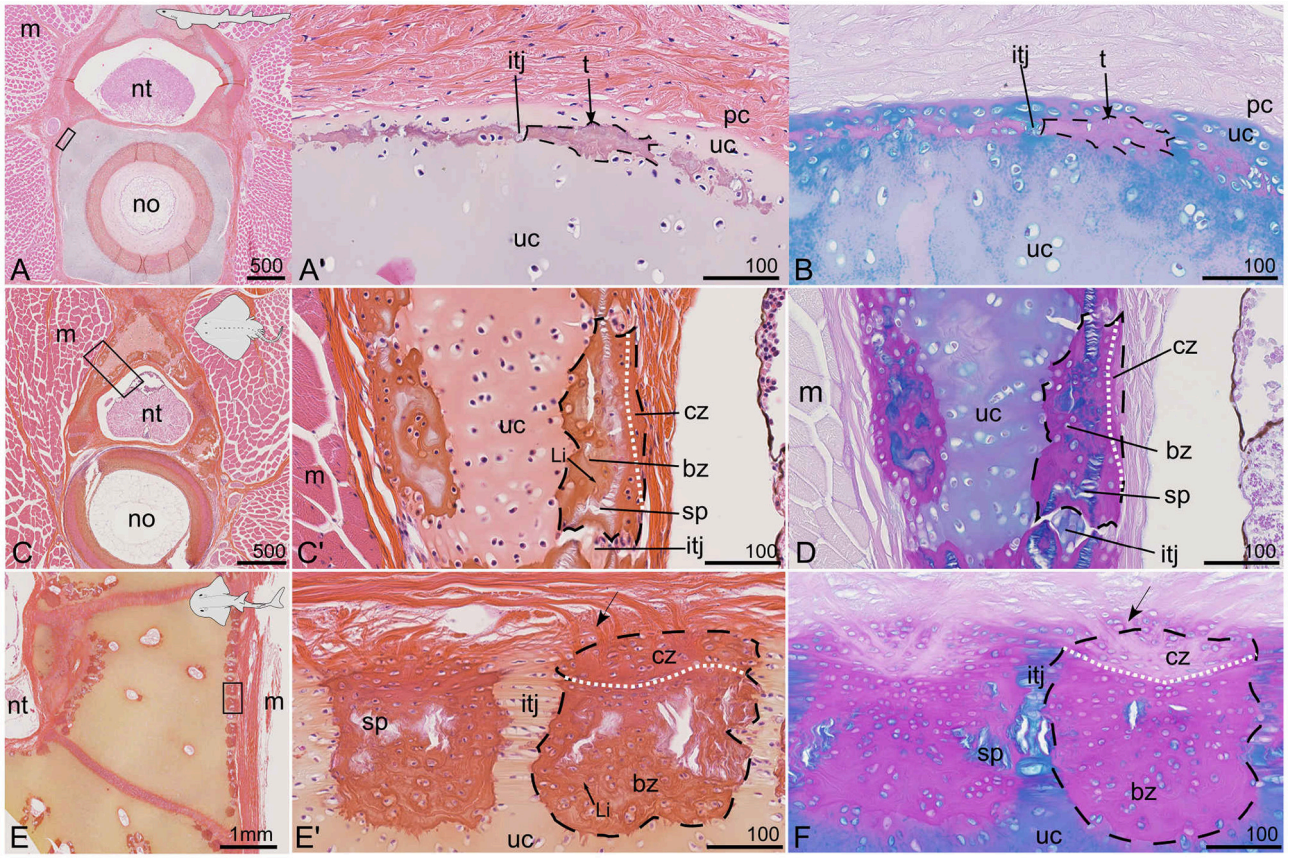

FIGURE 5 | Vertebral tissues with various tesseral mineralization patterns in selected species stained with HES **(A,C,E)** and PAS-AB **(B,D,F)**. **(A,B)** Subperichondrial tesserae in the cartilaginous vertebral body of a juvenile (20 cm TL) small-spotted catshark *S. canicula*; anterior vertebra. **(C,D)** Tesserae in the neural spine of a juvenile (13 cm DW) thornback ray *R. clavata*; posterior vertebra. **(E,F)** Tesserae in the neural arch of a (147 cm TL) bowmouth guitarfish *Rhina ancylostoma*; posterior vertebra. bz, body zone of a tessera; cz, cap zone of a tessera; itj, intertesseral joint; Li, Liesegang lines; m, muscle tissue; no, notochord; nt, neural tube; pc, perichondrium; t, tesserae (dashed contours delineate single tessera); sp, spoke; uc, unmineralized cartilage. The white dotted line separates bz and cz. Arrows point to Sharpey's fibers. **(A',B,C',D,E',F)** are close-ups of the zones located by the rectangles in **(A,C,E)**, respectively. Scale bars are in μm except in **(E)**.

the Haller's round ray *Urobatis halleri* (Dean et al., 2009), although their size relative to the closest tesserae is higher than that of previously observed "corner tesserae" (**Figure 3F**). Histological staining showed the occurrence of mineralized globular cartilage in the center of these elements and layers of fibrous perichondrial mineralization on their proximal and distal surface (**Figures 3L,M**).

As a consequence, the interneural elements and neural arches of *S. canicula* and *R. clavata* in the caudal zone of the vertebral column display continuous mineralization, while the anterior vertebrae of *R. clavata* (immediately posterior to the synarcual) display a combination of tesserae and massive "corner tesserae". All these mineralized structures are characterized by a mineralized perichondrial tissue that covers a partly (*S. canicula*) or more extensively (*R. clavata*) mineralized cartilaginous rod. Perichondrial mineralization occurs as lamellar mineralization only in the proximal zone of the neural arches of *S. canicula* and as fibrous mineralization in all other occurrences.

3.1.3. Synarcual Mineralization in *Hydrolagus colliei*

The synarcual of *H. colliei* is a post-cranial element pierced by dorsal and ventral nerve foramina (**Figures 4A,B**) that develops from the fusion of successive embryonic vertebrae and that does not display discrete neural arch or interneural elements (Johanson et al., 2015). The equivalent zone of elasmobranch neural arches in the synarcual is considered to be the zone dorsal to a ventral foramen (Goodrich, 1930; Eames et al., 2007; Criswell et al., 2017). We hypothesized a similar situation for chimaeras, and focused on the portion of the synarcual located dorsally to a ventral foramen, although our observations were similar in all other parts of the synarcual (including in the vertebral body, see **Figures 4A,D,E,G**). Previous studies showed poorly developed cartilaginous tissue in the posterior vertebrae of juvenile *H. colliei*, where histology displayed no sign of modified cartilaginous matrix that could be linked to cartilage mineralization (Debiais-Thibaud, 2019). However, more recent publications pointed out the thin layer of mineralized matrix in the synarcual of the elephant shark *Callorhinchus milii* (Pears

et al., 2020) and recognized thin tesserae in the adult *C. milii* and rabbit fishes *Chimaera monstrosa* (Pears et al., 2020; Seidel et al., 2020). In our *H. colliei* sample, we detect a similar thin layer of mineralized tissue in the synarcual of a hatchling and a juvenile specimen (**Figures 4A,G**). This pattern is found as a peripheral delineation of the ventral part (corresponding to the vertebral body) and the dorsal part (corresponding to the neural arches) of the synarcual, but also in the inner contact with the notochord (**Figures 4A,D,G**). Most tesserae are not more than 10 μm wide in their chondral-perichondrial axis (**Figures 4E',F,G',H**). The line of modified cartilaginous matrix can be observed at the hatching stage and is more obvious in the juvenile specimen (**Figures 4E–H**). The matrix stains deep purple with HES (**Figures 4E',G'**) and does not stain with Alcian blue (**Figures 4F,H**), suggesting a difference in the glycosaminoglycan content at this mineralization location. This site of mineralization is located in the subperichondrial zone of the cartilaginous unit. The cells located on the perichondrial side of this line are enclosed in lacunae in a matrix of cartilaginous nature [as supported by positive Alcian blue staining (**Figures 4F,H**)], although the cells are flattened (**Figures 4E',G'**). Moreover, no cells can be observed fully embedded in the mineralized cartilaginous matrix, either at the hatching or juvenile stage and the mineralized layer appears discontinuous (**Figures 4G',H**), supporting the presence of aligned tesserae as described in other holocephalan species (Pears et al., 2020).

3.1.4. Diverse Combinations of Histotypes in Chondrichthyan Tesserae

To better compare our observations with literature data on tesserae, these mineralized structures were also illustrated in selected species (**Figure 5**). As previously noted, focal cartilage mineralization is detected with microCT outside the neural arches and surrounding the vertebral body of *S. canicula* (**Figures 1A,B**). Such sites also appear on histology sections, they are stained dark pink with HES and purple with PAS-AB and occur in a subperichondrial location within the cartilaginous matrix (**Figures 5A,B**). Although poorly developed, these sites can be interpreted as thin tesserae engulfing chondrocytes and display intertesseral joint regions (**Figures 5A',B**), as previously described (Seidel et al., 2016). The tesserae are separated from the perichondrium by a subperichondrial and unmineralized cartilaginous layer (**Figures 5A',B**). They are comparable to the discontinuous pattern of mineralization described in *H. colliei* (**Figures 4G',H**) but are thicker (up to 50 μm) and engulf chondrocytes in the mineralized matrix (**Figure 5A'**) in *S. canicula*.

The neural spines of *R. clavata*, as well as the neural arches of the bowmouth guitarfish *Rhina ancylostoma* are covered by tesserae (**Figures 3B**, **5C–F**). The tesserae are separated by unmineralized intertesseral joints (itj in **Figures 5C',D,E',F**) and display internal spokes (sp in **Figures 5C',D,E',F**) as defined by Seidel et al. (2016). Two zones can further be distinguished in the tesserae that correspond to the previously defined body and cap zones of a tessera (Kemp and Westrin, 1979; Seidel et al., 2016, 2017). In both species, the cap zone is characterized by flat cells, a higher content in collagen fibers, and a matrix poorly stained by Alcian blue except in the pericellular layer (**Figures 5D,F**). The cells in the body zone are subspherical and surrounded by an extracellular matrix displaying Liesegang lines with HES staining (**Figures 5C',E'**). In both batoids (*R. clavata* and *R. ancylostoma*), the maximum width of a tessera (tangential axis) is about 200 μm and does not seem to depend on the specimen body size as *R. clavata* is a young juvenile of 13 cm DW and 21 cm TL, while *R. ancylostoma* is 147 cm long. However, the depth of the tesserae (along the chondral-perichondrial axis) is less than 100 μm in *R. clavata*, while it is more than 200 μm in *R. ancylostoma* (compare **Figures 5D,F**). There are no obvious Sharpey's fibers radiating from the tesserae of *R. clavata*, whereas they are well-defined in the tesserae of *R. ancylostoma* (**Figures 5C',D,E'F**). Sharpey's fibers are thick collagenous fibers previously described in tesserae (Kemp and Westrin, 1979; Seidel et al., 2017).

3.2. Neural Arch Mineralization and Elasmobranch Diversity

In the following, we describe the variation of neural arch mineralized histotypes and architectures in several species covering a broad part of the elasmobranch taxonomic diversity.

3.2.1. Batoids

Most of the neural arch of the smooth butterfly ray *Gymnura micrura* and *Torpedo* sp. is covered by tesserae that are 250 μm wide in their tangential axis (**Figures 6A,B,E,F**). Two larger mineralized elements are found on the anteriormost and posteriormost surfaces of each neural arch, similar to the corner tesserae described in *R. clavata*. These elements are more than 500 μm in their longer dimension (**Figures 6A,E**). The virtual sections made through the center of the neural arches show regular-sized tesserae on the neural arch surface (**Figures 6B,F**). The histological sections made through the corner tesserae (**Figures 6C,G**) show a central zone of globular mineralized cartilage covered by fibrous mineralization (**Figures 6C',D,G',H**).

The neural arches of the shovelnose guitarfish *Pseudobatos productus* are covered by classically organized tesserae with no massive corner tesserae (**Figure 6I**). The tesserae of the neural arch reach 400 μm long (in their tangential axis) and 100 μm wide (along the chondral-perichondrial axis, **Figure 6J**) and display intertesseral joints (**Figures 6K',L**). The cap zone of a tessera contains elongated cells in a fibrous (Saffron-positive) matrix with little acidic glycosaminoglycan content (**Figures 6K',L**), while cells in the body zone are similar in shape to chondrocytes in the unmineralized matrix (**Figures 6K',L**). The neural arch of *R. ancylostoma* also is covered by standard tesserae only (**Figures 6E,F**) without enlarged elements (data not shown).

3.2.2. Selachians, Squalomorphs, Order: Squaliformes

In both the velvet belly *Etmopterus spinax* and the longnose velvet dogfish *Centroscymnus crepidater*, the neural arches display thin zones of mineralization dorsal to the centra (**Figures 7A,B,E,F**). Virtual sections passing through the neural arches show a thin, discontinuous layer of mineralization (**Figures 7B,F**). The histological staining results show that the

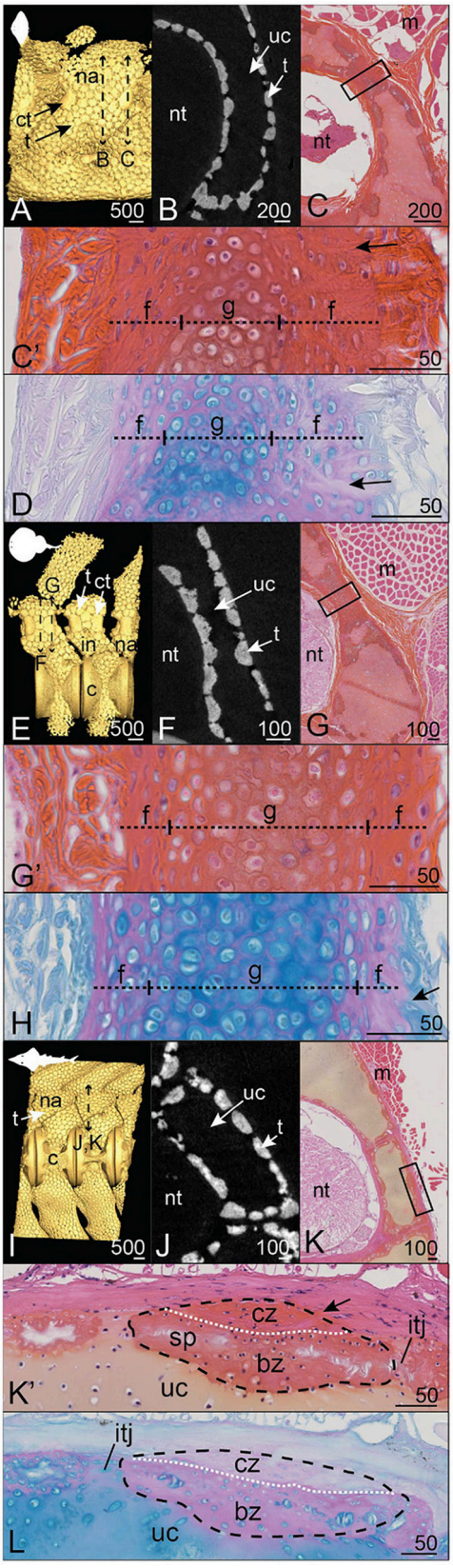

FIGURE 6 | (Continued)

FIGURE 6 | Mineralization patterns in the neural arches of posterior vertebrae in batoids. **(A–D)** Smooth butterfly ray *Gymnura micrura* (40.5 cm DW). **(E–H)** *Torpedo* sp. (16 cm DW). **(I–L)** Shovelnose guitarfish *Pseudobatos productus* (60 cm TL). **(A,E,I)** 3D isosurfaces. **(B,F,J)** Virtual cross sections following the plane indicated by the double sided dashed arrow in **(A,E,I)**. **(C,G,K)** HES staining on transverse sections following the plane indicated by the double sided dashed arrow in **(A,E,I)**. **(C',G',K')** Close-ups of the boxes in **(C,G,K)**. **(D,H,L)** PAS-AB staining of similar zones as in **(C',G',K')**, respectively. Legends as in **Figures 1**–**5**.

thin mineralization layer is both proximal (facing the neural tube) and subperichondrial (**Figures 7C,D,G,H**). Although the majority of the neural arch is composed of unmineralized cartilage matrix containing round chondrocytes (**Figures 7D,H**), the HES staining shows thin purple-stained blocks within the cartilaginous matrix that do not embed any cells (**Figures 7C',G'**), similar to the thin tesserae described in *H. colliei*. The tesserae are 10 μm wide (in their chondral-perichondrial axis, **Figures 7C',G'**) and are separated from the neural tube by a layer of cartilaginous matrix in *C. crepidater* (**Figure 7G'**), while it occurs in contact with the very thin perichondrium in *E. spinax* (**Figure 7C'**).

3.2.3. Selachians, Squalomorphs, Order: Squatiniformes

In the Pacific angelshark *Squatina californica*, the dorsal neural arches and interneural elements appear as continuously mineralized structures that are contiguous with the tesserae covering the neural spine and the basidorsal and basiventral elements (**Figure 8I**). The virtual section of the *S. californica* vertebra shows an internal variation in the mineral density of this structure, with denser peripheral mineralization than in the core (**Figure 8J**). On the histological sections, the cartilaginous tissue core contains round chondrocytes in a modified matrix (**Figures 8K',L**), similar to our previous description of globular mineralization. This central cartilaginous zone is covered proximally and distally by a fibrous mineralized tissue that contains flattened cells, similar to what we already described for fibrous mineralization of the perichondrium (**Figures 8K',L**).

3.2.4. Selachians, Galeomorphs, Order: Carcharhiniformes

In all three Carcharhiniformes considered in the following, neural arch and interneural mineralization builds up continuous structures (**Figures 8A,E,I**). Neural arch mineralization is ventrally contiguous with tesserae from the vertebral body in the tope shark *Galeorhinus galeus* and the scalloped hammerhead *Sphyrna lewini* (**Figures 8A,B,E,F**).

The continuously mineralized elements of *G. galeus* and *S. lewini* include neural arches and interneural elements (**Figures 8A,E**). In both species, neural arch mineralization encloses an unmineralized core and appears denser on the proximal and distal faces than on the dorsal zone (**Figures 8B,F**). The dorsal zone and the contact zone with the mineralized perichondrium are composed of globular mineralization (g in **Figures 8C',D,G',H**). The perichondrial layer of the mineralized tissue is similar to the fibrous mineralization sites described in the

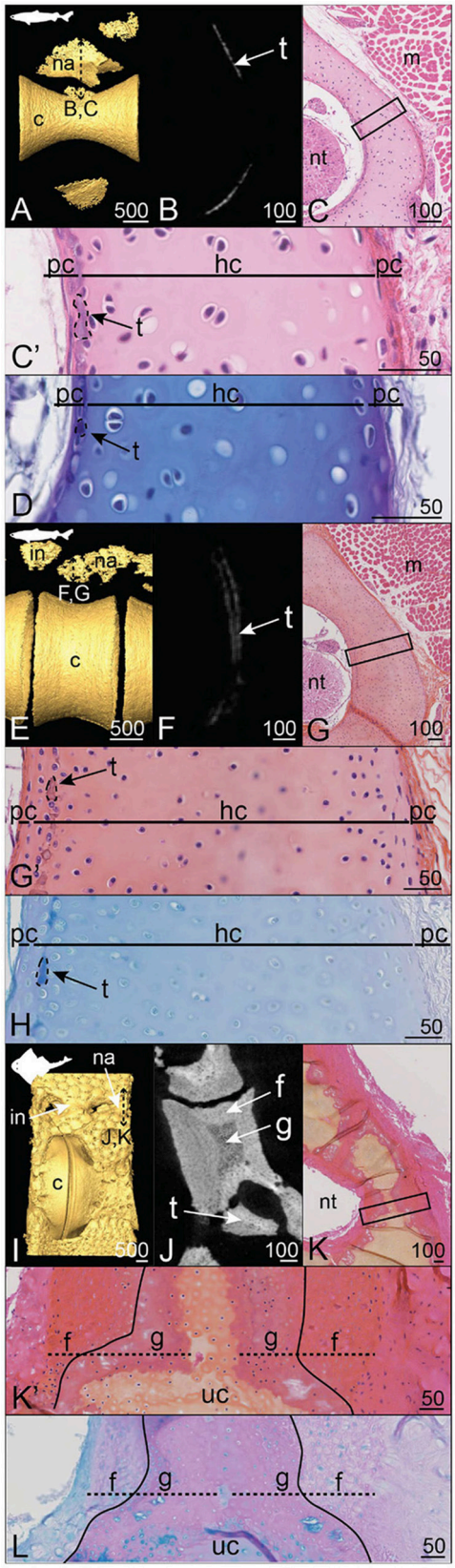

FIGURE 7 | (Continued)

FIGURE 7 | Mineralization patterns in the neural arches of posterior vertebrae in Squaliformes. **(A–D)** Velvet belly *Etmopterus spinax* (23 cm TL). **(E–H)** Longnose velvet dogfish *Centroscymnus crepidater* (31 cm TL). **(I–L)** Pacific angelshark *Squatina californica* (75 cm TL). **(A,E,I)** 3D isosurfaces. **(B,F,J)** Virtual cross sections following the plane indicated in **(A,E,I)**, respectively. **(C,G,K)** HES staining on transverse sections following the plane indicated in **(A,E,I)**. **(C',G',K')** Close-ups of the boxes in **(C,G,K)**. **(D,H,L)** PAS-AB staining of similar zones as in **(C',G',K')**, respectively. Legends as in **Figures 1**–**5**.

distal side of the *S. canicula* neural arch, with enclosed fibrocyte-shaped cells and no observable lamellae (**Figures 8C',D,G',H**).

In the blue shark *Prionace glauca*, neural arch and interneural mineralization sites alternate dorsal to the large centrum and no tesserae can be observed on the whole vertebral unit (**Figure 8I**). Mineralization is very restricted to the dorsoventral axis of the neural arch. The neural arch mineralization is superficial to only one location of the unmineralized cartilaginous neural arch (**Figure 8K**). The mineralized tissue includes globular mineralization in its innermost zone, together with outer perichondrial layers on both proximal and distal sides of the neural arch (**Figures 8K',L**). These perichondrial layers are not homogeneous because the cells undergo a morphological transition from flat—in the contact zone with globular mineralization—to subspherical—in the external zone (**Figures 8K',L**). Besides, the extracellular matrix of the external zone shows HES and Alcian blue staining similar to unmineralized cartilage, suggesting the presence of hyaline cartilaginous matrix in this perichondrial zone (**Figures 8K',L**). However, this external layer also displays numerous bundles of collagen fibers similar to Sharpey's fibers (**Figure 8K'**). The progressive centrifugal transition from a fibrous to a cartilaginous nature of the outer layers corresponds to a progressive decrease of mineralization, as shown in the virtual section (**Figure 8J**).

3.2.5. Selachians, Galeomorphs, Orders: Heterodontiformes, Orectolobiformes, and Lamniformes

In the horn shark *Heterodontus francisci* and the brownbanded bambooshark *Chiloscyllium punctatum*, alternate neural arches and interneural elements display a fully mineralized surface (**Figures 9A,E**). Tesseral mineralization is also located ventral to the neural and interneural elements of *H. francisci* (**Figure 9A**). In both species, the neural arch displays an unmineralized central core (**Figures 9B,F**) made of cartilage (**Figures 9C',G'**). However, globular mineralization is detected in the cartilaginous core in contact with the mineralized perichondrial layers (**Figures 9C',G'**). In *H. francisci*, the perichondrial mineralized layers are highly fibrous, in particular in the distal layer where numerous Sharpey's fibers are observed and incorporate numerous flattened cells (arrows, **Figures 9C',D**). On the contrary, the proximal perichondrium of the *C. punctatum* neural arch contains very few cells and the matrix is arranged in lamellae (**Figures 9G',H**). Overall, the organization and composition of the *C. punctatum* neural arch are very similar to what is observed in the *S. canicula* neural arch (compare with **Figures 1C, 2A',B,C',D**).

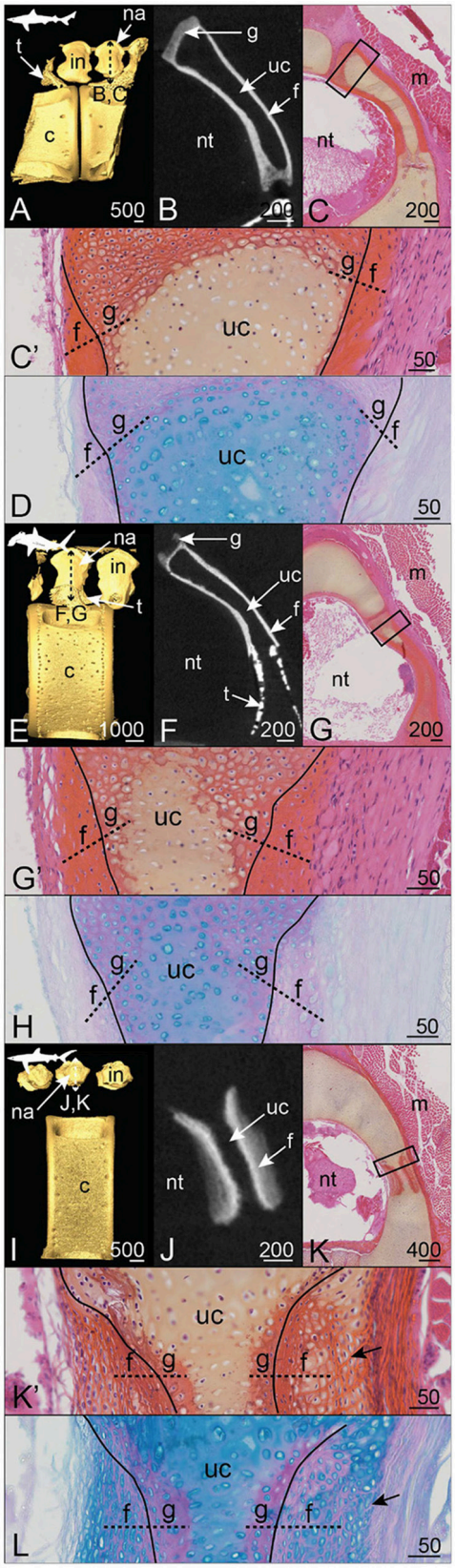

FIGURE 8 | (Continued)

FIGURE 8 | Mineralization patterns of the neural arches in Carcharhiniformes. **(A–D)** Anterior vertebra of a tope shark *Galeorhinus galeus* (50 cm TL). **(E–H)** Posterior vertebra of a scalloped hammerhead *Sphyrna lewini* (60 cm TL). **(I–L)** Posterior vertebra of a blue shark *Prionace glauca* (80 cm TL). **(A,E,I)** 3D isosurfaces. **(B,F,J)** virtual cross sections following the plane indicated in **(A,E,I)**. **(C,G,K)** HES staining on transverse sections following the plane indicated in **(A,E,I)**. **(C',G',K')** Close-ups of the boxes in **(C,G,K)**. **(D,H,L)** PAS-AB staining of similar zones as in **(C',G',K')**, respectively. Legends as in **Figures 1**–**5**.

The neural arch of the bull shark *Carcharias taurus* displays superficial mineralization in the form of standard size tesserae, while the core of the neural arch remains unmineralized (**Figures 9I,J**) and cartilaginous (**Figure 9K**). The tesserae are about 300 μm long (tangential axis) and 150 μm wide (along the chondral-perichondrial axis, **Figures 9K',L**). The cap and body zones cannot be properly distinguished from our sample, probably because of a tilted section plan (**Figures 9K',L**). However, we observe Sharpey's fibers anchoring the tesserae to the distal fibrous layer of the neural arch (arrows, **Figures 9K',L**) and unmineralized intertesseral joints (**Figures 9K',L**).

4. DISCUSSION

In the following, we discuss our results at two scales of organization, as previously defined by Dean and Summers (2006). The description of the cells and extracellular matrices involved in the mineralization (microscale description) allows defining three histotypes: globular mineralization (as reported by Ørvig, 1951), fibrous mineralization, and lamellar mineralization (as reported by Peignoux-Deville et al., 1982). On the other hand, the description of the whole skeletal elements (mesoscale description) provides insights into three mineralization architectures: discontinuous with tessellated cartilage, continuous over the whole neural arch, and semi-discontinuous in which tesserae are found associated with larger elements that we herein named corner tesserae.

4.1. Microscale Characterization of the Diversity of the Chondrichthyan Mineralized Tissues

In this work, we described the distribution of three histotypes in the neural arches of a wide taxonomic range of cartilaginous fishes. These results highlight the combined contribution of cartilaginous and perichondrial tissues in building the mineralized skeletal units of most chondrichthyans.

First, we identified globular mineralization that initiates in the hyaline cartilaginous matrix of the neural arches of all sampled species, in all architectures. It occurs in poorly developed tesserae of a holocephalan and the two Squaliformes examined in this study, in the body zone of tesserae of several elasmobranch species, in the most internal layer of the corner tesserae, and in the continuously mineralized neural arches of the other species. The classical description of tessellated cartilage includes such globular mineralization in the body zone (Kemp and Westrin, 1979; Seidel et al., 2016, 2017; Maisey et al., 2020), where the

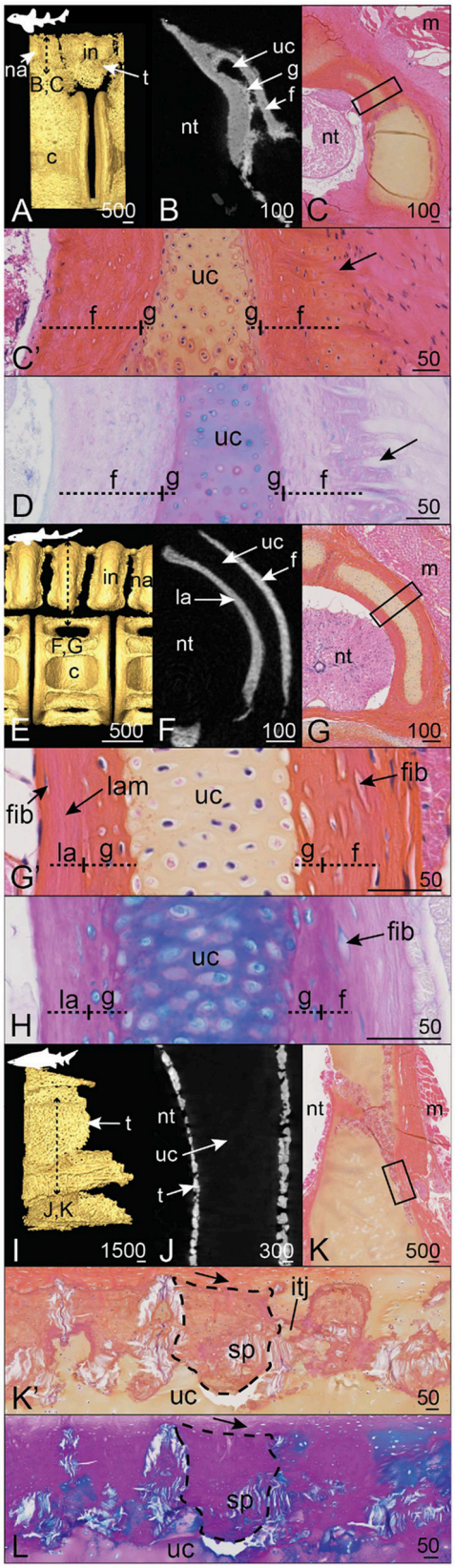

FIGURE 9 | (Continued)

FIGURE 9 | Mineralization patterns of the neural arches in galeomorphs (excluding Carcharhiniformes). **(A–D)** posterior vertebra of a horn shark *Heterodontus francisci* (55 cm TL). **(E–H)** Anterior vertebra of a brownbanded bambooshark *Chiloscyllium punctatum* (19.3 cm TL). **(I–L)** Anterior vertebra of a bull shark *Carcharias taurus* (270 cm TL). **(A,E,I)** 3D isosurfaces. **(B,F,J)** Virtual cross sections following the plane indicated in **(A,E,I)**. **(C,G,K)** HES staining on transverse sections following the plane indicated in **(A,E,I)**. **(C',G',K')** Close-ups of the boxes in **(C,G,K)**. **(D,H,L)** PAS-AB staining of similar zones as in **(C',G',K')**, respectively. Legends as in **Figures 1**–**5**.

surrounding matrix is hyaline and cells display a chondrocyte morphology with some shape variations (Chaumel et al., 2020). In both standard and corner tesserae, our observations are consistent with globular mineralization, from the observation of heterogeneous staining marking the presence of Liesegang lines. Although the exact nature of these Liesegang lines is not clear, they were hypothesized to be produced by the rhythmic activity of chondrocytes in their matrix (Kemp and Westrin, 1979). Because chondrocytes are not embedded in the mineralized matrix of the poorly developed tesserae of *E. spinax*, *C. crepidater*, and *H. colliei*, we could not detect Liesegang lines. However, Liesegang lines have been described in the thin tesserae of other holocephalan species (Pears et al., 2020; Seidel et al., 2020), defining these tesserae as sites of globular mineralization. Previous studies also showed that fully developed tesserae first appear only as subperichondrial focal mineralization sites (Enault et al., 2015; Seidel et al., 2016). This suggests that tesserae remain in an "under-developed" stage in holocephalan species as they do not engulf chondrocytes and are devoid of cap zone mineralization (Pears et al., 2020; Seidel et al., 2020), although chondrocytes in the mineralized matrix were described at an early stage of tesseral growth in *C. milii* (Pears et al., 2020). Our findings extend the occurrence of this thin globular mineralization outside of holocephalans, in selachian species with secondarily poorly mineralized skeletons (*E. spinax* and *C. crepidater*) but also in sites of poor development of these tesserae (in the *S. canicula* vertebral body).

Although they did not study and precisely describe neural arches, Ridewood and MacBride (1921) first illustrated several transverse sections of vertebrae that showed the diversity of mineralized tissues in elasmobranchs. More recent studies have interpreted some aspects of the mineralized neural arch tissues as "bone-like" in few elasmobranch species (Eames et al., 2007; Enault et al., 2015; Atake et al., 2019). Here we show that such tissues may be of at least two different types that we both hypothesize to be of perichondrial origin. Of these two types, fibrous mineralization is found in all occurrences of a continuously mineralized neural arch, is defined by the presence of fibrocyte-shaped cells enclosed in a fibrous matrix often crossed by Sharpey's fibers, and stands in continuity with the peripheral unmineralized connective tissue that links the neural arches to the surrounding muscles. Our histological results support a perichondrial nature of the tissue and therefore a growth by external apposition, as previously suggested (Atake et al., 2019). Also, we show that the inner cartilaginous core keeps a stable thickness in embryonic and

juvenile stages of development, supporting the fact that growth of the outer layers of the neural arches is generated through the activity of perichondrial cells (**Figures 2**, **3**). In our histological assays, there is no staining difference between the fibrous continuous mineralization in neural arches and the cap zone of fully developed tesserae. The cap zone has classically been described as a tissue with a derived type of mineralization (prismatic mineralization in Ørvig, 1951). Because prismatic mineralization can only be identified through polarized light microscopy, our sample preparation does not allow identifying the prismatic nature of the observed mineralization. However, the perichondrial characteristics of the cap zone have also been discussed recurrently in both the continuous neural arch tissues and the cap zone of tesserae because of the presence of type I collagen fibers and the observation of fibrocyte-shaped cells (Kemp and Westrin, 1979; Dean and Summers, 2006; Seidel et al., 2017). Further comparison to bone tissue was also often raised about the cap zone because of its dense mineralization and because of its topological location, similar to the perichondrial bone described in early vertebrates (Ørvig, 1951; Donoghue and Sansom, 2002). In our microCT images, we also detected internal variation of mineral density, suggesting lower density in globular mineralization as compared to fibrous mineralization. A more detailed tissue characterization, including recognition of cellular and lacunar shape or density, would have involved microCT scans of a much higher resolution than those analyzed here.

The third mineralized tissue identified in our samples is another type of perichondrial tissue that we named lamellar mineralization and that is only observed on the proximal side of the neural arches of *S. canicula* and *C. punctatum*. This lamellar tissue in *C. punctatum* is thin and our sampled individual was a young juvenile (19.3 cm TL) so it remains difficult to be properly compared to our observation in *S. canicula*. In *S. canicula*, the extracellular matrix content of this tissue appears more linearly organized than in fibrous mineralization (hence the lamellar denomination). The cell density is extremely low as compared to both cartilaginous and fibrous tissues and the rare cells observed in the matrix are similar to fibrocytes encased in the lamellar matrix, which is particularly visible in the elder *S. canicula* sample (**Figures 1C',D,C1,D1**). The growth of this tissue has to be appositional from cells located on the proximal surface of the neural arch, facing the neural tube, where no thick unmineralized perichondrium was apparent in our samples but only a monolayer of fibrocytes (see **Figure 9G'**). This observation highlights the potential for very different growth processes between the fibrous and lamellar mineralized tissues, as cells do not seem to behave similarly, being either engulfed and kept alive (distal side) or dead or excluded from the mineralized matrix (proximal side).

4.2. Mesoscale Mineralization Patterns: Continuous vs. Discontinuous Architectures

At mesoscale, we chose to classify our observations into several types. We defined the mineralization architecture as discontinuous when the neural surface is covered by tesserae of homogeneous size, either fully developed with a body and cap zones (Dean et al., 2009; Seidel et al., 2020) as in *C. taurus* and in Rhinopristiformes, or reduced in size and acellular (Maisey et al., 2020; Pears et al., 2020) as in Squaliformes and in *H. colliei* (**Table 2** and **Figure 10**, yellow silhouettes). We further observed discontinuous architecture in the neural arches of the posterior vertebrae of another batoid (in the white-blotched river stingray *Potamotrygon leopoldi*, data not shown). On the opposite extreme, we termed continuous architecture the neural arch surface that is mineralized as a whole (**Figure 10**, green silhouettes). Continuous mineralization involves globular, fibrous, and eventually lamellar mineralizations and is reported in Squatiniformes, Rajiformes, and all galeomorphs except in Lamniformes (**Table 2** and **Figure 10**, green silhouettes).

The third mesoscale architectural pattern is characterized by the co-occurrence of homogeneous tesserae covering most of the neural arch surface in addition to two larger elements located on the anteriormost and posteriormost sides of the neural arch, which we named corner tesserae after Dean et al. (2009). From histology, these large elements are comparable both to tesserae and to continuously mineralized neural arches because they involve an internal (chondral) globular mineralization and an external (perichondrial) fibrous mineralization. However, they differ from standard tesserae because of their size and also because they cover the surface of the proximo-distal face of the element, in addition to having two parallel faces, one on the proximal surface and the other one on the distal surface of the neural arch, making them U-shaped in their anterior-posterior axis (**Figure 3K**). As a result, they could be interpreted either as highly modified and enlarged tesserae, or as continuous mineralization that is restricted to only part of the neural arch surface. We termed this situation a semi-discontinuous architecture, considering it an intermediate state between discontinuous and continuous architectures (**Figure 10**, red silhouettes).

We described the semi-discontinuous architecture only in batoids, in the posterior vertebrae of *G. micrura* (Myliobatiformes) and *Torpedo* sp. (Torpediniformes) (**Table 2** and **Figure 10**, red silhouettes). Besides, we report its occurrence in the anterior vertebrae of *R. clavata* (Rajiformes), whereas the posterior vertebrae displayed continuous mineralization. Within Rajiformes, a semi-discontinuous architecture was reported in the Eaton's skate anterior vertebrae *Bathyraja eatonii* (Rajiformes) (Atake et al., 2019), while continuously mineralized neural arches were observed in the little skate posterior vertebrae *Leucoraja erinacea* (Criswell et al., 2017). The co-occurrence of continuous and semi-discontinuous architectures in *R. clavata* calls for more complete descriptions of the mineralized structures in vertebral columns in a wider range of Rajiformes, and other batoids, to allow making any inference on the ancestral state of mineralization architecture in this group.

4.3. Prospects on the Evolution of Mineralized Histotypes in Vertebrates

4.3.1. The Putative Nature of Fibrous Mineralization

Our work provides a histological examination in an unprecedented taxonomic range of elasmobranch fishes. We uncover the occurrence of fibrous mineralization in

TABLE 2 | Description and categorization of the mineralized tissues in the neural arches of the chondrichthyan species examined in this study.

Species	Order	Mineralization histotypes (microscale)			Mineralization architecture (mesoscale)
		Globular (c)	Fibrous (pc)	Lamellar (pc)	
S. canicula	Carcharhiniformes	+	+, dist	+, prox	Continuous
C. punctatum	Orectolobiformes	+	+, dist	+, prox	
P. glauca	Carcharhiniformes	+	+	–	
G. galeus	Carcharhiniformes	+	+	–	
S. lewini	Carcharhiniformes	+	+	–	
H. francisci	Heterodontiformes	+	+	–	
S. californica	Squatiniformes	+	+	–	
R. clavata	Rajiformes	+	+	–	Continuous and semi-discontinuous (corner tesserae)
G. micrura	Myliobatiformes	+	+	–	Semi-discontinuous (corner tesserae)
Torpedo sp.	Torpediniformes	+	+	–	
R. ancylostoma	Rhinopristiformes	+, t	+, t	–	Discontinuous (tessellated)
P. productus	Rhinopristiformes	+, t	+, t	–	
C. taurus	Lamniformes	+, t	+, t	–	
H. colliei	Chimaeriformes	+, t	–	–	Discontinuous (reduced)
C. crepidater	Squaliformes	+, t	–	–	
E. spinax	Squaliformes	+, t	–	–	

+ indicates that the mineralized tissue is detected, as opposed to –, t indicates that the tissue is located within a tessera, and prox and dist are specified when the tissue is restricted to the proximal (facing the neural tube) and distal (facing muscular attachments) sides of the neural arch, respectively. c, cartilage; pc, perichondrium.

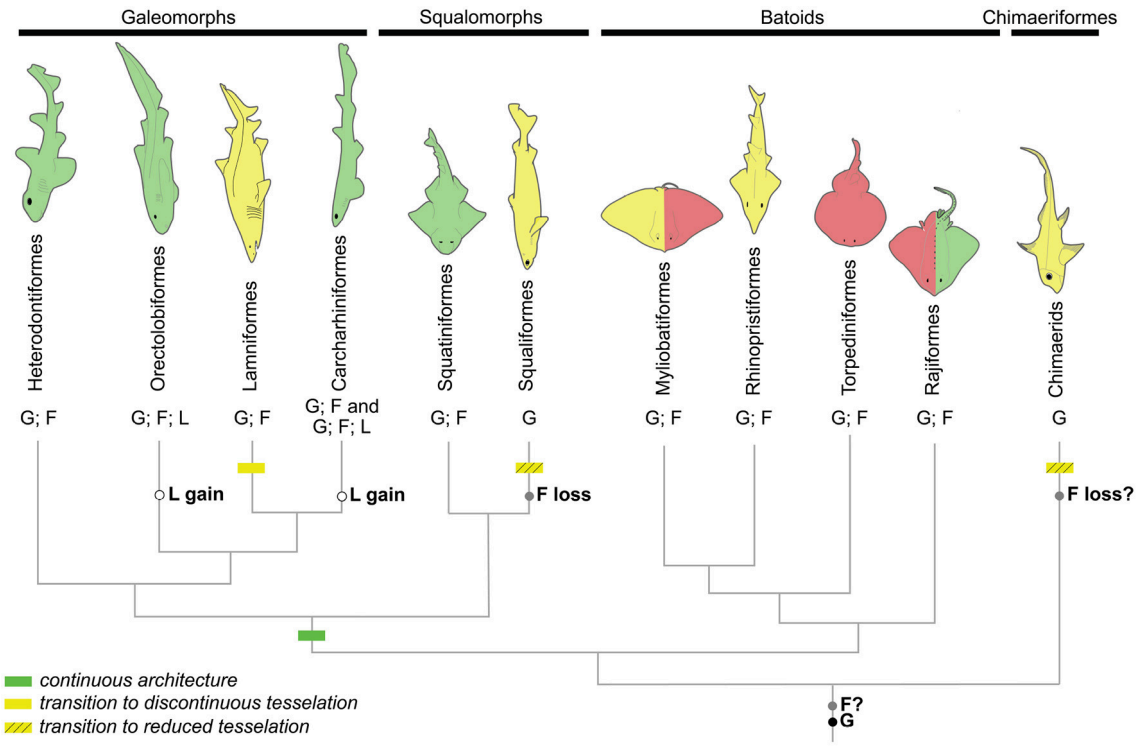

FIGURE 10 | Phylogenetic relationships of the main chondrichthyan groups sampled in this study showing the distribution of neural arch mineralization architecture (silhouettes: green, continuous mineralization; red, semi-discontinuous mineralization; yellow, discontinuous mineralization) and histotypes (F, fibrous mineralization; G, globular mineralization; L, lamellar mineralization). Evolutionary events are located on the tree branches based on reconstructions following a most parsimonious model.

continuously mineralized neural arches in an Heterodontiform, a Squatiniform, most Carcharhiniformes examined in this study, and a Rajiform (**Figure 10**). Fibrous mineralization is also identified in the perichondrial zone of both corner and standard tesserae (**Table 2**). Here we wish to discuss the hypothesis of fibrous mineralization to be naturally mineralizing fibrocartilage, as previously suggested by Ørvig (1951) and Eames et al. (2007). Mineralized fibrocartilages were described in tetrapod entheses that join tendons to bones (Benjamin and Ralphs, 1998) and surrounding rib cartilage (Claassen et al., 1996). Fibrocartilage histology shows strong variation, ranging from almost hyaline to highly fibrous (similar to tendons) in mammals (Wachsmuth et al., 2006) and bony fishes (Benjamin, 1990). Similar variation is observed in our sample, where fibrous mineralization resembles more hyaline-type cartilage crossed by fibers in *P. glauca* (**Figures 8K,L**). This hypothesis would also explain the presence of type II collagen and a thin layer identified as "supra-tesseral cartilage" in the perichondrial surface of tesserae in some species (Seidel et al., 2017). Further histochemical, histological, and cellular characterization is therefore needed to better define the nature of this tissue and compare it to tetrapod tissues.

Beyond the nature of this tissue, we show that perichondrial fibrous mineralization is widely present in skeletal tissues of elasmobranchs. Ancestral character state reconstruction by a most-parsimonious model (**Supplementary Material 1** and summarized in **Figure 10**) suggests that this histotype is ancestral to elasmobranchs (as previously hypothesized by Atake et al., 2019). This scenario implies a secondary loss of fibrous mineralization in *C. crepidater* and *E. spinax*. Considering the secondary loss of mineralization observed in extant holocephalans (Maisey et al., 2020; Pears et al., 2020), it is also plausible that fibrous mineralization is ancestral to all chondrichthyans but lost in holocephalans. Fibrous mineralization may then be a remnant of forms of mineralization found in early vertebrates. As a consequence, a review of the paleontological data is needed, especially in stem gnathostomes and agnathan taxa where several forms of perichondrial bone (cellular or acellular, as described in placoderm taxa Ørvig, 1951 or galeaspid and osteostracan taxa, as reviewed by Donoghue and Sansom, 2002) may be revised in light of this fibrous mineralization that covers cartilaginous skeletal units. Further comparison with extant and extinct taxa of bony fishes may also uncover similar tissues outside of chondrichthyans. Only this information may shed light on the evolution of fibrous mineralization and its significance to the evolution of a mineralized skeleton in vertebrates.

4.3.2. Lamellar Mineralization and Putative Bone in Cartilaginous Fishes

The continuous architecture always includes fibrous mineralization in the distal part of the neural arch but we identified lamellar, instead of fibrous, mineralization in the proximal side of the neural arch of two galeomorph species (**Table 2**). The fibrous and lamellar mineralizations histologically differ in that the former contains numerous cells, as opposed to the latter where only very few cells are observed, and by the arrangement of fibers. Another difference is the lack of a thick unmineralized connective tissue surrounding the lamellar mineralization (see **Figure 2C'**, as opposed to the situation in other galeomorphs, see **Figures 9G',K'**). Bone-like tissue was previously reported in the neural arches of Carcharhiniformes (Peignoux-Deville et al., 1982; Eames et al., 2007) and Rajiformes (Atake et al., 2019). These previous studies did not distinguish the cellular from almost acellular tissues and the histological staining results in the work of Atake et al. (2019) better support the presence of fibrous mineralization in both the proximal and distal sides of the neural arches of *L. erinacea* and *B. eatonii*. As a consequence, the lamellar mineralized pattern as defined in our work has only been described so far in *S. canicula* and most probably in *C. ventriosum* (Eames et al., 2007) (both Carcharhiniformes), and in *C. punctatum* (Orectolobiformes). Considering these results, ancestral character state reconstruction with a most-parsimonious model suggests parallel evolution of this lamellar pattern in Carcharhiniformes and Orectolobiformes (**Supplementary Material 2**, summarized in **Figure 10**). Still, our observations and hypothesis need to be confirmed with broader sampling among Orectolobiform species, including older specimens. As a broader conclusion, our results support a recent evolution of this trait, making it unlikely to be homologous to any bone type found in early vertebrates.

4.4. Concluding Remarks

Tessellated cartilage is considered a synapomorphy of chondrichthyans (reviewed in Maisey, 2013) and displays a high variety of tessera morphologies and spatial arrangements (Summers et al., 1998; Seidel et al., 2016; Maisey et al., 2020; Pears et al., 2020). What could be considered classical, polygonal and flat tesserae as described in extant batoids are assumed to be the ancestral morphology of chondrichthyan tesserae and to have further undergone size and shape alterations during the evolution of different groups, including strong size regression as found in holocephalans (Pears et al., 2020). Here we have described other mineralization architectures in elasmobranchs, where cartilage surfaces can be continuously mineralized or covered by a combination of tesserae and larger mineralized elements. The reconstruction of an ancestral state for the architecture character under maximum parsimony only suggests that mineralization of the neural arches was ancestrally continuous in selachians, considering a secondary reduction of mineralization in our sampled Lamniform (**Supplementary Material 3**). More samples are necessary to generate hypotheses on chondrichthyans and elasmobranchs.

Besides, we never observed any complete absence of mineralization in our samples. What could be considered a minimal state of mineralization was located in a subperichondrial zone of the hyaline cartilaginous matrix of neural arches (in *H. colliei*, *E. spinax*, and *C. crepidater*). This zone was previously considered as the initiator for further mineralization that would propagate from the hyaline cartilage toward the perichondrium (Ørvig, 1951). It is plausible that the process and pattern of tissue mineralization in elasmobranchs (microscale analysis) might be completely independent of the process of architecture regulation (mesoscale analysis) that has led to

the derived evolution of tesserae in chondrichthyans. As a consequence, if mineralized tissues are comparable in continuous and discontinuous mineralized architectures, evolution between these two states may simply entail a variation in the intensity of one regulatory signal (as suggested by Maisey et al., 2020) that would constrain the size of the mineralized elements, from tesserae as minimal objects to fully mineralized structures, with intermediate states involving the massive elements described in some neural arches of batoids.

Finally, the occurrence of a reduced tessellated pattern in phylogenetically distant groups (Squaliformes and holocephalans) questions the existence of ecological signals able to drive such convergent evolution. Deep-water shark species are known to display reduced mineralization of the endoskeleton as compared to shallower species (Dean et al., 2015; Seidel et al., 2016). *H. colliei* is not restricted to deep water habitats (Barnett et al., 2012) but holocephalans are characterized by a reduction of mineralized structures (Pears et al., 2020) and are the chondrichthyan group found in deepest waters (Priede and Froese, 2013). As a conclusion, ecological constraints, such as deep-water habitat may have convergently driven loss of mineralization in chondrichthyans. It is assumed that such a reduced amount of mineralization could contribute to energetic trade-offs by impacting buoyancy and metabolic costs of locomotion (Blaxter et al., 1971; Blaxter, 1980), however, more data on chondrichthyans are needed to challenge this hypothesis.

DATA AVAILABILITY STATEMENT

The original contributions presented in the study are included in the article/**Supplementary Material**, further inquiries can be directed to the corresponding author/s.

ETHICS STATEMENT

Ethical review and approval was not required for the animal study because no handling of live specimens was necessary for this study.

AUTHOR CONTRIBUTIONS

FB and MD-T designed the experimental setup, prepared the samples, imaged and analyzed the results, and drafted the manuscript. SE, MB, and NP performed the histological sections and staining. FAL-R collected the samples. All authors agree to be accountable for the content of the work.

FUNDING

NP and MB are members of the Réseau d'Histologie Expérimentale de Montpellier (RHEM) facility, supported by SIRIC Montpellier Cancer (Grant INCa Inserm DGOS 12553), the European regional development foundation and the occitanian region (FEDER-FSE 2014-2020 Languedoc Roussillon).

ACKNOWLEDGMENTS

We thank Sylvain Adnet, Henri Cappetta, and Guillaume Guinot from the Institut des Sciences de l'Evolution de Montpellier and the aquaria Planet Ocean, Montpellier (Nicolas Hirel) and Marineland Parcs, Antibes (Jean-Philippe Cateau) for providing biological samples. We thank Renaud Lebrun for his help with microCT scans and Camille Martinand-Mari, Nicolas Leurs, and Yann Bayle for insightful proofreading. 3D data acquisitions (microCT facilities) and slide scanning (nanozoomer) are hosted in the MRI platform, a member of the national infrastructure France-BioImaging supported by the French National Research Agency (ANR-10-INBS-04, Investments for the future), and of the Labex CEMEB (ANR-10-LABX-0004) and NUMEV (ANR-10-LABX-0020).

SUPPLEMENTARY MATERIAL

The Supplementary Material for this article can be found online at: https://www.frontiersin.org/articles/10.3389/fevo.2021.660767/full#supplementary-material

REFERENCES

Applegate, S. (1967). "A survey of shark hard parts," in *Sharks, Skates and Rays*, eds P. Gilbert, R. Mathewson, and D. Rall (Baltimore, MD: The Johns Hopkins Press), 37–67.

Atake, O. J., Cooper, D. M. L., and Eames, B. F. (2019). Bone-like features in skate suggest a novel elasmobranch synapomorphy and deep homology of trabecular mineralization patterns. *Acta Biomater.* 84, 424–436. doi: 10.1016/j.actbio.2018.11.047

Barnett, L. A., Earley, R. L., Ebert, D. A., and Cailliet, G. M. (2009). Maturity, fecundity, and reproductive cycle of the spotted ratfish, *Hydrolagus colliei*. *Mar. Biol.* 156, 301–316. doi: 10.1007/s00227-008-1084-y

Barnett, L. A. K., Ebert, D. A., and Cailliet, G. M. (2012). Evidence of stability in a chondrichthyan population: case study of the spotted ratfish *Hydrolagus colliei* (Chondrichthyes: Chimaeridae). *J. Fish Biol.* 80, 1765–1788. doi: 10.1111/j.1095-8649.2011.03216.x

Bejarano-Álvarez, M., Galván-Magaña, F., and Ochoa-Báez, R. I. (2011). Reproductive biology of the scalloped hammerhead shark *Sphyrna lewini* (Chondrichthyes: Sphyrnidae) off southwest Mexico. *Aqua Int. J. Ichthyol.* 17, 11–22.

Benjamin, M. (1990). The cranial cartilages of teleosts and their classification. *J. Anat.* 169, 153–172.

Benjamin, M., and Ralphs, J. R. (1998). Fibrocartilage in tendons and ligaments–an adaptation to compressive load. *J. Anat.* 193, 481–494. doi: 10.1046/j.1469-7580.1998.19340481.x

Blaxter, J. H. S. (1980). "The effect of hydrostatic pressure on fishes," in *Environmental Physiology of Fishes. NATO Advanced Study Institutes Series (Series A: Life Science)*, Vol. 35, ed M. A. Ali (Boston, MA: Springer). doi: 10.1007/978-1-4899-3659-2_13

Blaxter, J. H. S., Wardle, C. S., and Roberts, B. L. (1971). Aspects of the circulatory physiology and muscle systems of deep-sea fish. *J. Mar. Biol. Assoc.* 51, 991–1006. doi: 10.1017/S0025315400018105

Bustamante, C., and Bennett, M. B. (2013). Insights into the reproductive biology and fisheries of two commercially exploited species, shortfin mako (*Isurus oxyrinchus*) and blue shark (*Prionace glauca*), in the south-east Pacific Ocean. *Fish. Res.* 143, 174–183. doi: 10.1016/j.fishres.2013.02.007

Capapé, C., Guélorget, O., Siau, Y., Vergne, Y., and Quignard, J. P. (2007). Reproductive biology of the thornback ray *Raja clavata* (Chondrichthyes: Rajidae) from the coast of Languedoc (southern France, northern Mediterranean). *Vie Milieu* 57, 83–90.

Capapé, C., Reynaud, C., Vergne, Y., and Quignard, J. P. (2008). Biological observations on the smallspotted catshark *Scyliorhinus canicula* (Chondrichthyes: Scyliorhinidae) off the Languedocian coast (southern France, northern Mediterranean). *Pan Am. J. Aquat. Sci.* 3, 282–289.

Chaumel, J., Schotte, M., Bizzarro, J. J., Zaslansky, P., Fratzl, P., Baum, D., et al. (2020). Co-aligned chondrocytes: zonal morphological variation and structured arrangement of cell lacunae in tessellated cartilage. *Bone* 134:115264. doi: 10.1016/j.bone.2020.115264

Claassen, H., Kampen, W. U., and Kirsch, T. (1996). Localization of collagens and alkaline phosphatase activity during mineralization and ossification of human first rib cartilage. *Histochem. Cell Biol.* 105, 213–219. doi: 10.1007/BF01462294

Compagno, L. J. V. (1984). Sharks of the world: an annotated and illustrated catalogue of shark species known to date. *FAO Species Catalog. Fish. Purposes* 2, 175–176.

Criswell, K. E., Coates, M. I., and Gillis, J. A. (2017). Embryonic development of the axial column in the little skate, *Leucoraja erinacea*. *J. Morphol.* 278, 300–320. doi: 10.1002/jmor.20637

Dean, M. N., Ekstrom, L., Monsonego-Ornan, E., Ballantyne, J., Witten, P. E., Riley, C., et al. (2015). Mineral homeostasis and regulation of mineralization processes in the skeletons of sharks, rays and relatives (Elasmobranchii). *Semin. Cell Dev. Biol.* 46, 51–67. doi: 10.1016/j.semcdb.2015.10.022

Dean, M. N., Mull, C. G., Gorb, S. N., and Summers, A. P. (2009). Ontogeny of the tessellated skeleton: insight from the skeletal growth of the round stingray *Urobatis halleri*. *J. Anat.* 215, 227–239. doi: 10.1111/j.1469-7580.2009.01116.x

Dean, M. N., and Summers, A. P. (2006). Mineralized cartilage in the skeleton of chondrichthyan fishes. *Zoology* 109, 164–168. doi: 10.1016/j.zool.2006.03.002

Debiais-Thibaud, M. (2019). "The evolution of endoskeletal mineralisation in chondrichthyan fish," in *Evolution and Development of Fishes, Chapter 6*, eds Z. Johanson, C. Underwood, and M. Richter (Cambridge: Cambridge University Press), 110–125. doi: 10.1017/9781316832172.007

Debiais-Thibaud, M., Simion, P., Ventéo, S., Muñoz, D., Marcellini, S., Mazan, S., et al. (2019). Skeletal mineralization in association with type x collagen expression is an ancestral feature for jawed vertebrates. *Mol. Biol. Evol.* 36, 2265–2276. doi: 10.1093/molbev/msz145

Donoghue, P. C. J., and Sansom, I. J. (2002). Origin and early evolution of vertebrate skeletonization. *Microsc. Res. Tech.* 59, 352–372. doi: 10.1002/jemt.10217

Eames, B. F., Allen, N., Young, J., Kaplan, A., Helms, J. A., and Schneider, R. A. (2007). Skeletogenesis in the swell shark *Cephaloscyllium ventriosum*. *J. Anat.* 210, 542–554. doi: 10.1111/j.1469-7580.2007.00723.x

Ebert, D. A., Fowler, S., and Compagno, L. J. V. (2013). *Sharks of the World: A Fully Illustrated Guide*. Plymouth: Wild Nature Press.

Enault, S., Adnet, S., and Debiais-Thibaud, M. (2016). Skeletogenesis during the late embryonic development of the catshark *Scyliorhinus canicula* (Chondrichthyes; Neoselachii). *MorphoMuseuM* 1:e2. doi: 10.18563/m3.1.4.e2

Enault, S., Muñoz, D. N., Silva, W. T. A. F., Borday-birraux, V., Bonade, M., Oulion, S., et al. (2015). Molecular footprinting of skeletal tissues in the catshark Scyliorhinus canicula and the clawed frog *Xenopus tropicalis* identifies conserved and derived features of vertebrate calcification. *Front. Genet.* 6:283. doi: 10.3389/fgene.2015.00283

Finarelli, J. A., and Coates, M. I. (2014). Chondrenchelys problematica (Traquair 1888) redescribed: a Lower Carboniferous, eel-like holocephalan from Scotland. *Earth Environ. Sci. Trans. R. Soc. Edinb.* 105, 35–59. doi: 10.1017/S1755691014000139

Goodrich, E. S. (1930). *Studies on the Structure & Development of Vertebrates*. London: Macmillan and Co.

Hall, B. K. (2015). *Bones and Cartilage, 2nd Edn*. Oxford: Elsevier-Academic Press.

Hall, B. K., and Witten, P. E. (2019). "Plasticity and variation of skeletal cells and tissues and the evolutionary development of actinopterygian fishes," in *Evolution and Development of Fishes, Chapter 7*, eds Z. Johanson, C. Underwood, and M. Richter (Cambridge: Cambridge Université Press), 126–143. doi: 10.1017/9781316832172.008

Hasse, C. (1879). *Das natürliche System der Elasmobranchier auf Grundlage des Baues und der Entwicklung ihrer Wirbelsäule*, Vol. I Allgemei. Jena: Eine morphologische und paläontologische Studie.

Hilton, M. J., Tu, X., Cook, J., Hu, H., and Long, F. (2005). Ihh controls cartilage development by antagonizing Gli3, but requires additional effectors to regulate osteoblast and vascular development. *Development* 132, 4339–4351. doi: 10.1242/dev.02025

Johanson, Z., Boisvert, C. A., Maksimenko, A., Currie, P., and Trinajstic, K. (2015). Development of the synarcual in the elephant sharks (Holocephali; Chondrichthyes): implications for vertebral formation and fusion. *PLoS ONE* 10:e0135138. doi: 10.1371/journal.pone.0135138

Kemp, N. E., and Westrin, S. K. (1979). Ultrastructure of calcified cartilage in the endoskeletal tesserae of sharks. *J. Morphol.* 160, 75–109. doi: 10.1002/jmor.1051600106

Last, P., Naylor, G., Séret, B., White, W., de Carvalho, M., and Stehmann, M. (2016). *Rays of the World*. Clayton South, VIC: CSIRO Publishing.

Leurs, N., Martinand-Mari, C., Vento, S., Haitina, T., and Debiais-Thibaud, M. (2021). Evolution of matrix gla and bone gla protein genes in jawed vertebrates. *Front. Genet.* 12:245. doi: 10.3389/fgene.2021.620659

Licht, M., Schmuecker, K., Huelsken, T., Hanel, R., Bartsch, P., and Paeckert, M. (2012). Contribution to the molecular phylogenetic analysis of extant holocephalan fishes (Holocephali, Chimaeriformes). *Organ. Divers. Evol.* 12, 421–432. doi: 10.1007/s13127-011-0071-1

Lucifora, L. O., Menni, R. C., and Escalante, A. H. (2002). Reproductive ecology and abundance of the sand tiger shark, *Carcharias taurus*, from the southwestern Atlantic. *ICES J. Mar. Sci.* 59, 553–561. doi: 10.1006/jmsc.2002.1183

Lucifora, L. O., Menni, R. C., and Escalante, A. H. (2004). Reproductive biology of the school shark, *Galeorhinus galeus*, off Argentina: support for a single south western Atlantic population with synchronized migratory movements. *Environ. Biol. Fishes* 71, 199–209. doi: 10.1007/s10641-004-0305-6

Maddison, W. P., and Maddison, D. R. (2019). *Mesquite: A Modular System for Evolutionary Analysis*. Available online at: http://www.mesquiteproject.org

Maisey, J. G. (2013). The diversity of tessellated calcification in modern and extinct chondrichthyans. *Rev. Paléobiol.* 32, 355–371.

Maisey, J. G., Denton, J. S. S., Burrow, C., and Pradel, A. (2020). Architectural and ultrastructural features of tessellated calcified cartilage in modern and extinct chondrichthyan fishes. *J. Fish Biol.* 98, 919–941. doi: 10.1111/jfb.14376

Márquez-Farías, J. F. (2007). Reproductive biology of shovelnose guitarfish Rhinobatos productus from the eastern Gulf of California México. *Mar. Biol.* 151, 1445–1454. doi: 10.1007/s00227-006-0599-3

Mayoral, E. E., Schultz, R., Rosemberg, S., Suzuki, L., Nunes de Oliveira, L. A., and Kay, F. U. (2014). Thanatophoric dysplasia : case report of an autopsy complemented by postmortem computed tomographic study. *Autopsy Case Rep.* 4, 35–41. doi: 10.4322/acr.2014.019

Meese, E. N., and Lowe, C. G. (2020). Environmental effects on daytime sheltering behaviors of California horn sharks (*Heterodontus francisci*). *Environ. Biol. Fishes* 103, 703–717. doi: 10.1007/s10641-020-00977-6

Moore, D. M., Neat, F. C., and McCarthy, I. D. (2013). Population biology and ageing of the deep water sharks *Galeus melastomus*, *Centroselachus crepidater* and *Apristurus aphyodes* from the Rockall Trough, north-east Atlantic. *J. Mar. Biol. Assoc.* 93, 1941–1950. doi: 10.1017/S0025315413000374

Naylor, G. J. P., Caira, J. N., Jensen, K., Rosana, K. A. M., Straube, N., and Lakner, C. (2012). "Elasmobranch phylogeny: a mitochondrial estimate based on 595 species," in *Biology of Sharks and Their Relatives, Chapter 2, 2nd Edn.*, eds J. C. Carrier, J. A. Musick, and M. R. Heithaus (Boca Raton, FL: CRC Press), 31–56. doi: 10.1201/b11867-4

Ørvig, T. (1951). Histologic studies of Placoderms and fossil Elasmobranchs. I: the endoskeleton, with remarks on the hard tissues of lower vertebrates in general. *Arkiv Zool.* 2:322.

Pears, J., Johanson, Z., Trinajstic, K., Dean, M. N., and Boisvert, C. A. (2020). Mineralization of the callorhinchus vertebral column (Holocephali; Chondrichthyes). *Front. Genet.* 11:1477. doi: 10.3389/fgene.2020.571694

Peignoux-Deville, J., Lallier, F., and Vidal, B. (1982). Evidence for the presence of osseous tissue in dogfish vertebrae. *Cell Tissue Res.* 222, 605–614. doi: 10.1007/BF00213858

Porcu, C., Marongiu, M. F., Follesa, M. C., Bellodi, A., Mulas, A., Pesci, P., et al. (2014). Reproductive aspects of the velvet belly *Etmopterus spinax*

(Chondrichthyes: Etmopteridae), from the central western Mediterranean Sea. Notes on gametogenesis and oviducal gland microstructure. *Mediterr. Mar. Sci.* 15, 313–326. doi: 10.12681/mms.559

Priede, I. G., and Froese, R. (2013). Colonization of the deep sea by fishes. *J. Fish Biol.* 83, 1528–1550. doi: 10.1111/jfb.12265

Ridewood, W. G., and MacBride, E. W. (1921). VIII. On the calcification of the vertebral centra in sharks and rays. *Philos. Trans. R. Soc. Lond. B* 210, 311–407. doi: 10.1098/rstb.1921.0008

Romero-Caicedo, A. F., Galván-Magaña, F., Hernández-Herrera, A., and Carrera-Fernández, M. (2016). Reproductive parameters of the Pacific angel shark *Squatina californica* (Selachii: Squatinidae). *J. Fish Biol.* 88, 1430–1440. doi: 10.1111/jfb.12920

Ryll, B., Sanchez, S., Haitina, T., Tafforeau, P., and Ahlberg, P. E. (2014). The genome of Callorhinchus and the fossil record: a new perspective on scpp gene evolution in gnathostomes. *Evol. Dev.* 16, 123–124. doi: 10.1111/ede.12071

Seidel, R., Blumer, M., Chaumel, J., Amini, S., and Dean, M. N. (2020). Endoskeletal mineralization in chimaera and a comparative guide to tessellated cartilage in chondrichthyan fishes (sharks, rays and chimaera). *J. R. Soc. Interface* 17:20200474. doi: 10.1098/rsif.2020.0474

Seidel, R., Blumer, M., Pechriggl, E.-J., Lyons, K., Hall, B. K., Fratzl, P., et al. (2017). Calcified cartilage or bone? Collagens in the tessellated endoskeletons of cartilaginous fish (sharks and rays). *J. Struct. Biol.* 200, 54–71. doi: 10.1016/j.jsb.2017.09.005

Seidel, R., Lyons, K., Blumer, M., Zaslansky, P., Fratzl, P., Weaver, J. C., et al. (2016). Ultrastructural and developmental features of the tessellated endoskeleton of elasmobranchs (sharks and rays). *J. Anat.* 229, 681–702. doi: 10.1111/joa.12508

Smith, M. M., Underwood, C., Goral, T., Healy, C., and Johanson, Z. (2019). Growth and mineralogy in dental plates of the holocephalan *Harriotta raleighana* (Chondrichthyes): novel dentine and conserved patterning combine to create a unique chondrichthyan dentition. *Zool. Lett.* 5, 1–30. doi: 10.1186/s40851-019-0125-3

Summers, A. P., Koob, T. J., and Brainerd, E. L. (1998). Stingray jaws strut their stuff. *Nature* 395, 450–451. doi: 10.1038/26649

Tarazona, O. A., Slota, L. A., Lopez, D. H., Zhang, G., and Cohn, M. J. (2016). The genetic program for cartilage development has deep homology within Bilateria. *Nature* 533, 86–89. doi: 10.1038/nature 17398

Wachsmuth, L., Söder, S., Fan, Z., Finger, F., and Aigner, T. (2006). Immunolocalization of matrix proteins in different human cartilage subtypes. *Histol. Histopathol.* 21, 477–485. doi: 10.14670/HH-21.477

Whiteman, P. (1973). The quantitative measurement of Alcian Blue-glycosaminoglycan complexes. *Biochem. J.* 131, 343–350. doi: 10.1042/bj1310343

Witten, P. E., and Huysseune, A. (2009). A comparative view on mechanisms and functions of skeletal remodelling in teleost fish, with special emphasis on osteoclasts and their function. *Biol. Rev. Camb. Philos. Soc.* 84, 315–346. doi: 10.1111/j.1469-185X.2009.00077.x

Witten, P. E., Huysseune, A., and Hall, B. K. (2010). A practical approach for the identification of the many cartilaginous tissues in teleost fish. *J. Appl. Ichthyol.* 26, 257–262. doi: 10.1111/j.1439-0426.2010.01416.x

Xiong, H., Rabie, A. B. M., and Hagg, U. (2005). Mechanical strain leads to condylar growth in adult rats. *Front. Biosci.* 10, 65–73. doi: 10.2741/1507

Yokota, L., Goitein, R., Gianeti, M. D., and Lessa, R. T. (2012). Reproductive biology of the smooth butterfly ray *Gymnura micrura*. *J. Fish Biol.* 81, 1315–1326. doi: 10.1111/j.1095-8649.2012.03413.x

Zhang, G., and Cohn, M. J. (2006). Hagfish and lancelet fibrillar collagens reveal that type II collagen-based cartilage evolved in stem vertebrates. *Proc. Natl. Acad. Sci. U.S.A.* 103, 16829–16833. doi: 10.1073/pnas.0605630103

Conflict of Interest: The authors declare that the research was conducted in the absence of any commercial or financial relationships that could be construed as a potential conflict of interest.

4.3 Conclusions of the article

The project highlights the occurrence of three types of architecture for neural arch mineralisation at mesoscale: continuous, when the neural arch is mineralised as a whole element, discontinuous when the neural arch is covered by regular tesserae, and semi-discontinuous when tesserae cover most element but when through-tesserae also cross the neural arch at discrete locations. All these mineralisation architectures contain the globular mineralisation histotype, which is found in neoselachians, batoids, and holocephalans. The bone-like tissue as previously reported in some elasmobranch neural arches can be subdivided into two mineralisation types, based on histological features. We named the first type fibrous mineralisation, which is characterised by numerous elongated cells enclosed in a fibrous mineralised matrix and is bordered by unmineralised connective tissue. We showed that fibrous mineralisation occurs in most of the elasmobranch species considered but has been probably secondarily lost in Squaliformes. Lamellar mineralisation is the second type of bone-like tissue we recognise, it contains no cells or fewer cells than in fibrous mineralisation and is bordered by a very thin and unmineralised layer of connective tissue. It only occurs in the neural arch of one Carcharhiniforme and one Orectolobiforme and we suggest a parallel evolution of this lamellar pattern in these two lineages. Altogether, these results refine the mineralised histotypes previously described in the neural arches of chondrichthyans and allow speculating on the evolution of different bone-like tissues within the group. This work finally reminds us that the mineralisation patterns of the chondrichthyan endoskeleton are probably much more diverse than currently known and that they offer promising research prospects to understand the evolution of this group and vertebrates.

Chapter 5
Conclusions and prospects

In this chapter, I discuss in more details the major findings and the prospects of my PhD work but my main contributions can be summarised as follows. I highlighted and detailed for the first time the emergence of gynandric heterodonty during growth in two shark species. I gathered a large and reusable dataset on shark tooth shapes and combined a 3D geometric morphometric approach with the use of Random Forests in an original framework to assess tooth form differences between shark populations. I provided a detailed examination of tooth crowns in *S. canicula*, a model species among sharks, which dental pattern diversity had not been investigated hitherto. I compared the *S. canicula* tooth morphologies with those of *S. stellaris* for which very few data on dental forms were already available and highlighted shape overlaps that could lead to taxonomic misclassifications. I designed a protocol to perform functional tests on *S. canicula* embryos by inserting microbeads next to developing tooth buds. These experiments aim at providing the first clues on the role of specific proteins on the acquisition of a particular tooth shape in sharks. I finally deciphered the occurrence of bone-like tissue in the neural arches of several chondrichthyan groups and species. I evidenced that this tissue is synthesised in more elasmobranch groups than previously thought, which contributes having an overview of the evolution of mineralised tissues of vertebrates.

5.1 Shark "dental impressions": Stability and variation of tooth forms and developmental trajectories

Various groups of organisms display intraindividual variability in their serial structures: leaf forms can depend on their location along a partly submerged stalk, foliar shade, interaction between temperature and the node at which the leaf is produced, and ontogeny [Winn, 1996; Chitwood et al., 2012; Spriggs et al., 2018]. Benthic colonial invertebrates such as corals and gorgonians also display flexible architecture according to the patterning of modular colonies [Hughes, 2005]. Models have been developed to understand the patterning of such colonies and have included environmental contraints, proximity of neighbouring branches, and endogenous factors such as diffusion-limitation parameters [Hughes, 2005]. These models highlighted the potential for endo- and exogenous factors to generate intraindividual variability.
My PhD work first aimed at detailing intraindividual variability in the dental sets of two scyliorhinid species (*S. canicula* and *S. stellaris*). I used 3D tooth surfaces to perform geometric morphometrics and describe tooth form and shape patterns along the jaw

of a specimen and between palatoquadrate and Meckelian teeth. I documented the modification of intraindividual variability over ontogeny, to the condition one accepts that the specimens I examined are not the same for each developmental stage considered. Based on these observations, I proposed hypotheses on the factors that can generate such intraindividual variability: the mesio-distal modifications of number of accessory cusps and bending can be related to gradients of protein receptors along the jaw and cartilage folding, while the slight differences of tooth forms between jaws might more be due to mesio-distal and labio-lingual shape differences between both cartilages. Dental patterning in sharks is dynamic, not only because of the permanent renewal of dental sets, but also because teeth can display changing morphologies that depend on the ontogenetic stage and allow specific mating behaviours in which males bite and hold females. Thus, I also report the emergence of gynandric heterodonty during the ontogeny of *S. canicula* and *S. stellaris*. In *S. stellaris*, the developmental trajectories of dental sets are similar in both sexes from the hatching to juvenile ontogenetic stage but differ in older specimens because mature males develop less accessory cusps as compared to mature females, which retain a juvenile-like morphology. The emergence of gynandric heterodonty between the juvenile and mature stages could be controlled by the production of different sex hormones, such as androgens, after sexual maturation. The characteristics of intraspecific dental trajectories in *S. canicula* and *S. stellaris* should be statistically compared to assess which, among these characteristics, are species-specific. The inclusion of other scyliorhinid species in a broader comparative work would also question the occurrence of such developmental trajectories within the group, as well as with close-related species with respect to the phylogeny (e.g., in *Scoliodon* sp.) [Amaral et al., 2017] and the dental morphology (e.g., in *Leptocharias smithii*). By including and comparing more species in trajectory analyses, it could be tested if distinct shark groups exhibiting the same tooth type (e.g., grasping in scyliorhinids and chlamydoselachids [Cappetta, 1986]) but phylogenetically far related share similar ontogenetic and sexual differences in tooth shape. Such comparisons among selachians coupled with data on species' ecology should shed light on the potential factors (e.g., trophic, reproductive) that could explain consistent trajectory patterns among sharks and shifts of these patterns that are species- or taxa-specific.
Overall, there is currently a need for detailed descriptions of shark teeth because of their crucial use for extant and extinct species determination, as well as for understanding the implications of specific tooth morphologies in the trophic habits and mating behaviour of species and my work contributes to bridging this gap.

5.2 A fresh identification framework for shark conservation

The need for fast and reliable identification tools for shark species is growing with the increase of illegal fishing and trade. The identification of shark species is currently based on DNA analyses notably on fishmarkets, because a small sample of each specimen is enough to perform the analyses and because in several cases, only pieces are sold, which are insufficient to identify a species with certainty. However, this is not always true, as some fishmarkets still exhibit species whose jaw and teeth have been retained.

In this thesis, I aimed at deciphering subtle tooth form differences between two shark populations by combining GM and Random Forests. The study conducted for these populations is a proof of concept, as the origin of specimens was already labelled but the framework I used performed better at classifying the *S. canicula* populations than the traditional one. These results offer promising prospects for species delineation, which could complement DNA-based identification of species in the field, which is an expensive process that needs time to be performed. Then, they highlight dental differences for the first time in two *S. canicula* populations, a species whose genetic structure is still unclear [Barbieri et al., 2014] and question the ecological aspects that could correlate with the interpopulational differences observed.

The framework I used provides good classification performances but the landmarking process is laborious and time consuming and can be improved. First, the 3D coordinates provided to the Random Forests could be replaced by raw images of the teeth or by topographic information automatically extracted from 3D tooth surfaces [Lazzari and Guy, 2014; MacLeod, 2017, 2018; Thiery et al., 2019], which would drastically reduce the time allocated to data pre-processing. The replacement of GM data by raw images also provides equivalent to better results to those obtained when working with GM data and toolkit [MacLeod, 2017, 2018].
Second, the use of topographic information instead of landmark data would overcome the problem of phylogenetic and topographic homology of landmarks. The homology problem excluded, tooth crowns that do not exhibit remarkable topographic points could be included in the classification analyses. This would allow to include shark species with crushing teeth in these classification analyses such as smooth-hound sharks *Mustelus schmitti* [Belleggia et al., 2014] and bonnethead sharks *Sphyrna tiburo* [Wilga and Motta, 2000] but also to generate a dataset for the elasmobranch group, by including several batoid species with crushing teeth [Cappetta, 1986; Herman et al., 1995; Underwood et al., 2015].

5.3 Molecular control of tooth development in sharks

The ontogenetic stage and sex factors are intricately linked together, which leads to question the causes of the emergence of gynandric heterodonty. In addition to the molecular factors I focused on in the manuscript (Shh, Fgf3, and Bmp4), I wish to emphasize on the suspected role of sex hormones in gynandric heterodonty in sharks. O'Shaughnessy et al. [2015] have evidenced the role of androgen receptors in maintaining *Shh* expression during clasper development in the little skate *Leucoraja erinacea* by binding androgen response elements of *Hand2*, a *Shh* regulator. The detection of *Shh* expression in shark teeth and the known pleiotropic effects of Shh allow to hypothesize that *Shh* regulates the tooth shape in elasmobranchs and could be partly controlled by androgens. Such hypothesis is being challenged by ongoing experiments: *S. canicula* embryos were raised in 11-ketotestosterone supplied seawater to investigate the impact of this hormone on tooth development.
According to these results, the models for tooth development in mammals could be tuned to adapt to the contraints that most likely shape shark teeth. The ToothMaker model made for mammals [Salazar-Ciudad and Jernvall, 2010] has been adapted during my PhD by a postdoctoral researcher to fit to *Scyliorhinus* teeth and the preliminary results are the following. Bending forces were for example added in the shark tooth

model to mimic the mesio-distal changes of tooth morphologies along the jaw, whereas mammalian teeth rarely display such variation. The original activator-inhibitor system of ToothMaker does not produce the morphologies observed in *Scyliorhinus* and a second inhibitory signalling centre of cell differentiation needs to be added to the system. Furthermore, parameters such as sex hormones that were not initially included in ToothMaker would be included in the shark tooth model to try mimicking the emergence of gynandric heterodonty. Several data types are thus missing to accurately model shark tooth development and to confirm that the set of parameters producing the more promising tooth morphologies is also confirmed by experimental work. Experimental work notably still has to assess the correlation between a specific tooth shape and the dental lamina conformation. In a preliminary work with a Master student, we have explored the labio-lingual bending along the mesio-distal axis of *S. canicula* Meckelian cartilage. We found that this bending is gradually modified along the jaw but it remains to be tested if and how this gradient correlates with the one observed between parasymphyseal and commissural tooth shapes. The experimental protocol used to perform the functional tests with bead implantation could be used to investigate the impact of different gene expression levels on shark tooth shape. The beads inserted next to developing tooth buds could be soaked in a gradient of concentrations of one specific protein, which could be correlated with the potentially different tooth phenotypes observed. Also, complementary experiments involving known inhibitors of the tested molecules are still to be performed, to further test the functional implication of these signalling factors. The influence of sex hormones on tooth shape, and especially of the 11-ketotestosterone that is currently ongoing could also be investigated by quantifying the occurrence of androgen receptors on tooth buds of *S. canicula* embryos. The tooth phenotypes resulting from the functional tests performed in my PhD have been examined with raw microCT images. The data analysis could be completed by performing geometric morphometrics on isolated 3D tooth surfaces in the case of bead implantation experiments, and on the whole dental set in the case of tests with sex hormones.

5.4 Dermal denticles: the great forgotten ones?

The development of teeth and dermal denticles of elasmobranchs is patterned by common genes and these structures share similar stages during development, and similar tissular composition and organisation [Debiais-Thibaud et al., 2011, 2015; Berio and Debiais-Thibaud, 2019]. Whether or not teeth arose from dermal odontodes is still an ongoing debates that continues to be challenged by recent work [Haridy et al., 2019]. In this context, it would be reckless to not discuss the possibilities of my PhD analyses to be adapted to the study of dermal denticles. The morphology and spacing of shark dermal denticles has already been investigated in several species and often correlated with the swimming performance [Wen et al., 2015] and habitat preference along the water column [Dillon et al., 2017], as well as with a species' mating behaviour [Crooks et al., 2013]. It has, however, not being detailed with a GM framework. The analyses performed in GM on *S. canicula* and *S. stellaris* teeth could be applied to the dermal denticles of these species to quantify the denticle shape and form over different body locations, over the ontogeny and between sexes, and within and between species.

Despite multiple similarities common to elasmobranch teeth and placoid scales, these structures still exhibit differences, notably regarding the tissues both structure

types develop into. Teeth develop and are continuously replaced within tooth files that are linked through a dental lamina [Fraser et al., 2020]. Dermal denticles also develop *via* the interplay between epithelium and mesenchyme, however, when shed, they are not systematically replaced at the exact same location [Reif, 1978, 1980; Fraser et al., 2020]. The gaps created by newly formed skin or dermal denticle loss are progressively filled by new denticles that do not belong to successional families [Reif, 1978, 1980; Fraser et al., 2020; Popp et al., 2020]. Shark teeth and placoid scales also slightly differ in their gene expressions [Debiais-Thibaud et al., 2015; Berio and Debiais-Thibaud, 2019]. As in teeth, shark scale development and regeneration depend on molecular parameters (signalling factors and the resulting inhibitory fields) [Reif, 1978; Cooper et al., 2017, 2018] but their form might also depend on the skin folding and thickness. Dermal denticles can display a broader intraindividual diversity of forms than teeth and develop above tissues of different hardness (e.g., cartilage, eye, muscles) and functions [Pratt and Carrier, 2001; Crooks and Waring, 2013; Tomita et al., 2020]. The impact of the underlying tissue softness and folding might be easier to investigate in dermal denticles than in teeth and would provide a larger picture of the physical, putative parameters participating to shape a denticle.

5.5 Cartilage or bone: Are chondrichthyans more subtle?

The dichotomous classification of cartilage and bone is highly mammal-centered and has long been used as such notably in teleosts, which, however, display a variety of cartilage types that differ from the classical idea of the mammalian hyaline cartilage [Witten et al., 2010]. Chondrichthyans, which are named after their mostly cartilaginous endoskeleton, display three types of cartilage mineralisation: tesselated, areolar, and lamellar or bone-like. The microstructure of tesserae can also be subdivided into the globular (in the body zone) and the prismatic (in the cap zone) mineralisations [Kemp and Westrin, 1979; Dean and Summers, 2006]. The secreting cells of the cap zone matrix have first been identified as osteoblasts in sharks (e.g., in the lemon shark *Negaprion brevirostris* and in the whitetip reef shark *Triaenodon obesus*) [Kemp and Westrin, 1979] and the cap zone of tesserae is covered by hydroxyapatite cristallites, which is notably observed in bone. The occurrence of several types of cartilage mineralisation, as well as the detection of bone-like tissue in elasmobranchs [Kemp and Westrin, 1979; Peignoux-Deville et al., 1982; Clement, 1992; Eames et al., 2007; Atake et al., 2019] well illustrate the continuum between cartilage and bone in this group, as already discussed in teleosts [Witten et al., 2014]. This continuum is still difficult to comprehend in chondrichthyans as most studies focus on a species or a specific taxon [Kemp and Westrin, 1979; Peignoux-Deville et al., 1982; Eames et al., 2007; Dean et al., 2009; Atake et al., 2019] and it still needs to be examined in details. The search for bone-like tissue in chondrichthyans has been restricted to isolated species hitherto and no big picture has been drawn about the evolution of bone-like tissue in the whole chondrichthyan group. In my PhD, I wished to identify the occurrence of bone-like tissue and to refine the existing description and classification of the neural arch mineralisation patterns in the main chondrichthyan groups. Within bone-like tissue, a new distinction of tissues is proposed and fibrous and lamellar mineralisations are recognised. The former is identified in most elasmobranch species examined, while the latter is restricted to the Orectolobiformes

and the Carcharhiniformes, suggesting evolutionary convergence of this histotype within galeomorphs.
In addition, assuming that lamellar mineralisation resembles mammalian bone, it would have a strenghtening role greater than the other mineralisation patterns found in chondrichthyans (tesseral and areolar) and thus would have been retained in species with a specific ecology. The endoskeleton of coldwater and deep-sea sharks is thought to be less mineralised than the one of coastal species, probably related to ambient temperature, pressure, and available phosphate sources in the environment [Dean et al., 2015]. Deep-sea sharks also exhibit physical characteristics such as a smaller heart, a greater buoyancy, and less aerobic fibers in the tail as compared to shallower species with greater metabolic rates [Pinte et al., 2019; Larsen et al., 2020]. The lesser extent of mineralisation (thinner tesserae and no lamellar mineralisation) in the deep-sea chondrichthyan species considered in my thesis could then be explained by their adaptation to these particular habitats. In order to evaluate the ecological implications of bone-like tissue in elasmobranchs, the robustness of lamellar and tesseral mineralisations could be compared for example by measuring their compressive stiffness and densities [Balaban et al., 2015; Di Santo, 2019].

5.6 Chondrichthyans facing global climate change

The ocean acidification has negative impacts on biological processes in marine species, notably on molluscan shell formation [McClintock et al., 2009; Welladsen et al., 2010; Gazeau et al., 2013] and on teleost skeletogenesis and mineralisation [Bignami et al., 2013; Chambers et al., 2014; Coll-Lladó et al., 2018; Holmberg et al., 2019]. The consequences of a pH decrease have been less studied in the skeleton of elasmobranchs, yet a change in this parameter induces dermal denticle corrosion and is expected to have similar effects on teeth [Dziergwa et al., 2019] and an increase of hydroxyapatite density in the cartilage of crura (leg-like structures modified from the anterior lobes of the pelvic fins) and jaws in a skate [Di Santo, 2019]. However, the interplay between temperature, pH, and the mineralisation processes in elasmobranchs is complex and a fall in temperature induces a mineralisation decrease in the pectoral fins of a skate [Di Santo, 2019].
As stated before, deep-sea sharks are believed to have less mineralised endoskeletons than their shallow counterparts [Dean et al., 2015]. However, this broad trend has not been tested yet in chondrichthyans and is more the result of sparse personal observations that should be examined in details in several species of this group. If confirmed, this trend would be challenged by the global environmental modifications oceans are facing due to anthropogenic activities. Shallow and deep-sea chondrichthyans would experience uneven modifications of their cartilage mineralisation patterns because of differential temperature changes and basins. These temperature changes are for example expected to be more important in bathyal depths as compared to abyssal depths and in the Atlantic basin as compared to the Indian one in 100 years [Sweetman et al., 2017]. Species mechanics in similar habitats would also be affected differently depending on the specific structures and behaviour they display: skates species exhibiting denser crura due to ocean acidification would shift their locomotory behaviour to more punting but would also experience a decrease in locomotor efficiency due to a heavier skeleton [Di Santo, 2019]. A detailed examination of the uneven skeletal condition of chondrichthyan

species facing global climate change could provide strong decisionary tools to identify the species whose survival is the most likely to be endangered in the next few years.

Appendices

6.1 Journal article — Scyland3D: Processing 3D landmarks

The Journal of Open Source Software

Scyland3D: Processing 3D landmarks

Fidji Berio[1, 2] **and Yann Bayle**[3]

1 ISEM, UMR 5554, CNRS-IRD-UM, 34095 Montpellier, France **2** IGFL, UMR 5242, CNRS-ENS de Lyon, 69007 Lyon, France **3** LaBRI, UMR 5800, CNRS, 33400 Talence, France

DOI: 10.21105/joss.01262

Software

- Review
- Repository
- Archive

Editor: Kevin M. Moerman

Reviewers:

- @r-barnes
- @patrikhuber

Submitted: 03 January 2019
Published: 08 February 2020

Abstract

`Scyland3D` is a Python tool for converting 3D raw landmark and semilandmark coordinates exported from landmark acquisition software to a CSV best suited for geometric morphometric analyses. Processing schemes to mirror and reorder these points are provided to address further symmetry issues. This is useful when working on left-right differences in a given species. This tool is designed to pre-process the raw extracted landmarks and to generate a database-like CSV for statistical analyses. The main targeted audience are biologists looking for an easy and quick parser for raw landmarks.

Background

Living organisms display a high diversity of shapes and sizes that are used to characterise ontogenetic stages and phylogenies (Guinot et al., 2018; Jones, Smaers, & Goswami, 2015; Musa, Czachur, & Shiels, 2018). Shape similarities are used as phylogenetic signal —mostly in extinct species— and, when combined with ecological data, allow describing trophic habits of species (Randau, Goswami, Hutchinson, Cuff, & Pierce, 2016).

Traditional 2D morphometrics, *i.e. in situ* or picture measurements of structural element dimensions, have long been favoured to quantitatively compare extant and extinct shapes of organisms (Adams, Rohlf, & Slice, 2013). However, part of these measurements did not reflect the geometry of the structures and depended for example on their relative size. Landmark-based geometric morphometrics in 2D allows separating a form into size and shape within a set of measures. In this method, landmarks define comparable points within a set of objects and capture their geometry. A Procrustes superimposition then rescales, rotates and translates these landmarks to virtually superimpose all object geometries (Adams et al., 2013; Zelditch, Swiderski, Sheets, & Fink, 2004). Each measured variable, however, is partly independent of other ones on the same structure as all may have been quantified in different 2D views of the same object. Then, merging morphometric datasets for global analyses may bring noise in the results.

Landmark-based geometric morphometrics in 3D emerged with recent imaging techniques among other X-ray microtomography (Adams et al., 2013). 3D surfaces are created based on scanned organisms and landmarks can be set on all views of interest of a given specimen and belong to the same dataset, with the same reference space.
Among software allowing digitizing (data acquisition of) 3D landmarks and semilandmarks, there are few free software and they do not offer complete tools for subsequent shape and size analyses. A landmark is a point set up by hand as opposed to a semilandmark that is interpolated by the computer between two landmarks by following the curvature of the studied form. Most morphometricians use R packages to perform size and shape analyses but input data must already be in package-specific formats that often highly differ from the

output formats generated by landmark acquisition software products. Moreover, the rise of intra- and interspecific asymmetry questions involves post-processing steps of morphometric datasets that are not managed by current R packages.

`Scyland3D` details

`Scyland3D` can be installed from pip https://pypi.org/project/Scyland3D or from the Github repository https://github.com/ybayle/Scyland3D.

We introduce `Scyland3D` to convert .pts files (format defined on page 37 in https://web.cs.ucdavis.edu/~amenta/LandmarkDoc_v3_b6.pdf), exported by the Landmark software (v3.6 cf https://web.cs.ucdavis.edu/~amenta/LandmarkDoc_v3_b6.pdf) or any landmark processing software, into CSV. `Scyland3D` first removes duplicated coordinates because landmarks and semilandmarks may coincide in the Landmark software. We then allow to mirror the landmark and semilandmark coordinates for a subset of 3D objects and to reorder these points. This allows performing 3D geometric morphometric analyses between previously asymmetrical objects (Figure 1).

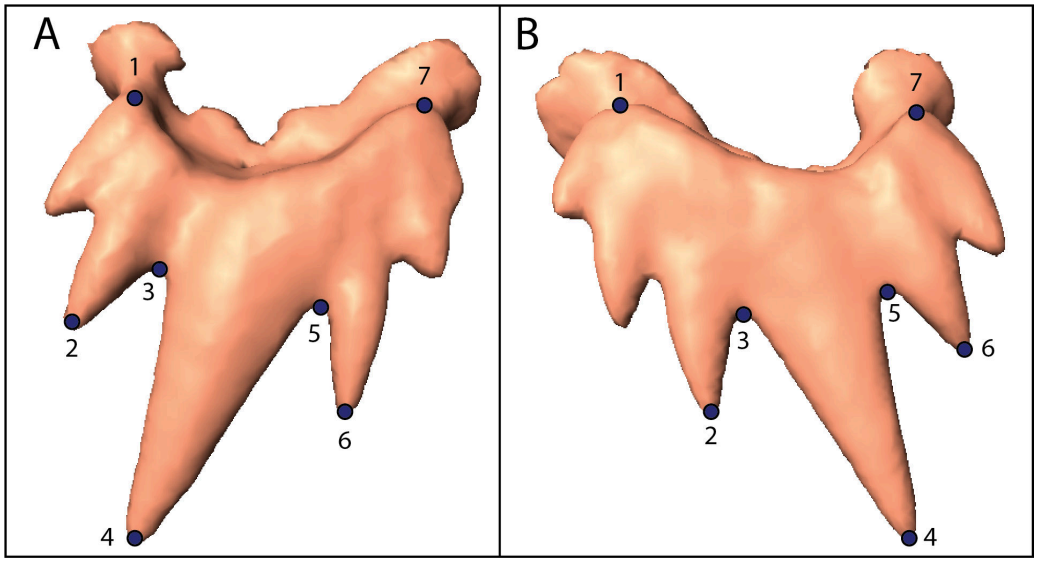

Figure 1: Landmarked small-spotted catshark *Scyliorhinus canicula* (A) upper tooth and (B) lower tooth. Only landmarks are drawn but semilandmarks can be set between them. Numbers indicate their relative order of setting. Surfaces were generated based on 3D X-ray microtomography scans.

Manual landmarking might generate coordinate duplicates or missing landmarks and semilandmarks. Before processing the data, `Scyland3D` checks their integrity because setting landmarks in 3D is an error-prone manual operation. `Scyland3D` thus checks and reports the:

- Consistency of folder and file names (one folder per specimen with an underscore between features in the folder and file's name),
- Number of landmarks and semilandmarks across all structures,
- Presence of duplicate landmarks and semilandmark coordinates exported by the Landmark software.

Processing options can be specified in order to modify the dataset asymmetry. In this case, landmark and semilandmark coordinates of elements characterised by a given feature can be

sequentially mirrored and reordered. Mirror processing involves the use of the Least Squares method and generates a regression plane through all the landmark and semilandmark coordinates of an object. This plane is subsequently used as a symmetry plane and a projection of landmark and semilandmark coordinates is generated for each 3D object. For the mirrored objects, a reorder of landmarks and semilandmarks can be done and the software needs a vector containing their new relative positions specified. Indeed, geometric morphometrics aim at comparing shape objects after a standardization process (Procrustes superimposition). During the latter step, the space distance is minimized between equivalent landmarks. This equivalence is given by their relative order of placement, e.g. a minimized distance is calculated between the first landmark placed in object 1 and the first landmark placed in object 2. Such a process implies that landmarks must be placed in the exact same order in all comparable objects of the dataset. Thus, mirrored objects have reverted bending compared to others and this must be compensated by reordering the mirrored landmarks.

`Scyland3D` is currently used on larger datasets with different specimens to compare upper and lower tooth shapes at intraspecific scale and deciphering symmetry patterns. We aim at characterising tooth shape transformations across growth stages and emerging sexual dimorphism in *S. canicula* and unravel ontogenetic and evolutionary processes. We provide an example use-case with a subset of our dataset in our Github repository to help newcomers handle `Scyland3D`.

Acknowledgements

We acknowledge the contribution of SFR Biosciences (UMS3444/CNRS, US8/Inserm, ENS de Lyon, UCBL) facilities: AniRA-ImmOs and Mathilde Bouchet for her help with X-ray microtomography. We are thankful to Patrik Huber and Richard Barnes, the two reviewers who helped improve the code and the documentation a lot.

References

Adams, D. C., Rohlf, F. J., & Slice, D. E. (2013). A field comes of age: Geometric morphometrics in the 21st century. *Hystrix*, *24*(1), 7. doi:10.4404/hystrix-24.1-6283

Guinot, G., Adnet, S., Shimada, K., Underwood, C. J., Siversson, M., Ward, D. J., Kriwet, J., et al. (2018). On the need of providing tooth morphology in descriptions of extant elasmobranch species. *Zootaxa*, *4461*(1), 118–126. doi:10.11646/zootaxa.4461.1.8

Jones, K. E., Smaers, J. B., & Goswami, A. (2015). Impact of the terrestrial-aquatic transition on disparity and rates of evolution in the carnivoran skull. *BMC Evolutionary Biology*, *15*(1), 8. doi:10.1186/s12862-015-0285-5

Musa, S. M., Czachur, M. V., & Shiels, H. A. (2018). Oviparous elasmobranch development inside the egg case in 7 key stages. *PLOS One*, *13*(11), e0206984. doi:10.1371/journal.pone.0206984

Randau, M., Goswami, A., Hutchinson, J. R., Cuff, A. R., & Pierce, S. E. (2016). Cryptic complexity in felid vertebral evolution: shape differentiation and allometry of the axial skeleton. *Zoological Journal of the Linnean Society*, *178*(1), 183–202. doi:10.1111/zoj.12403

Zelditch, M. L., Swiderski, D. L., Sheets, H. D., & Fink, W. L. (2004). Superimposition. In *Geometric morphometrics for biologists: A primer* (p. 457). San Diego: Elsevier Academic Press. doi:10.1016/B978-012778460-1/50007-7

6.2 Mean Decrease Accuracy values obtained by Random Forests with tooth shape data

TABLE 6.1: Details of Mean Decrease Accuracy values obtained by Random Forests with tooth shape data. The teeth belong to *Scyliorhinus canicula* specimens sampled in one Atlantic and one Mediterranean populations. L, landmark; SL, semilandmark.

Point	x	y	z
L-1	0.5	1.5	0.1
SL-2	0.5	0.2	0.2
SL-3	0.6	0.2	0.2
SL-4	0.3	0.1	0.7
SL-5	0.2	0.1	0.2
SL-6	0.3	0.2	0.2
SL-7	0.1	0.2	0.1
SL-8	0.2	0.1	0.1
SL-9	0.2	0.2	0.2
SL-10	0.4	0.1	0.1
SL-11	5.2	0.3	0.2
SL-12	1.1	0.7	0.1
L-13	0.3	1.9	0.2
SL-14	0.3	0.2	0.3
L-15	0.4	0.6	1.1
SL-16	0.5	0.3	0.3
L-17	0.2	0.4	0.5
SL-18	0.3	0.2	0.4
L-19	1.0	0.9	0.1
SL-20	0.2	0.6	0.3
L-21	0.3	0.6	0.1
SL-22	0.1	0.9	0.1
SL-23	0.5	1.1	0.1
SL-24	1.1	1.7	0.1
SL-25	0.9	0.7	0.1
SL-26	0.3	0.1	0.1
SL-27	0.2	0.3	0.1
SL-28	0.3	0.7	0.1
SL-29	0.1	0.2	0.2
SL-30	0.1	0.1	0.2
SL-31	0.1	0.1	0.2
SL-32	0.1	0.2	0.2
L-33	0.2	0.3	0.2
SL-34	0.4	0.5	0.2
SL-35	0.4	0.7	0.2
SL-36	0.2	0.2	0.5
SL-37	0.2	0.3	0.2
SL-38	0.3	0.8	0.2

6.3 Mean Decrease Accuracy values obtained by Random Forests with tooth form data

TABLE 6.2: Details of Mean Decrease Accuracy values obtained by Random Forests with tooth shape data. The teeth belong to *Scyliorhinus canicula* specimens sampled in one Atlantic and one Mediterranean populations. L, landmark; SL, semilandmark.

Point	x	y	z
L-1	0.2	1.2	0.2
S-L2	0.2	0.2	0.1
SL-3	0.3	0.1	0.3
SL-4	0.2	0.1	0.2
SL-5	0.1	0.1	0.2
SL-6	0.1	0.3	0.2
SL-7	0.1	0.2	0.1
SL-8	0.1	0.1	0.2
SL-9	0.1	0.1	0.2
SL-10	0.4	0.2	0.2
SL-11	5.5	1.7	0.3
SL-12	0.7	1.3	0.2
L-13	0.2	1.0	0.7
SL-14	0.2	0.2	0.4
L-15	0.9	0.7	0.9
SL-16	0.5	0.3	0.4
L-17	0.3	0.5	0.5
SL-18	0.2	0.2	0.3
L-19	1.0	1.7	0.1
SL-20	0.2	0.3	0.2
L-21	0.3	0.5	0.1
SL-22	0.2	0.8	0.2
SL-23	1.7	0.9	0.1
SL-24	2.2	0.8	0.1
SL-25	0.4	0.2	0.1
SL-26	0.1	0.1	0.1
SL-27	0.3	0.3	0.1
SL-28	0.4	0.6	0.1
SL-29	0.3	0.2	0.1
SL-30	0.1	0.1	0.1
SL-31	0.2	0.1	0.1
SL-32	0.5	0.2	0.1
L-33	0.7	0.4	0.2
SL-34	0.3	0.3	0.2
SL-35	0.1	0.5	0.2
SL-36	0.1	0.2	0.6
SL-37	0.4	0.2	0.6
SL-38	0.2	0.5	0.9

6.4 Details of the specimens and conditions used for the bead experiments

TABLE 6.3: Details of the functional tests performed on the teeth of *Scyliorhinus canicula* embryos. An asterisk indicates an embryo did not survive until the end of the experiment. A slash (/) indicates that two beads have been inserted, one per hemi-jaw. B, beginning of the experiment; E, end of the experiment; F, female; M, male; Shh, Sonic Hedgehog; na, not available; XP, type of the experiment.

ID	Sex	Size B:E (cm)	XP	Beads	Beginning	End
1	M	7.0:na	Shh	PBS	05.07.18	06.08.18
2	M	6.9:na	Shh	Shh	05.07.18	na*
3	M	7.0:na	Shh	Shh	05.07.18	09.07.18*
4	F	6.6:na	Shh	Shh	05.07.18	12.07.18*
5	M	7.0:na	Shh	Shh	05.07.18	12.07.18*
6	F	7.0:na	Shh	Shh	05.07.18	06.08.18
7	M	6.9:na	Shh	Shh	05.07.18	12.07.18*
8	F	7.0:na	Shh	Shh	05.07.18	06.08.18
9	M	6.8	Shh	Shh/hole	05.07.18	06.08.18
10	M	7.0:na	Shh	Shh	05.07.18	06.08.18
11	M	6.7:na	Shh	Shh/PBS	05.07.18	06.08.18
12	M	6.5:na	Shh	Shh/PBS	05.07.18	06.08.18
13	M	7.1:na	Shh	Shh/PBS	05.07.18	12.07.18*
14	M	6.5:na	Shh	Shh/PBS	05.07.18	12.07.18*
15	F	6.9	Shh	PBS	06.07.18	12.07.18*
16	F	6.8:na	Shh	PBS	06.07.18	06.08.18
17	M	6.6:na	Shh	PBS	06.07.18	06.08.18
18	F	7.0	Shh	PBS	06.07.18	12.07.18*
19	M	6.9:na	Shh	PBS	06.07.18	06.08.18
28	M	8.5:na	Bmp4	HCl+BSA	09.10.19	28.10.19*
29	M	8.5:9.9	Bmp4	HCl+BSA	09.10.19	12.11.19
30	M	8.5:10.0	Bmp4	HCl+BSA	09.10.19	12.11.19
31	M	7.5:9.5	Bmp4	HCl+BSA	09.10.19	12.11.19
32	F	7.5:9.0	Bmp4	HCl+BSA	09.10.19	12.11.19
33	F	8.2:9.5	Bmp4	HCl+BSA	09.10.19	12.11.19
34	F	7.5:9.3	Bmp4	HCl+BSA	09.10.19	12.11.19
35	M	8.3:9.6	Bmp4	HCl+BSA	09.10.19	12.11.19
36	M	7.5:9.1	Bmp4	HCl+BSA	09.10.19	12.11.19
37	M	8.0:8.5	Bmp4	HCl+BSA	09.10.19	12.11.19
38	M	8.2:na	Bmp4	HCl+BSA	09.10.19	04.11.19*
39	F	7.7:9.6	Bmp4	Bmp4+HCl+BSA	16.10.19	18.11.19
40	F	7.5:na	Bmp4	Bmp4+HCl+BSA	16.10.19	04.11.19*
41	M	8.3:9.4	Bmp4	Bmp4+HCl+BSA	16.10.19	18.11.19
42	M	7.7:9.6	Bmp4	Bmp4+HCl+BSA	16.10.19	18.11.19
43	M	8.3:9.6	Bmp4	Bmp4+HCl+BSA	16.10.19	18.11.19
44	M	8.4:9.5	Bmp4	Bmp4+HCl+BSA	16.10.19	18.11.19

Continued on next page

Table 6.3 – *Continued from previous page*

ID	Sex	Size B:E (cm)	XP	Beads	Beginning	End
45	M	7.8:9.9	Bmp4	Bmp4+HCl+BSA	16.10.19	18.11.19
46	M	8.4:9.7	Bmp4	Bmp4+HCl+BSA	16.10.19	18.11.19
47	F	8.2:na	Bmp4	Bmp4+HCl+BSA	16.10.19	28.10.19*
48	M	7.7:9.0	Bmp4	Bmp4+HCl+BSA	16.10.19	18.11.19
49	M	8.3:9.7	Bmp4	Bmp4+HCl+BSA	16.10.19	18.11.19
50	F	6.2:8.4	Bmp4	Bmp4+HCl+BSA	16.10.19	18.11.19
51	M	6.9:na	Bmp4	Bmp4+HCl+BSA	16.10.19	04.11.19*
52	M	6.0:8.1	Bmp4	Bmp4+HCl+BSA	16.10.19	18.11.19
53	M	6.6:na	Bmp4	Bmp4+HCl+BSA	16.10.19	04.11.19*
54	M	6.8:na	Bmp4	Bmp4+HCl+BSA	16.10.19	28.10.19*
55	F	7.2:8.4	Bmp4	Bmp4+HCl+BSA	16.10.19	18.11.19
56	F	6.8:na	Bmp4	Bmp4+HCl+BSA	16.10.19	28.10.19*
57	M	6.7:na	Bmp4	Bmp4+HCl+BSA	16.10.19	04.11.19*
58	M	6.5:8.2	Bmp4	Bmp4+HCl+BSA	16.10.19	18.11.19
71	F	7.6:na	Fgf3	Fgf3/PBS+BSA	13.11.19	04.12.19*
72	M	7.8:8.7	Fgf3	Fgf3/PBS+BSA	13.11.19	13.12.19
73	F	7.4:na	Fgf3	Fgf3	13.11.19	25.11.19*
74	M	8.2:na	Fgf3	Fgf3/PBS+BSA	13.11.19	10.12.19*
75	F	8.0:9.0	Fgf3	Fgf3/hole	13.11.19	13.12.19
76	F	8.1:9.3	Fgf3	Fgf3/PBS+BSA	13.11.19	13.12.19
77	F	8.2:9.0	Fgf3	Fgf3/PBS+BSA	13.11.19	13.12.19
78	M	8.0:na	Fgf3	Fgf3/PBS+BSA	13.11.19	10.12.19*
79	M	7.3:na	Fgf3	Fgf3/hole	13.11.19	04.12.19*
80	F	8.4:9.1	Fgf3	Fgf3/PBS+BSA	13.11.19	13.12.19
81	M	7.7:8.2	Fgf3	Fgf3/PBS+BSA	13.11.19	13.12.19
82	F	7.5:8.8	Fgf3	Fgf3/PBS+BSA	13.11.19	13.12.19
83	M	8.1:na	Fgf3	Fgf3/PBS+BSA	13.11.19	04.12.19*
84	F	7.2:9.1	Fgf3	Fgf3/PBS+BSA	13.11.19	13.12.19
85	F	8.1:9.5	Fgf3	Fgf3/PBS+BSA	13.11.19	13.12.19
86	F	7.6:9.0	Fgf3	Fgf3/PBS+BSA	13.11.19	13.12.19
87	F	7.8:na	Fgf3	Fgf3/hole/PBS+BSA	13.11.19	25.11.19*
88	M	7.1:na	Fgf3	Fgf3/PBS+BSA	13.11.19	10.12.19*
89	F	7.6:9.1	Fgf3	Fgf3/PBS+BSA	13.11.19	13.12.19
90	F	7.5:9.3	Fgf3	Fgf3/PBS+BSA	13.11.19	13.12.19
91	F	7.0:8.4	Fgf3	Fgf3/PBS+BSA	13.11.19	13.12.19
92	M	7.0:8.5	Fgf3	Fgf3/PBS+BSA	13.11.19	13.12.19
93	M	7.0:8.1	Fgf3	Fgf3/PBS+BSA	13.11.19	13.12.19
94	M	7.0:8.3	Fgf3	Fgf3/PBS+BSA	13.11.19	13.12.19
95	M	7.6:9.0	Fgf3	Fgf3/hole	14.11.19	13.12.19
96	M	7.0:8.3	Fgf3	Fgf3/PBS+BSA	14.11.19	13.12.19
97	M	7.3:na	Fgf3	Fgf3/PBS+BSA	14.11.19	04.12.19*
98	M	7.0:8.5	Fgf3	Fgf3/PBS+BSA	14.11.19	13.12.19
99	F	7.7:9.3	Fgf3	Fgf3/PBS+BSA	14.11.19	13.12.19
100	F	6.8:8.5	Fgf3	Fgf3/PBS+BSA	14.11.19	13.12.19
101	F	7.1:8.7	Fgf3	Fgf3/PBS+BSA	14.11.19	13.12.19

6.5 Extraits traduits en français

Table des matières

6.5.1 Résumé de la thèse

Les dents sont des structures répétées dont l'histoire évolutive est étroitement liée à celle de l'émergence des tissus minéralisés des vertébrés. Les dents des vertébrés actuels présentent une importante diversité de tissus, de formes et donc de développement, ce qui permet de les étudier dans un contexte de diversification des espèces. Les dents des sélaciens se renouvellent en permanence et présentent des morphologies variées en lien avec les comportements reproducteur et alimentaire.

Ce travail aborde dans un premier temps la variation des formes dentaires de deux scyliorhinidés en utilisant de la morphométrie géométrique en 3D et un algorithme d'apprentissage automatique. Il décrit pour la première fois en détail l'émergence de l'hétérodontie gynandrique au cours de l'ontogénie chez des requins et discute des implications de cette variation pour la taxonomie.

Les tests fonctionnels réalisés au cours de cette thèse suggèrent par ailleurs que les facteurs de signalisation Shh et Fgf influencent la morphogenèse des cuspides et la minéralisation dentaire. Ces résultats sont discutés dans le cadre de la divergence entre espèces et de l'acquisition de certains comportements reproducteur et alimentaire.

Les données histologiques de vertèbres révèlent enfin une proportion inattendue d'élasmobranches actuels dont les arcs neuraux présentent de la minéralisation fibreuse, un tissu similaire à l'os dont la présence au sein de ce clade a longtemps été supposée perdue. Ces résultats permettent de discuter de l'évolution des tissus squelettiques et de questionner quels pourraient être les facteurs écologiques expliquant la restriction de tissus minéralisés particuliers à certains groupes de requins et de raies.

Mots-clés chondrichtyens; évo-dévo; morphologie dentaire; morphométrie géométrique; histologie; apprentissage automatique; scyliorhinidés; vertèbres

6.5.2 Chapitre introductif L'émergence des odontodes et des dents

Origine évolutive et diversité des odontodes

L'exosquelette des premiers vertébrés À l'origine des Vertébrés était l'exosquelette, une version minéralisée du squelette qui couvrait la tête et le corps des espèces [Sire and Huysseune, 2003]. La plupart de l'exosquelette des premiers vertébrés était composé d'os dermique, cependant des éléments isolés et très minéralisés de dentine et d'émailloïde étaient attachés à ces plaques osseuses et couvraient le corps et la tête à des degrés variés en fonction des espèces [Janvier, 1996; Sire and Huysseune, 2003; Giles et al., 2013]. Les caractéristiques histologiques de ces premiers exosquelettes ont souvent révélé des structures organisées en couches et composées de nodules superficiels de dentine et d'émailloïde ou d'une couche superficielle de tissu similaire à l'os, d'une couche médiane d'os spongieux et d'une couche basale d'os lamellaire compact [Donoghue et al., 2006; Giles et al., 2013]. Bien que la position phylogénétique de certains des gnathostomes souches est toujours débattue, l'organisation ancestrale de l'exosquelette peut être définie comme étant organisée suivant trois couches dont la superficielle est composée de dentine recouverte d'émailloïde, la médiane est composée d'ostéons et la couche basale est composée d'une couche similaire à de l'os lamellaire [Keating et al.,

2015]. Par conséquent, l'une des caractéristiques les plus marquantes émergeant des données paléontologiques réside dans le fait que plusieurs tissus minéralisés ont évolué de façon concomitante chez les premiers vertébrés. Ces premiers tissus sont liés à ceux composant les dents et les os des organismes actuels.
La diversité actuelle des vertébrés comprend les agnathes et les gnathostomes au sein desquels se trouvent les chondrichtyens et les ostéichtyens, deux groupes ayant divergé l'un de l'autre il y a environ 422 millions d'années [Benton et al., 2009] (Figure 1.1). Mon travail de thèse a été centré sur les chondrichtyens actuels, un groupe qui comprend les néosélaciens ou requins (galéomorphes et squalomorphes), les batoïdes ou batomorphes (ces deux groupes formant celui des élasmobranches) et les holocéphales (chimères) (Figure 1.2) [Inoue et al., 2010; Janvier and Pradel, 2015; Last et al., 2016].

Le squelette minéralisé des vertébrés actuels peut-être composé de quatre types de tissus caractérisés par différentes natures de matrices extracellulaires et synthétisés par des types cellulaires distincts [Hall, 2015]. Les tissus les plus minéralisés sont l'émail ou l'émailloïde et la dentine des dents et des denticules dermiques et qui sont respectivement produits par les améloblastes d'origine ectodermique et les odontoblastes dérivés de cellules mésenchymateuses elles-mêmes issues de la crête neurale. L'os lamellaire est composé d'os spongieux cortical ou trabéculaire et d'os compact. L'os spongieux est organisé en lamelles aplaties parallèles à la surface de l'élément osseux et qui s'entrelacent avec la moelle osseuse et les vaisseaux sanguins tandis que l'os compact se présente sous forme de lamelles concentriques formant des ostéons. Le tissu osseux est produit par des ostéoblastes d'origine mésodermique, excepté dans la plupart des éléments du crâne. Ces ostéoblastes sont progressivement inclus dans la matrice qu'ils sécrètent et sont alors qualifiés d'ostéocytes. Le cartilage minéralisé constitue un état de transition tissulaire, notamment au cours de l'ossification endochondrale, ou n'est présent qu'en des zones restreintes chez la plupart des vertébrés. Chez les chondrichtyens, ce tissu représente pourtant la condition normale de consolidation de l'endosquelette.
Les cellules de la crête neurale participent à la production de l'os et du cartilage au niveau du crâne des vertébrés. Les cellules sécrétrices de la matrice cartilagineuse sont les chondroblastes et les chondrocytes et la minéralisation du cartilage peut être effectuée par des chondrocytes de forme sub-sphérique ou par des chondrocytes présentant une morphologie similaire à celle des fibrocytes au sein du fibrocartilage.

Les odontodes ont originellement été définis par la présence d'émail ou d'émailloïde recouvrant de la dentine, elle-même disposée autour d'une cavité vascularisée et innervée, ainsi que par l'ancrage de ces structures à de l'os cellulaire ou acellulaire (selon la définition d'Ørvig [1977] ensuite modifiée par Reif [1982]).

Les denticules dermiques, également appelés écailles placoïdes, des chondrichtyens (Figure 1.2) sont des structures répétées qui forment l'exosquelette (Figure 1.3). Ils sont considérés comme étant dérivés des couches superficielles d'émailloïde et de dentine présentes au niveau de l'état ancestral d'un odontode, dont la couche osseuse basale n'a pas été conservée.

Chez la plupart des ostéichtyens, les éléments répétés de l'exosquelette qui recouvrent le corps et la tête se déclinent en une importante diversité d'écailles, notamment élasmoïdes et ganoïdes [Sire et al., 2009; Sasagawa et al., 2013; Schultze, 2016; Quan et al., 2018]. Les premiers poissons osseux présentaient de grandes plaques osseuses formant une armure, cette dernière s'étant divisée en plaques de taille inférieure au cours de l'évolution et étant représentée par les écailles ganoïdes des polyptéridés et

des lépisostés [Sasagawa et al., 2013; Quan et al., 2018]. Les écailles élasmoïdes se sont développées à partir des écailles ganoïdes et sont notamment présentes chez les téléostéens et les dipneustes [Schultze, 2016]. Contrairement aux écailles placoïdes, les écailles élasmoïdes se forment sans la contribution d'une couche épithéliale et sont faiblement minéralisées [Sire and Akimenko, 2004; Mondéjar Fernández and Meunier, 2020]. Les écailles rhomboïdes (ganoïdes et cosmoïdes) conservent par ailleurs de l'émail et de la dentine ou des tissus similaires à de l'émail recouvrant une couche osseuse alors que les écailles élasmoïdes sont composées d'une plaque osseuse superficielle recouvrant une couche interne de tissu conjonctif composé de fibres de collagène [Sasagawa et al., 2013; Schultze, 2016; Quan et al., 2018].
La distinction fondamentale entre les écailles élasmoïdes de la plupart des téléostéens, les denticules dermiques et les dents réside dans le fait que les premières structures ont une origine mésodermique comme celle des tissus endosquelettiques du tronc (cartilage et os), alors que les principaux constituants tissulaires des deux autre types de structures proviennent de l'ectomésenchyme, un tissu dérivé de la crête neurale (voir la sous-section 3.1.1 pour plus de détails) [Lee et al., 2013; Mongera and Nüsslein-Volhard, 2013; Shimada et al., 2013; Gillis et al., 2017]. Plusieurs similarités ont été mises en évidence entre les denticules dermiques et les dents des élasmobranches. Ces structures ont des expressions de gènes similaires au cours de leur développement, elles partagent une même origine embryonnaire (voir la sous-section 3.1.1), présentent des stades de morphogenèse et de différentiation équivalents et requièrent une interaction étroite entre l'épithélium et le mésenchyme au cours de leur développement [Debiais-Thibaud et al., 2011, 2015; Smith et al., 2015; Martin et al., 2016; Enault et al., 2018; Berio and Debiais-Thibaud, 2019] (voir également le chapitre 3). Cependant et contrairement aux denticules dermiques, les dents des élasmobranches se développent à partir d'une lame dentaire [Reif, 1982; Witten et al., 2014].

Diversité des formes de denticules dermiques chez les élasmobranches actuels
Les élasmobranches constituent un groupe d'importance cruciale afin de comprendre l'évolution des odontodes. Contrairement à la majorité des vertébrés actuels, ils conservent en effet des écailles placoïdes qui ont servi de modèle afin de représenter l'état ancestral d'un odontode. Le développement et les formes des écailles placoïdes et des dents des élasmobranches fournissent des indications quant à l'évolution des voies de régulation contrôlant la présence de ces structures au sein des chondrichtyens et des vertébrés. Les batoïdes (Figure 1.2) et les requins ont des écailles placoïdes sur la tête et le corps (Figure 1.3), dans la cavité orale et parfois sur la membrane nictitante de l'œil et certaines espèces ont également des épines dorsales [Poscai et al., 2017; de Sousa Rangel et al., 2019a; Tomita et al., 2020]. Contrairement aux élasmobranches (Figure 1.2), les chimères adultes conservent un nombre réduit de denticules dermiques, notamment à proximité de l'épine dorsale et de la ligne latérale [Didier and Stehmann, 1996; Didier, 2004; Møller et al., 2004].
Les morphologies des écailles placoïdes des élasmobranches sont contraintes par la phylogénie des espèces mais également par l'écologie de ces dernières. La faible quantité d'ornementations sur les denticules dermiques est par exemple considérée comme étant la condition plésiomorphe chez les requins et l'augmentation du nombre de stries et de la complexité de la microstructure est supposée être apparue au cours de l'évolution du groupe [Mello et al., 2013]. Toutefois, les différences morphologiques des

denticules dermiques aux échelles intra- et interspécifique suggèrent également que les facteurs biotiques et abiotiques exercent une pression de sélection sur la forme finale des denticules [Raschi and Tabit, 1992; Deynat and Séret, 1996; Chernova and Vorob'eva, 2012; Crooks et al., 2013; Mello et al., 2013; Dillon et al., 2017].
Les patrons de disposition, de densité et de morphologie des écailles placoïdes des élasmobranches le long du corps ont un rôle de protection et influencent également l'hydrodynamisme [Raschi and Tabit, 1992; Dillon et al., 2017; Ankhelyi et al., 2018]. Les stries présentes sur les denticules de la cavité oropharyngée sont supposées augmenter l'efficacité de la ventilation par exemple chez les requins disposant d'une petite ouverture buccale tels que les requins-marteaux [Atkinson and Collin, 2012; de Sousa Rangel et al., 2019b]. Leur absence peut résulter en une augmentation des forces de frottement hydrodynamiques chez des espèces présentant de grandes surfaces branchiales, ce qui est notamment le cas chez les requins mako [Atkinson and Collin, 2012; de Sousa Rangel et al., 2019b]. De même, des denticules dermiques fins, comportant plusieurs cuspides et des stries parallèles au sens de circulation de l'eau réduisent les turbulences au cours de la nage chez les espèces se déplaçant rapidement alors que les espèces benthiques présentent plutôt des denticules larges et peu ornementés qui sont supposés les protéger de l'abrasion par les structures au fond de la mer [Raschi and Tabit, 1992; Dillon et al., 2017]. L'arrangement spatial des denticules dermiques influence également l'hydrodynamisme des espèces puisque les prédateurs pélagiques rapides tels que les requins mako ont des densités de denticules 100 fois supérieures à celles observées chez les espèces démersales et sédentaires [Díez et al., 2015; Dillon et al., 2017].

Les denticules des élasmobranches forment une armure dermique constamment renouvelée. Ils peuvent par exemple empêcher l'installation des ectoparasites, bien que cette hypothèse est débattue, et protéger des morsures de prédateurs et de congénères au cours de la reproduction [Raschi and Tabit, 1992; Dillon et al., 2017]. Les marques de morsure dues au comportement reproducteur des élasmobranches sont souvent observées sur la peau des individus puisque les mâles mordent les femelles au cours de l'accouplement [Stevens, 1974; Young, 1993; Kajiura et al., 2000; Pratt and Carrier, 2001; Calich and Campana, 2015; Ritter and Amin, 2019].

Les denticules dermiques modifiés en épines alaires sur les nageoires pectorales des batoïdes et particulièrement des Rajidae permettent également aux mâles de maintenir les femelles sous leur emprise durant l'accouplement [de Sousa Rangel et al., 2016]. Les cuspides des denticules des mâles subissent de plus une transition depuis une morphologie plane à pointue après la maturité sexuelle et cette modification est concomitante de la transition morphologique des dents au cours de la maturation sexuelle [McEachran, 1977; Braccini and Chiaramonte, 2002; Vinu et al., 2017]. Chez les espèces de petits requins tels que le requin dormeur cornu *Heterodontus francisci*, le requin à chaîne *Scyliorhinus retifer* et la petite roussette *Scyliorhinus canicula*, les mâles s'enroulent autour des femelles avant et pendant l'accouplement et il a été suggéré que les denticules dermiques en des zones spécifiques, notamment au niveau des nageoires pectorales et de la ceinture pelvienne, pourraient faciliter le maintien d'une telle position afin de faciliter l'intromission des ptérygopodes [Pratt and Carrier, 2001; Crooks et al., 2013].

La régionalisation des écailles placoïdes sur le corps des élasmobranches a donc été observée à plusieurs reprises et a été estimée être le résultat de spécialisations fonctionnelles [Daniel, 1934; Raschi and Tabit, 1992; Díez et al., 2015; de Sousa Rangel et al., 2016; Dillon et al., 2017; Ankhelyi et al., 2018; Soares and de Carvalho, 2019]. La relation entre

le développement et la structure des différentes morphologies des denticules dermiques à différentes localisations sur le corps a été étudiée chez très peu d'élasmobranches. Les premiers denticules dermiques se développent en fonction d'un patron séquentiel au cours de l'ontogénie. Chez la petite raie *Leucoraja erinacea*, le requin dormeur de Port-Jackson *Heterodontus portusjacksoni*, le requin dormeur à crête *Heterodontus galeatus* et *S. canicula*, plusieurs rangées de denticules plats et lisses comportant des contours irréguliers se développent les premiers le long de la nageoire caudale de l'embryon et des denticules plus longs et larges se développent ensuite suivant une rangée dorsale [Grover, 1974; Ballard et al., 1993; Mellinger and Wrisez, 1993; Miyake et al., 1999; Johanson et al., 2007, 2008; Debiais-Thibaud et al., 2011, 2015; Cooper et al., 2018]. Une fois ces denticules développés, de nouveaux denticules émergent sur l'ensemble du corps suivant des patrons en apparence moins réguliers et tous disparaissent ensuite dans l'ensemble de l'exosquelette en développement [Cooper et al., 2018]. Les divergences existant entre les durées de développement, les formes, les patrons séquentiels ou épars et les structures des denticules dermiques ont conduit à considérer que les denticules primaires et ceux plus tardifs et épars constituent des modules développementaux distincts [Johanson et al., 2007, 2008]. Les patrons d'expressions de gènes qui caractérisent les denticules primaires caudaux et ceux épars du reste du corps demeurent toutefois peu connus et les données actuellement disponibles n'ont pas permis de tester l'hypothèse de l'existence de modules développementaux [Debiais-Thibaud et al., 2011, 2015; Martin et al., 2016; Cooper et al., 2017, 2018; Berio and Debiais-Thibaud, 2019]. Des questions similaires peuvent être posées au sujet de l'existence de modules dentaires, il est cependant nécessaire, afin d'y répondre, de disposer de descriptions détaillées des formes dentaires suivant différentes conditions telles que le stade ontogénétique et la position de la dent dans la mâchoire. Un cadre comparatif est également requis, dont l'élaboration et l'utilisation sont discutées dans cette thèse.

La question controversée de l'homologie La morphologie des éléments biologiques peut être comparée entre les espèces et les individus. De ce besoin de comparaison émerge le problème des structures qui peuvent être comparées au sein des organismes et entre ceux-ci. Ceci questionne l'homologie sous-jacente existant entre les éléments qui sont donc comparés et ce problème peut être illustré par les deux questions suivantes : les éléments sont-ils comparables du point de vue topologique, c'est-à-dire présentent-ils des connections anatomiques semblables au sein d'espèces et d'organes différents [Panchen, 2001] ou dérivent-ils d'une structure unique présente chez leur dernier ancêtre commun et est-ce que ces éléments comparables au point de vue topologique résultent de l'hypothèse évolutive la plus parcimonieuse [Schmitt, 1995] ? Cette dernière version de l'homologie est celle utilisée en biologie évolutive, cependant elle n'est pas toujours définie ni considérée en tant que telle lorsque des analyses de morphométrie géométrique sont menées. Cette supposition implicite est souvent discutée après avoir réalisé des analyses fondées sur des homologies topologiques, notamment entre des structures répétées chez un même individu.

Plusieurs tentatives ont été effectuées afin de définir des homologies dentaires entre des espèces de requins et de grouper les dents le long de l'axe mésio-distal de la mâchoire. L'exemple le plus saisissant de cette catégorisation dentaire concerne le patron dentaire des Lamniformes, dont la description implique l'utilisation de formules dentaires inspirées du travail des mammalogistes [Shimada, 2002]. Ce patron

a originellement été divisé entre les dents symphysaires, antérieures, intermédiaires et latérales au niveau du palatocarré (mâchoire supérieure) et entre les dents symphysaires, antérieures et latérales au niveau du cartilage de Meckel (mâchoire inférieure) [Leriche, 1905]. Ces familles dentaires sont fondées sur les patrons d'occlusion des files dentaires ainsi que sur les modifications brutales de morphologies et tailles des dents notamment impactées par la bulle dentaire sous-jacente, un renflement du cartilage de la mâchoire [Leriche, 1905; Shimada, 2002; Purdy and Francis, 2007]. La dénomination de ces familles dentaires a toutefois été l'objet de querelles intestines à cause des relations d'homologie entre les dents des Lamniformes et de l'établissement de leur « vrai » patron dentaire [Shimada, 2002, 2005a; Purdy and Francis, 2007; Bemis et al., 2015]. Dans ces études, le concept d'homologie est défini selon un point de vue phylogénétique qui implique que les structures homologues chez différentes espèces dérivent nécessairement d'une structure unique présente chez leur dernier ancêtre commun [Gans, 1985]. Les relations d'homologie entre les files dentaires des Lamniformes demeurent néanmoins débattues puisque des variations dans l'identification d'une seule file dentaire peuvent décaler l'ensemble du patron dentaire des Lamniformes et amener à reconsidérer le patron d'homologie dentaire des Lamniformes déjà établi [Shimada, 2002; Purdy and Francis, 2007].

Dans tous les cas, l'homologie de files dentaires chez un requin, entre différents stades ontogénétiques, entre individus de la même espèce et entre espèces est fortement perturbée par la variabilité de l'insertion de files dentaires au sein d'une dentition. Chez *Heterodontus*, des divisions spontanées de familles dentaires sont par exemple reportées dans une hémi-mâchoire et ne surviennent pas dans la seconde moitié. De nouvelles familles dentaires peuvent également être insérées en deux zones de la mâchoire : il s'agit par exemple d'une zone située entre les dents symphysaires et celles de type broyeur ou encore au niveau des commissures [Reif, 1976, 1980]. Chez les batoïdes, de nouvelles files dentaires peuvent également émerger après qu'un bourgeon a été lésé mais également de façon plus attendue, à proximité des dents symphysaires comme par exemple chez la raie guitare à nez rond *Rhina ancylostoma* [Smith et al., 2013]. De plus, il existe chez les Carcharhinidae de fréquentes différences intraspécifiques quant à la présence et à l'absence de dents symphysaires, de même qu'au niveau du nombre de files dentaires intermédiaires chez les Lamniformes. Les éléments topologiques utilisés afin de déterminer des homologies au niveau interspécifique ne sont par ailleurs pas toujours évidents à déceler au sein d'un clade, c'est notamment le cas de la bulle dentaire du requin pèlerin *Cetorhinus maximus* et du requin grande-gueule *Megachasma pelagios*, ce qui questionne la fiabilité des hypothèses d'homologie [Shimada, 2002; Smith et al., 2013]. Une telle variabilité nécessite d'adapter les règles utilisées afin de déterminer des homologies au niveau interspécifique. Chez le requin-lutin *Mitsukurina owstoni*, la reconnaissance du patron dentaire des Lamniformes ne s'appuie que sur les tailles relatives des dents et sur l'occlusion de ces dernières puisque la délimitation de la bulle dentaire classiquement utilisée afin de déterminer la limite entre les dents antérieures et intermédiaires des Lamniformes est difficile à apprécier [Shimada, 2002].

Il existe également un manque d'études *in vivo* quant à l'insertion de files dentaires et la faible quantité de données développementales disponibles à ce jour tend à indiquer que le développement de nouvelles files dentaires s'effectue selon différents patrons au sein d'une seule mâchoire [Reif, 1976; Smith et al., 2013; Underwood et al., 2015]. Chez les élasmobranches, bien que les files dentaires sont généralement ajoutées après la file

dentaire existante la plus distale, ce patron peut être modifié par l'émergence occasionnelle de files dentaires à tous niveaux mésio-distaux, ce qui perturbe l'établissement de patrons d'homologie stricts entre les files dentaires [Smith et al., 2013; Underwood et al., 2015, 2016]. Les homologies strictes entre les files dentaires devraient donc être restreintes aux espèces qui subissent un ajout de files dentaires distales jusqu'à un certain stade ontogénétique. Un tel stade demeure toutefois à déterminer pour chaque espèce d'élasmobranche.
Les tentatives de détermination d'homologies entre les dents de requins ont historiquement été élaborées afin d'étudier la pertinence des homologies entre files dentaires au-delà du cadre d'étude traditionnel des mammifères [Shimada, 2002]. Il est heureusement advenu que la dénomination de files dentaires individuelles ou de familles de dents constitue plus aujourd'hui un outil afin de comparer des types dentaires dans des zones de la mâchoire que le reflet de véritables homologies [Straube et al., 2007; Cullen and Marshall, 2019; Berio et al., 2020]. La dénomination de groupes dentaires au sein des clades de requins, excepté celui des Lamniformes, est plus flexible et ceci est nécessairement dû aux appréciations subjectives par l'observateur des modifications de patrons dentaires le long d'une mâchoire. Ces jugements subjectifs concernent par exemple la définition des dents symphysaires qui peuvent être des dents localisées à proximité de la symphyse de la mâchoire mais également des dents sur la symphyse elle-même, des dents qui sont nécessairement petites pour certains auteurs alors que cette condition n'est pas requise pour d'autres [Shimada, 2002]. Dans la plupart des cas, la terminologie quant à la définition d'une famille dentaire est utilisée différemment entre les espèces et dépend également souvent du bon vouloir des auteurs, c'est pourquoi certains auteurs préfèrent s'affranchir d'une telle catégorisation en utilisant le cadre plus sécuritaire de la numérotation des dents selon l'axe mésio-distal [Straube et al., 2007; Bemis et al., 2015].

Au cours de ma thèse, j'ai choisi d'analyser les files dentaires le long de l'axe mésio-distal du palatocarré et du cartilage de Meckel et de numéroter les dents selon le même principe. La numérotation des dents a seulement été effectuée afin de faciliter les analyses de gradient de conformation et de taille des dents le long de la mâchoire et entre les individus. Les analyses de trajectoire ont nécessairement impliqué une hypothèse d'homologie entre files mais l'interprétation des résultats a été effectuée sous l'hypothèse de files dentaires comparables du point de vue topologique, entre plusieurs individus ou au sein de l'un d'entre eux. Cette dernière hypothèse n'implique donc pas que les files dentaires et les dents comparées dans les analyses de trajectoire de développement partagent une même structure ancestrale. Les numérotations de files dentaires équivalentes entre plusieurs stades ontogénétiques et entre des individus de sexes différents n'ont pas été utilisées au sens évolutif du concept d'homologie et n'ont donc pas été discutées dans un contexte de spéciation. Cependant, ces files dentaires impliquent la continuité des contraintes topologiques et de l'information moléculaire au niveau du site à partir duquel les nouvelles dents sont produites au cours du temps.

Origine développementale des odontodes et des dents

Des dents à partir des odontodes ou des odontodes à partir des dents ? Des similarités morphologiques et développementales existant entre les denticules dermiques et les

dents émergent les questions évolutives concernant (i) la relation embryologique commune entre ces structures et (ii) si une telle relation existe, quelle structure, de la dent ou du denticule dermique, est apparue en premier ? La théorie *outside-in* (Figure 1.4A) a été la première à avoir été proposée. Cette théorie stipule que les dents sont apparues à partir d'un tissu épithélial ectodermique externe capable d'odontogenèse et que les cellules capables de former des odontodes ont ensuite envahi la cavité oropharyngée [Huysseune et al., 2009, 2010]. Cette théorie est soutenue par les similarités développementales existant entre les dents et les denticules dermiques ainsi que par les morphologies intermédiaires des denticules autour de la cavité orale (voir le chapitre 3) [Daniel, 1934; Blais et al., 2011; Debiais-Thibaud et al., 2011, 2015; Martin et al., 2016; Enault et al., 2018; Berio and Debiais-Thibaud, 2019]. À propos de l'orientation de la cuspide principale de ces denticules, Daniel [1934] reporte au sujet de l'aiguillat commun *Squalus acanthias* que certaines morphologies de denticules sont si généralistes qu'une modification de l'orientation de leur cuspide permettrait alternativement de les considérer comme des denticules ou des dents. La théorie *outside-in* a néanmoins encore besoin de support de la part du registre fossile afin qu'une continuité anatomique soit observée entre les dents et les denticules dermiques [Blais et al., 2011].

La théorie *inside-out* (Figure 1.4B) stipule que (i) les dents d'origine endodermique se sont développées en premier, de façon concomitante avec le mésenchyme dérivé de la crête neurale dans le pharynx postérieur des vertébrés, (ii) qu'elles ont évolué indépendamment dans la cavité orale de lignages variés et (iii) qu'elles n'ont pas généré les denticules dermiques [Smith and Coates, 1998; Smith, 2003; Johanson and Smith, 2005; Fraser et al., 2010; Huysseune et al., 2009; Witten et al., 2014]. Selon cette hypothèse, la compétence odontogène a été acquise *de novo* par la cavité orale et s'est répandue à l'endoderme oral et à l'ectoderme externe, ce qui a permis le développement des dents et des denticules dermiques respectivement, ce qui est cohérent avec les expressions génétiques communes observées durant le développement de ces deux types de structures [Smith and Coates, 1998, 2001; Fraser et al., 2010; Donoghue and Rücklin, 2016]. La théorie *inside-out* est fondée sur l'hypothèse selon laquelle les dents sont apparues avant les mâchoires et avant le squelette dermique [Smith and Coates, 1998, 2001; Murdock et al., 2013]. Pourtant, la relation d'homologie a été réfutée entre les odontodes pharyngiens des thélodontes (agnathes), les éléments des conodontes (agnathes) et les dents des eugnathostomes et ceci s'oppose à l'hypothèse selon laquelle les vraies dents orales sont apparues avant les denticules dermiques [Blais et al., 2011; Donoghue and Rücklin, 2016].

Une théorie *outside-in* modifiée (Figure 1.4C) a tenté de concilier les données paléontologiques et embryologiques bien que les conodontes, dont l'appartenance au clade des vertébrés demeure débattue, n'y ont pas été inclus [Huysseune et al., 2009, 2010]. Selon cette théorie, l'émergence des dents a précédé celle des mâchoires au cours de l'évolution et les dents seraient apparues suite à la migration par les fentes branchiales et jusqu'à la cavité orale d'un ectoderme capable de former des odontodes [Huysseune et al., 2009, 2010]. La capacité à produire des odontodes aurait été transférée de l'ectoderme à l'endoderme en ces zones et les dents seraient donc apparues suite à l'interaction entre l'endoderme et du mésenchyme dérivé de la crête neurale [Huysseune et al., 2009, 2010]. Une fois établie, cette hypothèse a été supportée par l'absence de dents pharyngiennes chez des espèces ne possédant pas de fentes branchiales. Des tétrapodes avec des fentes branchiales tels que les salamandres et les têtards de grenouilles ne

présentent néanmoins pas de dents pharyngiennes [Huysseune et al., 2009; Berkovitz and Shellis, 2016].

Fraser et al. [2010] ont proposé une quatrième théorie intitulée *inside and out* (Figure 1.4D), centrée sur une réseau de régulation de gènes plutôt que sur un tissu ou un type cellulaire. Les auteurs ont suggéré qu'un groupe de gènes localisés au niveau des placodes sensorielles telles que les papilles et co-exprimés au niveau de l'épithélium interagissent avec un groupe de gènes co-exprimés au niveau de cellules ectomésenchymateuses dérivées de la crête neurale [Fraser et al., 2010]. Ce nouveau réseau de gènes de régulation aurait pu permettre le développement d'un odontode ou d'une dent en tout point du corps qui aurait présenté des cellules ectomésenchymateuses dérivées de la crête neurale en lien étroit avec un épithélium [Fraser et al., 2010].

Chen et al. [2020] ont récemment proposé, à partir de données sur un ostéichtyen souche, que des odontodes primaires et fondateurs couvraient originellement la peau et la cavité oropharyngée et qu'ils ont ensuite permis aux odontodes et aux dents de se développer, selon qu'ils étaient en présence d'épithélium oral ou dermique, respectivement. Toutefois, ce résultat est nouveau dans la littérature et un plus grand nombre de fossiles est nécessaire afin d'évaluer la solidité de l'hypothèse proposée.

Le principal crédit est généralement attribué à l'hypothèse *outside-in*. Tout d'abord, les éléments des euconodontes ne sont pas homologues aux dents des vertébrés puisque le tissu similaire à de l'émail au niveau de leur couronne n'était pas présent chez leurs ancêtres paraconodontes [Murdock et al., 2013]. L'existence de structures similaires à des dents ainsi que le remplacement successif de spires dentaires dans le pharynx et la cavité orale de *Loganellia*, un genre dérivé des thélodontes, a également favorisé l'hypothèse selon laquelle les dents sont apparues avant les mâchoires au cours de l'évolution [Van Der Brugghen and Janvier, 1993; Donoghue and Rücklin, 2016].

La relation phylogénétique existant entre les thélodontes et les groupes d'organismes, gnathostomes compris, présentant un remplacement dentaire successif et des structures similaires à des dents favorise néanmoins une hypothèse de convergence entre ces structures plutôt qu'une hypothèse d'homologie [Donoghue and Rücklin, 2016]. La relation d'homologie entre les dents des placodermes et des gnathostomes couronnes a donc été établie, ce qui a réfuté l'hypothèse de convergence entre ces groupes et celui des placodermes [Rücklin et al., 2012]. La plupart des études s'accordent enfin sur le fait que les dents ont évolué à partir des odontodes dermiques et qu'elles sont apparues une seule fois au cours de l'évolution [Rücklin et al., 2011; Murdock et al., 2013; Witten et al., 2014; Donoghue and Rücklin, 2016; Martin et al., 2016; Haridy et al., 2019].

Le domaine de la Biologie est toutefois empreint d'exceptions et l'existence de denticules extra-oraux a été reportée au niveau des os dermiques du crâne chez plusieurs espèces actuelles de téléostéens non apparentés, notamment chez *Denticeps*, *Atherion* et *Xiphias* [Huysseune and Sire, 1998; Sire, 2001; Sire and Allizard, 2001]. Il s'avère néanmoins que ces denticules ne sont pas directement dérivés des odontodes ancestraux, c'est-à-dire qu'il ne sont pas issus de la ré-expression de facteurs odontogènes latents au niveau de la peau [Sire, 2001]. Ils résultent plus probablement de l'interaction étroite entre des cellules épidermiques situées sur le corps avec des cellules de la crête neurale odontogènes ayant migré hors de la cavité orale [Sire, 2001].

La question de qui, de la dent ou de l'odontode est apparu en premier illustre parfaitement le besoin qui existe de découvrir et de décrire de nouveaux fossiles afin de tester les hypothèses évolutives élaborées et de tenter de décider laquelle est la plus

probable. Les études développementales peuvent toutefois fournir des indications quant aux similarités observées au cours de la croissance des odontodes et dents au sein des espèces et entre celles-ci.

> **Diversité des formes dentaires et patrons de dentition chez les élasmobranches** *Of the Heterodontus francisci biology: « May bite back when harassed. »*
>
> – *www.fishbase.se*, read 02/09/2020

Chez les mammifères, les dents se développent exclusivement sur les os de la mâchoire. Les dents sont remplacées une seule fois au cours de la vie des individus de la plupart des espèces, qui sont donc qualifiées de diphyodontes et présentent souvent des formes de dents différentes entre la symphyse et les commissures, un caractère qui se nomme hétérodontie monognathique [Jernvall and Thesleff, 2012]. Il existe néanmoins des exceptions à ces patrons, notamment chez certains rongeurs, chauve-souris et odontocètes qui sont monophyodontes et donc ne renouvellent jamais leurs dents [Jernvall and Thesleff, 2012]. Les pétrogales des rochers et les lamantins sont de rares espèces parmi les mammifères à être polyphyodontes et donc à présenter un renouvellement perpétuel de leur dentition [Jernvall and Thesleff, 2012]. Dans le cas de ces espèces, ce remplacement a lieu par l'ajout distal de nouvelles molaires [Jernvall and Thesleff, 2012]. Contrairement aux mammifères, la plupart des autres vertébrés sont polyphyodontes et cette caractéristique est considérée comme étant la condition plésiomorphe du remplacement dentaire chez les gnathostomes couronnes [Rücklin et al., 2012]. Les poissons osseux, amphibiens, reptiles et élasmobranches renouvellent leurs dents à plusieurs reprises au cours de la vie des individus et leurs dents peuvent se développer au niveau de plusieurs sites de la cavité oropharyngée, ce qui génère une importante diversité de formules dentaires et de types de remplacement dentaire [Davit-Béal et al., 2007; Cappetta, 2012; Jernvall and Thesleff, 2012; Underwood et al., 2015; Smith et al., 2018]. Les dents peuvent par exemple se développer sur les os du palais des salamandres [Ungar and Sues, 2019] et sur les arcs pharyngiens des téléostéens [Wautier et al., 2001] et des variants ont été identifiés quant au nombre de rangées dentaires chez les cécilies [Ungar and Sues, 2019].

Au cours de leur évolution, les chimères ont perdu la capacité à produire des dents individuelles, elles possèdent néanmoins six plaques dentaires à croissance continue composées de dentine trabéculaire, hyperminéralisée (whitlockine) et sclérotique (incluant l'ostéodentine) [Smith et al., 2020]. La question de l'existence d'émailloïde recouvrant ou non cette dentine chez les chimères a longtemps été débattue [Ishiyama et al., 1984; Ørvig, 1985; Enault et al., 2015a], cependant l'hyperminéralisation des plaques dentaires est plus probablement due à la présence du biominéral whitlockite dans la matrice de dentine [Johanson et al., 2020].

La plupart des élasmobranches possèdent des dents exclusivement sur le cartilage de Meckel et sur le palatocarré. La couche minéralisée la plus externe des dents de requins est composée d'émailloïde, dont la matrice est produite par les améloblastes, d'origine ectodermique, et par les odontoblastes, d'origine mésenchymateuse, contrairement aux mammifères dont l'émail a une origine exclusivement ectodermique [Sasagawa, 2002; Gillis and Donoghue, 2007; Enault et al., 2015a; Lübke et al., 2015]. L'émailloïde des élasmobranches n'est pas équivalent à l'émail des tétrapodes [Kemp, 1999; Enault

et al., 2015a]. Il diffère par exemple de ce dernier en cela que la phase minérale de l'émailloïde est composée de fluorapatite alors que l'émail contient de l'hydroxyapatite [Enax et al., 2014; Lübke et al., 2015]. De plus, contrairement à l'émail, l'émailloïde des élasmobranches est minéralisé avant que la dentine ne le soit [Kemp, 1999]. Les émailloïdes présents chez les élasmobranches sont homologues mais diffèrent dans leur patrons d'organisation et de minéralisation [Sasagawa, 2002; Gillis and Donoghue, 2007]. Chez les téléostéens, l'émailloïde est parsemé de vésicules matricielles contenant des cristaux participant ensuite à la minéralisation alors que chez les élasmobranches, le site de minéralisation initial se situe au niveau des vésicules tubulaires mises en place à partir des processus cellulaires des odontoblastes [Sasagawa, 2002]. L'émailloïde des élasmobranches contient également moins de fibrilles de collagène que l'émailloïde des téléostéens et les cristaux ne s'accumulent pas spécifiquement le long de ces fibrilles [Sasagawa, 2002]. Les cristaux initiaux participant à la minéralisation de l'émailloïde chez les élasmobranches ne se rassemblent enfin pas selon un patron spécifique alors que chez les téléostéens le processus de minéralisation débute à la limite entre la dentine et l'émailloïde et progresse vers la limite externe de l'émailloïde [Sasagawa, 2002].

Les dents des requins actuels ont été classées selon des caractéristiques histologiques concernant notamment la présence ou non de certains types de dentine dans la couronne dentaire. L'histologie des dents de requins actuels et fossiles a constitué le cœur de plusieurs études ayant pour objectif de comprendre la diversification de la minéralisation dentaire au sein de ce groupe et d'établir des corrélations entre les histotypes, ou patrons histologiques de la couronne dentaire, et des signaux phylogénétiques ou fonctionnels [Moyer et al., 2015; Jambura et al., 2018, 2019, 2020].

Trois histotypes dentaires différents sont définis chez les requins (Figure 1.5). Les dents orthodontes sont composées d'émailloïde recouvrant une couche d'orthodentine qui englobe elle-même une cavité pulpaire [Moyer et al., 2015; Jambura et al., 2020]. Celles-ci sont notamment présentes chez la plupart des Carcharhiniformes, chez le requin-lézard *Chlamydoselachus anguineus* et chez le requin-baleine *Rhincodon typus* (Figure 1.5A) [Moyer et al., 2015; Jambura et al., 2020]. Les dents pseudo-ostéodontes sont supposées être la condition plésiomorphe pour tous les requins actuels et sont composées d'un centre d'ostéodentine entouré d'une couche d'orthodentine recouverte d'émailloïde (Figure 1.5B) [Jambura et al., 2018, 2020]. Les dents pseudo-ostéodontes sont notamment présentes chez les Echinorhiniformes, les Squaliformes et chez certains Orectolobiformes [Jambura et al., 2020]. Les dents ostéodontes possèdent une couronne remplie d'ostéodentine et ne comprennent pas d'orthodentine (Figure 1.5C) [Moyer et al., 2015; Jambura et al., 2019, 2020]. Cet histotype est retrouvé chez la plupart des Lamniformes tels que le petit requin taupe *Isurus paucus* et le grand requin blanc *Carcharodon carcharias* [Moyer et al., 2015; Jambura et al., 2019, 2020].

Les dents des élasmobranches sont régulièrement perdues et remplacées au cours de la vie d'un individu, selon des durées spécifiques aux espèces, aux mâchoires et aux taux métaboliques associés aux saisons [Luer et al., 1990; Correia, 1999; Motta and Wilga, 2001; Botella et al., 2009]. Ces taux métaboliques sont souvent influencés par des conditions environnementales telles que la température de l'eau mais n'ont pas été corrélés à des pertes dentaires accidentelles, notamment au cours de la prise alimentaire ou de la reproduction [Luer et al., 1990; Correia, 1999; Motta and Wilga, 2001]. Lorsque les dents ne sont pas perdues accidentellement, le remplacement dentaire constitue également un patron en lui-même. Les dents usées sont remplacées au moyen d'un «

tapis roulant » dont le patron diverge entre les espèces. Les dents peuvent être perdues sporadiquement au sein de files individuelles, c'est par exemple le cas du requin bleu *Prionace glauca*, du requin longimane *Carcharhinus longimanus*, de *I. paucus* et de *C. carcharias*, selon des phases sinusoïdales le long de l'axe mésio-distal du palatocarré chez le squale-chagrin commun *Centrophorus granulosus* ou peuvent être perdues au cours du renouvellement de l'ensemble des dents les plus âgées comme cela est observé chez le squalelet féroce *Isistius brasiliensis*, l'aiguillat commun *Squalus acanthias* et au niveau des dents meckeliennes de *C. granulosus* [Bigelow and Schroeder, 1948; Strasburg, 1963; Motta and Wilga, 2001; Bemis et al., 2015; Moyer and Bemis, 2016] (Figure 1.6).

Les types dentaires peuvent être modifiés au cours du processus de remplacement ontogénétique chez les élasmobranches. Les dents peuvent subir une variation en termes de nombre d'éléments et notamment d'ajout de cuspides accessoires, ce qui est le cas entre les stades juvéniles et sexuellement matures chez le squale bouclé *Echinorhinus brucus* [Herman et al., 1989] ou entre ces mêmes stades chez les mâles *S. canicula* [Ellis and Shackley, 1995] et *S. stellaris* [Berio et al., 2020] (voir aussi la sous-section 2.1.2). L'ajout de crénulations est également observable entre les stades juvéniles et sexuellement matures du requin de nuit *Carcharhinus signatus* [Raschi et al., 1982] ainsi qu'une perte de ces crénulations chez les individus sexuellement matures de *C. carcharias* [Bemis et al., 2015]) (Figure 1.7).

La dentition peut également être modifiée en fonction des types dentaires dont elle est constituée. Les juvéniles de *Heterodontus* possèdent par exemple une majorité de dents agrippeuses alors que les individus matures présentent plus de dents molariformes [Reif, 1976; Powter et al., 2010]. Les embryons précoces de *C. carcharias* ont par ailleurs des dents en forme de crochets sans crénulations alors que les embryons tardifs ont des dents tricuspides avec des crénulations latérales [Tomita et al., 2017]. Chez les élasmobranches, les dents peuvent comporter des cuspides au niveau de la symphyse et être molariformes au niveau des commissures et la dentition peut subir des transitions en termes de types dentaires au cours de l'ontogénie qui peuvent être corrélées avec des modifications du régime alimentaire [Reif, 1976; Wilga and Motta, 2000; Motta and Wilga, 2001; Powter et al., 2010; Cappetta, 2012]. Au-delà de son importance dans l'écologie trophique des espèces, le remplacement dentaire au cours de l'ontogénie est étroitement lié au comportement reproducteur, au moins chez certains batoïdes [McEachran, 1977; Kajiura and Tricas, 1996; Schmitt et al., 2015; Vinu et al., 2017; Rutledge et al., 2019]. Des tests mécaniques avec des mâchoires de batoïdes ont démontré que l'efficacité des dents avec les cuspides chez les mâles sexuellement matures était supérieure à celle des dents sans cuspides des juvéniles pour agripper les nageoires pectorales (tests réalisés avec les mâchoires de *Hypanus sabinus* et de *Aptychotrema rostrata* [Kajiura and Tricas, 1996; Gutteridge and Bennett, 2014]). Il est également curieux de constater que les modifications ontogénétiques des morphologies dentaires peuvent affecter uniquement certaines dents à des emplacements précis le long de la mâchoire. Le cas le plus extrême concerne les dents supérieures une et trois de *C. carcharias*, dont la largeur et l'angle sont respectivement et significativement modifiés après la maturation sexuelle des mâles, contrairement à celles des femelles [French et al., 2017]. Chez *H. portusjacksoni*, les dents de type broyeur sont plus nombreuses chez les femelles matures par rapport aux mâles matures et les dents antérieures sont plus pointues chez certains batoïdes mâles matures par rapport aux juvéniles chez lesquels elles demeurent de type broyeur, c'est notamment le cas chez les raies *Hemitrygon akajei*, *H. sabinus* et *A. rostrata*

[Taniuchi and Shimizu, 1993; Kajiura and Tricas, 1996; Powter et al., 2010; Gutteridge and Bennett, 2014].

Très peu d'élasmobranches présentent une homodontie monognathique mais c'est notamment le cas des Squaliformes au niveau des dents meckeliennes, de la raie bouclée *Raja clavata*, du requin-baleine et du requin pèlerin [Karbhari and Josekutty, 1986; Motta and Wilga, 2001; Underwood et al., 2015, 2016] (Figure 1.6). Chez la plupart des requins et des batoïdes, les morphologies dentaires subissent des modifications subtiles et continues le long de l'axe mésio-distal, ce qui se traduit par une faible hétérodontie monognathique et rend difficile le fait de déterminer des familles dentaires [Reif, 1976; Straube et al., 2007] (Figure 1.6 et voir la sous-section 2.1.2). L'un des problèmes relatifs à ces propos concerne donc la caractérisation des changements morphologiques au sein d'une mâchoire et la comparaison de ces derniers entre spécimens. J'ai abordé cette problématique au cours de ma thèse en utilisant de la morphométrie géométrique (voir le chapitre 2).

L'un des principaux avantages de l'exploration de la grande diversité morphologique des dents de requins aux niveaux intraspécifique et intra-individuel est de fournir une vue d'ensemble des formes dentaires qu'une seule espèce peut produire et ce en fonction de la population d'origine d'un individu, de son stade ontogénétique, de son sexe et de la position dentaire le long de la mâchoire. La gamme de morphologies qui caractérise une espèce peut donc être corrélée à des paramètres développementaux dont les influences génétique et physique sur les conformations dentaires demeurent peu étudiées au sein des requins.

On commence par les dents puis on découvre l'endosquelette

> *« [...] it may be pointed out that until the vertebrae of any particular fish are examined one cannot decide whether they are of interest or not; when the examination has been made, the author is performing a service to science by placing his observations on record, for even if the structures prove to have no very direct bearing on the elucidation of the problem, he spares his successors the labour of an independent examination of the vertebrae. »*
>
> – *On the Calcification of the Vertebral Centra in Sharks and Rays*, Walter G. Ridewood, 1921

Toute personne ayant jamais étudié les dents sait qu'il existe un risque non négligeable d'être irrésistiblement attirée par la moindre petite forme de minéralisation se trouvant sur son chemin. Ceci est probablement dû au fait que les approches expérimentales utilisées afin d'étudier les odontodes et l'endosquelette sont similaires ainsi qu'au fait que des données paléontologiques et développementales, y compris génétiques, ont montré que l'histoire évolutive de ces deux ensembles était étroitement liée.

Certains des gènes exprimés durant les stades de différentiation des bourgeons dentaires sont responsables du processus de minéralisation. Les protéines et molécules associées à ce processus contrôlent la sécrétion de dentine par les odontoblastes d'origine mésenchymateuse et de l'émailloïde, ou de l'émail chez les mammifères, par les améloblastes d'origine épithéliale. Or, les odontoblastes partagent des caractéristiques avec les cellules productrices de tissu osseux dont la synthèse de collagène de type 1 et plusieurs autres marqueurs [James et al., 2004; Simon et al., 2009; Enault et al., 2015b; Hisham Zainal Ariffin et al., 2017; Enault et al., 2018] (voir la sous-section 3.1.1).

Jusqu'aux années 1980, l'endosquelette des élasmobranches était considéré comme étant dépourvu de tissu osseux, toutefois des patrons de minéralisation dans les arcs neuraux ainsi qu'une partie des tessères présentent des cellules allongées semblables à des ostéoblastes ainsi que des marqueurs similaires à ceux connus dans les tissus osseux [Kemp and Westrin, 1979; Peignoux-Deville et al., 1982, 1989; Eames et al., 2007; Atake et al., 2019]. La capacité des chondrichtyens à produire des odontoblastes ainsi que le fait que certaines espèces présentent du tissu lamellaire, semblable au tissu osseux interroge quant aux similarités entre les tissus dentaires et ceux des arcs neuraux en termes d'expressions de gènes, de types cellulaires et de composition de matrice extracellulaire. Puisque les odontoblastes et les ostéoblastes partagent des expressions de gènes similaires, la présence chez les élasmobranches de tissu semblable au tissu osseux pourrait résulter de (i) la perte de l'os chez une partie des groupes ancestraux seulement ou (ii) une possibilité de perte et de réacquisition de voies de développement chez certains fibroblastes qui contrôlent le développement de la dentine et de l'os. Au cours de ma thèse, j'ai choisi de commencer à étudier cette question complexe en recherchant la présence de tissu lamellaire au sein des ordres principaux de chondrichtyens actuels.

L'étude de l'occurrence et de la diversité des composants squelettiques des chondrichtyens est étroitement liée à la recherche de l'origine des tissus minéralisés des vertébrés. L'origine et l'absence supposée de tissu osseux chez les chondrichtyens actuels est encore débattue. Deux hypothèses s'opposent à ce sujet, la première stipule que l'ossification endochondrale est une innovation des poissons osseux [Donoghue and Sansom, 2002] alors que la seconde stipule que les chondrichtyens ont perdu la capacité à synthétiser du tissu osseux après la divergence entre ce groupe et celui des ostéichtyens [Donoghue et al., 2006; Brazeau et al., 2020]. Cette dernière hypothèse demeure la plus probable en raison de son soutien par le registre fossile, ce qui implique que le tissu « osseux » dont la présence a été reportée chez certains chondrichtyens actuels ne constitue pas l'état ancestral de l'os endochondral des vertébrés. Ce tissu « osseux » serait donc un vestige de tissu osseux ou un caractère dérivé dont l'existence serait limitée à certains groupes d'élasmobranches actuels.

Structure de la thèse

Dans le chapitre 2, je décris les morphologies dentaires de la grande roussette *Scyliorhinus stellaris* en détails et couple les avantages de la microtomographie à rayons X et de la morphométrie géométrique en 3D. Je discute des résultats préliminaires que j'ai obtenus avec le même protocole sur les dents de *S. canicula* et effectue une comparaison des patrons dentaires observés pour ces deux espèces de scyliorhinidés. Je commente la contribution de ces descriptions pour la taxonomie et insiste quant à l'importance de considérer que les morphologies dentaires des requins sont dynamiques dans le temps et entre les individus de sexe différent.

Lorsque ces morphologies dentaires sont caractérisées en détail, elles peuvent être utilisées pour traiter diverses questions. J'ai choisi de m'intéresser au potentiel des dents de *S. canicula* afin de discriminer des populations génétiquement et écologiquement différenciées. J'ai élaboré un protocole original en couplant les avantages de la morphométrie géométrique et du *Random Forests* [Breiman, 2001], un algorithme

d'apprentissage automatique, afin de classer les dents de *S. canicula* provenant d'une population de l'Océan Atlantique et d'une population de la Mer Méditerranée.

La diversité morphologique des dents de requins fait émerger une autre question, qui concerne les facteurs pouvant influencer la forme finale d'une dent. Ces facteurs peuvent être de nature physique ou génétique et ces derniers ont été abordés au cours de ma thèse. Dans le chapitre 3, je discute de l'importance de coupler des approches théoriques et expérimentales afin de comprendre le rôle de protéines spécifiques dans l'acquisition d'une forme de dent particulière. Je commente également les avantages de la comparaison entre les patrons observés chez les requins et ceux reportés chez les mammifères afin de comprendre l'histoire évolutive des dents. Je présente les résultats préliminaires de tests fonctionnels réalisés sur des bourgeons dentaires d'embryons de *S. canicula* et discute de la méthode d'implantation des billes ainsi que des expérimentations futures qui pourraient être effectuées afin de confirmer ou d'infirmer les résultats que j'ai jusqu'ici obtenus.

Le chapitre 4 est enfin consacré à la description de la diversité des types de minéralisation au niveau des arcs neuraux des chondrichtyens. Le projet développé dans ce chapitre questionne notamment la fréquence à laquelle un tissu similaire au tissu osseux est présent dans les arcs neuraux des poissons cartilagineux. Les résultats fournis par des analyses histologiques et de la microtomographie à rayons X sont discutés à la lumière de l'histoire évolutive des tissus minéralisés des vertébrés.

6.5.3 Résumé du chapitre 2 : Caractérisation des formes dentaires et des dentitions chez les requins

Ce chapitre présente l'intérêt de caractériser les diversités de formes des dents chez les requins, aux niveaux de l'individu, de la population et de l'espèce. Ce travail de thèse est primordial puisqu'il permet de fournir des éléments de réflexion quant aux facteurs moléculaires responsables de l'acquisition des formes dentaires chez les requins, un aspect qui est ensuite développé dans le chapitre 3. Les méthodes couramment utilisées afin d'analyser les changements de forme ou de conformation d'une structure sont la morphométrie classique et la morphométrie géométrique. La première méthode est la plus ancienne et consiste à réaliser des mesures linéaires sur un objet afin de comparer celles-ci à celles d'un objet homologue par exemple. Néanmoins, ces mesures peuvent s'avérer être redondantes et ne permettent pas, une fois collectées, de reconstituer la forme de l'objet en question. La morphométrie géométrique pallie ces problèmes en se fondant notamment sur la collecte de points homologues entre deux structures. Le problème sous-jacent soulevé par cette méthode provient précisément de la nécessité originelle de placer des points homologues, au sens évolutif, puisque la plupart des relations d'homologies entre les structures de plusieurs espèces n'ont pas été prouvées bien qu'elles sont souvent suspectées. Les points homologues peuvent donc être réduits à des points correspondants du point de vue topologique, par exemple entre la cuspide principale d'une dent de requin et celle d'un individu de la même espèce ou d'une espèce dont les dents sont morphologiquement proches. L'hétérodontie gynandrique constitue un patron récurrent chez les scyliorhinidés et cet aspect n'avait jusqu'alors pas été étudié en détails. L'utilisation d'un cadre traditionnel de morphométrie géométrique sur des données de conformation et de forme des dents en 3D a, pour la première fois, permis de suivre l'émergence de l'hétérodontie gynandrique chez une espèce de requin

et un article a été publié à ce sujet dans le cadre de ma thèse (voir [Berio et al., 2020]). Cet article a permis de montrer que les dents de *S. stellaris* subissent une augmentation du nombre de leurs cuspides accessoires lorsque les embryons des deux sexes deviennent des juvéniles. En revanche, si au cours de la maturation sexuelle les dents des femelles connaissent aussi une faible augmentation du nombre de cuspides accessoires, celles des mâles en subissent une réduction ainsi qu'une augmentation de la taille relative de leur cuspide principale. Les analyses des trajectoires de développement corroborent ces observations morphologiques, dont l'une des causes probables pourrait être le taux différentiel d'hormones sexuelles circulantes entre mâles et femelles après maturation sexuelle. Chez certaines espèces de requins, le mâle mord la femelle afin de la maintenir durant l'accouplement et de plus grandes cuspides chez les mâles de ces espèces pourraient être liées à l'efficacité d'une telle morphologie pour la reproduction. Une étude similaire a été initiée en ce qui concerne les dents de *S. canicula* et les résultats comparatifs préliminaires avec les dents de *S. stellaris* sont également présentés dans ce chapitre. Les néosélaciens sont victimes d'un accroissement de l'intensité de la pêche et du commerce illégal. Les fraudes sont recherchées au moyen d'analyses d'ADN sur les criées mais sont coûteuses et chronophages. Dans ma thèse, j'ai proposé un protocole de reconnaissance des dents de requins sous la forme d'une preuve de concept.

Les populations de *S. canicula* sont génétiquement et morphologiquement différenciées entre l'Océan Atlantique et la Mer Méditerranée. Cependant, aucune étude n'a encore été réalisée afin de caractériser d'éventuelles différences dentaires entre ces populations. Au cours de ce projet, j'ai couplé une approche de morphométrie géométrique en 3D avec une approche de classification supervisée, le *Random Forests*. Cela m'a permis d'exploiter les bénéfices des deux approches et ensuite de comparer les résultats d'une Analyse Discriminante Linéaire classiquement utilisée en morphométrie géométrique avec ceux obtenus avec le *Random Forests*. J'ai d'abord montré que les cuspides des spécimens de la population méditerranéenne sont plus pointues que celle des individus d'Atlantique et que les dents des individus matures sont plus grandes chez la population atlantique par rapport à la population méditerranéenne. Les performances de classification sont environ 20 % meilleures avec le *Random Forests* qu'avec une Analyse Linéaire Discriminante et l'utilisation de données de forme et non uniquement de conformation permet également d'accroître les performances de classification. Ce protocole d'analyse pourrait donc être substitué à celui traditionnellement utilisé en morphométrie géométrique afin d'identifier à quelle population ou espèce appartient une dent de requin. Les différences de morphologies dentaires proviennent enfin probablement de différences génétiques plus que de régimes alimentaires divergents puisque *S. canicula* est opportuniste et que les populations considérées vivent dans des environnements similaires. Dans ce chapitre, je souligne enfin l'extraordinaire diversité de formes dentaires au sein d'une seule espèce de requin et donc l'importance de fournir des descriptions morphologiques et quantitatives des dents de requins actuels afin de réaliser des travaux de taxonomie fiables.

6.5.4 Résumé du chapitre 3 : Développement dentaire, une approche moléculaire

Le chapitre 3 discute des aspects moléculaires du développement dentaire et des denticules dermiques chez les requins au regard des données déjà disponibles chez les

téléostéens et les mammifères. Le développement dentaire des mammifères est celui ayant été le plus étudié. Cependant, bien que les patrons d'expression des facteurs de prolifération et de différentiation cellulaires chez les requins diffèrent de ceux des mammifères, plusieurs protéines impliquées peuvent être considérées comme étant homologues à celles reportées chez la souris. Un article de revue de littérature publié au cours de ma thèse permet de comparer les expressions de nombreux gènes exprimés durant la morphogenèse dentaire de *S. canicula*, de la souris et de plusieurs téléostéens ainsi que durant le développement des denticules dermiques de *S. canicula* [Berio and Debiais-Thibaud, 2019]. Cette revue met en évidence les nombreux patrons d'expression communs entre les espèces considérées et ce en fonction de stades de développement équivalents entre les structures. Plusieurs hypothèses sont fournies quant aux différences inter- et intraspécifiques observées, en termes de localisation et d'occurrence d'expression. Elles concernent notamment les biais dus au fait d'attribuer des stades de développement stricts au cours de processus dynamiques mais également des hétérochronies de développement et redondances fonctionnelles au sein d'une famille de gènes. La revue souligne enfin le manque de données d'expression à tous les stades de développement dentaire chez une espèce, ce qui constitue une entrave à la compréhension de l'évolution de ces structures chez les vertébrés. L'étude des causes du changement de forme des dents peut être réalisée au moyen de modèles informatiques. Ceux-ci ont néanmoins été fondés sur le développement dentaire des mammifères et ne sont donc pas adaptés aux contraintes spécifiques exercées sur les bourgeons dentaires des requins. Les requins ne présentent par exemple pas de nœud d'émail tel qu'il est défini chez les mammifères et les patrons de forme dentaire le long de la mâchoire des requins diffèrent largement de ceux, moins visibles, des mammifères. Des tests fonctionnels ont donc été réalisés afin de fournir à ces modèles des données spécifiques aux dents de requins. Les tests fonctionnels ont consisté à insérer des microbilles imprégnées de protéines d'intérêt, dans ce cas Shh, Fgf3 et Bmp4, à proximité de bourgeons dentaires chez des embryons de *S. canicula* en développement. Shh et Fgf3 sont des activateurs de la prolifération cellulaire alors que Bmp4 induit la différentiation cellulaire. Les résultats préliminaires suggèrent que la présence de Shh et de Fgf3 affecte négativement le développement de cuspides accessoires et que Fgf3 affecte également négativement le processus de minéralisation des dents. Les résultats obtenus avec Bmp4 ne montrent pas de différence fiable entre les dents contrôles et les dents traitées. Plusieurs améliorations peuvent être apportées au protocole expérimental mis en place. Elles concernent le maintien des individus en aquarium une fois ceux-ci sortis de leur capsule, ce qui permettrait d'augmenter le taux de survie des embryons et d'atteindre un échantillonnage suffisant pour effectuer des tests statistiques fiables. De plus, la localisation exacte de la bille dans la lame dentaire demeure incertaine en raison de la difficulté de la manipulation physique et certains bourgeons ont pu être endommagés, ce qui a pu produire des morphologies non attendues. Les concentrations de protéines utilisées ont par ailleurs été choisies en fonction de données de la littérature concernant des dents de mammifères ou d'amphibiens ou des ptérygopodes de raies et les effets observés sur les dents de *S. canicula* peuvent donc différer des effets de ces protéines dans des conditions physiologiques normales. De plus, les stades de développement des bourgeons dentaires sont impossibles à évaluer sans coupes histologiques. Or, des études ont montré que les protéines d'intérêt ne sont sécrétées qu'au cours de certains stades de développement des bourgeons. Dans le cas selon lequel la bille aurait été

insérée à proximité d'un bourgeon n'exprimant pas les récepteurs correspondants à la protéine, aucun effet sur la morphologie dentaire n'aura donc pu être observé. Cette étude préliminaire demeure à améliorer selon plusieurs aspects, toutefois le protocole mis en place est original et les résultats obtenus sont encourageants et offrent des perspectives prometteuses quant à l'étude du rôle de certaines protéines sur l'acquisition d'une forme spécifique de dent de requin.

6.5.5 Résumé du chapitre 4 : Des odontodes et de l'endosquelette des chondrichtyens

Les chondrichtyens ont ainsi été nommés en raison de leur endosquelette dont la nature a longtemps été supposée être uniquement cartilagineuse. Néanmoins, il est établi que les chondrichtyens ont perdu la capacité à fabriquer de l'os dermique et périchondral il y a 400 millions d'années. Le cartilage des chondrichtyens subit cependant un processus de minéralisation, le plus souvent superficiel, au cours de la croissance permanente de l'individu afin de renforcer les éléments squelettiques. Cette minéralisation est dite tessérale lorsqu'elle consiste en l'apposition de petits blocs d'hydroxyapatite sur la superficie des éléments cartilagineux et elle concerne la plupart de l'endosquelette, par exemple les rayons des nageoires et les éléments du crâne. La minéralisation aréolaire est restreinte aux seuls corps vertébraux, lorsque ceux-ci sont présents. La minéralisation lamellaire ou plus généralement la minéralisation similaire à du tissu osseux a été historiquement le dernier type à avoir été défini. Sa présence a uniquement été reportée dans les arcs neuraux de deux espèces de requins appartenant à l'ordre des Carcharhiniformes ainsi qu'à deux raies de l'ordre des Rajidae. Elle présente plusieurs caractéristiques qui semblent être similaires à celles du tissu osseux tel qu'il est défini chez les tétrapodes. Elle est décrite dans la littérature comme étant organisée en lamelles entre lesquelles une faible densité de cellules très allongées, similaires morphologiquement à des ostéocytes, sont réparties. La matrice extracellulaire contient de plus du collagène de type 1, comme cela est également le cas dans le tissu osseux, alors que le cartilage hyalin comprend du collagène de type 2. Le fait que cette minéralisation a dans un premier temps été nommée tissu osseux a généré deux questionnements majeurs : (i) à partir de quelles caractéristiques est-il possible d'assimiler un tissu à de l'os, notamment si celui-ci diffère de celui défini à partir du modèle des tétrapodes et (ii) s'il existe du tissu osseux chez certains élasmobranches, qu'en-est-il de sa présence au sein des chondrichtyens et de son histoire évolutive subséquente ? Afin de fournir des éléments de réponse à cette seconde question, je présente dans ce chapitre 4 une étude histologique de la minéralisation des arcs neuraux au sein de la majorité des ordres de chondrichtyens. L'approche histologique est utilisée afin de comprendre l'organisation structurelle des arcs neuraux, de caractériser les formes cellulaires synthétisant les matrices minéralisées et d'élaborer des hypothèses quant à la nature des tissus observés. Cette approche est couplée avec des images produites par de la microtomographie à rayons X afin de visualiser les parties de matrice minéralisées ainsi que de qualifier la topographie de la surface des arcs neuraux. Les résultats obtenus permettent d'appréhender la diversité des patrons de minéralisation des arcs neuraux des chondrichtyens et d'en proposer une nouvelle catégorisation. La minéralisation globulaire est présente dans les arcs neuraux de toutes les espèces de chondrichtyens considérées et constitue donc un caractère ancestral du groupe. Le tissu similaire à de

l'os et dont la présence a été reportée chez plusieurs espèces d'élasmobranches peut être subdivisée en deux tissus distincts en fonction de leurs caractéristiques histologiques. La minéralisation fibreuse est le premier type histologique défini, elle est caractérisée par la présence de nombreuses cellules disposées dans une matrice fibreuse et minéralisée qui est bordée par une épaisse couche de tissu conjonctif non minéralisé. Elle est observée chez la plupart des espèces d'élasmobranches étudiées et a probablement été perdue au cours de l'évolution des Squaliformes et des holocéphales. La minéralisation lamellaire est le second type de tissu similaire à de l'os. La densité cellulaire y est beaucoup moins importante par rapport à celle observée dans la minéralisation fibreuse et aucun tissu conjonctif non minéralisé ne la borde. Mon projet confirme la présence de minéralisation lamellaire chez *S. canicula*, un Carcharhiniforme, et met pour la première fois en évidence ce type de minéralisation des arcs neuraux chez un Orectolobiforme. L'hypothèse évolutive la plus parcimonieuse dans cette étude suggère que la présence de minéralisation lamellaire dans les arcs neuraux de ces deux espèces est le résultat d'une évolution convergente plutôt que de la perte secondaire de ce caractère chez les Lamniformes, les Hétérodontiformes et certains Carcharhiniformes. Ce travail démontre également qu'il existe une diversité de tissus minéralisés dans les arcs neuraux des chondrichtyens dont la caractérisation peut être précisée en couplant la microtomographie à rayons X et l'histologie. Par ailleurs, la minéralisation aréolaire n'a jusqu'alors été décrite qu'au niveau des corps vertébraux des élasmobranches et peu d'études ont exploré la diversité des patrons qu'elle présente. Des travaux d'anatomie publiés il y a un siècle suggèrent toutefois qu'il existe une importante variation de ces patrons chez les élasmobranches et cette dernière pourrait être analysée avec les mêmes méthodes que celles décrites dans ce chapitre 4.

6.5.6 Chapitre 5 Conclusions et perspectives

Dans cette sous-section, je discute en détail des contributions majeures et des perspectives de ma thèse mais les principales contributions de mon travail sont exposées dans ce paragraphe. J'ai montré pour la première fois l'émergence de l'hétérodontie gynandrique au cours de la croissance de deux espèces de requins. J'ai pour cela élaboré un important jeu de données en 3D relatif aux formes de dents de requins. J'ai analysé ce jeu de données en couplant de façon originale des méthodes de morphométrie géométrique avec des modèles de *Random Forests*. Ces analyses m'ont permis de fournir une description détaillée des couronnes dentaires chez *S. canicula*, une espèce modèle chez les requins dont la diversité des patrons dentaires n'avait jusqu'alors jamais été décrite. J'ai de plus comparé les morphologies dentaires de *S. canicula* avec celles de *S. stellaris*, une espèce chez laquelle très peu de données de formes dentaires étaient disponibles. Cette comparaison a permis de déceler des morphologies dentaires communes à ces deux espèces et de discuter de leurs implications, en termes de classification taxonomique. Par ailleurs, j'ai élaboré un nouveau protocole expérimental afin d'effectuer des tests fonctionnels sur les bourgeons dentaires d'embryons de *S. canicula* au moyen de microbilles. Ces expérimentations ont fourni les premiers résultats concernant le rôle de certaines protéines au cours de l'acquisition d'une forme de dent particulière chez les requins. J'ai enfin étudié l'occurrence d'un tissu similaire à de l'os au niveau des arcs neuraux de plusieurs espèces de chondrichtyens et ai montré que celui-ci est présent

chez un plus grand nombre de ces espèces que supposé jusqu'alors. Ces nouvelles données permettent de discuter quant à l'évolution des tissus minéralisés des vertébrés.

Stabilité et variation des formes dentaires et de leurs trajectoires de développement chez les requins

Il existe plusieurs organismes présentant de la variabilité intra-individuelle dans la forme de leurs structures répétées. Chez certaines plantes, c'est par exemple le cas des feuilles immergées ou non le long d'une tige ou des feuilles d'âges différents [Winn, 1996; Chitwood et al., 2012; Spriggs et al., 2018]. Certains invertébrés benthiques tels que les coraux et les gorgones présentent également des patrons architecturaux intra-individuels variables en raison des colonies modulaires qui les composent [Hughes, 2005]. Les modèles qui ont été développés pour appréhender l'acquisition de forme de telles colonies reposent sur des contraintes environnementales, la proximité de branches coralliennes voisines et certains facteurs endogènes tels que des paramètres de diffusion [Hughes, 2005] et soulignent le potentiel de facteurs endo- et exogènes à générer de la variabilité intra-individuelle.
Mon travail de thèse a tout d'abord eu pour objectif de détailler la variabilité intra-individuelle au sein des dentitions de deux espèces de scyliorhinidés, *S. canicula* et *S. stellaris*. J'ai utilisé des surfaces dentaires en 3D et de la morphométrie géométrique afin de décrire les patrons de forme et de conformation dentaires le long de la mâchoire d'un individu, ainsi qu'entre le palatocarré et le cartilage de Meckel. J'ai détaillé la modification de variabilité intra-individuelle au cours de l'ontogénie et ai proposé des hypothèses quant aux facteurs pouvant générer cette variabilité. Les modifications du nombre de cuspides accessoires et de la courbure de la couronne des dents peuvent par exemple être liés à des gradients de récepteurs aux protéines le long de la mâchoire alors que les différences de forme dentaire entre les mâchoires supérieure et inférieure pourraient plutôt être attribuées à des différences de courbure mésio-distale et labio-linguale entre les deux cartilages. La dentition des requins est dynamique, non seulement du fait du renouvellement permanent des dents au cours de la vie d'un individu mais également parce que les dents présentent des morphologies différentes en fonction des stades ontogénétiques de l'individu. Cela permet notamment aux individus d'adopter un comportement reproducteur particulier, au cours desquels les mâles mordent les femelles. J'ai donc, au cours de ma thèse, décrit l'émergence de l'hétérodontie gynandrique au cours de l'ontogénie chez *S. canicula* et *S. stellaris*. Chez *S. stellaris*, les trajectoires de développement des dentitions sont similaires chez les mâles et les femelles entre les stades éclos et juvénile. Ils diffèrent en revanche chez les spécimens plus âgés puisque les mâles sexuellement matures possèdent moins de cuspides accessoires que les femelles au même stade de développement qui, elles, conservent une morphologie dentaire proche de celle des juvéniles. La mise en place de l'hétérodontie gynandrique entre les stades juvénile et sexuellement mature pourrait être contrôlée par la production d'hormones sexuelles différentes, telles que les androgènes, après la maturation sexuelle. Les trajectoires de développement dentaire chez *S. canicula* et *S. stellaris* devraient par la suite être comparées statistiquement afin de déterminer quelles en sont les différences. L'incorporation d'autres espèces de scyliorhinidés dans une comparaison à plus large échelle permettrait par ailleurs de déterminer quelles sont les caractéristiques des trajectoires de développement communes à ce groupe ainsi que

celles communes aux espèces phylogénétiquement (par exemple chez *Scoliodon* sp.) et aux morphologies dentaires (par exemple chez *Leptocharias smithii*) proches. L'inclusion et la comparaison d'un plus grand nombre d'espèces dans les analyses de trajectoires pourrait de plus permettre de tester si des groupes de requins aux types dentaires similaires, par exemple les scyliorhinidés et les chlamydosélachidés qui possèdent un type agrippeur [Cappetta, 1986], mais phylogénétiquement éloignés partagent les mêmes modifications de forme dentaire au cours de l'ontogénie et en fonction des sexes. De telles comparaisons parmi les néosélaciens, couplées à des données relatives à leurs écologies pourraient permettre de comprendre les impacts du mode de reproduction et du régime trophique sur les patrons de trajectoire développementale communs au groupe et ceux spécifiques à certains taxons ou espèces.

Il existe plus généralement un manque de descriptions détaillées des dents de requins en raison de leur importance cruciale pour la détermination des espèces actuelles et fossiles ainsi que pour appréhender le rôle de morphologies dentaires spécifiques dans certains comportements alimentaires et reproducteurs et mon travail contribue à combler cette lacune.

Un nouveau protocole d'identification pour la conservation des requins

Dans le contexte d'accroissement de l'intensité de pêche et du commerce illégal, il existe une demande de méthodes rapides et fiables d'identification des espèces de requins. L'identification des espèces de requins repose actuellement sur des analyses ADN, notamment sur les criées parce que de petits échantillons suffisent à effectuer les analyses et que, dans de nombreux cas, seules certaines parties des individus sont vendues et sont insuffisantes pour identifier les espèces morphologiquement. Cela n'est néanmoins pas toujours le cas puisque sur certaines criées, les mâchoires et dents des individus sont préservées.
Dans cette thèse, j'ai souhaité étudier les différences subtiles de forme de dents entre deux populations de requins en couplant de la morphométrie géométrique et du *Random Forests*. Les analyses effectuées s'intègrent dans une preuve de concept puisque l'origine des individus était connue, cependant elles ont permis de montrer que le protocole de classification des dents de *S. canicula* que j'ai mis en place était plus performant que celui traditionnellement utilisé. Ces résultats offrent des perspectives prometteuses quant à la délimitation d'espèces et le cadre d'analyse proposé pourrait être couplé aux identifications fondées sur l'analyse de l'ADN, qui demeure un processus coûteux et chronophage. Ces résultats montrent donc, pour la première fois, des différences de morphologies dentaires entre deux populations de *S. canicula*, une espèce dont la structure génétique demeure controversée [Barbieri et al., 2014] et interrogent les aspects écologiques qui pourraient être corrélés aux différences inter-populationnelles observées.

Le protocole que j'ai utilisé atteint des performances de classification élevées, cependant le processus de pose de points repères est laborieux, chronophage et peut être amélioré. Les coordonnées 3D fournies au *Random Forests* pourraient tout d'abord être remplacées par les images non traitées des dents ou par une information topographique extraite automatiquement des surfaces 3D [Lazzari and Guy, 2014; MacLeod, 2017, 2018; Thiery et al., 2019], ce qui réduirait drastiquement le temps alloué au pré-traitement des données. L'utilisation d'images brutes fournit également de meilleurs résultats que

ceux obtenus en utilisant des données de morphométrie géométrique et les méthodes associées [MacLeod, 2017, 2018].

L'utilisation d'informations topographiques plutôt que de données de points remarquables devrait ensuite résoudre le problème posé par l'homologie phylogénétique et topographique de ces points remarquables. Ce problème d'homologie exclu, les couronnes dentaires ne présentant pas de points topographiques remarquables pourraient également être intégrées aux analyses de classification. Ceci pourrait permettre d'inclure aux analyses de classification des espèces de requins aux dents de type broyeur tels que les émissoles *Mustelus schmitti* [Belleggia et al., 2014] et les requins marteaux *Sphyrna tiburo* [Wilga and Motta, 2000]. Cela pourrait également permettre de générer un jeu de données à l'échelle des élasmobranches en incluant plusieurs espèces de batoïdes aux dents de type broyeur [Cappetta, 1986; Herman et al., 1995; Underwood et al., 2015].

Contrôle moléculaire du développement dentaire chez les requins

Le stade ontogénétique et les caractères sexuels sont intimement liés, ce qui interroge quant aux causes de l'émergence de l'hétérodontie gynandrique. Au-delà des facteurs moléculaires sur lesquels j'ai concentré mon travail de thèse (Shh, Fgf3 et Bmp4), les hormones sexuelles sont de très bonnes candidates quant à la régulation de l'hétérodontie gynandrique chez les requins. O'Shaughnessy et al. [2015] ont mis en évidence le rôle des récepteurs d'androgènes dans le maintien de l'expression de *Shh* durant le développement des ptérygopodes chez la petite raie *Leucoraja erinacea* par le lien à des éléments de réponse à *Hand2*, qui est un régulateur de *Shh*. La détection de l'expression de *Shh* au niveau des dents de requins ainsi que les effets pléiotropes de Shh permettent de supposer que *Shh* régule la forme des dents chez les élasmobranches et pourrait être partiellement contrôlé par les androgènes. Cette hypothèse est actuellement testée en laboratoire puisque des embryons de *S. canicula* ont été élevés dans un milieu contenant de la 11-kétotestostérone afin d'étudier l'impact de cette hormone sur le développement dentaire.

D'après les données de la littérature et les résultats des tests fonctionnels de ma thèse, les modèles de développement dentaire chez les mammifères pourraient être adaptés aux contraintes qui sont le plus susceptibles de réguler l'acquisition de formes dentaires chez les requins. Le modèle ToothMaker [Salazar-Ciudad and Jernvall, 2010] élaboré pour les mammifères a été modifié au cours de ma thèse par un collaborateur afin de correspondre aux dents de *Scyliorhinus* et les résultats préliminaires obtenus sont présentés ci-après. Des compressions physiques ont par exemple été ajoutées au modèle de développement dentaire chez les requins afin de mimer les modifications mésio-distales des morphologies dentaires le long de la mâchoire, une caractéristique qui est moins visible chez les mammifères. Le système originel d'activation-diffusion de ToothMaker ne génère pas non plus les morphologies dentaires observées chez *Scyliorhinus* et un second inhibiteur de la différentiation cellulaire, tel que Shh, a été ajouté au système. De plus, des paramètres tels que les hormones sexuelles qui n'étaient pas présents dans le modèle ToothMaker seront également ajoutés afin d'essayer de reproduire l'émergence de l'hétérodontie gynandrique au cours de l'ontogénie. Plusieurs types de données sont donc manquants afin de modéliser précisément le développement dentaire chez les requins et d'évaluer la pertinence de certaines combinaisons de paramètres, au moyen

de travaux expérimentaux. Des travaux expérimentaux sont notamment nécessaires afin de tester une éventuelle corrélation entre une forme dentaire particulière et une conformation de lame dentaire associée. Des travaux préliminaires avec une étudiante en Master ont permis d'explorer la courbure labio-linguale le long de l'axe mésio-distal du cartilage de Meckel de *S. canicula*. Les résultats suggèrent que cette courbure subit une modification graduelle le long de la mâchoire mais la corrélation entre ce gradient de courbure et celui de changement de forme observé entre les dents parasymphysaires et commissurales doit à présent être testée. Le protocole expérimental proposé pour les tests fonctionnels avec les implantations de billes pourrait être utilisé afin d'étudier l'impact de différents niveaux d'expression de gènes sur la morphologie dentaire des requins. Les billes insérées à proximité des bourgeons dentaires en développement pourraient être imprégnées de plusieurs concentrations d'une protéine donnée et de telles concentrations pourraient être corrélées aux éventuels et différents phénotypes dentaires observés. De plus, des expérimentations complémentaires impliquant les inhibiteurs des protéines utilisées au cours de cette thèse doivent encore être réalisées afin d'étudier leurs implications fonctionnelles. L'influence des hormones sexuelles sur la forme des dents et notamment celle de la 11-kétotestostérone pourrait également être questionnée en quantifiant l'occurrence de récepteurs aux androgènes sur les bourgeons dentaires des embryons de *S. canicula*. Les phénotypes dentaires résultant des tests fonctionnels réalisés au cours de ma thèse ont été analysés au moyen de la microtomographie à rayons X. L'analyse de ces phénotypes pourrait également être complétée par de la morphométrie géométrique sur les surfaces en 3D de dents isolées dans le cas des expérimentations avec les billes et sur la dentition complète des individus dans le cas des expérimentations avec les hormones sexuelles.

Denticules dermiques : les grands oubliés ?

Le développement des dents et denticules dermiques des élasmobranches est contrôlé par des gènes communs et ces structures partagent également des stades de développement, des compositions tissulaires ainsi que des organisations similaires [Debiais-Thibaud et al., 2011, 2015; Berio and Debiais-Thibaud, 2019]. La question de l'origine des dents à partir des odontodes dermiques ou l'inverse est toujours source de débats et les hypothèses proposées sont régulièrement remises en question [Haridy et al., 2019]. Dans ce contexte, il semble pertinent de discuter des analyses effectuées durant ma thèse qui pourraient être transposées à l'étude des denticules dermiques. La morphologie et l'espacement des denticules dermiques chez les requins ont déjà été étudiés chez plusieurs espèces et ont souvent été corrélés avec la performance de nage [Wen et al., 2015], la préférence pour une profondeur spécifique le long de la colonne d'eau [Dillon et al., 2017], ainsi qu'avec le comportement reproducteur de certaines espèces [Crooks et al., 2013]. Ces caractéristiques des denticules n'ont pourtant pas encore été décrites avec un protocole de morphométrie géométrique. Les analyses de morphométrie géométrique effectuées sur les dents de *S. canicula* et de *S. stellaris* pourraient par exemple être appliquées aux denticules dermiques de ces mêmes espèces afin de quantifier la forme et la conformation des denticules en différents points le long du corps des spécimens, au cours de leur ontogénie, entre différents sexes et plus généralement aux niveaux intra- et interspécifiques.

En dépit des similarités multiples qui existent entre les dents et les denticules dermiques des élasmobranches, ces structures présentent néanmoins certaines différences, notamment en ce qui concerne les tissus dans lesquelles elles se développent. Les dents se développent et sont remplacées continuellement au cours de la vie d'un individu et ce au sein de files dentaires qui sont liées par une lame dentaire [Fraser et al., 2020]. Les denticules dermiques se développent également *via* l'interaction entre un épithélium et un mésenchyme, cependant lorsque ces denticules sont perdus ils ne sont pas systématiquement remplacés à l'endroit exact où ils ont été perdus [Reif, 1978, 1980; Fraser et al., 2020]. Les interstices de peau nue créés lors de la croissance d'un individu ou lors de la perte d'un denticule sont progressivement réinvestis par de nouveaux denticules dont le développement n'est pas inféodé à des files telles que celles existant pour les dents [Reif, 1978, 1980; Fraser et al., 2020; Popp et al., 2020]. Les dents et denticules des requins diffèrent également en termes d'expressions de gènes [Debiais-Thibaud et al., 2015; Berio and Debiais-Thibaud, 2019]. Le développement et le remplacement des denticules, comme celui des dents de requins, dépend de paramètres moléculaires –facteurs de signalisation et champs d'inhibition– [Reif, 1978; Cooper et al., 2017, 2018], cependant les formes qu'ils acquièrent dépendent probablement aussi de l'épaisseur et de la topographie de la peau. Les denticules dermiques peuvent présenter une diversité de formes au sein d'un individu plus importante que celle observée pour les dents et se développer au-dessus de tissus et structures présentant différentes fonctions ainsi que différents niveaux de dureté tels qu'au niveau du cartilage, de l'œil ou des muscles [Pratt and Carrier, 2001; Crooks and Waring, 2013; Tomita et al., 2020]. L'impact de la dureté et de la conformation du tissu sur l'acquisition de la forme particulière d'une structure serait plus facile à étudier en considérant les denticules puisque ces structures recouvrent une plus grande diversité de tissus que les dents.

Cartilage ou os : les chondrichtyens sont-ils plus subtils que cela ?

> *« We divide the Pisces into Chondrichthyes (sharks and rays), with a purely cartilaginous skeleton, and Osteichthyes, in which bone is present. »*
>
> – Edwin Stephen Goodrich, 1868-1946

La classification dichotomique des tissus osseux et cartilagineux est largement fondée sur les observations effectuées sur les mammifères et a longtemps été utilisée comme telle chez les téléostéens qui présentent cependant une diversité de types de cartilages différents de ceux identifiés chez les mammifères [Witten et al., 2010]. Les chondrichtyens, dont le nom rappelle que leur endosquelette est principalement cartilagineux, présentent trois types de cartilage minéralisé : les cartilages tesséral, aréolaire et lamellaire ou similaire à l'os. La microstructure des tessères peut également être subdivisée en cartilage minéralisé globulaire, dans sa zone interne, et en cartilage minéralisé prismatique, dans sa zone externe [Kemp and Westrin, 1979; Dean and Summers, 2006]. Les cellules sécrétrices de la matrice externe des tessères des requins ont initialement été identifiées comme étant des ostéoblastes, par exemples chez le requin citron *Negaprion brevirostris* et le requin-corail *Triaenodon obesus* [Kemp and Westrin, 1979]. La matrice externe de cette zone est recouverte par des cristaux d'hydroxyapatite qui sont de plus présents dans le tissu osseux. La présence de plusieurs types de cartilages minéralisés ainsi que la détection de tissu similaire à l'os chez les élasmobranches [Kemp and Westrin, 1979; Peignoux-Deville et al., 1982; Clement, 1992; Eames et al.,

2007; Atake et al., 2019] illustrent parfaitement le continuum qui existe entre le cartilage et l'os chez ce groupe, tel qu'également décrit chez les téléostéens [Kemp and Westrin, 1979]. Ce continuum est cependant peu compris chez les chondrichtyens puisque la plupart des études se concentrent sur une espèce ou un taxon [Kemp and Westrin, 1979; Peignoux-Deville et al., 1982; Eames et al., 2007; Dean et al., 2009; Atake et al., 2019]. La recherche de l'occurrence de la minéralisation similaire à l'os chez les chondrichtyens a été restreinte à des espèces isolées jusqu'alors et aucune vision globale n'a été fournie quant à l'évolution de ce tissu au sein des chondrichtyens. Au cours de ma thèse, j'ai identifié la présence de minéralisation similaire à celle observée au niveau du tissu osseux et ai décrit ce patron plus en détails dans les arcs neuraux de nombreux groupes de chondrichtyens. Au sein du tissu similaire à l'os identifié chez les élasmobranches, la distinction entre une minéralisation fibreuse et une minéralisation lamellaire est proposée. La première est présente chez la plupart des espèces d'élasmobranches considérées alors que la seconde est restreinte aux groupes des Orectolobiformes et des Carcharhiniformes, ce qui suggère une convergence évolutive de cet histotype au sein des galéomorphes.

De plus, si l'on suppose que la minéralisation lamellaire ressemble au tissu osseux des mammifères, elle devrait posséder des propriétés de renforcement supérieures à celles des autres patrons de minéralisation présents chez les chondrichtyens (minéralisations tessérale et aréolaire) et pourrait donc avoir été conservée chez certaines espèces pour des raisons écologiques. Par ailleurs, l'endosquelette des requins vivant en eaux froides et en eaux profondes est supposé être moins minéralisé que celui des espèces côtières et ce probablement à cause de la température de l'eau, de la pression dans la colonne d'eau et de la disponibilité des sources de phosphate dans le milieu [Dean et al., 2015]. Les requins vivant en eaux profondes présentent des caractéristiques physiques incluant un volume cardiaque et un nombre de fibres aérobies réduit ainsi qu'une flottabilité accrue par rapport aux espèces d'eaux moins profondes avec des taux métaboliques plus importants [Pinte et al., 2019; Larsen et al., 2020]. La minéralisation moindre (tessères plus fines et absence de minéralisation lamellaire) des arcs neuraux des espèces profondes de chondrichtyens que j'ai échantillonnées durant ma thèse pourrait donc être expliquée par l'adaptation de ces espèces à leurs habitats aux conditions extrêmes. Afin d'évaluer les implications écologiques de la présence de tissu similaire au tissu osseux chez les chondrichtyens, la robustesse des minéralisations lamellaire et tessérale pourrait être comparée en mesurant par exemple leurs résistances à la compression ainsi que leurs densités [Balaban et al., 2015; Di Santo, 2019].

Les chondrichtyens face au changement climatique global

L'acidification des océans présente plusieurs impacts délétères sur les processus biologiques des espèces marines, notamment en ce qui concerne la formation de la coquille des mollusques [McClintock et al., 2009; Welladsen et al., 2010; Gazeau et al., 2013] et les squelettogenèse et minéralisation chez les téléostéens [Bignami et al., 2013; Chambers et al., 2014; Coll-Lladó et al., 2018; Holmberg et al., 2019]. Les conséquences d'une diminution de pH ont été beaucoup moins étudiées chez les élasmobranches par rapport à ces deux derniers groupes, pourtant une modification de ce paramètre provoque la corrosion des denticules dermiques et pourrait également affecter les dents [Dziergwa et al., 2019]. Une diminution de pH engendre également une augmentation

de la densité d'hydroxyapatite dans le cartilage des nageoires pelviennes modifiées de certaines raies ainsi que dans celui de leurs mâchoires [Di Santo, 2019]. Néanmoins, l'interaction entre la température, le pH et les processus de minéralisation chez les élasmobranches demeure complexe et une diminution de la température induit également une réduction de la minéralisation au niveau des nageoires pectorales chez une Rajidae [Di Santo, 2019].

Tel que mentionné précédemment, les requins d'eaux profondes sont supposés présenter des endosquelettes moins minéralisés que ceux des espèces phylogénétiquement proches vivant en eaux côtières [Dean et al., 2015]. Cependant, cette tendance n'a à ce jour pas encore été testée chez les chondrichtyens et résulte d'observations personnelles et sporadiques qui devraient être décrites et consignées rigoureusement afin de tester ladite tendance. Dans l'hypothèse où cette tendance se révèlerait fondée scientifiquement, elle serait probablement modulée par les modifications environnementales d'origine anthropique auxquelles sont confrontés les océans. Les chondrichtyens d'eaux côtières et profondes pourraient en effet subir des modifications inégales de leurs patrons de minéralisation de cartilage et ce à cause des changements différents de température dans plusieurs zones océaniques. Dans 100 ans, ces modifications de température pourraient par exemple être plus importantes dans le domaine bathyal comparé au domaine abyssal, ainsi que dans le bassin Atlantique comparé au bassin Indien [Sweetman et al., 2017]. La motricité des espèces occupant les mêmes niches écologiques pourrait également être affectée différemment en fonction de leur anatomie et de leur comportement. Les espèces de Rajidae présentant une densité accrue des cartilages modifiés au niveau des nageoires pelviennes à cause de l'acidification océanique pourraient adopter un mode de locomotion similaire à de la marche mais pourraient aussi être confrontées à une diminution de leur efficacité de locomotion résultant d'une augmentation de la densité de leur squelette [Di Santo, 2019]. Une étude détaillée de la vulnérabilité différentielle du squelette de plusieurs chondrichtyens dans le contexte du changement climatique global pourrait fournir de précieux outils afin d'identifier les espèces dont la survie est la plus susceptible d'être menacée au cours des prochaines années.

References

Åberg, T., Wozney, J., and Thesleff, I. (1997). Expression patterns of bone morphogenetic proteins (*Bmps*) in the developing mouse tooth suggest roles in morphogenesis and cell differentiation. *Developmental Dynamics*, 210(4):383–396.

Adams, D., Collyer, M., and Kaliontzopoulou, A. (2019). Geomorph: Software for geometric morphometric analyses. R package version 3.1.0.

Adams, D., Rohlf, F. J., and Slice, D. E. (2004). Geometric morphometrics: ten years of progress following the "revolution". *Italian Journal of Zoology*, 71(1):5–16.

Adams, D. C. and Collyer, M. L. (2009). A general framework for the analysis of phenotypic trajectories in evolutionary studies. *Evolution*, 63(5):1143–1154.

Adelabu, S., Mutanga, O., and Adam, E. (2015). Testing the reliability and stability of the internal accuracy assessment of random forest for classifying tree defoliation levels using different validation methods. *Geocarto International*, 30(7):810–821.

Ahnelt, H., Sauberer, M., Ramler, D., Koch, L., and Pogoreutz, C. (2020). Negative allometric growth during ontogeny in the large pelagic filter-feeding basking shark. *Zoomorphology*, 139(1):71–83.

Alain, G. and Bengio, J. (2016). Understanding intermediate layers using linear classifier probes. *arXiv preprint*, page arXiv:1610.01644v4.

Almerón-Souza, F., Sperb, C., Castilho, C. L., Figueiredo, P. I. C. C., Gonçalves, L. T., Machado, R., Oliveira, L. R., Valiati, V. H., and Fagundes, N. J. R. (2018). Molecular identification of shark meat from local markets in southern Brazil based on DNA barcoding: Evidence for mislabeling and trade of endangered species. *Frontiers in Genetics*, 9:138.

Amaral, C. R. L., Pereira, F., Silva, D. A., Amorim, A., and de Carvalho, E. F. (2017). The mitogenomic phylogeny of the Elasmobranchii (Chondrichthyes). *Mitochondrial DNA Part A*, 29(6):867–878.

Ankhelyi, M. V., Wainwright, D. K., and Lauder, G. V. (2018). Diversity of dermal denticle structure in sharks: Skin surface roughness and three-dimensional morphology. *Journal of Morphology*, 279(8):1132–1154.

Šantić, M and RaĐa, B and Pallaoro, A (2012). Feeding habits of small-spotted catshark (*Scyliorhinus canicula* Linnaeus, 1758) from the eastern central Adriatic Sea. *Marine Biology Research*, 8(10):1003–1011.

Applegate, S. P. (1967). A survey on shark hard parts. In Gilbert, P., Mathewson, R., and Rall, D., editors, *Sharks, Skates and Rays*, pages 37–67. John Hopkins Press.

Archer, K. J. and Kimes, R. V. (2008). Empirical characterization of random forest variable importance measures. *Computational Statistics and Data Analysis*, 52(4):2249–2260.

Atake, O. J., Cooper, D. M. L., and Eames, B. F. (2019). Bone-like features in skate suggest a novel elasmobranch synapomorphy and deep homology of trabecular mineralization patterns. *Acta Biomaterialia*, 84:424–436.

Atkinson, C. J. L. and Collin, S. P. (2012). Structure and topographic distribution of oral denticles in elasmobranch fishes. *The Biological bulletin*, 222(1):26–34.

Bailleul, A. M., Hall, B. K., and Horner, J. R. (2012). First evidence of dinosaurian secondary cartilage in the post-hatching skull of *Hypacrosaurus stebingeri* (Dinosauria, Ornithischia). *PLOS One*, 7(4):e36112.

Balaban, J. P., Summers, A. P., and Wilga, C. A. (2015). Mechanical properties of the hyomandibula in four shark species. *Journal of Experimental Zoology Part A: Ecological Genetics and Physiology*, 323(1):1–9.

Ballard, W. W., Mellinger, J., and Lechenault, H. (1993). A series of normal stages for development of *Scyliorhinus canicula*, the lesser spotted dogfish (Chondrichthyes: Scyliorhinidae). *Journal of Experimental Zoology*, 267(3):318–336.

Barbieri, M., Maltagliati, F., Roldán, M. I., and Castelli, A. (2014). Molecular contribution to stock identification in the small-spotted catshark, *Scyliorhinus canicula* (Chondrichthyes, Scyliorhinidae). *Fisheries Research*, 154:11–16.

Barbuto, M., Galimberti, A., Ferri, E., Labra, M., Malandra, R., Galli, P., and Casiraghi, M. (2010). DNA barcoding reveals fraudulent substitutions in shark seafood products: The Italian case of "palombo" (*Mustelus* spp.). *Food Research International*, 43(1):376–381.

Bardua, C., Felice, R. N., Watanabe, A., Fabre, A. C., and Goswami, A. (2019). A practical guide to sliding and surface semilandmarks in morphometric analyses. *Integrative Organismal Biology*, 1(1):obz016.

Baylac, M., Villemant, C., and Simbolotti, G. (2003). Combining geometric morphometrics with pattern recognition for the investigation of species complexes. *Biological Journal of the Linnean Society*, 80(1):89–98.

Belleggia, M., Figueroa, D. E., and Bremec, C. (2014). The dentition of the narrownose smooth-hound shark, *Mustelus schmitti*. *Marine and Freshwater Research*, 65(8):688.

Bemis, W. E., Moyer, J. K., and Riccio, M. L. (2015). Homology of lateral cusplets in the teeth of lamnid sharks (Lamniformes: Lamnidae). *Copeia*, 103(4):961–972.

Bendiab, A. A. T., Mouffok, S., and Boutiba, Z. (2012). Reproductive biology and growth of lesser spotted dogfish *Scyliorhinus canicula* (Linnaeus, 1758) in western Algerian coasts (Chondrichthyes, Scyliorhinidae). *Biodiversity Journal*, 3(1):41–48.

Benton, M., Donoghue, P. C. J., and Asher, R. J. (2009). Calibrating and constraining molecular clocks. In Hedges, S. B. and Kumar, S., editors, *The Timetree of Life*, pages 35–86. Oxford University Press.

Berio, F. and Bayle, Y. (2020). Scyland3D: Processing 3D landmarks. *Journal of Open Source Software*, 5(46):1262.

Berio, F. and Debiais-Thibaud, M. (2019). Evolutionary developmental genetics of teeth and odontodes in jawed vertebrates: a perspective from the study of elasmobranchs. *Journal of Fish Biology*.

Berio, F., Evin, A., Goudemand, N., and Debiais-Thibaud, M. (2020). The intraspecific diversity of tooth morphology in the large-spotted catshark *Scyliorhinus stellaris*: insights into the ontogenetic cues driving sexual dimorphism. *Journal of Anatomy*, 237(5):960–978.

Berkovitz, B. K. and Shellis, R. P. (2016). Amphibia. In *The Teeth of non-Mammalian Vertebrates*, chapter 5, pages 113–152. Academic Press.

Bethea, D. M., Carlson, J. K., Buckel, J. A., and Satterwhite, M. (2006). Ontogenetic and site-related trends in the diet of the Atlantic sharpnose shark *Rhizoprionodon terraenovae* from the northeast Gulf of Mexico. *Bulletin of Marine Science*, 78(2):287–307.

Bigelow, H. B. and Schroeder, W. C. (1948). Sharks. In Tee-Van, J., Bredr, C. M., Hildebrand, S. F., Parr, A. E., and Schroeder, W. C., editors, *Fishes of the Western North Atlantic*, chapter 3, pages 59–546. Sears Foundation for Marine Research, New Heaven.

Bignami, S., Enochs, I. C., Manzello, D. P., Sponaugle, S., and Cowen, R. K. (2013). Ocean acidification alters the otoliths of a pantropical fish species with implications for sensory function. *Proceedings of the National Academy of Sciences of the United States of America*, 110(18):7366–7370.

Blackburn, T. M., Gaston, K. J., and Loder, N. (2008). Geographic gradients in body size: a clarification of Bergmann's rule. *Diversity and distributions*, 5(4):165–174.

Blais, S. A., MacKenzie, L. A., and Wilson, M. V. H. (2011). Tooth-like scales in early Devonian eugnathostomes and the "outside-in" hypothesis for the origins of teeth in vertebrates. *Journal of Vertebrate Paleontology*, 31(6):1189–1199.

Bookstein, F. L. (1989). Principal warps: Thin-plate splines and the decomposition of deformations. *IEEE Transactions on Pattern Analysis and Machine Intelligence*, 11(6):567–585.

Bookstein, F. L. (1991a). Features of shape comparison. In *Morphometric Tools for Landmark Data: Geometry and Biology*, chapter 7, pages 258–357. Cambridge University Press, Cambridge, 1 edition.

Bookstein, F. L. (1991b). Landmarks. In *Morphometric Tools for Landmark Data: Geometry and Biology*, chapter 3, pages 55–87. Cambridge University Press, Cambridge.

Bookstein, F. L. (1991c). *Morphometric Tools for Landmark Data: Geometry and Biology*. Cambridge University Press, Cambridge, 1 edition.

Bookstein, F. L. (1997). Landmark methods for forms without landmarks: Morphometrics of group differences in outline shape. *Medical Image Analysis*, 1(3):225–243.

Borrell, A., Aguilar, A., Gazo, M., Kumarran, R. P., and Cardona, L. (2011). Stable isotope profiles in whale shark (*Rhincodon typus*) suggest segregation and dissimilarities in the diet depending on sex and size. *Environmental Biology of Fishes*, 92(4):559–567.

Botella, H., Valenzuela-Rios, J. I., and Martinez-Pérez, C. (2009). Tooth replacement rates in early chondrichthyans: a qualitative approach. *Lethaia*, 42(3):365–376.

Box, G. E. P. (1976). Science and statistics. *Journal of the American Statistical Association*, 71(356):791–799.

Box, G. E. P. (1979). Robustness in the Strategy of Scientific Model Building. In *Robustness in Statistics*, pages 201–236. Elsevier.

Braccini, J. M. and Chiaramonte, G. E. (2002). Intraspecific variation in the external morphology of the sand skate. *Journal of Fish Biology*, 61(4):959–972.

Brazeau, M. D., Giles, S., Dearden, R. P., Jerve, A., Ariunchimeg, Y., Zorig, E., Sansom, R., Guillerme, T., and Castiello, M. (2020). Endochondral bone in an Early Devonian "placoderm" from Mongolia. *Nature Ecology and Evolution*, pages 1–8.

Breiman, L. (2001). Random forests. *Machine learning*, 45(1):5–32.

Breiman, L., Friedman, J. H., Olshen, R. A., and Stone, C. J. (1984). Introduction to tree classification. In Breiman, L., Friedman, J. H., Olshen, R. A., and Stone, C. J., editors, *Classification and Regression Trees*, chapter 2, pages 18–58. Chapman & Hall, Boca Raton, 1 edition.

Buser, T. J., Sidlauskas, B. L., and Summers, A. P. (2018). 2D or Not 2D? Testing the Utility of 2D Vs. 3D Landmark Data in Geometric Morphometrics of the Sculpin Subfamily Oligocottinae (Pisces; Cottoidea). *The Anatomical Record*, 301(5):806–818.

Butler, P. M. (1995). Ontogenetic aspects of dental evolution. *The International Journal of Developmental Biology*, 39(1):25–34.

Calich, H. J. and Campana, S. E. (2015). Mating scars reveal mate size in immature female blue shark *Prionace glauca*. *Journal of Fish Biology*, 86(6):1845–1851.

Capapé, C., Mnasri-Sioudi, N., El Kamel-Moutalibi, O., Boumaïza, M., Amor, M. B., and Reynaud, C. (2014). Production, maturity, reproductive cycle and fecundity of small-spotted catshark, *Scyliorhinus canicula* (Chondrichthyes: Scyliorhinidae) from the northern coast of Tunisia (Central Mediterranean). *Journal of ichthyology*, 54(1):111–126.

Cappetta, H. (1986). Types dentaires adaptatifs chez les sélaciens actuels et post-paléozoïques. *Palaeovertebrata*, 16(2):57–76.

Cappetta, H. (2012). *Handbook of Paleoichthyology, Vol 3E: Chondrichthyes - Mesozoic and Cenozoic Elasmobranchii: Teeth*. Verlag Dr. Friedrich Pfeil.

Cardini, A. L. (2014). Missing the third dimension in geometric morphometrics: how to assess if 2D images really are a good proxy for 3D structures? *Hystrix*, 25:73–81.

Carlson, J. K. and Parsons, G. R. (1997). Age and growth of the bonnethead shark, *Sphyrna tiburo*, from northwest Florida, with comments on clinal variation. *Environmental Biology of Fishes*, 50(3):331–341.

Caruana, R. and Niculescu-Mizil, A. (2006). An empirical comparison of supervised learning algorithms. In *Proceedings of the 23rd international conference on Machine learning*, pages 161–168.

Chai, Y., Jiang, X., Ito, Y., Bringas, P., Han, J., Rowitch, D. H., Soriano, P., McMahon, A. P., and Sucov, H. M. (2000). Fate of the mammalian cranial neural crest during tooth and mandibular morphogenesis. *Development*, 127(8):1671–1679.

Chambers, R. C., Candelmo, A. C., Habeck, E. A., Poach, M. E., Wieczorek, D., Cooper, K. M., Greenfield, C. E., and Phelan, B. A. (2014). Effects of elevated CO2 in the early life stages of summer flounder, *Paralichthys dentatus*, and potential consequences of ocean acidification. *Biogeosciences*, 11(6):1613–1626.

Chawla, N. V., Bowyer, K. W., Hall, L. O., and Kegelmeyer, W. P. (2002). SMOTE: Synthetic Minority Over-sampling Technique. *Journal of Artificial Intelligence Research*, 16:321–357.

Chen, D., Blom, H., Sanchez, S., Tafforeau, P., Märss, T., and Ahlberg, P. E. (2020). The developmental relationship between teeth and dermal odontodes in the most primitive bony fish *Lophosteus*. *eLife*, 9.

Chernova, O. F. and Vorob'eva, E. I. (2012). Polymorphism of the surface sculpture of placoid scales of sharks (Selachomorpha, Elasmobranchii). *Doklady Biological Sciences*, 446(1):316–319.

Chitwood, D. H., Headland, L. R., Kumar, R., Peng, J., Maloof, J. N., and Sinha, N. R. (2012). The developmental trajectory of leaflet morphology in wild tomato species. *Plant Physiology*, 158(3):1230–1240.

Clement, J. G. (1992). Re-examination of the fine structure of endoskeletal mineralization in Chondrichthyans: Implications for growth, ageing and calcium homeostasis. *Marine and Freshwater Research*, 43(1):157–181.

Cobourne, M. T., Hardcastle, Z., and Sharpe, P. T. (2001). *Sonic hedgehog* regulates epithelial proliferation and cell survival in the developing tooth germ. *Journal of Dental Research*, 80(11):1974–1979.

Coll-Lladó, C., Giebichenstein, J., Webb, P. B., and Bridges, C. R. (2018). Ocean acidification promotes otolith growth and calcite deposition in gilthead sea bream (*Sparus aurata*) larvae. *Scientific Reports*, 8(1):1–10.

Collyer, M. L. and Adams, D. C. (2013). Phenotypic trajectory analysis: comparison of shape change patterns in evolution and ecology. *Hystrix, the Italian Journal of Mammalogy*, 24(1):75–83.

Compagno, L. J. V. (1984). FAO species catalogue: vol 4 Sharks of the world an annotated and illustrated catalogue of shark species known to date Part 2-Carcharhiniformes. *FAO Fisheries Synopsis*, 4:251–265.

Coolen, M., Menuet, A., Chassoux, D., Compagnucci, C., Henry, S., Lévèque, L., Da Silva, C., Gavory, F., Samain, S., Wincker, P., Thermes, C., D'Aubenton-Carafa, Y., Rodriguez-Moldes, I., Naylor, G., Depew, M., Sourdaine, P., and Mazan, S. (2008). The dogfish *Scyliorhinus canicula*: A reference in jawed vertebrates. *CSH protocols*, 2008(12):pdb–emo111.

Cooper, R. L., Martin, K. J., Rasch, L. J., and Fraser, G. J. (2017). Developing an ancient epithelial appendage: FGF signalling regulates early tail denticle formation in sharks. *EvoDevo*, 8(1):8–19.

Cooper, R. L., Thiery, A. P., Fletcher, A. G., Delbarre, D. J., Rasch, L. J., and Fraser, G. J. (2018). An ancient Turing-like patterning mechanism regulates skin denticle development in sharks. *Science Advances*, 4(11):eaau5484.

Correia, J. P. (1999). Tooth loss rate from two captive sandtiger sharks (*Carcharias taurus*). *Zoo Biology*, 18(4):313–317.

Cortés, E. (2000). Life history patterns and correlations in sharks. *Reviews in Fisheries Science*, 8(4):299–344.

Courtenay, L. A., Yravedra, J., Huguet, R., Aramendi, J., Maté-González, M. Á., González-Aguilera, D., and Arriaza, M. C. (2019). Combining machine learning algorithms and geometric morphometrics: A study of carnivore tooth marks. *Palaeogeography, Palaeoclimatology, Palaeoecology*, 522:28–39.

Crooks, N., Babey, L., Haddon, W. J., Love, A. C., and Waring, C. P. (2013). Sexual dimorphisms in the dermal denticles of the Lesser-spotted catshark, *Scyliorhinus canicula* (Linnaeus, 1758). *PLOS One*, 8(10):e76887.

Crooks, N. and Waring, C. P. (2013). Sexual dimorphisms in the dermal structure of the lesser-spotted catshark, *Scyliorhinus canicula* (Linnaeus, 1758). *Acta Zoologica*, 94:331–334.

Cullen, J. A. and Marshall, C. D. (2019). Do sharks exhibit heterodonty by tooth position and over ontogeny? A comparison using elliptic Fourier analysis. *Journal of Morphology*, 280(5):687–700.

Daniel, J. F. (1934). Integument. In *The Elasmobranch Fishes*, chapter 2, page 332. University of California press, Berkeley, 3 edition.

Davit-Béal, T., Chisaka, H., Delgado, S., and Sire, J.-Y. (2007). Amphibian teeth: current knowledge, unanswered questions, and some directions for future research. *Biological Reviews*, 82(1):49–81.

de Sousa Rangel, B., Amorim, A. F., Kfoury Jr, J. R., and Rici, R. E. G. (2019a). Microstructural morphology of dermal and oral denticles of the sharpnose sevengill shark *Heptranchias perlo* (Elasmobranchii: Hexanchidae), a deep-water species. *Microscopy Research and Technique*, 82(8):1243–1248.

de Sousa Rangel, B., Salmon, T., Poscai, A. N., Kfoury Jr, J. R., and Rici, R. E. G. (2019b). Comparative investigation into the morphology of oral papillae and denticles of four species of lamnid and sphyrnid sharks. *Zoomorphology*, 138(1):127–136.

de Sousa Rangel, B., Wosnick, N., Magdanelo Leandro, R., de Amorim, A. F., Kfoury Jr, J. R., and Rici, R. E. G. (2016). Thorns and dermal denticles of skates *Atlantoraja cyclophora* and *A. castelnaui* : Microscopic features and functional implications. *Microscopy Research and Technique*, 79(12):1133–1138.

Dean, M. N., Ekstrom, L., Monsonego-Ornan, E., Ballantyne, J., Witten, P. E., Riley, C., Habraken, W., and Omelon, S. (2015). Mineral homeostasis and regulation of mineralization processes in the skeletons of sharks, rays and relatives (Elasmobranchii). *Seminars in Cell & Developmental Biology*, 46:51–67.

Dean, M. N., Mull, C. G., Gorb, S. N., and Summers, A. P. (2009). Ontogeny of the tessellated skeleton: insight from the skeletal growth of the round stingray *Urobatis halleri*. *Journal of Anatomy*, 215(3):227–239.

Dean, M. N. and Summers, A. P. (2006). Mineralized cartilage in the skeleton of chondrichthyan fishes. *Zoology*, 109(2):164–168.

Debiais-Thibaud, M. (2019). The Evolution of Endoskeletal Mineralisation in Chondrichthyan Fish. In Johanson, Z., Underwood, C. J., and Richter, M., editors, *Evolution and Development of Fishes*, chapter 6, pages 110–125. Cambridge University Press, 1 edition.

Debiais-Thibaud, M., Chiori, R., Enault, S., Oulion, S., Germon, I., Martinand-Mari, C., Casane, D., and Borday-Birraux, V. (2015). Tooth and scale morphogenesis in shark: an alternative process to the mammalian enamel knot system. *BMC Evolutionary Biology*, 15(1):292.

Debiais-Thibaud, M., Oulion, S., Bourrat, F., Laurenti, P., Casane, D., and Borday-Birraux, V. (2011). The homology of odontodes in gnathostomes: insights from *Dlx* gene expression in the dogfish, *Scyliorhinus canicula*. *BMC Evolutionary Biology*, 11(1):307.

Deynat, P. P. and Séret, B. (1996). Le revêtement cutané des raies (Chondrichthyes, Elasmobranchii, Batoidea). I-Morphologie et arrangement des denticules cutanés. *Annales des sciences naturelles-Zoologie et biologie animale*, 17(2):65–83.

Di Santo, V. (2019). Ocean acidification and warming affect skeletal mineralization in a marine fish. *Proceedings of the Royal Society B: Biological Sciences*, 286(1894):20182187.

Díaz-Uriarte, R. and Alvarez de Andrés, S. (2006). Gene selection and classification of microarray data using random forest. *BMC Bioinformatics*, 7(1):1–13.

Didier, D. A. (2004). Phylogeny and classification of extant Holocephali. In Carrier, J. C., Musick, J. A., and Heithaus, M. R., editors, *Biology of Sharks and Their Relatives*, chapter 4, pages 115–138. CRC Press, 1 edition.

Didier, D. A. and Stehmann, M. (1996). *Neoharriotta pumila*, a new species of lLongnose chimaera from the Northwestern Indian Ocean (Pisces, Holocephali, Rhinochimaeridae). *Copeia*, 4(1996):955–965.

Díez, G., Soto, M., and Blanco, J. M. (2015). Biological characterization of the skin of shortfin mako shark *Isurus oxyrinchus* and preliminary study of the hydrodynamic behaviour through computational fluid dynamics. *Journal of Fish Biology*, 87(1):123–137.

Dillon, E. M., Norris, R. D., and O'Dea, A. (2017). Dermal denticles as a tool to reconstruct shark communities. *Marine Ecology Progress Series*, 566:117–134.

Domi, N., Poncin, P., and Voss, J. (2000). A new observed pre-copulatory behaviour of the lesser-spotted dogfish, *Scyliorhinus canicula*,in captivity. In *Proceedings of the 3rd European Elasmobranch Association Meeting, Boulogne-sur-Mer*, pages 67–71. Société Française d'Ichtyologie et de l'Institut de Recherche pour le Développement.

Domínguez-Rodrigo, M. and Baquedano, E. (2018). Distinguishing butchery cut marks from crocodile bite marks through machine learning methods. *Scientific Reports*, 8(1):1–8.

Donoghue, P. C. J., Graham, A., and Kelsh, R. N. (2008). The origin and evolution of the neural crest. *BioEssays*, 30(6):530–541.

Donoghue, P. C. J. and Rücklin, M. (2016). The ins and outs of the evolutionary origin of teeth. *Evolution & Development*, 18(1):19–30.

Donoghue, P. C. J. and Sansom, I. J. (2002). Origin and early evolution of vertebrate skeletonization. *Microscopy Research and Technique*, 59(5):352–372.

Donoghue, P. C. J., Sansom, I. J., and Downs, J. P. (2006). Early evolution of vertebrate skeletal tissues and cellular interactions, and the canalization of skeletal development. *Journal of experimental zoology. Part B: Molecular and developmental evolution*, 306B(1):278–294.

Doyle, D., Gammell, M. P., and Nash, R. (2018). Morphometric methods for the analysis and classification of gastropods: A comparison using *Littorina littorea*. *Journal of Molluscan Studies*, 84(2):190–197.

Dryden, I. L. and Mardia, K. V. (1998). *Statistical Shape Analysis*. Wiley, 1 edition.

Du, W., Du, W., and Yu, H. (2018). The role of Fibroblast Growth Factors in tooth development and incisor renewal. *Stem Cells International*, pages 1–14.

Dulvy, N. K., Fowler, S. L., Musick, J. A., Cavanagh, R. D., Kyne, P. M., Harrison, L. R., Carlson, J. K., Davidson, L. N. K., Fordham, S. V., Francis, M. P., Pollock, C. M., Simpfendorfer, C. A., Burgess, G. H., Carpenter, K. E., Compagno, L. J. V., Ebert, D. A., Gibson, C., Heupel, M. R., Livingstone, S. R., Sanciangco, J. C., Stevens, J. D., Valenti, S., and White, W. T. (2014). Extinction risk and conservation of the world's sharks and rays. *eLife*, 3:e00590.

Dziergwa, J., Singh, S., Bridges, C. R., Kerwath, S. E., Enax, J., and Auerswald, L. (2019). Acid-base adjustments and first evidence of denticle corrosion caused by ocean acidification conditions in a demersal shark species. *Scientific Reports*, 9(1):1–10.

Eames, B. F., Allen, N., Young, J., Kaplan, A., Helms, J. A., and Schneider, R. A. (2007). Skeletogenesis in the swell shark *Cephaloscyllium ventriosum*. *Journal of Anatomy*, 210(5):542–554.

Ellis, J. K. and Musick, J. A. (2007). Ontogenetic changes in the diet of the sandbar shark, *Carcharhinus plumbeus*, in lower Chesapeake Bay and Virginia (USA) coastal waters. *Environmental Biology of Fishes*, 80:51–67.

Ellis, J. R. and Shackley, S. E. (1995). Ontogenic changes and sexual dimorphism in the head, mouth and teeth of the lesser spotted dogfish. *Journal of Fish Biology*, 47(1):155–164.

Ellis, J. R. and Shackley, S. E. (1997). The reproductive biology of *Scyliorhinus canicula* in the Bristol Channel, U.K. *Journal of Fish Biology*, 51(2):361–372.

Enault, S., Guinot, G., Koot, M. B., and Cuny, G. (2015a). Chondrichthyan tooth enameloid: past, present, and future. *Zoological Journal of the Linnean Society*, 174(3):549–570.

Enault, S., Muñoz, D., Simion, P., Ventéo, S., Sire, J.-Y., Marcellini, S., and Debiais-Thibaud, M. (2018). Evolution of dental tissue mineralization: an analysis of the jawed vertebrate *SPARC* and *SPARC-L* families. *BMC Evolutionary Biology*, 18(1):127.

Enault, S., Muñoz, D. N., Silva, W. T. A. F., Borday-Birraux, V., Bonade, M., Oulion, S., Ventéo, S., Marcellini, S., and Debiais-Thibaud, M. (2015b). Molecular footprinting of skeletal tissues in the catshark *Scyliorhinus canicula* and the clawed frog *Xenopus tropicalis* identifies conserved and derived features of vertebrate calcification. *Frontiers in Genetics*, 6:283.

Enax, J., Janus, A. M., Raabe, D., Epple, M., and Fabritius, H. O. (2014). Ultrastructural organization and micromechanical properties of shark tooth enameloid. *Acta Biomaterialia*, 10(9):3959–3968.

Evin, A., Cucchi, T., Cardini, A., Vidarsdottir, U. S., Larson, G., and Dobney, K. (2013). The long and winding road: identifying pig domestication through molar size and shape. *Journal of Archaeological Science*, 40(1):735–743.

Fort, G. and Lambert-Lacroix, S. (2005). Classification using partial least squares with penalized logistic regression. *Bioinformatics*, 21(7):1104–1111.

Fraser, G. J., Cerny, R., Soukup, V., Bronner-Fraser, M., and Streelman, J. T. (2010). The odontode explosion: the origin of tooth-like structures in vertebrates. *Bioessays*, 32(9):808–17.

Fraser, G. J., Standing, A., Underwood, C., and Thiery, A. P. (2020). The dental lamina: An essential structure for perpetual tooth regeneration in sharks. *Integrative and comparative biology*, 60(3):644–655.

French, G. C. A., Stürup, M., Rizzuto, S., van Wyk, J. H., Edwards, D., Dolan, R. W., Wintner, S. P., Towner, A. V., and Hughes, W. O. H. (2017). The tooth, the whole tooth and nothing but the tooth: tooth shape and ontogenetic shift dynamics in the white shark *Carcharodon carcharias*. *Journal of Fish Biology*, 91(4):1032–1047.

Fruciano, C. (2016). Measurement error in geometric morphometrics. *Development Genes and Evolution*, 226(3):139–158.

Gans, C. (1985). Differences and similarities: Comparative methods in mastication. *American Zoologist*, 25(2):291–302.

Gans, C. and Northcutt, R. G. (1983). Neural crest and the origin of vertebrates: A new head. *Science*, 220(4594):268–273.

Gazeau, F., Parker, L. M., Comeau, S., Gattuso, J.-P., O'Connor, W. A., Martin, S., Pörtner, H. O., and Ross, P. M. (2013). Impacts of ocean acidification on marine shelled molluscs. *Marine Biology*, 160(8):2207–2245.

Gilbert, S. F. and Barresi, M. J. F. (2016). Neural Tube Formation and Patterning. In *Developmental Biology*, chapter 13, pages 413–437. Sinauer Associates, Inc, Sunderland, 11 edition.

Giles, S., Rücklin, M., and Donoghue, P. C. J. (2013). Histology of "placoderm" dermal skeletons: Implications for the nature of the ancestral gnathostome. *Journal of Morphology*, 274(6):627–644.

Gillis, J. A., Alsema, E. C., and Criswell, K. E. (2017). Trunk neural crest origin of dermal denticles in a cartilaginous fish. *Proceedings of the National Academy of Sciences of the United States of America*, 114(50):13200–13205.

Gillis, J. A. and Donoghue, P. C. J. (2007). The homology and phylogeny of chondrichthyan tooth enameloid. *Journal of Morphology*, 268(1):33–49.

Gillis, J. A., Witten, P. E., and Hall, B. K. (2006). Chondroid bone and secondary cartilage contribute to apical dentary growth in juvenile Atlantic salmon. *Journal of Fish Biology*, 68(4):1133–1143.

Gleiss, A. C., Potvin, J., and Goldbogen, J. A. (2017). Physical trade-offs shape the evolution of buoyancy control in sharks. *Proceedings of the Royal Society B: Biological Sciences*, 284(1866):20171345.

Goldring, S. R. and Goldring, M. B. (2006). Clinical aspects, pathology and pathophysiology of osteoarthritis. *Journal of Musculoskeletal and Neuronal Interactions*, 6(4):376.

Golub, E. E. (2011). Biomineralization and matrix vesicles in biology and pathology. In *Seminars in immunopathology*, volume 33, pages 409–417.

Goren, M. (2014). The Fishes of the Mediterranean: A Biota Under Siege. In *The Mediterranean Sea*, pages 385–400. Springer Netherlands, Dordrecht.

Goswami, A. (2006). Cranial modularity shifts during mammalian evolution. *American Naturalist*, 168(2):270–280.

Graveson, A. C. (1993). Neural crest contributions to the development of the vertebrate head. *American Zoologist*, 33(4):424–433.

Green, S. A., Simoes-Costa, M., and Bronner, M. E. (2015). Evolution of vertebrates as viewed from the crest. *Nature*, 520(7548):474–482.

Gritli-Linde, A., Bei, M., Maas, R., Zhang, X. M., Linde, A., and McMahon, A. P. (2002). Shh signaling within the dental epithelium is necessary for cell proliferation, growth and polarization. *Development*, 129(23):5323–5337.

Grover, C. A. (1974). Juvenile denticles of the swell shark *Cephaloscyllium ventriosum*: Function in hatching. *Canadian Journal of Zoology*, 52(3):359–363.

Gruber, S. H. and Compagno, L. J. V. (1981). Taxonomic status and biology of the bigeye thresher *Alopias superciliosus* (Mediterranean Sea, New Zealand). *Fishery Bulletin*, 79(4):617–640.

Guinot, G., Adnet, S., Shimada, K., Underwood, C. J., Siversson, M., Ward, D. J., Kriwet, J., and Cappetta, H. (2018). On the need of providing tooth morphology in descriptions of extant elasmobranch species. *Zootaxa*, 4461(1):118–126.

Gunz, P. and Mitteroecker, P. (2013). Semilandmarks: a method for quantifying curves and surfaces. *Hystrix, the Italian Journal of Mammalogy*, 24(1):103–109.

Gunz, P., Mitteroecker, P., and Bookstein, F. L. (2005). Semilandmarks in Three Dimensions. In Slice, D. E., editor, *Modern Morphometrics in Physical Anthropology*, chapter 4, pages 73–98. Springer US.

Gutteridge, A. N. and Bennett, M. B. (2014). Functional implications of ontogenetically and sexually dimorphic dentition in the eastern shovelnose ray, *Aptychotrema rostrata*. *The Journal of experimental biology*, 217(2):192–200.

Hall, B. K. (2001). The neural crest as a fourth germ layer and vertebrates as quadroblastic not triploblastic. *Evolution & Development*, 2(1):3–5.

Hall, B. K. (2015). *Bones and cartilage: Developmental and Evolutionary Skeletal Biology*. Elsevier Academic Press, 2 edition.

Hall, B. K. and Gillis, J. A. (2013). Incremental evolution of the neural crest, neural crest cells and neural crest-derived skeletal tissues. *Journal of Anatomy*, 222(1):19–31.

Haridy, Y., Gee, B. M., Witzmann, F., Bevitt, J. J., and Reisz, R. R. (2019). Retention of fish-like odontode overgrowth in Permian tetrapod dentition supports outside-in theory of tooth origins. *Biology Letters*, 15(9):20190514.

Hastie, T., Tibshirani, R., and Friedman, J. (2009). Overview of Supervised Learning. In *The Elements of Statistical Learning: Data Mining, Inference, and Prediction*, chapter 2, pages 9–41. Springer-Verlag, 2 edition.

Henderson, A. C. and Casey, A. (2001). Reproduction and growth in the lesser-spotted dogfish *Scyliorhinus canicula* (Elasmobranchii; Scyliorhinidae), from the west coast of Ireland. *Cahiers de Biologie Marine*, 42(4):397–405.

Herman, J., Hovestadt-Euler, M., and Hovestadt, D. C. (1989). Contributions to the study of the comparative morphology of teeth and other relevant ichthyodorulites in living supraspecific taxa of chondrichthyan fishes. Part A: Selachii. No. 3: Order: Squaliformes—Families: Echinorhinidae, Oxynotidae and Squalidae. *Bulletin de l'Institut royal des Sciences naturelles de Belgique, Biologie*, 59:101–158.

Herman, J., Hovestadt-Euler, M., and Hovestadt, D. C. (1990). Contributions to the study of the comparative morphology of teeth and other relevant ichthyodorulites in living supraspecific taxa of Chondrichthyan fishes. Part A: Selachii. No. 2b: Order: Carcharhiniformes - Family: Scyliorhinidae. *Bulletin de l'Institut Royal des Sciences Naturelles de Belgique, Biologie*, 60:181–230.

Herman, J., Hovestadt-Euler, M., Hovestadt, D. C., and Stehmann, M. (1995). Contributions to the study of the comparative morphology of teeth and other relevant ichthyodorulites in living supra-specific taxa of Chondrichthyan fishes. Part B. Batomorphii. 1b: Order Rajiformes-Suborder Rajoidei-Family: Rajidae-Genera and Subgenera:. *Bulletin de l'Institut Royal des Sciences Naturelles de Belgique. Biologie*, 65:237–307.

Hirouchi, H., Kitamura, K., Yamamoto, M., Odaka, K., Matsunaga, S., Sakiyama, K., and Abe, S. (2018). Developmental characteristics of secondary cartilage in the mandibular condyle and sphenoid bone in mice. *Archives of Oral Biology*, 89:84–92.

Hisham Zainal Ariffin, S., Manogaran, T., Zarina Zainol Abidin, I., Megat Abdul Wahab, R., and Senafi, S. (2017). A perspective on stem cells as biological systems that produce differentiated osteoblasts and odontoblasts. *Current Stem Cells Research & Therapy*, 12(3):247–259.

Holmberg, R. J., Wilcox-Freeburg, E., Rhyne, A. L., Tlusty, M. F., Stebbins, A., Nye, S. W., Honig, A., Johnston, A. E., San Antonio, C. M., Bourque, B., and Hannigan, R. E. (2019). Ocean acidification alters morphology of all otolith types in Clark's anemonefish (*Amphiprion clarkii*). *PeerJ*, 2019(1):e6152.

Horie, T. and Tanaka, S. (2002). Geographic variation of maturity size of the cloudy catshark, *Scyliorhinus torazame*, in Japan. *Journal of the Faculty of Marine Science and Technology-Tokai University*.

Hughes, R. N. (2005). Lessons in modularity: the evolutionary ecology of colonial invertebrates. *Scientia Marina*, 69(S1):169–179.

Hulsey, C. D., Cohen, K. E., Johanson, Z., Karagic, N., Meyer, A., Miller, C. T., Sadier, A., Summers, A. P., and Fraser, G. J. (2020). Grand challenges in comparative tooth biology. *Integrative and Comparative Biology*, 60(3):563–580.

Huysseune, A. and Sire, J.-Y. (1998). Evolution of patterns and processes in teeth and tooth-related tissues in non-mammalian vertebrates. *European Journal of Oral Sciences*, 106(S1):437–481.

Huysseune, A., Sire, J.-Y., and Witten, P. E. (2009). Evolutionary and developmental origins of the vertebrate dentition. *Journal of Anatomy*, 214(4):465–476.

Huysseune, A., Sire, J.-Y., and Witten, P. E. (2010). A revised hypothesis on the evolutionary origin of the vertebrate dentition. *Journal of Applied Ichthyology*, 26(2):152–155.

Ifft, J. D. and Zinn, D. J. (1948). Tooth succession in the smooth dogfish, *Mustelus canis*. *The Biological Bulletin*, 95(1):100–106.

Inoue, J. G., Miya, M., Lam, K., Tay, B.-H., Danks, J. A., Bell, J., Walker, T. I., and Venkatesh, B. (2010). Evolutionary origin and phylogeny of the modern holocephalans (Chondrichthyes: Chimaeriformes): A Mitogenomic Perspective. *Molecular Biology and Evolution*, 27(11):2576–2586.

Ishiyama, M., Sasagawa, I., and Akai, J. (1984). The inorganic content of pleromin in tooth plates of the living holocephalan, *Chimaera phantasma*, consists of a crystalline calcium phosphate known as β-Ca3 (PO4) 2 (Whitlockite). *Archivum histologicum japonicum*, 47(1):89–94.

Ivory, P., Jeal, F., Nolan, C. P., and Jeal, P. F. (2004). Age determination, growth and reproduction in the lesser-spotted dogfish, *Scyliorhinus canicula* (L.). *Journal of Northwest Atlantic Fishery Science*, 35:89–106.

Jambura, P. L., Kindlimann, R., López-Romero, F., Marramà, G., Pfaff, C., Stumpf, S., Türtscher, J., Underwood, C. J., Ward, D. J., and Kriwet, J. (2019). Micro-computed tomography imaging reveals the development of a unique tooth mineralization pattern in mackerel sharks (Chondrichthyes; Lamniformes) in deep time. *Scientific Reports*, 9(1):9652.

Jambura, P. L., Pfaff, C., Underwood, C. J., Ward, D. J., and Kriwet, J. (2018). Tooth mineralization and histology patterns in extinct and extant snaggletooth sharks, *Hemipristis* (Carcharhiniformes, Hemigaleidae)—Evolutionary significance or ecological adaptation? *PLOS One*, 18(3):e0200951.

Jambura, P. L., Türtscher, J., Kindlimann, R., Metscher, B., Pfaff, C., Stumpf, S., Weber, G. W., and Kriwet, J. (2020). Evolutionary trajectories of tooth histology patterns in modern sharks (Chondrichthyes, Elasmobranchii). *Journal of Anatomy*, 236(5):753–771.

James, M. J., Järvinen, E., and Thesleff, I. (2004). *Bono1*: A gene associated with regions of deposition of bone and dentine. *Gene Expression Patterns*, 4(5):595–599.

James, W. W. (1953). The succession of teeth in elasmobranchs. *Proceedings of the Zoological Society of London*, 123(2):419–474.

Janvier, P. (1996). *Early Vertebrates*. Oxford University Press, Oxford.

Janvier, P. and Pradel, A. (2015). Elasmobranchs and their extinct relatives: diversity, relationships, and adaptations through time. *Fish Physiology*, 34(A):1–17.

Jennings, S., Greenstreet, S. P. R., and Reynolds, J. D. (1999). Structural change in an exploited fish community: a consequence of differential fishing effects on species with contrasting life histories. *Journal of Animal Ecology*, 68(3):617–627.

Jernvall, J. (2000). Linking development with generation of novelty in mammalian teeth. *Proceedings of the National Academy of Sciences of the United States of America*, 97(6):2641–2645.

Jernvall, J., Keränen, S. V. E., and Thesleff, I. (2000). Evolutionary modification of development in mammalian teeth: quantifying gene expression patterns and topography. *Proceedings of the National Academy of Sciences of the United States of America*, 97(26):14444–14448.

Jernvall, J., Kettunen, P., Karavanova, I., Martin, L. B., and Thesleff, I. (1994). Evidence for the role of the enamel knot as a control center in mammalian tooth cusp formation: non-dividing cells express growth stimulating *Fgf-4* gene. *The International journal of developmental biology*, 38(3):463–469.

Jernvall, J. and Thesleff, I. (2000). Reiterative signaling and patterning during mammalian tooth morphogenesis. *Mechanisms of Development*, 92(1):19–29.

Jernvall, J. and Thesleff, I. (2012). Tooth shape formation and tooth renewal: evolving with the same signals. *Development*, 139(19):3487–3497.

Johanson, Z., Manzanares, E., Underwood, C., Clark, B., Fernandez, V., and Smith, M. (2020). Evolution of the dentition in holocephalans (Chondrichthyes) through tissue disparity. *Integrative and Comparative Biology*, 60(3):630–643.

Johanson, Z. and Smith, M. M. (2005). Origin and evolution of gnathostome dentitions: a question of teeth and pharyngeal denticles in placoderms. *Biological Reviews*, 80(2):303–345.

Johanson, Z., Smith, M. M., and Joss, J. M. P. (2007). Early scale development in *Heterodontus* (Heterodontiformes; Chondrichthyes): a novel chondrichthyan scale pattern. *Acta Zoologica*, 88(3):249–256.

Johanson, Z., Tanaka, M., Chaplin, N., and Smith, M. (2008). Early Palaeozoic dentine and patterned scales in the embryonic catshark tail. *Biology Letters*, 4(1):87–90.

Kajiura, S. M., Sebastian, A. P., and Tricas, T. C. (2000). Dermal bite wounds as indicators of reproductive seasonality and behaviour in the Atlantic stingray, *Dasyatis sabina*. *Environmental Biology of Fishes*, 58(1):23–31.

Kajiura, S. N. and Tricas, T. C. (1996). Seasonal dynamics of dental sexual dimorphism in the Atlantic stingray *Dasyatis sabina*. *Journal of Experimental Biology*, 199(10):2297–2306.

Karbhari, J. P. and Josekutty, C. J. (1986). On the largest whale shark *Rhincodon typus* Smith landed alive at Cuffe Parade, Bombay. *Marine Fisheries Information Service, Technical and Extension Series*, 66:31–35.

Karl, S. A., Castro, A. L. F., and Garla, R. C. (2012). Population genetics of the nurse shark (*Ginglymostoma cirratum*) in the western Atlantic. *Marine Biology*, 159(3):489–498.

Keating, J., Marquart, C. L., and Donoghue, P. C. J. (2015). Histology of the heterostracan dermal skeleton: Insight into the origin of the vertebrate mineralised skeleton. *Journal of Morphology*, 276(6):657–680.

Kemp, N. E. (1999). Integumentary system and teeth. In *Sharks, Skates and Rays. The Biology of Elasmobranch Fishes*, chapter 2, pages 43–68. Baltimore : Johns Hopkins University Press.

Kemp, N. E. and Westrin, S. K. (1979). Ultrastructure of calcified cartilage in the endoskeletal tesserae of sharks. *Journal of Morphology*, 160(1):75–101.

Kemsley, E. K. (1996). Discriminant analysis of high-dimensional data: A comparison of principal components analysis and partial least squares data reduction methods. *Chemometrics and Intelligent Laboratory Systems*, 33(1):47–61.

Kettunen, P., Laurikkala, J., Itäranta, P., Vainio, S., Itoh, N., and Thesleff, I. (2000). Associations of FGF-3 and FGF-10 with signaling networks regulating tooth morphogenesis. *Developmental Dynamics*, 219(3):322–332.

Klingenberg, C. P. (2016). Size, shape, and form: concepts of allometry in geometric morphometrics. *Development genes and evolution*, 226(3):113–137.

Klingenberg, C. P. and Zimmermann, M. (1992). Static, ontogenetic, and evolutionary allometry: a multivariate comparison in nine species of water striders. *The American Naturalist*, 140(4):601–620.

Kousteni, V., Karachle, P. K., and Megalofonou, P. (2017). Diet of the small-spotted catshark *Scyliorhinus canicula* in the Aegean Sea (eastern Mediterranean). *Marine Biology Research*, 13(2):161–173.

Kousteni, V., Kasapidis, P., Kotoulas, G., and Megalofonou, P. (2015). Strong population genetic structure and contrasting demographic histories for the small-spotted catshark (*Scyliorhinus canicula*) in the Mediterranean Sea. *Heredity*, 114(3):333–343.

Kousteni, V., Kontopoulou, M., and Megalofonou, P. (2010). Sexual maturity and fecundity of *Scyliorhinus canicula* (Linnaeus, 1758) in the Aegean Sea. *Marine Biology Research*, 6(4):390–398.

Kurpinski, K., Chu, J., Hashi, C., and Li, S. (2006). Anisotropic mechanosensing by mesenchymal stem cells. *Proceedings of the National Academy of Sciences of the United States of America*, 103(44):16095–16100.

Kurpinski, K., Chu, J., Wang, D., and Li, S. (2009). Proteomic profiling of mesenchymal stem cell responses to mechanical strain and TGF-beta1. *Cellular and Molecular Bioengineering*, 2(4):606–614.

Lachenbruch, P. A. and Goldstein, M. (1979). Discriminant analysis. *Biometrics*, 35(1):85.

Lagler, K. F., Bardach, J. E., and Miller, R. R. (1962). Systematics and Nomenclature. In *Ichthyology*, chapter 13, page 545. Wiley, New York.

Larsen, M. E., Abel, D. C., Crane, D. P., and Grubbs, R. D. (2020). Differences in relative heart mass among deep-sea and coastal sharks with increasing depth. *Marine Biology*, 167(11):1–8.

Last, P., Naylor, G., Séret, B., White, W., de Carvalho, M., and Stehmann, M. (2016). *Rays of the World*. CSIRO publishing, Clayton South.

Lazzari, V. and Guy, F. (2014). Quantitative three-dimensional topography in taxonomy applied to the dental morphology of catarrhines. *Bulletins et Memoires de la Societe d'Anthropologie de Paris*, 26(3-4):140–146.

Le Douarin, N. M., Creuzet, S., Couly, G., and Dupin, E. (2004). Neural crest cell plasticity and its limits. *Development*, 131(19):4637–4650.

Le Douarin, N. M. and Dupin, E. (2018). The "beginnings" of the neural crest. *Developmental Biology*, 444:S3–S13.

Lee, R. T. H., Knapik, E. W., Thiery, J. P., and Carney, T. J. (2013). An exclusively mesodermal origin of fin mesenchyme demonstrates that zebrafish trunk neural crest does not generate ectomesenchyme. *Development*, 140(14):2923–2932.

Leloup, J. and Olivereau, M. (1951). Données biométriques comparatives sur la Roussette (*Scyllium canicula* L.) de la Manche et de la Méditerranée. *Vie et milieu*, 2(2):182–206.

Leriche, M. (1905). Les poissons Eocène de la Belgique. *Mémoires du Musée Royal d'Histoire Naturelle de la Belgique*, 3:49–228.

Li, J., Wang, P., and Liu, X. (2018). Research based on unbalanced data set classification algorithm. In *AIP Conference Proceedings*, page 040054.

Li, T., Zhu, S., and Ogihara, M. (2006). Using discriminant analysis for multi-class classification: An experimental investigation. *Knowledge and Information Systems*, 10(4):453–472.

Liaw, A. and Wiener, M. (2002). Classification and Regression by randomForest. *R News*, 2(3):18–22.

Lingham-Soliar, T. (2005). Caudal fin allometry in the white shark *Carcharodon carcharias*: implications for locomotory performance and ecology. *Naturwissenschaften*, 92(5):231–235.

Lombardi-Carlson, L. A., Cortés, E., Parsons, G. R., and Manire, C. A. (2003). Latitudinal variation in life-history traits of bonnethead sharks, *Sphyrna tiburo*, (Carcharhiniformes : Sphyrnidae) from the eastern Gulf of Mexico. *Marine and Freshwater Research*, 54(7):875–883.

Lorenz, C., Ferraudo, A. S., and Suesdek, L. (2015). Artificial Neural Network applied as a methodology of mosquito species identification. *Acta Tropica*, 152:165–169.

Lübke, A., Enax, J., Loza, K., Prymak, O., Gaengler, P., Fabritius, H. O., Raabe, D., and Epple, M. (2015). Dental lessons from past to present: Ultrastructure and composition of teeth from plesiosaurs, dinosaurs, extinct and recent sharks. *RSC Advances*, 5(76):61612–61622.

Lucifora, L. O., Cione, A. L., Menni, R. C., and Escalante, A. H. (2003). Tooth row counts, vicariance, and the distribution of the sand tiger shark *Carcharias taurus*. *Ecography*, 26(5):567–572.

Luer, C. A., Blum, P. C., and Gilbert, P. W. (1990). Rate of tooth replacement in the Nurse shark, *Ginglymostoma cirratum*. *Copeia*, 1990(1):182–191.

Lyle, J. M. (1983). Food and feeding habits of the lesser spotted dogfish, *Scyliorhinus canicula* (L.), in Isle of Man waters. *Journal of Fish Biology*, 23(6):725–737.

MacLeod, N. (2017). On the use of machine learning in morphometric analysis. In *Biological shape analysis: proceedings of the 4th international symposium*, pages 134–171.

MacLeod, N. (2018). The quantitative assessment of archaeological artifact groups: Beyond geometric morphometrics. *Quaternary Science Reviews*, 201:319–348.

MacLeod, N. and Kolska Horwitz, L. (2020). Machine-learning strategies for testing patterns of morphological variation in small samples: sexual dimorphism in gray wolf (*Canis lupus*) crania. *BMC biology*, 18(1):113.

Malik, Z., Alexiou, M., Hallgrímsson, B., Economides, A. N., Luder, H. U., and Graf, D. (2018). Bone Morphogenetic Protein 2 coordinates early tooth mineralization. *Journal of Dental Research*, 97(7):835–843.

Malik, Z., Roth, D. M., Eaton, F., Theodor, J. M., and Graf, D. (2020). Mesenchymal Bmp7 controls onset of tooth mineralization: A novel way to regulate molar cusp shape. *Frontiers in Physiology*, 11:698.

Marcus, L. F. (1990). Traditional Morphometrics. In Rohlf, F. J. and Bookstein, F. L., editors, *Proceedings of he Michigan Morphometrics Workshop*, pages 77–122.

Märkel, V. K. and Laubier, L. (1969). Zum Zahnerzatz bei Elasmobranchiern. *Zoologische Beitraege*, 15:41–44.

Marramà, G. and Kriwet, J. (2017). Principal component and discriminant analyses as powerful tools to support taxonomic identification and their use for functional and phylogenetic signal detection of isolated fossil shark teeth. *PLOS One*, 12(11):e0188806.

Martin, K. J., Rasch, L. J., and Cooper, R. L. (2016). Sox2+ progenitors in sharks link taste development with the evolution of regenerative teeth from denticles. *PNAS*, 113(51):14769–14774.

Mayor, R. and Theveneau, E. (2012). The neural crest. *Development*, 140(11):2247–2251.

McClintock, J. B., Angus, R. A., Mcdonald, M. R., Amsler, C. D., Catledge, S. A., and Vohra, Y. K. (2009). Rapid dissolution of shells of weakly calcified Antarctic benthic macroorganisms indicates high vulnerability to ocean acidification. *Antarctic Science*, 21(5):449–456.

McCourt, R. M. and Kerstitch, A. N. (1980). Mating behavior and sexual dimorphism in dentition in the stingray, *Urolophus concentricus*, from the Gulf of California. *Copeia*, pages 900–901.

McEachran, J. D. (1977). Reply to "Sexual dimorphism in skates (Rajidae)". *Evolution*, 31(1):218–220.

McEachran, J. D. and Martin, C. O. (1977). Possible occurrence of character displacement in the sympatric skates *Raja erinacea* and *R. ocellata* (Pisces: Rajidae). *Environmental Biology of Fishes*, 2(2):121–130.

McGonnell, I. M. and Graham, A. (2002). Trunk neural crest has skeletogenic potential. *Current Biology*, 12(9):767–771.

McNamara, K. J. (2012). Heterochrony: The evolution of development. *Evolution: Education and Outreach*, 5(2):203–218.

Mellinger, J. and Wrisez, F. (1993). Etude des écailles primaires de l'embryon de la roussette *Scyliorhinus canicula* (Chondrichthyes: Scyliorhinidae) au microscope électronique à balayage. *Annales des sciences naturelles-Zoologie et biologie animale*, 14(1):13–22.

Mellinger, J., Wrisez, F., and Alluchon-Gérard, M.-J. (1984). Caractères biométriques distinctifs de l'embryon et de ses annexes chez la roussette (*Scyliorhinus canicula*) de la Manche, comparée à celle de la Méditerranée, et détermination précise du stade d'éclosion. *Cahiers de biologie marine*, 25(3):305–317.

Mello, W. C., de Carvalho, J. J., and Brito, P. M. M. (2013). Microstructural morphology in early dermal denticles of hammerhead sharks (Elasmobranchii: Sphyrnidae) and related taxa. *Acta Zoologica*, 94(2):147–153.

Melo Palmeira, C. A., da Silva Rodrigues-Filho, L. F., de Luna Sales, J. B., Vallinoto, M., Schneider, H., and Sampaio, I. (2013). Commercialization of a critically endangered species (largetooth sawfish, *Pristis perotteti*) in fish markets of northern Brazil: Authenticity by DNA analysis. *Food Control*, 34(1):249–252.

Meulemans, D. and Bronner-Fraser, M. (2002). Amphioxus and lamprey AP-2 genes: implications for neural crest evolution and migration patterns. *Development*, 129:4953–4962.

Miletich, I. and Sharpe, P. T. (2004). Neural crest contribution to mammalian tooth formation. *Birth Defects Research Part C: Embryo Today: Reviews*, 72(2):200–212.

Mitteroecker, P. and Bookstein, F. (2011). Linear discrimination, ordination, and the visualization of selection gradients in modern morphometrics. *Evolutionary Biology*, 38:100–114.

Mitteroecker, P. and Gunz, P. (2009). Advances in Geometric morphometrics. *Evolutionary Biology*, 36(2):235–247.

Mitteroecker, P., Gunz, P., Bernhard, M., Schaefer, K., and Bookstein, F. L. (2004). Comparison of cranial ontogenetic trajectories among great apes and humans. *Journal of Human Evolution*, 46(6):679–698.

Mitteroecker, P., Gunz, P., Windhager, S., and Schaefer, K. (2013). A brief review of shape, form, and allometry in geometric morphometrics, with applications to human facial morphology. *Hystrix, the Italian Journal of Mammalogy*, 24(1):59–66.

Miyake, T., Vaglia, J. L., Taylor, L. H., and Hall, B. K. (1999). Development of dermal denticles in skates (Chondrichthyes, Batoidea): Patterning and cellular differentiation. *Journal of Morphology*, 241(1):61–81.

Mnasri, N., El-Kamel, O., Boumaïza, M., Reynaud, C., and Capapé, C. (2012). Food and feeding habits of the small-spotted catshark, *Scyliorhinus canicula* (Chondrichthyes: Scyliorhinidae) from the northern coast of Tunisia (central Mediterranean). *Cahiers de Biologie Marine*, 53(1):139–150.

Møller, P. R., Kullberg, T., and Jørgensen, O. A. (2004). New records of chimaeroid fishes from Greenland waters (North Atlantic), with description of juvenile *Chimaera monstrosa* and *Hydrolagus affinis* (Holocephali, Chimaeridae). *Cybium*, 28(1):55–60.

Mondéjar Fernández, J. and Meunier, F. J. (2020). New histological information on *Holoptychius* Agassiz, 1839 (Sarcopterygii, Porolepiformes) provides insights into the palaeoecological implications and evolution of the basal plate of the scales of osteichthyans. *Historical Biology*, pages 1–13.

Mongera, A. and Nüsslein-Volhard, C. (2013). Scales of fish arise from mesoderm. *Current Biology*, 23(9):R338–R339.

Moss, S. A. (1967). Tooth replacement in the lemon shark, *Negaprion brevirostris*. In Gilbert, P. W., Mathewson, R. F., and Rall, D. P., editors, *Sharks, skates and rays*, pages 319–329. Johns Hopkins Press.

Motta, P. J. and Wilga, C. D. (2001). Advances in the study of feeding behaviors, mechanisms, and mechanics of sharks. In *The behavior and sensory biology of elasmobranch fishes: an anthology in memory of Donald Richard Nelson*, pages 131–156. Springer, Dordrecht.

Moyer, J. K. and Bemis, W. E. (2016). Tooth microstructure and replacement in the Gulper shark, *Centrophorus granulosus* (Squaliformes: Centrophoridae). *Copeia*, 104(2):529–538.

Moyer, J. K., Riccio, M. L., and Bemis, W. E. (2015). Development and microstructure of tooth histotypes in the blue shark, *Prionace glauca* (Carcharhiniformes: Carcharhinidae) and the great white shark, *Carcharodon carcharias* (Lamniformes: Lamnidae). *Journal of Morphology*, 276(7):797–817.

Müller, T. (2006). Neural Development. In *Encyclopedic Reference of Genomics and Proteomics in Molecular Medicine*, pages 1258–1266. Springer, 1 edition.

Murdock, D. J. E., Dong, X.-P., Repetski, J. E., Marone, F., Stampanoni, M., and Donoghue, P. C. J. (2013). The origin of conodonts and of vertebrate mineralized skeletons. *Nature*, 502(7472):546–549.

Nguyen, H. and Bui, X. N. (2018). Predicting blast-induced air overpressure: A robust artificial intelligence system based on artificial neural networks and random forest. *Natural Resources Research*, 28(3):893–907.

Nijhout, H. F. and McKenna, K. Z. (2019). Allometry, scaling, and ontogeny of form—An introduction to the symposium. *Integrative and Comparative Biology*, 59(5):1275–1280.

Olaso, I. (1998). Importance of discarded blue whiting (*Micromesistius poutassou*) in the diet of lesser spotted dogfish (*Scyliorhinus canicula*) in the Cantabrian Sea. *ICES Journal of Marine Science*, 55(3):331–341.

Ørvig, T. (1977). A survey of odontodes ('dermal teeth') from developmental, structural, functional and phyletic points of view. In Mahala Andrews, S., Miles, R. S., and Walker, A. D., editors, *Problems in Vertebrate Evolution*, page 411. Academic Press, London and New York, 4 edition.

Ørvig, T. (1985). Histologic studies of ostracoderms, placoderms and fossil elasmobranchs. 5. Ptyctodontid tooth plates and their bearing on holocephalan ancestry: the condition of chimaerids. *Zoologica Scripta*, 14(1):55–79.

O'Shaughnessy, K. L., Dahn, R. D., and Cohn, M. J. (2015). Molecular development of chondrichthyan claspers and the evolution of copulatory organs. *Nature Communications*, 6(1):6698.

Ota, K. G., Fujimoto, S., Oisi, Y., and Kuratani, S. (2011). Identification of vertebra-like elements and their possible differentiation from sclerotomes in the hagfish. *Nature Communications*, 2:373.

Oxnard, C. and O'Higgins, P. (2009). Biology clearly needs morphometrics. Does morphometrics need biology? *Biological Theory*, 4(1):84–97.

Ozcan, E. I. and Başusta, N. (2018). Some population parameters of *Scyliorhinus canicula* (Linnaeus, 1758) from the northeastern Mediterranean Sea. *Journal of the Black Sea/Mediterranean Environment*, 24(1):51–64.

Panchen, A. L. (2001). Étienne Geoffroy St.-Hilaire: Father of "evo-devo"? *Evolution and Development*, 3(1):41–46.

Pang, H., Lin, A., Holford, M., Enerson, B. E., Lu, B., Lawton, M. P., Floyd, E., and Zhao, H. (2006). Pathway analysis using random forests classification and regression. *Bioinformatics*, 22(16):2028–2036.

Parsons, G. R. (1993). Geographic variation in reproduction between two populations of the bonnethead shark, *Sphyrna tiburo*. In Demski, L. S. and Wourms, J. P., editors, *The reproduction and development of sharks, skates, rays and ratfishes*, chapter 3, pages 25–35. Springer.

Pazzaglia, U. E., Congiu, T., Sibilia, V., Pagani, F., Benetti, A., and Zarattini, G. (2016). Relationship between the chondrocyte maturation cycle and the endochondral ossification in the diaphyseal and epiphyseal ossification centers. *Journal of Morphology*, 277(9):1187–1198.

Pechenizkiy, M., Puuronen, S., and Tsymbal, A. (2006). The impact of sample reduction on PCA-based feature extraction for supervised learning. In *Proceedings of the ACM Symposium on Applied Computing*, volume 1, pages 553–558, New York, New York, USA. ACM Press.

Peignoux-Deville, J., Bordat, C., and Vidal, B. (1989). Demonstration of bone resorbing cells in elasmobranchs: Comparison with osteoclasts. *Tissue and Cell*, 21(6):925–933.

Peignoux-Deville, J., Lallier, F., and Vidal, B. (1982). Evidence for the presence of osseous tissue in dogfish vertebrae. *Cell and tissue research*, 222(3):605–614.

Pélabon, C., Bolstad, G. H., Egset, C. K., Cheverud, J. M., Pavlicev, M., and Rosenqvist, G. (2013). On the relationship between ontogenetic and static allometry. *American Naturalist*, 181(2):195–212.

Perdiguero-Alonso, D., Montero, F. E., Kostadinova, A., Raga, J. A., and Barrett, J. (2008). Random forests, a novel approach for discrimination of fish populations using parasites as biological tags. *International Journal for Parasitology*, 38(12):1425–1434.

Pinte, N., Godefroid, M., Abbas, O., Baeten, V., and Mallefet, J. (2019). Deep-sea sharks: Relation between the liver's buoyancy and red aerobic muscle volumes, a new approach. *Comparative Biochemistry and Physiology Part A: Molecular & Integrative Physiology*, 236:110520.

Pistore, A. E., Barry, T. N., Vanderzwan, S. L., Schutz, H., Rogers, S. M., and Jamniczky, H. A. (2019). The role of genetic and environmental background driving ontogenetic trajectories of skeletal variation in the Threespine stickleback (Gasterosteus aculeatus L.). *Evolutionary Ecology Research*, 20(1):27–50.

Pollerspöck, J. and Straube, N. (2019). An identification key to elasmobranch genera based on dental morphological characters Part A: Squalomorph sharks (Superorder Squalomorphii). *Bulletin of Fish Biology Volume*, 18(1/2):77–105.

Popp, M., White, C. F., Bernal, D., Wainwright, D. K., and Lauder, G. V. (2020). The denticle surface of thresher shark tails: Three-dimensional structure and comparison to other pelagic species. *Journal of Morphology*, 281(8).

Portnoy, D. S., McDowell, J. R., Heist, E. J., Musick, J. A., and Graves, J. E. (2010). World phylogeography and male-mediated gene flow in the sandbar shark, *Carcharhinus plumbeus*. *Molecular Ecology*, 19(10):1994–2010.

Poscai, A. N., de Sousa Rangel, B., da Silva Casas, A. L., Wosnick, N., Rodrigues, A., Rici, R. E. G., and Kfoury, Jr, J. R. (2017). Microscopic aspects of the nictitating membrane in Carcharhinidae and Sphyrnidae sharks: A preliminary study. *Zoomorphology*, 136(3):359–364.

Powter, D. M., Gladstone, W., and Platell, M. (2010). The influence of sex and maturity on the diet, mouth morphology and dentition of the Port Jackson shark, *Heterodontus portusjacksoni*. *Marine and Freshwater Research*, 61(1):74.

Pratt, H. L. and Carrier, J. C. (2001). A review of elasmobranch reproductive behavior with a case study on the Nurse shark, *Ginglymostoma Cirratum*. *Environmental Biology of Fishes*, 60(1/3):157–188.

Pratt, H. L., Carrier, J. C., and Hamlett, W. C. (2005). Elasmobranch courtship and mating behavior. In Hamlett, W. C., editor, *Reproductive biology and phylogeny of Chondrichthyes: sharks, batoids and chimaeras*, chapter 5, pages 129–169. Science Publishers, Enfield, 1 edition.

Purdy, R. W. and Francis, M. P. (2007). Ontogenetic development of teeth in *Lamna nasus* (Bonnaterre, 1758) (Chondrichthyes: Lamnidae) and its implications for the study of fossil shark teeth. *Journal of Vertebrate Paleontology*, 27(4):798–810.

Püschel, T. A., Marcé-Nogué, J., Gladman, J. T., Bobe, R., and Sellers, W. I. (2018). Inferring locomotor behaviours in Miocene New World monkeys using finite element analysis, geometric morphometrics and machine-learning classification techniques applied to talar morphology. *Journal of the Royal Society Interface*, 15(146).

Qiu, M., Bulfone, A., Ghattas, I., Meneses, J. J., Christensen, L., Sharpe, P. T., Presley, R., Pedersen, R. A., and Rubenstein, J. L. R. (1997). Role of the Dlx homeobox genes in proximodistal patterning of the branchial arches: Mutations of *Dlx-1*, *Dlx-2*, and *Dlx-1* and -2 alter morphogenesis of proximal skeletal and soft tissue structures derived from the first and second arches. *Developmental Biology*, 185(2):165–184.

Quan, H., Yang, W., Schaible, E., Ritchie, R. O., and Meyers, M. A. (2018). Novel defense mechanisms in the armor of the scales of the "living fossil" coelacanth fish. *Advanced Functional Materials*, 28(46):1804237.

Quenu, M., Trewick, S. A., Brescia, F., and Morgan-Richards, M. (2020). Geometric morphometrics and machine learning challenge currently accepted species limits of the land snail *Placostylus* (Pulmonata: Bothriembryontidae) on the Isle of Pines, New Caledonia. *Journal of Molluscan Studies*, 86(1):35–41.

Ramírez-Amaro, S., Picornell, A., Arenas, M., Castro, J. A., Massutí, E., Ramon, M. M., and Terrasa, B. (2018). Contrasting evolutionary patterns in populations of demersal sharks throughout the western Mediterranean. *Marine Biology*, 165(1):1–16.

Rasch, L. J., Martin, K. J., Cooper, R. L., Metscher, B. D., Underwood, C. J., and Fraser, G. J. (2016). An ancient dental gene set governs development and continuous regeneration of teeth in sharks. *Developmental Biology*, 415(2):347–370.

Raschi, W., Musick, J. A., and Compagno, L. J. V. (1982). *Hypoprion bigelowi*, a synonym of *Carcharhinus signatus* (Pisces: Carcharhinidae), with a description of ontogenetic heterodonty in this species and notes on its natural history. *Copeia*, 1982(1):102–109.

Raschi, W. and Tabit, C. (1992). Functional aspects of placoid scales: A review and update. *Marine and Freshwater Research*, 43(1):123–147.

Reif, W.-E. (1976). Morphogenesis, pattern formation and function of the dentition of *Heterodontus* (Selachii). *Zoomorphologie*, 83(1):1–47.

Reif, W.-E. (1978). Wound healing in sharks - Form and arrangement of repair scales. *Zoomorphologie*, 90(2):101–111.

Reif, W.-E. (1980). A mechanism for tooth pattern reversal in sharks: the polarity switch model. *Wilhelm Roux's archives of developmental biology*, 188(2):115–122.

Reif, W.-E. (1982). Evolution of Dermal Skeleton and Dentition in Vertebrates: The Odontode Regulation Theory. In Hecht, M. K., Wallace, B., and Prance, G. T., editors, *Evolutionary Biology*, chapter 7, pages 287–368. Plenum Press, New York.

Ritter, E. K. and Amin, R. W. (2019). Mating scars among sharks: evidence of coercive mating? *acta ethologica*, 22(1):9–16.

Rodríguez-Cabello, C., Cabello, F., Olaso, I., and Olaso, I. (1998a). Reproductive biology of lesser spotted dogfish *Scyliorhinus canicula* (L., 1758) in the Cantabrian Sea. *Scientia Marina*, 62(3):187–191.

Rodríguez-Cabello, C., de la Gándara, F., and Sánchez, F. (1998b). Preliminary results on growth and movements of dogfish *Scyliorhinus canicula* (Linnaeus, 1758) in the Cantabrian Sea. *Oceanologica Acta*, 21(2):363–370.

Rodríguez-Cabello, C., Sánchez, F., Fernández, A., and Olaso, I. (2004). Is the lesser spotted dogfish (*Scyliorhinus canicula*) from the Cantabrian Sea, a unique stock? *Fisheries research*, 69(1):57–71.

Rodríguez-Cabello, C., Sánchez, F., and Olaso, I. (2007). Distribution patterns and sexual segregations of *Scyliorhinus canicula* (L.) in the Cantabrian Sea. *Journal of Fish Biology*, 70(5):1568–1586.

Rodríguez-Cabello, C., Sánchez, F., and Velasco, F. (2005). Growth of lesser spotted dogfish (*Scyliorhinus canicula* L., 1758) in the Cantabrian Sea, based on tag-recapture data. *Journal of Northwest Atlantic Fishery Science*, 35:131–140.

Rohlf, F. J. and Marcus, L. F. (1993). A revolution morphometrics. *Trends in Ecology and Evolution*, 8(4):129–132.

Rohlf, F. J. and Slice, D. (1990). Extensions of the Procrustes method for the optimal superimposition of landmarks. *Systematic Zoology*, 39(1):40.

Rücklin, M., Donoghue, P. C. J., Johanson, Z., Trinajstic, K., Marone, F., and Stampanoni, M. (2012). Development of teeth and jaws in the earliest jawed vertebrates. *Nature*, 491(7426):748–751.

Rücklin, M., Giles, S., Janvier, P., and Donoghue, P. C. J. (2011). Teeth before jaws? Comparative analysis of the structure and development of the external and internal scales in the extinct jawless vertebrate *Loganellia scotica*. *Evolution & Development*, 13(6):523–532.

Rutledge, K. M., Summers, A. P., and Kolmann, M. A. (2019). Killing them softly: Ontogeny of jaw mechanics and stiffness in mollusk-feeding freshwater stingrays. *Journal of Morphology*, 280(6):796–808.

Sahlberg, C. (2015). Gene expression in tooth.

Salazar-Ciudad, I. and Jernvall, J. (2002). A gene network model accounting for development and evolution of mammalian teeth. *PNAS*, 99(12):8116–8120.

Salazar-Ciudad, I. and Jernvall, J. (2010). A computational model of teeth and the developmental origins of morphological variation. *Nature*, 464(7288):583.

Sasagawa, I. (2002). Mineralization patterns in elasmobranch fish. *Microscopy Research and Technique*, 59(5):396–407.

Sasagawa, I., Ishiyama, M., Yokosuka, H., and Mikami, M. (2013). Teeth and ganoid scales in *Polypterus* and *Lepisosteus*, the basic actinopterygian fish: An approach to understand the origin of the tooth enamel. *Journal of Oral Biosciences*, 55(2):76–84.

Sasai, N., Mizuseki, K., and Sasai, Y. (2001). Requirement of *FoxD3*-class signaling for neural crest determination in *Xenopus*. *Development*, 128(13):2525–2536.

Schmitt, J. D., Gedamke, T., DuPaul, W. D., and Musick, J. A. (2015). Ontogenetic and sex-specific shifts in the feeding habits of the Barndoor skate. *Marine and Coastal Fisheries*, 7(1):409–418.

Schmitt, M. (1995). The homology concept - still alive. In *The Nervous Systems of Invertebrates: An Evolutionary and Comparative Approach*, pages 425–438. Birkhäuser Basel.

Schultze, H. P. (2016). Scales, enamel, cosmine, ganoine, and early osteichthyans. *Comptes Rendus - Palevol*, 15(1-2):83–102.

Schwartz-Ziv, R. and Tishby, N. (2017). Opening the black box of deep neural networks via information. *arXiv preprint*, page arXiv:1703.00810.

Scornet, E. (2018). Tuning parameters in random forests. *ESAIM: Proceedings and Surveys*, 60:144–162.

Seidel, R., Blumer, M., Pechriggl, E.-J., Lyons, K., Hall, B. K., Fratzl, P., Weaver, J. C., and Dean, M. N. (2017). Calcified cartilage or bone? Collagens in the tessellated endoskeletons of cartilaginous fish (sharks and rays). *Journal of Structural Biology*, 200(1):54–71.

Seidel, R., Lyons, K., Blumer, M., Zaslansky, P., Fratzl, P., Weaver, J. C., and Dean, M. N. (2016). Ultrastructural and developmental features of the tessellated endoskeleton of elasmobranchs (sharks and rays). *Journal of Anatomy*, 229(5):681–702.

Shang, X. and Chisholm, L. A. (2014). Classification of Australian native forest species using hyperspectral remote sensing and machine-learning classification algorithms. *IEEE Journal of Selected Topics in Applied Earth Observations and Remote Sensing*, 7(6):2481–2489.

Sheets, H. D., Covino, K. M., Panasiewicz, J. M., and Morris, S. R. (2006). Comparison of geometric morphometric outline methods in the discrimination of age-related differences in feather shape. *Frontiers in Zoology*, 3(1):15.

Sheets, H. D. and Zelditch, M. L. (2013). Studying ontogenetic trajectories using resampling methods and landmark data. *Hystrix, the Italian Journal of Mammalogy*, 24(1):67–73.

Shimada, A., Kawanishi, T., Kaneko, T., Yoshihara, H., Yano, T., Inohaya, K., Kinoshita, M., Kamei, Y., Tamura, K., and Takeda, H. (2013). Trunk exoskeleton in teleosts is mesodermal in origin. *Nature Communications*, 4(1):1–8.

Shimada, K. (2002). Dental homologies in lamniform sharks (Chondrichthyes: Elasmobranchii). *Journal of Morphology*, 251(1):38–72.

Shimada, K. (2005a). Phylogeny of lamniform sharks (Chondrichthyes: Elasmobranchii) and the contribution of dental characters to lamniform systematics. *Paleontological Research*, 9(1):55–72.

Shimada, K. (2005b). Types of tooth sets in the fossil record of sharks, and comments on reconstructing dentitions of extinct sharks. *Journal of Fossil Research*, 38(2):141–145.

Simon, S., Smith, A. J., Lumley, P. J., Berdal, A., Smith, G., Finney, S., and Cooper, P. R. (2009). Molecular characterization of young and mature odontoblasts. *Bone*, 45(4):693–703.

Sire, J.-Y. (2001). Teeth outside the mouth in teleost fishes: How to benefit from a developmental accident. *Evolution and Development*, 3(2):104–108.

Sire, J.-Y. and Akimenko, M.-A. (2004). Scale development in fish: a review, with description of *sonic hedgehog* (*shh*) expression in the zebrafish (*Danio rerio*). *The International Journal of Developmental Biology*, 48(2-3):233–47.

Sire, J.-Y. and Allizard, F. (2001). A fourth teleost lineage possessing extra-oral teeth: the genus *Atherion* (Teleostei; Atheriniformes). *European journal of morphology*, 39(5):295–305.

Sire, J.-Y., Donoghue, P. C. J., and Vickaryous, M. K. (2009). Origin and evolution of the integumentary skeleton in non-tetrapod vertebrates. *Journal of Anatomy*, 214(4):409–440.

Sire, J.-Y. and Huysseune, A. (2003). Formation of dermal skeletal and dental tissues in fish: a comparative and evolutionary approach. *Biological Reviews of the Cambridge Philosophical Society*, 78(2):219–249.

Smith, M., Manzanares, E., Underwood, C., Healy, C., Clark, B., and Johanson, Z. (2020). Holocephalan (Chondrichthyes) dental plates with hypermineralized dentine as a substitute for missing teeth through developmental plasticity. *Journal of Fish Biology*, 97(1):16–27.

Smith, M. M. (2003). Vertebrate dentitions at the origin of jaws: when and how pattern evolved. *Evolution and Development*, 5(4):394–413.

Smith, M. M. and Coates, M. I. (1998). Evolutionary origins of the vertebrate dentition: Phylogenetic patterns and developmental evolution. *European Journal of Oral Sciences*, 106(S1):482–500.

Smith, M. M. and Coates, M. I. (2001). Evolutionary origins of teeth and jaws: developmental models and phylogenetic patterns. In Teaford, M. F., Smith, M. M., and Ferguson, M. W. J., editors, *Development, Function and Evolution of Teeth*, chapter 10, pages 133–151. Cambridge University Press, Cambridge.

Smith, M. M. and Hall, B. K. (1990). Development and evolutionary origins of vertebrate skeletogenic and odontogenic tissues. *Biological Reviews*, 65(3):277–373.

Smith, M. M., Hickman, A., Amanze, D., Lumsden, A., and Thorogood, P. (1994). Trunk neural crest origin of caudal fin mesenchyme in the zebrafish *Brachydanio rerio*. *Proceedings of the Royal Society B*, 256(1346):137–145.

Smith, M. M., Johanson, Z., Butts, T., Ericsson, R., Modrell, M., Tulenko, F. J., Davis, M. C., and Fraser, G. J. (2015). Making teeth to order: conserved genes reveal an ancient molecular pattern in paddlefish (Actinopterygii). *Proceedings of the Royal Society B: Biological Sciences*, 282(1805):20142700.

Smith, M. M., Johanson, Z., Underwood, C., and Diekwisch, T. G. H. (2013). Pattern formation in development of chondrichthyan dentitions: a review of an evolutionary model. *Historical Biology*, 25(2):127–142.

Smith, M. M., Underwood, C., Clark, B., Kriwet, J., and Johanson, Z. (2018). Development and evolution of tooth renewal in neoselachian sharks as a model for transformation in chondrichthyan dentitions. *Journal of Anatomy*, 232(6):891–907.

Smith, S. E., Au, D. W., and Show, C. (1998). Intrinsic rebound potentials of 26 species of Pacific sharks. *Marine and Freshwater Research*, 49(7):663–678.

Soares, K. D. A. and de Carvalho, M. R. (2019). The catshark genus *Scyliorhinus* (Chondrichthyes: Carcharhiniformes: Scyliorhinidae): taxonomy, morphology and distribution. *Zootaxa*, 4601(1):1–147.

Soda, K. J., Slice, D. E., and Naylor, G. J. P. (2017). Artificial neural networks and geometric morphometric methods as a means for classification: A case-study using teeth from *Carcharhinus* sp. (Carcharhinidae). *Journal of Morphology*, 278(1):131–141.

Soldo, A., Dulcic, J., Cetinic, P., and Cetinic, P. (2000). Contribution to the study of the morphology of the teeth of the nursehound *Scyliorhinus stellaris* (Chondrichthyes: Scyliorhinidae). *Scientia Marina*, 64(3):355–356.

Som, P. M. and Miletich, I. (2018). Review of the embryology of the teeth. *Neurographics*, 8(5):369–393.

Sonnenschein, A., VanderZee, D., Pitchers, W. R., Chari, S., and Dworkin, I. (2015). An image database of *Drosophila melanogaster* wings for phenomic and biometric analysis. *GigaScience*, 4(1):25.

Spriggs, E. L., Schmerler, S. B., Edwards, E. J., and Donoghue, M. J. (2018). Leaf form evolution in *Viburnum* parallels variation within individual plants. *American Naturalist*, 191(2):235–249.

Stalling, D., Westerhoff, M., and Hege, H.-C. (2005). Amira: a highly interactive system for visual data analysis. In *The Visualization Handbook*, pages 749–767. Elsevier.

Stevens, J. D. (1974). The occurrence and significance of tooth cuts on the Blue shark (*Prionace Glauca* L.) from British waters. *Journal of the Marine Biological Association of the United Kingdom*, 54(2):373–378.

Stewart, R. A., Arduini, B. L., Berghmans, S., George, R. E., Kanki, J. P., Henion, P. D., and Look, A. T. (2006). Zebrafish foxd3 is selectively required for neural crest specification, migration and survival. *Developmental Biology*, 292(1):174–188.

Strasburg, D. W. (1963). The diet and dentition of *Isistius brasiliensis*, with remarks on tooth replacement in other sharks. *Copeia*, pages 33–40.

Straube, N., Schliewen, U., and Kriwet, J. (2007). Dental structure of the Giant lantern shark *Etmopterus baxteri* (Chondrichthyes: Squaliformes) and its taxonomic implications. *Environmental Biology of Fishes*, 82(2):133–141.

Sweetman, A. K., Thurber, A. R., Smith, C. R., Levin, L. A., Mora, C., Wei, C. L., Gooday, A. J., Jones, D. O. B., Rex, M., Yasuhara, M., Ingels, J., Ruhl, H. A., Frieder, C. A., Danovaro, R., Würzberg, L., Baco, A., Grupe, B. M., Pasulka, A., Meyer, K. S., Dunlop, K. M., Henry, L. A., and Roberts, J. M. (2017). Major impacts of climate change on deep-sea benthic ecosystems. *Elementa: Science of the Anthropocene*, 5:4.

Takigawa-Imamura, H., Morita, R., Iwaki, T., Tsuji, T., and Yoshikawa, K. (2015). Tooth germ invagination from cell–cell interaction: Working hypothesis on mechanical instability. *Journal of Theoretical Biology*, 382:284–291.

Taniuchi, T. and Shimizu, M. (1993). Dental sexual dimorphism and food habits in the stingray *Dasyatis akajei* from Tokyo Bay, Japan. *Nippon Suisan Gakkaishi*, 59(1):53–60.

Taniuchi, T. and Tachikawa, H. (1997). Geographical variation in age and growth of *Squalus mitsukurii* (Elasmobranchii: Squalidae) in north Pacific. In *Proceedings of 5th Indo-Pacific Fish Conference, Nouméa*, pages 321–328.

Templeman, W. (1984). Variations in numbers of median dorsal thorns and rows of teeth in thorny skate (*Raja radiata*) of the Northwest Atlantic. *Journal of Northwest Atlantic Fishery Science*, 5(2):171–179.

Thesleff, I. and Sharpe, P. (1997). Signalling networks regulating dental development. *Mechanisms of Development*, 67(2):111–123.

Thiery, G., Guy, F., and Lazzari, V. (2019). A comparison of relief estimates used in three-dimensional dental topography. *American Journal of Physical Anthropology*, 170(2):260–274.

Thomas, B. L., Tucker, A. S., Qui, M., Ferguson, C. A., Hardcastle, Z., Rubenstein, J. L., and Sharpe, P. T. (1997). Role of *Dlx-1* and *Dlx-2* genes in patterning of the murine dentition. *Development*, 124(23):4811–4818.

Thompson, D. W. (1917). *On Growth and Form*. Cambridge University Press.

Tomita, T., Miyamoto, K., Kawaguchi, A., Toda, M., Oka, S.-I., Nozu, R., and Sato, K. (2017). Dental ontogeny of a white shark embryo. *Journal of Morphology*, 278(2):215–227.

Tomita, T., Murakumo, K., Komoto, S., Dove, A., Kino, M., Miyamoto, K., and Toda, M. (2020). Armored eyes of the whale shark. *PLOS One*, 15(6):e0235342.

Torok, M. A., Gardiner, D. M., Izpisúa-Belmonte, J. C., and Bryant, S. V. (1999). Sonic Hedgehog (*shh*) expression in developing and regenerating axolotl limbs. *Journal of Experimental Zoology*, 284(2):197–206.

Tucker, A. S., Matthews, K. L., and Sharpe, P. T. (1998). Transformation of tooth type induced by inhibition of BMP signaling. *Science*, 282(5391):1136–1138.

Tucker, A. S. and Sharpe, P. T. (1999). Molecular genetics of tooth morphogenesis and patterning: The right shape in the right place. *Journal of Dental Research*, 78(4):826–834.

Underwood, C., Johanson, Z., and Smith, M. M. (2016). Cutting blade dentitions in squaliform sharks form by modification of inherited alternate tooth ordering patterns. *Open Science*, 3(11):160385.

Underwood, C. J., Johanson, Z., Welten, M., Metscher, B., Rasch, L. J., Fraser, G. J., and Smith, M. M. (2015). Development and evolution of dentition pattern and tooth order in the skates and rays (Batoidea; Chondrichthyes). *PLOS One*, 10(4):e0122553.

Ungar, P. S. and Sues, H.-D. (2019). Tetrapod Teeth: Diversity, Evolution, and Function. In Bels, V. and Whishaw, I., editors, *Feeding in Vertebrates*, pages 385–429. Springer, Cham.

Vaahtokari, A., Åberg, T., Jernvall, J., Keränen, S., and Thesleff, I. (1996). The enamel knot as a signaling center in the developing mouse tooth. *Mechanisms of Development*, 54(1):39–43.

Van Der Brugghen, W. and Janvier, P. (1993). Denticles in thelodonts. *Nature*, 364(6433):107.

Venables, W. N. and Ripley, B. D. (2002). *Modern Applied Statistics with S*. Springer New York, fourth edition.

Veríssimo, A., McDowell, J. R., and Graves, J. E. (2010). Global population structure of the spiny dogfish *Squalus acanthias*, a temperate shark with an antitropical distribution. *Molecular Ecology*, 19(8):1651–1662.

Vickaryous, M. K. and Hall, B. K. (2006). Human cell type diversity, evolution, development, and classification with special reference to cells derived from the neural crest. *Biological Reviews of the Cambridge Philosophical Society*, 81(3):425–455.

Vinu, J., Rajeeshkumar, M. P., Parmeswaran, U. V., Sumod, K. S., Akhilesh, K. V., Manjebrayakath, H., and Sanjeevan, V. N. (2017). Redescription and sexual dimorphism of Andaman leg-skate *Cruriraja andamanica* (Chondrichthyes: Rajiformes) with comments on the zoogeography of the genus *Cruriraja*. *Journal of Fish Biology*, 91(2):587–602.

Von der Mark, K. and Von der Mark, H. (1977). The role of three genetically distinct collagen types in endochondral ossification and calcification of cartilage. *The Journal of Bone and Joint Surgery. British volume*, 59(4):458–464.

Wasiljew, B. D., Pfaender, J., Wipfler, B., Utama, I. V., and Herder, F. (2020). Do we need the third dimension? Quantifying the effect of the *z*-axis in 3D geometric morphometrics based on sailfin silversides (Telmatherinidae). *Journal of Fish Biology*, 97(2):537–545.

Wass, R. C. (1973). Size, growth, and reproduction of the Sandbar shark, *Carcharhinus milberti*, in Hawaii. *Pacific Science*, 27(4):305–318.

Wautier, K., Van der heyden, C., and Huysseune, A. (2001). A quantitative analysis of pharyngeal tooth shape in the zebrafish (*Danio rerio*, Teleostei, Cyprinidae). *Archives of Oral Biology*, 46(1):67–75.

Webster, M. and Sheets, H. D. (2010). A practical introduction to landmark-based geometric morphometrics. *The Paleontological Society Papers*, 16:163–188.

Welladsen, H. M., Southgate, P. C., and Heimann, K. (2010). The effects of exposure to near-future levels of ocean acidification on shell characteristics of *Pinctada fucata* (Bivalvia: Pteriidae). *Molluscan Research*, 30(3):125.

Welton, B. J. and Farish, R. F. (1993). *The collector's guide to fossil sharks and rays from the Cretaceous of Texas*. Before Time.

Wen, L., Weaver, J. C., Thornycroft, P. J., and Lauder, G. V. (2015). Hydrodynamic function of biomimetic shark skin: effect of denticle pattern and spacing. *Bioinspiration & biomimetics*, 10(6):066010.

White, W. T., Ebert, D. A., Naylor, G. J. P., Ho, H.-C., Clerkin, P., Veríssimo, A., and Cotton, C. F. (2013). Revision of the genus Centrophorus (Squaliformes: Centrophoridae): Part 1—Redescription of *Centrophorus granulosus* (Bloch & Schneider), a senior synonym of *C. acus* Garman and *C. niaukang* Teng. *Zootaxa*, 3752:35–72.

Whitenack, L. B. and Gottfried, M. D. (2010). A morphometric approach for addressing tooth-based species delimitation in fossil mako sharks, *Isurus* (Elasmobranchii: Lamniformes). *Journal of Vertebrate Paleontology*, 30(1):17–25.

Wiley, D. F., Amenta, N., Alcantara, D. A., Ghosh, D., Kil, Y. J., Delson, E., Harcourt-Smith, W., Rohlf, F. J., St. John, K., and Hamann, B. (2005). Evolutionary Morphing. In *Proceedings of the 5th IEEE Conference on Visualization*, pages 431–438. Institute of Electrical and Electronics Engineers (IEEE).

Wilga, C. D. and Motta, P. J. (2000). Durophagy in sharks: feeding mechanics of the hammerhead *Sphyrna tiburo*. *The Journal of Experimental Biology*, 203(18):2781–2796.

Winn, A. A. (1996). The contributions of programmed developmental change and phenotypic plasticity to within-individual variation in leaf traits in *Dicerandra linearifolia*. *Journal of Evolutionary Biology*, 9(6):737–752.

Witten, P. E., Huysseune, A., and Hall, B. K. (2010). A practical approach for the identification of the many cartilaginous tissues in teleost fish. *Journal of Applied Ichthyology*, 26(2):257–262.

Witten, P. E., Sire, J.-Y., and Huysseune, A. (2014). Old, new and new-old concepts about the evolution of teeth. *Journal of Applied Ichthyology*, 30(4):636–642.

Wolpert, D. H. (1996). The lack of a priori distinctions between learning algorithms. *Neural Computation*, 8(7):1341–1390.

Wolpert, D. H. and Macready, W. G. (1997). No free lunch theorems for optimization. *IEEE Transactions on Evolutionary Computation*, 1(1):67–82.

Yamaguchi, A., Taniuchi, T., and Shimizu, M. (1998). Geographic variation in growth of the starspotted dogfish *Mustelus manazo* from five localities in Japan and Taiwan. *Fisheries Science*, 64(5):732–739.

Yamaguchi, A., Taniuchi, T., and Shimizu, M. (2000). Geographic Variations in Reproductive Parameters of the Starspotted Dogfish, *Mustelus manazo*, from Five Localities in Japan and in Taiwan. *Environmental Biology of Fishes*, 57(2):221–233.

Yang, Y., Drossopoulou, G., Chuang, P. T., Duprez, D., Marti, E., Bumcrot, D., Vargesson, N., Clarke, J., Niswander, L., McMahon, A., and Tickle, C. (1997). Relationship between dose, distance and time in *Sonic Hedgehog*-mediated regulation of anteroposterior polarity in the chick limb. *Development*, 124(21):4393–4404.

Young, R. F. (1993). Observation of the mating behavior of the yellow stingray, *Urolophus jamaicensis*. *Copeia*, 1993(3):879–880.

Zelditch, M. L., Swiderski, D. L., Sheets, H. D., and Fink, W. L. (2004). *Geometric Morphometrics for Biologists: A Primer*. Elsevier Academic Press, San Diego.

Zhang, L., Hua, F., Yuan, G. H., Zhang, Y. D., and Chen, Z. (2008). Sonic hedgehog signaling is critical for cytodifferentiation and cusp formation in developing mouse molars. *Journal of Molecular Histology*, 39(1):87–94.